

**ISOLATION OF DIOSGENIN FROM *Smilax kraussiana* MEISN EX.  
KRAUSS AND SYNTHESIS OF ITS DERIVATIVES AS  
ANTICANCER AGENTS**

**By**

**Abdulumumeen Amao HAMID**

**B.Sc. (Hons) CHEMISTRY, ILORIN,  
M.Sc. ORGANIC CHEMISTRY, IBADAN  
MATRIC NO.: 129951**

**a thesis in the Department of Chemistry**

**Submitted to**

**the Faculty of Science  
In partial fulfillment of the requirements for**

**the degree of**

**DOCTOR OF PHILOSOPHY**

**of the**

**UNIVERSITY OF IBADAN**

**AUGUST, 2015**

## ABSTRACT

Plants remain a major source of novel drugs for the treatment of various diseases like cancer. The search for safe anticancer drugs from plants has led to the discovery of camptothecin and taxol. *Smilax kraussiana* is used in herbal medicine to treat tumors, venereal and skin diseases. Many plants including *S. kraussiana* are still underexploited despite their ethnomedicinal properties. This study was designed to isolate and characterise the constituents of *S. kraussiana*, synthesise active derivatives from the most bioactive isolate and evaluate the anticancer activities of the extracts and compounds.

The leaves and stems of *S. kraussiana* were collected from Onigambari Forest Reserve, Ibadan and authenticated at Forestry Research Institute of Nigeria (Voucher number: FHI 108799), Ibadan, Oyo State. The samples were air-dried, pulverized and successively extracted with hexane, ethyl acetate and methanol. The extracts were subjected to chromatographic techniques to obtain pure isolates. Structural elucidation of the isolated compounds was done using 1D, 2D Nuclear Magnetic Resonance and Mass Spectroscopic methods. Isolated diosgenin was synthetically modified by oxidation, reduction, and condensation reactions. The extracts, isolates and synthesised compounds were evaluated for anticancer activities against four human cancer cell lines; leukaemic (K-562), hepatic (WRL), breast (MCF-7) and colorectal carcinoma (COLO) at 20, 50 and 100  $\mu\text{M}$  concentrations using 3-(4,5-dimethylthiazol-2-yl)-2,5-diphenyltetrazolium bromide and Sorphordamine assays. Tamoxifen was used as positive control for both assays. Data were analysed using descriptive statistics.

The successive extraction of *S. kraussiana* with hexane, ethyl acetate and methanol yielded 14.0, 20.0 and 11.5 g of the extracts respectively. Chromatographic separation of hexane, ethyl acetate and methanol extracts resulted in four, nine and six compounds respectively. The isolates are mainly triterpenoids, steroids and fatty acids, while the most abundant isolate was diosgenin (3 $\beta$ -hydroxy-5-spirostene) (80.0 mg = 0.5 %). The modification of diosgenin via two synthetic reaction schemes yielded fifteen and twelve compounds respectively. The new analogues obtained from the first scheme included (22 $\beta$ )-25-oxo-27-nor-furost-5-en-3 $\beta$ -acetate, (22 $\beta$ )-25-hydroxy-3 $\beta$ -yl-27-nor-furost-5-en-3 $\beta$ -acetate, (22 $\beta$ )-(Z)-26-(4'-nitrobenzylidene)-3 $\beta$ -yl-furost-5-en-3 $\beta$ -acetate, (22 $\beta$ )-26-(3',4',5'-

trimethoxybenzylidene)-3 $\beta$ -yl-furost-5-en-3 $\beta$ -acetate, 3 $\beta$ -acetoxy-furost-5-en-26-aldoxime and 3 $\beta$ -acetoxy-27-nor-furost-5-en-25-ketoxime. The new compounds from the second scheme included (22 $\beta$ ,25R)-3 $\beta$ -acetoxy-spirost-5-en-7-one, (22 $\beta$ ,25R)-3 $\beta$ -acetoxy-spirost-5-en-7-ketoxime, (22 $\beta$ ,25R)-spirost-3,5-dien-7-one, (22 $\beta$ ,25R)-3 $\beta$ -acetoxy-7-(4'-nitrobenzylidene)-spirost-5-en-3 $\beta$ -yl, (22 $\beta$ ,25R)-3 $\beta$ -acetoxy-spirost-5-en-3 $\beta$ -yl-7-(ethyl-3'-propanoate)-ketoxime and (22 $\beta$ ,25R)-3 $\beta$ -acetoxy-spirost-5-en-3 $\beta$ -yl-7-(ethyl-4'-butyrate)-ketoxime. Nineteen out of the 27 synthesised compounds are reported for the first time. Ethyl acetate and methanol extracts of *S. kraussiana* exhibited cytotoxic activity against WRL and COLO cell lines with IC<sub>50</sub> of 46.1 and 90.0  $\mu$ M, but showed low inhibition on K-562 and MCF-7 with IC<sub>50</sub> of 113.0 and 236.0  $\mu$ M respectively. Hexane extract exhibited low activity against the four cell lines with IC<sub>50</sub> between 130.0 and 310.0  $\mu$ M. The most bioactive isolate, diosgenin showed cytotoxic activity against the four cell lines by suppressing the viability of cells with IC<sub>50</sub> between 12.3 and 38.0  $\mu$ M, while active synthesised compounds inhibited the growth of the four cell lines with IC<sub>50</sub> between 7.5 and 35.5  $\mu$ M.

The phytochemical constituents of *Smilax kraussiana* extracts justify their use in herbal medicine. The isolated compounds are reported for the first time from the plant. The synthesised diosgenin derivatives could serve as lead compounds for further investigation as anticancer agents.

**Keywords:** *Smilax kraussiana*, Diosgenin, (22 $\beta$ )-26-(3',4',5'-trimethoxybenzylidene)-3 $\beta$ -yl-furost-5-en-3 $\beta$ -acetate, (22 $\beta$ )-25-oxo-27-nor-furost-5-en-3 $\beta$ -acetate, (22 $\beta$ ,25R)-3 $\beta$ -acetoxy-spirost-5-en-3 $\beta$ -yl-7-(ethyl-3'-propanoate)-ketoxime, Human cell-lines.

**Word count:** 490

## **DEDICATION**

This research work is dedicated to Almighty God, The beginning and the end.

## ACKNOWLEDGEMENTS

My sincere gratitude goes to Almighty God, the most beneficent and merciful, for His divine protection over my life, God may your name be exalted.

I express my immense gratitude and appreciation to my supervisor, Dr. Olapeju O. Aiyelaagbe for her ability to disseminate information, patience, guidance, encouragement, steadfastness and for freely allowing me to learn abundantly from her fountain of wisdom, knowledge and experience throughout this research work. You are a Mother and a rare gem. Thank you for everything Ma.

I acknowledge and appreciate the entire Staff of the Department of Chemistry, University of Ibadan especially the head of department, Prof. A.A. Adesomoju for all they have imparted to my life during the course of this study. for the support given to me during the course of this work. I am indebted to all the organic group lecturers, especially Prof. O. Ekundayo and Dr Ibrahim Oladosu for their guidance and encouragement, and also for creating time despite his tight schedules to inspire me academically. You are always active and reliable. My thanks go to my Labmates in Organic unit, Department of Chemistry, University of Ibadan for their encouragement and support.

My appreciation goes to the entire staff of the Department of Chemistry, University of Ilorin, especially the head of department, Dr. N. Abdus-Salam, Organic unit lecturers and colleagues, Drs. Lamidi Usman, Stephen Oguntayo, My friends and brothers Dr. Sunday Elaigwu, Mr. M. A. Adebayo and Dr. Baba Alafara for their support and encouragement during the work. I am indebted to the Administration of University of Ilorin for giving me staff development award (study leave with pay) to pursue this research work.

My gratitude goes to a rare guide, Dr. Arvind S. Negi of Central Institute of Medicinal and Aromatic Plants (CIMAP), Lucknow, India for encouragement, support and his immense academic contribution which proved indispensable as confirmed in his academic and moral skills. My thanks go to my CIMAP labmates Kidwai sir, Satish, Yashveer, Balo, Ravi, Aastha, Tanu, Seema and Fatima for their support and the harmonious working

relationship throughout my stay with them during the course of this work. The caring and hospitality of Kidwai's family at CIMAP Staff Colony, Lucknow (India), can never be forgotten. Thank you so much Faiz, Owaiz and other family members for your support. My gratitude goes to the Director, entire Staff and Research fellows of CSIR-CIMAP, Lucknow, India for their support. I acknowledge the TWAS-CSIR and CSIR-CIMAP Fellowships for providing all the funds and facilities needed for this research work.

My Parents, Alh. and Mrs. Hamid A. Amao, thank you for your kindness, encouragement, moral and financial support, and everything. I thank all those who might have helped me at every stage of this work either personally or in their various official capacities.

I thank and appreciate my wife, Mrs. Hamid Bola Rahmat and our children, Halimah, Imam Hassan, Zainab (Taiwo) and Aisha (Kehinde) for their support.

## **CERTIFICATION**

I certify that this work was carried out by Mr. Abdulmumeen A. HAMID in the Department of Chemistry, University of Ibadan, Ibadan, Nigeria.

.....

Supervisor

Dr. Olapeju O. Aiyelaagbe,

B.Sc., M.Sc., Ph.D (Ibadan),

Reader, Department of Chemistry,

University of Ibadan, Ibadan, Nigeria

## TABLE OF CONTENTS

	Page
Abstract	ii
Dedication	iv
Acknowledgements	v
Certification	vii
Table of Contents	viii
List of figures	xvii
List of Tables	xxv
List of Schemes	xxviii
List of Abbreviation	xxix
<b>CHAPTER ONE: INTRODUCTION</b>	<b>1</b>
1.1 Plants as source of Pharmaceuticals	1
1.2 Drugs developed from Plants	2
1.3 Research objectives	6
<b>CHAPTER TWO: LITERATURE REVIEW</b>	<b>7</b>
2.1 The Smilax genus	7
2.2 Species of Smilax	7
2.2.1 <i>Smilax kraussiana</i>	7



2.2.2	<i>Smilax aspera</i>	9
2.2.3	<i>Smilax china</i>	9
2.3	Isolated compounds from <i>Smilax</i> species	10
2.4	Biological potentials of <i>Smilax</i> species	19
2.4.1	Antimicrobial activity	19
2.4.2	Antimalarial and antipyretic activities	19
2.4.3	Antioxidant activity	20
2.4.4	Antiproliferative activity	23
2.4.5	Anti-HIV, antihepatotoxic and contraceptive activities	23
2.5	Cancer	26
2.6	Antiproliferative drugs	26
2.6.1	Camptothecin	27
2.6.2	Combretastatin A-4	31
2.6.3	Podophylloxin	34
2.7	Secondary metabolites	36
2.7.1	Terpenoids	36
2.7.2	Flavonoids	38
2.7.3	Alkaloids	40
2.7.4	Saponins	41
2.7.5	Tannins	44

2.8	Chromatography	45
2.8.1	Column chromatography	45
2.8.2	Thin layer chromatography (TLC)	45
2.8.3	High performance liquid chromatography (HPLC)	46
2.8.4	Gas chromatography	46
2.9	Spectroscopic Techniques	47
2.9.1	Nuclear Magnetic Resonance (NMR) Spectroscopy	47
2.9.1.1	Two-dimensional nuclear magnetic resonance spectroscopy (2D NMR)	47
2.9.2	Mass Spectroscopy (MS)	49
2.9.3	Infrared Spectroscopy (IR)	50
2.9.4	Ultra violet Spectroscopy (UV)	51
2.9.5	X-ray crystallography	51
	<b>CHAPTER THREE: MATERIALS AND METHODS</b>	<b>53</b>
3.1	General Experimental Procedures	53
3.2	Collection of plant materials	53
3.3	Extraction of plant materials	54
3.4	Antiproliferative assays of Extracts	54
3.4.1	3-(4,5-dimethylthiazol-2-yl)-2,5-diphenyl-2H-tetrazolium bromide (MTT) assay	54
3.4.2	Sulphorhodamine assay	55

3.5	Phytochemical Screening	55
3.5.1	Flavonoids Test	55
3.5.2	Tannins Test	55
3.5.3	Saponins Test	55
3.5.4	Anthocyanins Test	56
3.5.5	Anthraquinone Test	56
3.5.6	Cardiac glycoside Test	56
3.5.7	Alkaloids Test	56
3.5.8	Carbohydrates Test	56
3.6	Column chromatography of hexane extract of <i>S. kraussiana</i> (aerial parts)	57
3.7	Column chromatography of ethyl acetate extract of <i>S. kraussiana</i> (aerial parts)	59
3.8	Column chromatography of methanol extract of <i>S. kraussiana</i> (aerial parts)	59
3.9	Antiproliferative activity of isolated compounds	60
3.10	Chemical synthesis of Diosgenin (Haske-9) analogues	60
3.10.1.	Synthesis of (22 $\beta$ ,25R)-spirost-5-en-3 $\beta$ -yl-3-acetate (Haad-1)	60
3.10.2.	Synthesis of (22 $\beta$ ,25R)-3 $\beta$ ,26-dihydroxyfurost-5-en-3 $\beta$ -acetate (Haad-2a)	60
3.10.3	Synthesis of (22 $\beta$ ,25R)-furost-5-en-3 $\beta$ ,26-diacetate (Haad-2b)	62
3.10.4	Synthesis of (22 $\beta$ ,25R)-3 $\beta$ -hydroxy,26-formyl-furost-5-en-3 $\beta$ -acetate (Haad-3)	62
3.10.5	Synthesis of (22 $\beta$ )-3 $\beta$ -hydroxy,25-oxo-27-nor-furost-5-en-3 $\beta$ -acetate (Haad-4)	62
3.10.6	Wittig reaction on (22 $\beta$ )-3 $\beta$ -hydroxy,25-oxo-27-nor-furost-5-en-3 $\beta$ -acetate, (Haad-3)	63

3.10.6.1 Synthesis of (22 $\beta$ )-(E)-26-Benzylidene-3 $\beta$ -yl-furost-5-en-3-acetate (Haad-5)	63
3.10.6.2 Synthesis of (22 $\beta$ )-(Z)-26-(4'-Nitrobenzylidene)-3 $\beta$ -yl-furost-5-en-3-acetate (Haad-6)	63
3.10.6.3 Synthesis of (22 $\beta$ )-(E)-26-(3',4',5'-Trimethoxybenzylidene)-3 $\beta$ -yl-furost-5-en-3-acetate (Haad-7a) and (22 $\beta$ )-(Z)-26-(3',4',5'-Trimethoxybenzylidene)-3 $\beta$ -yl-furost-5-en-3-acetate (Haad-7b).	63
3.10.7 Synthesis of (22 $\beta$ )-3 $\beta$ -Acetoxy-furost-5-en-26-aldoxime (Haad-8)	63
3.10.8 Synthesis of (22 $\beta$ )-3 $\beta$ -Acetoxy-furost-5-en-26-aldoxime acetate (Haad-9)	64
3.10.9 Synthesis of (22 $\beta$ )-3 $\beta$ -Acetoxy-27-nor-furost-5-en-25-ketoxime (Haad-10)	64
3.10.10 Synthesis of (22 $\beta$ )-3 $\beta$ -Hydroxy-27-nor-furost-5-en-25-ketoxime-3 $\beta$ ,26-diacetate (Haad-11)	64
3.10.11 Synthesis of (22 $\beta$ )-25 $\alpha$ -Hydroxy-3 $\beta$ -yl-27-nor-furost-5-en-3-acetate and (22 $\beta$ )-25 $\beta$ -Hydroxy-3 $\beta$ -yl-27-nor-furost-5-en-3-acetate (Haad-12)	64
3.10.12 Synthesis of (22 $\beta$ ,25R)-7-oxo-spirost-5-en-3 $\beta$ -yl-3-acetate (Hak-1)	66
3.10.13 Synthesis of (22 $\beta$ ,25R)-3 $\beta$ -Acetoxy-spirost-5-en-3 $\beta$ -yl-7-ketoxime (Hak-2)	66
3.10.14 Synthesis of (22 $\beta$ ,25R)-3 $\beta$ -Acetoxy-spirost-5-en-3 $\beta$ -yl-7-(ethyl-2'-acetate)-ketoxime (Hak-3)	66
3.10.15 Synthesis of (22 $\beta$ ,25R)-3 $\beta$ -Acetoxy-spirost-5-en-3 $\beta$ -yl-7-(ethyl-3'-propanoate)-ketoxime (Hak-4)	67
3.10.16 Synthesis of (22 $\beta$ ,25R)-3 $\beta$ -Acetoxy-spirost-5-en-3 $\beta$ -yl-7-(ethyl-4'-butyrate)-ketoxime (Hak-5)	67
3.10.17 Synthesis of (22 $\beta$ ,25R)-3 $\beta$ -Acetoxy-spirost-5-en-3 $\beta$ -yl-7-(ethyl-5'-pentanoate)-ketoxime (Hak-6)	67
3.10.18 Synthesis of (22 $\beta$ ,25R)-3 $\beta$ -Acetoxy-spirost-5-en-3 $\beta$ -yl-7-(ethyl-6'-hexanoate)-ketoxime (Hak-7)	67
3.10.19 Synthesis of (22 $\beta$ ,25R)-3 $\beta$ -Acetoxy-spirost-5-en-3 $\beta$ -yl-7-(ethyl-7 <sup>1</sup> -heptanoate)-ketoxime (Hak-8)	67
3.10.20 Synthesis of (22 $\beta$ ,25R)-3 $\beta$ -Acetoxy-spirost-5-en-3 $\beta$ -yl-7-benzyketoxime (Hak-9)	67

3.10.21	Synthesis of (22 $\beta$ ,25R)-3 $\beta$ -Acetoxy-spirost-5-en-3 $\beta$ -yl-7-(4'-butanoic)-ketoxime (Hak-10)	68
3.10.22	Synthesis of (22 $\beta$ ,25R)-3 $\beta$ -Acetoxy-7-(4-nitrobenzylidene)-spirost-5-en-3 $\beta$ -yl (Hak-11)	68
3.10.23	Synthesis of (22 $\beta$ ,25R)- 7-oxo-spirost-3,5-diene (Hak-12)	68
<b>CHAPTER FOUR: RESULTS AND DISCUSSION</b>		69
4.1	Extraction procedure	69
4.2	Antiproliferative assay	69
4.3	Phytochemical screening	72
4.4	Column chromatography of hexane extract of <i>S. kraussiana</i> (aerial parts)	74
4.4.1	Characterisation of Haskh-1	74
4.4.2	Characterisation of Haskh-2	77
4.4.3	Characterisation of Haskh-3	80
4.4.4	Characterisation of Haskh-4	94
4.5	Column chromatography of ethyl acetate extract of <i>S. kraussiana</i> (aerial parts)	109
4.5.1	Characterisation of Haske-1	109
4.5.2	Characterisation of Haske-2	117
4.5.3	Characterisation of Haske-3	130
4.5.4	Characterisation of Haske-4	142
4.5.5	Characterisation of Haske-5	145
4.5.6	Characterisation of Haske-6	148
4.5.7	Characterisation of Haske-7	151

4.5.8	Characterisation of Haske-8	154
4.5.9	Characterisation of Haske-9	157
4.6	Column chromatography of methanol extract of <i>S. kraussiana</i> (aerial parts)	164
4.6.1	Characterisation of Haskm-1	164
4.6.2	Characterisation of Haskm-2	167
4.6.3	Characterisation of Haskm-3	179
4.6.4	Characterisation of Haskm-4	182
4.6.5	Characterisation of Haskm-5	185
4.7	Antiproliferative activity of isolated compounds obtained from <i>Smilax kraussiana</i> (Aerial parts)	188
4.8	Synthetic modification of diosgenin (First reaction scheme)	190
4.8.1.	Synthesis and characterisation of (22 $\beta$ ,25R)-spirost-5-en-3 $\beta$ -yl-3-acetate (Haad-1)	190
4.8.2	Synthesis and characterisation of (22 $\beta$ ,25R)-3 $\beta$ ,26-dihydroxyfurost-5-en-3 $\beta$ -acetate (Haad-2a)	197
4.8.3	Synthesis and characterisation of (22 $\beta$ ,25R)-furost-5-en-3 $\beta$ ,26-diacetate (Haad-2b)	203
4.8.4	Synthesis and characterisation of (22 $\beta$ ,25R)-3 $\beta$ -hydroxy,26-formyl-furost-5-en-3 $\beta$ -acetate (Haad-3)	209
4.8.5	Synthesis and characterisation of (22 $\beta$ )-3 $\beta$ -hydroxy,25-oxo-27-nor-furost-5-en-3 $\beta$ -acetate (Haad-4)	215
4.8.6	Synthesis and characterisation of (22 $\beta$ )-(E)-26-Benzylidene-3 $\beta$ -yl-furost-5-en-3 $\beta$ -acetate (Haad-5)	229
4.8.7	Synthesis and characterisation of (22 $\beta$ )-(Z)-26-(4'-Nitrobenzylidene)-3 $\beta$ -yl-3 $\beta$ -yl-furost-5-en-3 $\beta$ -acetate (Haad-6)	235
4.8.8	Synthesis and characterisation of (22 $\beta$ )-(E)-26-(3',4',5'-Trimethoxybenzylidene)-3 $\beta$ -yl-furost-5-en-3 $\beta$ -acetate (Haad-7a)	241

4.8.9	Synthesis and characterisation of (22 $\beta$ )-(Z)-26-(3',4',5'-Trimethoxy benzylidene)-3 $\beta$ -yl-furost-5-en-3-acetate (Haad-7b)	247
4.8.10	Synthesis and characterisation of (22 $\beta$ )-3 $\beta$ -Acetoxy-furost-5-en-26-aldoxime (Haad-8)	253
4.8.11	Synthesis and characterisation of (22 $\beta$ )-3 $\beta$ -Acetoxy-furost-5-en-26-aldoxime acetate (Haad-9)	259
4.8.12	Synthesis and characterisation of (22 $\beta$ )-3 $\beta$ -Acetoxy-27-nor-furost-5-en-25-ketoxime (Haad-10)	265
4.8.13	Synthesis and characterisation of (22 $\beta$ )-3 $\beta$ -Hydroxy-27-nor-furost-5-en-25-ketoxime-3 $\beta$ ,26-diacetate (Haad-11)	271
4.8.14	Synthesis and characterisation of (22 $\beta$ )-25 $\alpha$ -Hydroxy-3 $\beta$ -yl-27-nor-furost-5-en-3-acetate and (22 $\beta$ )-25 $\beta$ -Hydroxy-3 $\beta$ -yl-27-nor-furost-5-en-3-acetate (Haad-12a and Haad-12b)	277
4.9	Synthetic modification of Diosgenin (Second reaction scheme)	284
4.9.1.	Synthesis and characterization of (22 $\beta$ ,25R)-7-oxo-spirost-5-en-3 $\beta$ -yl-3-acetate (Hak-1)	284
4.9.2	Synthesis and characterization of (22 $\beta$ ,25R)-3 $\beta$ -Acetoxy-spirost-5-en-3 $\beta$ -yl-7-ketoxime (Hak-2)	290
4.9.3	Synthesis and characterization of (22 $\beta$ ,25R)-3 $\beta$ -Acetoxy-spirost-5-en-3 $\beta$ -yl-7-(ethyl-2'-acetate)-ketoxime (Hak-3)	296
4.9.4	Synthesis and characterization of (22 $\beta$ ,25R)-3 $\beta$ -Acetoxy-spirost-5-en-3 $\beta$ -yl-7-(ethyl-3'-propanoate)-ketoxime (Hak-4)	301
4.9.5	Synthesis and characterization of (22 $\beta$ ,25R)-3 $\beta$ -Acetoxy-spirost-5-en-3 $\beta$ -yl-7-(ethyl-4'-butyrate)-ketoxime (Hak-5)	307
4.9.6	Synthesis and characterization of (22 $\beta$ ,25R)-3 $\beta$ -Acetoxy-spirost-5-en-3 $\beta$ -yl-7-(ethyl-5'-pentanoate)-ketoxime (Hak-6)	313
4.9.7	Synthesis and characterization of (22 $\beta$ ,25R)-3 $\beta$ -Acetoxy-spirost-5-en-3 $\beta$ -yl-7-(ethyl-6'-hexanoate)-ketoxime (Hak-7)	319
4.9.8	Synthesis and characterization of (22 $\beta$ ,25R)-3 $\beta$ -Acetoxy-spirost-5-en-3 $\beta$ -yl-7-(ethyl-7'-heptanoate)-ketoxime (Hak-8)	325
4.9.9	Synthesis and characterization of (22 $\beta$ ,25R)-3 $\beta$ -Acetoxy-spirost-5-en-3 $\beta$ -yl-7-benzyketoxime (Hak-9)	331
4.9.10	Synthesis and characterization of (22 $\beta$ ,25R)-3 $\beta$ -Acetoxy-spirost-5-en-3 $\beta$ -yl-7-(4'-butanoic)-ketoxime (Hak-10)	337

4.9.11	Synthesis and characterization of (22 $\beta$ ,25R)-3 $\beta$ -Acetoxy-7-(4'-nitrobenzylidene)-spirost-5-en-3 $\beta$ -yl (Hak-11)	343
4.9.12	Synthesis and characterization of (22 $\beta$ ,25R)-7-oxo-spirost-3,5-diene (Hak-12)	349
4.10	Antiproliferative activity of synthesized compounds	355
4.11	Conclusion and Recommendations	359
	References	360
	Appendices	



## LIST OF FIGURES

	Page	
Fig. 4.0	ESI Mass spectrum of Haskh-3 in MeOH	83
Fig. 4.1	$^1\text{H}$ NMR spectrum of Haskh-3 in $\text{CDCl}_3$	84
Fig. 4.2	$^{13}\text{C}$ NMR spectrum of Haskh-3 in $\text{CDCl}_3$	85
Fig. 4.3	Expanded $^{13}\text{C}$ NMR spectrum of Haskh-3 in $\text{CDCl}_3$	86
Fig. 4.4	DEPT spectrum of Haskh-3 in $\text{CDCl}_3$	87
Fig. 4.5	Expanded DEPT spectrum of Haskh-3 in $\text{CDCl}_3$	88
Fig. 4.6	$^1\text{H}$ - $^1\text{H}$ COSY spectrum of Haskh-3 in $\text{CDCl}_3$	89
Fig. 4.7	HSQC spectrum of Haskh-3 in $\text{CDCl}_3$	90
Fig. 4.8	Expanded HSQC spectrum of Haskh-3 in $\text{CDCl}_3$	91
Fig. 4.9	HMBC spectrum of Haskh-3 in $\text{CDCl}_3$	92
Fig. 4.10	Expanded HMBC spectrum of Haskh-3 in $\text{CDCl}_3$	93
Fig. 4.11	$^1\text{H}$ NMR spectrum of Haskh-4 in $\text{CDCl}_3$	97
Fig. 4.12	$^{13}\text{C}$ NMR spectrum of Haskh-4 in $\text{CDCl}_3$	98
Fig. 4.13	Expanded $^{13}\text{C}$ NMR spectrum of Haskh-4 in $\text{CDCl}_3$	99
Fig. 4.14	DEPT spectrum of Haskh-4 in $\text{CDCl}_3$	100
Fig. 4.15	Expanded DEPT spectrum of Haskh-4 in $\text{CDCl}_3$	101
Fig. 4.16	$^1\text{H}$ - $^1\text{H}$ COSY spectrum of Haskh-4 in $\text{CDCl}_3$	102
Fig. 4.17	Expanded $^1\text{H}$ - $^1\text{H}$ COSY spectrum of Haskh-4 in $\text{CDCl}_3$	103
Fig. 4.18	HSQC spectrum of Haskh-4 in $\text{CDCl}_3$	104
Fig. 4.19	Expanded HSQC spectrum of Haskh-4 in $\text{CDCl}_3$	105

Fig. 4.20	$^1\text{H}$ - $^{13}\text{C}$ HMBC spectrum of Haskh-4 in $\text{CDCl}_3$	106
Fig. 4.21	Expanded $^1\text{H}$ - $^{13}\text{C}$ HMBC spectrum of Haskh-4 in $\text{CDCl}_3$ (1)	107
Fig. 4.22	Expanded $^1\text{H}$ - $^{13}\text{C}$ HMBC spectrum of Haskh-4 in $\text{CDCl}_3$ (2)	108
Fig. 4.23	ESI-MS spectrum of Haske-1 in MeOH	112
Fig. 4.24	$^1\text{H}$ NMR spectrum of Haske-1 in $\text{CDCl}_3$	113
Fig. 4.25	$^{13}\text{C}$ NMR spectrum of Haske-1 in $\text{CDCl}_3$	114
Fig. 4.26	$^1\text{H}$ - $^1\text{H}$ COSY spectrum of Haske-1 in $\text{CDCl}_3$	115
Fig. 4.27	$^1\text{H}$ - $^{13}\text{C}$ HMBC spectrum of Haske-1 in $\text{CDCl}_3$	116
Fig. 4.28	ESI-MS spectrum of Haske-2 in MeOH	120
Fig. 4.29	$^1\text{H}$ NMR spectrum of Haske-2 in $\text{CDCl}_3$	121
Fig. 4.30	$^{13}\text{C}$ NMR spectrum of Haske-2 in $\text{CDCl}_3$	122
Fig. 4.31	DEPT spectrum of Haske-2 in $\text{CDCl}_3$	123
Fig. 4.32	$^1\text{H}$ - $^1\text{H}$ COSY spectrum of Haske-2 in $\text{CDCl}_3$	124
Fig. 4.33	HSQC spectrum of Haske-2 in $\text{CDCl}_3$	125
Fig. 4.34	Expanded HSQC spectrum of Haske-2 in $\text{CDCl}_3$	126
Fig. 4.35	$^1\text{H}$ - $^{13}\text{C}$ HMBC spectrum of Haske-2 in $\text{CDCl}_3$	127
Fig. 4.36	Expanded $^1\text{H}$ - $^{13}\text{C}$ HMBC spectrum of Haske-2 in $\text{CDCl}_3$ (1)	128
Fig. 4.37	Expanded $^1\text{H}$ - $^{13}\text{C}$ HMBC spectrum of Haske-2 in $\text{CDCl}_3$ (2)	129
Fig. 4.38	ESI MS spectrum of Haske-3 in MeOH	133
Fig. 4.39	$^1\text{H}$ NMR spectrum of Haske-3 in $\text{CDCl}_3$	134
Fig. 4.40	$^{13}\text{C}$ NMR spectrum of Haske-3 in $\text{CDCl}_3$	135
Fig. 4.41	DEPT spectrum of Haske-3 in $\text{CDCl}_3$	136

Fig. 4.42	$^1\text{H}$ - $^1\text{H}$ COSY spectrum of Haske-3 in $\text{CDCl}_3$	137
Fig. 4.43	HSQC spectrum of Haske-3 in $\text{CDCl}_3$	138
Fig. 4.44	Expanded HSQC spectrum of Haske-3 in $\text{CDCl}_3$	139
Fig. 4.45	$^1\text{H}$ - $^{13}\text{C}$ HMBC spectrum of Haske-3 in $\text{CDCl}_3$	140
Fig. 4.46	Expanded $^1\text{H}$ - $^{13}\text{C}$ HMBC spectrum of Haske-3 in $\text{CDCl}_3$	141
Fig. 4.47	ESI MS spectrum of Haske-9 in MeOH	160
Fig. 4.48	$^1\text{H}$ NMR spectrum of Haske-9 in $\text{CDCl}_3$	161
Fig. 4.49	$^{13}\text{C}$ NMR spectrum of Haske-9 in $\text{CDCl}_3$	162
Fig. 4.50	DEPT spectrum of Haske-9 in $\text{CDCl}_3$	163
Fig. 4.51	Mass spectrum of Haskm-2 in MeOH	170
Fig. 4.52	IR spectrum of Haskm-2 in $\text{CCl}_4$ and KBr	171
Fig. 4.53	$^1\text{H}$ NMR spectrum of Haskm-2 in $\text{CDCl}_3$	172
Fig. 4.54	$^{13}\text{C}$ NMR spectrum of Haskm-2 in $\text{CDCl}_3$	173
Fig. 4.55	Expanded $^{13}\text{C}$ NMR spectrum of Haskm-2 in $\text{CDCl}_3$	174
Fig. 4.56	DEPT spectrum of Haskm-2 in $\text{CDCl}_3$	175
Fig. 4.57	$^1\text{H}$ - $^1\text{H}$ COSY spectrum of Haskm-2 in $\text{CDCl}_3$	176
Fig. 4.58	HSQC spectrum of Haskm-2 in $\text{CDCl}_3$	177
Fig. 4.59	$^1\text{H}$ - $^{13}\text{C}$ HMBC spectrum of Haskm-2 in $\text{CDCl}_3$	178
Fig. 4.60	ESI-MS spectrum of Haad-1 in MeOH	193
Fig. 4.61	$^1\text{H}$ NMR spectrum of Haad-1 in $\text{CDCl}_3$	194
Fig. 4.62	$^{13}\text{C}$ NMR spectrum of Haad-1 in $\text{CDCl}_3$	195
Fig. 4.63	DEPT spectrum of Haad-1 in $\text{CDCl}_3$	196

Fig. 4.64	ESI-MS spectrum of Haad-2a in MeOH	199
Fig. 4.65	$^1\text{H}$ NMR spectrum of Haad-2a in $\text{CDCl}_3$	200
Fig. 4.66	$^{13}\text{C}$ NMR spectrum of Haad-2a in $\text{CDCl}_3$	201
Fig. 4.67	DEPT spectrum of Haad-2a in $\text{CDCl}_3$	202
Fig. 4.68	ESI-MS spectrum of Haad-2b in MeOH	205
Fig. 4.69	$^1\text{H}$ NMR spectrum of Haad-2b in $\text{CDCl}_3$	206
Fig. 4.70	$^{13}\text{C}$ NMR spectrum of Haad-2b in $\text{CDCl}_3$	207
Fig. 4.71	DEPT spectrum of Haad-2b in $\text{CDCl}_3$	208
Fig. 4.72	ESI-MS spectrum of Haad-3 in MeOH	211
Fig. 4.73	$^1\text{H}$ NMR spectrum of Haad-3 in $\text{CDCl}_3$	212
Fig. 4.74	$^{13}\text{C}$ NMR spectrum of Haad-3 in $\text{CDCl}_3$	213
Fig. 4.75	DEPT spectrum of Haad-3 in $\text{CDCl}_3$	214
Fig. 4.76	Plausible mechanism of conversion of aldehyde (Haad-3) to ketone (Haad-4).	218
Fig. 4.77	ESI-MS spectrum of Haad-4 in MeOH	221
Fig. 4.78	$^1\text{H}$ NMR spectrum of Haad-4 in $\text{CDCl}_3$	222
Fig. 4.79	$^{13}\text{C}$ NMR spectrum of Haad-4 in $\text{CDCl}_3$	223
Fig. 4.80	DEPT spectrum of Haad-4 in $\text{CDCl}_3$	224
Fig. 4.81	$^1\text{H}$ - $^1\text{H}$ COSY spectrum of Haad-4 in $\text{CDCl}_3$	225
Fig. 4.82	HSQC spectrum of Haad-4 in $\text{CDCl}_3$	226
Fig. 4.83	$^1\text{H}$ - $^{13}\text{C}$ HMBC spectrum of Haad-4 in $\text{CDCl}_3$	227
Fig. 4.84	COSY and HMBC correlations of Haad-4	228

Fig. 4.85	Molecular conformation (X-ray) of Haad-4 in crystals.	228
Fig. 4.86	ESI-MS spectrum of Haad-5 in MeOH	231
Fig. 4.87	$^1\text{H}$ NMR spectrum of Haad-5 in $\text{CDCl}_3$	232
Fig. 4.88	$^{13}\text{C}$ NMR spectrum of Haad-5 in $\text{CDCl}_3$	233
Fig. 4.89	DEPT spectrum of Haad-5 in $\text{CDCl}_3$	234
Fig. 4.90	ESI-MS spectrum of Haad-6 in MeOH	237
Fig. 4.91	$^1\text{H}$ NMR spectrum of Haad-6 in $\text{CDCl}_3$	238
Fig. 4.92	$^{13}\text{C}$ NMR spectrum of Haad-6 in $\text{CDCl}_3$	239
Fig. 4.93	DEPT spectrum of Haad-6 in $\text{CDCl}_3$	240
Fig. 4.94	ESI-MS spectrum of Haad-7a in MeOH	243
Fig. 4.95	$^1\text{H}$ NMR spectrum of Haad-7a in $\text{CDCl}_3$	244
Fig. 4.96	$^{13}\text{C}$ NMR spectrum of Haad-7a in $\text{CDCl}_3$	245
Fig. 4.97	DEPT spectrum of Haad-7a in $\text{CDCl}_3$	246
Fig. 4.98	ESI-MS spectrum of Haad-7b in MeOH	249
Fig. 4.99	$^1\text{H}$ NMR spectrum of Haad-7b in $\text{CDCl}_3$	250
Fig. 5.00	$^{13}\text{C}$ NMR spectrum of Haad-7b in $\text{CDCl}_3$	251
Fig. 5.01	DEPT spectrum of Haad-7b in $\text{CDCl}_3$	252
Fig. 5.02	ESI-MS spectrum of Haad-8 in MeOH	255
Fig. 5.03	$^1\text{H}$ NMR spectrum of Haad-8 in $\text{CDCl}_3$	256
Fig. 5.04	$^{13}\text{C}$ NMR spectrum of Haad-8 in $\text{CDCl}_3$	257
Fig. 5.05	DEPT spectrum of Haad-8 in $\text{CDCl}_3$	258
Fig. 5.06	ESI-MS spectrum of Haad-9 in MeOH	261

Fig. 5.07	$^1\text{H}$ NMR spectrum of Haad-9 in $\text{CDCl}_3$	262
Fig. 5.08	$^{13}\text{C}$ NMR spectrum of Haad-9 in $\text{CDCl}_3$	263
Fig. 5.09	DEPT spectrum of Haad-9 in $\text{CDCl}_3$	264
Fig. 5.10	ESI-MS spectrum of Haad-10 in MeOH	267
Fig. 5.11	$^1\text{H}$ NMR spectrum of Haad-10 in $\text{CDCl}_3$	268
Fig. 5.12	$^{13}\text{C}$ NMR spectrum of Haad-10 in $\text{CDCl}_3$	269
Fig. 5.13	DEPT spectrum of Haad-10 in $\text{CDCl}_3$	270
Fig. 5.14	ESI-MS spectrum of Haad-11 in MeOH	273
Fig. 5.15	$^1\text{H}$ NMR spectrum of Haad-11 in $\text{CDCl}_3$	274
Fig. 5.16	$^{13}\text{C}$ NMR spectrum of Haad-11 in $\text{CDCl}_3$	275
Fig. 5.17	DEPT spectrum of Haad-11 in $\text{CDCl}_3$	276
Fig. 5.18	ESI-MS spectrum of Haad-12 in MeOH	280
Fig. 5.19	$^1\text{H}$ NMR spectrum of Haad-12 in $\text{CDCl}_3$	281
Fig. 5.20	$^{13}\text{C}$ NMR spectrum of Haad-12 in $\text{CDCl}_3$	282
Fig. 5.21	DEPT spectrum of Haad-12 in $\text{CDCl}_3$	283
Fig. 5.22	ESI-MS spectrum of Hak-1 in MeOH	286
Fig. 5.23	$^1\text{H}$ NMR spectrum of Hak-1 in $\text{CDCl}_3$	287
Fig. 5.24	$^{13}\text{C}$ NMR spectrum of Hak-1 in $\text{CDCl}_3$	288
Fig. 5.25	DEPT spectrum of Hak-1 in $\text{CDCl}_3$	289
Fig. 5.26	ESI-MS spectrum of Hak-2 in MeOH	292
Fig. 5.27	$^1\text{H}$ NMR spectrum of Hak-2 in $\text{CDCl}_3$	293
Fig. 5.28	$^{13}\text{C}$ NMR spectrum of Hak-2 in $\text{CDCl}_3$	294

Fig. 5.29	DEPT spectrum of Hak-2 in CDCl <sub>3</sub>	295
Fig. 5.30	<sup>1</sup> H NMR spectrum of Hak-3 in CDCl <sub>3</sub>	298
Fig. 5.31	<sup>13</sup> C NMR spectrum of Hak-3 in CDCl <sub>3</sub>	299
Fig. 5.32	DEPT spectrum of Hak-3 in CDCl <sub>3</sub>	300
Fig. 5.33	Mass spectrum of Hak-4 in MeOH	303
Fig. 5.34	<sup>1</sup> H NMR spectrum of Hak-4 in CDCl <sub>3</sub>	304
Fig. 5.35	<sup>13</sup> C NMR spectrum of Hak-4 in CDCl <sub>3</sub>	305
Fig. 5.36	DEPT spectrum of Hak-4 in CDCl <sub>3</sub>	306
Fig. 5.37	Mass spectrum of Hak-5 in MeOH	309
Fig. 5.38	<sup>1</sup> H NMR spectrum of Hak-5 in CDCl <sub>3</sub>	310
Fig. 5.39	<sup>13</sup> C NMR spectrum of Hak-5 in CDCl <sub>3</sub>	311
Fig. 5.40	DEPT spectrum of Hak-5 in CDCl <sub>3</sub>	312
Fig. 5.41	Mass spectrum of Hak-6 in MeOH	315
Fig. 5.42	<sup>1</sup> H NMR spectrum of Hak-6 in CDCl <sub>3</sub>	316
Fig. 5.43	<sup>13</sup> C NMR spectrum of Hak-6 in CDCl <sub>3</sub>	317
Fig. 5.44	DEPT spectrum of Hak-6 in CDCl <sub>3</sub>	318
Fig. 5.45	Mass spectrum of Hak-7 in MeOH	321
Fig. 5.46	<sup>1</sup> H NMR spectrum of Hak-7 in CDCl <sub>3</sub>	322
Fig. 5.47	<sup>13</sup> C NMR spectrum of Hak-7 in CDCl <sub>3</sub>	323
Fig. 5.48	DEPT spectrum of Hak-7 in CDCl <sub>3</sub>	324
Fig. 5.49	Mass spectrum of Hak-8 in MeOH	327
Fig. 5.50	<sup>1</sup> H NMR spectrum of Hak-8 in CDCl <sub>3</sub>	328

Fig. 5.51	$^{13}\text{C}$ NMR spectrum of Hak-8 in $\text{CDCl}_3$	329
Fig. 5.52	DEPT spectrum of Hak-8 in $\text{CDCl}_3$	330
Fig. 5.53	Mass spectrum of Hak-9 in MeOH	333
Fig. 5.54	$^1\text{H}$ NMR spectrum of Hak-9 in $\text{CDCl}_3$	334
Fig. 5.55	$^{13}\text{C}$ NMR spectrum of Hak-9 in $\text{CDCl}_3$	335
Fig. 5.56	DEPT spectrum of Hak-9 in $\text{CDCl}_3$	336
Fig. 5.57	Mass spectrum of Hak-10 in MeOH	339
Fig. 5.58	$^1\text{H}$ NMR spectrum of Hak-10 in $\text{CDCl}_3$	340
Fig. 5.59	$^{13}\text{C}$ NMR spectrum of Hak-10 in $\text{CDCl}_3$	341
Fig. 5.60	DEPT spectrum of Hak-10 in $\text{CDCl}_3$	342
Fig. 5.61	Mass spectrum of Hak-11 in MeOH	345
Fig. 5.62	$^1\text{H}$ NMR spectrum of Hak-11 in $\text{CDCl}_3$	346
Fig. 5.63	$^{13}\text{C}$ NMR spectrum of Hak-11 in $\text{CDCl}_3$	347
Fig. 5.64	DEPT spectrum of Hak-11 in $\text{CDCl}_3$	348
Fig. 5.65	Mass spectrum of Hak-12 in MeOH	351
Fig. 5.66	$^1\text{H}$ NMR spectrum of Hak-12 in $\text{CDCl}_3$	352
Fig. 5.67	$^{13}\text{C}$ NMR spectrum of Hak-12 in $\text{CDCl}_3$	353
Fig. 5.68	DEPT spectrum of Hak-12 in $\text{CDCl}_3$	354



## LIST OF TABLES

	Page
Table 2.1: Anticancer activities of camptothecin analogues	29
Table 2.2: Cytotoxicities of sulfonate derivatives of CA-4	33
Table 4.1: The yields of extracts obtained from successive extraction of <i>S. kraussiana</i> aerial parts	70
Table 4.2: <i>In-vitro</i> cytotoxicities of extracts obtained from successive extraction of <i>S. kraussiana</i> aerial parts	71
Table 4.3: Results of the Phytochemical screening of the extracts from successive extraction of <i>S. kraussiana</i> aerial parts.	73
Table 4.41: $^{13}\text{C}$ and $^1\text{H}$ NMR ( $\text{CDCl}_3$ ) spectra data of Haskh-1	75
Table 4.42: $^{13}\text{C}$ and $^1\text{H}$ NMR ( $\text{CDCl}_3$ ) spectra data of Haskh-2	78
Table 4.43: $^{13}\text{C}$ and $^1\text{H}$ NMR ( $\text{CDCl}_3$ ) spectra data of Haskh-3	81
Table 4.44: $^{13}\text{C}$ and $^1\text{H}$ NMR ( $\text{CDCl}_3$ ) spectra data of Haskh-4	95
Table 4.45: $^{13}\text{C}$ and $^1\text{H}$ NMR ( $\text{CDCl}_3$ ) spectra data of Haske-1 and oleana-9(11),12-dien-3-ol	110
Table 4.46: $^{13}\text{C}$ and $^1\text{H}$ NMR ( $\text{CDCl}_3$ ) spectra data of Haske-2	118
Table 4.47: $^{13}\text{C}$ and $^1\text{H}$ NMR ( $\text{CDCl}_3$ ) spectra data of Haske-3 and $\beta$ -sitosterol	131
Table 4.48: $^{13}\text{C}$ and $^1\text{H}$ NMR ( $\text{CDCl}_3$ ) spectra data of Haske-4	143
Table 4.49: $^{13}\text{C}$ NMR and $^1\text{H}$ ( $\text{CDCl}_3$ ) spectra data of Haske-5	146
Table 4.50: $^{13}\text{C}$ and $^1\text{H}$ NMR ( $\text{CDCl}_3$ ) spectra data of Haske-6	149
Table 4.51: $^{13}\text{C}$ and $^1\text{H}$ NMR ( $\text{CDCl}_3$ ) spectra data of Haske-7 and Z9-octadecenoic acid	152
Table 4.52: $^{13}\text{C}$ and $^1\text{H}$ NMR ( $\text{CDCl}_3$ ) spectra data of Haske-8 and cis-hexadec-9-enoic acid	155
Table 4.53: $^{13}\text{C}$ and $^1\text{H}$ NMR ( $\text{CDCl}_3$ ) spectra data of Haske-9 and Diosgenin	158

Table 4.54: $^{13}\text{C}$ and $^1\text{H}$ NMR ( $\text{CDCl}_3$ ) spectra data of Haskm-1 and 1,2,3-Propanetriyl (7Z, 7'Z, 7''Z)tris(-7-tetradecenoate)	165
Table 4.55: $^{13}\text{C}$ and $^1\text{H}$ NMR ( $\text{CDCl}_3$ ) spectra data of Haskm-2 and Campesterol	168
Table 4.56: $^{13}\text{C}$ and $^1\text{H}$ NMR ( $\text{CDCl}_3$ ) spectra data of Haskm-3 and Hexadec-9-enoic acid	180
Table 4.57: $^{13}\text{C}$ and $^1\text{H}$ NMR ( $\text{CDCl}_3$ ) spectra data of Haskm-4	183
Table 4.58: $^{13}\text{C}$ and $^1\text{H}$ NMR ( $\text{CDCl}_3$ ) spectra data of Haskm-5 and Z5, 8-eicosdienoic acid	186
Table 4.59: Antiproliferative activities of isolated compounds from extracts of <i>S. kraussiana</i> (aerial parts)	189
Table 4.60: Comparison of $^{13}\text{C}$ and $^1\text{H}$ NMR data of Diosgenin and Haad-1	192
Table 4.61: Comparison of $^{13}\text{C}$ and $^1\text{H}$ NMR data of Haad-1 and Haad-2a	198
Table 4.62: Comparison of $^{13}\text{C}$ and $^1\text{H}$ NMR data of Haad-2a and Haad-2b	204
Table 4.63: Comparison of $^{13}\text{C}$ and $^1\text{H}$ NMR data of Haad-2a and Haad-3	210
Table 4.64: Effect of various amines on transformation of Haad-3 to Haad-4	219
Table 4.65: Effect of solvent polarity on transformation of compound Haad-3 to Haad-4.	219
Table 4.66: Comparison of $^{13}\text{C}$ and $^1\text{H}$ NMR data of Haad-3 and Haad-4	220
Table 4.67: Comparison of $^{13}\text{C}$ and $^1\text{H}$ NMR data of Haah-3 and Haad-5	230
Table 4.68: Comparison of $^{13}\text{C}$ and $^1\text{H}$ NMR data of Haad-3 and Haad-6	236
Table 4.69: Comparison of $^{13}\text{C}$ and $^1\text{H}$ NMR data of Haad-3 and Haad-7a	242
Table 4.70: Comparison of $^{13}\text{C}$ and $^1\text{H}$ NMR data of Haad-3 and Haad-7b	248
Table 4.71: Comparison of $^{13}\text{C}$ and $^1\text{H}$ NMR data of Haad-3 and Haad-8	254
Table 4.72: Comparison of $^{13}\text{C}$ and $^1\text{H}$ NMR data of Haad-8 and Haad-9	260
Table 4.73: Comparison of $^{13}\text{C}$ and $^1\text{H}$ NMR data of Haad-4 and Haad-10	266

Table 4.74: Comparison of $^{13}\text{C}$ and $^1\text{H}$ NMR data of Haad-10 and Haad-11	272
Table 4.75: Comparison of $^{13}\text{C}$ and $^1\text{H}$ NMR data of Haad-4 and Haad-12( $\alpha$ and $\beta$ )	279
Table 4.76: Comparison of $^{13}\text{C}$ and $^1\text{H}$ NMR data of Haad-1 and Hak-1	285
Table 4.77: Comparison of $^{13}\text{C}$ and $^1\text{H}$ NMR data of Hak-1 and Hak-2	291
Table 4.78: Comparison of $^{13}\text{C}$ and $^1\text{H}$ NMR data of Hak-2 and Hak-3	297
Table 4.79: Comparison of $^{13}\text{C}$ and $^1\text{H}$ NMR data of Hak-2 and Hak-4	302
Table 4.80: Comparison of $^{13}\text{C}$ and $^1\text{H}$ NMR data of Hak-2 and Hak-5	308
Table 4.81: Comparison of $^{13}\text{C}$ and $^1\text{H}$ NMR data of Hak-2 and Hak-6	314
Table 4.82: Comparison of $^{13}\text{C}$ and $^1\text{H}$ NMR data of Hak-2 and Hak-7	320
Table 4.83: Comparison of $^{13}\text{C}$ and $^1\text{H}$ NMR data of Hak-2 and Hak-8	326
Table 4.84: Comparison of $^{13}\text{C}$ and $^1\text{H}$ NMR data of Hak-2 and Hak-9	332
Table 4.85: Comparison of $^{13}\text{C}$ and $^1\text{H}$ NMR data of Hak-3 and Hak-10	338
Table 4.86: Comparison of $^{13}\text{C}$ and $^1\text{H}$ NMR data of Hak-4 and Hak-11	344
Table 4.87: Comparison of $^{13}\text{C}$ and $^1\text{H}$ NMR data of Hak-5 and Hak-12	350
Table 4.88: Antiproliferative activities of synthesized compounds from the first reaction scheme	357
Table 4.89: Antiproliferative activities of synthesized compounds from the second reaction scheme	358

## LIST OF SCHEMES

	Page
Scheme 1: Biosynthesis of terpenoids	37
Scheme 2: Biosynthesis of flavonoids	39
Scheme 3: Biosynthesis of saponins	43
Scheme 4: Extraction and Isolation of compounds from <i>S. kraussiana</i>	58
Scheme 5: Modification of Diosgenin at spiroketal position, C <sub>22</sub>	61
Scheme 6: Modification of Diosgenin at position 7	65

## LIST OF ABBREVIATIONS

$\mu$  - Micro

$\mu\text{M}$  – Micromole

$^{13}\text{C}$  NMR – Carbon-13 Nuclear Magnetic Resonance

$^1\text{H}$  NMR – Proton Nuclear Magnetic Resonance

$^1\text{H}$ - $^1\text{H}$  COSY – Homonuclear Correlation spectroscopy

2D NMR – Two-dimensional Nuclear Magnetic Resonance

A549 - Lung cancer cell line

Ara- $\alpha$ -L – Arabinopyranosyl

C33A - Cervical cancer cell line

CIMAP – Central Institute of Medicinal and Aromatic Plants

COLO – Colorectal cancer cell line

DU145 - prostate cancer cell line

ESI-MS – Electrospray Ionisation-Mass Spectroscopy

FaDu - hypopharyngeal cancer cell line

Glc- $\beta$ -D-dlucopyranosyl

HMBC – Heteronuclear multiple bond correlation

HSQC – Heteronuclear single quantum correlation

IC<sub>50</sub> – 50% inhibition concentration

IPP – Isopentenyl pyrophosphate

IR – Infrared

J – Coupling constant

K562 – Leukemia cancer cell line

KB - HeLa contaminant of mouth epidermal carcinoma

L – Litres

m/z – Mass to Charge ratio

M<sup>+</sup> - Molecular ion

MCF-7 – Breast cancer cell line

MeOH – Methanol

mg – Milligram

MS – Mass Spectroscopy

MVA – Mevalonic acid

NMR – Nuclear Magnetic Resonance

PTLC – Preparative Thin Layer Chromatography

Rha- $\alpha$ -L – Rhamnopyranosyl

TLC – Thin Layer Chromatography

UV – Ultraviolet

WHO – World Health Organisation

WRL – Hepatic blood cancer cell lines

# CHAPTER ONE

## INTRODUCTION

### 1.1 Plants as source of Pharmaceuticals

The primordial significance of plants in creation has continuously given limitless satisfaction to mankind. Although man domesticated plants at early date, he did not study them seriously for a long time afterwards. Without plants there would be no other form of life on earth (Rothwell *et al.*, 1989). Plants are the basis for the development of most modern drugs, and medicinal plants have been used for many years in daily life to treat diseases all over the world. Throughout the ages, humans have relied on nature for their basic needs, for the production of food, shelter, clothing, transportation, fertilizers, flavors, fragrances, and medicine (Newman *et al.*, 2003; Cragg and Newman, 2005). Plants have formed the basis of some sophisticated traditional medicine systems that have been in existence for thousands of years and continue to provide mankind with new remedies. Although some of the therapeutic properties attributed to plants have been proven to be erroneous, medicinal plant therapy is based on the empirical findings of hundreds and probably thousands of years of use. The first records written on clay tablets in cuneiform are from Mesopotamia about 2600 BC (Heinrich *et al.*, 2004). Among the substances that were used are oils of *Cedrus* species (cedar) and *Cupressus sempervirens* (cypress), *Glycyrrhiza glabra* (licorice), *Commiphora* Species (myrrh) and *Papaver somniferum* (opium poppy), all of which are still in use today for the treatment of ailments ranging from coughs and cold, to parasitic infections and inflammation (Heinrich *et al.*, 2004).

Sick animals tend to search for plants that are rich in secondary metabolites, such as terpenoids, steroids, tannins and alkaloids (Hutchings *et al.*, 2003). Since these metabolites often have antiviral, antibacterial, antifungal and antihelminthic properties,

a plausible case can be made for self-medication by animals in the wild (Engel and Mifflin, 2002).

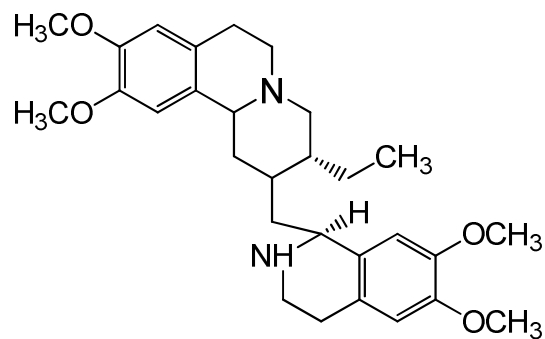
## 1.2. Drugs developed from Plants

Historically, plants have provided a source for novel drug compounds and have made tremendous contributions to human health and well being (Chin *et al.*, 2006). The isoquinoline alkaloid, emetine (**1**) isolated from the underground part of *Cephaelis ipecacuanha* and related species has been used for many years as an amoebicidal drug and also for the treatment of abscesses due to the spread of *Entamoeba histolytica* infections. Another important drug isolated from plant is quinine. This alkaloid occurs naturally in the bark of Cinchona tree. Quinine (**2**) was widely used for the treatment of malaria (Cragg and Newman, 2005). Yohimbine (**3**) is another drug obtained from the bark of *Pausinystalia yohimbine*. It possesses antihypertensive properties.

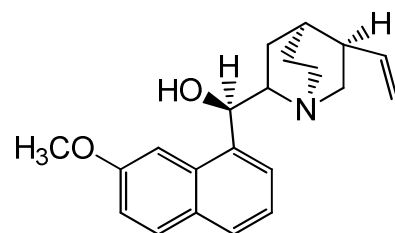
In the last 40 years, many potent drugs have been derived from flowering plants; including for example diosgenin (**4**) (from *Dioscorea* species), from which all anovulatory contraceptive agents have been derived; reserpine (**5**) and other anti-hypertensive and tranquilizing alkaloids from *Rauwolfia* species, and two powerful anti-cancer agents, vincristine (**6**) and vinblastine (**7**) from the Rosy Periwinkle (*Catharanthus roseus*) (Gurib-Fakim, 2006). Tropical rain forests continue to support a vast reservoir of potential drug species because they contain half of the world's flowering plant species. They continue to provide natural product chemists with invaluable compounds as starting points for the development of new drugs. These medicinal plants contain secondary metabolites, of which at least 12,000 have been isolated and the number was estimated to be less than 10% of the total. Many of the plants and spices used by human as seasoning in food yields useful medicinal compounds (Sofowora, 1982<sup>a</sup>; Sofowora, 1982<sup>b</sup>; Harvey, 2001; Lai and Roy, 2004; Tapsell *et al.*, 2006).

Phytochemical investigation of *Artemisia annua* led to isolation of an active compound, sesquiterpene endoperoxide named artemisinin (**8**) (Newman *et al.*, 2000). In Wall and Wani National Cancer Institute, USA, an anticancer agent taxol (**9**), a diterpene was obtained from the bark of *Taxus brevifolia* (Suffness, 1995).

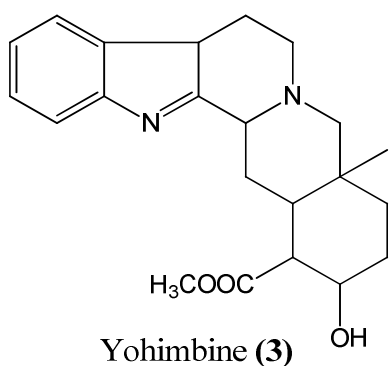




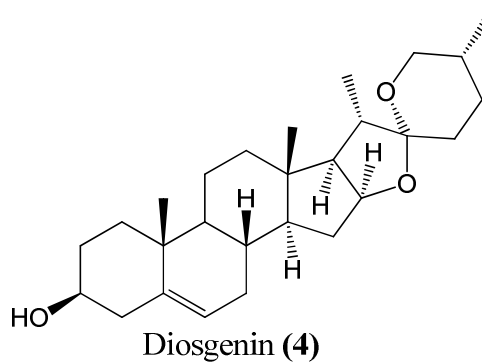
Emetine (1)



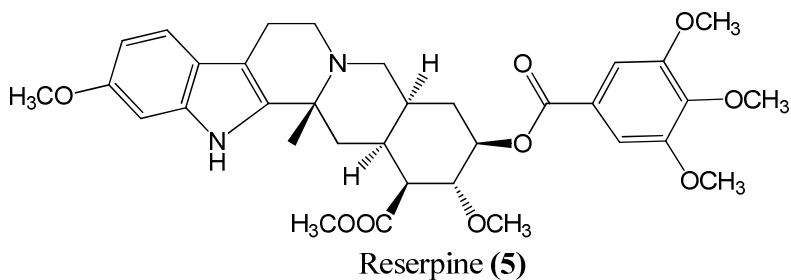
Quinine (2)



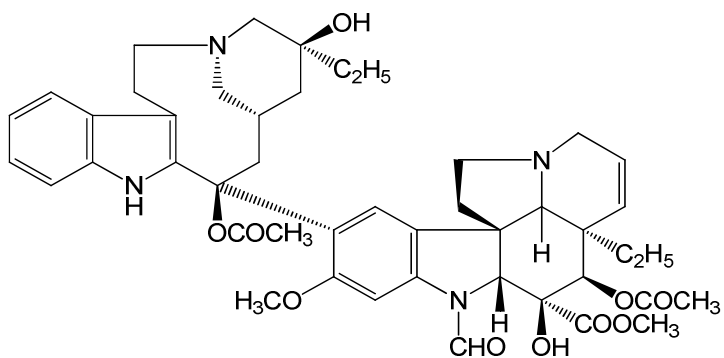
Yohimbine (3)



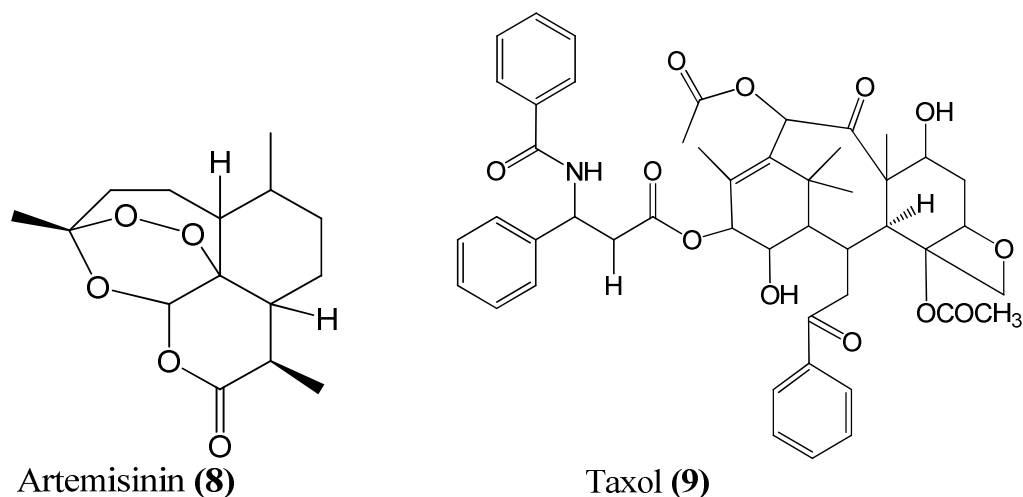
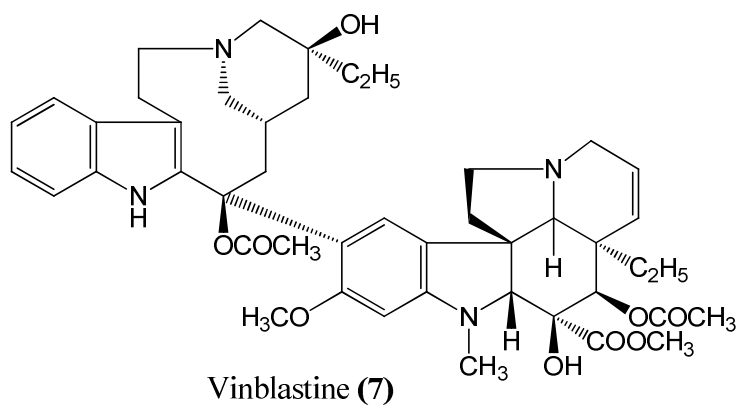
Diosgenin (4)



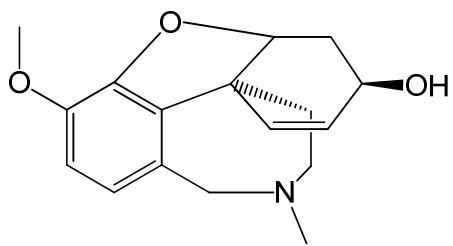
Reserpine (5)



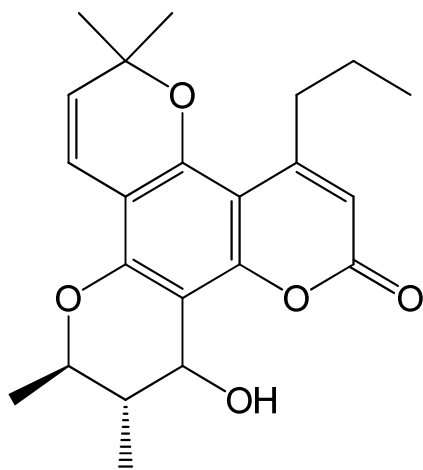
Vincristine (6)



Many compounds that have pharmacological properties have been synthesized from taxol and are currently in use. *Galanthus nivalis* from the Amaryllidaceous family has a long history of use in the traditional medicine of Bulgaria and Turkey for neurological conditions. Investigation of the plant led to the isolation of galantamine (10) which was launched into the market in 2001 as a selective acetylcholinesterase inhibitor for Alzheimer's disease (Shu, 1998). Calanide A (11) isolated from *Calophyllum lanmigerium*, a tree from the Malaysian rain forest is a reverse-transcriptase inhibitor. An in-vitro study of the compound showed that it is effective against, including strains resistant to AZT and other non-nucleoside reverse-transcriptase (Butler, 2004).



Galantamine (10)



Calanide A (11)

### 1.3 Research objectives

In view of the foregoing the research objectives of this work will include the following:

- (a) To prepare extracts of *Smilax kraussiana* aerial parts and evaluate the antiproliferative activities of the plant extracts.
- (b) To isolate the chemical constituents of the plant extracts and elucidate the structures of the isolated compounds.
- (c) To determine the antiproliferative activities of the pure compounds.
- (d) Structural modification of the most active isolate of *Smilax kraussiana* by synthesis and bioevaluation of synthesized molecules

## CHAPTER TWO

### LITERATURE REVIEW

Since plants are known as source of pharmaceuticals, it is necessary to discuss some of them with promising ethnomedicinal applications. One of the plant genus that has shown interest is *Smilax* L.

#### 2.1 The *Smilax* genus

*Smilax* is one of the 10 genera of Smilacaceae. It is a genus of about 225 species, found in temperate, tropical and subtropical zones of Africa, Asia worldwide. In China for example about 80 species are found (39 of which are endemic), while there are 20 in North America north of Mexico (Mabberley, 1987; Raven and Zengyi, 2000). They are climbing flowering plants, many of which are woody and/or thorny. Common names include catbriers, greenbriers, prickly-ivys and smilaxes. "Sarsaparilla" (also zarzaparrilla, sarsparilla) is a name used specifically for the Jamaican *S. regelli* as well as American species. *Smilax* species have long been used in traditional medicine in many countries for the treatment of infectious diseases, skin disorders and liver inflammation (Burkill, 1985; Kubo *et al.*, 1992; Ng and Yu, 2001). The chief components are sarsaparilloside along with parillin as a breakdown product, including desglucorhamno parillin and aglycone sarsapogenin (Fukunaga *et al.*, 1997).

#### 2.2 Species of *Smilax*

Some species of smilax are *Smilax kraussiana*, *Smilax aspera* and *Smilax china*. These species are discussed below.

**2.2.1 *Smilax kraussiana*** (Synonym *Smilax korthalsii* A.D.C.), is an evergreen shrub or semi-shrub, climbing branches, stapler tendrils, thorny, flowering and ornamental plant (Mabberley, 1987; Brummitt, 1992; Inyang, 2000; Mifsud, 2002; Inyang 2003). It is commonly known as West African Sarsaparilla. It is known as *Odufat* by the

Ibibios, *Uruk – ekwong* by the Efiks, *Jiabanammuo* by the Ibos, *Kurangawofi* by the Hausas and *Ekanamagbo/Egun-igbao* by the Yoruba of Nigeria. Earlier preliminary work on the root of the plant revealed that it contained saponins, tannins, simple sugar, cardiac glycosides and flavonoids (Nwafor et al, 2006). *Smilax kraussiana* is a widely used shrub in traditional medicine. The leaf is an excellent antidote in the treatment of poison and for the treatment of infertility in the Eastern Tanzania tribes of South Africa (Chhabra *et al.*, 1993), and inflammation among the Ibibios of South Eastern Nigeria. It is used as a cure for gout in Latin American countries and decoction of the twig is employed to hasten delivery while the root is applied for rheumatism, gout (Dalziel, 1937; Irvine, 1961), kidney problems, gonorrhoea and syphilis (Irvine, 1961; Mitchell and Rook, 1979; Ravens and Zengyi, 2000), febrifuge, malaria and skin diseases (Irvine, 1961; Ravens and Zengyi, 2000; Odugbemi and Akinsulire, 2008). Some of the therapeutic properties of the plant have been established by various researchers. The acute toxicity potential of the leaves, the anti-inflammatory as well as its analgesic activities have been reported (Iwu and Anyanwu 1982; Nwafor *et al.*, 2006; Nwafor *et al.*, 2010). Okokon *et al.*, (2012) reported the antiplasmodial and antipyretic activities of the plant. The root is used as a contraceptive. The root of *Smilax kraussiana* was investigated for its contraceptive activity in rodents with the aim of ascertaining the scientific basis for the use of this plant for family planning and to establish if any, its mechanism of action (Nwafor *et al.*, 2012; Nwafor *et al.*, 2013).



***Smilax kraussiana* (Aerial parts)**

**2.2.2 *Smilax aspera*** (Synonym *Smilax mauritanica* var. *vesperilionis*) is an evergreen, creeping, extremely tough shrub that belongs to the Liliaceae (Smilacaceae) family. The climbing stem is 1 – 4 metres (3 ft 3 in – 13 ft 1 in) long. The leaves are 8 – 10 centimetres (3.1 – 3.9 in) long, petiolated, alternate, tough and leathery, heart-shaped, with toothed and spiny margins. Also the midribs of the underside of the leaves are provided with spines. The flowers, (very fragrant) are small, yellowish or greenish, gathered in axillary racemes. The flowering period in Mediterranean regions extends from September to November. The fruits are globose berries, gathered in clusters, which ripen in Autumn. They are initially red, later turn black. They have a diameter of 8 – 10 millimetres (0.31 – 0.39 in) and contain one to three tiny and round seeds (Pignatti, 1982; Longo and Vasapollo, 2006). They are used in herbal medicine for muscle relaxation, skin ailment, rheumatic pain, depurative, diuretic, diaphoretic, antigout, dropsy, stimulant and for its tonic properties (Longo and vasapollo, 2006; Aburjai *et al.*, 2007). *S. aspera* has also used traditionally for the treatment of syphilis (Vermani and Garg, 2002), diabetes (Fukunaga *et al.*, 1997), rheumatism (Ageel *et al.*, 1989), as an antioxidant (Demo *et al.*, 1998) and to treat symptoms of menopause in women (Weil *et al.*, 2000). In fact, several species of genus *Smilax* are well-known in Chinese traditional medicines, and are used as anti-inflammatory, anticancer and analgesic agents (Shu *et al.*, 2006).

**2.2.3 *Smilax china*** (Synonyms *Smilax nipponica* Miq, *Smilax riparia* DC, *Smilax seiboldii* Miq) is a hard tendril climbing vine with sparsely prickled or unarmed stems and thick tuberous rhizomes. It is called China Sasparilla, China Root (Da Orta, 1895). The main part of the plant used is the rhizome which is considered to be an alternative antiscrofulatic, carminative, depurative, diuretic, tonic and antivenereal. It came into prominence when Da Orta reported success in treating syphilis, a disease introduced by the Portuguese into India in the mid fifteenth century, in Goa. As its fame spread far and wide as an effective treatment for this rapidly spreading disease globally, it fell to disrepute due to the poor quality of the drug being exported. However, it remains the best treatment for syphilis to the east of India because of its quality. A decoction of the roots of *Smilax china* has been used to treat all stages of syphilis. It has also been advocated in the treatment of leprosy, scrofula and many skin infections developing into ulcers (Kimura and But, 1996). In the Far East the roots had been used to treat

abscesses, pyoderma and burns (Da Orta, 1895). The roots of the plant are considered carminative, depurative, laxative and digestive and are being prescribed for treatment of dyspepsia, constipation, flatulence and colic by the Indians who received the drug from Chinese merchants. The Chinese on the other hand made use of this drug to treat cases of gastroenteritis and dysentery. In Korea it was one of the drugs used in the treatment of acute appendicitis, taeniasis and constipation (Warrier *et al.*, 1994; Kimura and But, 1996).

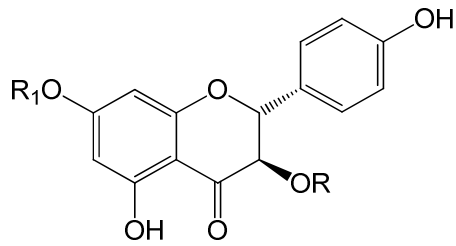
The root has been employed to treat cases of paralysis and sciatica. Its tonic effect has been taken advantage of and was prescribed in cases of general weakness and debilitating diseases. It has also been considered an aphrodisiac and was used to treat impotency. Emperor Charles the fifth was treated successfully for gout using this drug and from thence on it has acquired much esteem for treatment of this and other rheumatic complaints apart from its use to treat syphilis in Europe. It was also advocated in the treatment of insanity and neuralgias. Its diuretic properties had made the Indians use it to treat urinary tract infection, stone and ulcers of the bladder and even chyluria by the physicians of Hong Kong. It helps in relieving strangury and also seminal weakness (Warrier *et al.*, 1994; Kimura and But, 1996). Apart from infective skin conditions this root has been used to treat other dermatological conditions and amongst them is psoriasis. In its native land it was also used to treat diabetes. Both Chinese and Indians consider it an expectorant and used them for treatment of cough with phlegm. It is also given sometimes to treat fever and other inflammatory conditions associated with fever like acute lymphadenitis (Kimura and But, 1996).

### **2.3 Isolated compounds from Smilax species**

Smilax species are rich in saponins. Previous phytochemical investigation of this genus yielded flavonoids, fats, tannins, alkaloids, saponins, and glycosides. Wang *et al.*, 2014 isolated five phenolic compounds, dihydrokaempferol (**12**), dihydrokaempferol-3-O- $\alpha$ -L-rhamnoside (**13**), kaempferol-7-O- $\beta$ -D-glucoside (**14**), resveratrol (3, 5, 4'-trihydroxystibene) (**15**) and oxyresveratrol (**16**) from dried tuber of *Smilax china*. A flavonoid, Quercetin (**17**) was isolated from the rhizome of the plant (Vijayalakshmi *et al.*, 2012). Steroidal saponins, Tigogenin (**18**), neo-tigogenin (Sarsasapogenin) (**19**), laxogenin (**20**), isonarthogenin (**21**), pseudoprotodioscin (**22**), dioscin (**23**), diosgenin (**4**), oleic acid (**24**) and rutin (**25**) were also reported from the plant (James, 2001;



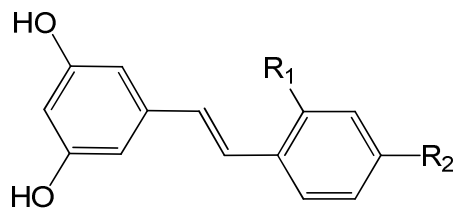
Thomas, 2002; Khare. 2004; Xu *et al.*, 2008). Xu *et al.*, (2008) isolated kaempferol-7-O-beta-D-glucopyranoside (**26**), engeletin (**27**), kaempferol (**28**), dihydrokaempferol (**12**), dihydrokaempferol-5-O-β-D-glucopyranoside (**29**), kaempferol-5-O-beta-D-glucopyranoside (**30**), vanillic acid (**31**), β-sitosterol (**32**), and beta-daucosterol (**33**). Shao *et al.*, (2007) also isolated six stilbenes and flavonoids from *S. china*, they include taxifolin-3-O-glycoside (**34**), piceid (**35**), engeletin (**27**), resveratrol (**13**) and scirpusin A (**36**). Phenylpropanoids were also obtained from the plant. These include smiglaside E (**37**), heloniosides B (**38**), and 2',6'-diacetyl-3,6-diferuloylsucrose (**39**) (Kuo *et al.*, 2005). Five Amino acids; 4-methylene- 4-methyl-glutamic acid (**40**), 4-hydroxy-4-methyl-glutamic acid (**41**), arginine (**42**), N-a-acylarginine (**43**), and acidic N-a-acylarginine derivatives were also reported from rhizome of *S. China* (Kimura and Paul, 1996). Diosgenin (**4**) is reported from *S. menispermoides*. Other active compounds reported from various greenbrier species are parillin (also sarsaparillin or smilacin), sarsapic acid, sarsapogenin and sarsaponin. Xu *et al.*, (2013) isolated six new phenolic compounds, named smiglabrone A (**44**), smiglabrone B (**45**), smilachromanone (**46**), smiglastilbene (**47**), smiglactone (**48**) and smiglabrol (**49**) from the rhizomes of *Smilax glabra*.



Dihydrokaempferol (**12**): R = H

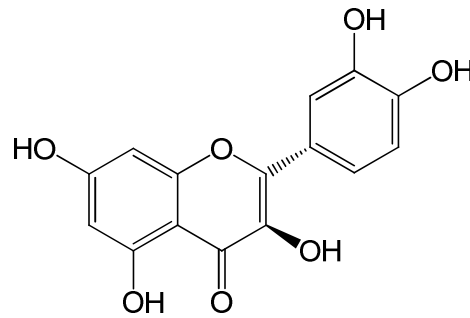
Dihydrokaempferol-3-O- $\alpha$ -L-rhamnoside (**13**): R =  $\alpha$ -L-rhamnoside

Kaempferol-7-O- $\beta$ -D-glucoside (**14**): R<sub>1</sub> =  $\beta$ -D-glucose

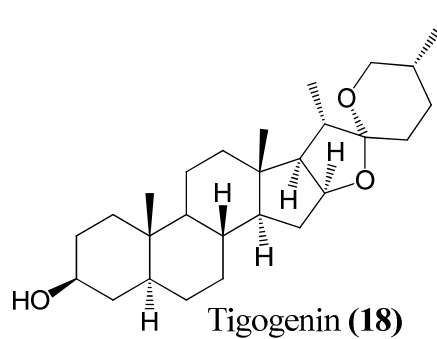


Resveratrol (**15**): R<sub>1</sub> = H, R<sub>2</sub> = OH

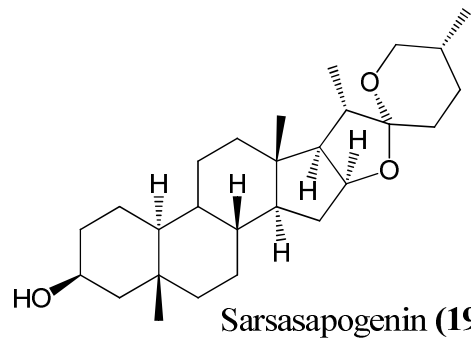
Oxyresveratrol (**16**): R<sub>1</sub> = OH, R<sub>2</sub> = OH



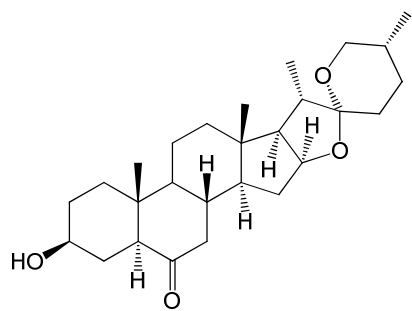
Quercetin (**17**)



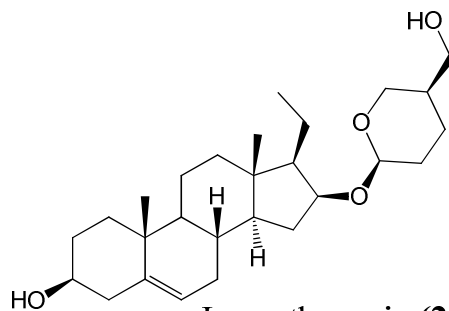
Tigogenin (**18**)



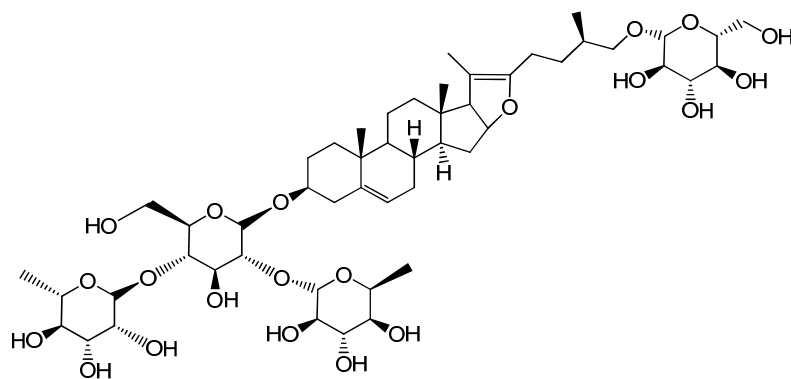
Sarsasapogenin (**19**)



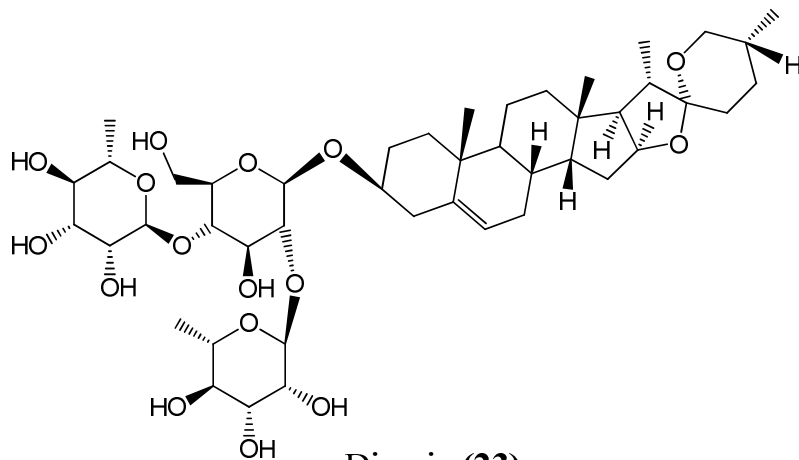
Laxogenin (20)



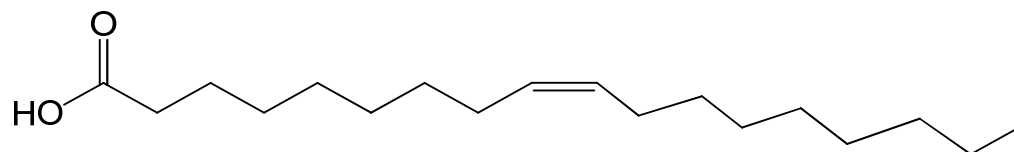
Isonarthogenin (21)



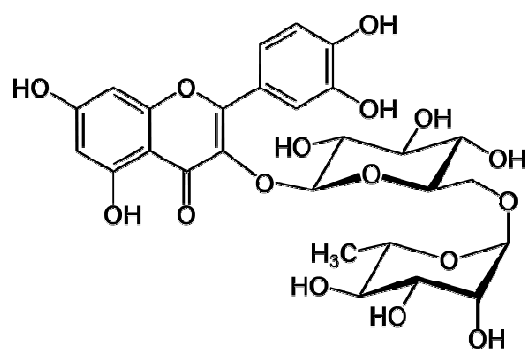
Pseudoprotodioscin (22)



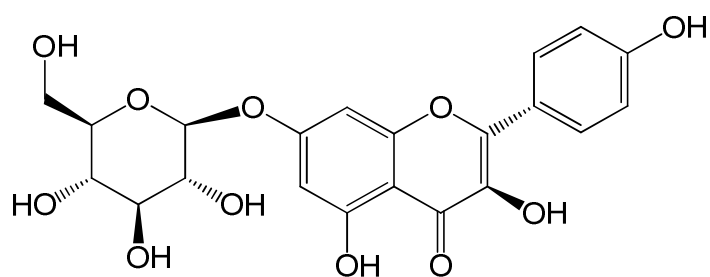
Dioscin (23)



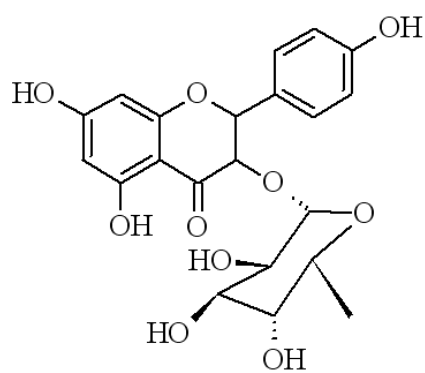
Oleic acid (24)



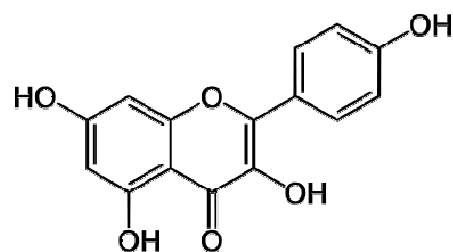
Rutin (25)



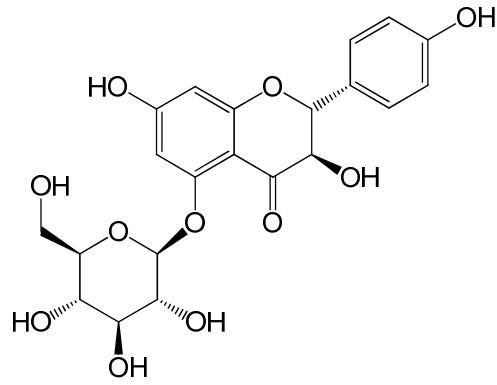
Kaempferol-7-O-beta-D-glucopyranoside (26)



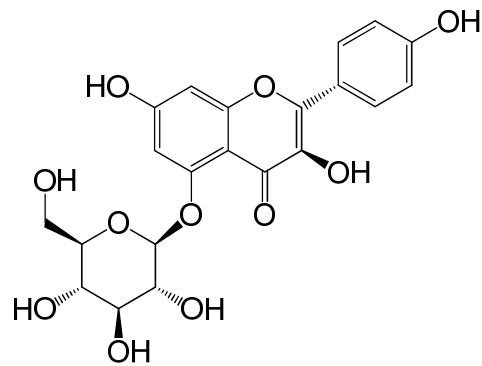
Engeletin (27)



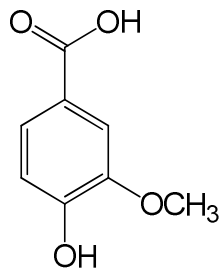
Kaempferol (28)



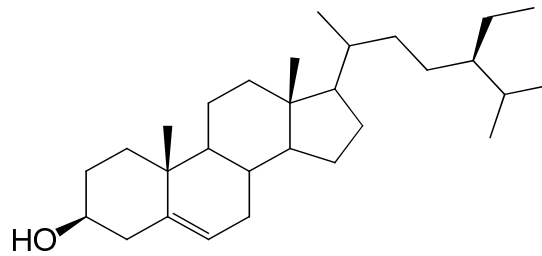
Dihydrokaempferol-5-O- $\beta$ -D-glucopyranoside (29)



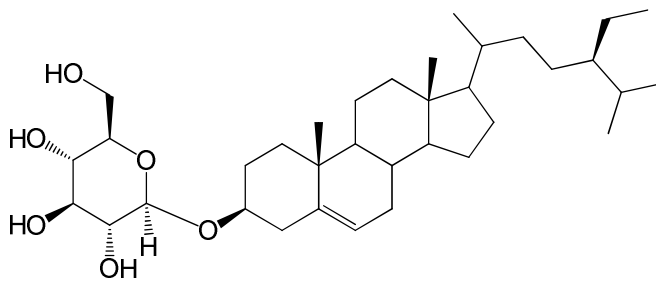
Kaempferol-5-O-beta-D-glucopyranoside (30)



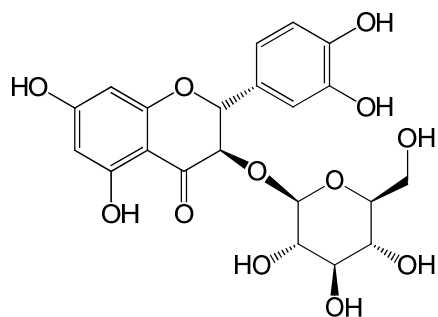
Vanillic acid (31)



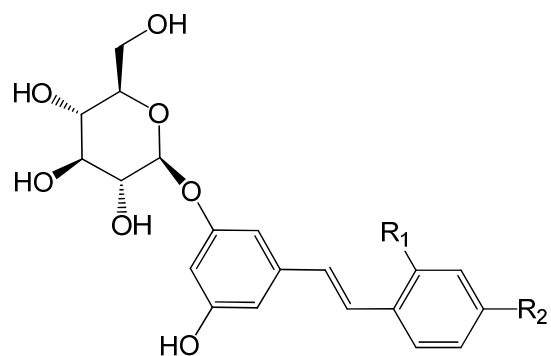
$\beta$ -sitosterol (32)



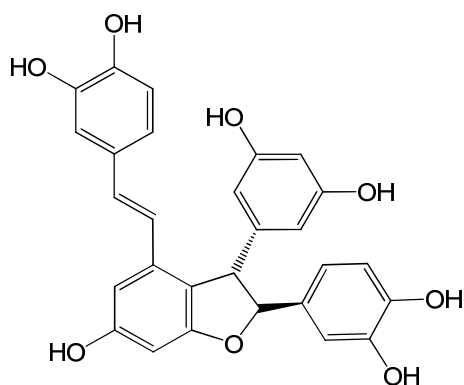
$\beta$ -daucosterol (33)



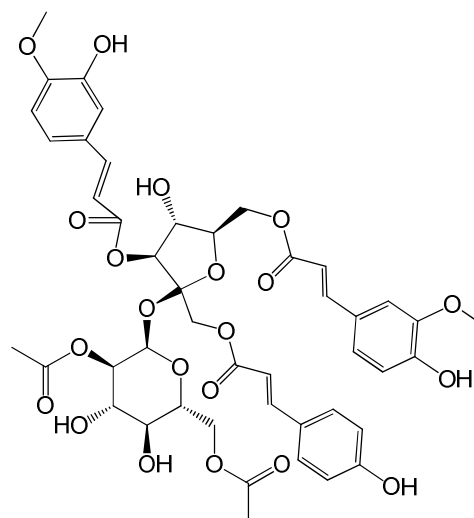
Taxifolin-3-O-glycoside (34)



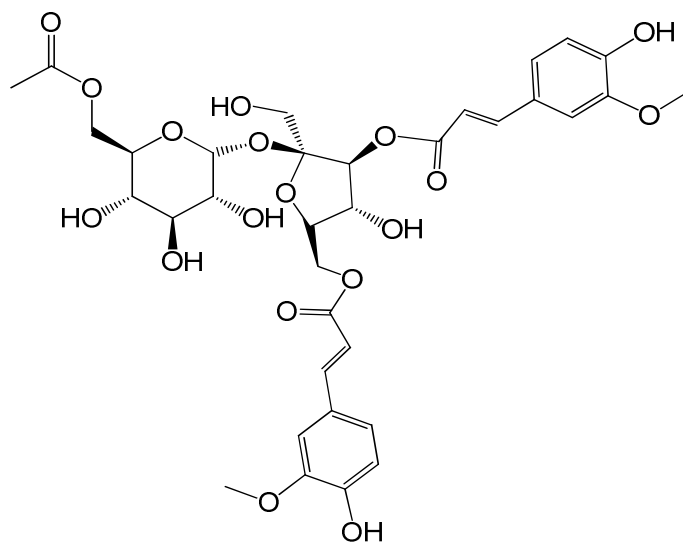
Piceid (35)



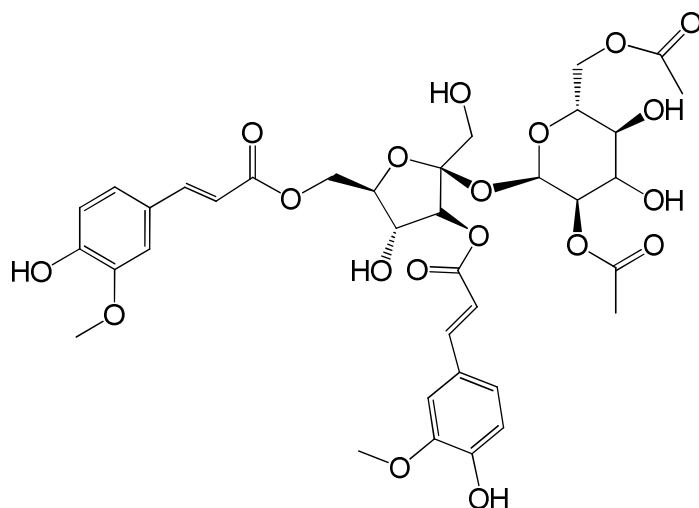
Scirpusin A (36)



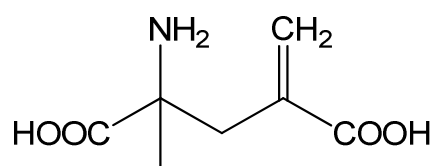
Smiglaside E (37)



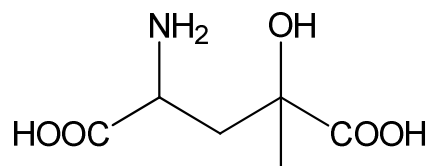
Helonioside B (38)



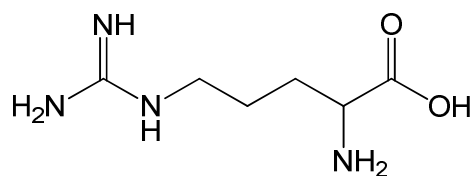
2',6'-diacetyl-3,6-diferuloylsucrose (**39**)



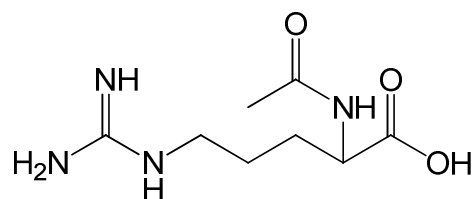
4-methylene-4-methylglutamic acid (**40**)



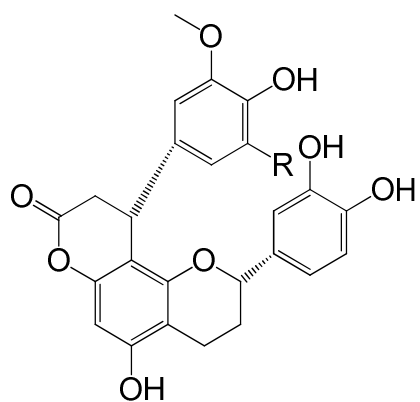
4-hydroxy-4-methylglutamic acid (**41**)



Arginine (**42**)

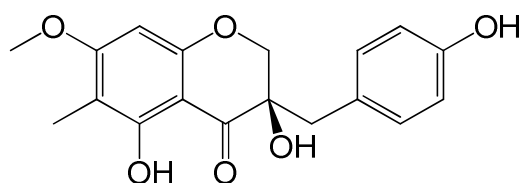


N- $\alpha$ -acylarginine (**43**)

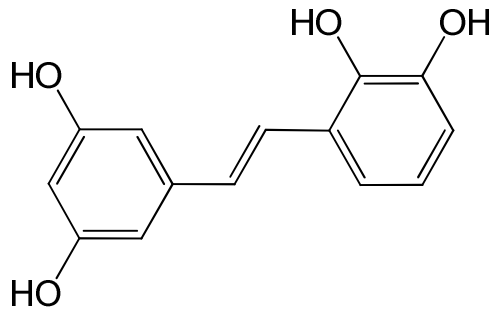


Smiglabrone A (**44**): R = OCH<sub>3</sub>

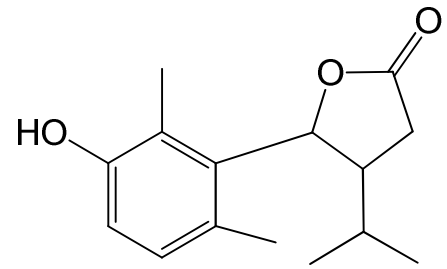
Smiglabrone B (**45**): R = H



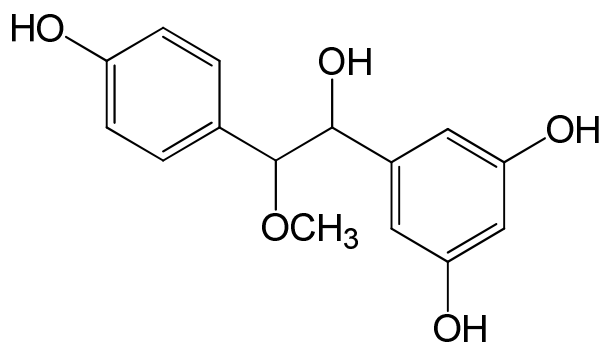
Smilachromanone (**46**)



Smiglastilbebe (47)



Smiglactone (48)



Smiglabrol (49)



## 2.4 Biological potentials of *Smilax* species

Some of the reported pharmacological properties of *Smilax* species are antimicrobial, antimalarial, antipyretic, antioxidant, antiproliferative, anti-HIV, antihepatotoxic and contraceptive activities. These are discussed below.

### 2.4.1 Antimicrobial activity

Hexane and methanol extracts of *Smilax kraussiana* leaves showed inhibition on *Staphylococcus aureus* and *Bacillus subtilis* (gram positive) than ethylacetate extract at concentrations between 25 and 200mg/mL, while hexane, ethyl acetate and methanol extracts of the plant possess lower antibacterial properties on *Escherichia coli*, *Pseudomonas aeruginosa*, *Klebsiellae pneumoniae* and *Salmonellae typhii* (gram negative). However, hexane, ethylacetate and methanol extracts of *Smilax kraussiana* leaves exhibited higher antifungal activities on *Candida albicans*, *Aspergillus niger*, *Rhizopus stolon*, *Penicillum notatum*, *Tricophyton rubrum* and *Epidermophyton floccosum* with activity comparable to that of the reference drug Tioconazole (Hamid and Aiyelaagbe, 2011). Xu *et al.*, (2013) reported the antibacterial and antifungal properties of ethanol, ethyl acetate and *n*-butanol fractions of rhizomes of *Smilax glabra*. Seventeen of the isolated compounds from the plant exhibited antibacterial activities against gram-negative bacteria; ten compounds inhibited the growth of tested fungi while eight isolated compounds inhibited the growth of gram-positive bacteria. These compounds were stilbenes, flavonols, flavan-3ols, spiro-acetal steroids and their derivatives (Xu *et al.*, 2013). Jagessar *et al.*, (2009) also reported the antimicrobial activities of ethanol and ethyl acetate extracts of *Smilax schombrugiana* leaves against *S. aureus* (gram+ve), *E. coli* (gram-ve) and *C. albicans* using the stokes disc diffusion, well diffusion, streak plate and dilution methods. Diosgenin (**1**), which has been isolated from *Smilax* species possesses antifungal properties (Zubair *et al.*, 2011).

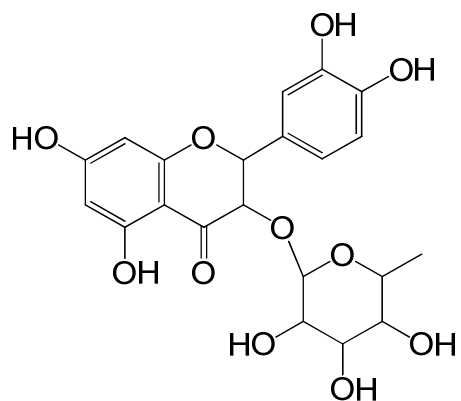
### 2.4.2 Antimalarial and antipyretic activities

Okokon *et al.*, (2012) investigated the antiplasmodial and antipyretic properties of the extract and fractions of *Smilax krausiana*. It was found that both the extract and its fractions significantly reduced the parasitaemia in prophylactic, suppressive and curative models in a dose dependent fashion. Some secondary metabolites of *S. krausiana* may be responsible for the plasmocidal activity of its extract and therefore

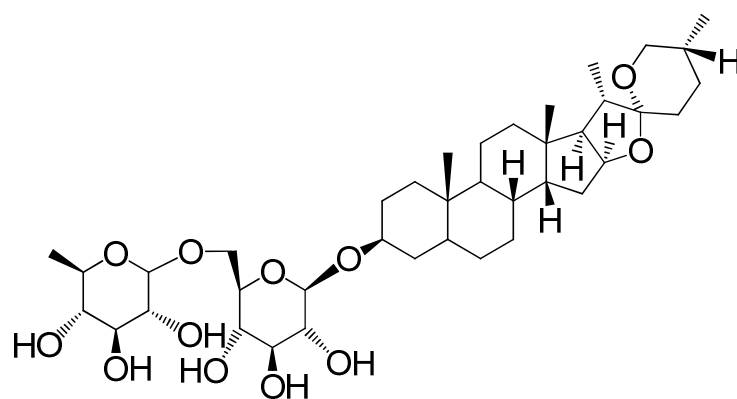
explained the mechanism of antiplasmodial effect of the plant extract and its fractions. On antipyretic activity, the extract inhibited significantly dinitrophenol, amphetamine and yeast-induced pyrexia. Dinitrophenol induces hyperthermia by uncoupling oxidative phosphorylation causing release of calcium from mitochondrial stores and also prevent calcium reuptake. This results in increased level of intracellular calcium, muscle contraction and hyperthermia (Kumar *et al.*, 2002). The hypothermic activity of the extract could have also been mediated by vasodilatation of superficial blood vessels leading to increased dissipation of heat following resetting of hypothalamic temperature control center (Rang *et al.*, 2007). This action may be due to the phytochemical compounds in this plant. Therefore, the temperature lowering activity of the extract may not be unconnected with the inhibition of one or combination of the mechanisms mentioned above.

### **2.4.3 Antioxidant activity**

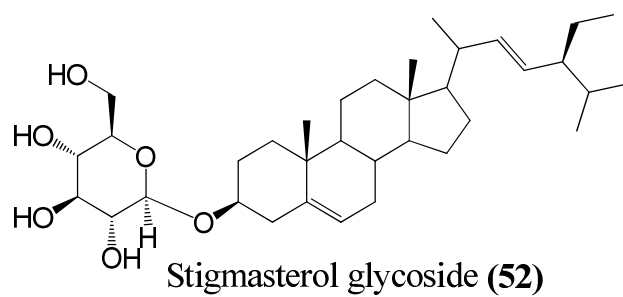
The methanol extract of *Smilax lanceaeifolia* root showed relatively high di(phenyl)-(2,4,6-trinitrophenyl) iminoazanium (DPPH) radical scavenging activity, with an average of 67.6%. The DPPH radical scavenging activity of isolated compounds, apigenin glycoside (**50**), neotigogenin (**19**), neotigogenin-3-*O*- $\alpha$ -L-rhamnopyranosyl-(1 $\rightarrow$ 6)- $\beta$ -D-glucopyranoside (**51**) and stigmasterol glycoside (**52**) from the plant were found to be in the order of 34.88%, 2.33%, 2.30% and 47.44%, respectively (Warjeet *et al.*, 2011). Thirugnanasampandan *et al.*, (2009) reported the *in vitro* antioxidant activities of leaf and stem extracts of *Smilax zeylanica* Vent. Among the extracts tested, ethanol extract of the stem showed maximum DPPH (52.361%) scavenging activity and chloroform extract of stem inhibited hydroxyl radical mediated linoleic acid oxidation up to 50.87%. Ethanol extract of leaves showed maximum reducing power of 0.53. The total free phenolics were found to be 293.3  $\mu$ g in the ethanol extract of leaf. Chen *et al.*, (2012) also established the antioxidant properties of constituents from *Smilax riparia*. Thirteen compounds were isolated from the plant. 5-methoxy-[6]-gingerol (**53**), 3,5-dimethoxy-4-hydroxybenzoic acid (**54**), isovanillin (**55**), vanillic acid (**31**), p-hydroxycinnamic acid (**56**), p-hydroxycinnamic methyl ester (**57**), p-hydroxybenzaldehyde (**58**) and ferulic acid methyl ester (**59**) showed antioxidant activities on DPPH method.



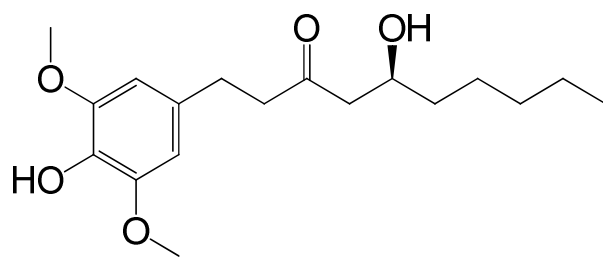
Apigenin glycoside (**50**)



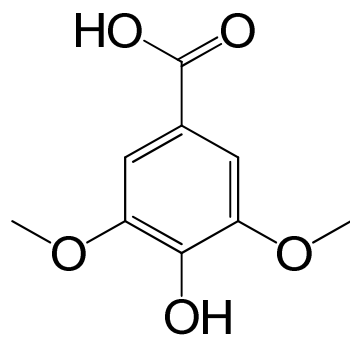
Neotigogenin-3-*O*- $\alpha$ -L-rhamnopyranosyl-(1 $\rightarrow$ 6)- $\beta$ -D-glucopyranoside (**51**)



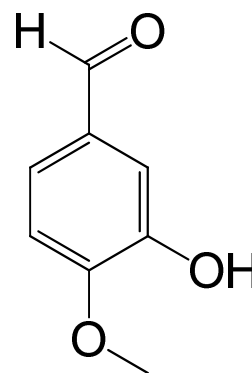
Stigmasterol glycoside (**52**)



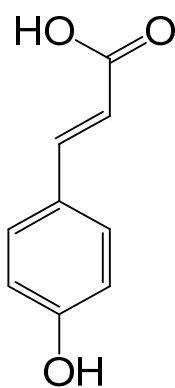
5-methoxy-[6]-gingerol (**53**)



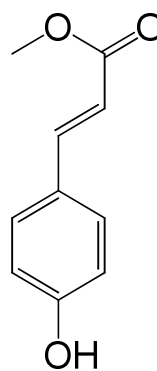
3,5-dimethoxy-4-hydroxybenzoic acid (54)



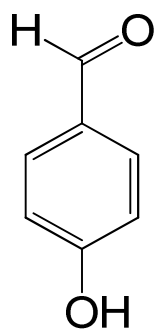
Isovanillin (55)



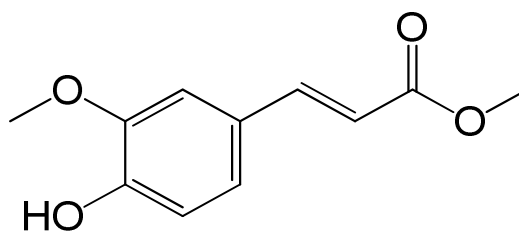
p-hydroxycinnamic acid (56)



p-hydroxycinnamic methyl ester (57)



p-hydroxybenzaldehyde (58)



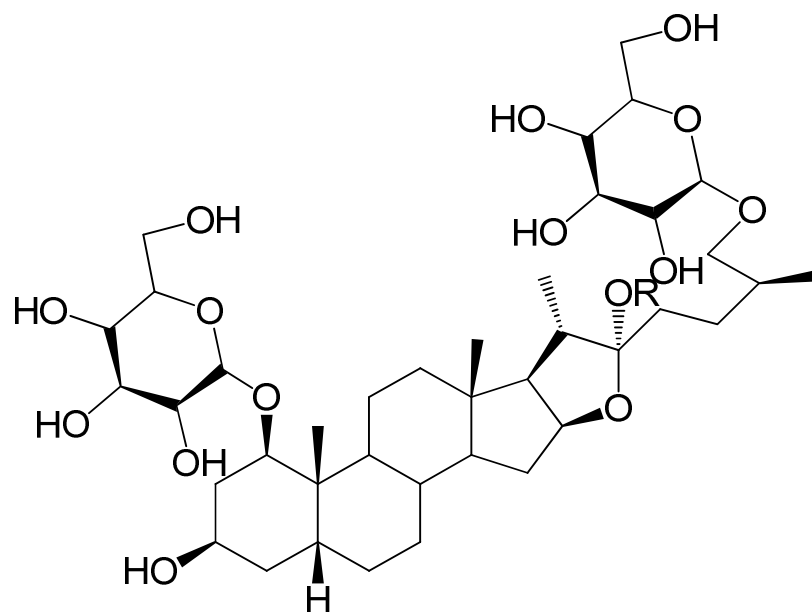
Ferulic acid methyl ester (59)

#### 2.4.4 Antiproliferative activity

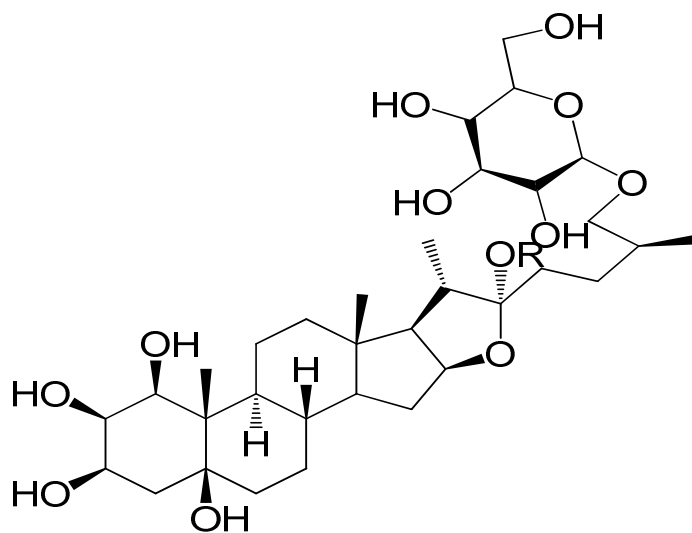
Ivanova *et al.*, (2011) reported the isolation of furostanol saponins; (25S)-26-O- $\beta$ -D-glucopyranosyl-5 $\beta$ -furostan-1 $\beta$ ,3 $\beta$ ,22 $\alpha$ ,26-tetraol-1-O- $\beta$ -D-glucopyranoside (**60**), (25S)-26-O- $\beta$ -D-glucopyranosyl-5 $\beta$ -furostan-1 $\beta$ ,2 $\beta$ ,3 $\beta$ ,5 $\beta$ ,22 $\alpha$ ,26-hexaol (**61**), (25S)-26-O- $\beta$ -D-glucopyranosyl-5 $\beta$ -furostan-3 $\beta$ ,22 $\alpha$ ,26-triol-3-O- $\alpha$ -L-rhamnopyranosyl-(1 $\rightarrow$ 2)-O- $\beta$ -D-glucopyranosyl-(1 $\rightarrow$ 2)-O- $\beta$ -D-glucopyranoside (**62**) and (25S)-26-O- $\beta$ -D-glucopyranosyl-5 $\beta$ -furostan-3 $\beta$ ,22 $\alpha$ ,26-triol-3-O- $\beta$ -D-glucopyranosyl-(1 $\rightarrow$ 2)-O- $\beta$ -D-glucopyranoside (**63**), from the rhizomes of *Smilax aspera*. All saponins have been isolated as their 22-OMe derivatives, which were further subjected to extensive spectroscopic analysis. The isolated furostanol saponins were evaluated for cytotoxic activity against human normal amniotic and human lung carcinoma cell lines using neutral red and MTT assays. In vitro experiments showed significant cytotoxicity in a dose dependent manner with IC<sub>50</sub> values in the range of 32.98 - 94.53  $\mu$ M. The antiproliferative properties of butanol, ethanol, ethylacetate and chloroform extracts of *Smilax china* L. were also reported. The extracts showed cytotoxicity at concentrations ranged from 0.8  $\mu$ g/mL to 100  $\mu$ g/mL (Wang *et al.*, 2014). Jan *et al.* (2007) and Raju and Bird (2007) demonstrated that diosgenin (**4**) exhibited antiproliferative activity and induce apoptosis in several cell lines.

#### 2.4.5 Anti-HIV, antihepatotoxic and contraceptive activities

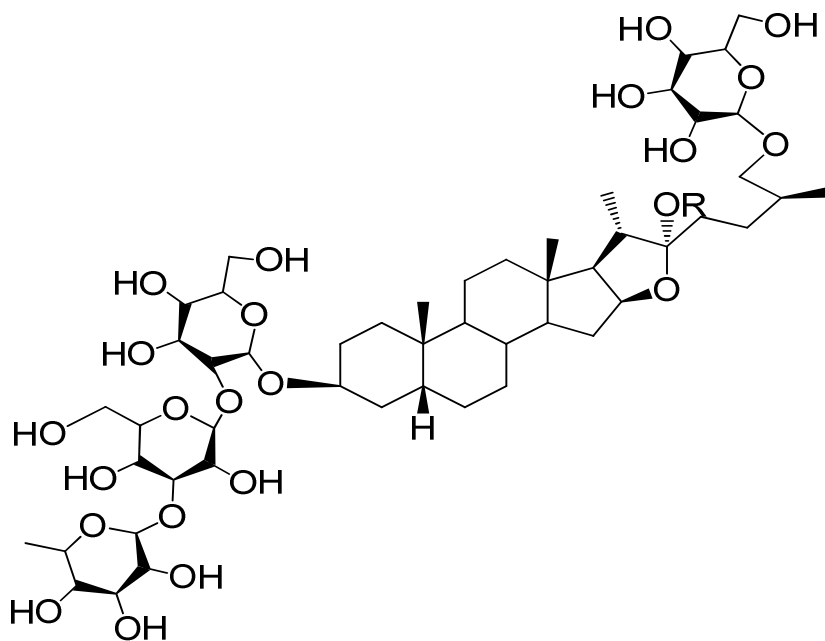
Wang *et al.*, (2014) reported the anti-HIV-1 properties of butanol, ethanol, ethylacetate and chloroform extracts as well as five phenolic compounds (dihydrokaempferol (**12**), dihydrokaempferol-3-O- $\alpha$ -L-rhamnoside (**13**), kaempferol-7-O- $\beta$ -D-glucoside (**14**), resveratrol (**15**) and oxyresveratrol (**16**)) isolated from *Smilax china* L. Butanol extract and resveratrol showed higher anti-HIV-1 activities than other extracts and compounds in the tested concentrations. EtOAc extract and compound **12** and **14** showed moderate anti-HIV-1 activities at a concentration higher than 4 $\mu$ g/mL. The acute toxicity of methanol extract of *Smilax kraussiana* leaves investigated. The extract possesses antihepatotoxic activities. The results of non-protein nitrogen compounds and ionic analysis showed that the integrity of the kidney was not compromised (Nwafor *et al.*, 2006). The anticonceptive, estrogenic and progestational properties as well as its copulatory behaviours of *Smilax kraussiana* root are also reported to be due to the presence of its phytochemical constituents which includes alkaloids, saponins and flavonoids (Nwafor *et al.*, 2013).



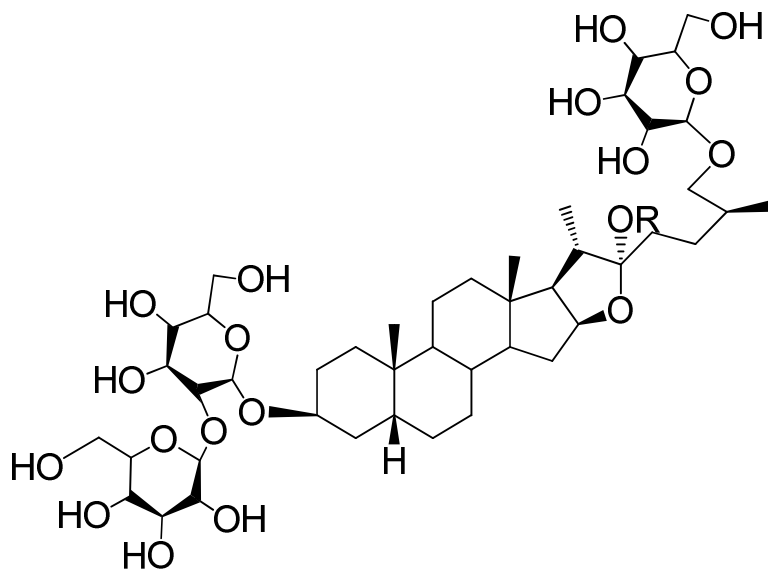
(25S)-26-O-β-D-glucopyranosyl-5β-furostan-1β,3β,22α,26-tetraol-1-O-β-D-glucopyranoside (**60**)



(25S)-26-O-β-D-glucopyranosyl-5β-furostan-1β,2β,3β,5β,22α,26-hexaol (**61**)



(25S)-26-O-β-D-glucopyranosyl-5β-furostan-3β,22α,26-triol-3-O-α-L-rhamnopyranosyl-(1→2)-O-β-D-glucopyranosyl-(1→2)-O-β-D-glucopyranoside (**62**)



(25S)-26-O-β-D-glucopyranosyl-5β-furostan-3β,22α,26-triol-3-O-β-D-glucopyranosyl-(1→2)-O-β-D-glucopyranoside (**63**)

## **2.5 Cancer**

Cancer is a disease characterized by unregulated proliferation of cells. The morbidity and mortality of cancer is so high that it is an economic concern to the society. It involves about 6 million cases per year and is the second major cause of death after cardiovascular diseases. There are more than 100 types of cancers. Some of which are lung, stomach, leukaemia, hepatic, cervical, liver, colon and breast cancer. Lung, stomach, liver, colon and breast cancer cause the most deaths each year (Bishop and Weinberg, 1996). Tobacco use is the single largest preventable cause of cancer in the world causing 20% of cancer deaths. Cancers of major public health relevance such as breast, cervical and colorectal cancer can be cured if detected early and treated adequately. One fifth of all cancers worldwide are caused by a chronic infection, for example human papilloma virus (HPV) causes cervical cancer and hepatitis B virus (HBV) causes liver cancer (Bishop and Weinberg, 1996). The search for natural products as potential anticancer agents dates back, at least, to the Ebers papyrus in 1550 BC, but the scientific period of this search is much more recent, beginning with the investigations by Hartwell and co-workers in late 1960s on the application of podophyllotoxin and its derivatives as anticancer agents. A large number of plant, marine, and microbial sources have been tested as leads, and many compounds have survived the potential leads (Gupta *et al.*, 2013).

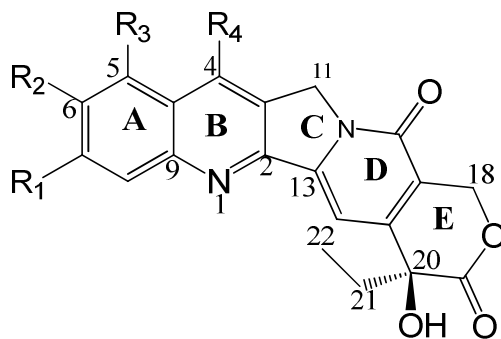
## **2.6 Antiproliferative drugs**

These are substances or drugs used to prevent or inhibit the spread or growth of cells, especially malignant cells, into surrounding tissues. A number of natural products, with diverse chemical structures, have been isolated as antiproliferative agents. Several potential lead molecules such as camptothecin, vincristine, vinblastine, taxol, podophyllotoxin, combretastatins, etc. have been isolated from plants and many of them have been modified to produce analogues for better activity, lower toxicity or higher solubility. Several successful molecules like topotecan, irinotecan, taxotere, etoposide, teniposide, etc. have emerged as drugs upon modification of these natural leads and many more are yet to come. Some of these compounds are discussed below.



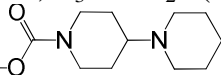
### 2.6.1 Camptothecin

In the early sixties, the discovery of camptothecin (CPT) (**64**) by Wall and Wani as an anticancer drug with a unique mode of action by inhibition of DNA topoisomerase I, added an entirely new dimension to the field of chemotherapy. This naturally occurring alkaloid was first isolated from the stem wood of the Chinese ornamental tree *Camptotheca acuminata*. It is a member of quinolino-alkaloid group. It consists of a pentacyclic ring structure which includes a pyrrole-quinoline moiety and one asymmetric centre within the hydroxyl lactone ring with 20(S) configuration (ring E). The planar pentacyclic ring structure (rings A-E) was suggested to be the most important structural features. The earlier report that the complete pentacyclic ring system is essential for its activity has been modified. Recently, reported results show that the E-ring (lactone) is not essential for its activity but, the ring in the present lactone form with specific C-20 configuration is required for better activity. A description of its structure activity relationship (SAR) is as follows (Jaxel *et al.*, 1989).



Camptothecin (**64**):  $R_1 = H$ ;  $R_2 = H$ ;  $R_3 = H$ ;  $R_4 = H$

Topotecan (**65**):  $R_1 = H$ ;  $R_2 = OH$ ;  $R_3 = CH_2N(CH_3)_2$ ;  $R_4 = H$

Irinotecan (**66**):  $R_1 = H$ ;  $R_2 =$  ;  $R_3 = H$ ;  $R_4 = CH_2CH_3$

Rubitecan (**67**):  $R_1 = H$ ;  $R_2 = H$ ;  $R_3 = NO_2$ ;  $R_4 = H$

Lurtotecan (**68**):  $R_1 = OCH_2O$ ;  $R_2 = H$ ;  $R_3 = H$ ;  $R_4 =$  

9-Aminocamptothecin (**69**):  $R_1 = H$ ;  $R_2 = H$ ;  $R_3 = NH_2$ ;  $R_4 = H$

- Rings A-D are essential for *in-vitro* and *in-vivo* activity.
- Saturation of ring B: compounds show little activity.
- A-Hydroxy lactone ring is necessary for activity.
- Oxygen at C-20 is crucial for better activity. Replacement of this oxygen with sulphur or nitrogen abolishes the activity of CPT.

- Conformation at C-20 is crucial for better activity as the 20(S) isomer is 10- to 100-fold more active than 20(R).
- D-ring pyridine is required for antitumor activity.
- Modifications in rings A and B are well tolerated and resulted in better activity than CPT in many cases.

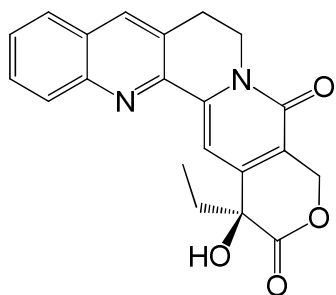
The first generation analogues of Camptothecin, hycamtin (topotecan) (**65**) and camptosar (irinotecan) (**66**) are used for the treatment of ovarian and colon cancers (Wall *et al.*, 1966; Wall, 1998; Saltz *et al.*, 2000; Gore *et al.*, 2001). CPT is a potent cytotoxic agent. It shows anticancer activity mainly on solid tumors. It inhibits DNA topoisomerase I (Redinbo *et al.*, 1998; Staker *et al.*, 2002). Although CPT exhibits antiproliferative activity mainly against colon and pancreatic cancer cells, it could not be used as a drug of choice due to its severe toxicity. Several groups have tried to synthesize derivatives having lower toxicity. Thus, the development of these synthetic and semisynthetic strategies has facilitated the study of the CPT mechanism, as well as the identification of analogues with improved properties (Table 2.1). Some of its modification in quinoline A and B rings (**66, 67, 68 and 69**), C and D rings (**70, 71, 72 and 73**), as well as derivatives/analogues obtained via modification at E ring (**74, 75, 76, 77, 78 and 79**) showed anticancer activities in breast, colorectal, lung, liver, pancreatic, leukemia and prostate cells (Moertel *et al.*, 1972; Muggia *et al.*, 1972; Hertzberg *et al.*, 1989; Kingsbury *et al.*, 1991; Potmesil and Kohn, 1991; Emerson *et al.*, 1995; Lackey *et al.*, 1995; Luzzio *et al.*, 1995; Pommier *et al.*, 1995; Potmesil and Pinedo, 1995; Ormrod and Spencer, 1999; Herzoq, 2002; Raymond *et al.*, 2002; Schoffski *et al.*, 2002 and Srivastava *et al.*, 2005).

**Table 2.1:** Anticancer activities of camptothecin analogues

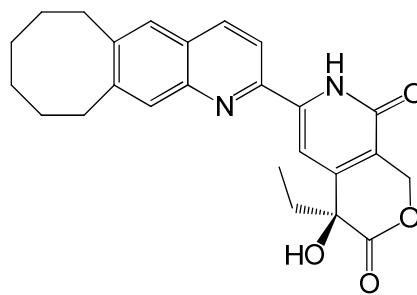
S/No	Analogues	1C <sub>50</sub> (μM) (Topo-1)	1C <sub>50</sub> (μM) (Topo-1)
64	CPT	0.6-1.4	23 (L1210), 0.046 (HT-29)
65	Topotecan	1.1	56 (L1210)
66	Irinotecan	>100	1200 (L1210)
67	Rubitecan	NA	
68	Lurtotecan	0.42	0.006 (HT-29)
69	9-Amino CPT	0.9	12(L1210)

L1210 – Leukemia cells;

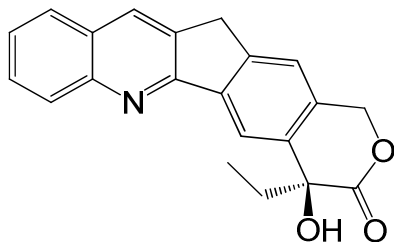
HT-29 – Human colorectal cells.



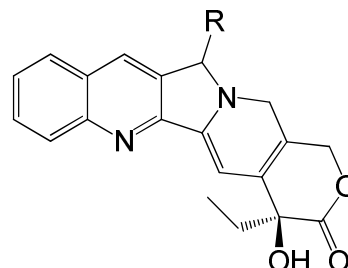
12-methylenecamptothecin (70)



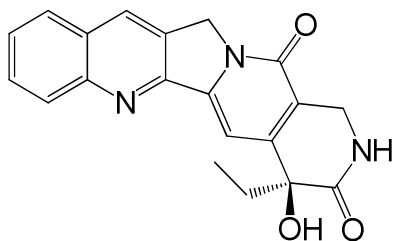
6,7-cyclooctyl camptothecin (71)



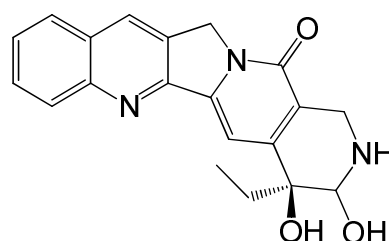
12-deaminocamptothecin (72)



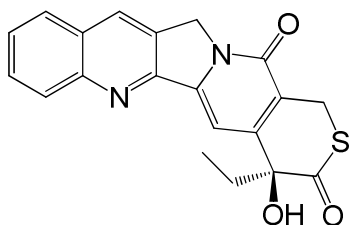
4-alkyl camptothecin (73)



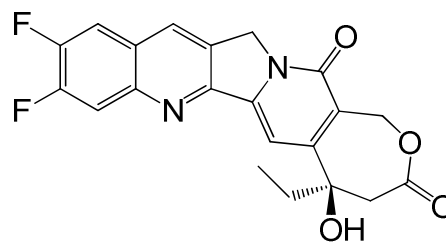
20-hydroxyaminocamptothecin (74)



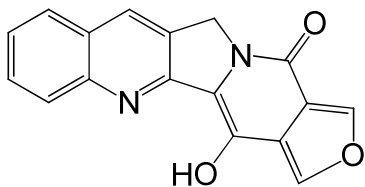
19,20-dihydroxyaminocamptothecin (75)



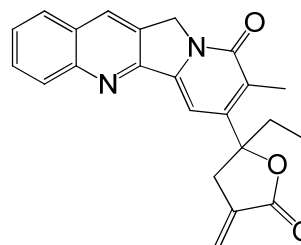
20-hydroxy thiocamptothecin (76)



6,7-difluoride-20-hydroxycamptothecin (77)



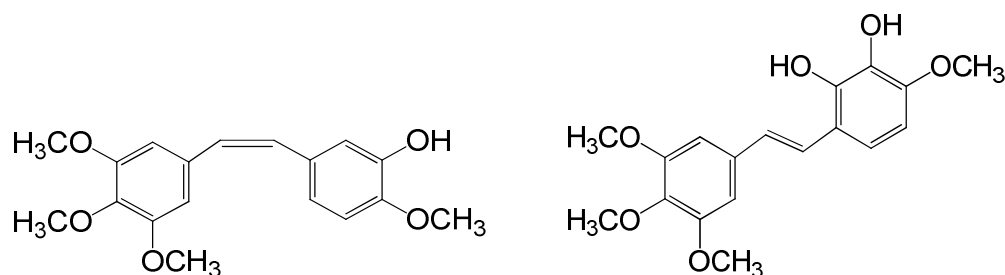
14-hydroxyl furacamptothecin (78)



18-ethyl-16-methyl-20-methylene-camptothecin (79)

### 2.6.2 Combretastatin A-4

The isolation of antiproliferative compound, Combretastatin from the bark of African willow tree *Combretum caffrum* at Arizona State University, USA was reported (Pettit *et al.*, 1982; Hamel and Lin, 1983; Pettit *et al.*, 1985). Combretastatins A-4 (**80**) (Pettit *et al.*, 1987a; Pettit *et al.*, 1989; Pettit *et al.*, 1995) and A-1 (**81**) (Pettit *et al.*, 1987b; Pettit *et al.*, 1987c; Pettit *et al.*, 1989) were isolated by the same group in 1987 and 1989, respectively. Chemically, they are stilbene derivatives having two phenyl rings separated by a C-C double bond. Ring-A has three methoxy groups in 3,4,5-positions while in ring B one hydroxyl group is at the C-3 position and one methoxy group at the C-4 position. CA-4 has been reported to possess antiproliferative activity against colon, lung and leukaemia cancers. The compound was the most cytotoxic phytomolecule with an LD<sub>50</sub> value of 0.007  $\mu$ M against murine L1210 leukaemia cell lines (Pettit *et al.*, 1995a; Pettit *et al.*, 1995b; Ohsumi *et al.*, 1998). A number of studies have been reported on the structure and activity relationship of combretastatins (Lin *et al.*, 1989; Brown *et al.*, 1995; Bedford *et al.*, 1996; Dorr *et al.*, 1996; Pettit *et al.*, 2000; Ducki *et al.*, 2005; Gwaltney II *et al.*, 2001). For a minimal cytotoxic activity of such compounds, a diaryl system should be separated through a double bond along with a trimethoxy system in one of the rings.



Combretastatins A-4 (**80**)

Combretastatins A-1 (**81**)

- Trimethoxy benzene moiety is essential for its activity (Talvitie *et al.*, 1992).
- The two aryl groups should be separated through a double bond and the cis (Z) isomer is preferred over the Trans (E) as cis is much more active than Trans (Cushman *et al.*, 1991).

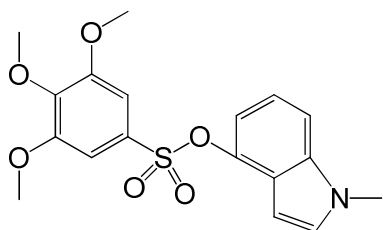
Various modifications have been reported in the CA-4 molecule. In some analogues, only the functional groups have been modified but in several analogues the total aryl ring is either replaced or modified by some other groups. However, in all cases

3,4,5-trimethoxy aryl or ring A was kept intact, which is considered to be indispensable for cytotoxicity of the molecule.

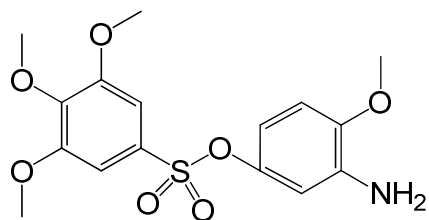
Several nitrogen-containing stilbene derivatives were synthesized (Pinney *et al.*, 2000) where the nitrogen atom was present as a nitro, amino or azide group and some of the derivatives exhibited excellent activity against the NCI 60 human cancer cell line. Similarly, Lawrence *et al.*, (2003) synthesized mono/difluoro derivatives of CA-4 at the C-3 and C-5 positions of ring B. Melero *et al.*, (2004) replaced one of the aryl groups with a naphthalene group and synthesized naphthylcombretastins, where they modified ring B of CA-4 to some quinoline and quinoxaline derivatives. All the compounds exhibited cytotoxicity comparable to or better than CA-4 and concluded that ring B in the present form is not essential for the cytotoxicity of CA-4. Several phosphate esters of CA-4 have been reported at phenolic hydroxyl of ring B, but none of the analogues showed better activity than CA-4 by MTT assay. From the SAR studies, it is concluded that the presence of an alkene is not necessary for activity. However, the restricted rotation of rings A and B of CA-4 can also be maintained by introducing suitable conformationally restricted arrangements. Sun *et al.*, (2004) reported 1,4-disubstituted azetidinone ring system having good cytotoxicity against MCF-7, CHO-K and NCI-H69 cancer cell lines. Thiophene-based analogues of CA-4 have shown tubulin polymerization inhibition activity comparable to CA-4, Gwaltney II *et al.*, (2001) used a sulfonate group between the aryl groups for restricted rotation, and compounds **(82)** and **(83)** showed cytotoxicity comparable to CA-4 (Table 2.2). In the place of a stilbene arrangement of the two aryl rings, several benzophenone type analogues have also been synthesized.

**Table 2.2:** Cytotoxicities of sulfonate derivatives of CA-4

<b>Compounds</b>	<b>HCT-15 Human colon carcinoma IC<sub>50</sub> (nM)</b>	<b>NCI-H460 Human lung carcinoma IC<sub>50</sub> (nM)</b>
<b>80</b> CA-4	1.7	3.0
<b>82</b> Methyl sulfonate CA-4	3.3	3.1
<b>83</b> Amino sulfonate CA-4	4.1	2.7



N-Methyl Indole combretastatin sulfonate (**82**)

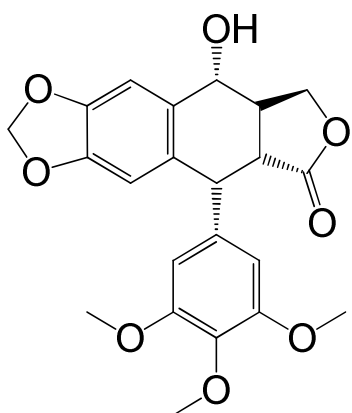


Combretastatin amino sulfonate (**83**)

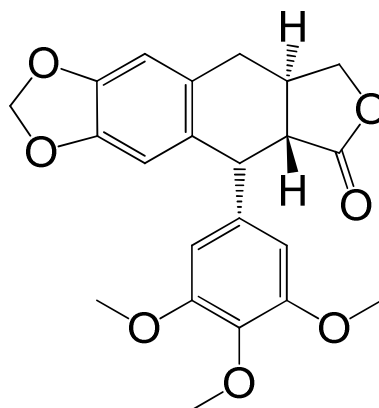
### 2.6.3 Podophyllotoxin

Podophyllotoxin (PDT, 37) (**84**) and deoxypodophyllotoxin (**85**) are two well-known naturally occurring aryltetralin lignans. Podophyllotoxin, a bioactive lignan, was first isolated by Podwyssotzki in 1880 from the North American plant *Podophyllum peltatum* Linnaeus (American *podophyllum*), commonly known as the American mandrake or May apple (Podwyssotzki, 1880). Later on, it was isolated from several other species like *P. emodi* Wall (Indian *podophyllum*, syn. *P. hexandrum* Royle) and *P. pleianthum* (Taiwanese *podophyllum*). Other than these, 4- deoxypodophyllotoxin has also been isolated (You *et al.*, 2004) from *Anthriscus sylvestris* and *Pulsatilla koreana*. It is a potent cytotoxic agent. Two of the semisynthetic derivatives of PDT, that is, etoposide (**86**) and teniposide (**87**), are currently used in frontline cancer chemotherapy against various cancers (O'Dwyer *et al.*, 1985). Chemically, it is an aryltetralin lignan, having a lactone ring. Podophyllotoxin contains a five-ring system (i.e., A, B, C, D and E rings). Only the A and E rings are essential for its activity. Earlier it was reported that all the rings are essential for its activity, but now the statement is modified. D-ring in lactone form is preferred for better activity. Modifications at the C-4 position in ring C are mostly acceptable and bulky groups at this position enhance both anticancer and topoisomerase activities. Podophyllotoxin shows strong cytotoxic property against various cancer cell lines. It is effective in the treatment of Wilms tumors, various genital tumours and in non-Hodgkinis and other lymphomas and lung cancer (Cassady *et al.*, 1980; Utsugi *et al.*, 1996; Subrahmanyam *et al.*, 1998). The attempts to use PDT in the treatment of human neoplasia were mostly unsuccessful due to complicated side effects (Kelly *et al.*, 1954) such as nausea, vomiting, damage of normal tissues, etc.

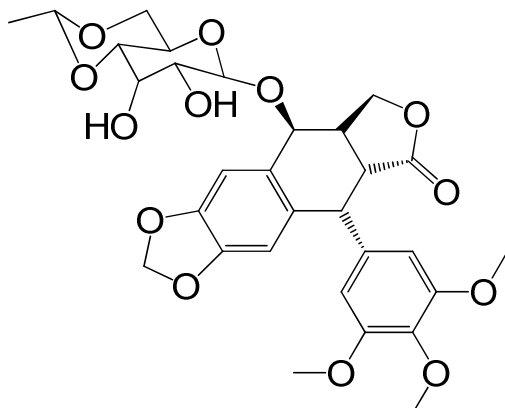




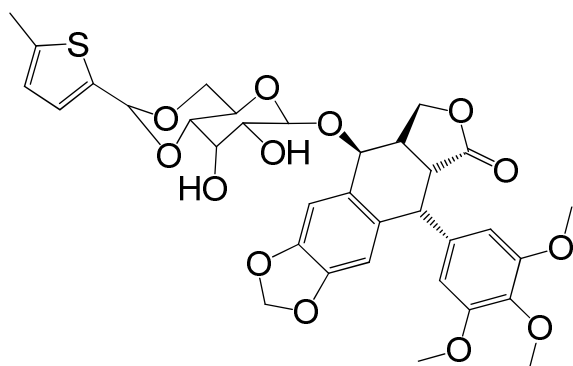
Podophyllotoxin (PDT, 37) **(84)**



Deoxypodophyllotoxin **(85)**



Etoposide **(86)**



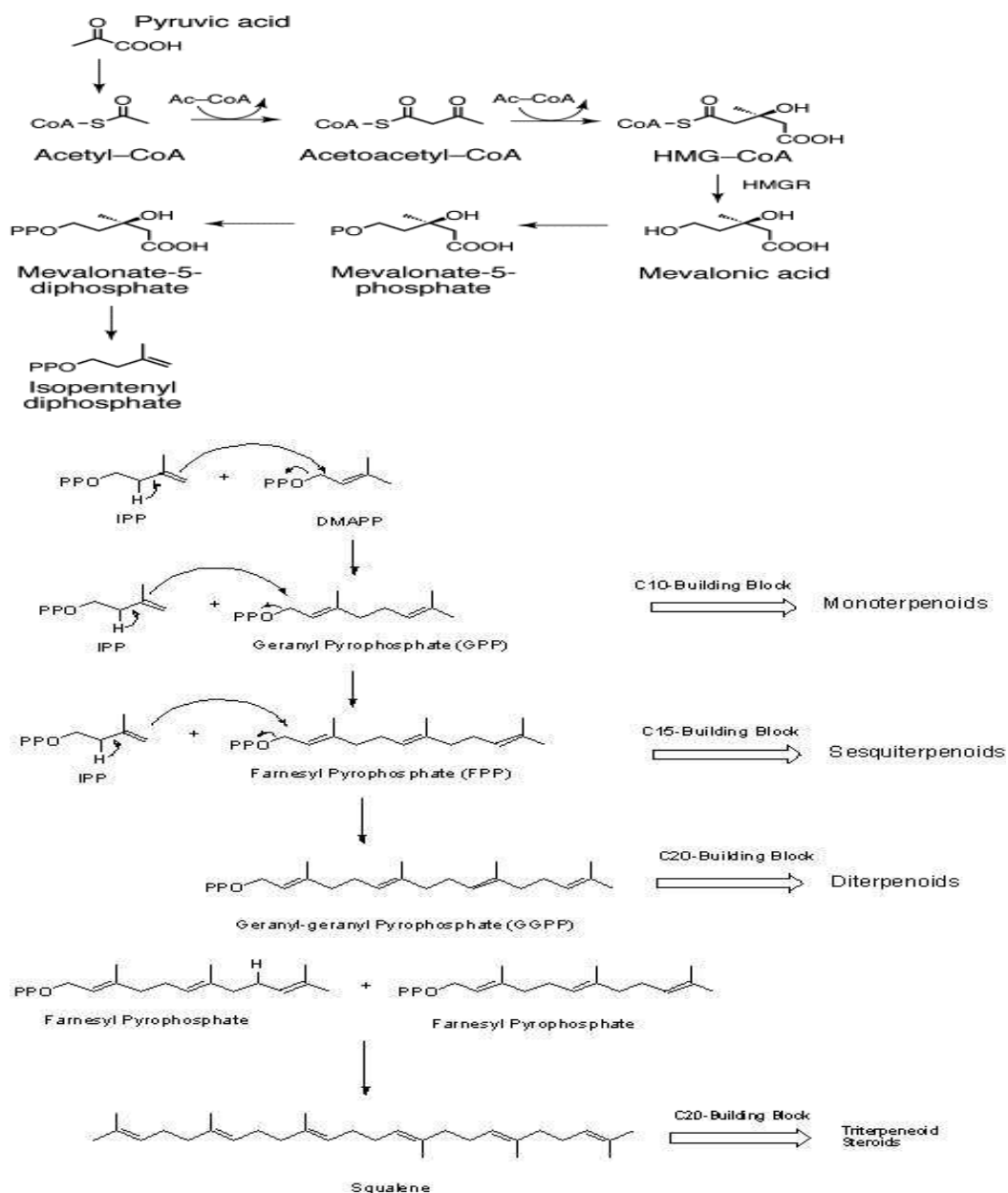
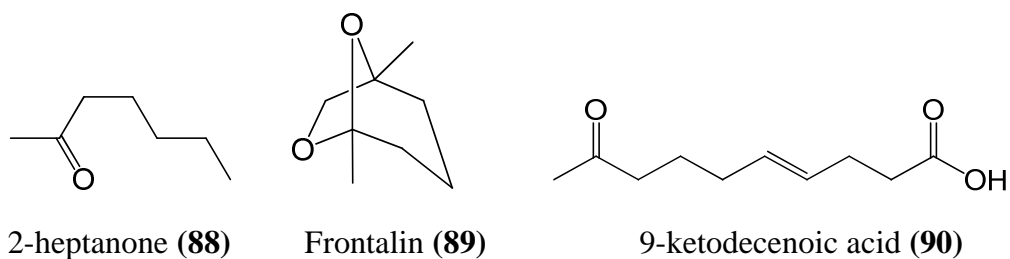
Teniposide **(87)**

## 2.7 Secondary metabolites

Plants produce a vast and diverse assortment of organic compounds, the great majority of which do not appear to participate directly in growth and development. These substances traditionally referred to as secondary metabolites, often differentially distributed among limited taxonomic groups within the plant kingdom. Their functions, many of which remain unknown, are being elucidated with increasing frequency. The primary metabolites, in contrast, such as phytosterols, acyl lipids, nucleotides, amino acids, and organic acids, are found in all plants and perform metabolic roles that are essential and usually evident (Croteau *et al.*, 2000). The secondary metabolite distribution in plants is far more limited than that of primary metabolites; often it is only found in a few species, or even within a few varieties within a species. The production of these compounds is often low (less than 1% dry weight), and it depends greatly on plant species and its physiological and developmental stage. Chemical synthesis of some of the secondary metabolites is either technically challenged or economically not feasible (Dixon, 2001).

### 2.7.1 Terpenoids

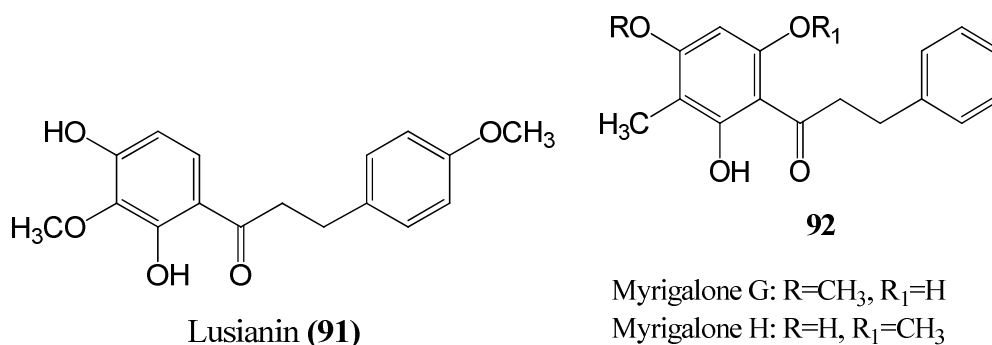
Terpenoids perhaps are the most structurally varied class of plant natural products. The name terpenoid, or terpene, derives from the fact that the first members of the class were isolated from turpentine. Many insects metabolize terpenes they have received with their plant food to growth hormones and pheromones. Pheromones are luring and signal compounds (sociohormones) that insects and other organisms excrete in order to communicate with others like them, e.g. 2-heptanone (**88**), an alarm pheromones from honey bees, frontalin (**89**) an aggregation pheromones from bark beetle and sexual pheromones, 9-ketodecenoic acid (**90**) produced by queen bee (Breitmaier, 2006). All terpenoids are derived by repetitive fusion of branched five-carbon (isoprene) units based on isopentane skeleton. The biosynthesis of terpenoids follows a mevalonic acid pathway (Scheme 1). These monomers generally are referred to as isoprene units, thus conferring the name isoprenoids on the terpenoid group (Croteau *et al.*, 2000). The isoprene units could assume head-to-tail, head-to-head and head-to-middle combination in the formation of different classes of terpenoids.

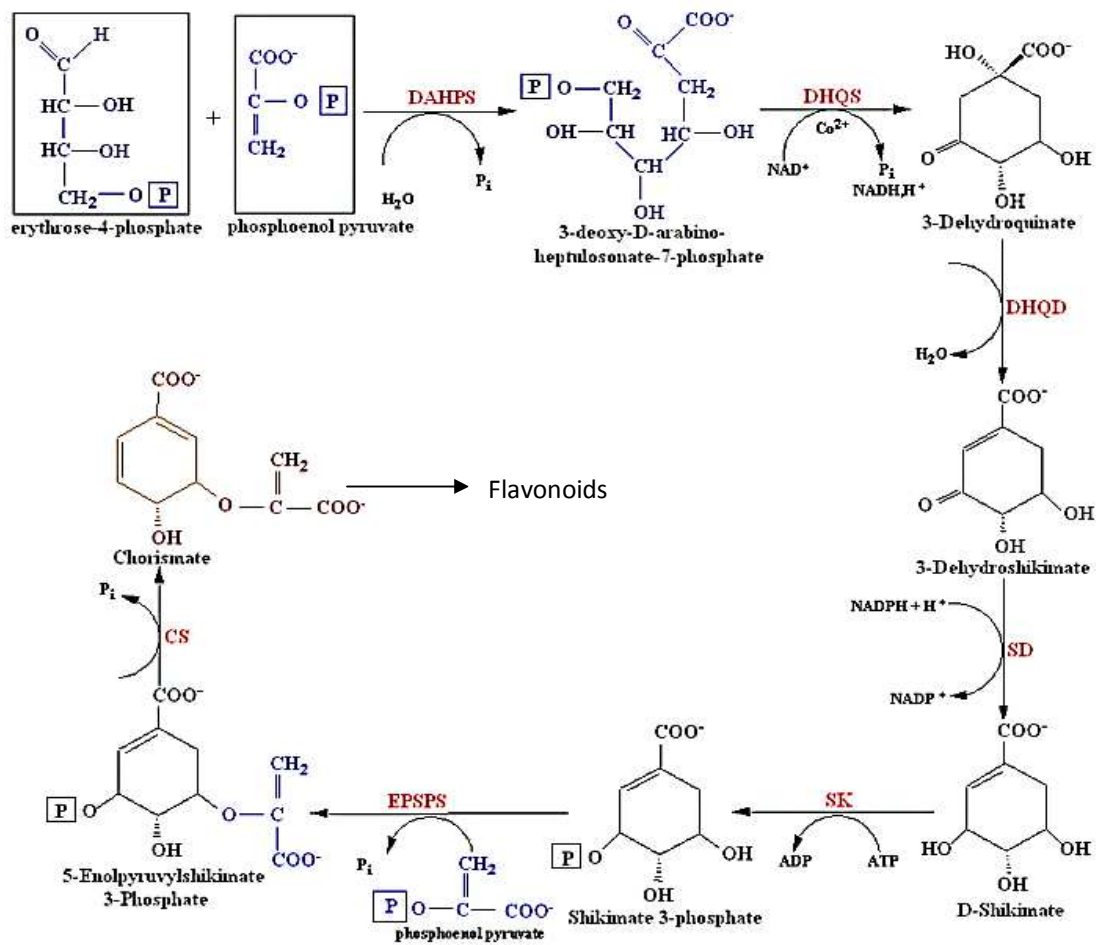


**Scheme 1:** Biosynthesis of terpenoids (Devon and Scott, 1972).

### 2.7.2 Flavonoids

Flavonoids are water soluble polyphenolic molecules containing 15 carbon atoms. They belong to the polyphenol family and originated from the shikimic acid biosynthetic pathway (Scheme 2). Most of the beneficial health effects of flavonoids are attributed to their antioxidant and chelating abilities. Their ability of scavenging hydroxyl radicals, superoxide anion radicals and lipid peroxyradicals highlights many of the flavonoid health-promoting functions in organism, which are important for prevention of diseases associated with an oxidative damage of membranes, proteins and DNA (Ferguson 2001). Flavonoids are classified into eight groups: flavans, flavanones, isoflavanones, flavones, isoflavones, anthocyanidines, chalcones and flavonolignans. The structures of these compounds are derived from a heterocyclic hydrocarbon, chromane, by substitution of its ring C in positions 2- or 3- with a phenyl-group (ring B) thereby forming flavans, and an oxo-group in the position 4 resulting in flavanones and isoflavanones. Frequently, a double bond between C2 and C3 in the ring C is present providing these compounds with quinone-like properties. These flavonoids are assigned as flavones (2-phenyl group) or isoflavones (3-phenyl group) depending on the ring C substitution. The presence of an additional double bond in the ring C instead of an oxo-group makes these compounds colourful and a well-known group of anthocyanidins. In addition, chalcones, bi-cyclic compounds possessing an opened C-ring are also classified as flavonoids. Examples are Lusianin (**91**) isolated from *Lusia volucris*, Myrigalone G and H (**92**) from *Myrica gale* and (Heim *et al.*, 2002; Hodek *et al.*, 2002).

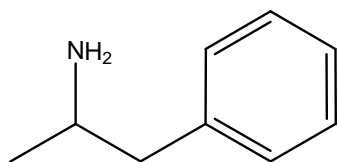




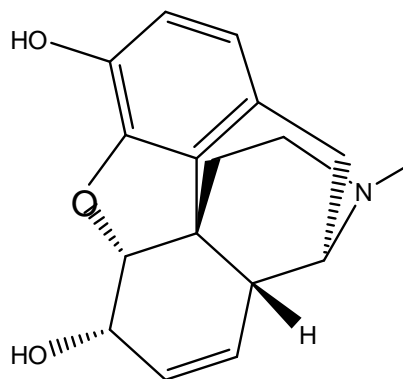
**Scheme 2** Biosynthesis of flavonoids (Filippou *et al.*, 2007)

### 2.7.3 Alkaloids

Alkaloids are a group of naturally occurring chemical compounds that contain mostly basic nitrogen atoms. Some alkaloid molecules, both natural and synthetic, can act as narcotics e.g. amphetamine (93) and morphine (94). The biosynthetic pathways of alkaloid are numerous. The biological precursors of most alkaloids are amino acids, such as ornithine, lysine and phenylalanine. Alkaloids are basic in nature, but some non-basic forms, such as quaternary compounds and *N*-oxides exist. Alkaloids are compounds needed for cell activity and gene code realization in the genotype. They are biologically significant as active stimulators, inhibitors and terminators of growth, part of an endogenous security and regulation mechanism. Some alkaloids have significance as haemoglobinizers of leukaemia cells and they can be biologically determined to be estrogenically active molecules. They display antimicrobial and anti-parasitic properties. Recent research has proved that alkaloids are not toxic to the organisms that produce them but selectively attack foreign organisms or cells (Aniszewski, 2007).



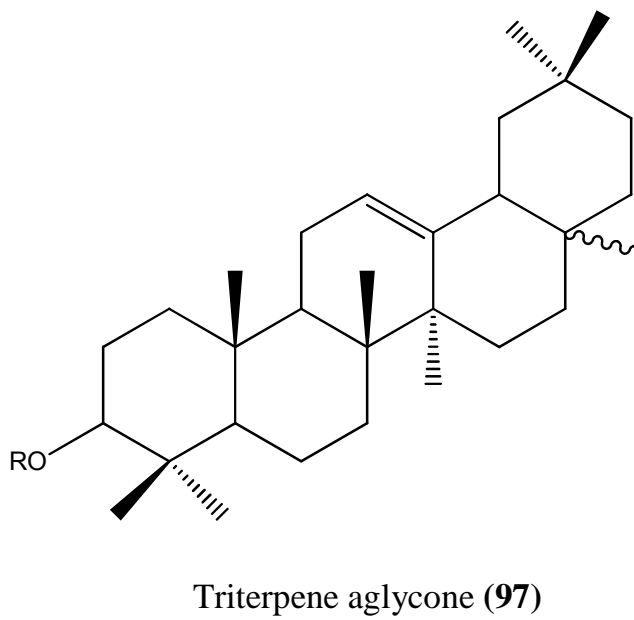
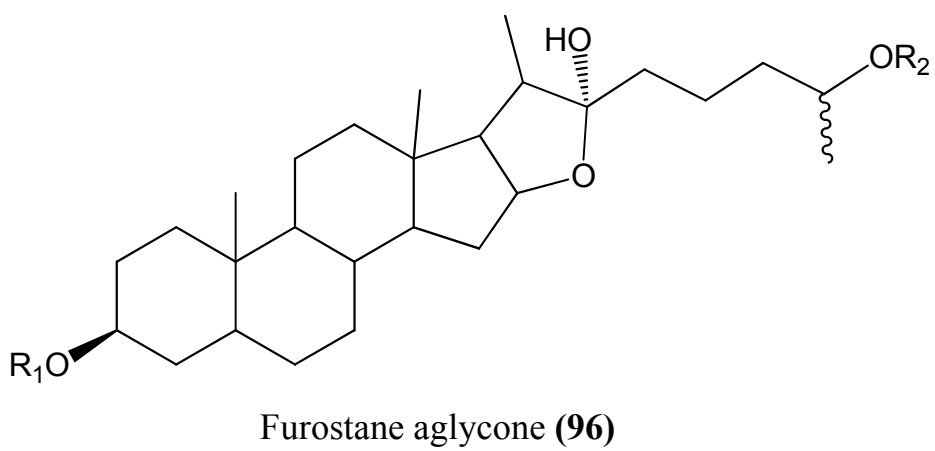
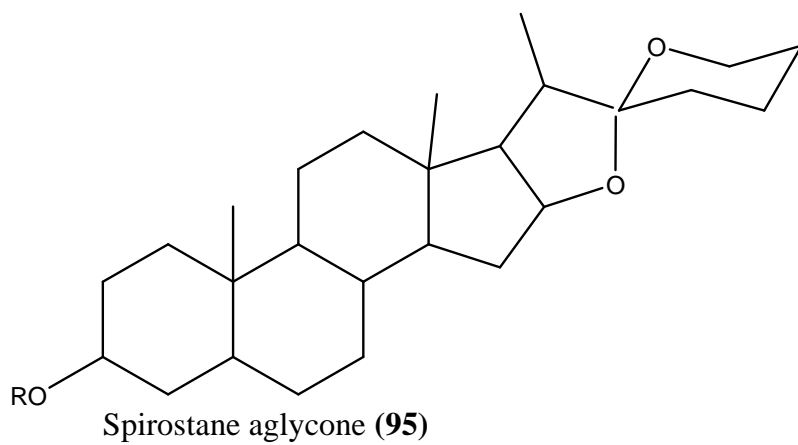
Amphetamine (93)



Morphine (94)

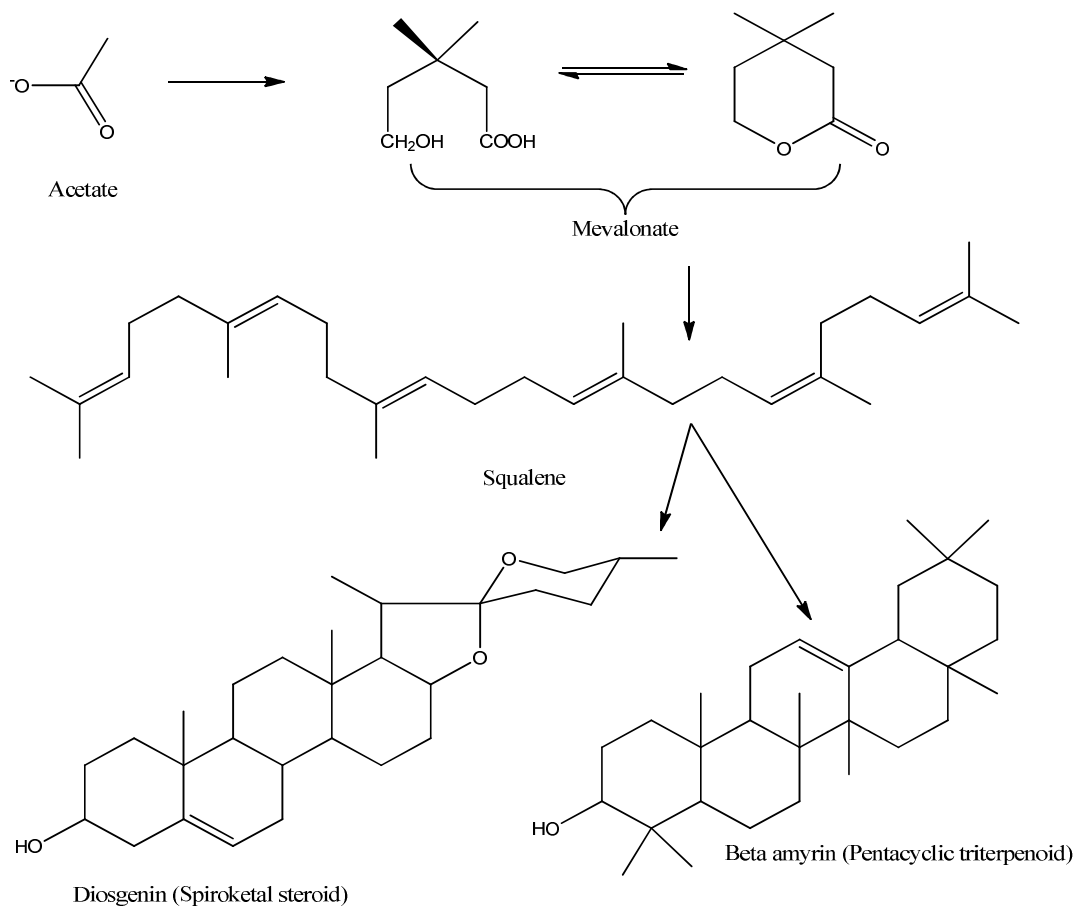
#### 2.7.4 Saponins

Saponins are generally known as non-volatile, surface active compounds that are widely distributed in nature, occurring primarily in the plant kingdom (Lasztity *et al.*, 1998; Oleszek, 2002; Hostettmann and Marston, 2005). They are structurally diverse molecules that are chemically referred to as steroid and triterpene glycosides. The steroidal saponins have either spirostane (**95**) or furostane (**96**) aglycone while the triterpenoid saponins have triterpene aglycone (**97**). Examples are diosgenin (**4**), tigogenin (**18**), sarsasapogenin (**19**) and laxogenin (**20**). The nonpolar aglycones are coupled with one or more monosaccharide moieties (Oleszek, 2002). This combination of polar and non-polar structural elements in their molecules explains their soap-like behaviour in aqueous solutions (Jean-Paul *et al.*, 2007). Saponins have also been sought after in the pharmaceutical industry because some form the starting point for the semi-synthesis of steroidal drugs. Many have pharmacological properties and are used in phytotherapy and in the cosmetic industry. They are believed to form the main constituents of many plant drugs and folk medicines, and are considered responsible for numerous pharmacological properties (Estrada *et al.*, 2000). Steroidal saponins are almost exclusively present in the monocotyledonous angiosperms while the triterpenoid saponins, which are the most common, occur mainly in the dicotyledonous angiosperms (Bruneton, 1995; Sparg *et al.*, 2004). The major biosynthetic pathways adopted by both types of saponins are identical. It involves head to tail coupling of various acetate units to form mevalonate. The enzymatic transformation of mevalonate forms triterpenoid hydrocarbon squalene, which ultimately leads to the spiroketal steroids or pentacyclic triterpenoids (Scheme 3).



R, R<sub>1</sub> and R<sub>2</sub> = Sugar moiety

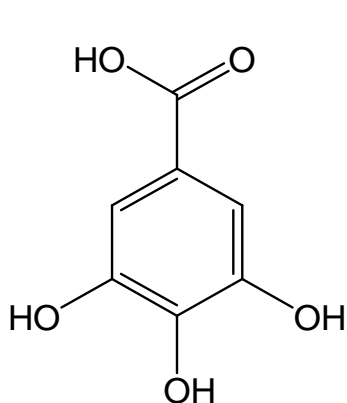




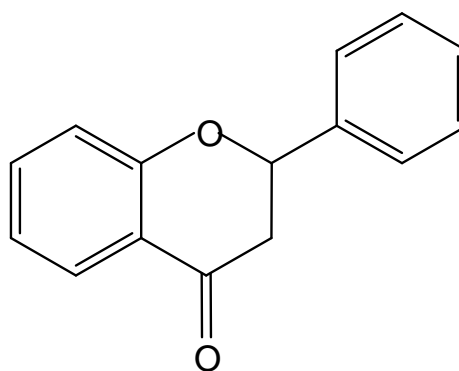
**Scheme 3** Biosynthesis of saponins (Bruneton, 1995; Sparg *et al.*, 2004).

### 2.7.5 Tannins

Tannins are very complex group of plant secondary metabolites, which are soluble in polar solution and distinguished from other polyphenolic compounds by their ability to precipitate protein. Their multiple phenolic hydroxyl groups lead to the formation of complexes with proteins, metal ions and other macromolecule like polysaccharides (Harborne, 1998; Van Acker *et al.*, 1998; Schofield *et al.*, 2001). The term tannin is used for structurally variable polymers which have been classified into two groups, the hydrolysable and the non hydrolysable (condensed) tannins with repeating units of gallic acid (**98**) and flavones (**99**) respectively. Condensed tannins are found in gymnosperms and angiosperms, whereas hydrolysable tannins are found only in dicotyledons (Haslam, 1981; Silanikove *et al.*, 2001). Biosynthesis of tannins follows shikimic acid pathways of flavonoids. For example, the proanthocyanidins are polymers of flavan-3-ol.



Gallic acid (**98**)



Flavones (**99**)

## **2.8 Chromatography**

Chromatography is a technique for separating the constituents of a mixture based on the difference in the interactions of the constituents with the mobile and stationary phase. The mobile phase may be either a liquid or a gas, while the stationary phase is either a solid or a liquid. The mobile phase carrying a mixture is caused to move in contact with a selectively absorbent stationary phase.

### **2.8.1 Column chromatography**

Column chromatography is a type of adsorption chromatography technique. The stationary phase is a solid material packed in a vertical column while the mobile phase is the eluting solvent. A small volume of the sample whose constituents are to be separated is introduced from top of the column, the individual components of mixture move with different rates based on their affinity to the solid phase and polarity of the eluting solvent. Those with lower affinity to stationary phase move faster and eluted out first while those with greater affinity move or travel slower and get eluted out last (Harbone, 1998).

### **2.8.2 Thin layer chromatography (TLC)**

Thin layer chromatography is a method used for identifying substances and testing the purity of compounds. The mobile phase is a solvent and the stationary phase is a thin layer of finely divided solid, such as silica gel or alumina, supported on glass or aluminium sheet. The separation depends on the relative affinity of compounds towards stationary and mobile phase. The compounds travel over the surface of stationary phase by capillary action under the influence of mobile phase. During this movement the compounds with higher affinity to stationary phase travel slowly while the others travel faster. Thus separation of components in the mixture is achieved. Once separation occurs individual components are visualized as spots at respective level of travel on the plate. Due to its rapidity of results, easy handling and inexpensive procedure, it finds its application as one of the most widely used chromatography techniques. High performance thin layer chromatography or high pressure thin layer chromatography is advancement in TLC. It is faster and as well gives better separation and resolution than the conventional TLC (Harbone, 1998).

### **2.8.3 High performance liquid chromatography (HPLC)**

The HPLC is a chromatographic technique used to separate a mixture of compounds with the purpose of identifying, quantifying or purifying the individual components of the mixture. Analyte molecules move through the porous packing beads and tend to interact with the surface adsorption sites. The different types of adsorption process include hydrophobic (non-specific) interactions in reversed-phase separations and dipole-dipole (polar) interactions in normal phase chromatography. In normal phase, the stationary bed is strongly polar in nature (e.g. silica gel) and the mobile phase is nonpolar (e.g n-hexane). Polar samples are thus retained on the polar surface of the column packing for longer than less polar materials. Reversed-phase chromatography has a non-polar stationary bed and a polar mobile phase such as mixtures of water and methanol or acetonitrile. The more nonpolar the material is, the longer it will be retained. Ionic interactions are responsible for the retention in ion-exchange chromatography. This technique is used almost exclusively with ionic or ionizable samples. The stronger the charge on the sample, the stronger it will be attracted to the ionic surface and thus, the longer it will take to elute. The mobile phase is an aqueous buffer, where both pH and ionic strength are used to control elution time. All these interactions are competitive; the analyte molecules are competing with the eluent molecules for the adsorption sites (Snyder *et al.*, 1997; Wilson *et al.*, 2005).

### **2.8.4 Gas chromatography (GC)**

This is used to detect the components based on the selective affinity of components towards the adsorbent materials. The sample is introduced into the machine with the help of GC syringe into the injection port, it gets vapourized at injection port then passes through column with the help of continuously flowing carrier gas stream (mobile phase), mainly H<sub>2</sub> or He, and gets separated/detected at the detection port with suitable temperature programming. Different chemical constituents of the sample travel through the column at different rates depending upon, physical and chemical properties, and interaction of the analytes with a stationary phase. As the chemicals exit the end of the column, they are detected and identified electronically (Snyder *et al.*, 1997).

## 2.9 Spectroscopic Techniques

### 2.9.1 Nuclear Magnetic Resonance (NMR) Spectroscopy

This is a research technique that exploits the magnetic properties of certain atomic nuclei to determine the structure of organic compounds. Common NMR active nuclei are  $^1\text{H}$ ,  $^{13}\text{C}$ ,  $^{15}\text{N}$ ,  $^{19}\text{F}$ ,  $^{31}\text{P}$ ,  $^{29}\text{Si}$  etc. NMR can provide detailed information about the structure, dynamics, reaction state, and chemical environment of molecules.

The principle behind NMR is that many nuclei have spin and all nuclei are electrically charged. If an external magnetic field is applied, an energy transfer is possible between the base energy to a higher energy level (generally a single energy gap). The energy transfer takes place at a wavelength that corresponds to radio frequencies and when the spin returns to its base level, energy is emitted at the same frequency. The signal that matches this transfer is measured in many ways and processed in order to yield an NMR spectrum for the nucleus concerned. The utility of NMR stems from the fact that chemically distinct nuclei differ in resonance frequency in the same magnetic field. This phenomenon is known as the chemical shift. In addition, the resonance frequencies are perturbed by the existence of neighbouring NMR active nuclei, in a manner dependent on the bonding electrons that connect the nuclei. This is known as spin-spin, or  $J$  coupling. Spin-spin coupling allows one to identify connections between atoms in a molecule, through the bonds that connect them (Pavia *et al.*, 2001; Kalsi, 2004).

#### 2.9.1.1 Two-dimensional nuclear magnetic resonance spectroscopy (2D NMR)

This is a set of nuclear magnetic resonance spectroscopy (NMR) methods which give data plotted in a space defined by two frequency axes rather than one. 2D NMR experiments include (i) Homonuclear through-bond correlation methods such as COrrrelation SpectroscopY (COSY), (ii) Heteronuclear through-bond correlation methods, such as Heteronuclear Single-Quantum Correlation spectroscopy (HSQC) and Heteronuclear Multiple-Bond Correlation spectroscopy (HMBC). (iii) Through-space correlation methods, like Nuclear Overhauser Effect SpectroscopY (NOESY) and Rotating frame nuclear Overhauser Effect SpectroscopY (ROESY). The most common types of 2D experiments are homonuclear correlation (COSY) and Heteronuclear COrrrelation (HETCOR) spectroscopy (Schram and Bellama, 1988).

**$^1\text{H}$ - $^1\text{H}$  COSY:** This is homonuclear correlation spectroscopy which shows correlation between protons that are coupled to each other. There are many modified version of the basic COSY experiment: DQF-COSY (Double-Quantum Filtered), COSY45, Long Range Correlation Spectroscopy (LRCOSY) and Exclusive Correlation Spectroscopy (ECOSY) (Macomber, 1998).

**HETCOR:** This 2D NMR indicates heteronuclear correlation, usually between  $^1\text{H}$  and  $^{13}\text{C}$  resonances mediated by  $J_{\text{C-H}}$ . The experiment can be run using either  $^1J_{\text{C-H}}$  or longer range couplings. It has poor sensitivity because the observed nucleus is  $^{13}\text{C}$  and has been largely replaced by the inverse detection experiments, Heteronuclear Multi-Quantum Coherence (HMQC) and Heteronuclear Single Quantum Coherence (HSQC) (Lamber and Mazzola, 2002).

**Heteronuclear Multi-Quantum Coherence (HMQC):** This experiment is similar to CH-COSY or HETCOR experiment, except that the inverse detection using a Distortionless Enhancement by Polarisation Transfer (DEPT) sequence provides much better sensitivity. It is used to correlate proton and carbon signals using either one bond or longer range couplings (Kalsi, 2004).

**Heteronuclear Single Quantum Coherence (HSQC):** This is a CH correlation experiment which uses proton detection of the  $^{13}\text{C}$  signals using an Insensitive Nuclear Enhancement by Polarisation Transfer (INEPT) sequence. It shows higher resolution in the C-dimension than does the related HMQC experiment (Schram and Bellama, 1988).

**Nuclear Overhauser Spectroscopy (NOESY):** This experiment shows the correlation between protons that are close in space. The nuclear overhauser effect arises throughout radio frequency saturation of one spin, the effect causes the perturbation via dipolar interactions with further nucleus spins. This enhances the intensity of other spins. This method is a very useful tool to study the conformation of molecules. This is a NMR technique for determining the 3-dimensional structure of molecules (Lamber and Mazzola, 2002).

### 2.9.2 Mass Spectrometry (MS)

Mass spectrometers use the difference in mass-to-charge ratio ( $m/z$ ) of ionized atoms or molecules to separate them. Therefore, mass spectroscopy allows quantitation of atoms or molecules and provides structural information by the identification of distinctive fragmentation patterns. Detection of compounds can be accomplished with very minute quantity of samples (Pavia *et al.*, 2001; Kalsi, 2004).

The general operation of a mass spectrometer is in three parts, creation of gas-phase ions, separation of the ions in space or time based on their mass-to-charge ratio and measurement of the quantity of ions of each mass-to-charge ratio. These three phases are carried out by suitable ionisation source, mass analysers and detector respectively.

**The Ionisation source:** This converts gas phase sample molecules into ions (or, in the case of electrospray ionization, move ions that exist in solution into the gas phase) examples include Chemical Ionisation (CI), Atmospheric Pressure CI (APCI), Electron Impact (EI), Electro-Spray Ionization (ESI), Fast Atom Bombardment (FAB), Field Desorption/Field Ionisation (FD/FI), Matrix Assisted Laser Desorption Ionisation (MALDI) and Thermospray Ionisation (TI).

**Electron Impact Ionisation (EI):** A beam of electrons passes through a gas-phase sample and collides with neutral analyte molecules to produce a positively charged ion or a fragment ion. Generally, electrons with energies of 70 eV are used. This method is applicable to all volatile compounds (>103 Da) and gives reproducible mass spectra with fragmentation to provide structural information (Rose and Johnstone, 2001).

**Chemical Ionisation (CI):** In this method, a reagent gas is first ionized by electron impact and then subsequently reacts with analyte molecules to produce analyte ions. This method gives molecular weight information and reduced fragmentation in comparison to EI.

**Fast Atom Bombardment (FAB):** Ions are produced by using a high current of bombarding particles is used to bombard the analyte which is in low volatile liquid matrix. This is a soft ionisation technique and is suitable for analysis of low volatility species. It produces large peaks for the pseudo-molecular ion species  $[M+H]^+$  and  $[M-$

H]<sup>-</sup> along with other fragment ions and some higher mass cluster ions and dimmers (Kalsi, 2004).

**Electro-Spray Ionization (ESI):** A solution is nebulized under atmospheric pressure and exposed to a high electrical field which creates a charge on the surface of the droplet. The production of multiple charged ions makes electrospray extremely useful for accurate mass measurement, particularly for thermally labile, high molecular mass substances (ie. proteins, oligonucleotides, synthetic polymers, etc.) (Hoffman and Stroobank, 2002).

**Matrix-Assisted Laser Desorption/Ionization (MALDI):** This is a soft ionization technique suitable for the analysis of molecules which tend to be fragile and fragment when ionized by more conventional ionization methods such as biomolecules (biopolymers e.g DNA, proteins, peptides and sugars) and large organic molecules (such as polymers, dendrimers and other macromolecules). It is similar in character to electrospray ionization both in relative softness and the ions produced (although it causes many fewer multiple charged ions). MALDI is also more tolerant of salts and complex mixture analysis than ESI (Rose and Johnstone, 2001).

**The mass analyzer:** This sorts the ions by their masses by applying electromagnetic fields. Examples include quadrupoles, Time-of-Flight (TOF), magnetic sectors, Fourier transform and quadrupole ion traps.

### 2.9.3 Infrared Spectroscopy (IR)

Infrared spectroscopy measures the vibrations of molecules. The infrared region of the electromagnetic spectrum is divided into three regions: the near-, mid-, and far-IR. The mid-IR (400-4000 cm<sup>-1</sup>) is the most commonly used region for analysis as all molecules possess characteristic absorbance frequencies and primary molecular vibrations in this range. Mid-infrared spectroscopy methods are based on studying the interaction of infrared radiation with samples. As IR radiation is passed through a sample, specific wavelengths are absorbed causing the chemical bonds in the material to undergo vibrations such as stretching, contracting, and bending. Functional groups present in a molecule tend to absorb IR radiation in the same wave number range regardless of other structures in the molecule, and spectral peaks are derived from the absorption of



bond vibrational energy changes in the IR region (Smith, 1996; Tolstoy *et al.*, 2003). IR spectroscopic analysis is mainly for determination of chemical functional groups in the sample.

#### **2.9.4 Ultra violet Spectroscopy (UV)**

Ultra violet spectroscopy (UV) is type of absorption spectroscopy in which light of ultra-violet region (200-400 nm.) is absorbed by the molecule. Absorption of the ultra-violet radiations results in the excitation of the electrons from the ground state to higher energy state. The energy of the ultra-violet radiation that are absorbed is equal to the energy difference between the ground state and higher energy states ( $\Delta E = hf$ ). Generally, the most favoured transition is from the highest occupied molecular orbital (HOMO) to lowest unoccupied molecular orbital (LUMO) (Pavia *et al.*, 2001; Kalsi, 2004).

UV spectroscopy employs the Beer-Lambert law, which states that when a beam of monochromatic light is passed through a solution of an absorbing substance, the rate of decrease of intensity of radiation with thickness of the absorbing solution is proportional to the incident radiation as well as the concentration of the solution or the greater the number of molecules capable of absorbing light of a given wavelength, the greater the extent of light absorption. This is the basic principle of UV spectroscopy. UV spectroscopy can be used for detection of chemical functional group and extent of conjugation, determination of purity of a substance and configuration of geometrical isomers, and as well as identification of unknown compound.

#### **2.9.5 X-ray crystallography**

X-ray crystallography is a technique in which the pattern produced by the diffraction of x-rays through the closely spaced lattice of atoms in a crystal is recorded and then analysed to reveal the nature of that lattice. X-ray crystallography allows precise determination of the atomic positions and consequently the bond lengths and angles of molecules within a single crystal. X-rays are electromagnetic radiation with wavelengths between about 0.02 Å and 100 Å ( $1\text{Å} = 10^{-10}$  meters).

When X-rays are beamed at the crystal, electrons diffract the X-rays, which cause a diffraction pattern. Through the use of the mathematical Fourier transform these patterns can be converted into electron density maps. These maps show contour lines of

electron density. Since electrons more or less surround atoms uniformly, it is possible to determine where atoms are located; only hydrogen is difficult to map because it has one electron thus resulting to very low electron density around it. The crystal is rotated while a computerized detector produces two dimensional electron density maps for each angle of rotation. The third dimension comes from comparing the rotation of the crystal with the series of images. Computer programs use this method to come up with three dimensional spatial coordinates (Rhodes, 1993; Carter, 1997).

## CHAPTER THREE

### MATERIALS AND METHODS

#### 3.1 General Experimental Procedures

All solvents were of analytical grade and were used as supplied. Column chromatography was performed on silica gel (Merck 120 - 200 mesh). Thin layer chromatography (TLC) was performed on aluminium plates coated with silica gel (Merck, 60 mesh). TLC bands were visualized under ultraviolet light (at 254 nm and 365 nm) and by exposure to iodine vapour.

$^1\text{H}$  and  $^{13}\text{C}$  NMR were recorded at 300 MHz (75 MHz for  $^{13}\text{C}$  NMR analysis) on Bruker Avance spectrophotometer at 300 K in deuterated solvents. Tetramethylsilane was used as internal reference and chemical shifts were expressed in parts per million (ppm). ESI mass spectra were recorded on API 3000 LC-MS-MS, Applied Biosystem, USA after dissolving the compounds in methanol or acetonitrile. FT-IR spectra were recorded on Perkin-Elmer Spectrum BX. Melting points were determined in open capillaries using E-Z Melt automated melting point apparatus, Stanford Research System, USA and were uncorrected.

#### 3.2 Collection of plant materials

The aerial parts of *Smilax kraussiana* were collected from Onigambari Forest Reserve, Ibadan, Oyo State in May 2010. The plant was identified and authenticated at Forestry Research Institute of Nigeria (FRIN) Ibadan, Oyo State of Nigeria. Voucher specimen of the plant was deposited at the herbarium of FRIN and identification number of FHI 108799 was assigned to *S. kraussiana*.

### **3.3 Extraction of Plant materials**

The air-dried, powdered plant materials: (1,200 g) aerial parts of *Smilax kraussiana* was successively extracted with hexane, ethyl acetate and methanol by maceration. The extracts were filtered with Whatmann No. 1 filter paper and separately concentrated on rotatory evaporator at 37° C to about 50 mL and freeze dried. The sequential extraction of the aerial parts of *Smilax kraussiana* with hexane yielded a yellowish brown solid (14 g) coded SKH. The marcs were air-dried to ensure that all residual hexane is evaporated, and then re-soaked in ethyl acetate for five days to give brown extract (20 g) coded SKE. The marc of the plant was air-dried and re-soaked in methanol for five days to give a dark brown extract (11.5 g). All the extracts were subjected to antiproliferative assay.

### **3.4 Antiproliferative Assays of Extracts**

#### **3.4.1 3-(4,5-dimethylthiazol-2-yl)-2,5-diphenyl-2H-tetrazolium bromide (MTT) assay**

Four human (K562 Leukemia, WRL hepatic, MCF-7 breast and COLO colon) cancer cells were obtained from the American Type Culture Collection (Lucknow, India), and cultured in DMEM/Ham's F-12 medium containing 10% heat-inactivated FBS, 5 mg/mL of penicillin, 10 mg/mL of neomycin and 5 mg/mL streptomycin. All cells were cultured at 37 °C in a humidified incubator containing 5% CO<sub>2</sub>. The suppressive effects of test agents on cell viability were assessed by using the 3-(4,5-dimethylthiazol-2-yl)-2,5-diphenyl-2H-tetrazolium bromide (MTT) assay in six replicates. Cells (5x10<sup>3</sup>/200 µL) were seeded and incubated in 96-well, flat-bottomed plates in 10% FBS-supplemented medium for 24 h and were exposed to various concentrations of test agents dissolved in DMSO (final DMSO concentration, 0.1%) in 5% FBS-supplemented medium. Controls received DMSO vehicle at a concentration equal to that of drug-treated cells. The medium was removed and replaced by 0.5 mM MTT (200 µL) in 10% FBS-containing DMEM/Ham's F-12 medium, and cells were incubated in the 5% CO<sub>2</sub> incubator at 37 °C for 2 h. Supernatants were removed from the wells, and the reduced MTT dye was solubilized in 200 µL/well DMSO. Absorbance at 570 nm was determined on a plate reader. The cell viability was expressed as a percentage to the viable cells of control culture condition and IC<sub>50</sub> values of each group were calculated (Woerdenbag *et al.*, 1993).

### **3.4.2 Sulphorhodamine assay**

Cytotoxic activity of the compounds was assessed by Sulphorhodamine B dye based plate assay (Adaramoye *et al.*, 2011). In brief,  $10^4$  cells/well were added in 96-well culture plates and incubated overnight at 37 °C in 5% CO<sub>2</sub>. Next day (at 80% confluency), serial dilutions of test compound were added to the wells. Untreated cells served as control. After 48h, cells were fixed with ice-cold 50% (w/v) Tri-chloroacetic acid (100µl/well) for 1h at 4 °C. Cells were then stained with SRB (0.4% w/v in 1% acetic acid, 50µl/well), washed and air-dried. Bound dye was solubilised with 10mM Tris base (150µl/ well) and absorbance was read at 540 nm on a plate reader (Biotek, USA). The cytotoxic effect of compound was calculated as % inhibition in cell growth as per formula:  $[1 - (\text{Absorbance of drug treated cells} / \text{Absorbance of untreated cells}) \times 100]$ . Determination of 50 % inhibitory concentration (IC<sub>50</sub>) was based on dose-response curves.

### **3.5 Phytochemical Screening**

Preliminary qualitative phytochemical screening of each extract was carried out using the following methods:

#### **3.5.1 Flavonoids Test**

About 5 mL of dilute ammonia solution were added to a portion of the aqueous filtrate of test extracts followed by addition of concentrated H<sub>2</sub>SO<sub>4</sub>. A yellow colouration observed in each extract indicated the presence of flavonoids. The yellow colouration may disappear on standing (Edeoga *et al.*, 2005).

#### **3.5.2 Tannins Test**

Few drops of 1% lead acetate were added to the test extract (2 mL). A yellowish precipitate indicating the presence of tannins was observed (Savithamma *et al.*, 2011).

#### **3.5.3 Saponins Test**

The test extract (5 mL) was mixed with 20 mL of distilled water and then agitated in a graduated cylinder for 15 minutes. Formation of foam indicates the presence of saponins (Kumar *et al.*, 2011).

#### **3.5.4 Anthocyanins Test**

About 2 mL of aqueous test extract was added to 2 mL of 2M HCl and ammonia. The pink-red colouration turned blue-violet. This showed the presence of anthocyanins (Savithramma *et al.*, 2011).

#### **3.5.5 Anthraquinone Test**

Borntrager's test was used for the detection of anthraquinones. Five grams of each plant extract was shaken with 10 mL benzene, filtered and 5 mL of 10% ammonia solution added to the filtrate. The mixture was then shaken and the appearance of a red colour in the ammoniacal phase (lower) indicated the presence of free hydroxyl-anthraquinones (Edeoga *et al.*, 2005).

#### **3.5.6 Cardiac glycoside Test**

The test extract (0.5 g) was dissolved in 2 mL of acetic anhydride and cooled in ice after which conc. sulphuric acid was carefully added. The colour change from violet to blue or green indicating the presence of a steroidal nucleus (i.e. aglycone portion of the cardiac glycoside).

#### **3.5.7 Alkaloids Test**

About 0.5 g test extract was stirred with 5 mL of 1% dilute hydrochloric acid on a water bath. The resulting solution was then filtered and 1 mL of the filtrate was then treated with a few drops of Mayer's reagent and a second 1 mL portion with Dragendorff's reagent. Turbidity or precipitation with either of these reagents was taken as evidence for the presence of alkaloids in the extract (Harborne, 1998; Trease and Evans, 1989).

#### **3.5.8 Carbohydrates Test**

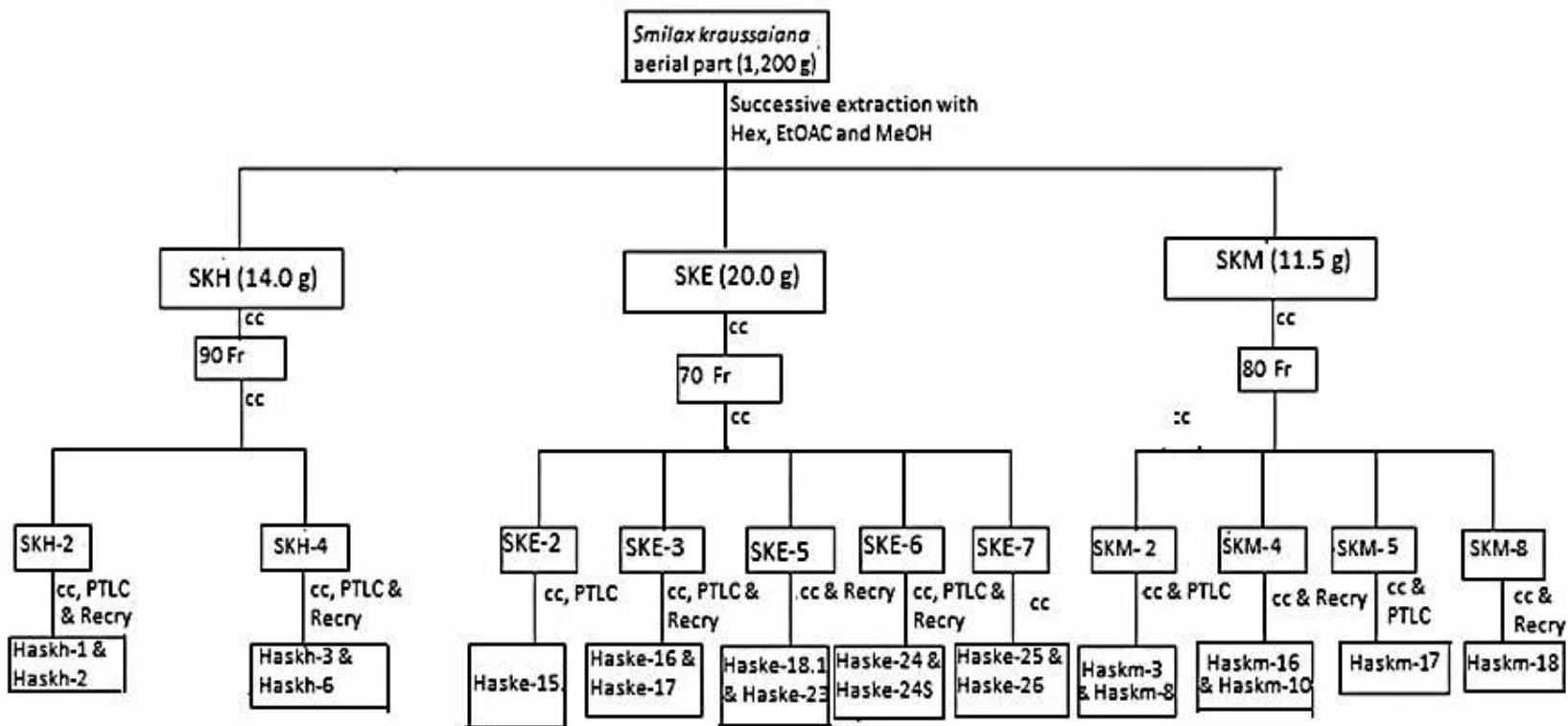
Two drops of the Molisch reagent (a solution of  $\alpha$ -naphthol in 95% ethanol) was added to 2 mL of a test solution in a test tube. The solution is then poured slowly into a test tube containing 2 mL of concentrated sulphuric acid to give two layers. The formation of a purple interface at the layer indicated the presence of carbohydrates. i.e a positive test is indicated by the formation of a purple product at the interface of the two layers.

### **3.6 Column chromatography of hexane extract of *S. kraussiana* (aerial parts)**

Hexane extract (11.0 g) of *S. kraussiana* aerial parts (SKH) was preadsorbed on silica gel (30 g) to form a homogenous solid which was subjected to column chromatography (silica gel, 700 g, 100-200 mesh size) using Hexane:CHCl<sub>3</sub> (19:1, 500 mL); (9:1, 500 mL); (17:3, 500 mL); (8:2, 500 mL); (7:3, 500 mL); (3:2, 500 mL); (1:1, 500 mL); (2:3, 500 mL); (3:7, 500 mL); (1:4, 500 mL); (1:9, 500 mL); (1:19, 500 mL); CHCl<sub>3</sub> (100%, 500 mL) and hexane: ethyl acetate (9:1, 500 mL); (17:3, 500 mL); (4:1, 500 mL); (7:3, 500 mL) and (3:2, 500 mL) separately. A total of 90 fractions (100 mL each) were collected and pooled to 4 sub-fractions (SKH-1-SKH-4) based on TLC analysis (Scheme 6). The sub-column chromatographic separation of SKH-2 and SKH-4 followed by preparative thin layer chromatography (PTLC) yielded two pure compounds each; a white crystalline solid Haskh-1 (30 mg), light yellow oily compound Haskh-2 (25 mg), creamy yellow solids Haskh-3 (21 mg) and Haskh-4 (15 mg).

#### **3.6.1 Characterisation of the Isolated compounds**

The pure compounds were characterized by subjecting them to Infra red (IR), Mass Spectrometry (MS), Proton and Carbon-13 Nuclear Magnetic Resonance (NMR) and analysis of the different spectra coupled with comparison with literature data.



Key:: Fraction (Fr), Column chromatography (cc), Preparative Thin Layer chromatography (PTLC), Recrystallisation (Recry)

SKH = Hexane extract of *Smilax kraussiana*, SKE = Ethyl acetate extract of *Smilax kraussiana*, SKM = Methanol extract of *Smilax kraussiana*,

#### Scheme 4: Extraction and Isolation of compounds from *S. kraussiana* (aerial parts)



### **3.7 Column chromatography of ethyl acetate extract of *S.kraussiana* (aerial parts)**

Ethyl acetate extract (17.0 g) of *S. kraussiana* aerial parts (SKE) was mixed with 40 g of silica gel and chromatographed on 800 g, 100-200 mesh silica gel. Elution was carried out using gradient of n-hexane and ethylacetate. A total of 70 fractions of 100 mL each were collected and pooled to 8 sub-fractions, SKE (1-8). The sub-column chromatographic separation of SKE- 2, 3, 5, 6 and 7 were purified by preparative TLC and crystallization using different eluting solvent ratios of n-hexane: ethylacetate. This yielded nine compounds: Creamy white solid, Haske-1; White crystal, Haske-2; Creamy white solid, Haske-3; white powdered solid, Haske-4; light yellow gelly-like solid, Haske-5; creamy yellow solid, Haske-6; white crystals, Haske-7; brown solid, Haske-8 and cream powdered solid, Haske-9.

#### **3.7.1 Characterisation of the Isolated compounds**

This was carried out as stated in 3.6.2

### **3.8 Column chromatography of methanol extract of *S.kraussiana* (aerial parts)**

The methanol extract (8.5 g) of *S. kraussiana* aerial parts (SKM) was mixed with silica gel (30 g) to form slurry. The extract slurry was chromatographed on silica gel and eluted with gradient of hexane and ethylacetate in order of hexane: ethylacetate (9:1, 500 mL); (4:1, 500 mL); (7:3, 500 mL); (3:2, 500 mL); (1:1, 500 mL); (2:3, 500 mL); (3:7, 500 mL); (1:4, 500 mL), (1:9, 500 mL), (1:19, 500 mL), ethyl acetate (100%, 500 mL), and ethyl acetate: methanol (98:2, 500 mL), (96:4, 500 mL), (95:5, 500 mL), (94:6, 500 mL) and (92:8, 500 mL) to give 80 fractions of 100 mL each. The fractions were pooled to 9 sub-fractions, SKM (1-9) using TLC analysis. Formation of dirty white solid was observed in the SKM-2 eluted with Hex: EtOAc, 4:1 and 7:3. The dirty white solid was purified with Preparative TLC in hexane-ethyl acetate 4:1 to give white crystals coded Haskm-1 (26 mg) and cream solid Haskm-2 (17 mg). The sub-column chromatography and preparative TLC of SKM-4, 5 and 8, followed by re-crystallization afforded one pure compound each. These are Haskm-3 (white crystals, 15 mg), Haskm-4 (light yellow gelly-like solid, 25 mg) and Haskm-5 (white powdered solid, 22 mg).

#### **3.8.1 Characterisation of the Isolated compounds**

This was carried out as stated in 3.6.2

### 3.9 Antiproliferative assay of Isolated compounds

The isolated compounds were tested against four human cancer cells (K562 Leukemia, WRL hepatic, MCF-7 breast and COLO colorectal) using 3-(4,5-dimethylthiazol-2-yl)-2,5-diphenyl-2H-tetrazolium bromide (MTT) and Sulphorhodamine assays as explained in 3.4.1 and 3.4.2.

### 3.10 Chemical synthesis of Diosgenin (Haske-9) analogues

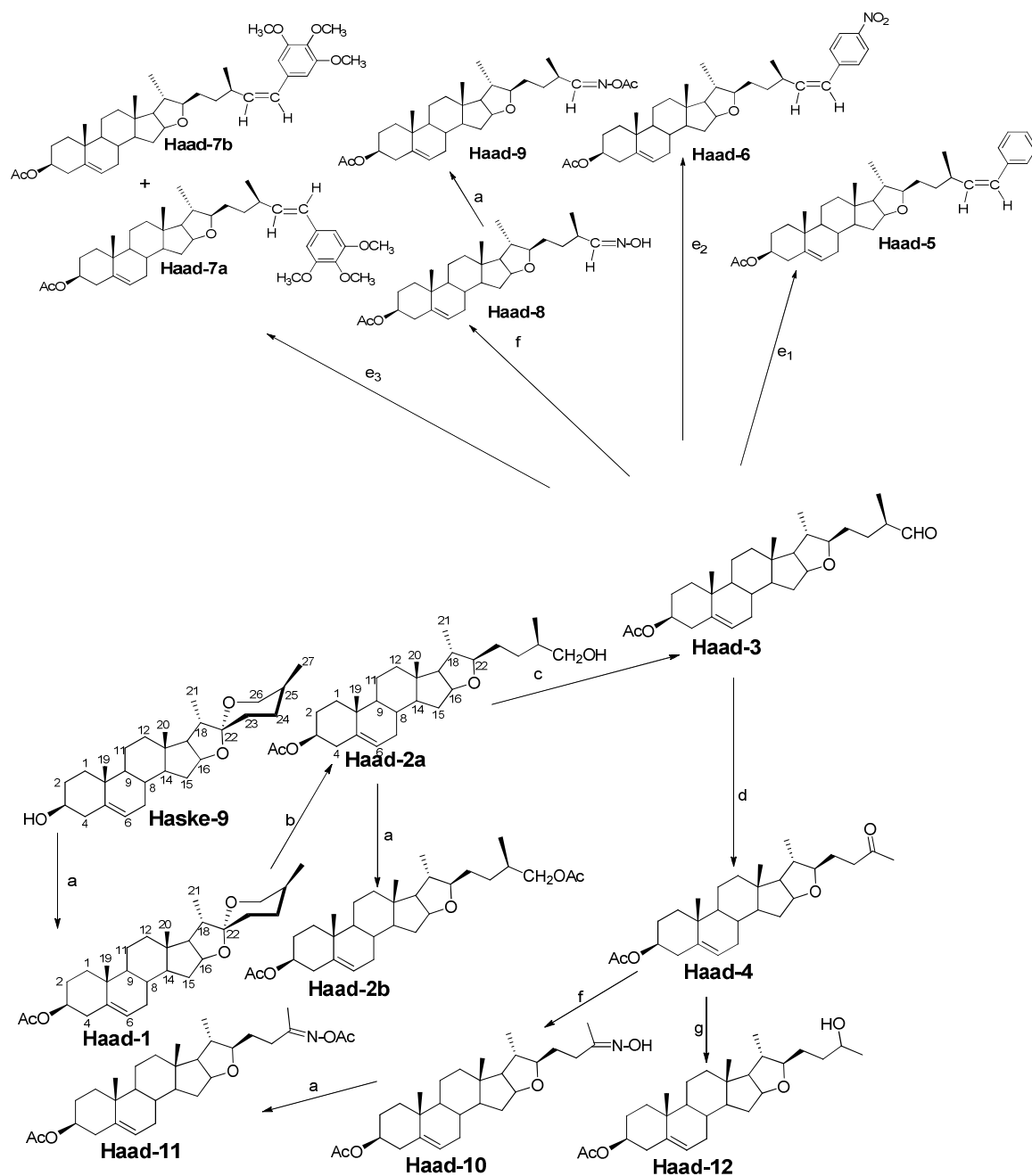
Diosgenin (Haske-9) is a C<sub>27</sub> spiroacetal steroidal sapogenin which has been isolated from *Smilax spp.* (Xu *et al.*, 2008), and other plant families (Gurib-Fakim, 2006). It was the most abundant and cytotoxic pure molecule isolated from the ethyl acetate extract of *S. kraussiana* aerial parts. Diosgenin was modified at spiroketal position, C<sub>22</sub> (Scheme 5) and at the 7<sup>th</sup> position (Scheme 6) to get new analogues.

#### 3.10.1. Synthesis of (22 $\beta$ ,25R)-spirost-5-en-3 $\beta$ -yl-3-acetate (Haad-1)

Diosgenin (Haske-9) (200 mg, 0.43 mmol) was acetylated when it was dissolved in the mixture of dry chloroform (5 mL), dry pyridine (1 mL) and acetic anhydride (0.5 mL), then stirred at room temperature for 6 hrs. The solvent was evaporated and the product mixture was cooled in ice bath. The residue was acidified with dil. HCl (5%, 10 mL), dissolved in ethyl acetate (30 mL) and washed with water. The organic layer was dried over anhydrous sodium sulphate and dried *in vacuo*. The crude solid was recrystallised with chloroform-hexane (1:3) to get Haad-1 as creamy white crystalline solid (Yield = 183 mg, 91%).

#### 3.10.2. Synthesis of (22 $\beta$ ,25R)-3 $\beta$ ,26-dihydroxyfurost-5-en-3 $\beta$ -acetate (Haad-2a)

Compound Haad-2a was synthesized when 200 mg of Haad-1 was dissolved in 5 mL glacial acetic acid with gradual addition of 200 mg sodium cyanoborohydride (NaCNBH<sub>3</sub>). The mixture was stirred at room temperature for 2 hrs. The product mixture was cooled in ice bath, dissolved in ethyl acetate (30 mL) and washed with water. The organic layer was dried over anhydrous sodium sulphate and dried *in vacuo*. The crude mass was then purified by column chromatography with ethyl acetate-hexane (1:12) to obtain cream crystalline solid (Yield = 164 mg, 81%).



- (a) Ac<sub>2</sub>O, dry pyridine, dry CHCl<sub>3</sub>, RT, 6 hrs. (b) AcOH, NaCNBH<sub>3</sub>, RT, 2 hrs.  
(c) Dry DCM, PCC, reflux, 1 h. (d) Ethanol, substituted aniline, RT, 3 hrs.  
(e<sub>1</sub>) Benzyltriphenylphosphonium bromide, NaH, dry toluene, RT, 4 hrs.  
(e<sub>2</sub>) 4-nitrobenzyltriphenylphosphonium bromide, NaH, dry toluene, RT, 4 hrs.  
(e<sub>3</sub>) 3,4,5-trimethoxybenzyltriphenylphosphonium bromide, NaH, dry toluene, RT, 3 hrs.  
(f) NH<sub>2</sub>OH.HCl, EtOH, reflux, 2 hrs.  
(g) Methanol, NaBH<sub>4</sub>, RT, 1 h.

**Scheme 5:** Modification of Diosgenin at spiroketal position, C<sub>22</sub>

### 3.10.3. Synthesis of (22 $\beta$ ,25R)-furost-5-en-3 $\beta$ ,26-diacetate (Haad-2b)

Compound Haad-2b was synthesized by acetylation of Haad-2a.

Haad-2a (200 mg, 0.44 mmol) was dissolved in the mixture of dry chloroform (5 mL), dry pyridine (1 mL) and acetic anhydride (0.5 mL), and then stirred at room temperature for 6 hrs. Solvent was evaporated and the product mixture was cooled in ice bath. The residue was acidified with dil. HCl (5%, 10 mL), dissolved in ethyl acetate (30 mL) and washed with water. The organic layer was dried over anhydrous sodium sulphate. The crude solid was recrystallised with chloroform-hexane (1:3) to get Haad-2b as creamy white crystalline solid (Yield = 100 mg, 35%).

### 3.10.4. Synthesis of (22 $\beta$ ,25R)-26-formyl-furost-5-en-3-yl-3 $\beta$ -acetate (Haad-3)

Alcohol Haad-2a (200 mg, 0.43 mmol) was dissolved in dry dichloromethane (10 mL) and stirred at room temperature. Pyridinium chlorochromate (PCC) (200 mg, 0.93 mmol) was added to the mixture and further stirred for an hour. Solvent was evaporated and residue was dissolved in ethyl acetate (30 mL). It was acidified with dil. HCl (5%, 10 mL) and washed with water. The organic layer was dried over anhydrous sodium sulphate and dried *in vacuo*. The crude product was recrystallised with chloroform-hexane (1:3) to get the aldehyde Haad-3 as brown crystalline solid (Yield = 182 mg, 91%).

### 3.10.5. Synthesis of (22 $\beta$ )-25-oxo-27-nor-furost-5-en-3-yl-3 $\beta$ -acetate (Haad-4)

Aldehyde Haad-3 (200 mg, 0.44 mmol) was taken in ethanol (10 mL) and stirred at ambient temperature (30 - 35°C). To this 3,4,5-trimethoxyaniline (200 mg, 1.09 mmol) was added and refluxed for 3 hrs. The solvent was evaporated, residue was dissolved in ethyl acetate (30 mL) and washed with water. The organic phase was dried over anhydrous sodium sulphate and dried *in vacuo*. The crude mass was purified through silica gel column eluting with ethyl acetate: hexane (1:10). The ketone Haad-4 was obtained at 8-10% ethyl acetate-hexane as creamy white solid (Yield = 163 mg, 84%).

### **3.10.6. Wittig reaction on (22 $\beta$ ,25R)-26-formyl-furost-5-en-3-yl-3 $\beta$ -acetate (Haad-3)**

#### **3.10.6.1 Synthesis of (22 $\beta$ )-(E)-26-Benzylidene-3 $\beta$ -yl-furost-5-en-3-acetate (Haad-5)**

Benzyltriphenylphosphonium bromide (Wittig salt, 200 mg) was taken in dry toluene (10 mL). To this stirred solution, pre-washed sodium hydride (200 mg, 8.33 mmol) was added and stirred for 20 min. Haad-3 (100 mg, 0.22 mmol) was added and the reaction mixture was further refluxed for 4 hrs. Toluene was evaporated under vacuum and residue was taken in ethyl acetate (20 mL x 3), washed with water and dried over anhydrous sodium sulphate. The organic layer was dried *in vacuo* to get a crude mass, which was purified through silica gel column eluting with ethyl acetate-hexane. The desired product was obtained as yellowish viscous liquid (Yield = 158 mg, 68%).

#### **3.10.6.2. Synthesis of (22 $\beta$ )-(Z)-26-(4'-Nitrobenzylidene)-3 $\beta$ -yl-furost-5-en-3-acetate (Haad-6)**

The procedure is same as for Haad-5. The Wittig salt used was 4-nitrobenzyltriphenylphosphonium bromide (200mg) (Yield = 157 mg, 62%).

#### **3.10.6.3. Synthesis of (22 $\beta$ )-(E)-26-(3',4',5'-Trimethoxybenzylidene)-3 $\beta$ -yl-furost-5-en-3-acetate (Haad-7a) and (22 $\beta$ )-(Z)-26-(3',4',5'-Trimethoxybenzylidene)-3 $\beta$ -yl-furost-5-en-3-acetate (Haad-7b).**

The procedure is same as for Haad-6. The Wittig salt used was 3,4,5-trimethoxybenzyltriphenylphosphonium bromide (200 mg) to get Haad-7a (Yield = 142 mg, 52%) and Haad-7b (Yield = 79 mg, 29%).

### **3.10.7. Synthesis of (22 $\beta$ )-3 $\beta$ -Acetoxy-furost-5-en-26-aldoxime (Haad-8)**

Haad-3 (100 mg, 0.22 mmol) was taken in ethanol (10 mL). To this dry pyridine (0.5 mL) and hydroxyaminehydrochloride (100 mg, 1.43 mmol) was added and refluxed for 2hrs. On completion ethanol was evaporated and dil HCl (10 mL) was added to it, extracted with ethyl acetate (20 mL x 3), washed with water and the organic layer was dried with anhydrous sodium sulphate. The residue thus obtained was purified through silica gel column using hexane-ethyl acetate as eluants. The desired aldoxime Haad-8 was obtained as creamy white solid (Yield = 73 mg, 70%).

### 3.10.8. Synthesis of (22 $\beta$ )-3 $\beta$ -Acetoxy-furost-5-en-26-aldoxime acetate (Haad-9)

Compound Haad-9 was also synthesized by acetylation of Haad-8. Compound Haad-8 (200 mg, 0.43 mmol) was dissolved in acetic anhydride (0.5 mL), in the presence of dry pyridine (1 mL) and chloroform (5 mL), and then stirred at room temperature for 5 hrs in dry condition. Solvent was evaporated and the product mixture was cooled in ice bath. The residue was acidified with dil. HCl (5%, 10 mL), dissolved in ethyl acetate (30 mL) and washed with water. The organic layer was dried over anhydrous sodium sulphate and dried *in vacuo*. The crude mass was recrystallised with chloroform-hexane (1:3) to get Haad-9 as creamy white crystalline solid (Yield = 1.0g, 92%).

### 3.10.9. Synthesis of (22 $\beta$ )-3 $\beta$ -Acetoxy-27-nor-furost-5-en-25-ketoxime (Haad-10).

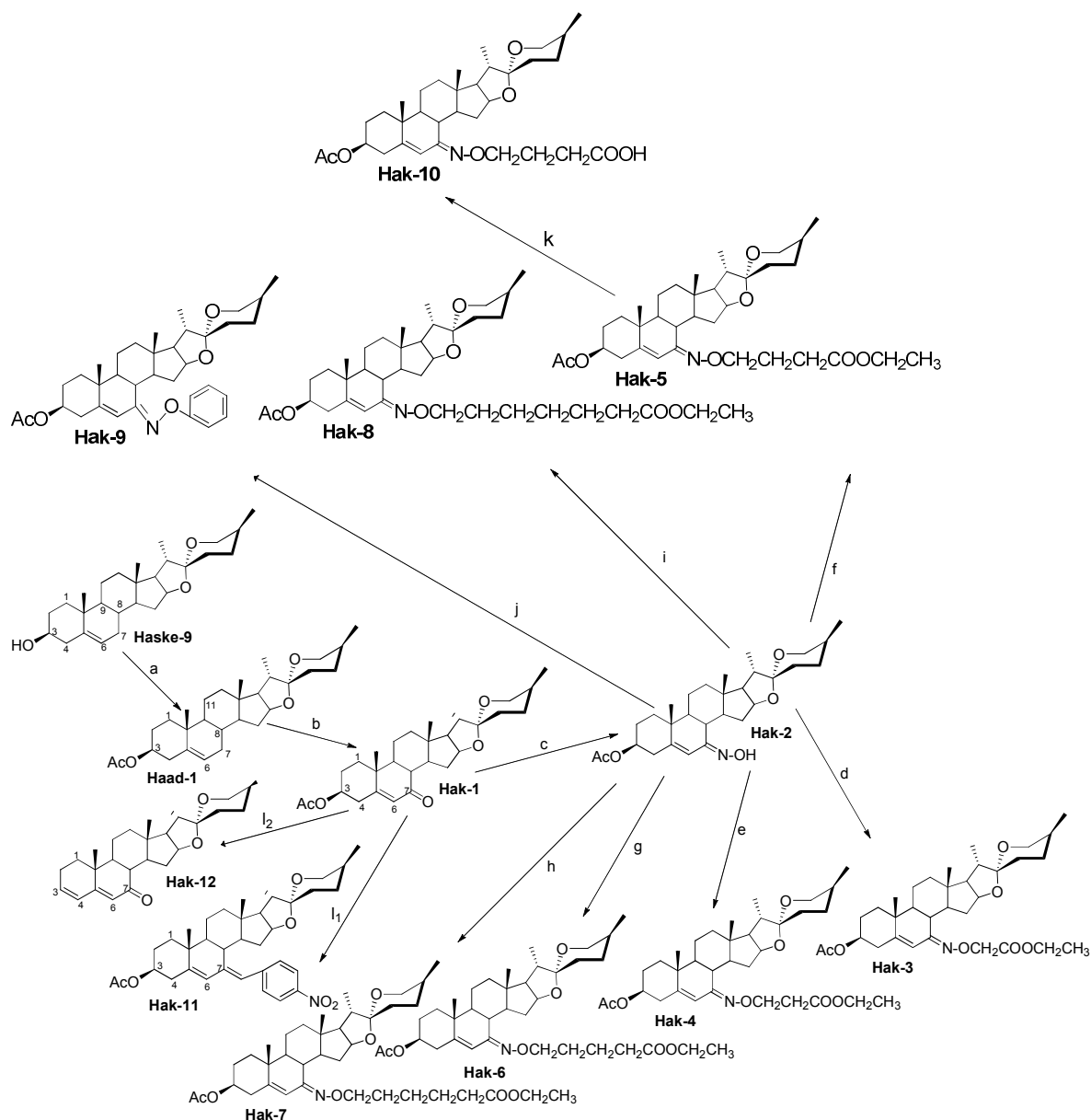
The ketoxime Haad-10 was prepared from Haad-4 using the same method as for aldoxime, Haad-8 (Yield = 87 mg, 84%).

### 3.10.10. Synthesis of (22 $\beta$ )-3 $\beta$ -Hydroxy-27-nor-furost-5-en-25-ketoxime-3 $\beta$ ,26-diacetate (Haad-11).

Compound Haad-11 was also synthesized by acetylation of Haad-10. 200 mg, 0.44 mmol of Haad-10 was dissolved in the mixture of dry chloroform (5 mL), dry pyridine (1 mL) and acetic anhydride (0.5 mL), and then stirred at room temperature for 5 hrs in dry condition. Solvent was evaporated and the product mixture was cooled in ice bath. The residue was acidified with dil. HCl (5%, 10 mL), dissolved in ethyl acetate (30 mL) and washed with water. The organic layer was dried over anhydrous sodium sulphate and dried *in vacuo*. The crude mass was recrystallised with chloroform-hexane (1:3) to get Haad-11 as creamy white solid (Yield = 57 mg, 52%).

### 3.10.11. Synthesis of (22 $\beta$ )-25 $\alpha$ -Hydroxy-3 $\beta$ -yl-27-nor-furost-5-en-3-acetate and (22 $\beta$ )-25 $\beta$ -Hydroxy-3 $\beta$ -yl-27-nor-furost-5-en-3-acetate (Haad-12)

Ketone Haad-4 (100 mg, 0.23 mmol) was stirred in methanol (5 mL). To this stirred solution sodium borohydride (30 mg, 0.79 mmol) was added and reaction mixture was further stirred for 1 hr. On completion, solvent was evaporated *in vacuo* and residue was taken in ethyl acetate (2 x 20 mL). It was acidified with dil. HCl (5%, 5 mL), washed with water (2 x 10 mL) and organic layer was dried over anhydrous sodium sulphate. The solvent was evaporated *in vacuo* and residue thus obtained was recrystallised with chloroform-hexane (1:4) to get Haad-12 as mixture of both 25 $\alpha$ / $\beta$ -hydroxy isomers (Yield = 86 mg, 86%).



- (a)  $\text{Ac}_2\text{O}$ , dry pyridine, dry  $\text{CHCl}_3$ , RT, 6 hrs; (b)  $\text{CrO}_3$ , dry pyridine, DCM, RT, 10 hrs  
(c)  $\text{NH}_2\text{OH}\cdot\text{HCl}$ , EtOH, reflux, 2 hrs; (d)  $\text{K}_2\text{CO}_3$ , acetone, ethyliodoacetate, reflux, 2 hrs  
(e)  $\text{K}_2\text{CO}_3$ , acetone, ethyl-3-bromopropanoate, reflux, 2 hrs;  
(f)  $\text{K}_2\text{CO}_3$ , acetone, ethyl-4-bromobutyrate, reflux, 3 hrs  
(g)  $\text{K}_2\text{CO}_3$ , acetone, ethyl-5-bromopentanoate, reflux, 3 hrs  
(h)  $\text{K}_2\text{CO}_3$ , acetone, ethyl-6-bromohexanoate, reflux, 4 hrs  
(i)  $\text{K}_2\text{CO}_3$ , acetone, ethyl-7-bromoheptanoate, reflux, 4 hrs  
(j)  $\text{K}_2\text{CO}_3$ , acetone, benzylbromide, reflux, 2 hrs; (k)  $\text{KOH}$ , 90% MeOH, RT, 1 h  
(l<sub>1</sub>) 4-nitrobenzyltriphenylphosphonium bromide, NaH, dry toluene, reflux, 4 hrs.  
(l<sub>2</sub>) 3,4-methylenedioxybenzyltriphenylphosphonium bromide, NaH, dry toluene, reflux, 4 hrs.

**Scheme 6:** Modification of Diosgenin at position 7

### 3.10.12. Synthesis of (22 $\beta$ ,25R)-7-oxo-spirost-5-en-3 $\beta$ -yl-3-acetate (Hak-1)

The addition of dry pyridine (4 mL) and dichloromethane (20 mL) was cooled in ice bath for 20 mins and chromium (VI) oxide (200 mg) was added and stirred in ice bath for 10 mins. Haad-1 (200 mg, 0.43 mmol) was taken in dichloromethane (5 mL) and added to the reaction mixture, then refluxed for 10 hrs. On completion dichloromethane was evaporated and dil. HCl (10 mL) was added to it, extracted with ethyl acetate (20 mL x 3), washed with water and dried over anhydrous sodium sulphate. The residue thus obtained was purified through silica gel column using hexane-ethyl acetate as eluants. The desired 7-keto analogue Hak-1 was obtained as white solid (Yield = 106 mg, 53%).

### 3.10.13. Synthesis of (22 $\beta$ ,25R)-3 $\beta$ -Acetoxy-spirost-5-en-3 $\beta$ -yl-7-ketoxime (Hak-2)

Ketone Hak-1 (100 mg, 0.24 mmol) was taken in ethanol (10 mL). To this dry pyridine (0.5 mL) and hydroxyaminehydrochloride (100 mg, 1.43 mmol) was added and refluxed for 2 hrs. On completion ethanol was evaporated and dil HCl (10 mL) was added to it, extracted with ethyl acetate (20 mL x 3), washed with water and dry *in vacuo*. The residue thus obtained was purified through silica gel column using hexane-ethyl acetate as eluants. The desired 7-ketoxime Hak-2 was obtained as light yellow oil (Yield = 90 mg, 90%).

### 3.10.14. Synthesis of (22 $\beta$ ,25R)-3 $\beta$ -Acetoxy-spirost-5-en-3 $\beta$ -yl-7-(ethyl-2'-acetate)-ketoxime (Hak-3)

The addition of potassium carbonate (1 g) to acetone (10 mL) was stirred for 20 mins, then ethyl iodoacetate (0.5 mL) was added and stirred for 10 mins. Hak-2 (100 mg, 0.22 mmol) was taken in acetone (1 mL) and added to the reaction mixture, then refluxed at 80 – 100°C for 2 hrs. On completion acetone was evaporated and the product was extracted with ethyl acetate (20 mL x 3), washed with water and dry *in vacuo*. The residue thus obtained was purified through silica gel column using hexane-ethyl acetate as eluants. The desired 7-oxime analogue Hak-3 was obtained as white crystals (Yield = 82 mg, 82%).



**3.10.15. Synthesis of (22 $\beta$ ,25R)-3 $\beta$ -Acetoxy-spirost-5-en-3 $\beta$ -yl-7-(ethyl-3'-propanoate)-ketoxime (Hak-4)**

The same procedure as for Hak-3. The reagent used is ethyl-3-bromopropanoate and the desired 7-oxime analogue Hak-4 was obtained as white crystals (Yield = 90 mg, 90%).

**3.10.16. Synthesis of (22 $\beta$ ,25R)-3 $\beta$ -Acetoxy-spirost-5-en-3 $\beta$ -yl-7-(ethyl-4'-butyrate)-ketoxime (Hak-5)**

The same procedure as for Hak-4. The reagent used is ethyl-4-bromobutyrate and the desired 7-oxime analogue Hak-5 was obtained as creamy white crystals (Yield = 82 mg, 82%).

**3.10.17. Synthesis of (22 $\beta$ ,25R)-3 $\beta$ -Acetoxy-spirost-5-en-3 $\beta$ -yl-7-(ethyl-5'-pentanoate)-ketoxime (Hak-6)**

The same procedure as for Hak-4. The reagent used is ethyl-5-bromopentanoate and the desired 7-oxime analogue Hak-6 was obtained as white crystals (Yield = 92 mg, 92%).

**3.10.18. Synthesis of (22 $\beta$ ,25R)-3 $\beta$ -Acetoxy-spirost-5-en-3 $\beta$ -yl-7-(ethyl-6'-hexanoate)-ketoxime (Hak-7)**

The same procedure as for Hak-6. The reagent used is ethyl-6-bromohexanoate and the desired 7-oxime analogue Hak-7 was obtained as creamy white crystals (Yield = 90 mg, 90%).

**3.10.19. Synthesis of (22 $\beta$ ,25R)-3 $\beta$ -Acetoxy-spirost-5-en-3 $\beta$ -yl-7-(ethyl-7'-heptanoate)-ketoxime Hak-8**

The same procedure as for Hak-5. The reagent used is ethyl-7-bromoheptanoate and the desired 7-oxime analogue Hak-8 was obtained as creamy white crystals (Yield = 51 mg, 51%).

**3.10.20. Synthesis of (22 $\beta$ ,25R)-3 $\beta$ -Acetoxy-spirost-5-en-3 $\beta$ -yl-7-benzyketoxime (Hak-9)**

The same procedure as for Hak-6. The reagent used is Benzylbromide and the desired 7-oxime analogue Hak-9 was obtained as brownish yellow solid (Yield = 95 mg, 95%).

### **3.10.21. Synthesis of (22 $\beta$ ,25R)-3 $\beta$ -Acetoxy-spirost-5-en-3 $\beta$ -yl-7-(4'-butanoic)-ketoxime (Hak-10)**

The addition of potassium hydroxide/sodium hydroxide (150 mg) to 90%MeOH (10 mL) was stirred for 20 mins. Hak-5 (100 mg, 0.21 mmol) was added to the reaction mixture, and stirred for 1 h at RT. On completion methanol was evaporated and the product was extracted with ethyl acetate (20 mL x 3), washed with water and dried *in vacuo*. The residue thus obtained was purified through silica gel column using hexane-ethyl acetate as eluants. The desired analogue Hak-10 was obtained as brownish yellow solid (Yield = 95 mg, 95%).

### **3.10.22. Synthesis of (22 $\beta$ ,25R)-3 $\beta$ -Acetoxy-7-(4'-nitrobenzylidene)-spirost-5-en-3 $\beta$ -yl (Hak-11)**

Procedure same as for Haad-6. 4-nitrobenzyltriphenylphosphonium bromide (Wittig salt, 200mg) was taken in dry toluene (10 mL). To this stirred solution, pre-washed sodium hydride (200 mg, 8.33 mmol) was added and stirred for 20 min. Hak-1 (100 mg, 0.22 mmol) was added and the reaction mixture was refluxed for 4 hrs. Toluene was evaporated under vacuum and residue was taken in ethyl acetate (20 mLx3), washed with water and dried over anhydrous sodium sulphate. The organic layer was dried *in vacuo* to get a crude mass, which was purified through silica gel column eluting with ethyl acetate-hexane. The desired 7-wittig analogue Hak-16 was obtained as orange solid (Yield = 65 mg, 65%).

### **3.10.23. Synthesis of (22 $\beta$ ,25R)-7-oxo-spirost-3,5-diene (Hak-12)**

3,4-methylenedioxybenzyltriphenylphosphine (Wittig salt, 200 mg) was taken in dry toluene (10 mL). To this stirred solution pre-washed sodium hydride (200 mg, 8.33 mmol) was added and stirred for 20 mins. 7-Keto Hak-1 (100 mg, 0.22 mmol) was added and the reaction mixture was further stirred for 4 hrs at 110-120°C. Toluene was evaporated under vacuum and residue was taken in ethyl acetate (20 mL x 3), washed with water and dried over anhydrous sodium sulphate. The organic layer was dried *in vacuo* to get a crude mass, which was purified through silica gel column eluting with ethyl acetate-hexane. The product Hak-12 was obtained as orange solid. Different wittig salts Benzyltriphenylphosphonium pentanoate; Benzyltriphenylphosphine and 3,4,5-trimethoxybenzyltriphenylphosphine) were also used with the same procedure, and the same desired product Hak-12 was yielded (Yield = 90 mg, 90%).

## CHAPTER FOUR

### RESULTS AND DISCUSSION

#### 4.1 Extraction procedure

*Smilax kraussiana* (aerial parts) was successively extracted with hexane, ethyl acetate and methanol by maceration. The extracts were filtered with whatmann No. 1 filter paper, separately concentrated on rotatory evaporator at 37° C and freeze dried. The yields of sequential extraction of the aerial parts of *Smilax kraussiana* (Scheme 4) are presented in Table 4.1.

#### 4.2 Antiproliferative assay

Various parts of *S. kraussiana* are traditionally used for the treatment of different diseases, especially fever, venereal diseases, fever, infertility, rheumatism and tumors without any scientific justification for this practice. Thus, the efficacy or otherwise and the toxicity profile of this plant are yet to be established. 3-(4,5-Dimethylthiazol-2-yl)-2,5-Diphenyltetrazolium Bromide (MTT) and Sulphorhodamine (SBR) assays were employed for cytotoxicity.

The cell viability was expressed as a percentage to the viable cells of control culture condition. Table 4.2 shows percentage inhibition of human cancer cell lines (leukaemia carcinoma (K562), breast carcinoma (MCF-7), hepatic liver (WRL) cell lines and colon carcinoma (COLO)) by the extracts at 50 and 100 µM concentrations. The ethyl acetate extract of *S. kraussiana* aerial parts coded SKE exhibited antiproliferative activities against WRL (IC<sub>50</sub> = 46.1 µM) and K562 (IC<sub>50</sub> = 113 µM), while methanol extract of the plant SKM, showed anticancer activities against WRL, COLO and K562 with IC<sub>50</sub> of 193.0, 90.0 and 201.0 µM respectively. Further, hexane extract of aerial parts of *S. kraussiana* coded SKH inhibited the growth of WRL, MCF-7 and COLO with IC<sub>50</sub> values of 130, 310 and 155 µM respectively.

**Table 4.1:** The yields of extracts obtained from successive extraction of *S. kraussiana* aerial parts

Plant sample	Sample weight (g)	n-Hexane extract (g)	% Yield	Ethyl acetate extract (g)	% Yield	Methanol extract (g)	% Yield
SKap	1200.0	14.0	1.17	20.0	1.67	11.5	0.98

Key: SKap = *S. kraussiana* aerial parts

**Table 4.2:** *In-vitro* cytotoxicities of extracts obtained from successive extraction of *S. kraussiana* aerial parts

S/No.	Extract code	Cell lines/IC <sub>50</sub> (ug/mL)			
		K562	WRL	MCF-7	COLO
1.	SKH	***	130	310	155
2.	SKE	113	46.1	***	160
3.	SKM	201	193	236	90

\*\*\* IC<sub>50</sub> (ug/mL) >500

K562 - leukaemia carcinoma

WRL - hepatic liver cell lines

MCF-7 – breast carcinoma

COLO – colorectal carcinoma

SKH- Hexane extract of *S. kraussiana* aerial parts

SKE- Ethyl acetate extract of *S. kraussiana* aerial parts

SKM- Methanol extract of *S. kraussiana* aerial parts

### **4.3 Phytochemical screening**

The crude extracts from *S. kraussiana* (aerial parts) were separately screened for secondary metabolites using various standard methods (Trease and Evans, 1989; Harborne, 1998; Edeoga *et al.*, 2005). The results of the phytochemical screening indicated the presence of flavonoids, steroids, glycosides and anthraquinones in all the extracts except in methanol extract of *S. kraussiana* aerial parts which showed the absence of flavonoids and steroids. Saponins and reducing sugars were found only in ethyl acetate and methanol extracts of *S. kraussiana* aerial parts while alkaloids and tannins were not detected in all the extracts. The detailed results of the phytochemical screening are presented in Table 4.3.

**Table 4.3:** Results of the Phytochemical screening of the extracts from successive extraction of *S. kraussiana* aerial parts.

Secondary metabolites	SKH	SKE	SKM
Reducing sugars	-	+	+
Alkaloids	-	-	-
Tannins	-	-	-
Saponins	-	+	+
Flavonoids	+	+	-
Steroids	+	+	-
Glycosides	+	+	+
Anthraquinones	+	+	+

+ indicates presence and – indicates absence

Key: SKH: Hexane extract of *S. kraussiana* aerial parts

SKE: Ethyl acetate extract of *S. kraussiana* aerial parts

SKM: Methanol extract of *S. kraussiana* aerial parts

#### 4.4 Column chromatography of hexane extract of *S. kraussiana* (aerial parts)

The chromatographic separation of hexane extract of *S. kraussiana* aerial parts SKH, (11.0 g) gave four compounds as described in section 3.6. The compounds are coded Haskh-1 (35.0 mg), Haskh-2 (25 mg), Haskh-3 (21 mg) and Haskh-4 (15 mg).

##### 4.4.1 Characterisation of Haskh-1

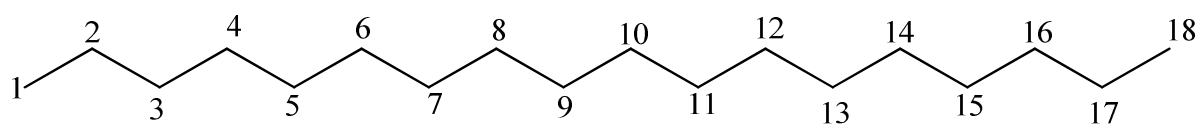
Compound Haskh-1 was obtained as white crystals (35.0 mg) with a melting point of 27 - 29°C. The ESI-MS fragment ions at  $m/z$  253.3  $[M-H]^+$ , 277.3  $[M+Na]^+$ , 509.4  $[2M+H]^+$  gave molecular formula  $C_{18}H_{38}$  (254.3). The IR  $\bar{\nu}$  ( $cm^{-1}$ ) spectrum showed absorption bands for C-H stretching and bending vibrations at 2923 and 1017  $cm^{-1}$  respectively. The  $^1H$  NMR spectrum of Haskh-1 showed peaks at  $\delta_H$  0.89 (6H, t,  $H_{1}$  &  $H_{18}$ ) correspond to terminal methyl protons [Table 4.41], while the multiplet peaks at  $\delta_H$  1.10 – 1.26 were assigned to cluster of methylene protons at 2-17 positions. The  $^{13}C$  NMR spectrum displayed eighteen carbon resonances and were sorted by DEPT experiment as sixteen methylene carbons and two methyl carbons [ $\delta_C$  14.49 ( $C_{-1}$ ) and 14.49 ( $C_{-187}$ )]. Based on the spectroscopic data of Haskh-1, its structure was elucidated to be octadecane (**100**).



**Table 4.41:**  $^{13}\text{C}$  and  $^1\text{H}$  NMR ( $\text{CDCl}_3$ ) spectral data of Haskh-1

Assignment	$^{13}\text{C}$	Multiplicity	$^1\text{H}$
1.	14.49	$\text{CH}_2$	0.89, t, 3H
2.	23.10	$\text{CH}_2$	1.10-1.26, m, 2H
3.	23.10	$\text{CH}_2$	1.10-1.26, m, 2H
4.	23.10	$\text{CH}_2$	1.10-1.26, m, 2H
5.	29.37	$\text{CH}_2$	1.10-1.26, m, 2H
6.	29.37	$\text{CH}_2$	1.10-1.26, m, 2H
7.	29.58	$\text{CH}_2$	1.10-1.26, m, 2H
8.	29.58	$\text{CH}_2$	1.10-1.26, m, 2H
9.	29.78	$\text{CH}_2$	1.10-1.26, m, 2H
10.	29.78	$\text{CH}_2$	1.10-1.26, m, 2H
11.	30.12	$\text{CH}_2$	1.10-1.26, m, 2H
12.	30.12	$\text{CH}_3$	1.10-1.26, m, 2H
13.	30.12	$\text{CH}_2$	1.10-1.26, m, 2H
14.	30.12	$\text{CH}_2$	1.10-1.26, m, 2H
15.	30.47	$\text{CH}_2$	1.10-1.26, m, 2H
16.	32.35	$\text{CH}_2$	1.10-1.26, m, 2H
17.	32.35	$\text{CH}_2$	1.10-1.26, m, 2H
18.	14.49	$\text{CH}_3$	0.89, t, 3H

Implied multiplicities of the carbons were determined from the DEPT experiment.



Octadecane (100)

#### 4.4.2 Characterisation of Haskh-2

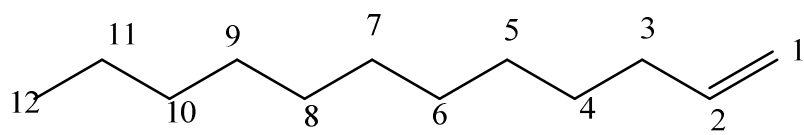
Compound Haskh-2 is a light yellow oily liquid (25.0 mg). The ESI-MS fragment ion at  $m/z$  437.2  $[2M+2K+Na]^+$  calculated for a molecular formula  $C_{12}H_{24}$  ( $M = 168.23$ ). The IR  $\bar{\nu}$  ( $cm^{-1}$ ) absorption bands for C-H  $sp^2$ , C-H  $sp^3$  and C=C stretching vibrations were seen at 3045, 2940 and  $1468\text{ cm}^{-1}$  respectively. The  $^1H$  NMR spectrum of Haskh-2 showed signals at  $\delta_H$  0.88 (3H, t,  $H_{12}$ ) corresponding to terminal methyl protons [Table 4.42], while the multiplet peaks at  $\delta_H$  1.26 – 1.47 were attributed to cluster of methylene protons at 5-11 positions. Olefinic protons were shown by the presence of  $\delta_H$  4.96 (2H, d,  $H_{11}$ ) and 5.02 (1H, m,  $H_{10}$ ). The  $^{13}C$  NMR spectrum indicated twelve carbon resonances and were sorted by DEPT experiment as two olefinic carbons [ $\delta_c$  114.46 ( $C_{11}$ ) and 130.05 ( $C_{10}$ )], nine methylene carbons and one methyl carbon [ $\delta_c$  14.50 ( $C_{12}$ )]. Haskh-2 was resolved to be Dodec-1-ene (**101**) based on the available spectral data.

**Table 4.42:**  $^{13}\text{C}$  and  $^1\text{H}$  NMR ( $\text{CDCl}_3$ ) spectra data of Haskh-2

Assignment	$^{13}\text{C}$	Multiplicity	$^1\text{H}$
1.	114.46	$\text{CH}_2$	4.96, d, 2H
2.	130.05	CH	5.02, m, 1H
3.	34.22	$\text{CH}_2$	2.05, m, 2H
4.	23.08	$\text{CH}_2$	1.58, m, 2H
5.	29.36	$\text{CH}_2$	1.26-1.47,m,2H
6.	29.56	$\text{CH}_2$	1.26-1.47,m,2H
7.	29.75	$\text{CH}_2$	1.26-1.47,m,2H
8.	29.91	$\text{CH}_2$	1.26-1.47,m,2H
9.	30.09	$\text{CH}_2$	1.26-1.47,m,2H
10.	30.09	$\text{CH}_2$	1.26-1.47,m,2H
11.	32.32	$\text{CH}_2$	1.26-1.47,m,2H
12.	14.50	$\text{CH}_3$	0.88, t, 3H

---

Implied multiplicities of the carbons were determined from the DEPT experiment.



Dodec-1-ene (**101**)

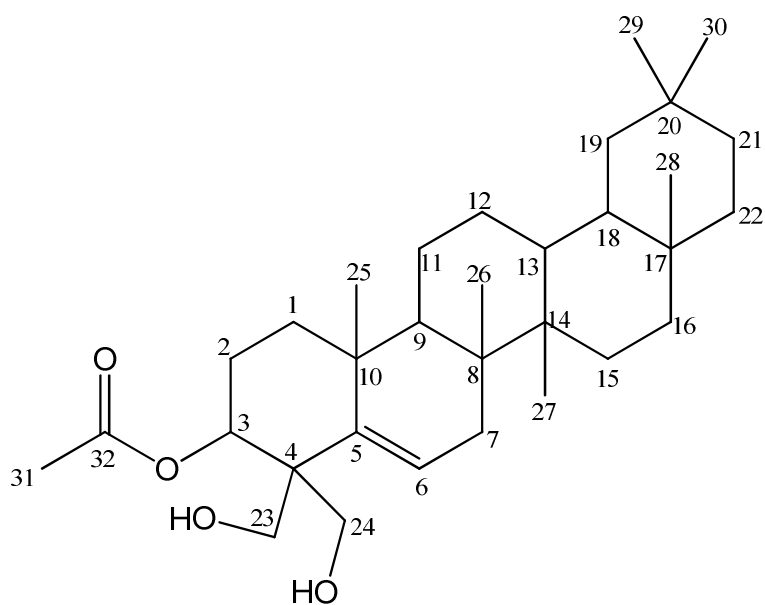
#### 4.4.3 Characterisation of Haskh-3

Compound Haskh-3 (21.0 mg) is a creamy yellow solid, (melting point 185 - 186°C). The ESI MS fragment ions 501.5 [M+H]<sup>+</sup>, 579.6 [M+2K+H]<sup>+</sup> correspond to a molecular formula C<sub>32</sub>H<sub>52</sub>O<sub>4</sub> (M = 500.3) [Fig. 4.0]. The IR  $\bar{\nu}$  (cm<sup>-1</sup>) absorptions at 3467, 2940, 1710 and 1468 cm<sup>-1</sup> revealed the presence of O-H, C-H, C=O and C=C functional groups respectively. The <sup>1</sup>H NMR spectrum signals at  $\delta_H$  0.86-0.93 (6H, m, 2 x CH<sub>3</sub>), 0.95-1.42 (27H, m, 3 x CH<sub>3</sub> & 9 x CH<sub>2</sub>) and 1.43-1.67 (3H, m, 3 x CH) are characteristics of methyl, methylene and methine protons of triterpenoids. The signals at  $\delta_H$  3.66 and 4.10 correspond to oxymethine proton at C-3 and oxymethylene protons at C-23 respectively [Fig. 4.1], while oxymethylene protons and olefinic methine proton at positions 24 and 6 were confirmed by the presence of  $\delta_H$  4.60 (s) and 5.35 (d) respectively. The <sup>13</sup>C NMR spectrum also indicates resonances consistent with polyhydroxy oleanane skeleton [Fig. 4.2 and 4.3]. The identified carbon skeleton were sorted by DEPT experiment [Fig. 4.4 and 4.5] into seven methyl carbons, ten methylene carbons, four methine carbons, one oxymethine and two oxymethylene carbons, and eight quaternary carbon resonances. In <sup>1</sup>H-<sup>1</sup>H COSY spectrum [Fig. 4.6], the correlation of oxymethylene protons at C-24 to methine proton at C-6 was observed, while methylene protons at C-1 was correlated with methylene protons at C-2. The <sup>1</sup>H-<sup>13</sup>C HMBC spectrum [Fig. 4.9 and 4.10] showed a long range correlation of methylene protons at C-2 with C-1, C-4 and C-32, while methyl protons at C-31 were also correlated with C-32. Further, methylene protons at C-23 revealed correlation with C-4, and oxymethylene protons at C-24 showed correlation with olefinic carbon C-5, C-6 and C-32, which confirm the presence of olefinic carbons at C-5 and C-6. The spectroscopic data of Haskh-3 [Table 4.43] was identical to oleana-5-en-ol derivatives (Toyota *et al.*, 1990) except the position of hydroxyl moieties at C-23 and C-24 which was confirmed by <sup>1</sup>H-<sup>1</sup>H COSY and <sup>1</sup>H-<sup>13</sup>C HMBC experiments. Therefore, Haskh-3 was elucidated as 23,24-dihydroxyoleana-5-en-3-acetate (**102**).

**Table 4.43:**  $^{13}\text{C}$  and  $^1\text{H}$  NMR ( $\text{CDCl}_3$ ) spectra data of Haskh-3

Assignment	$^{13}\text{C}$	Multiplicity	$^1\text{H}$ , multiplicity
1	23.08	$\text{CH}_2$	0.95-1.67, m, 2H
2	34.51	$\text{CH}_2$	0.95-1.67, m, 2H
3	51.79	CH	3.66, s, 3H
4	40.13	Q	-
5	142.94	Q	-
6	118.61	CH	5.35, d, 1H
7	32.32	$\text{CH}_2$	2.29, d, 2H
8	40.25	Q	-
9	39.70	CH	0.95-1.67, m, 1H
10	37.83	Q	-
11	25.43	$\text{CH}_2$	0.95-1.67, m, 2H
12	29.56	$\text{CH}_2$	0.95-1.67, m, 2H
13	33.19	CH	0.95-1.67, m, 1H
14	39.78	Q	-
15	26.34	$\text{CH}_2$	0.95-1.67, m, 2H
16	27.61	$\text{CH}_2$	0.95-1.67, m, 2H
17	37.03	Q	-
18	33.03	CH	0.95-1.67, m, 1H
19	30.10	$\text{CH}_2$	0.95-1.67, m, 2H
20	37.76	Q	-
21	34.80	$\text{CH}_2$	0.95-1.67, m, 2H
22	29.75	$\text{CH}_2$	0.95-1.67, m, 2H
23	61.58	$\text{CH}_2$	4.60, s, 2H
24	64.79	$\text{CH}_2$	4.10, s, 2H
25	24.87	$\text{CH}_3$	0.95-1.67, m, 3H
26	20.13	$\text{CH}_3$	0.95-1.67, m, 3H
27	23.01	$\text{CH}_3$	0.95-1.67, m, 3H
28	25.20	$\text{CH}_3$	0.65, d, 3H
29	14.50	$\text{CH}_3$	0.86-0.93, m, 3H
30	16.65	$\text{CH}_3$	0.86-0.93, m, 3H
31	37.70	$\text{CH}_3$	2.03, d, 1H
32	174.30	Q	-

Implied multiplicities of the carbons were determined from the DEPT experiment.



23,24-dihydroxyoleana-5-en-3-acetate (**102**)



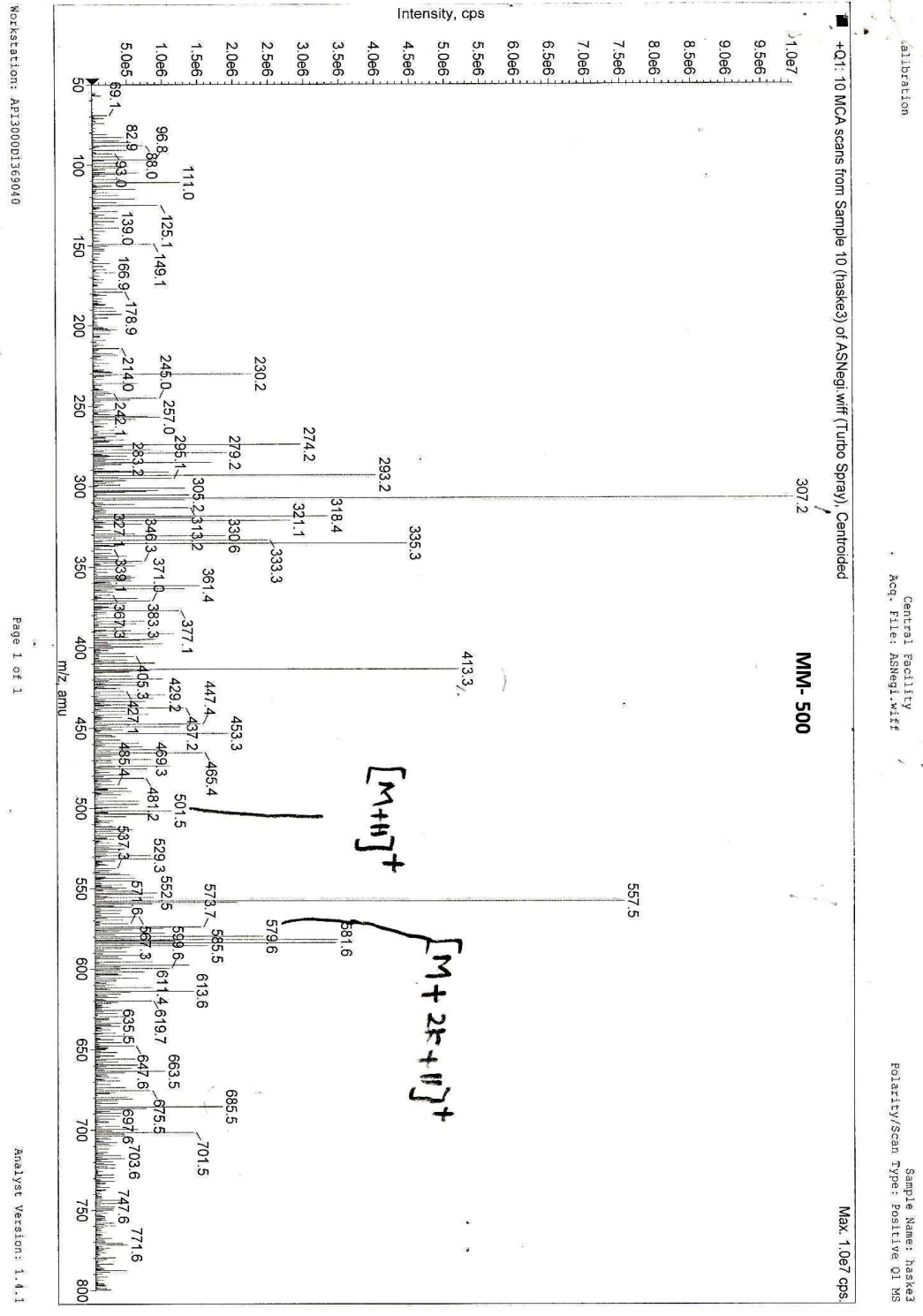


Fig. 4.0 ESI-MS spectrum of Haskh-3 in MeOH

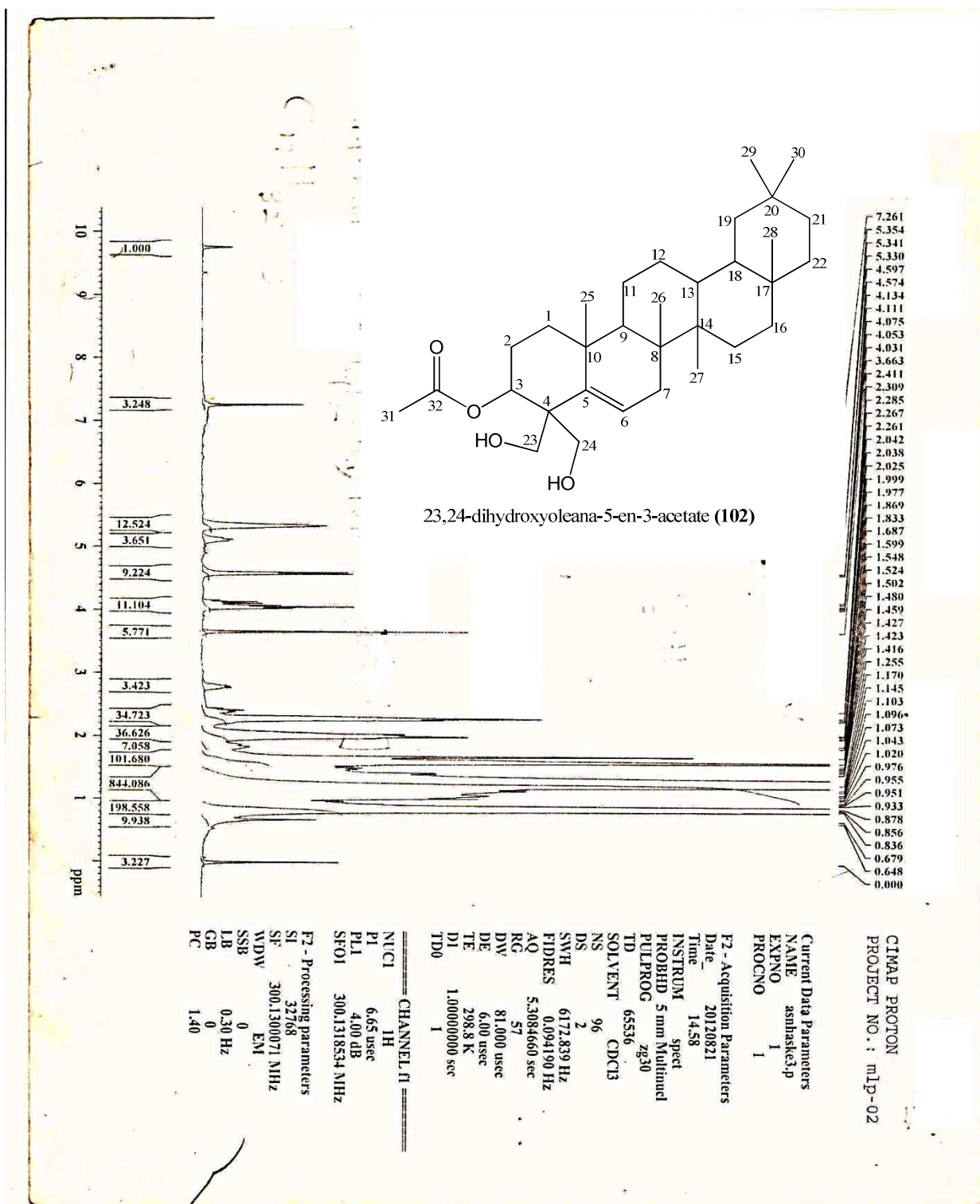


Fig. 4.1  $^1\text{H}$  NMR spectrum of Haskh-3 in  $\text{CDCl}_3$

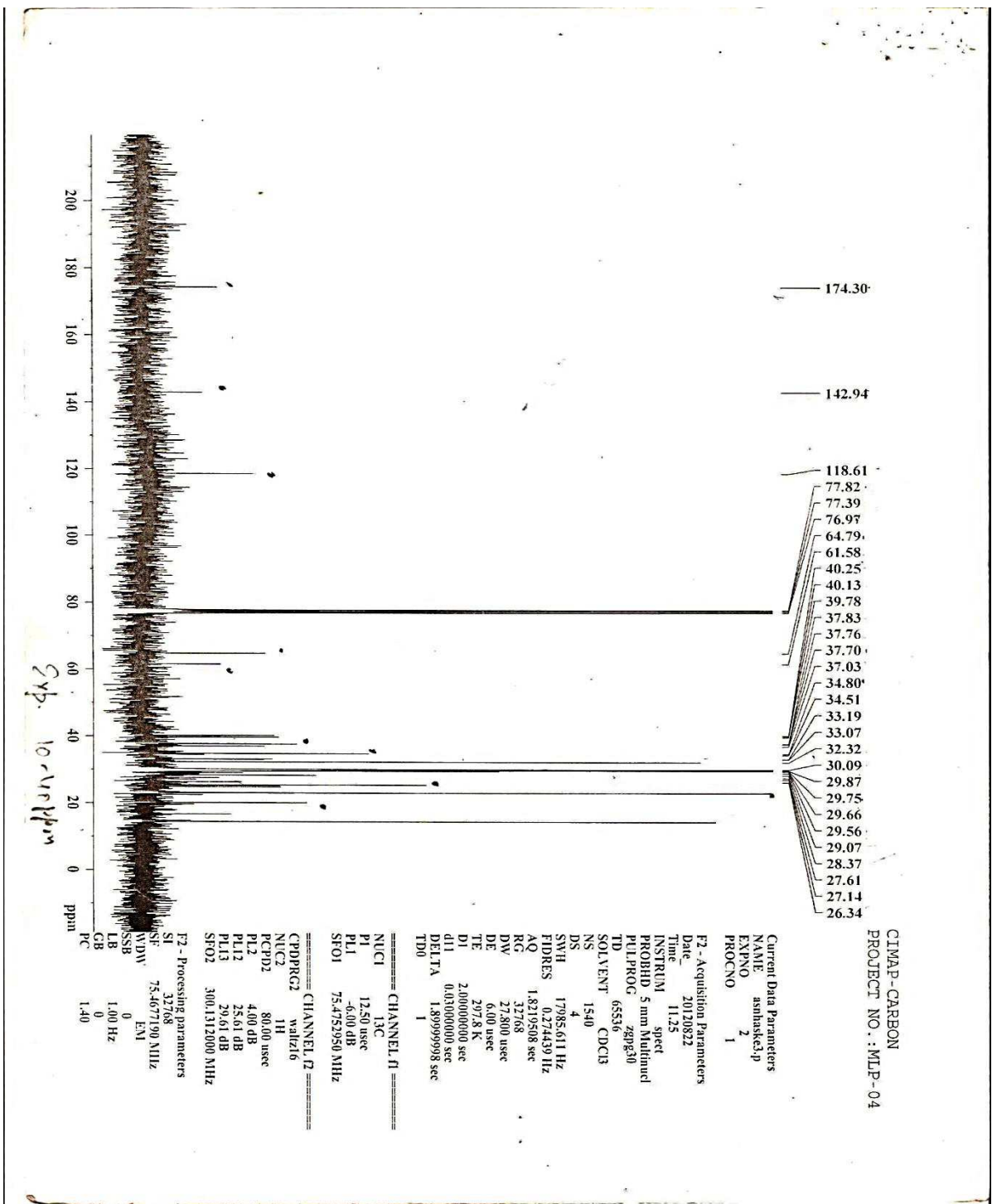


Fig. 4.2  $^{13}\text{C}$  NMR spectrum of Haskh-3 in  $\text{CDCl}_3$

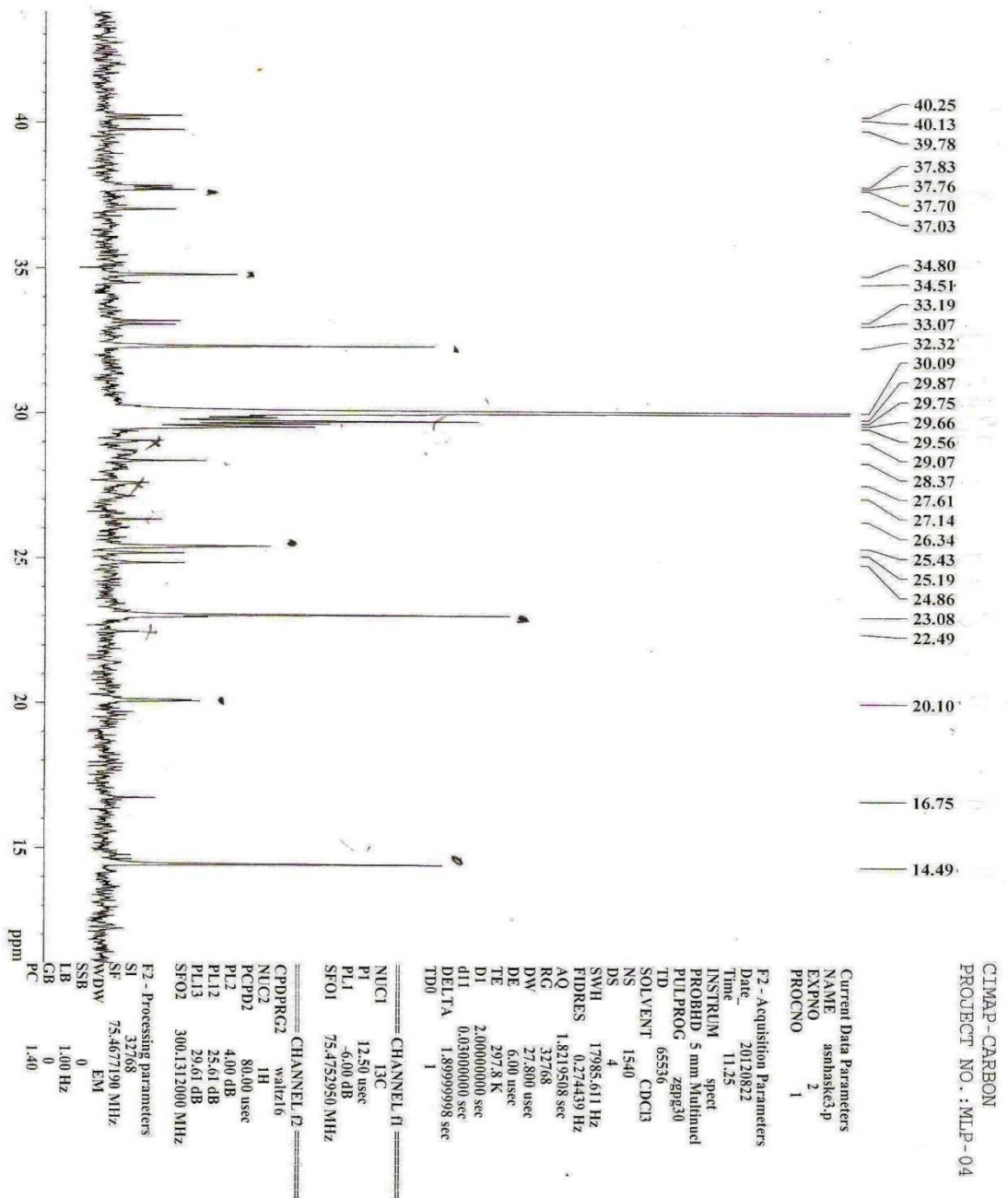


Fig. 4.3 Expanded  $^{13}\text{C}$  NMR spectrum of Haskh-3 in  $\text{CDCl}_3$

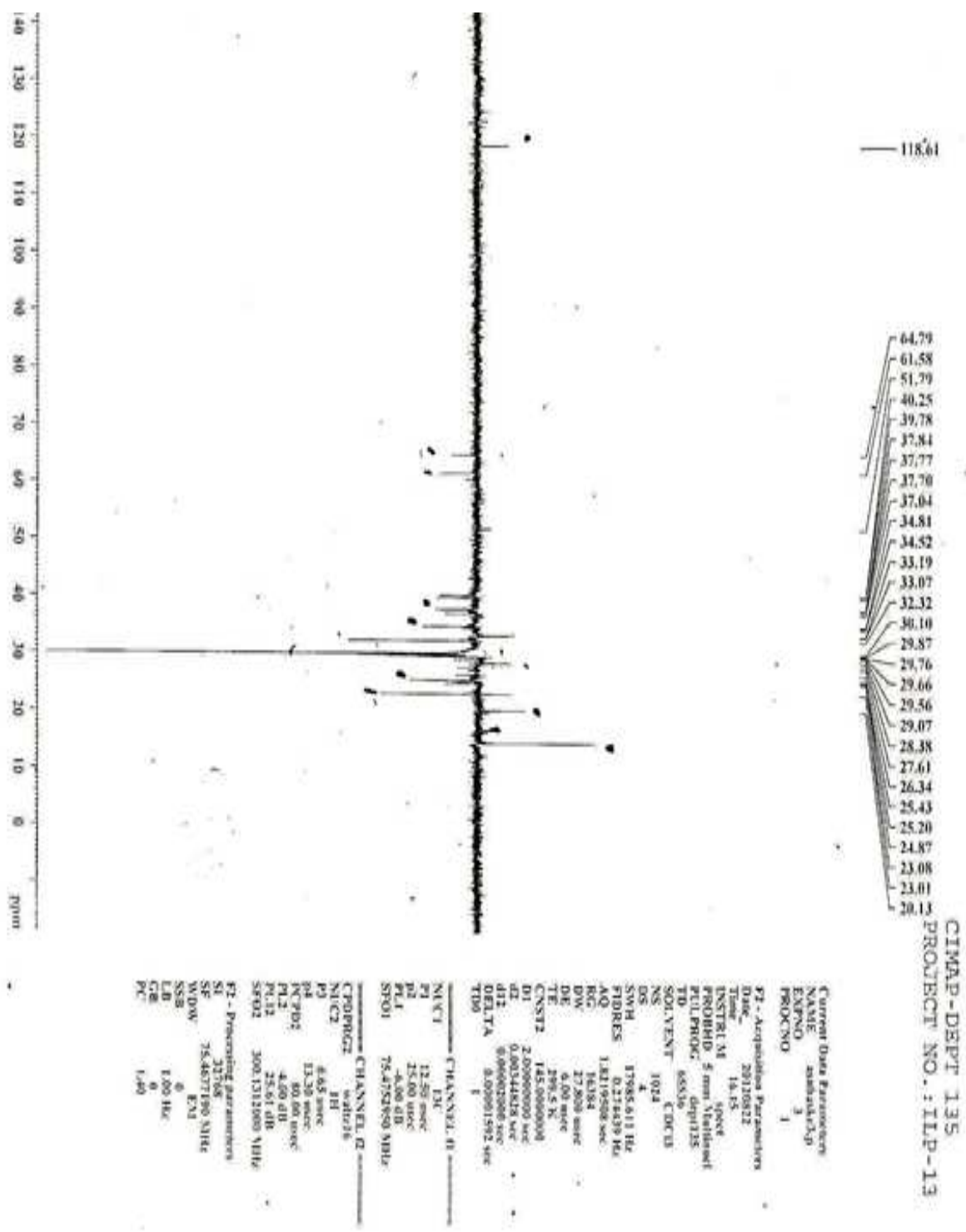


Fig. 4.4 DEPT spectrum of Haskh-3 in CDCl<sub>3</sub>

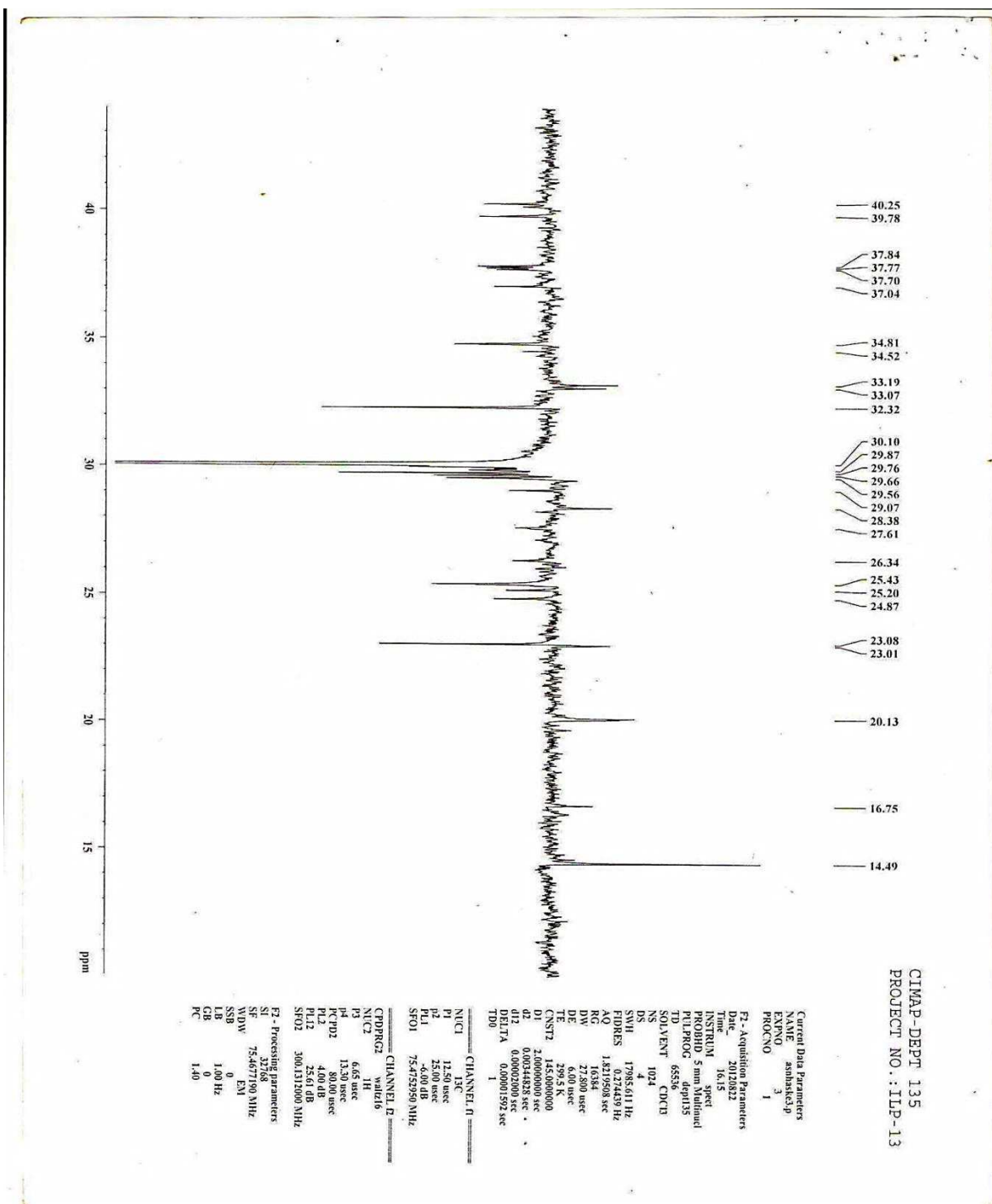
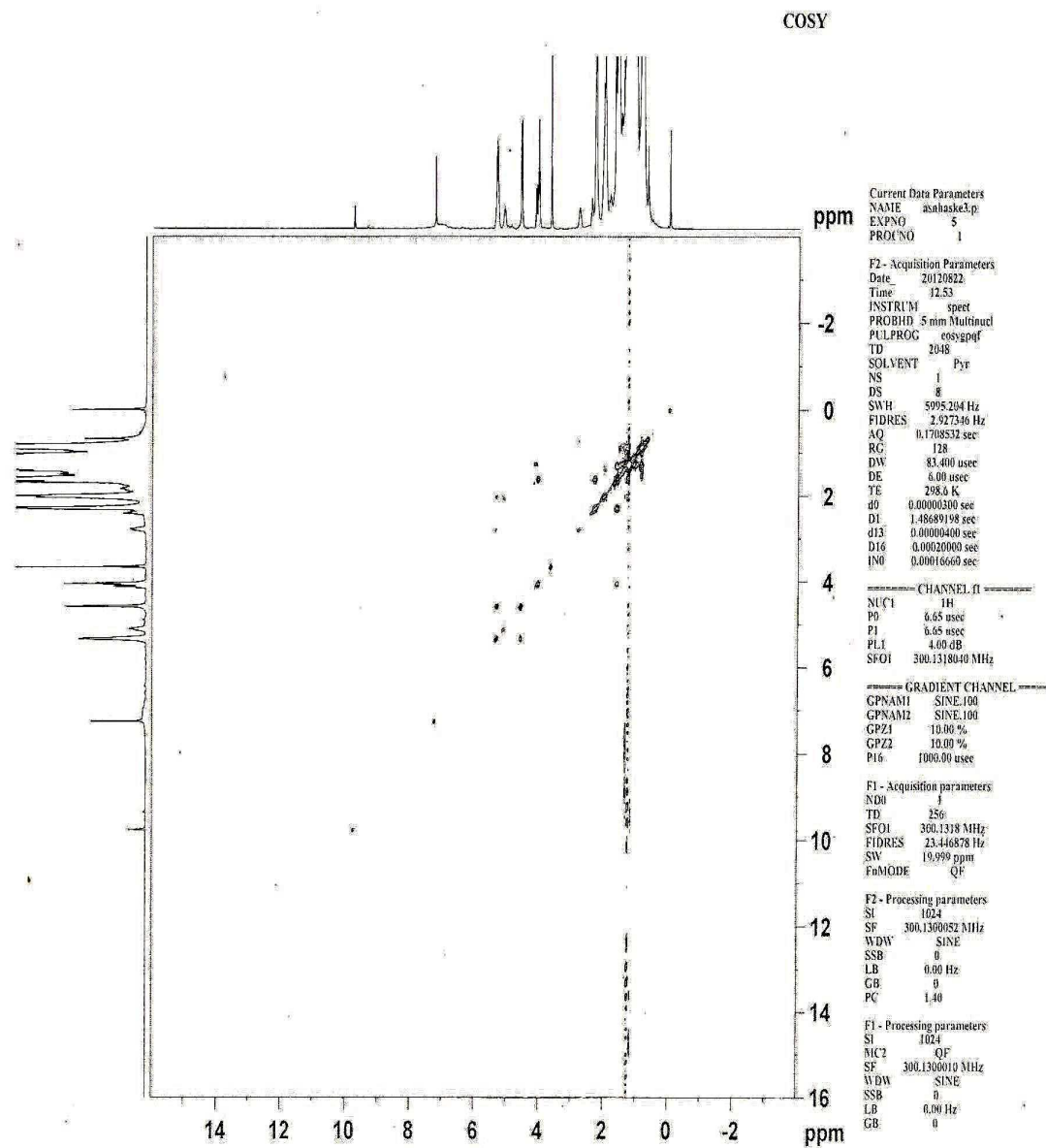


Fig. 4.5 Expanded DEPT spectrum of Haskh-3 in CDCl<sub>3</sub>



**Fig. 4.6**  $^1\text{H}$ - $^1\text{H}$  COSY spectrum of Haskh-3 in  $\text{CDCl}_3$

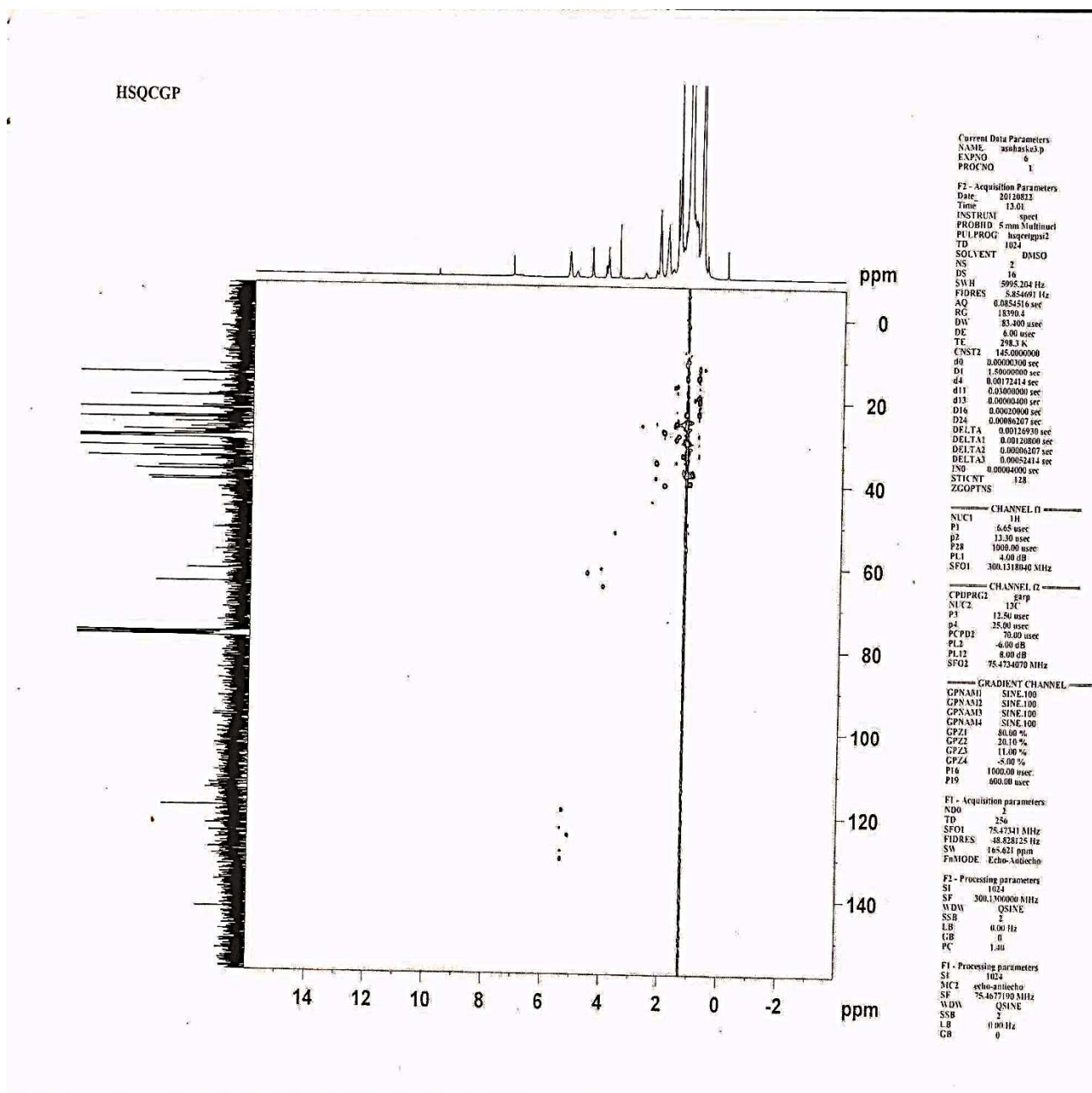


Fig. 4.7 HSQC spectrum of Haskh-3 in  $CDCl_3$



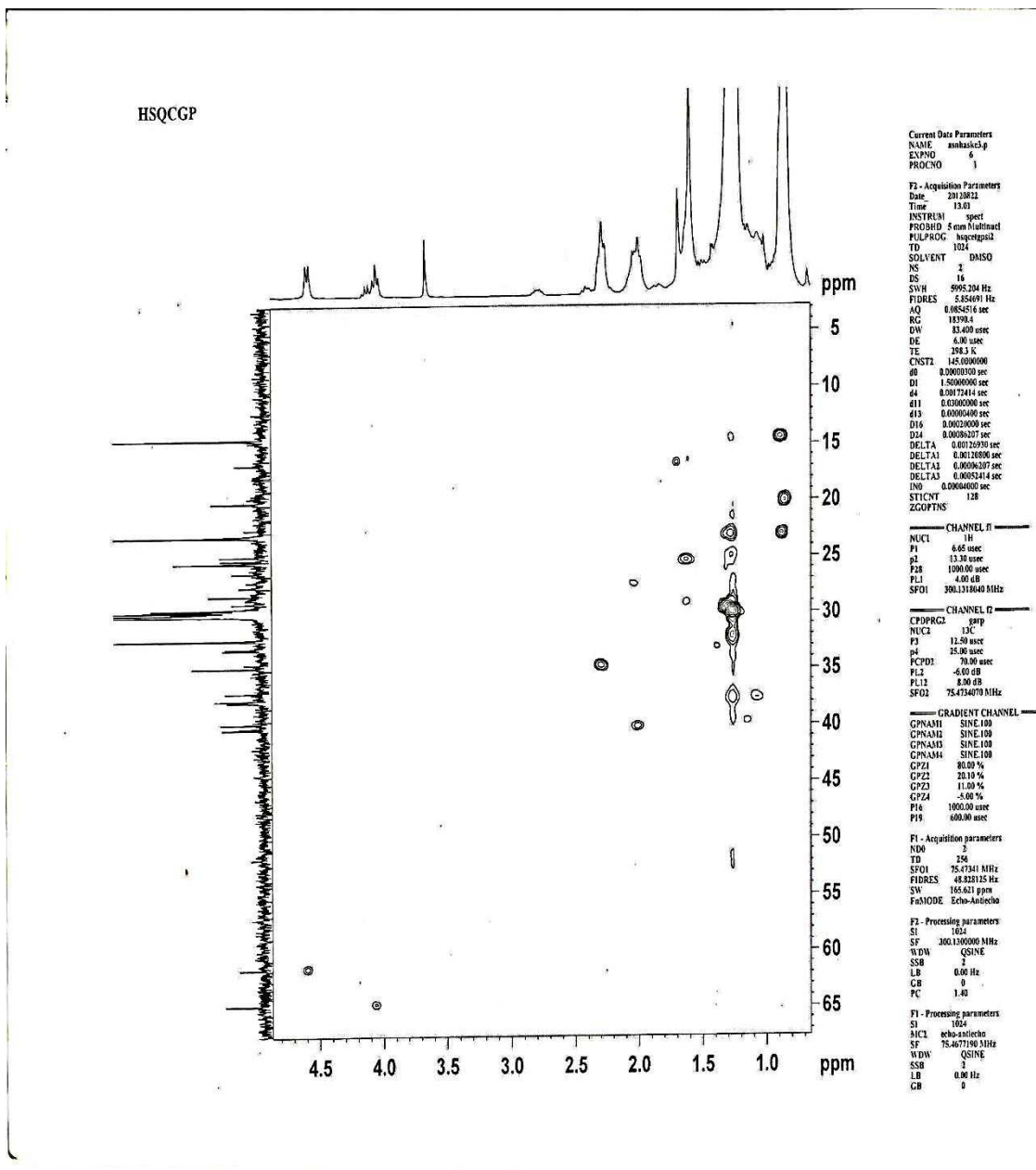
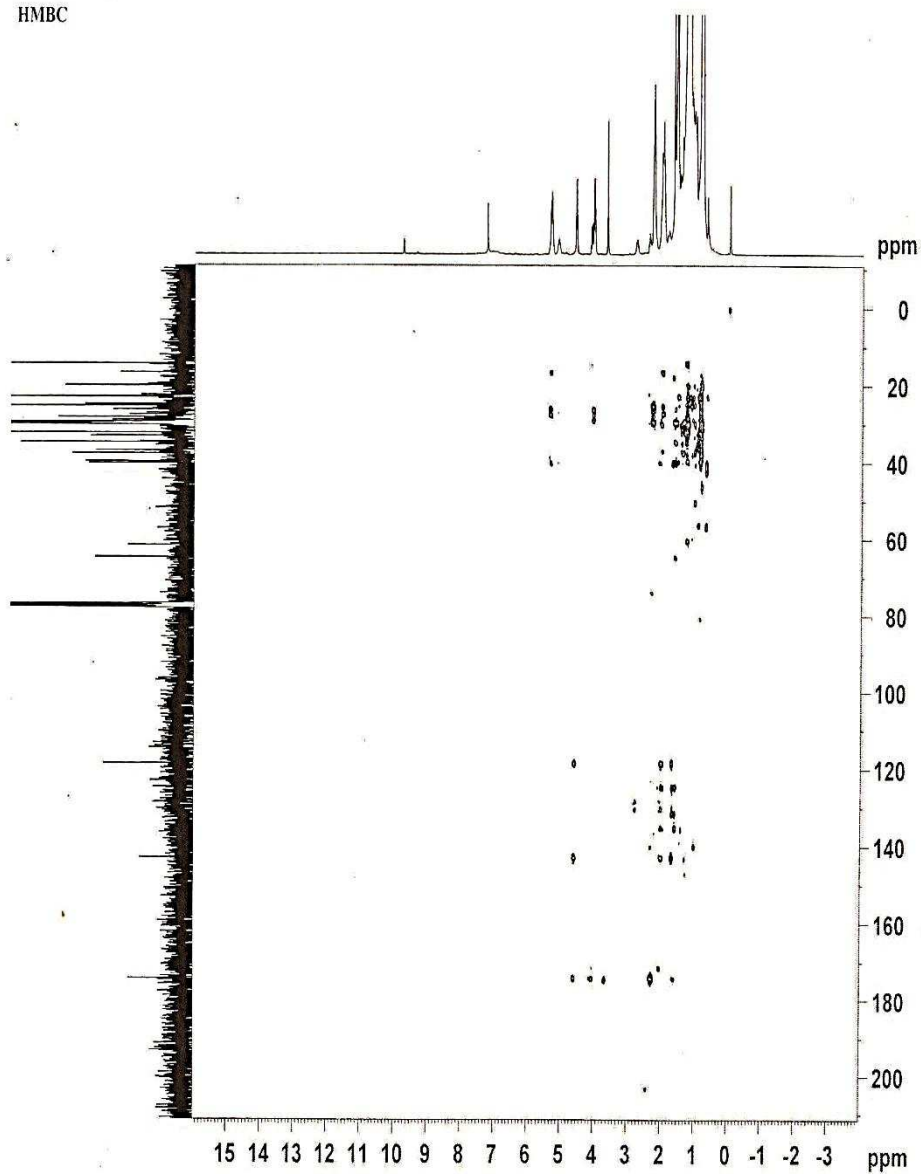


Fig. 4.8 Expanded HSQC spectrum of Haskh-3 in CDCl<sub>3</sub>

HMBC



Current Data Parameters  
NAME ashak3.p  
EXPNO 7  
PROCNO 1

F2 - Acquisition Parameters  
Date\_ 2012022  
Time 13.16  
INSTRUM spect  
PROBHD 5 mm Multinuc  
PULPROG hmcpg2ndqf  
TD 4096  
SOLVENT CDCl3  
NS 8  
DS 16  
SWH 5995.214 Hz  
FIDRES 1.463673 Hz  
AQ 0.3416564 sec  
RG 16384  
DW 83.400 usec  
DE 6.00 usec  
TE 299.4 K  
CNST6 135.0000000  
CNST7 165.0000000  
CNST13 7.0000000  
d0 0.0000300 sec  
D1 4.5000000 sec  
d6 0.07142857 sec  
D16 0.00020600 sec  
DELTA1 0.00250370 sec  
DELTA2 0.00618910 sec  
DELTA3 0.07023458 sec  
DNO 0.00002980 sec

----- CHANNEL f1 -----  
NUC1 1H  
P1 6.65 usec  
P2 13.30 usec  
PL1 4.00 dB  
SFO1 300.1318040 MHz

----- CHANNEL f2 -----  
NUC2 13C  
P3 12.50 usec  
PL2 -6.00 dB  
SFO2 75.4752830 MHz

----- GRADIENT CHANNEL -----  
GPNAM1 SINE.100  
GPNAM2 SINE.100  
GPNAM3 SINE.100  
GPNAM4 SINE.100  
GPNAM5 SINE.100  
GPNAM6 SINE.100  
GPZ1 50.00 %  
GPZ2 30.00 %  
GPZ3 40.00 %  
GPZ4 15.00 %  
GPZ5 -10.00 %  
GPZ6 -5.00 %  
P16 1000.00 usec

F1 - Acquisition parameters  
ND0 2  
TD 234  
SFO1 75.47528 MHz  
FIDRES 71.703094 Hz  
SV 222.305 ppm  
FaMODE QF

F2 - Processing parameters  
SI 1024  
SF 300.130037 MHz  
WDW SINE  
SSB 0  
LB 0.00 Hz  
GB 0  
PC 1.40

F1 - Processing parameters  
SI 1024  
MC1 QF  
SF 75.467190 MHz  
WDW SINE  
SSB 0  
LB 0.00 Hz  
GB 0

Fig. 4.9 HMBC spectrum of Haskh-3 in CDCl<sub>3</sub>

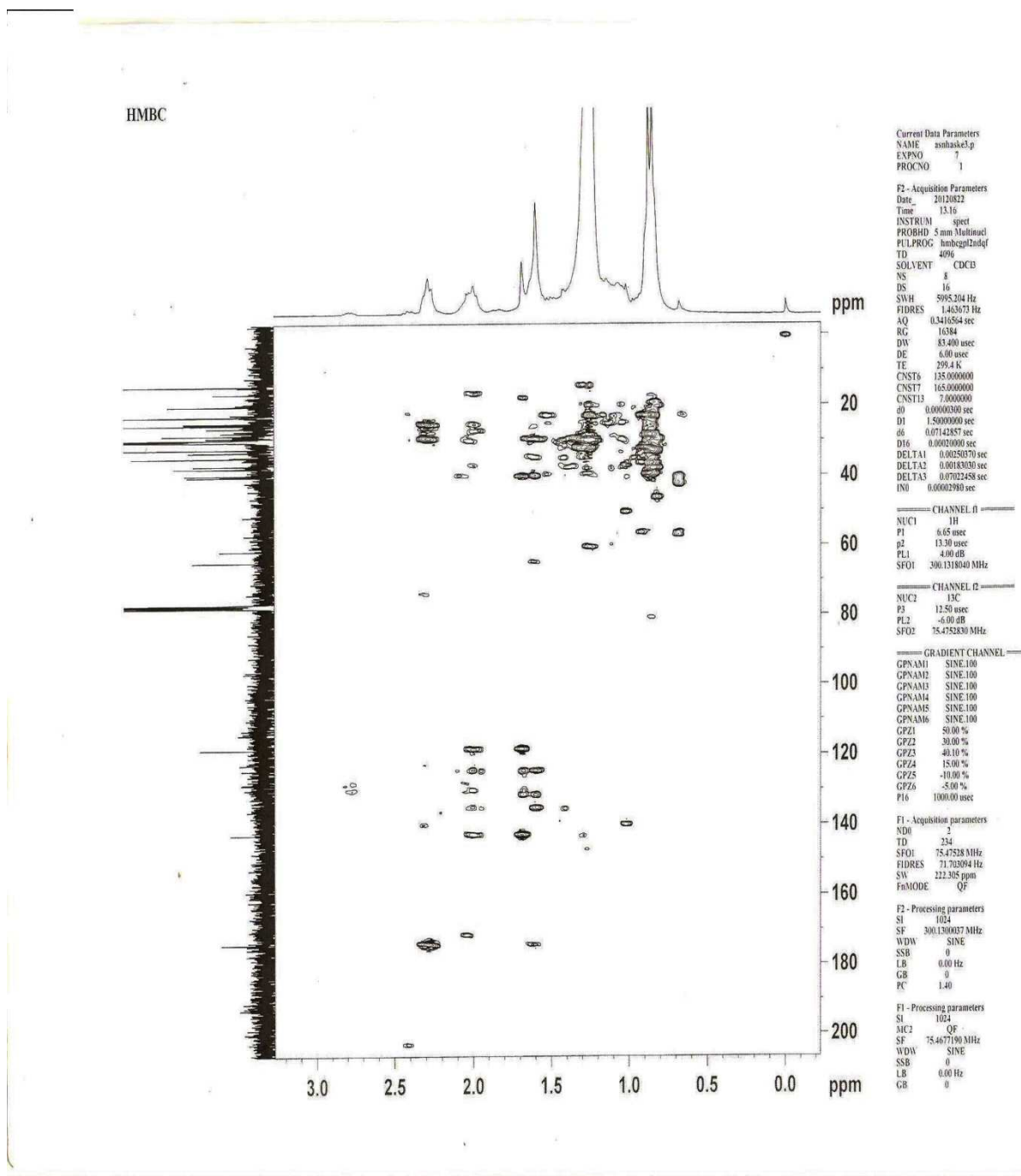


Fig. 4.10 Expanded HMBC spectrum of Haskh-3 in  $CDCl_3$

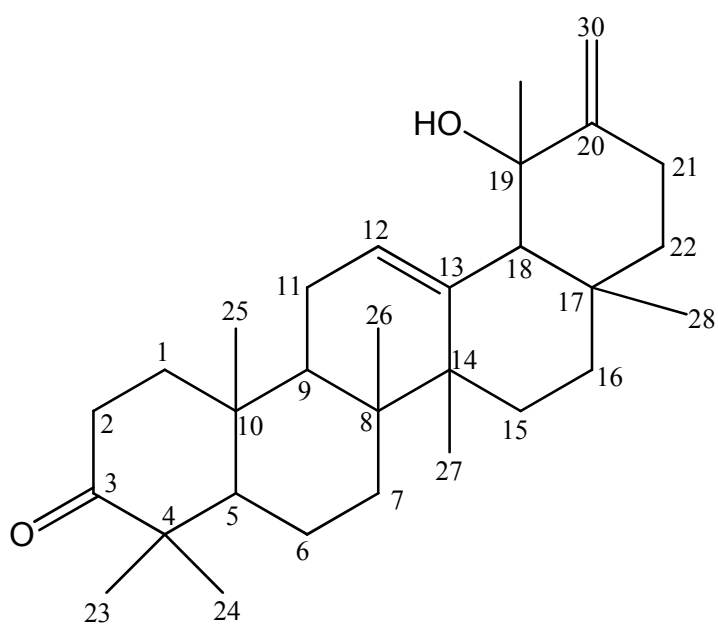
#### 4.4.4 Characterisation of Haskh-4

Compound Haskh-4 (15.0 mg) was obtained as a yellow solid which has a melting point of 190 - 193°C. The Mass fragment ions 436 [M]<sup>+</sup>, 437 [M+H]<sup>+</sup> gave the molecular formula C<sub>30</sub>H<sub>44</sub>O<sub>2</sub> (436). The IR  $\bar{\nu}$  (cm<sup>-1</sup>) absorption signals at 3368, 2924, 1719 and 1460 cm<sup>-1</sup> indicated the presence of O-H, C-H, C=O and C=C moieties respectively. The <sup>1</sup>H NMR spectrum signals at  $\delta_H$  0.85-0.87 (6H, d, 2 x CH<sub>3</sub>) and 2.03-2.24 (2H, d, H<sub>7</sub>) correspond to two angular methyl protons and methylene protons at C-24, C-28 and C-7, while  $\delta_H$  0.97-1.67 (31H, m, 5 x CH<sub>3</sub> & 8 x CH<sub>2</sub>) multiplet peaks are characteristics of methyl and methylene protons of triterpenoids. The signals at  $\delta_H$  4.72 (s) and 5.12 (t) revealed the presence of terminal olefinic methylene and methine protons at C-30 and C-12 respectively [Fig. 4.11]. <sup>13</sup>C NMR spectrum also showed resonances consistent with ursadiene skeleton [Fig. 4.12 and 4.13]. DEPT experiment [Fig. 4.14 and 4.15] classified the carbons into seven methyl carbons, ten methylene carbons, four methine carbons and nine quaternary carbon resonances. In <sup>1</sup>H-<sup>1</sup>H COSY spectrum [Fig. 4.16 and 4.17], the correlation of methine proton at C-12 to methylene protons at C-11 and methine proton at C-18 was shown, while methylene protons at C-1 were correlated with methylene protons at C-2. In <sup>1</sup>H-<sup>13</sup>C HMBC experiment [Fig. 4.20, 4.21 and 4.22], there was correlation of olefinic methylene protons at C-30 with C-19, which confirmed the presence of oxyquaternary carbon at C-19 revealed by HSQC [Fig. 4.18 and 4.19] experiment. HMBC spectrum also showed a long range correlation of methine proton at C-12 with C-11, C-18 and C-14, while methylene protons at C-2 and methine proton at C-5 were also correlated with keto-C-3 [Fig. 4.15]. Further, methylene protons at C-22 revealed correlations with C-20 and C-30. The spectroscopic data of Haskh-4 [Table 4.44] was identical to 3-keto-ursadiene derivatives (Reynolds *et al.*, 1986, Kojima *et al.*, 1987, Fujioka *et al.*, 1989, Numata *et al.*, 1990). Therefore, Haskh-4 was elucidated as Ursa-12,20-dien-19-ol-3-one (**103**).

**Table 4.44:**  $^{13}\text{C}$  and  $^1\text{H}$  NMR ( $\text{CDCl}_3$ ) spectral data of Haskh-4

Assignment	$^{13}\text{C}$	Multiplicity	$^1\text{H}$ , multiplicity
1	24.87	$\text{CH}_2$	0.99-1.67, m, 2H
2	27.11	$\text{CH}_2$	0.99-1.67, m, 2H
3	210.02	Q	-
4	39.78	Q	-
5	40.13	CH	2.03-2.24, d, 1H
6	23.02	$\text{CH}_2$	0.99-1.67, m, 2H
7	32.32	$\text{CH}_2$	0.99-1.67, m, 2H
8	41.87	Q	-
9	39.77	CH	2.03-2.24, d, 1H
10	41.72	Q	-
11	34.21	$\text{CH}_2$	0.99-1.67, m, 2H
12	124.67	CH	5.12, t, 1H
13	135.33	Q	-
14	37.68	Q	-
15	30.09	$\text{CH}_2$	0.99-1.67, m, 2H
16	29.57	$\text{CH}_2$	0.99-1.67, m, 2H
17	36.58	Q	-
18	40.14	CH	2.03-2.24, d, 1H
19	87.45	Q	-
20	139.68	Q	-
21	29.75	$\text{CH}_2$	0.99-1.67, m, 2H
22	27.88	$\text{CH}_2$	0.99-1.67, m, 2H
23	14.50	$\text{CH}_3$	0.67-0.97, s, 3H
24	16.42	$\text{CH}_3$	0.67-0.97, s, 3H
25	20.14	$\text{CH}_3$	0.67-0.97, s, 3H
26	23.10	$\text{CH}_3$	0.67-1.97, s, 3H
27	25.19	$\text{CH}_3$	0.67-1.97, s, 3H
28	23.10	$\text{CH}_3$	0.99-1.67, m, 3H
29	28.37	$\text{CH}_3$	0.99-1.67, m, 3H
30	114.46	$\text{CH}_2$	4.72, s, 2H

Implied multiplicities of the carbons were determined from the DEPT experiment.



Ursa-12,20-dien-19-ol-3-one (**103**)

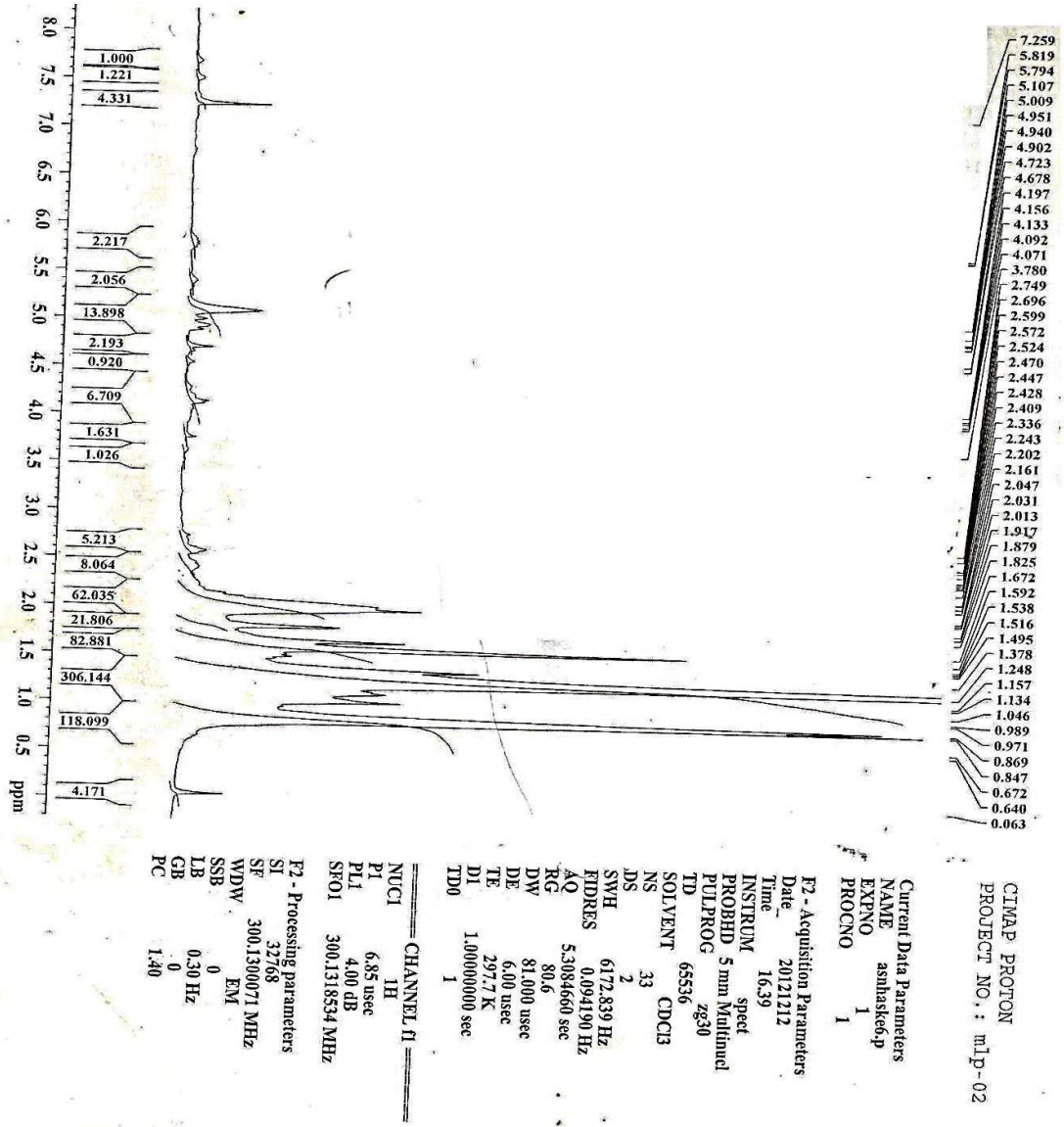


Fig. 4.11  $^1\text{H}$  NMR spectrum of Haskh-4 in  $\text{CDCl}_3$

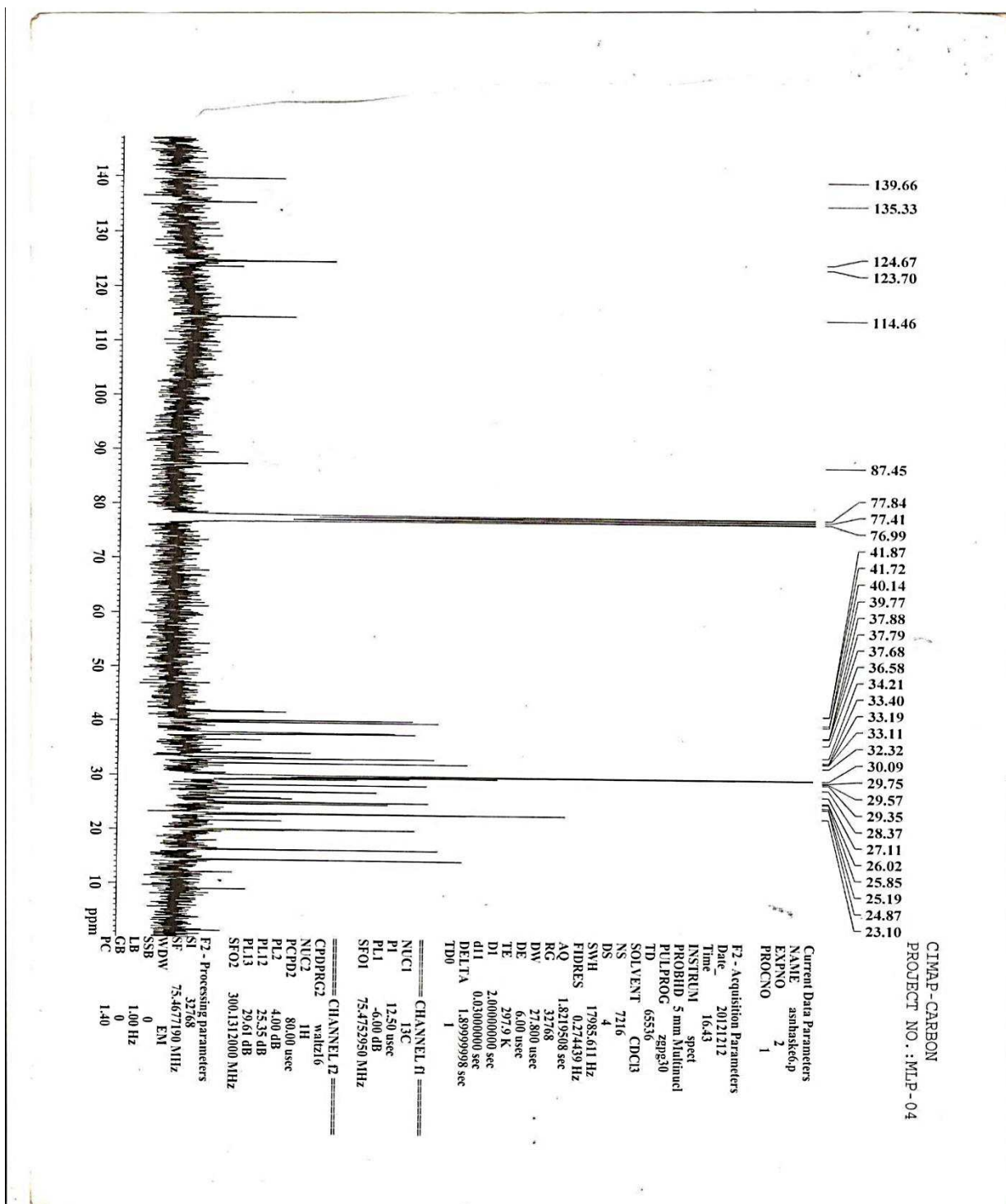
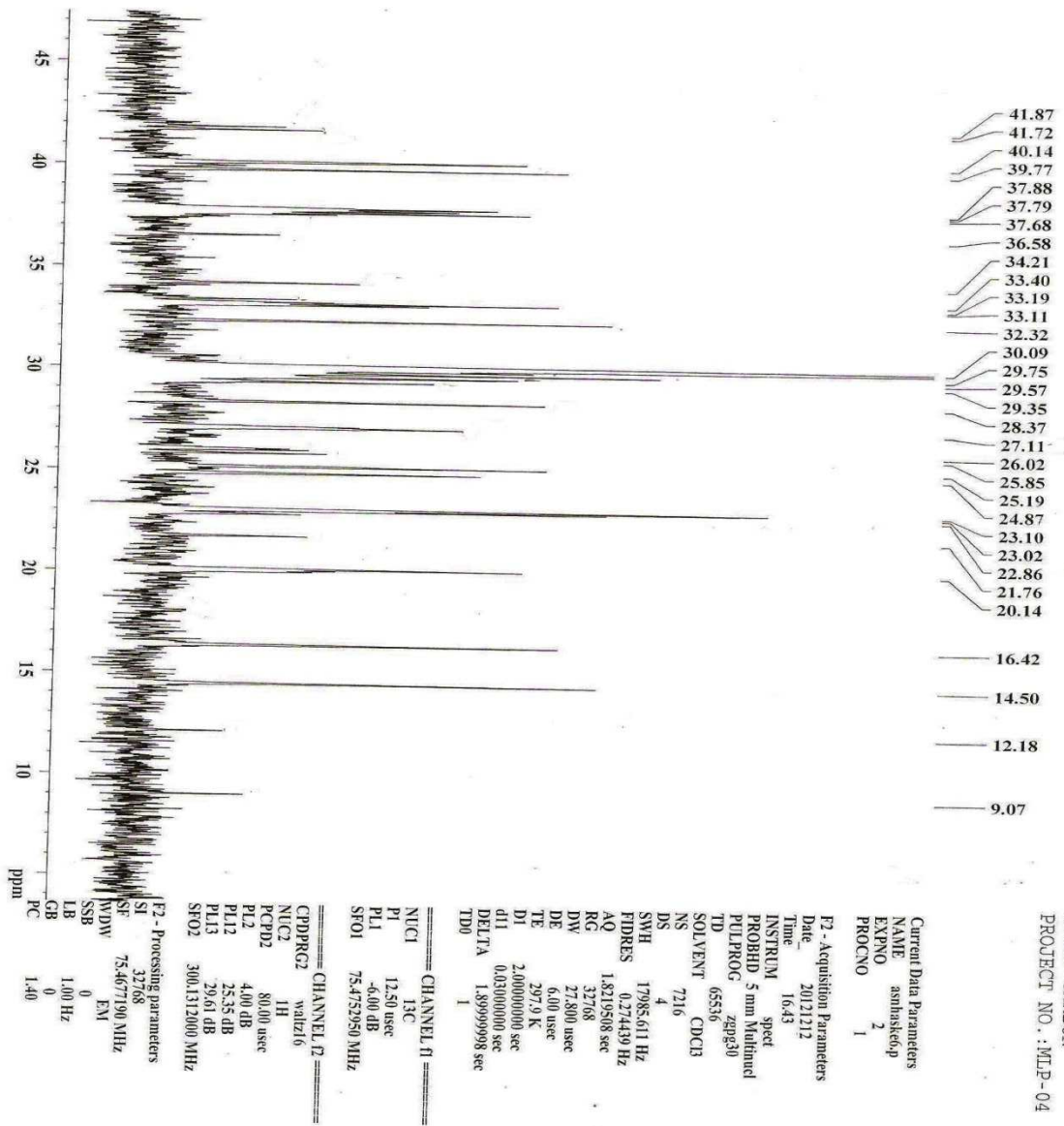


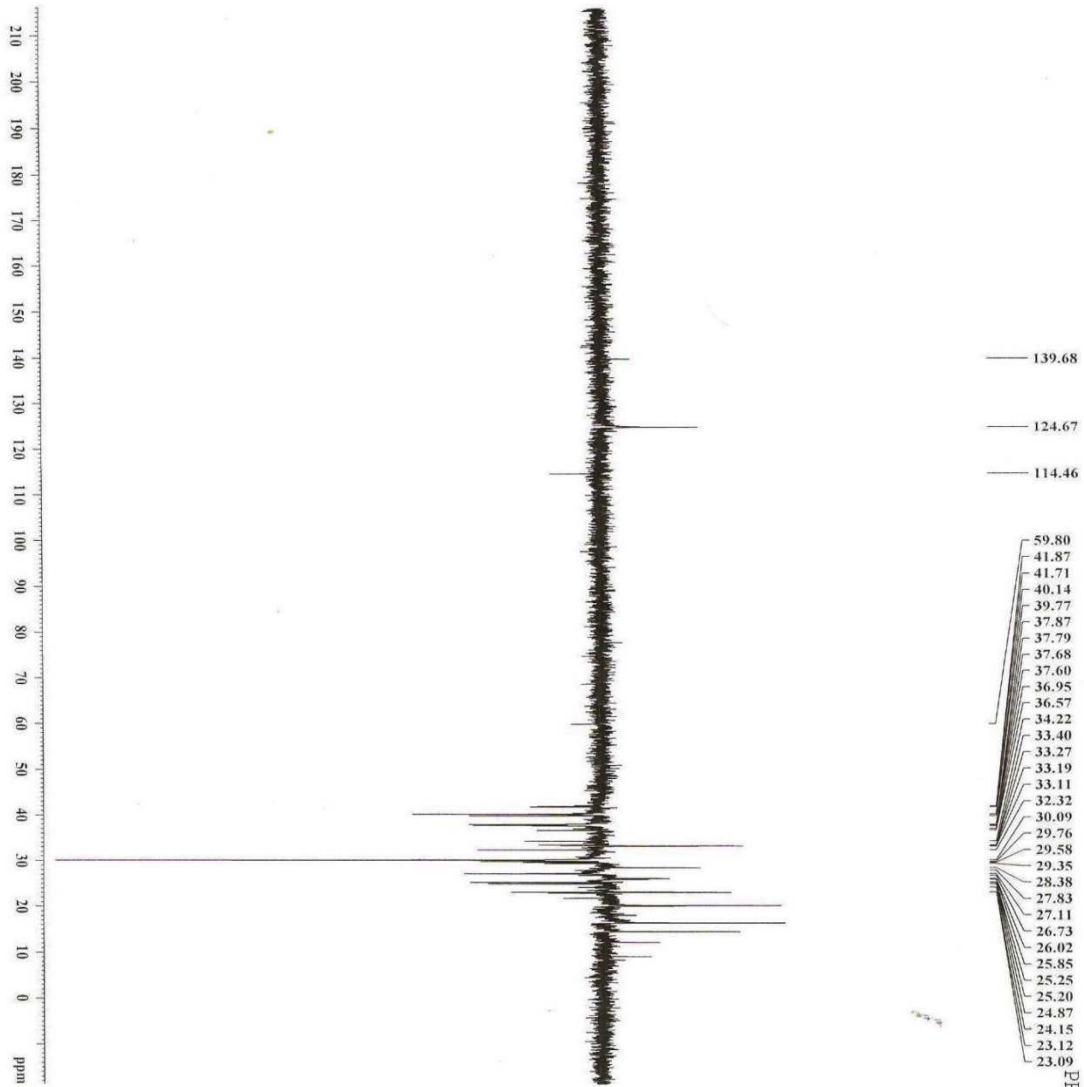
Fig. 4.12  $^{13}\text{C}$  NMR spectrum of Haskh-4 in  $\text{CDCl}_3$





CIMAP-CARBON  
PROJECT NO.: MLP-04

Fig. 4.13 Expanded  $^{13}\text{C}$  NMR spectrum of Haskh-4 in  $\text{CDCl}_3$



CIMAP-DEPT 135  
PROJECT NO.: ILP-13

```

Current Data Parameters
NAME      ashsk46j
EXPNO     3
PROCNO    1

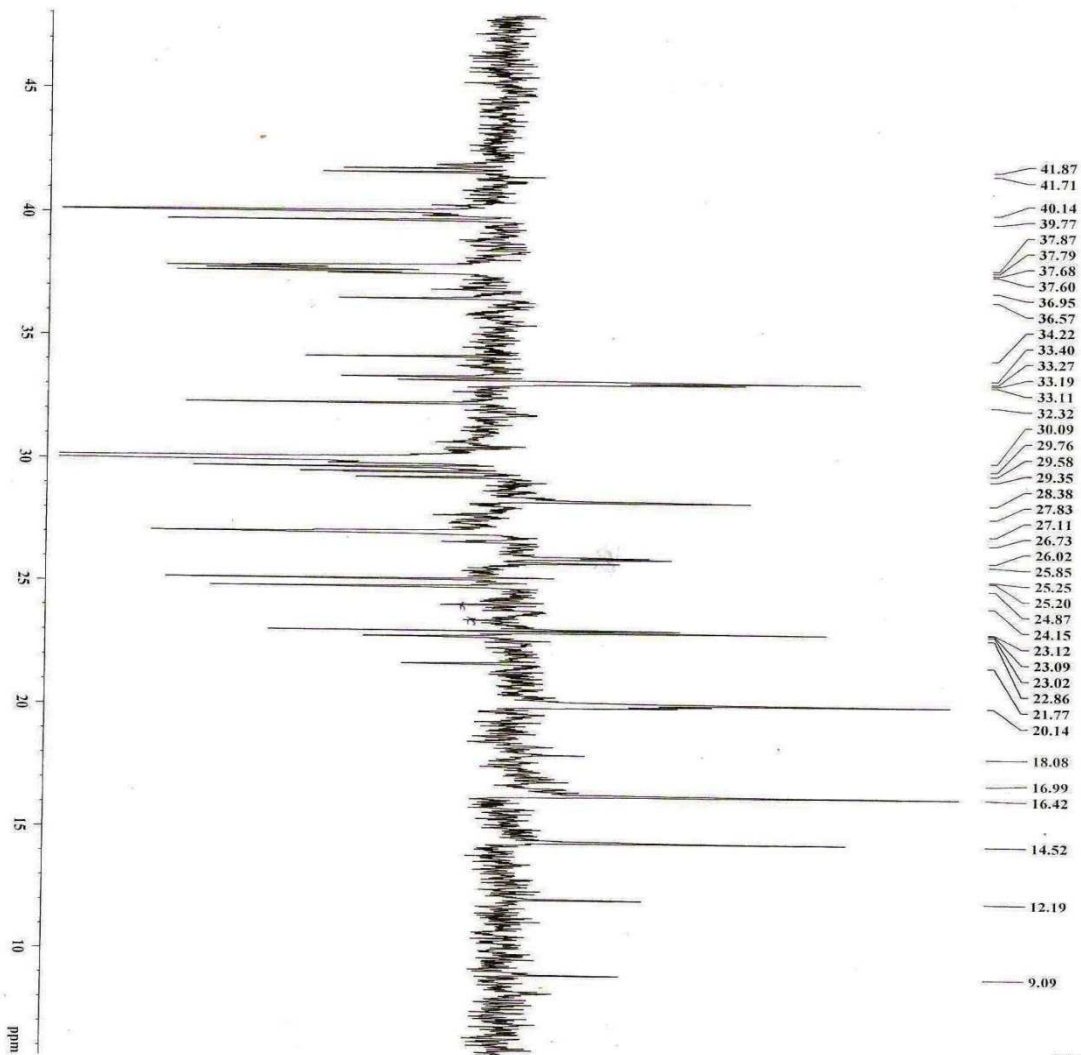
F2 - Acquisition Parameters
Date_     20121213
Time      5:57
INSTRUM   spect
PROBHD    5 mm VNP1H1
PULPROG   zgpg30
TD         65536
SOLVENT   CDCl3
NS         5120
DS         4
SWH        17985.611 Hz
FIDRES     0.274439 Hz
AQ         1.8219508 sec
RG         16384
DW         27.800 usec
DE         6.00 usec
TE         296.1 K
CST2      148.000000
d1         2.40000000 usec
d2         0.0034828 usec
d12        0.00002000 usec
DELTA     0.00001592 sec
TD0        1

===== CHANNEL f1 =====
NUC1       13C
P1         12.50 usec
P2         25.00 usec
PL1        -8.00 dB
PL12       75.4752590 MHz
SFO1       101.6261260 MHz

===== CHANNEL f2 =====
CPDPRG2   zgpg30
NUC2       1H
P3         6.85 usec
P4         13.70 usec
PCPD2     80.00 usec
PL2        4.00 dB
PL12       25.35 dB
SFO2       300.1372000 MHz

F2 - Processing parameters
SI         32768
SF         75467790 MHz
WDW        EM
SSB        0
LB         1.00 Hz
GB         0
PC         1.40
  
```

Fig. 4.14 DEPT spectrum of Haskh-4 in  $CDCl_3$



CIMAP-DEPT 135  
PROJECT NO.: ILP-13

```

Current Data Parameters
NAME      amhaskh.p
EXPNO     3
PROCNO    1

F2 - Acquisition Parameters
Date_     20121213
Time      5:57
INSTRUM   spect
PROBHD    5 mm Maltimed
PULPROG   dept135
TD         65536
SOLVENT   CDCl3
NS        5120
DS         4
SFO1      178541.1 Hz
FIDRES    1.8219508 sec
AQ         16384
RG         27.800 usec
DE         6.00 usec
TE         296.1 K
CNS12     145.0000000
D1         2.40000000 sec
d2         0.00348323 sec
DELTA     0.00002000 sec
TD0       1
===== CHANNEL f1 =====
NUC1       13C
P1         13.50 usec
P2         25.00 usec
PL1        -6.00 dB
SFO1      75.4752950 MHz

===== CHANNEL D =====
CPRPG2    walz16
NUC2       1H
P3         6.85 usec
P4         15.20 usec
PCPRD2    4.00 usec
PL2        4.00 dB
PL12       25.35 dB
SFO2      300.1312000 MHz

F2 - Processing parameters
SI         31768
SF         75.467190 MHz
WDW        EM
SSB        0
LB         1.00 Hz
GB         0
PC         1.40
  
```

Fig. 4.15 Expanded DEPT spectrum of Haskh-4 in CDCl<sub>3</sub>

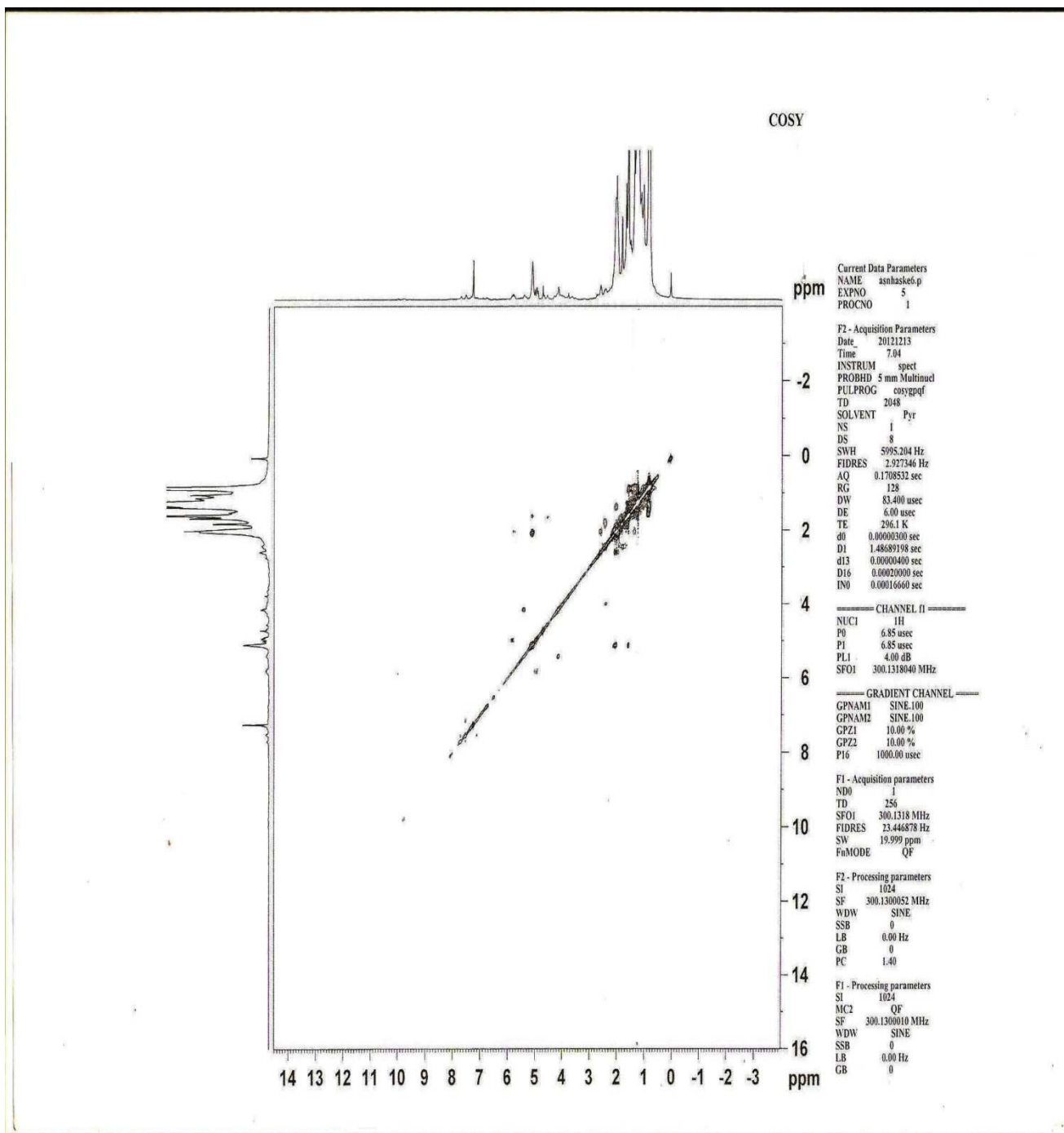


**Fig. 4.16**  $^1\text{H}$ - $^1\text{H}$  COSY spectrum of Haskh-4 in  $\text{CDCl}_3$

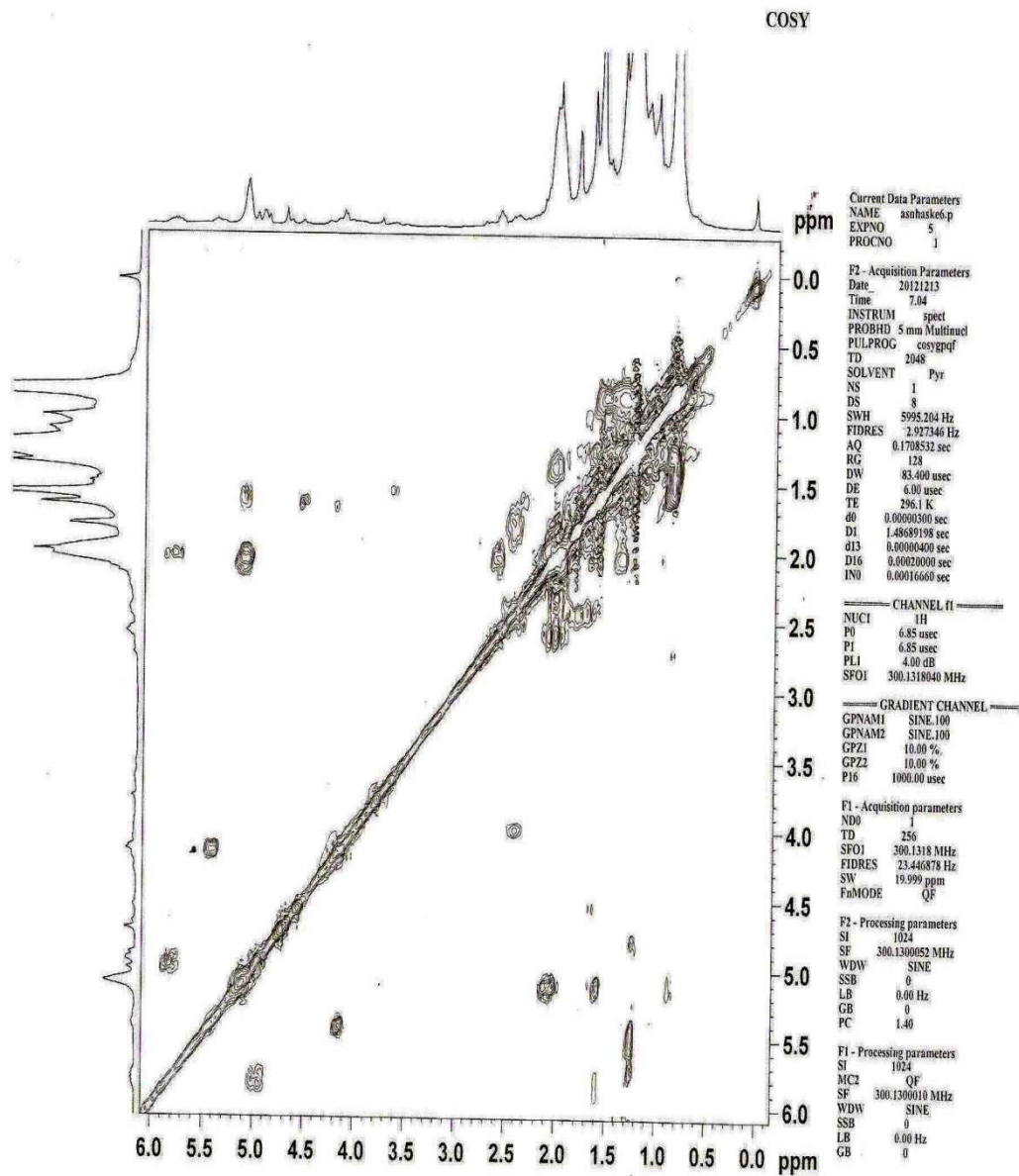


Fig. 4.17 Expanded  $^1\text{H}$ - $^1\text{H}$  COSY spectrum of Haskh-4 in  $\text{CDCl}_3$

HSQC

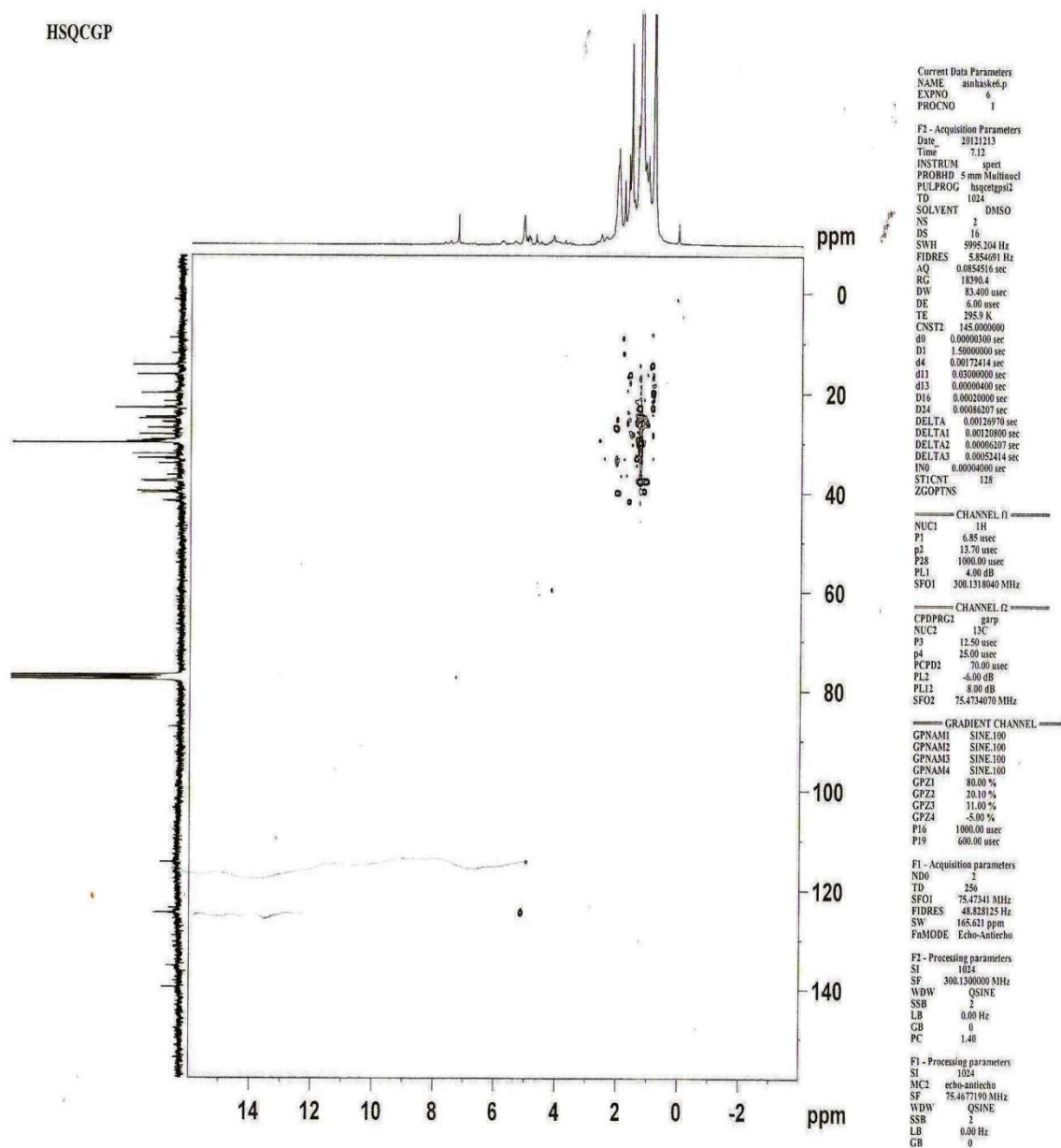
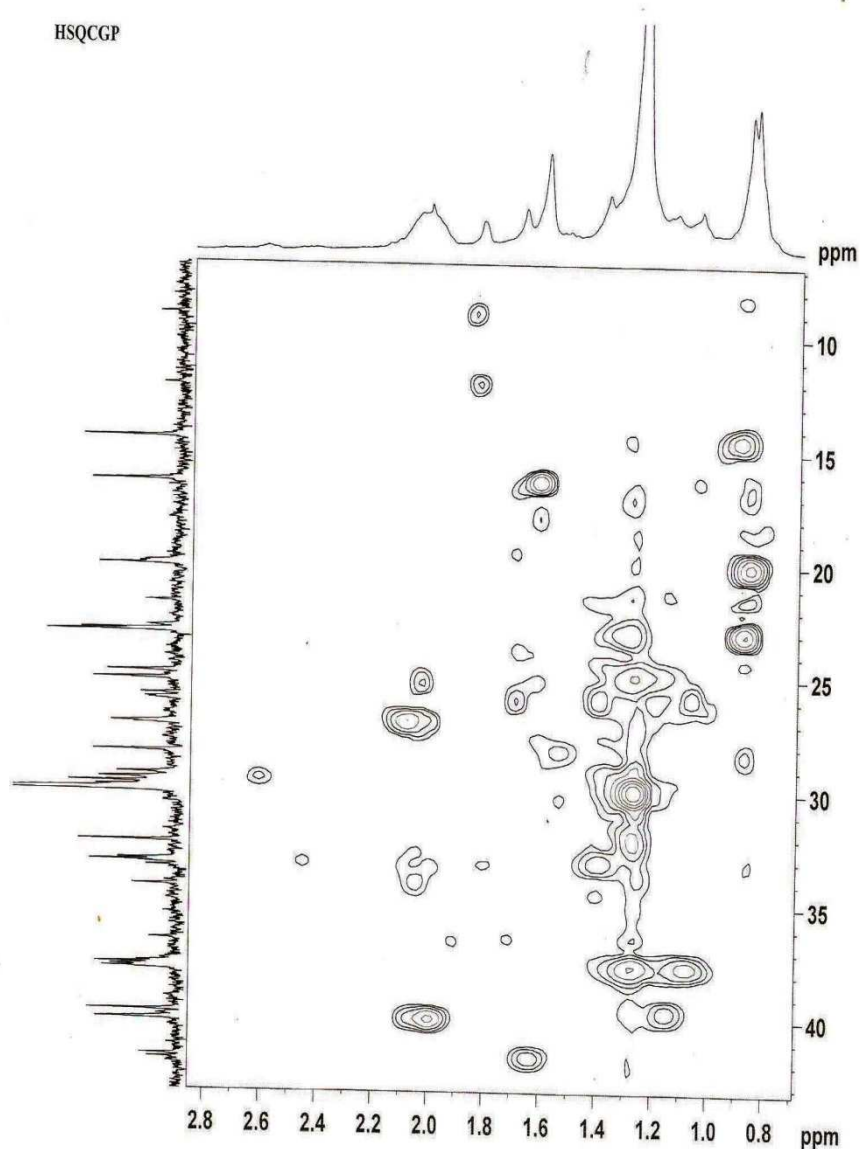


Fig. 4.18 HSQC spectrum of Haskh-4 in  $CDCl_3$

HSQCGP



Current Data Parameters  
 NAME amhax162.p  
 EXPNO 8  
 PROCNO 1

F2 - Acquisition Parameters  
 Date\_ 20121213  
 Time 7.12  
 INSTRUM spect  
 PROBHD 5 mm Multinuc  
 PULPROG hsqcqtgpsi2  
 TD 1024  
 SOLVENT DMSO  
 NS 2  
 DS 6  
 SWH 595.234 Hz  
 FIDRES 5.85491 Hz  
 AQ 0.0854516 sec  
 RG 18396.4  
 DW 83.400 usec  
 DE 6.00 usec  
 TE 295.9 K  
 CNST2 145.9000000  
 d0 0.00000300 sec  
 D1 1.5000000 sec  
 d4 0.0072414 sec  
 d11 0.0300000 sec  
 d13 0.0008400 sec  
 D16 0.0002000 sec  
 D21 0.0096207 sec  
 DELTA 0.0012070 sec  
 DELTA1 0.0012000 sec  
 DELTA2 0.0006207 sec  
 DELTA3 0.0005414 sec  
 LW 0.0000000 sec  
 ST1CNT 128  
 ZGOPTS

CHANNEL f1  
 NUC1 1H  
 P1 6.85 usec  
 P2 13.70 usec  
 P28 1000.00 usec  
 PL1 4.00 dB  
 SFO1 300.1318940 MHz

CHANNEL f2  
 CPDPRG2 garp  
 NUC2 13C  
 P3 12.50 usec  
 P4 25.00 usec  
 PCPD2 70.00 usec  
 PL2 -9.00 dB  
 PL11 8.00 dB  
 SFO2 75.4734070 MHz

GRADIENT CHANNEL  
 GPNAM1 SINE.100  
 GPNAM2 SINE.100  
 GPNAM3 SINE.100  
 GPNAM4 SINE.100  
 GPZ1 80.00 %  
 GPZ2 20.10 %  
 GPZ3 11.00 %  
 GPZ4 -5.00 %  
 P16 1000.00 usec  
 P19 600.00 usec

F1 - Acquisition parameters  
 ND0 2  
 TD 256  
 SFO1 75.47341 MHz  
 FIDRES 48.828125 Hz  
 SW 165.621 ppm  
 FaMODE Echo-Antiecho

F2 - Processing parameters  
 SI 1024  
 SF 300.1300000 MHz  
 WDW QSINE  
 SSB 2  
 LB 0.00 Hz  
 GB 0  
 PC 1.40

F1 - Processing parameters  
 SI 1024  
 MC2 echo-antiecho  
 SF 75.4677190 MHz  
 WDW QSINE  
 SSB 2  
 LB 0.00 Hz  
 GB 0

Fig. 4.19 Expanded HSQC spectrum of Haskh-4 in CDCl<sub>3</sub>

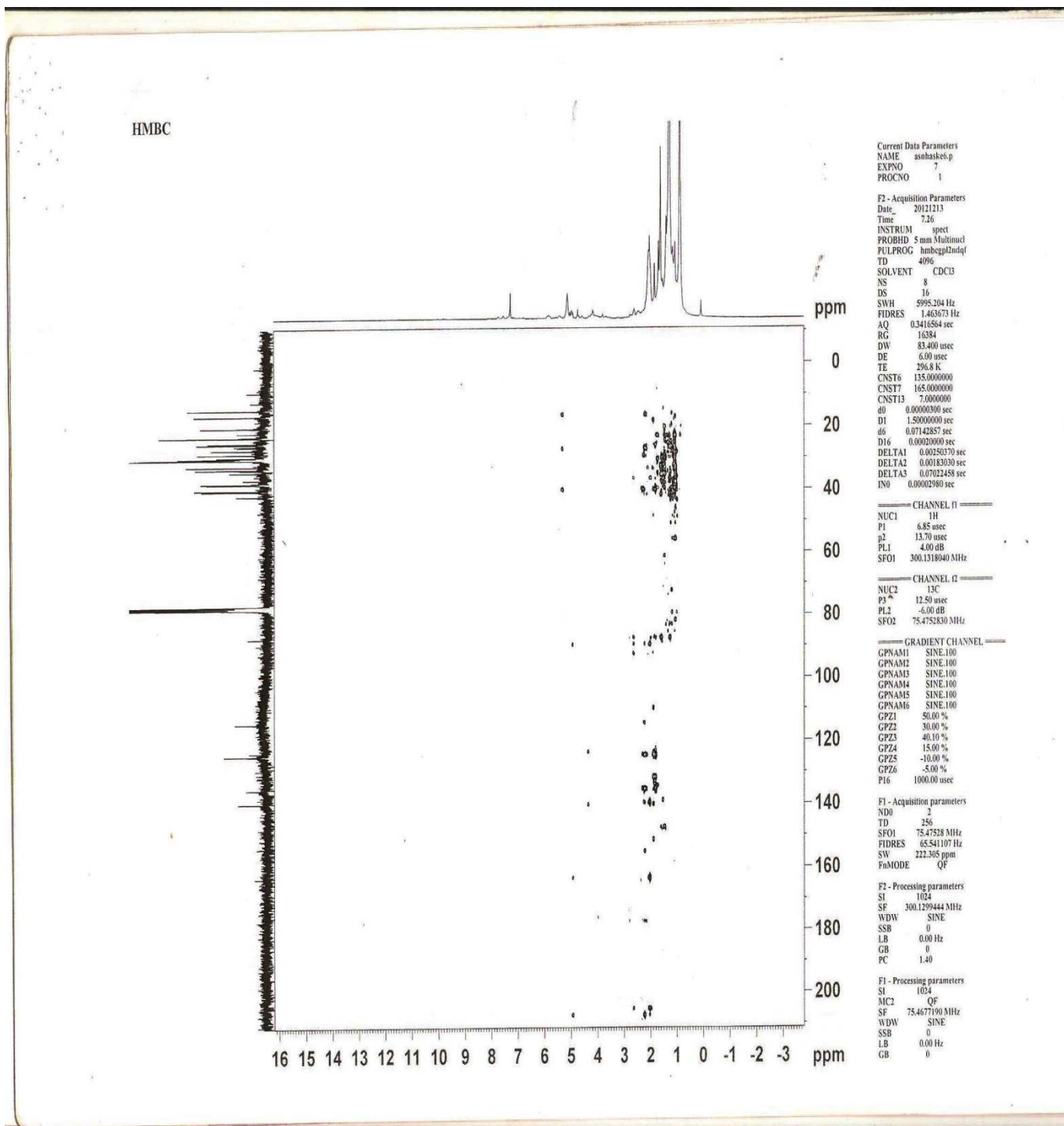


Fig. 4.20  $^1\text{H}$ - $^{13}\text{C}$  HMBC spectrum of Haskh-4 in  $\text{CDCl}_3$



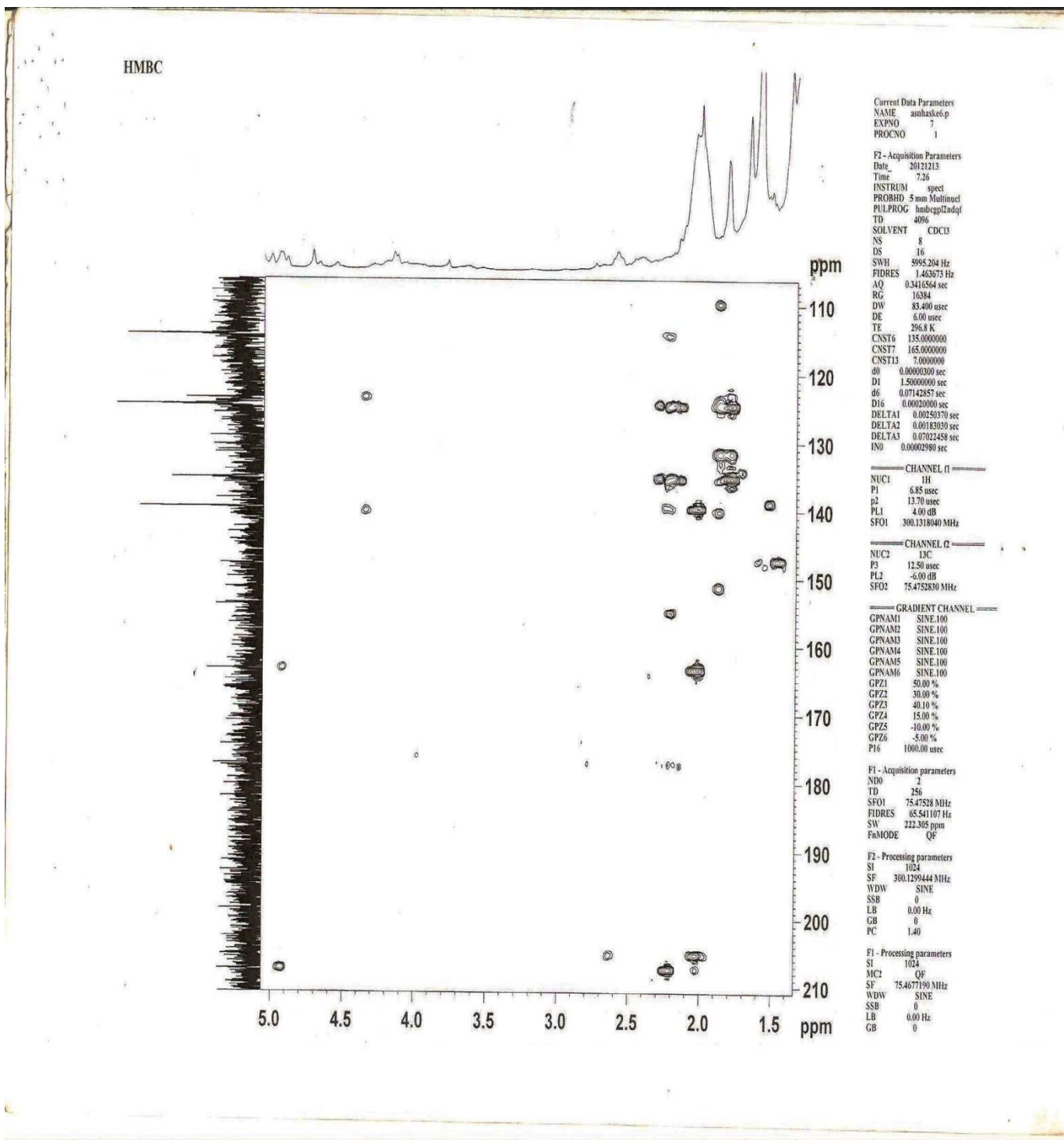


Fig. 4.21 Expanded  $^1\text{H}$ - $^{13}\text{C}$  HMBC spectrum of Haskh-4 in  $\text{CDCl}_3$  (1)

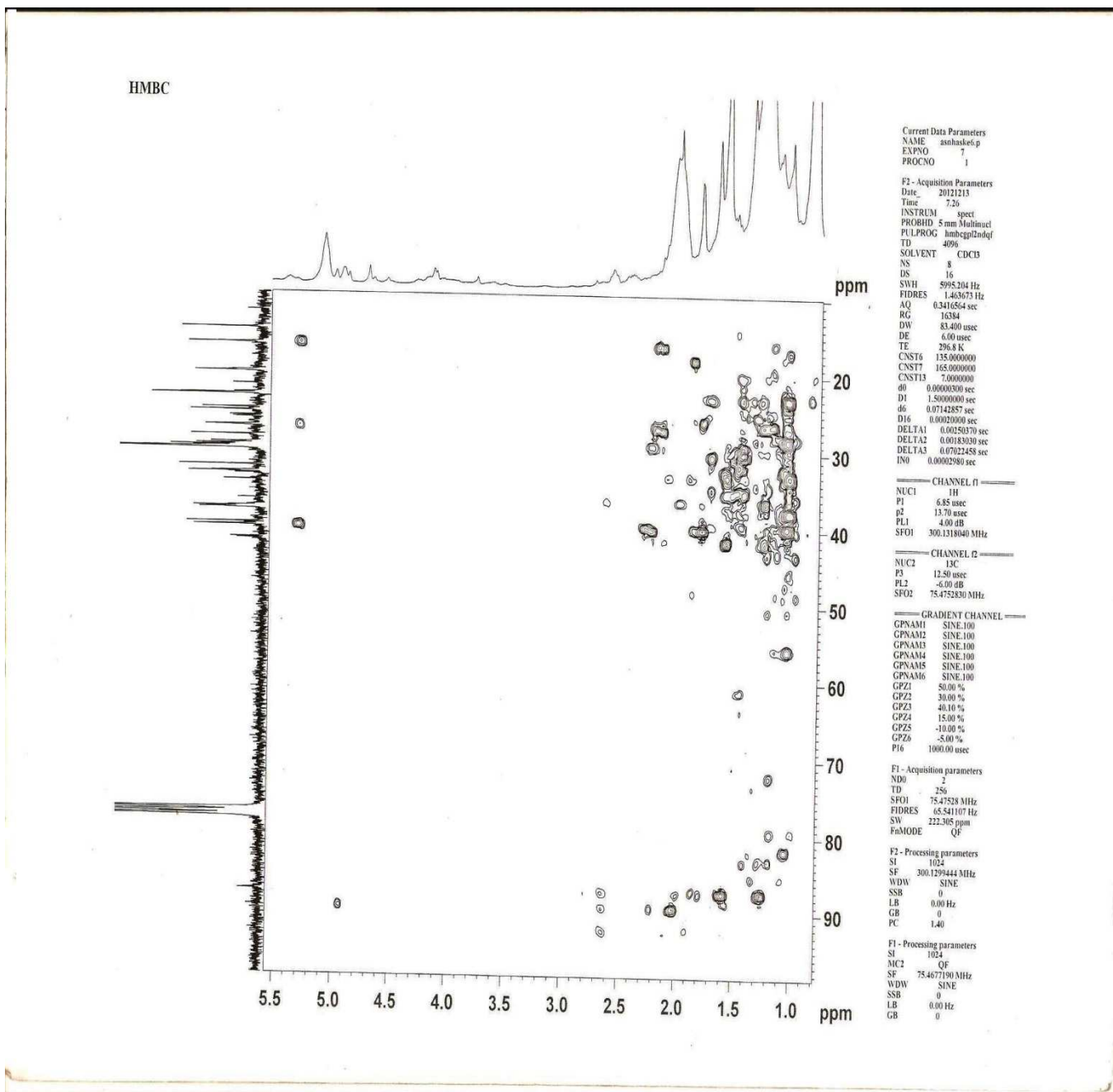


Fig. 4.22 Expanded  $^1\text{H}$ - $^{13}\text{C}$  HMBC spectrum of Haskh-4 in  $\text{CDCl}_3$  (2)

## 4.5 Column chromatography of ethyl acetate extract of *S.kraussiana* (aerial parts)

The ethyl acetate soluble extract (17.0 g) of *S. kraussiana* (aerial parts) was subjected to column chromatography (silica gel) and fractionated with hexane: ethyl acetate to obtain 70 fractions. The fractions were pooled together using TLC analysis to 8 sub-fractions, SKE (1-8). Fractions SKE-2 and SKE-3 were chromatographed on silica gel using appropriate solvent systems, followed by recrystallisation to obtain creamy white solid coded Haske-1 (15 mg); and a white crystalline compound coded Haske-2 (18 mg) and creamy white solid, Haske-3 (35 mg) respectively. The isolation of fractions SKE 5, 6 and 7 using column chromatography, preparative TLC and recrystallization yielded white powdered solid coded Haske-4 (20 mg) and light yellow gelly-like solid, Haske-5 (18 mg); creamy yellow solid, Haske-6 (35 mg) and white solid, Haske-7 (16 mg); and a brown solid coded Haske-8 (30 mg) and cream powdered solid, Haske-9 (80.0 mg) respectively.

### 4.5.1 Characterisation of Haske-1

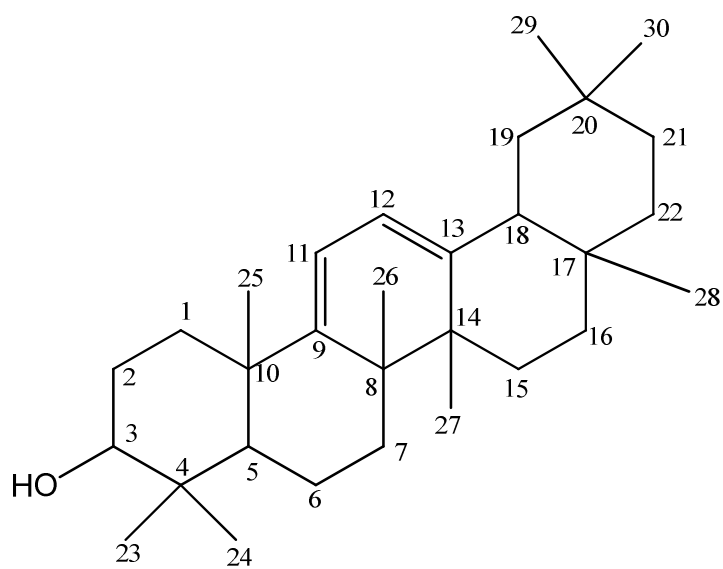
Compound Haske-1 (15.0 mg) is a creamy white solid (melting point 143 - 145°C). The molecular formula  $C_{30}H_{48}O$  (424.3) was obtained from ESI-MS fragment ions 447.3  $[M+Na]^+$ , 463.3  $[M+K]^+$  [Fig. 4.23]. The IR  $\bar{\nu}$  ( $cm^{-1}$ ) vibrational absorptions of O-H, C-H and C=C functions appeared at 3418, 2958 and 1426  $cm^{-1}$  respectively. The  $^1H$  NMR signals at  $\delta_H$  0.82-0.94 (24H, m, 8 x  $CH_3$ ), 1.17-1.40 (18H, m, 9 x  $CH_2$ ) and 1.43-1.61 (2H, bs, 2 x CH) are characteristics of methyl, methylene and methine protons of oleanane triterpenoids. The peaks at  $\delta_H$  3.64 (t) and 5.52 (dd) were attributed to oxymethine proton at C-3 and olefinic protons at C-11 and C-12 respectively [Fig. 4.24].  $^{13}C$  NMR spectrum also indicates resonances consistent with thirty carbon member-oleanane skeleton [Fig. 4.25]. The identified carbon skeleton were eight methyl carbons, nine methylene carbons, five methine carbons and eight quaternary carbon resonances. The spectroscopic data of Haske-1 [Table 4.45] was identical to oleana-9(11),12-dien-3-ol data reported previously (Kobayashi *et al.*, 1981). Hence, the structure of Haske-1 was identified as oleana-9(11),12-dien-3-ol (**104**).

**Table 4.45:**  $^{13}\text{C}$  and  $^1\text{H}$  NMR ( $\text{CDCl}_3$ ) spectra data of Haske-1 and Oleana-9(11),12-dien-3-ol

Assignment	$^{13}\text{C}$	Multiplicity	$^1\text{H}$ ,	* $^{13}\text{C}$
1	38.11	$\text{CH}_2$	1.17-1.40, m, 2H	38.8
2	29.20	$\text{CH}_2$	1.17-1.40, m, 2H	27.9
3	76.64	CH	3.64, t, 1H	78.6
4	38.45	Q	-	38.9
5	63.50	CH	1.43-1.61, bs, 1H	51.2
6	29.76	$\text{CH}_2$	1.17-1.40, m, 2H	18.4
7	32.33	$\text{CH}_2$	1.17-1.40, m, 2H	32.2
8	37.08	Q	-	37.0
9	157.04	Q	-	154.3
10	49.15	Q	-	40.7
11	117.15	CH	5.52, d, 1H	115.8
12	131.21	CH	5.52, d, 1H	120.8
13	147.90	Q	-	147.1
14	41.65	Q	-	42.8
15	34.16	$\text{CH}_2$	1.17-1.40, m, 2H	25.7
16	35.52	$\text{CH}_2$	1.17-1.40, m, 2H	27.3
17	39.56	Q	-	32.2
18	49.34	CH	1.43-1.61, bs, 1H	45.6
19	49.66	$\text{CH}_2$	1.17-1.40, m, 2H	46.9
20	36.18	Q	-	37.2
21	33.74	$\text{CH}_2$	1.17-1.40, m, 2H	34.7
22	32.65	$\text{CH}_2$	1.17-1.40, m, 2H	31.1
23	28.58	$\text{CH}_3$	0.82-0.94, m, 3H	28.8
24	16.67	$\text{CH}_3$	0.82-0.94, m, 3H	15.1
25	17.51	$\text{CH}_3$	0.82-0.94, m, 3H	20.1
26	19.80	$\text{CH}_3$	0.82-0.94, m, 3H	21.0
27	23.01	$\text{CH}_3$	0.82-0.94, m, 3H	25.3
28	23.75	$\text{CH}_3$	0.82-0.94, m, 3H	28.3
29	14.46	$\text{CH}_3$	0.82-0.94, m, 3H	23.7
30	14.90	$\text{CH}_3$	0.82-0.94, m, 3H	15.1

Implied multiplicities of the carbons were determined from the DEPT experiment.

\*Kobayashi *et al.*, (1981).



Oleana-9(11),12-dien-3-ol (104)

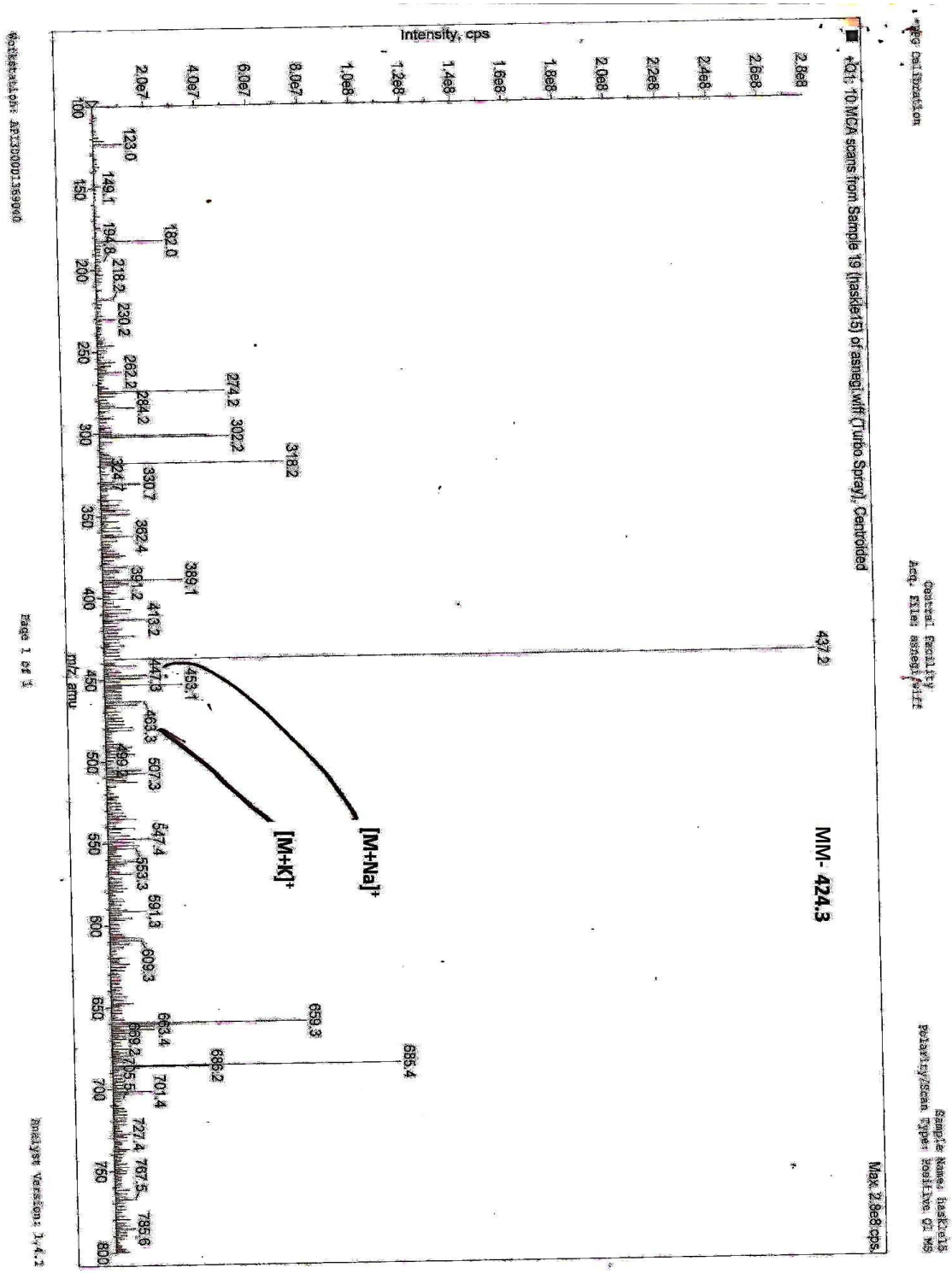


Fig. 4.23 ESI-MS spectrum of Haske-1 in MeOH

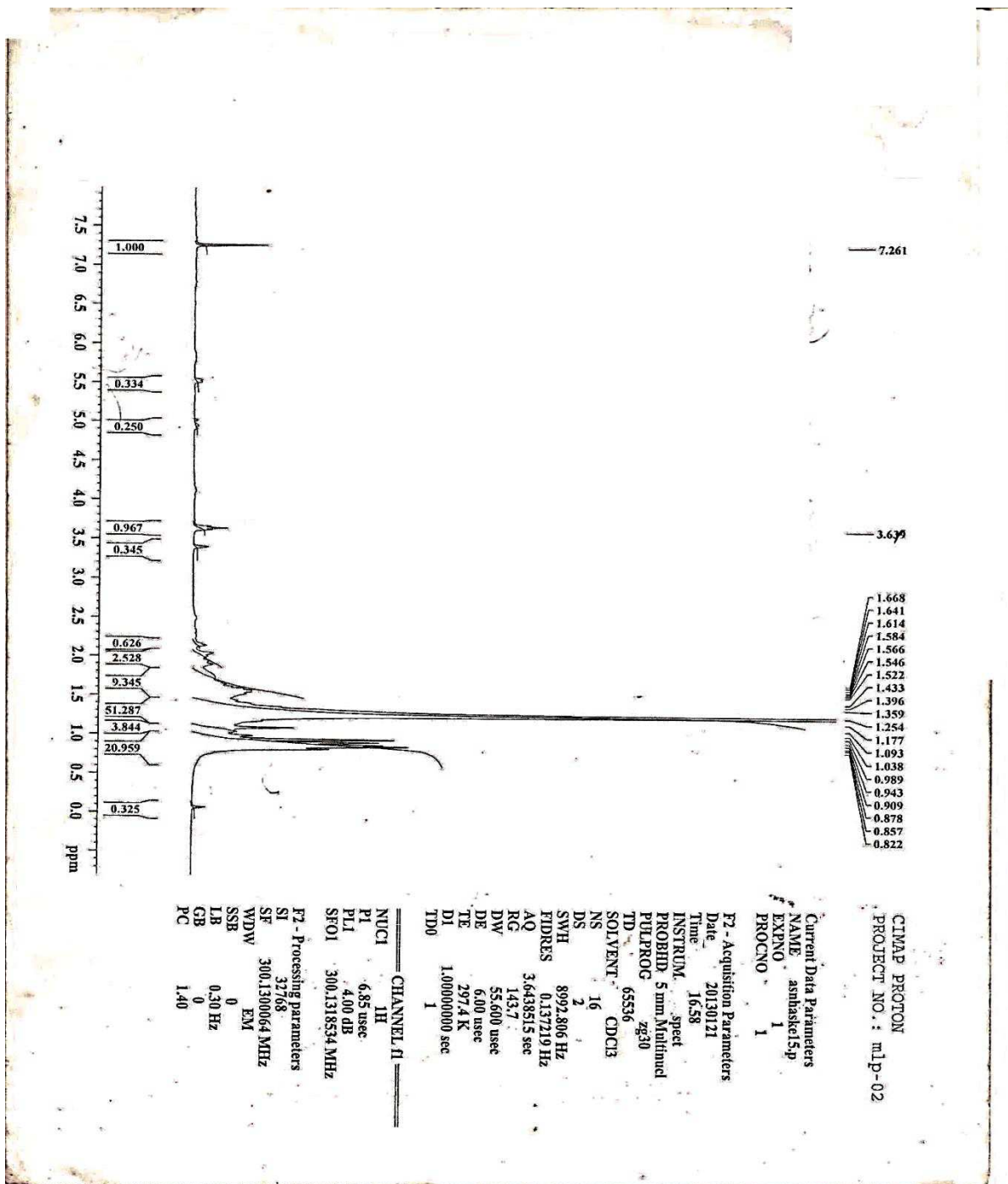


Fig. 4.24  $^1\text{H}$  NMR spectrum of Haske-1 in  $\text{CDCl}_3$

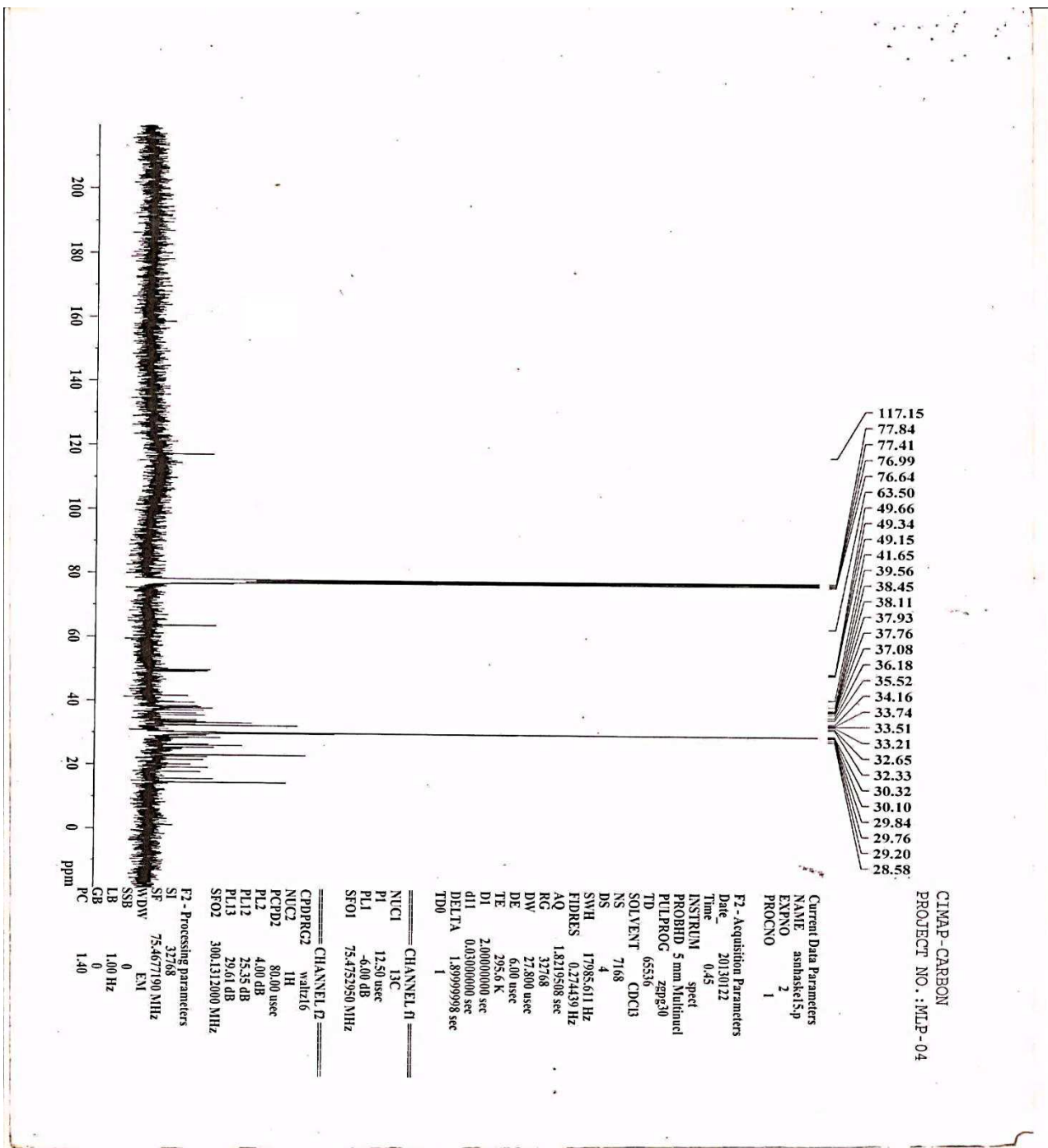


Fig. 4.25  $^{13}\text{C}$  NMR spectrum of Haske-1 in  $\text{CDCl}_3$



COSY

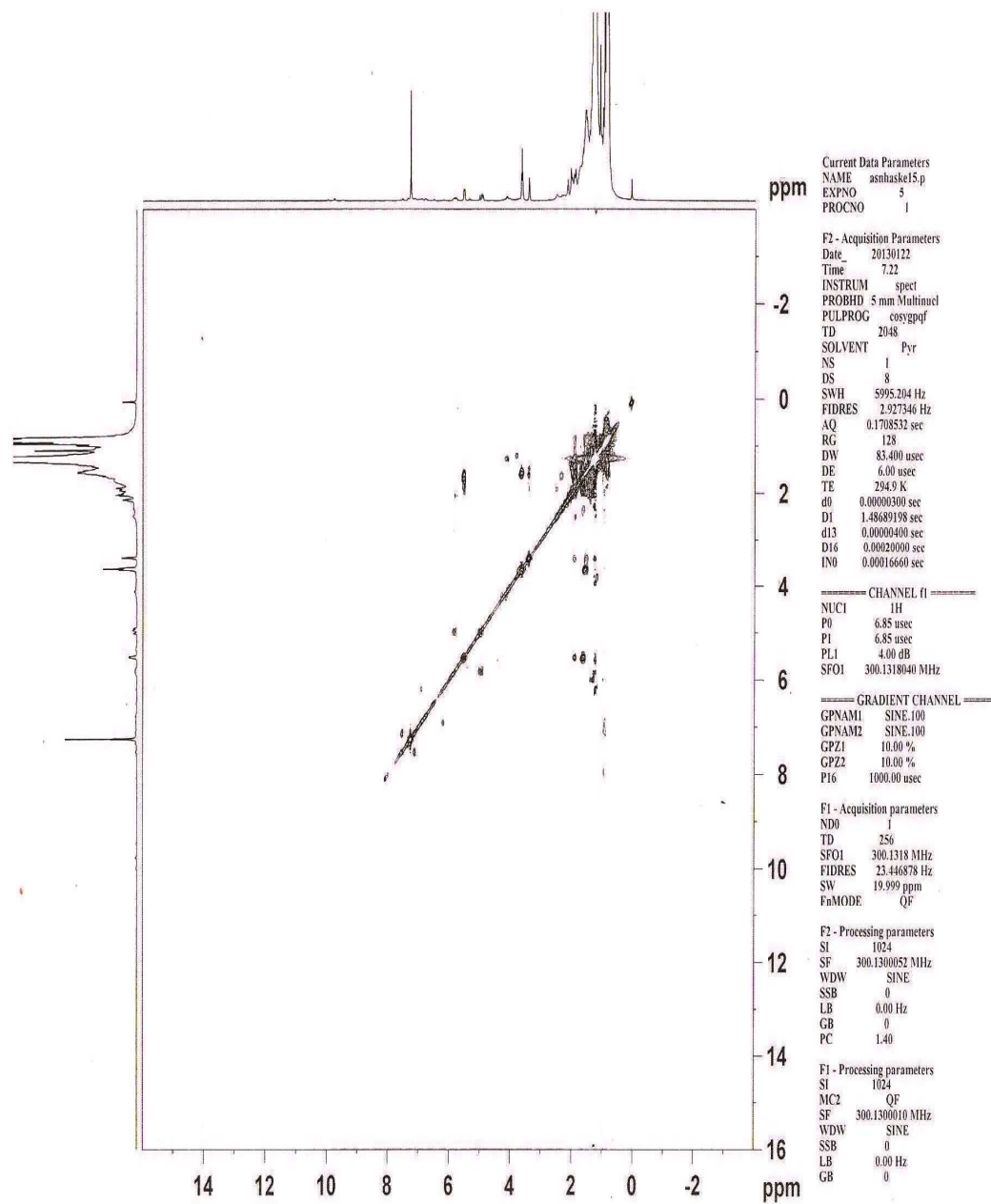


Fig. 4.26  $^1\text{H}$ - $^1\text{H}$  COSY spectrum of Haske-1 in  $\text{CDCl}_3$

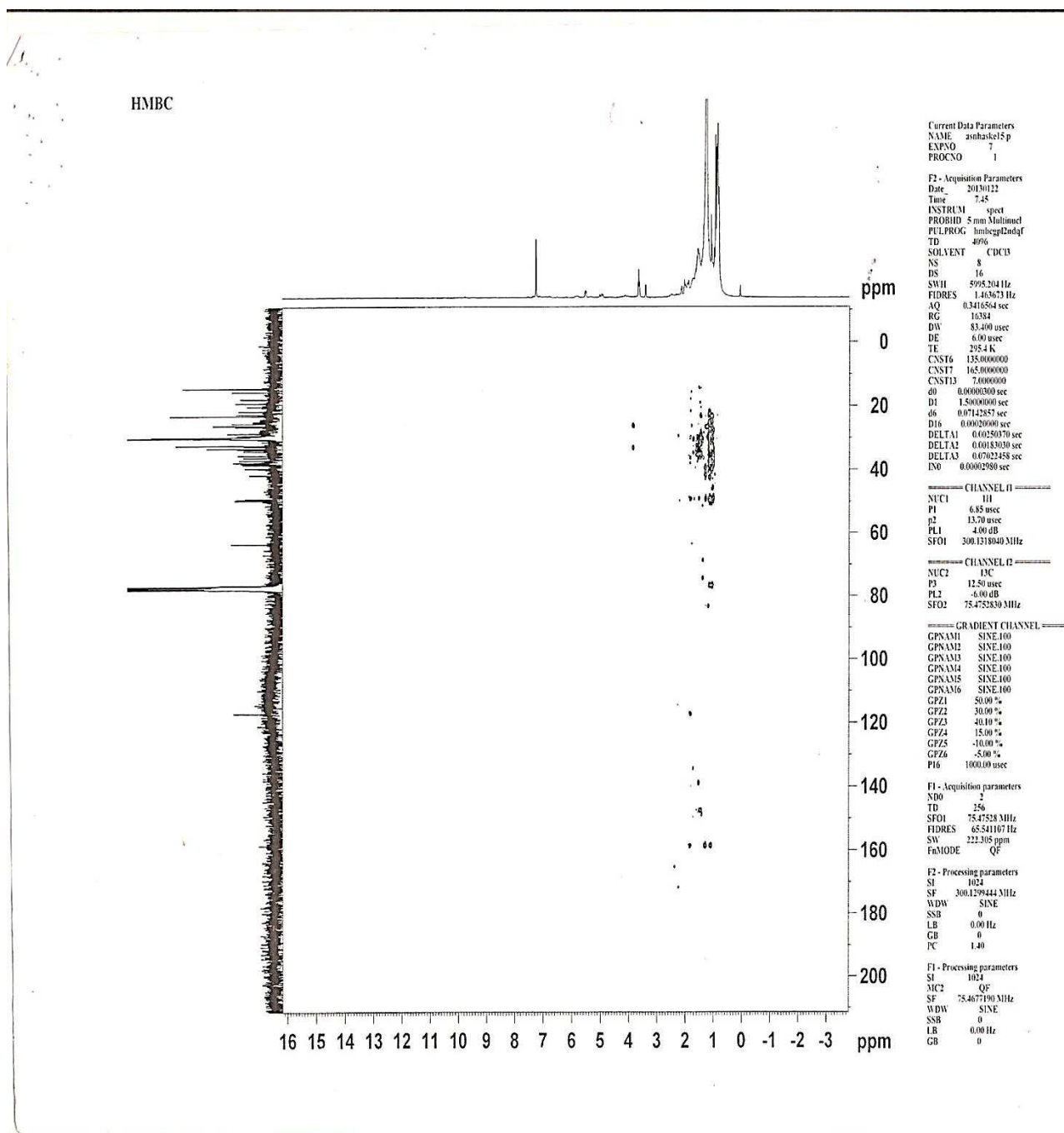


Fig. 4.27  $^1\text{H}$ - $^{13}\text{C}$  HMBC spectrum of Haske-1 in  $\text{CDCl}_3$

#### 4.5.2 Characterisation of Haske-2

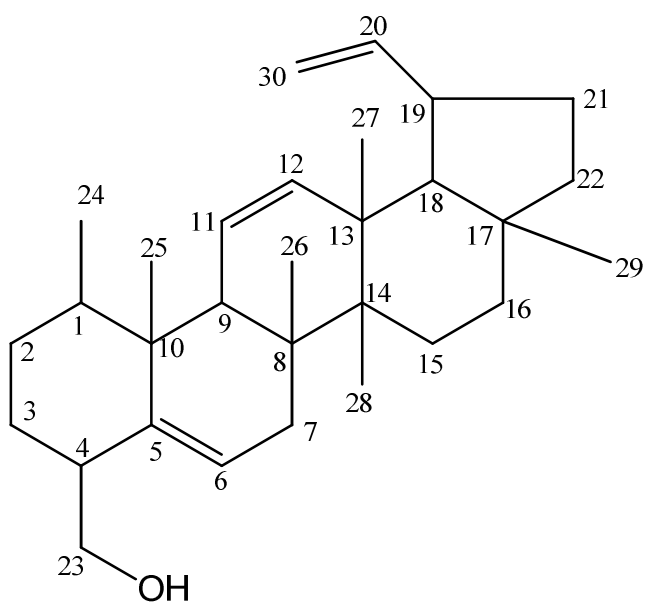
Compound Haske-2 (15.0 mg) was obtained as a white crystalline solid and has a melting point of 205 - 208°C. The Mass fragment ions 447.2 [M+2H+Na]<sup>+</sup>, 484.7 [M+K+Na]<sup>+</sup> gave the molecular formula C<sub>30</sub>H<sub>46</sub>O (422) [Fig. 4.28]. The IR  $\bar{\nu}$  (cm<sup>-1</sup>) absorptions at 3485, 2916, 1604 and 1324 cm<sup>-1</sup> revealed the presence of O-H, C-H, C=C and C-O functions respectively. The signals of <sup>1</sup>H NMR spectrum at  $\delta_H$  0.88-0.90 (6H, m, 2 x CH<sub>3</sub>) and 1.02-1.41 (14H, m, 6CH<sub>2</sub> & 2CH) correspond to cluster of methyl, methylene and methine protons of triterpenoids, while  $\delta_H$  4.16 (d) and 4.19 (d) were attributed to terminal olefinic methylene protons [Fig. 4.29]. The signals at  $\delta_H$  5.10 (m) and 5.43 (t) revealed the presence of olefinic methine protons at C-20 and C-6 respectively. Furthermore, olefinic methine protons at C-11 and C-12 were shown at  $\delta_H$  7.16 (dd) and 7.57 (t).

<sup>13</sup>C NMR experiment showed resonances consistent with Lupane skeleton [Fig. 4.30]. DEPT spectrum [Fig. 4.31] classified the carbons into one oxymethylene carbon, six methyl carbons, eight methylene carbons, nine methine carbons and six quaternary carbon resonances. <sup>1</sup>H-<sup>1</sup>H COSY spectrum [Fig. 4.32] revealed the correlation of oxymethylene protons at C-23 with methine proton at C-6 which confirm the presence of primary hydroxyl at C-23. In <sup>1</sup>H-<sup>13</sup>C HMBC experiment [Fig. 4.35, 4.36 and 4.37], there was correlation of oxymethylene protons at C-23 with C-5 and C-6. Methine proton at C-9 showed correlations with olefinic methine carbons at positions 11 and 12, while methylene protons at C-7 were also correlated with C-5 and C-6. Further, methylene protons at C-22 revealed correlation with C-20. The spectroscopic data of Haske-2 [Table 4.46] was similar to lupane derivatives (Reynolds *et al.*, 1986, Wenkert *et al.*, 1978). Haske-2 was elucidated as Lup-5,11,20(30)-trien-23-ol (**105**).

**Table 4.46:**  $^{13}\text{C}$  and  $^1\text{H}$  NMR ( $\text{CDCl}_3$ ) data of Haske-2

Assignment	$^{13}\text{C}$	Multiplicity	$^1\text{H}$ , multiplicity
1	34.21	CH	1.02-1.41, m, 1H
2	25.19	$\text{CH}_2$	1.02-1.41, m, 2H
3	25.54	$\text{CH}_2$	1.02-1.41, m, 2H
4	40.27	CH	1.50-1.69, t, 1H
5	140.64	Q	-
6	124.84	CH	5.43, t, 1H
7	33.19	$\text{CH}_2$	1.02-1.41, m, 2H
8	37.83	Q	-
9	39.77	CH	2.02-2.16, d, 1H
10	34.91	Q	-
11	124.37	CH	7.16, dd, 1H
12	123.50	CH	7.57, dd, 1H
13	35.26	Q	-
14	33.09	Q	-
15	23.11	$\text{CH}_2$	1.02-1.41, m, 2H
16	29.76	$\text{CH}_2$	1.02-1.41, m, 2H
17	37.07	Q	-
18	31.82	CH	1.02-1.41, s, 1H
19	37.69	CH	2.02-2.16, d, 1H
20	119.50	CH	5.10, m, 1H
21	32.32	$\text{CH}_2$	1.02-1.41, m, 2H
22	24.87	$\text{CH}_2$	1.02-1.41, m, 2H
23	59.80	$\text{CH}_2$	4.16 & 4.19, dd, 2H
24	16.42	$\text{CH}_3$	0.88-0.90, m, 3H
25	20.14	$\text{CH}_3$	0.88-0.90, m, 3H
26	23.08	$\text{CH}_3$	0.88-0.90, m, 3H
27	14.50	$\text{CH}_3$	0.88-0.90, m, 3H
28	30.59	$\text{CH}_3$	0.88-0.90, m, 3H
29	28.37	$\text{CH}_3$	0.88-0.90, m, 3H
30	114.45	$\text{CH}_2$	4.93, d, 2H

Implied multiplicities of the carbons were determined from the DEPT experiment.



Lup-5,11,20(30)-trien-23-ol (105).

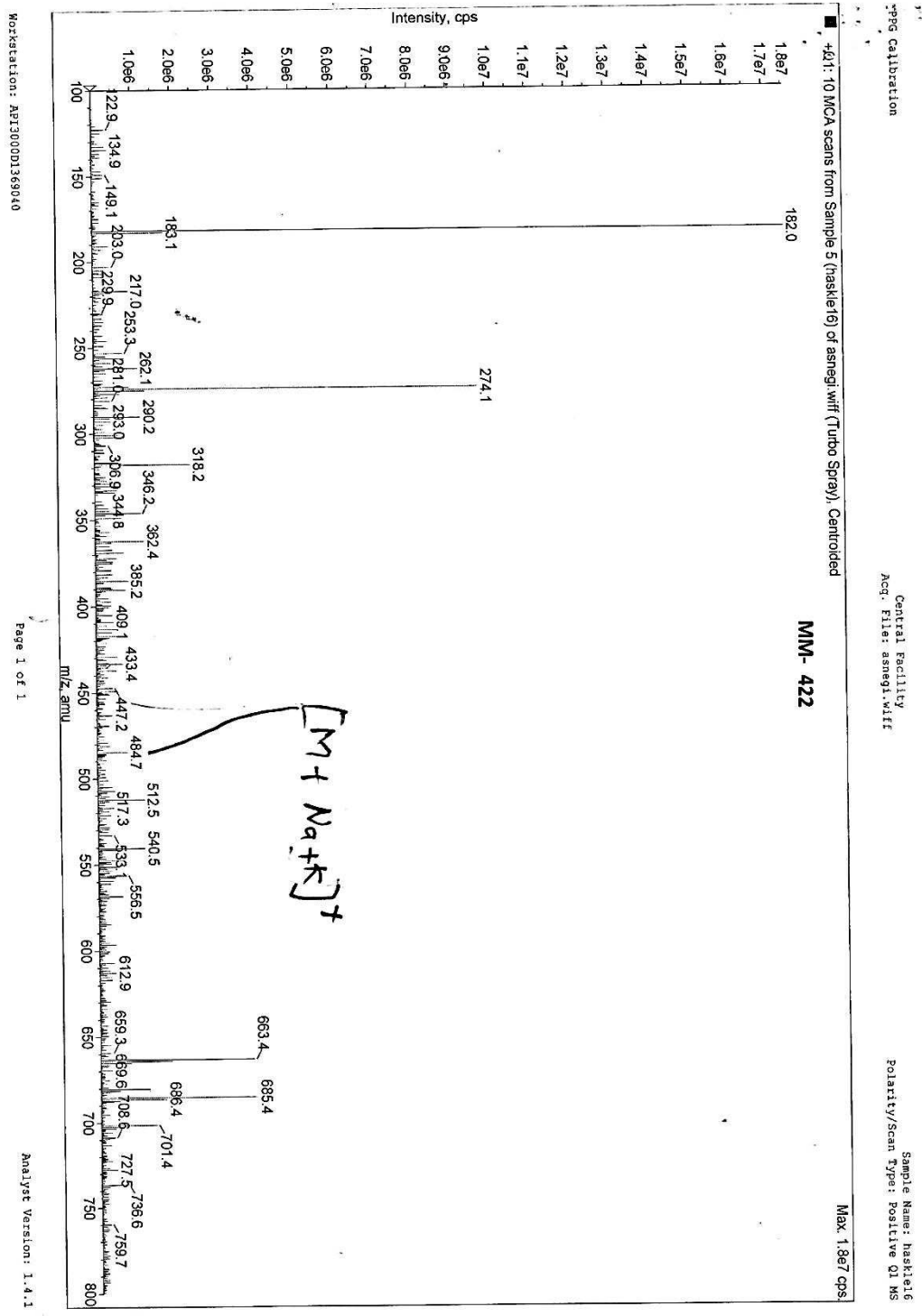


Fig. 4.28 ESI-MS spectrum of Haske-2 in MeOH

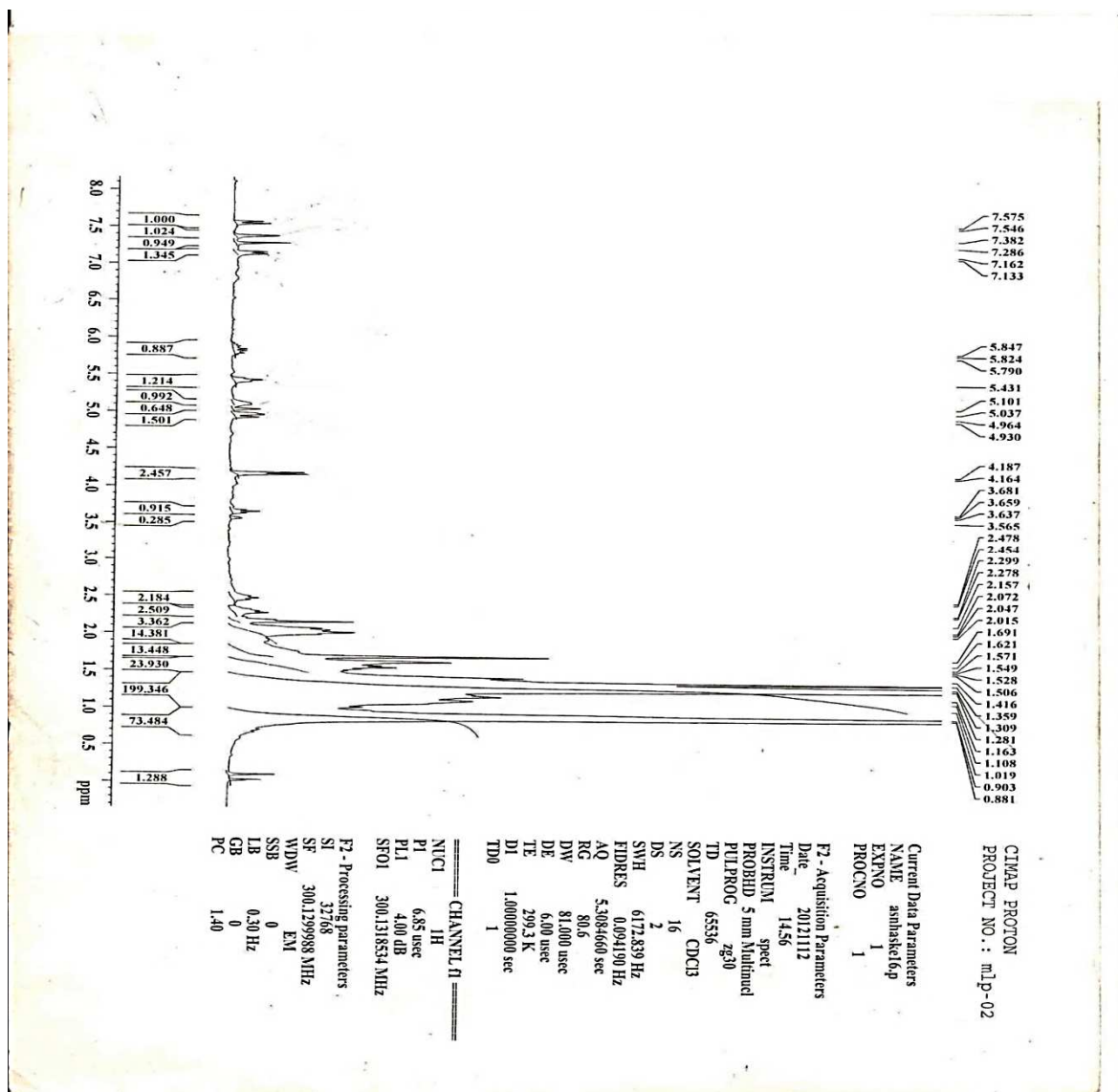


Fig. 4.29 <sup>1</sup>H NMR spectrum of Haske-2 in CDCl<sub>3</sub>

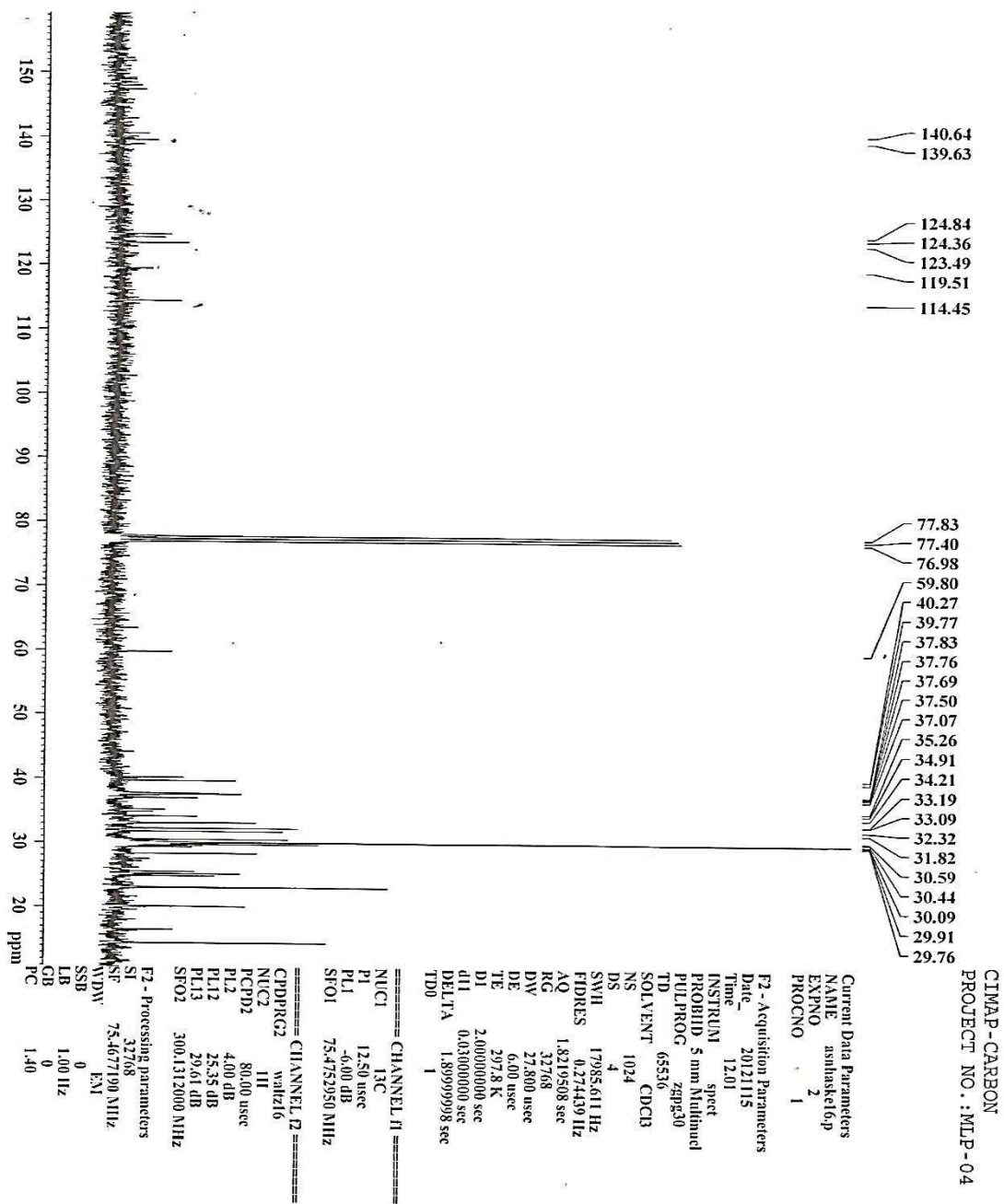


Fig. 4.30  $^{13}\text{C}$  NMR spectrum of Haske-2 in  $\text{CDCl}_3$



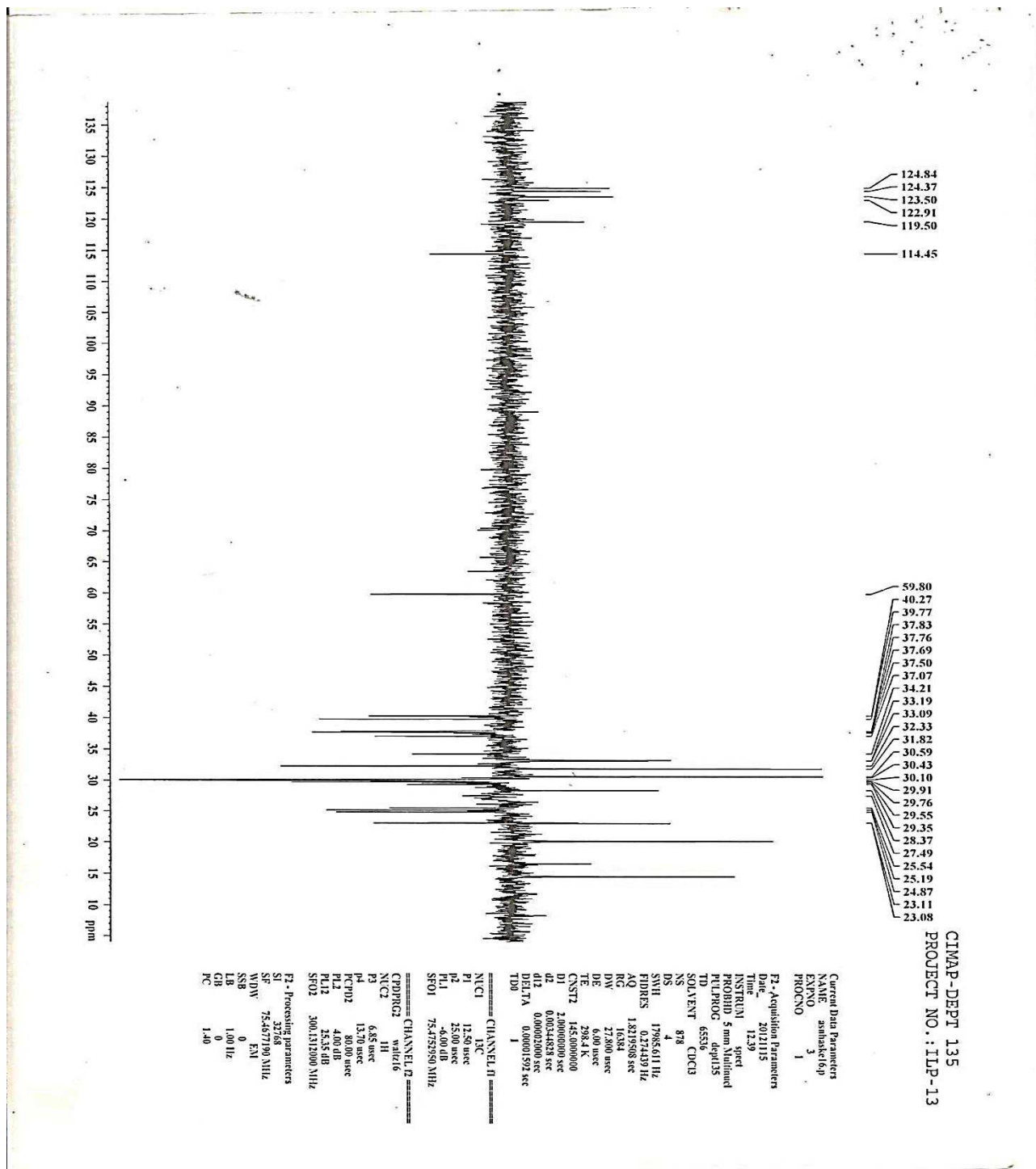


Fig. 4.31 DEPT spectrum of Haske-2 in CDCl<sub>3</sub>

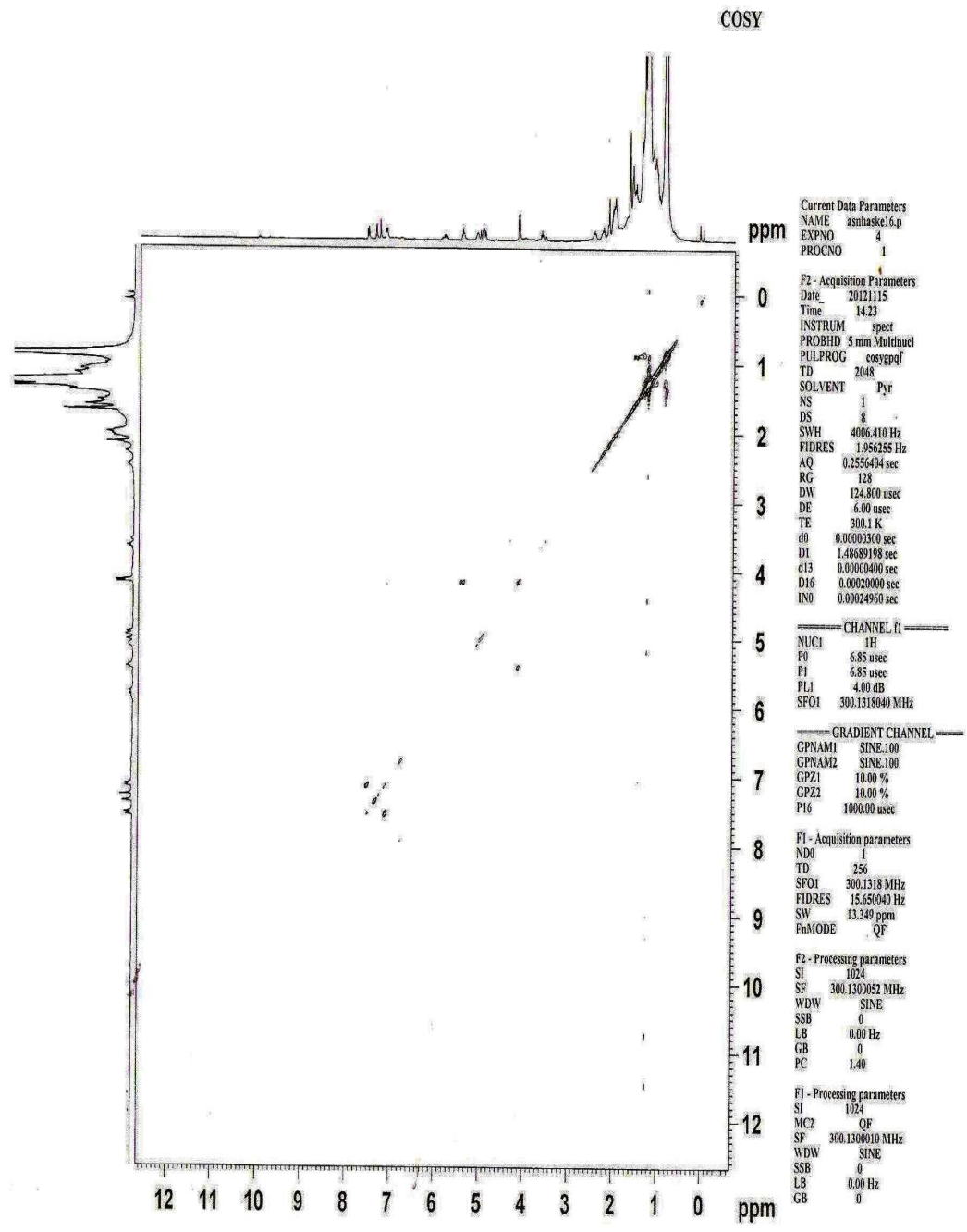
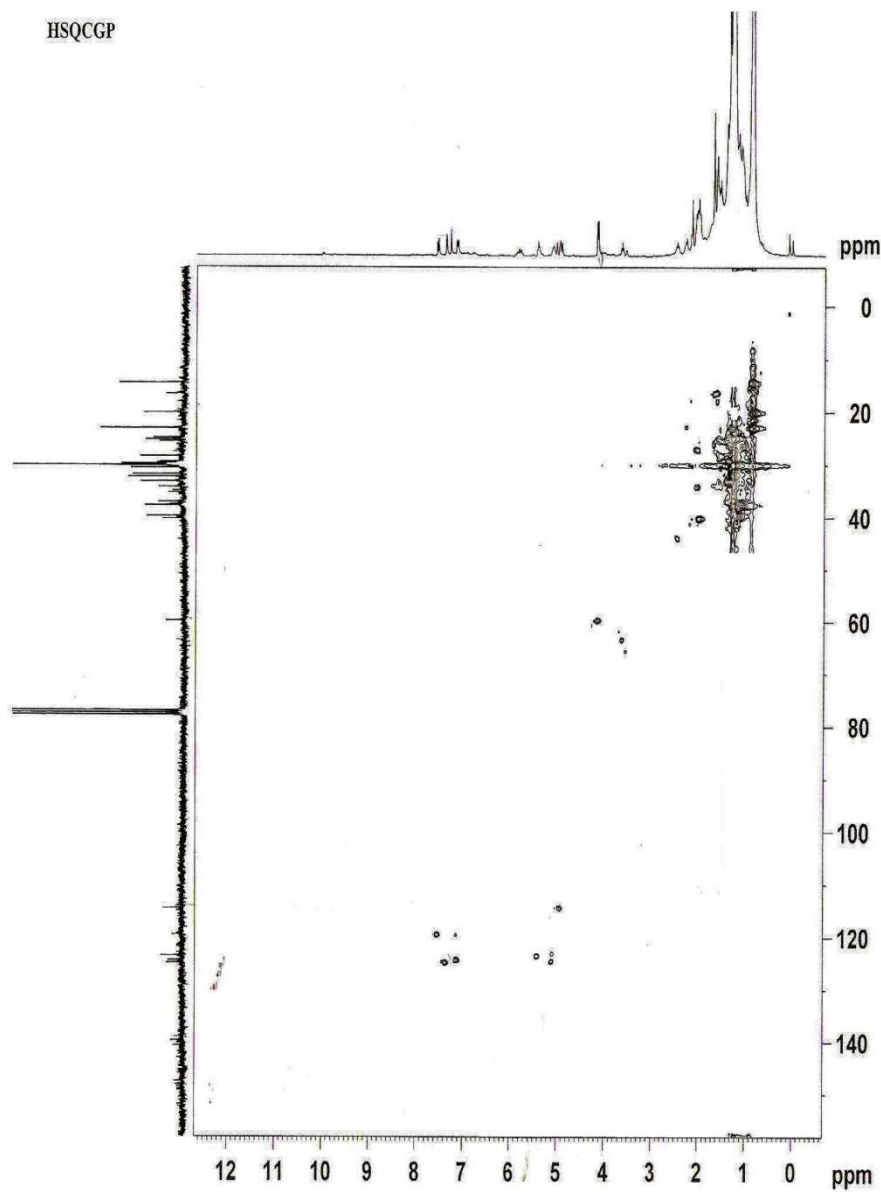


Fig. 4.32  $^1\text{H}$ - $^1\text{H}$  COSY spectrum of Haske-2 in  $\text{CDCl}_3$

HSQCGP



Current Data Parameters  
 NAME asnhaskel6.p  
 EXPNO 5  
 PROCNO 1

F2 - Acquisition Parameters  
 Date\_ 20121115  
 Time 14.34  
 INSTRUM spect  
 PROBHD 5mm Multinauc  
 PULPROG hsqcgpg2  
 TD 1024  
 SOLVENT DMSO  
 NS 2  
 DS 16  
 SWH 4006.410 Hz  
 FIDRES 3.912510 Hz  
 AQ 0.1278452 sec  
 RG 18390.4  
 DW 124.806 usec  
 DE 6.00 usec  
 TE 300.4 K  
 CNST2 145.000000  
 d0 0.0000500 sec  
 d1 1.5000000 sec  
 d4 0.00172414 sec  
 d11 0.03000000 sec  
 d13 0.00000400 sec  
 d16 0.00020000 sec  
 D24 0.0006207 sec  
 DELTA 0.00126970 sec  
 DELTA1 0.00120800 sec  
 DELTA2 0.00062070 sec  
 DELTA3 0.00023414 sec  
 INO 0.00004000 sec  
 STICNT 128  
 ZGPGTNS

CHANNEL 01  
 NUC1 1H  
 P1 6.85 usec  
 PL 13.70 usec  
 P2 1000.00 usec  
 PL1 4.00 dB  
 SFO1 300.1318040 MHz

CHANNEL 02  
 CPDPRG2 gprp  
 NUC2 13C  
 P3 12.50 usec  
 PL 25.00 usec  
 PCPD2 76.00 usec  
 PL1 -6.00 dB  
 PL12 8.00 dB  
 SFO2 75.4734070 MHz

GRADIENT CHANNEL  
 GPNAM1 SINE.100  
 GPNAM2 SINE.100  
 GPNAM3 SINE.100  
 GPNAM4 SINE.100  
 GFZ1 80.00 %  
 GFZ2 20.10 %  
 GFZ3 11.00 %  
 GFZ4 -5.00 %  
 P16 1000.00 usec  
 P19 600.00 usec

F1 - Acquisition parameters  
 ND0 2  
 TD 256  
 SFO1 75.47341 MHz  
 FIDRES 48.828125 Hz  
 SW 165.621 ppm  
 FMODE Echo-Antiecho

F1 - Processing parameters  
 SI 1024  
 SF 300.1300000 MHz  
 WDW QSINE  
 SSB 2  
 LB 0.00 Hz  
 GB 0  
 PC 1.40

F1 - Processing parameters  
 SI 1024  
 MC2 echo-antiecho  
 SF 75.4677190 MHz  
 WDW QSINE  
 SSB 2  
 LB 0.00 Hz  
 GB 0

Fig. 4.33 HSQC spectrum of Haske-2 in CDCl<sub>3</sub>

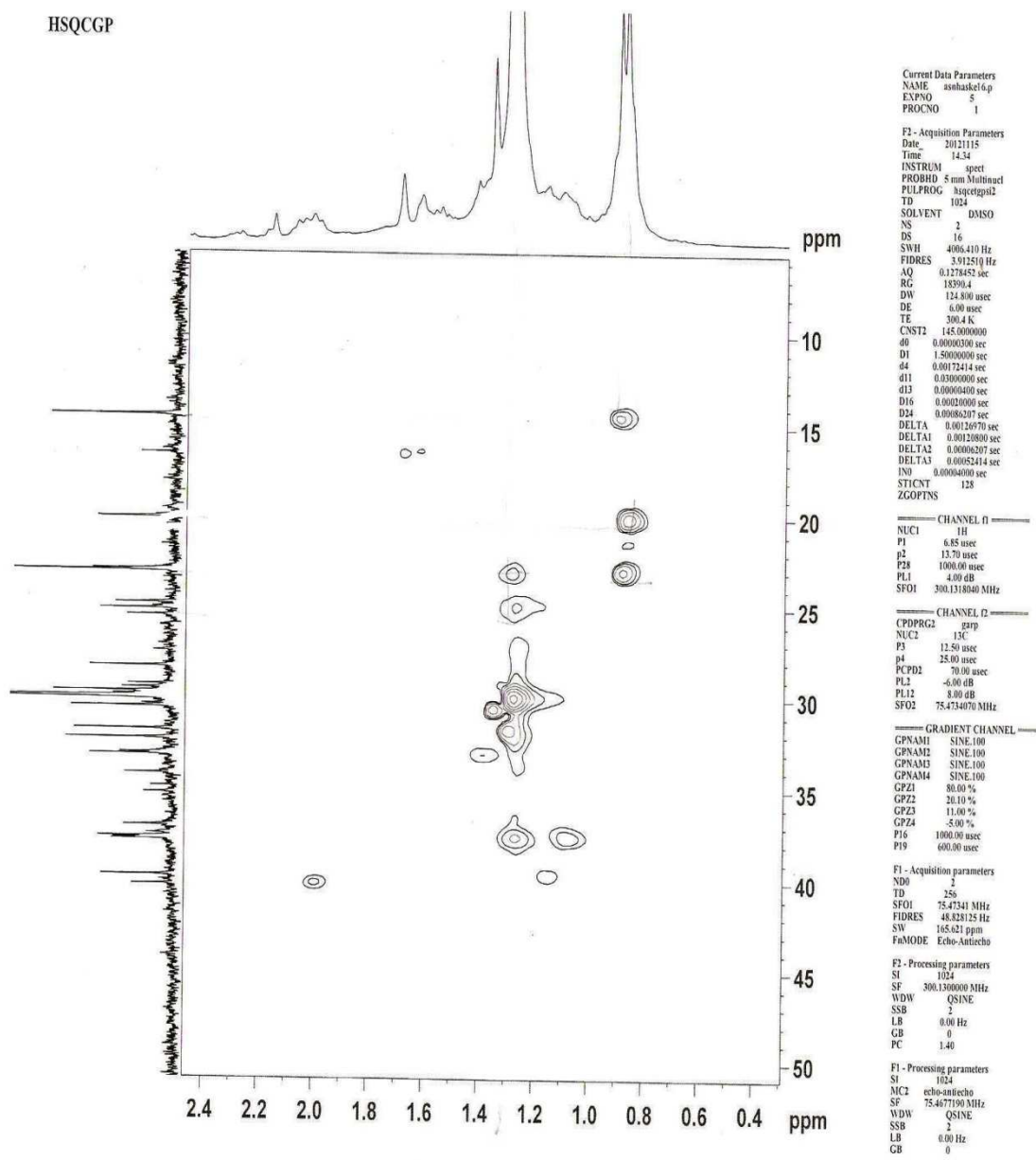


Fig. 4.34 Expanded HSQC spectrum of Haske-2 in  $CDCl_3$

HMBC

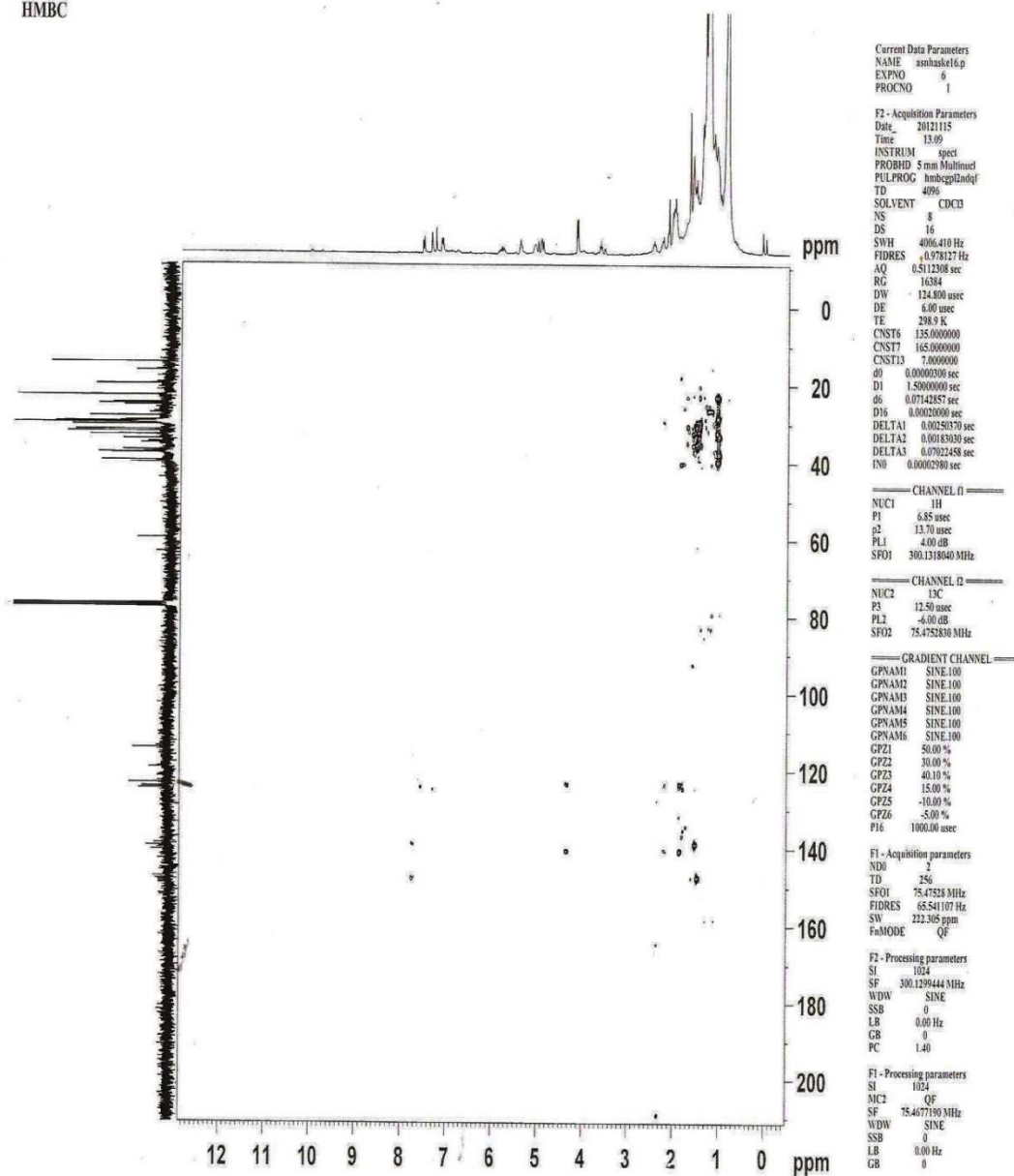


Fig. 4.35  $^1\text{H}$ - $^{13}\text{C}$  HMBC spectrum of Haske-2 in  $\text{CDCl}_3$

HMBC

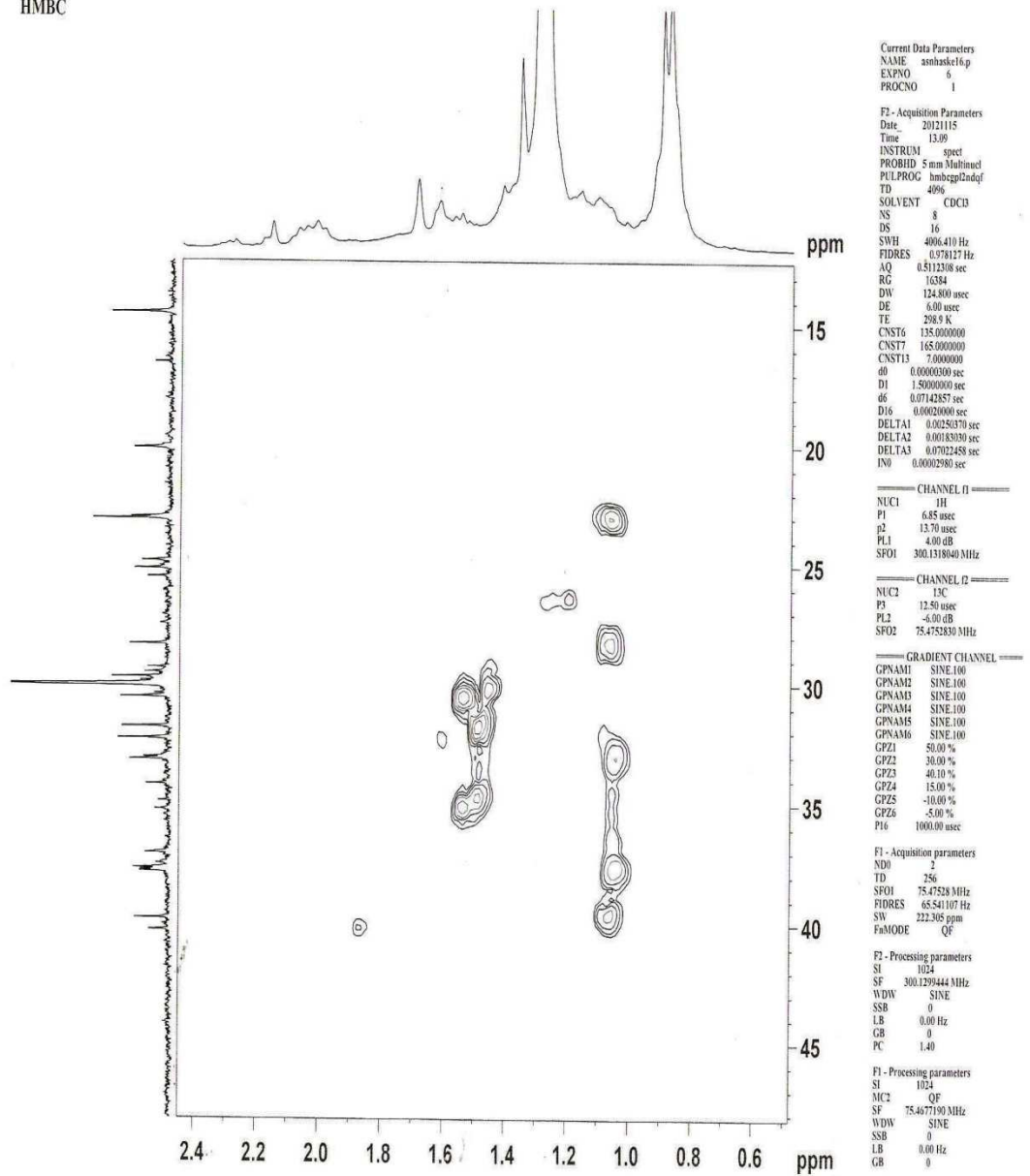


Fig. 4.36 Expanded  $^1\text{H}$ - $^{13}\text{C}$  HMBC spectrum of Haske-2 in  $\text{CDCl}_3$  (1)

HMBC

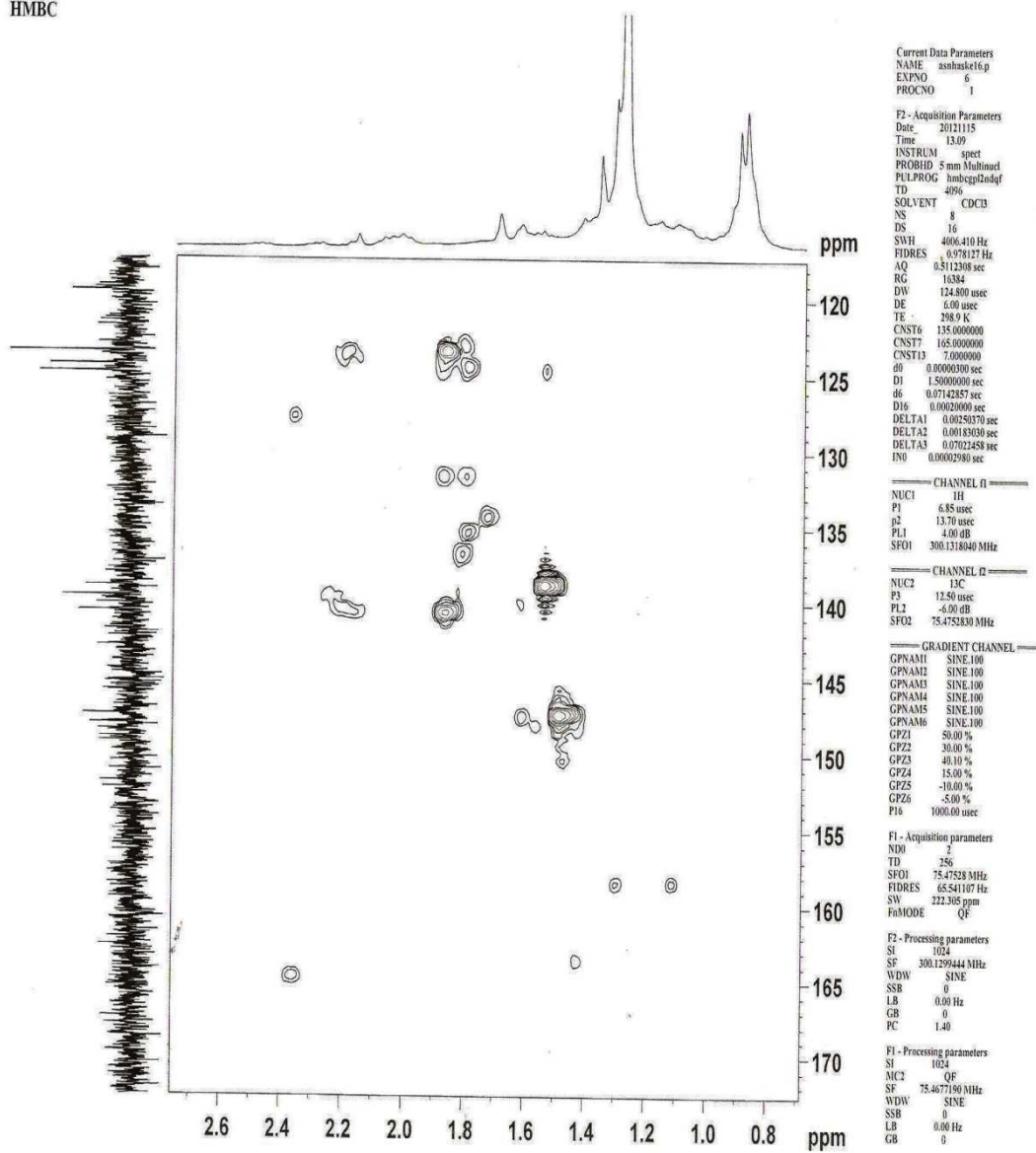


Fig. 4.37 Expanded  $^1\text{H}$ - $^{13}\text{C}$  HMBC spectrum of Haske-2 in  $\text{CDCl}_3$  (2)

### 4.5.3 Characterisation of Haske-3

Compound Haske-3 (35.0 mg) appeared as a white solid with a melting point of 123 - 126°C. The molecular formula C<sub>29</sub>H<sub>50</sub>O (414.3) was revealed by ESI MS fragment ions 182.1, 437.3 [M+Na]<sup>+</sup>, 453.1 [M+K]<sup>+</sup> [Fig. 4.38]. The IR  $\bar{\nu}$  (cm<sup>-1</sup>) absorptions at 3419, 2953, 1523 and 1326 cm<sup>-1</sup> correspond to the presence of O-H, C-H, C=C and C-O moieties respectively. The signals of <sup>1</sup>H NMR spectrum at  $\delta_{\text{H}}$  0.49-0.70 (6H, m, 2 x CH<sub>3</sub>) and 0.82-1.67 (18H, m, 9CH<sub>2</sub>) are characteristics of cluster of methyl and methylene protons of Stigmastane, while  $\delta_{\text{H}}$  2.02 (t) and 2.28 (d) were attributed to methylene protons at C-7 and C-4 respectively [Fig. 4.39]. The signals at  $\delta_{\text{H}}$  3.53 (m) and 5.36 (t) revealed the presence of oxymethine and olefinic methine protons at C-3 and C-6 respectively. <sup>13</sup>C NMR experiment showed resonances similar to stigmastane skeleton [Fig. 4.40]. There are twenty nine carbon resonances which were sorted by DEPT experiment [Fig. 4.41] into one oxymethine, six methyl, eleven methylene, eight methine and three quaternary carbon resonances. The signals at  $\delta_{\text{C}}$  71.58 (m), 121.57 (t) and 140.75 (m) were due to the presence of oxymethine carbon at C-3 and olefinic carbons at C-5 and C-6.

<sup>1</sup>H-<sup>1</sup>H COSY spectrum [Fig. 4.42] revealed the correlation of oxymethine proton at C-3 with methylene protons at C-2 and C-4, while olefinic methine proton at C-6 was correlated with methylene protons at C-7. The HSQC spectrum (Fig. 4.43 and 4.44) showed that methine protons at  $\delta_{\text{H}}$  3.53 (1H, m, H<sub>3</sub>) and 5.36 (1H, t, H<sub>6</sub>) were bonded to carbons at  $\delta_{\text{C}}$  71.58 (C-3), 121.57 (C-6) respectively. In <sup>1</sup>H-<sup>13</sup>C HMBC experiment [Fig. 4.45 and 4.46], there was correlation of methine proton at C-6 with C-4, C-7 and C-8. Methylene protons at C-1, C-2, C-4 and C-7 showed correlations with oxymethine carbon at C-3, while methylene protons at C-7 were also correlated with olefinic carbons C-5 and C-6. Further, methylene protons at C-4 also revealed correlation with C-5 and C-6. The spectroscopic data of Haske-3 [Table 4.47] was similar to stigmast-5-en-3-ol (Chaturvedula and Prakash, 2012, Jamal *et al.*, 2009, Jain and Bari, 2010, Habib *et al.*, 2007). Hence, Haske-3 was identified as Stigmast-5-en-3-ol ( $\beta$ -sitosterol) (**106**).

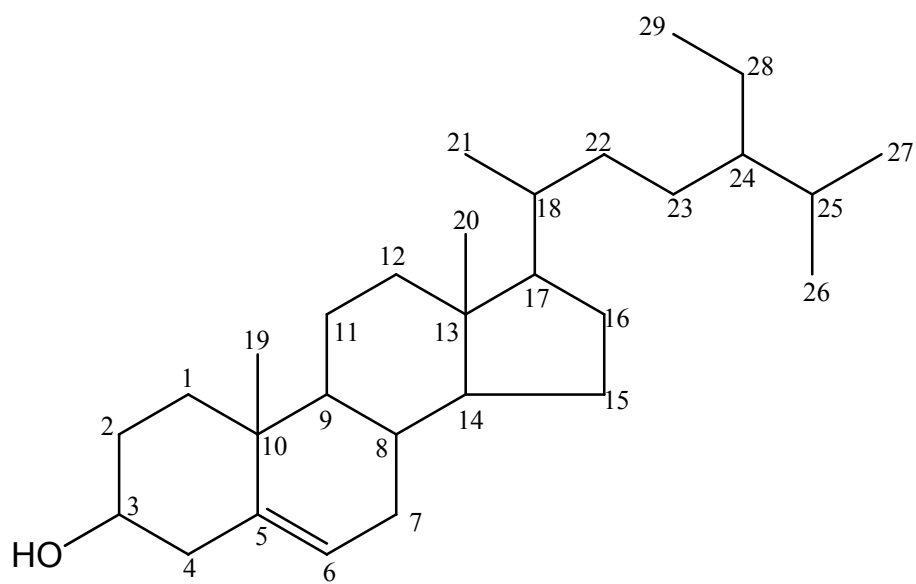


**Table 4.47:**  $^{13}\text{C}$  and  $^1\text{H}$  NMR ( $\text{CDCl}_3$ ) spectra data of Haske-3 and  $\beta$ -sitosterol

Assignment	$^{13}\text{C}$	Multiplicity	$^1\text{H}$	$^1\text{H}$	$^{13}\text{C}$
1	37.26	$\text{CH}_2$	0.82-1.67, m, 2H	1.47	37.5
2	31.38	$\text{CH}_2$	0.82-1.67, m, 2H	1.56	31.9
3	71.58	CH	3.53, m, 1H	3.52	72.0
4	42.24	$\text{CH}_2$	2.28, d, 2H	2.28	42.4
5	140.75	Q	-	-	140.9
6	121.57	CH	5.36, t, 1H	5.36	121.9
7	29.67	$\text{CH}_2$	2.02, t, 2H	2.03	32.1
8	45.82	CH	1.69-2.02, m, 1H	1.67	32.1
9	50.14	CH	1.69-2.02, m, 1H	1.48	50.3
10	36.46	Q	-	-	36.1
11	21.06	$\text{CH}_2$	0.82-1.67, m, 2H	1.52	21.3
12	23.05	$\text{CH}_2$	0.82-1.67, m, 2H	1.49	39.9
13	39.77	Q	-	-	42.6
14	56.07	CH	1.69-2.02, m, 1H	1.50	56.9
15	22.65	$\text{CH}_2$	0.82-1.67, m, 2H	1.60	26.3
16	28.21	$\text{CH}_2$	0.82-1.67, m, 2H	1.84	28.5
17	56.75	CH	1.69-2.02, m, 1H	1.49	56.3
18	36.11	CH	1.69-2.02, m, 1H	1.64	36.3
19	11.81	$\text{CH}_3$	0.49-0.70, m, 3H	0.68	19.2
20	11.93	$\text{CH}_3$	0.49-0.70, m, 3H	1.02	12.2
21	14.06	$\text{CH}_3$	0.49-0.70, m, 3H	0.94	12.0
22	24.26	$\text{CH}_2$	0.82-1.67, m, 2H	0.88	34.2
23	26.12	$\text{CH}_2$	0.82-1.67, m, 2H	1.04	26.3
24	33.93	CH	1.69-2.02, m, 1H	1.50	46.1
25	29.16	CH	1.69-2.02, m, 1H	1.65	29.4
26	19.03	$\text{CH}_3$	0.49-0.70, m, 3H	0.83	20.1
27	18.75	$\text{CH}_3$	0.49-0.70, m, 3H	0.85	19.6
28	19.76	$\text{CH}_2$	0.82-1.67, m, 2H	1.04	19.0
29	19.34	$\text{CH}_3$	0.49-0.70, m, 3H	0.88	23.3

Implied multiplicities of the carbons were determined from the DEPT experiment.

\* Chaturvedula and Prakash, 2012



$\beta$ -sitosterol (106)

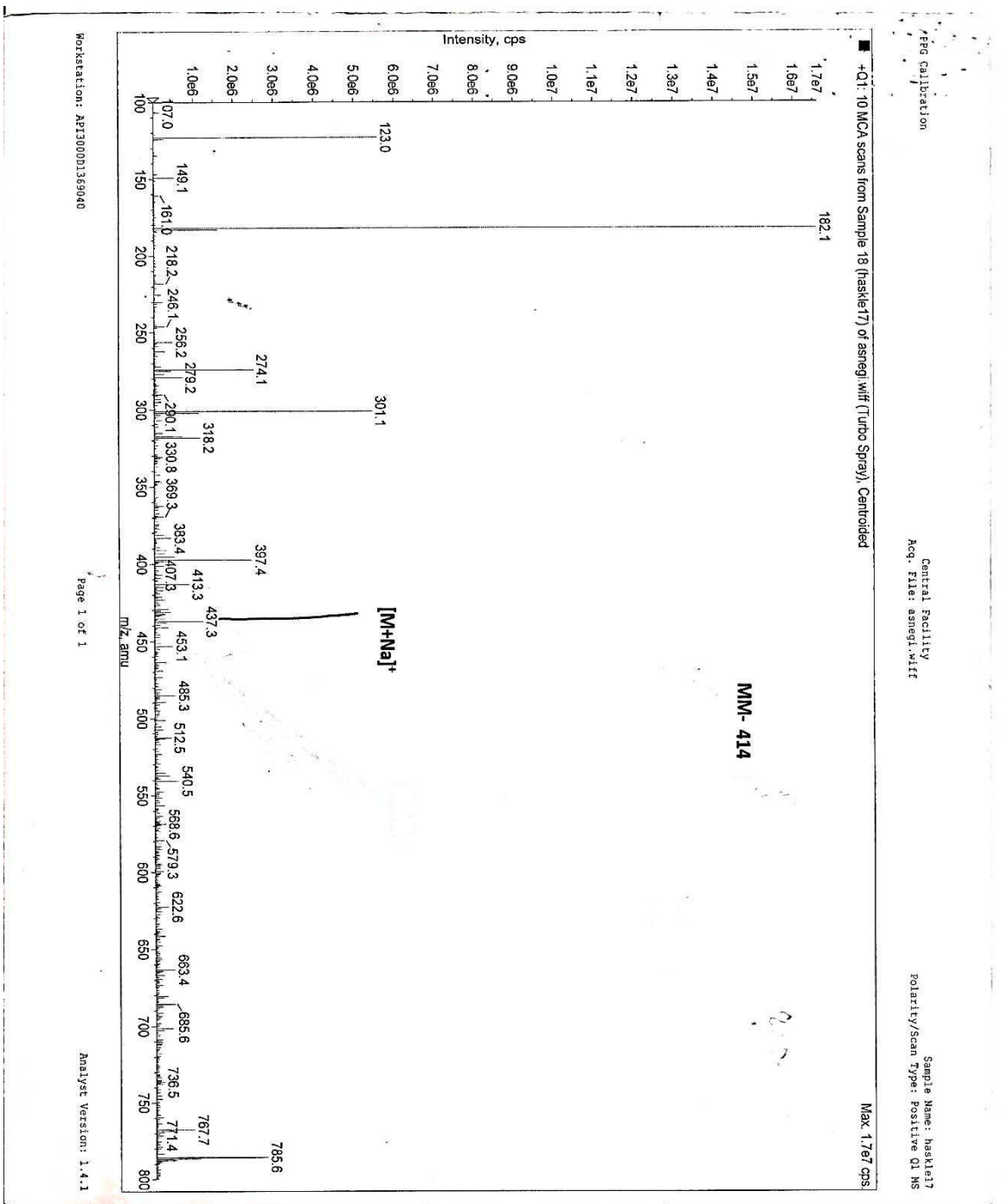


Fig. 4.38 ESI MS spectrum of Haske-3 in MeOH

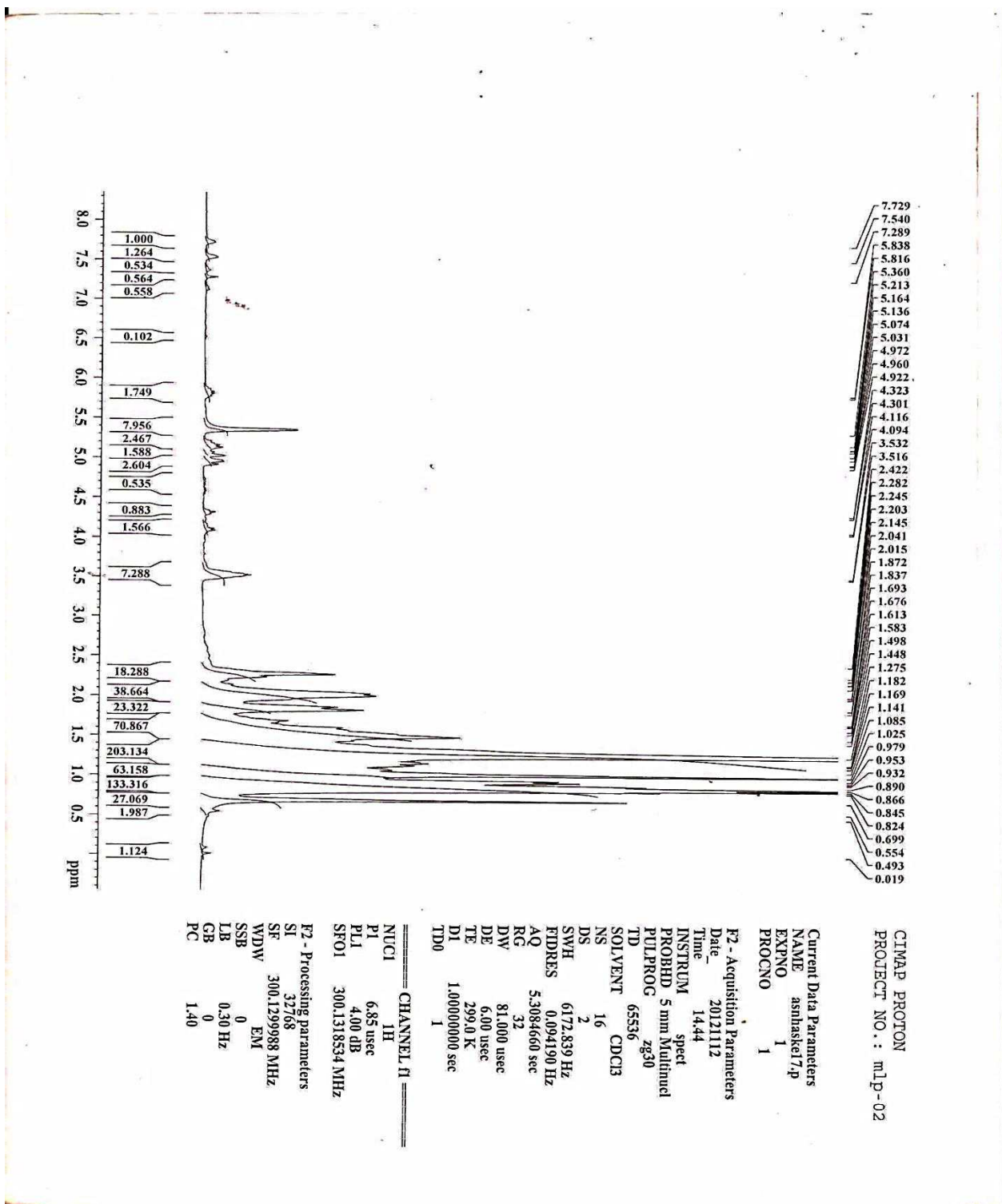


Fig. 4.39  $^1\text{H}$  NMR spectrum of Haske-3 in  $\text{CDCl}_3$

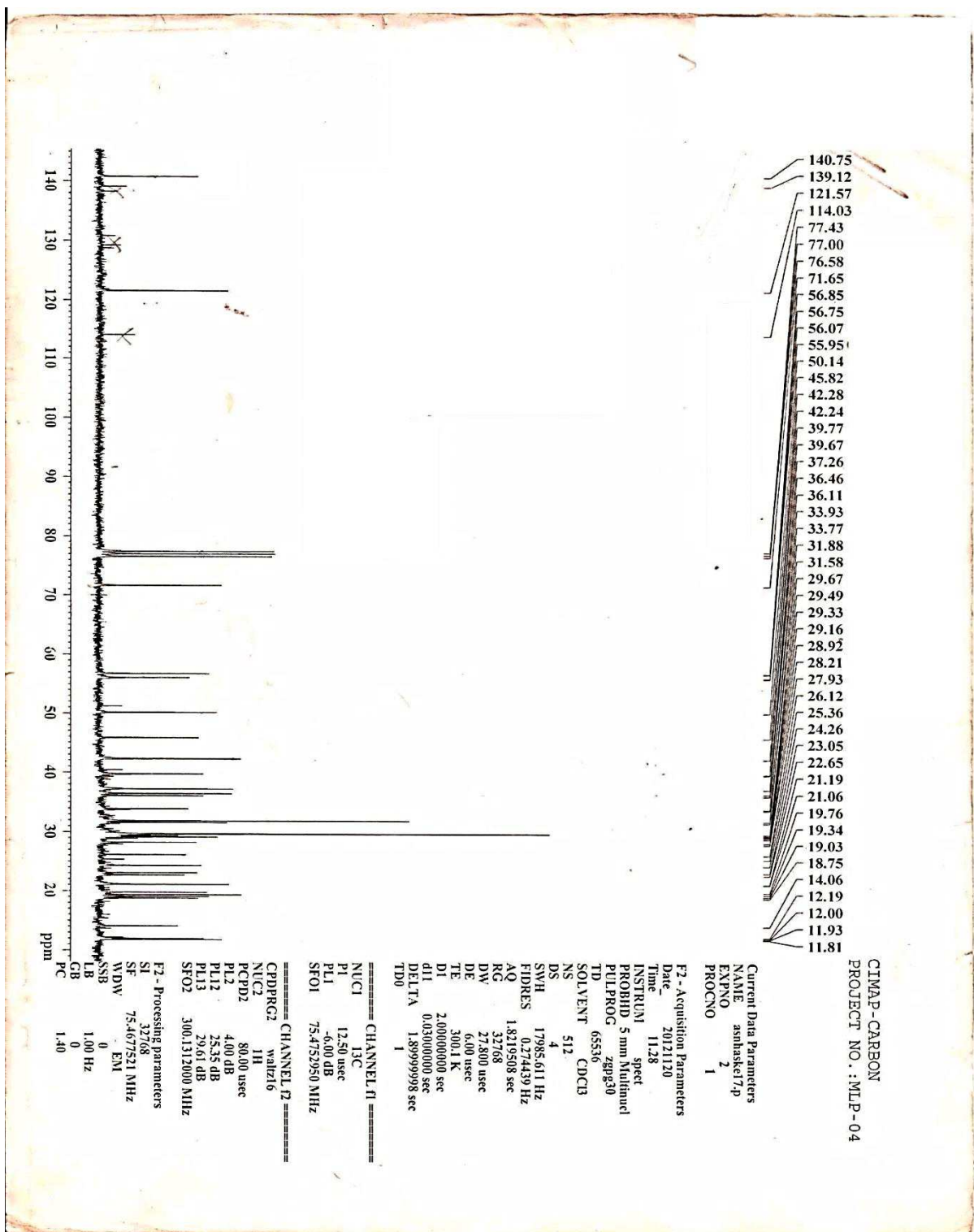


Fig. 4.40 <sup>13</sup>C NMR spectrum of Haske-3 in CDCl<sub>3</sub>

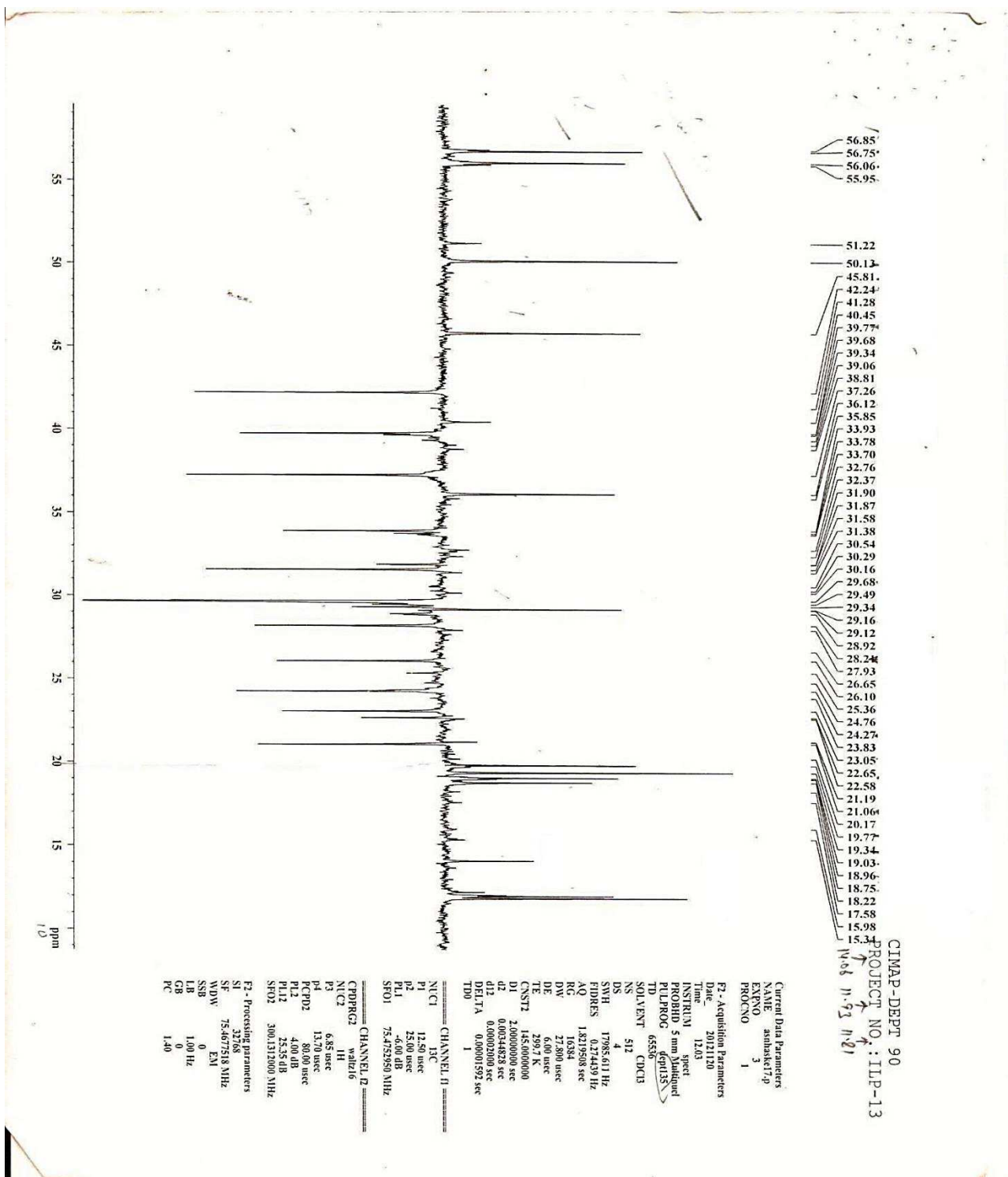


Fig. 4.41 DEPT spectrum of Haske-3 in CDCl<sub>3</sub>

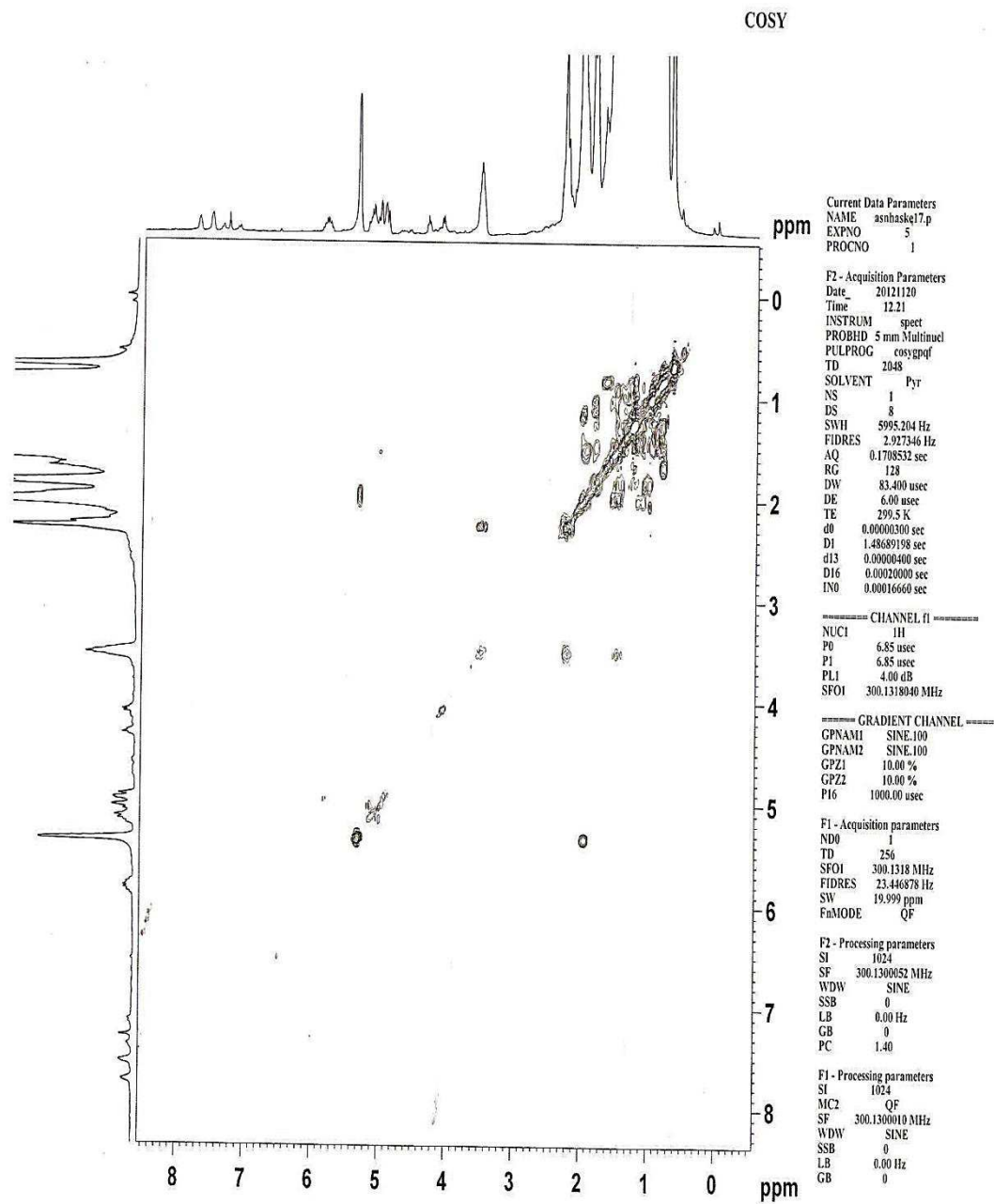


Fig. 4.42  $^1\text{H}$ - $^1\text{H}$  COSY spectrum of Haske-3 in  $\text{CDCl}_3$

HSQCGP

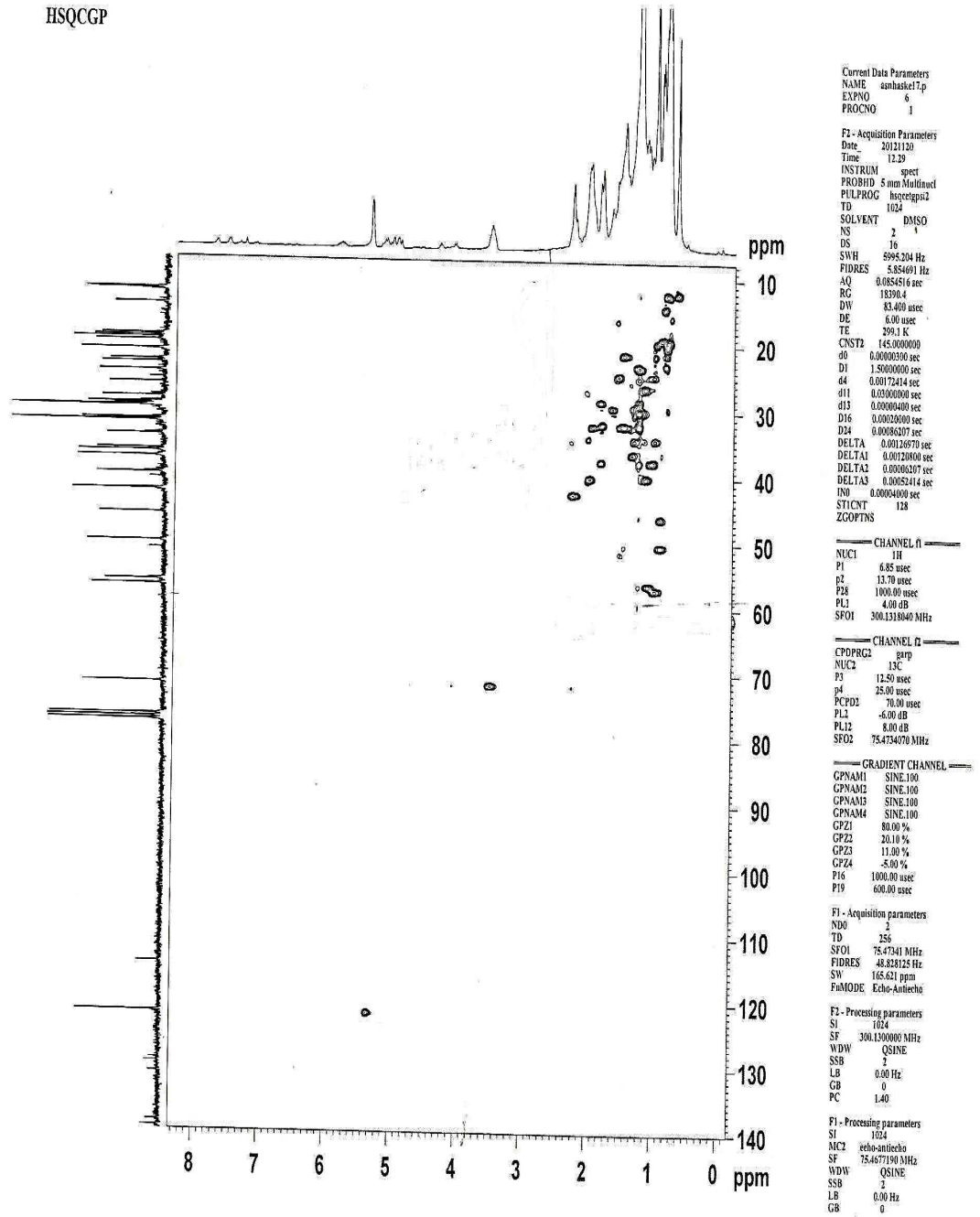


Fig. 4.43 HSQC spectrum of Haske-3 in CDCl<sub>3</sub>



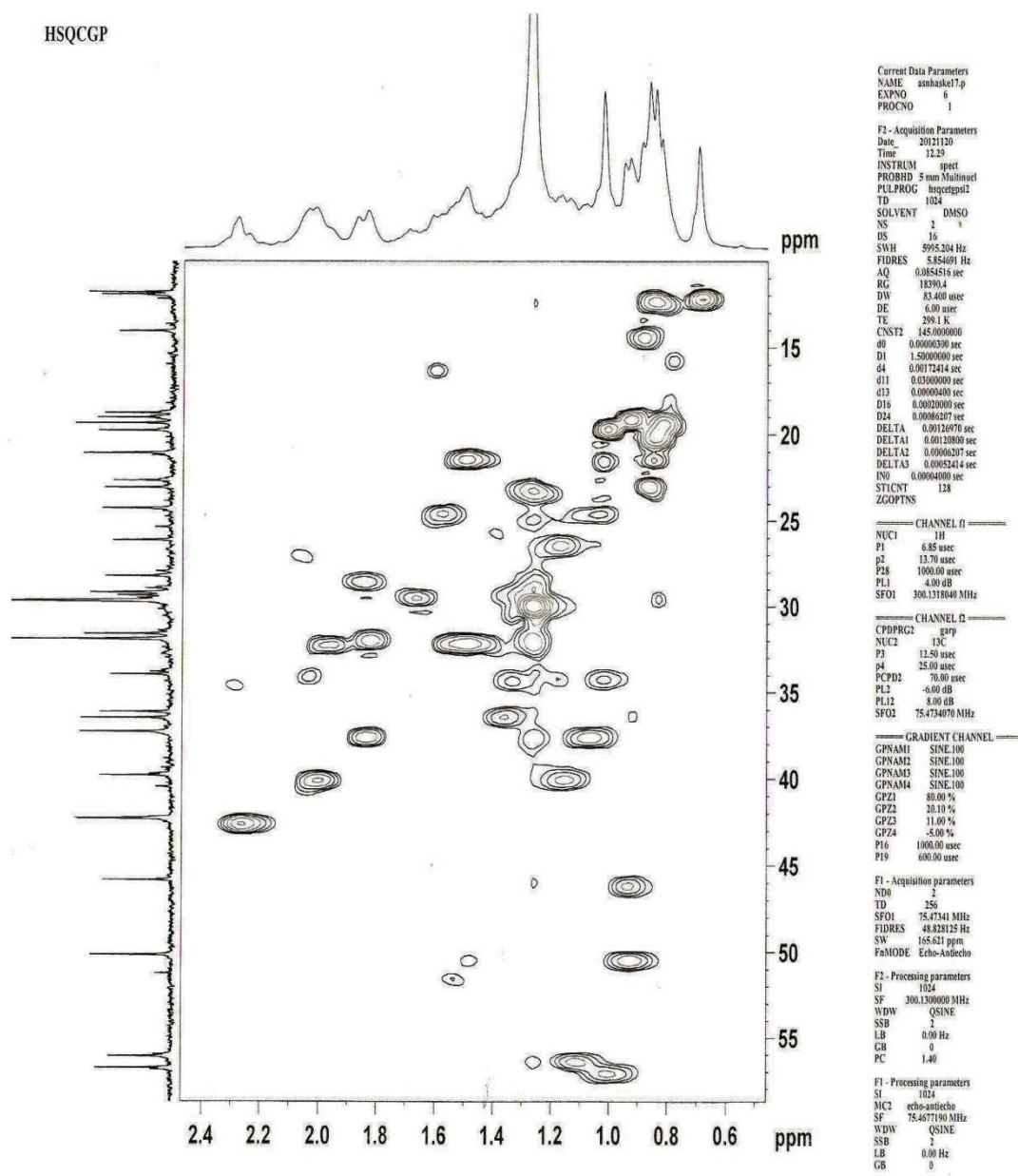


Fig. 4.44 Expanded HSQC spectrum of Haske-3 in  $CDCl_3$

HMBC

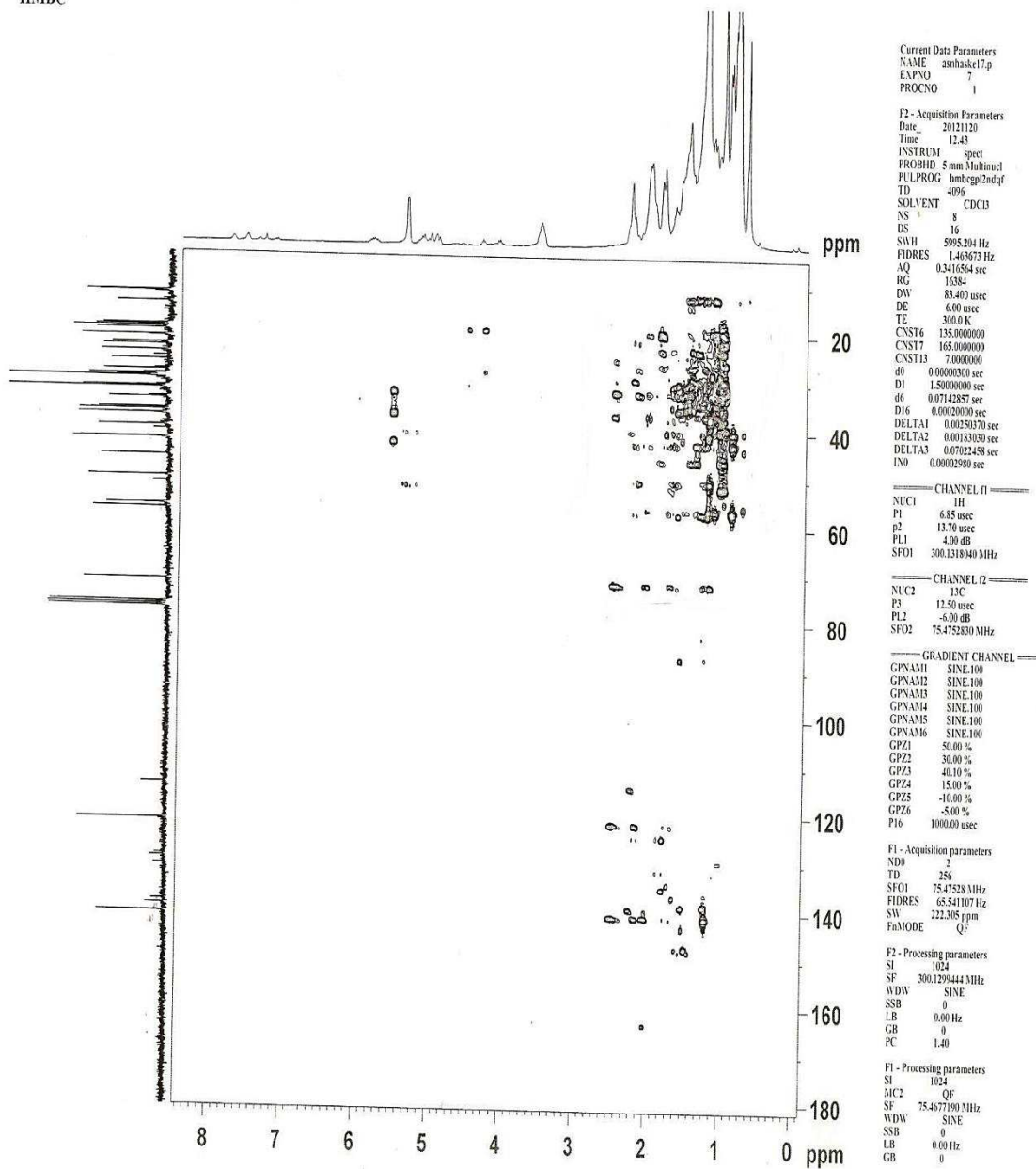


Fig. 4.45  $^1\text{H}$ - $^{13}\text{C}$  HMBC spectrum of Haske-3 in  $\text{CDCl}_3$

HMBC

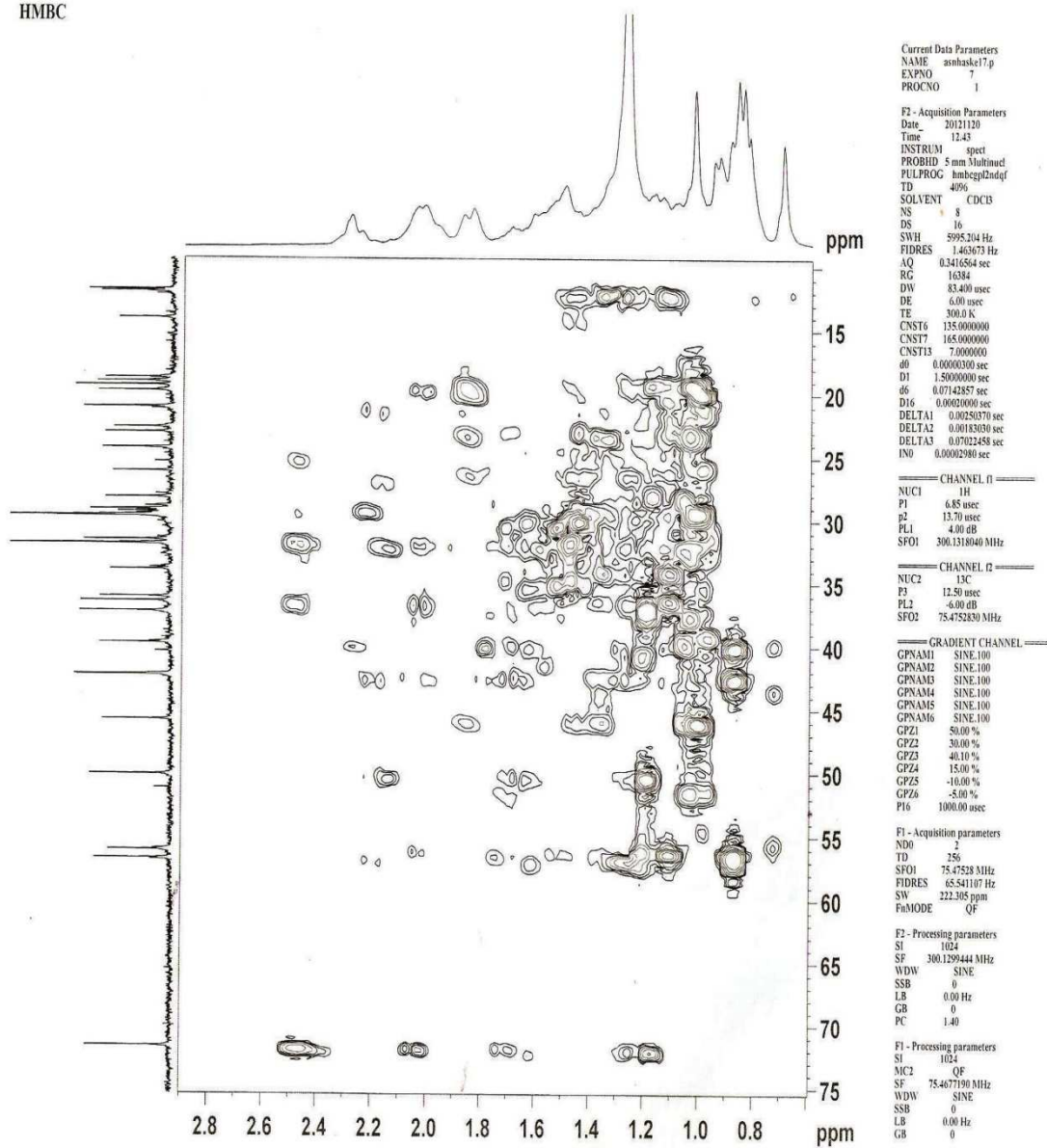


Fig. 4.46 Expanded  $^1\text{H}$ - $^{13}\text{C}$  HMBC spectrum of Haske-3 in  $\text{CDCl}_3$

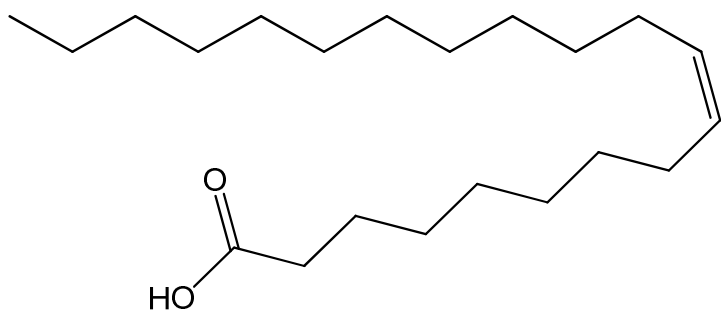
#### 4.5.4 Characterisation of Haske-4

Compound Haske-4 (20.0 mg) was obtained as a white powdered solid (melting point 73 - 76°C). The molecular formula  $C_{21}H_{40}O_2$  (324.2) was identified by ESI MS fragment ions 325.1  $[M+H]^+$ , 347.1  $[M+Na]^+$ , 363.2  $[M+K]^+$ . The IR  $\bar{\nu}$  ( $cm^{-1}$ ) signals at 3420, 2923, 1705 and 1462  $cm^{-1}$  correspond to O-H, C-H, C=O and C=C functional groups respectively. The signals of  $^1H$  NMR spectrum at  $\delta_H$  0.85-0.88 (3H, t,  $CH_3$ ,  $H_{21}$ ) and 1.17-1.25 (30H, m, 15 $CH_2$ ) are characteristics of methyl and cluster of methylene protons of fatty acid, while  $\delta_H$  1.63 (s) and 2.37 (t) were assigned to methylene protons at C-3 and C-2 respectively. The signal at  $\delta_H$  5.36 (t) were attributed to olefinic methine protons at C-9 and C-10 respectively.  $^{13}C$  NMR experiment showed resonances similar to fatty acid skeleton. There are twenty one carbon resonances, which were classified into one methyl carbon, seventeen methylene carbons, two methine carbon and one quaternary carbon resonances [Table 4.48]. The spectroscopic data of Haske-4 which include  $^1H$ - $^1H$  COSY and HMBC experiments, was identical to uneicos-9-enoic acid (Akita *et al.*, 2004, Siddiqui *et al.*, 2004). Hence, Haske-4 was elucidated as uneicos-9-enoic acid (**107**)

**Table 4.48:**  $^{13}\text{C}$  and  $^1\text{H}$  NMR ( $\text{CDCl}_3$ ) spectra data of Haske-4

Assignment	$^{13}\text{C}$	Multiplicity	$^1\text{H}$ , multiplicity
1	179.88	Q	-
2	34.38	$\text{CH}_2$	2.37, t, 2H
3	29.84	$\text{CH}_2$	1.17-1.25, m, 2H
4	29.77	$\text{CH}_2$	1.17-1.25, m, 2H
5	29.65	$\text{CH}_2$	1.17-1.25, m, 2H
6	29.65	$\text{CH}_2$	1.17-1.25, m, 2H
7	29.65	$\text{CH}_2$	1.17-1.25, m, 2H
8	28.57	$\text{CH}_2$	1.17-1.25, m, 2H
9	130.32	CH	5.36, t, 1H
10	130.08	CH	5.36, t, 1H
11	25.09	$\text{CH}_2$	1.17-1.25, m, 2H
12	29.47	$\text{CH}_2$	1.17-1.25, m, 2H
13	29.47	$\text{CH}_2$	1.17-1.25, m, 2H
14	30.10	$\text{CH}_2$	1.17-1.25, m, 2H
15	30.10	$\text{CH}_2$	1.17-1.25, m, 2H
16	30.10	$\text{CH}_2$	1.17-1.25, m, 2H
17	30.10	$\text{CH}_2$	1.17-1.25, m, 2H
18	30.10	$\text{CH}_2$	1.17-1.25, m, 2H
19	23.10	$\text{CH}_2$	1.17-1.25, m, 2H
20	32.33	$\text{CH}_2$	1.63, s, 2H
21	14.51	$\text{CH}_3$	0.85-0.88, t, 3H

Implied multiplicities of the carbons were determined from the DEPT experiment.



Uneicos-9-enoic acid **(107)**

#### 4.5.5 Characterisation of Haske-5

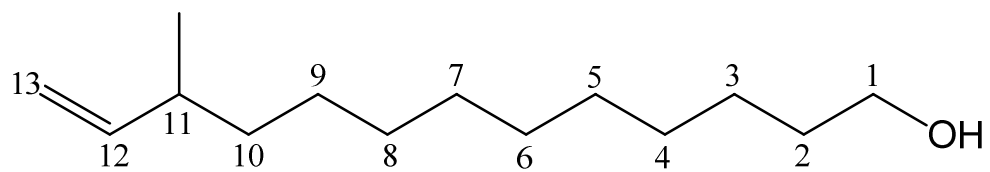
Compound Haske-5 (18.0 mg) was obtained as light yellow gel (melting point 76 - 77°C). The ESI-MS fragment ions at  $m/z$  182.0  $[M-2Na]^+$ , 274.34  $[M+2Na]^+$  calculated for a molecular formula  $C_{14}H_{28}O$  (228.12). The IR  $\bar{\nu}$  ( $cm^{-1}$ ) absorption bands for O-H, C-H, C=C and C-O moieties appeared at 3385, 2958, 1624 and 1368  $cm^{-1}$  respectively. The  $^1H$  NMR spectrum of Haske-5 showed signals at  $\delta_H$  0.87-0.90 (3H, t,) correspond to methyl protons [Table 4.49], while the multiplet peaks at  $\delta_H$  1.03 – 1.71 (16H, m, 8 x  $CH_2$ ) were attributed to cluster of methylene protons at 3-10 positions. Oxymethylene protons appeared at  $\delta_H$  4.13 (2H, t,  $H_{-1}$ ) while the signals at 4.96 (2H, t,  $H_{-13}$ ) and 5.02 (1H, m,  $H_{-12}$ ) correspond to olefinic methylene and methine protons. The  $^{13}C$  NMR spectrum revealed fourteen carbon resonances and were sorted by DEPT experiment as one oxymethylene carbon [ $\delta_c$  60.80], two olefinic carbons [ $\delta_c$  114.45 ( $C_{-13}$ ) and 139.65 ( $C_{-12}$ )], ten methylene carbons [ $\delta_c$  23.07 ( $C_{-3}$ ), 25.26 ( $C_{-7}$ ), 29.35 ( $C_{-5}$ ), 29.55 ( $C_{-6}$ ), 29.75 ( $C_{-4}$ ), 29.90 ( $C_{-8}$ ), 30.08 ( $C_{-9}$ ), 31.82 ( $C_{-11}$ ), 32.31 ( $C_{-10}$ ) and 34.20 ( $C_{-2}$ )] and one methyl carbon [ $\delta_c$  14.49 ( $C_{-14}$ )]. The structure of Haske-5 was identified as 11-methyl-tridec-12-enol (**108**).

**Table 4.49:**  $^{13}\text{C}$  NMR and  $^1\text{H}$  ( $\text{CDCl}_3$ ) spectra data of Haske-5

Assignment	$^{13}\text{C}$	Multiplicities	$^1\text{H}$
1.	60.80	$\text{CH}_2$	4.13, t, 2H
2.	34.20	$\text{CH}_2$	2.06, s, 2H
3.	23.07	$\text{CH}_2$	1.03-1.71,m,2H
4.	29.75	$\text{CH}_2$	1.03-1.71,m,2H
5.	29.35	$\text{CH}_2$	1.03-1.71,m,2H
6.	29.55	$\text{CH}_2$	1.03-1.71,m,2H
7.	29.26	$\text{CH}_2$	1.03-1.71,m,2H
8.	29.90	$\text{CH}_2$	1.03-1.71,m,2H
9.	30.09	$\text{CH}_2$	1.03-1.71,m,2H
10.	32.31	$\text{CH}_2$	1.03-1.71,m,2H
11.	31.82	CH	2.24, m, 1H
12.	139.65	CH	5.36, m, 1H
13.	114.45	$\text{CH}_2$	4.96, t, 2H
14.	14.49	$\text{CH}_3$	0.87-0.90,t,3H

Implied multiplicities of the carbons were determined from the DEPT experiment.





11-methyl-tridec-12-enol (**108**)

#### 4.5.6 Characterisation of Haske-6

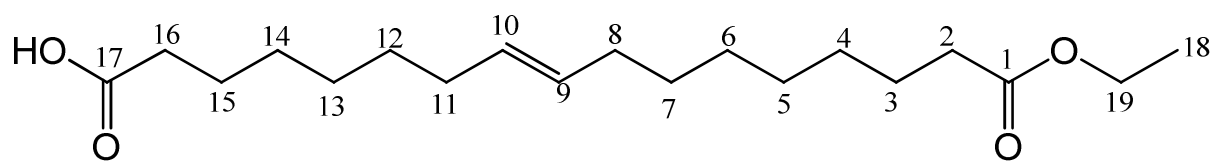
Haske-6 (35.0 mg) is a creamy yellow solid. It has a melting point of 113 - 116°C. The molecular formula  $C_{19}H_{34}O_4$  (326) was confirmed by ESI MS fragment ions 281.3 [M+H-2Na]<sup>-</sup>, 325.2 [M-H]<sup>-</sup>. The IR  $\bar{\nu}$  ( $cm^{-1}$ ) absorptions at 3489, 2840, 1694 and 1685  $cm^{-1}$  indicated the presence of O-H, C-H, C=O and C=C functions respectively. The <sup>1</sup>H NMR spectrum is identical to ester of fatty acid. The signals at  $\delta_H$  0.86-0.89 (3H, t, CH<sub>3</sub>) and 4.14 (2H, m, H<sub>19</sub>) were attributed to terminal methyl and oxymethylene protons of fatty ester, while  $\delta_H$  1.17-1.42 (m) was attributed to cluster of methylene protons of fatty acid. The signal at  $\delta_H$  5.35 (s) revealed the presence of olefinic methine protons at C-9 and C-10.

<sup>13</sup>C NMR experiment showed resonances consistent with fatty ester skeleton. DEPT spectrum classified the carbons into one oxymethylene carbon, one methyl carbon, thirteen methylene carbons, two methine carbons and two quaternary carbon resonances. The spectroscopic data of Haske-6 [Table 4.50] was however, used to elucidate the compound as Ethylheptadecan-17-oic-9-enoate (**109**).

**Table 4.50:**  $^{13}\text{C}$  and  $^1\text{H}$  NMR ( $\text{CDCl}_3$ ) spectra data of Haske-6

Assignment	$^{13}\text{C}$	Multiplicity	$^1\text{H}$ , multiplicity
1	171.72	Q	-
2	34.19	$\text{CH}_2$	2.05, s, 2H
3	23.06	$\text{CH}_2$	1.17-1.42, m, 2H
4	29.75	$\text{CH}_2$	1.17-1.42, m, 2H
5	29.45	$\text{CH}_2$	1.17-1.42, m, 2H
6	29.63	$\text{CH}_2$	1.17-1.42, m, 2H
7	30.08	$\text{CH}_2$	1.17-1.42, m, 2H
8	32.31	$\text{CH}_2$	1.63, m, 2H
9	130.06	CH	5.35, s, 1H
10	130.34	CH	5.35, s, 1H
11	27.58	$\text{CH}_2$	1.17-1.42, m, 2H
12	24.18	$\text{CH}_2$	1.17-1.42, m, 2H
13	25.07	$\text{CH}_2$	1.17-1.42, m, 2H
14	30.08	$\text{CH}_2$	1.17-1.42, m, 2H
15	29.82	$\text{CH}_2$	1.17-1.42, m, 2H
16	29.98	$\text{CH}_2$	2.32, t, 2H
17	180.47	Q	-
18	14.50	$\text{CH}_3$	0.86-0.89, t, 3H
19	60.84	$\text{CH}_2$	4.14, m, 2H

Implied multiplicities of the carbons were determined from the DEPT experiment.



Ethylheptadecan-17-oiс-9-enoate (**109**)

#### 4.5.7 Characterisation of Haske-7

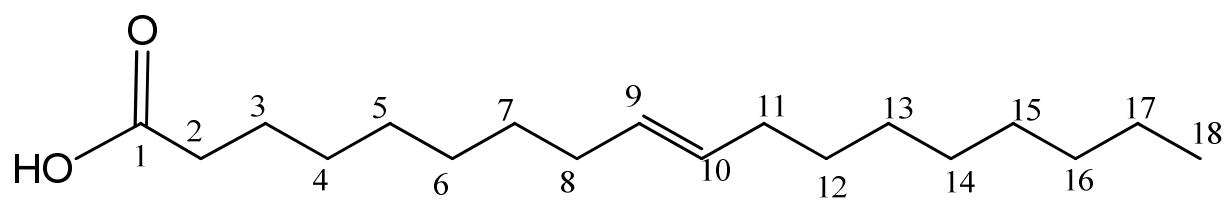
Compound Haske-7 (16.0 mg) was obtained as creamy gel. The ESI MS spectrum signals  $m/z$  282.2  $[M]^+$ , 305.4  $[M+Na]^+$  correspond to molecular formula  $C_{18}H_{34}O_2$  (282). The IR  $\bar{\nu}$  ( $cm^{-1}$ ) vibrations for O-H, C-H, C=O and C=C appeared at 3757, 2919, 1704 and 1461  $cm^{-1}$  respectively. The  $^1H$  NMR spectrum is identical to fatty acid. The signals at  $\delta_H$  0.89 (3H, t,  $H_{18}$ ) and 1.12-1.46 (22H, m, 11 x  $CH_2$ ) correspond to terminal methyl and cluster of methylene protons of fatty acid, while the signal at  $\delta_H$  5.38 (s) revealed the presence of olefinic methine protons at C-9 and C-10.  $^{13}C$  NMR spectrum data also showed resonances consistent with eighteen-carbon member fatty acid skeleton. The DEPT experiment sorted out the carbons into one methyl carbon, fourteen methylene carbons, two methine carbons and one quaternary carbon resonances. The spectroscopic data of Haske-7 [Table 4.51] was similar to Oleic acid data reported in the literature (Akita *et al.*, 2004, Siddiqui *et al.*, 2004, Tesemma *et al.*, 2013.). Therefore, Haske-7 was elucidated to be Z9-octadecenoic acid **(110)**.

**Table 4.51:**  $^{13}\text{C}$  and  $^1\text{H}$  NMR ( $\text{CDCl}_3$ ) spectra data of Haske-7 and Z9-octadecenoic acid

Assignment	$^{13}\text{C}$	Multiplicity	$^1\text{H}$	* $^{13}\text{C}$
1	180.32	Q	-	180.5
2	34.46	$\text{CH}_2$	2.35, t, 2H	34.12
3	23.08	$\text{CH}_2$	1.12-1.46, m, 2H	24.66
4	29.75	$\text{CH}_2$	1.12-1.46, m, 2H	29.14
5	29.46	$\text{CH}_2$	1.12-1.46, m, 2H	29.07
6	29.63	$\text{CH}_2$	1.12-1.46, m, 2H	29.05
7	30.08	$\text{CH}_2$	1.12-1.46, m, 2H	29.68
8	30.08	$\text{CH}_2$	2.10, s, 2H	27.16
9	130.11	CH	5.38, s, 1H	129.7
10	130.41	CH	5.38, s, 1H	130.0
11	27.55	$\text{CH}_2$	1.64, m, 2H	27.22
12	29.91	$\text{CH}_2$	1.12-1.46, m, 2H	29.78
13	25.08	$\text{CH}_2$	1.12-1.46, m, 2H	22.68
14	30.08	$\text{CH}_2$	1.12-1.46, m, 2H	29.53
15	29.83	$\text{CH}_2$	1.12-1.46, m, 2H	29.33
16	29.98	$\text{CH}_2$	1.12-1.46, m, 2H	29.33
17	32.31	$\text{CH}_2$	1.12-1.46, m, 2H	31.92
18	14.49	$\text{CH}_3$	0.89, t, 3H	14.07

Implied multiplicities of the carbons were determined from the DEPT experiment.

\* Tesemma *et al.*, 2013



*Z*9-octadecenoic acid (**110**)

#### 4.5.8 Characterisation of Haske-8

Compound Haske-8 (30.0 mg) is a creamy gel compound. The ESI MS fragment ions  $m/z$  255.2  $[M+H]^+$ , 277.4  $[M+Na]^+$  correspond to molecular formula  $C_{16}H_{30}O_2$  (254). The IR  $\bar{\nu}$  ( $cm^{-1}$ ) absorptions at 3650, 2858, 1728 and 1468  $cm^{-1}$  were assigned to O-H, C-H, C=O and C=C moieties respectively. The  $^1H$  NMR spectrum is also identical to fatty acid. The signals at  $\delta_H$  0.88 (3H, t,  $H_{16}$ ) and 1.17-1.41 (18H, m, 9 x  $CH_2$ ) were attributed to terminal methyl and cluster of methylene protons of fatty acid, while  $\delta_H$  5.35 (s) indicated the presence of olefinic methine protons at C-9 and C-10.  $^{13}C$  NMR spectrum data showed resonances consistent with sixteen-carbon member fatty acid skeleton, which was sorted by DEPT experiment into one methyl carbon, twelve methylene carbons, two methine carbons and one quaternary carbon resonances. The spectroscopic data of Haske-8 [Table 4.52] was identical to hexadec-9-enoic acid data previously reported in the literature (Akita *et al.*, 2004, Siddiqui *et al.*, 2004, Tesemma *et al.*, 2013). Hence, the structure of Haske-8 was identified as cis-hexadec-9-enoic acid (**111**).

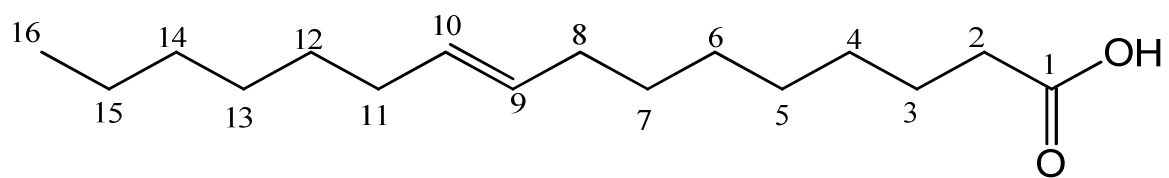


**Table 4.52:**  $^{13}\text{C}$  and  $^1\text{H}$  NMR ( $\text{CDCl}_3$ ) spectra data of Haske-8 and cis-hexadec-9-enoic acid

Assignment	$^{13}\text{C}$	Multiplicity	$^1\text{H}$	* $^{13}\text{C}$
1	180.41	Q	-	180.5
2	34.45	$\text{CH}_2$	2.37, t, 2H	34.12
3	23.06	$\text{CH}_2$	1.17-1.41,m, 2H	24.66
4	29.75	$\text{CH}_2$	1.17-1.41,m, 2H	29.14
5	29.45	$\text{CH}_2$	1.17-1.41,m, 2H	29.07
6	29.63	$\text{CH}_2$	1.17-1.41,m, 2H	29.05
7	29.83	$\text{CH}_2$	1.17-1.41,m, 2H	29.68
8	30.08	$\text{CH}_2$	2.14, s, 2H	27.16
9	130.12	CH	5.35, s, 1H	129.7
10	130.41	CH	5.35, s, 1H	130.0
11	27.55	$\text{CH}_2$	1.63, m, 2H	27.22
12	29.98	$\text{CH}_2$	1.17-1.41,m, 2H	29.78
13	30.08	$\text{CH}_2$	1.17-1.41,m, 2H	29.33
14	32.32	$\text{CH}_2$	1.17-1.41,m, 2H	31.92
15	25.08	$\text{CH}_2$	1.17-1.41,m, 2H	22.68
16	14.49	$\text{CH}_2$	0.88, t, 3H	14.07

Implied multiplicities of the carbons were determined from the DEPT experiment.

\*Teseemma *et al.*, 2013, Siddiqui *et al.*, 2004



**cis-hexadec-9-enoic acid (11)**

#### 4.5.9 Characterisation of Haske-9

Haske-9 (80.0 mg) appeared as a cream powdered solid with a melting point of 160-162°C. The ESI-MS fragment ions 415.3 [M+H]<sup>+</sup>, 437.4 [M+Na]<sup>+</sup> calculated for a molecular formula C<sub>27</sub>H<sub>42</sub>O<sub>3</sub> (414.3) [Fig. 4.47]. The IR  $\bar{\nu}$  (cm<sup>-1</sup>) absorptions at 3437, 2910, 1592 and 1327 cm<sup>-1</sup> correspond to O-H, C-H, C=C and C-O functions respectively. The signals of <sup>1</sup>H NMR spectrum at  $\delta_H$  0.79-1.31 (3H, m, 2 x CH<sub>3</sub>) and 1.44-2.03 (21H, m, 8CH<sub>2</sub> & 5CH) are characteristics of steroidal ring, while  $\delta_H$  3.38 (d) and 4.41 (m) were attributed to methylene and methine protons of spiroacetal bonds at C-26 and C-16 respectively [Fig. 4.48]. The signals at  $\delta_H$  3.58 (m) and 5.35 (t) indicated the presence of oxymethine and olefinic methine protons at C-3 and C-6 respectively.

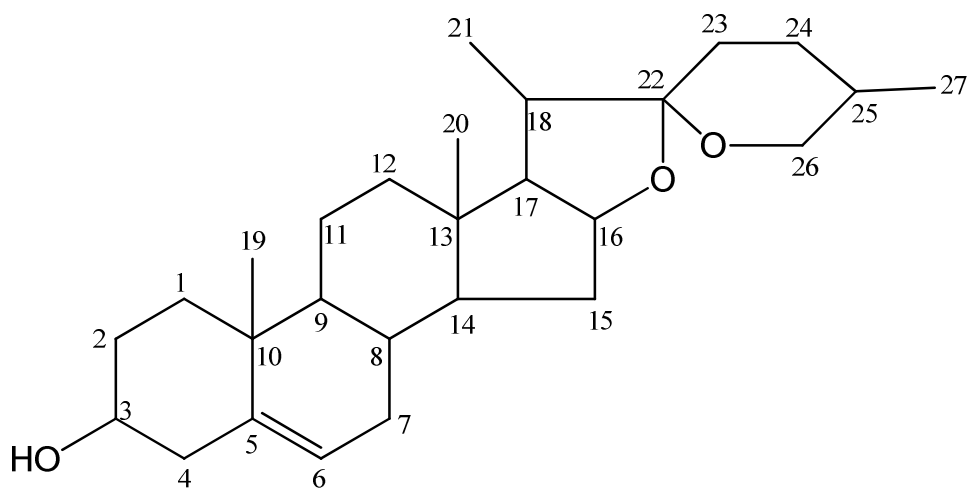
<sup>13</sup>C NMR spectrum also showed resonances similar to spirostene steroidal skeleton [Fig. 4.49]. There are twenty seven carbon resonances which were sorted by DEPT experiment [Fig. 4.50] into two oxymethine carbons, one oxymethylene carbon, four methyl carbons, nine methylene, seven methine carbons and four quaternary carbon resonances. The carbon signals at  $\delta_c$  72.11 (CH), 109.67 (Q), 121.57 (CH) and 140.75 (Q) were due to the presence of oxymethine carbon at C-3, a quaternary carbon at C-22 and olefinic methine and quaternary carbons at C-5 and C-6 respectively. The spectroscopic data of Haske-9 [Table 4.53] was similar to that of 3 $\beta$ -hydroxyspirost-5-ene (diosgenin) previously reported in the literature (Zubair *et al.*, 2011). Hence, Haske-9 was elucidated as 3 $\beta$ -hydroxyspirost-5-ene (diosgenin) (**4**).

**Table 4.53:**  $^{13}\text{C}$  and  $^1\text{H}$  NMR ( $\text{CDCl}_3$ ) spectra data of Haske-9 and Diosgenin

Assignment	$^{13}\text{C}$	Multiplicity	$^1\text{H}$ , multiplicity	* $^1\text{H}$	$^{13}\text{C}$
1	21.23	$\text{CH}_2$	1.44-2.03, m, 2H	1.61	20.9
2	37.63	$\text{CH}_2$	1.44-2.03, m, 2H	1.96	37.2
3	72.11	CH	3.58, m, 1H	3.46	71.7
4	42.68	$\text{CH}_2$	1.44-2.03, m, 2H	2.26	42.3
5	141.22	Q	-	-	140.8
6	121.80	CH	5.35, t, 1H	5.32	121.4
7	32.45	$\text{CH}_2$	2.30, t, 2H	1.82	32.1
8	31.79	CH	1.44-2.03, m, 1H	1.46	31.5
9	50.48	CH	1.44-2.03, m, 1H	0.80	50.1
10	37.04	Q	-	-	36.9
11	32.24	$\text{CH}_2$	1.44-2.03, m, 2H	1.36	31.9
12	29.20	$\text{CH}_2$	1.44-2.03, m, 2H	1.38	39.8
13	40.66	Q	-	-	41.9
14	40.19	CH	1.44-2.03, m, 1H	1.00	41.6
15	30.69	$\text{CH}_2$	1.44-2.03, m, 2H	1.96	31.6
16	81.22	CH	4.41, m, 1H	4.40	80.8
17	62.52	CH	1.44-2.03, m, 1H	1.61	62.1
18	56.93	CH	1.44-2.03, m, 1H	0.76	56.5
19	14.90	$\text{CH}_3$	0.97-1.31, m, 3H	0.75	16.3
20	16.67	$\text{CH}_3$	0.97-1.31, m, 3H	1.84	19.4
21	17.51	$\text{CH}_3$	0.79-0.81, m, 3H	0.95	14.5
22	109.67	Q	-	-	109.3
23	32.02	$\text{CH}_2$	1.44-2.03, m, 2H	1.58	31.4
24	30.69	$\text{CH}_2$	1.44-2.03, m, 2H	1.46	28.8
25	42.68	CH	1.44-2.03, m, 1H	1.54	30.3
26	67.24	$\text{CH}_2$	3.38, d, 3H	3.31	66.9
27	19.80	$\text{CH}_3$	0.97-1.31, m, 3H	1.06	17.1

Implied multiplicities of the carbons were determined from the DEPT experiment.

\* Zubair *et al.*, 2011



3β-hydroxyspirost-5-ene (4)

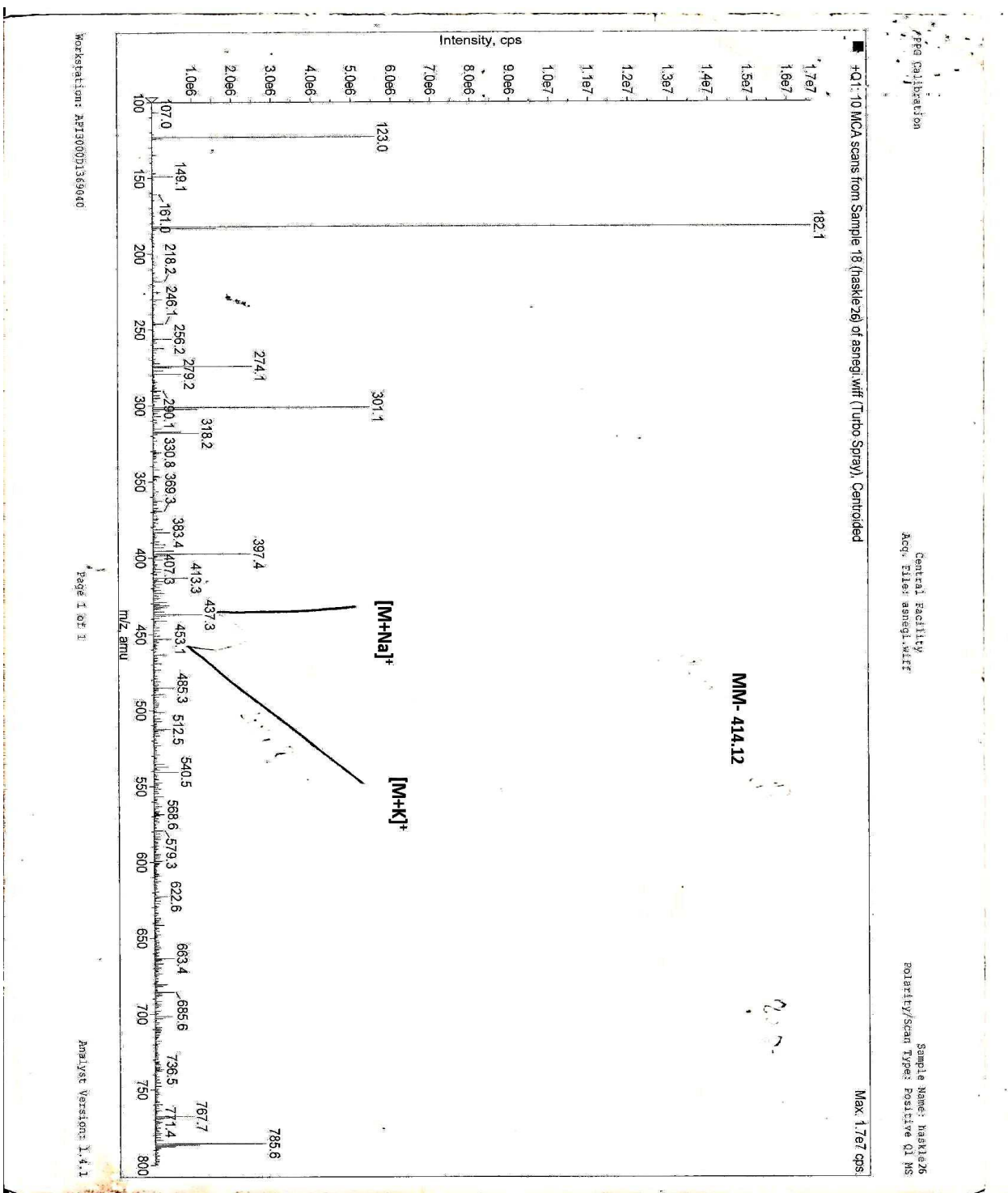


Fig. 4.47 ESI-MS spectrum of Haske-9 in MeOH

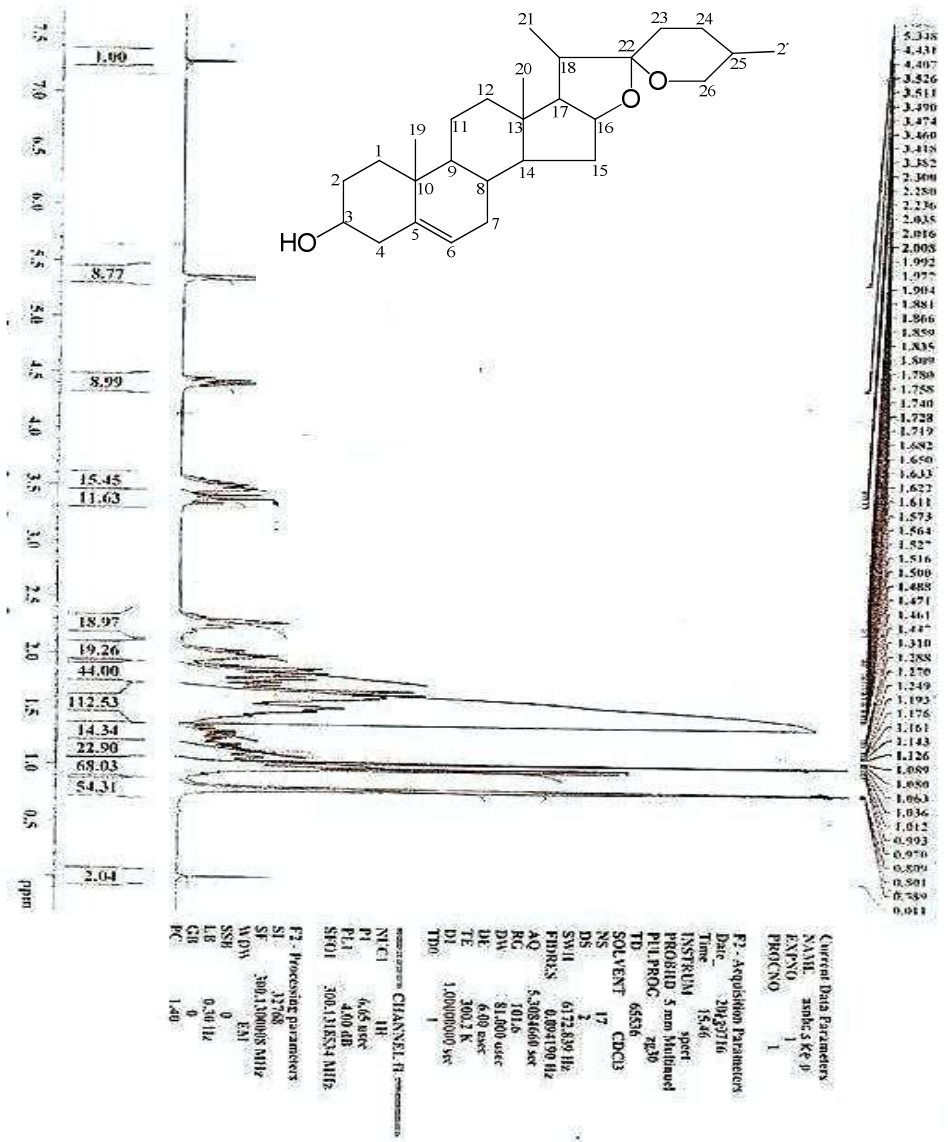


Fig. 4.48 <sup>1</sup>H NMR spectrum of Haske-9 in CDCl<sub>3</sub>

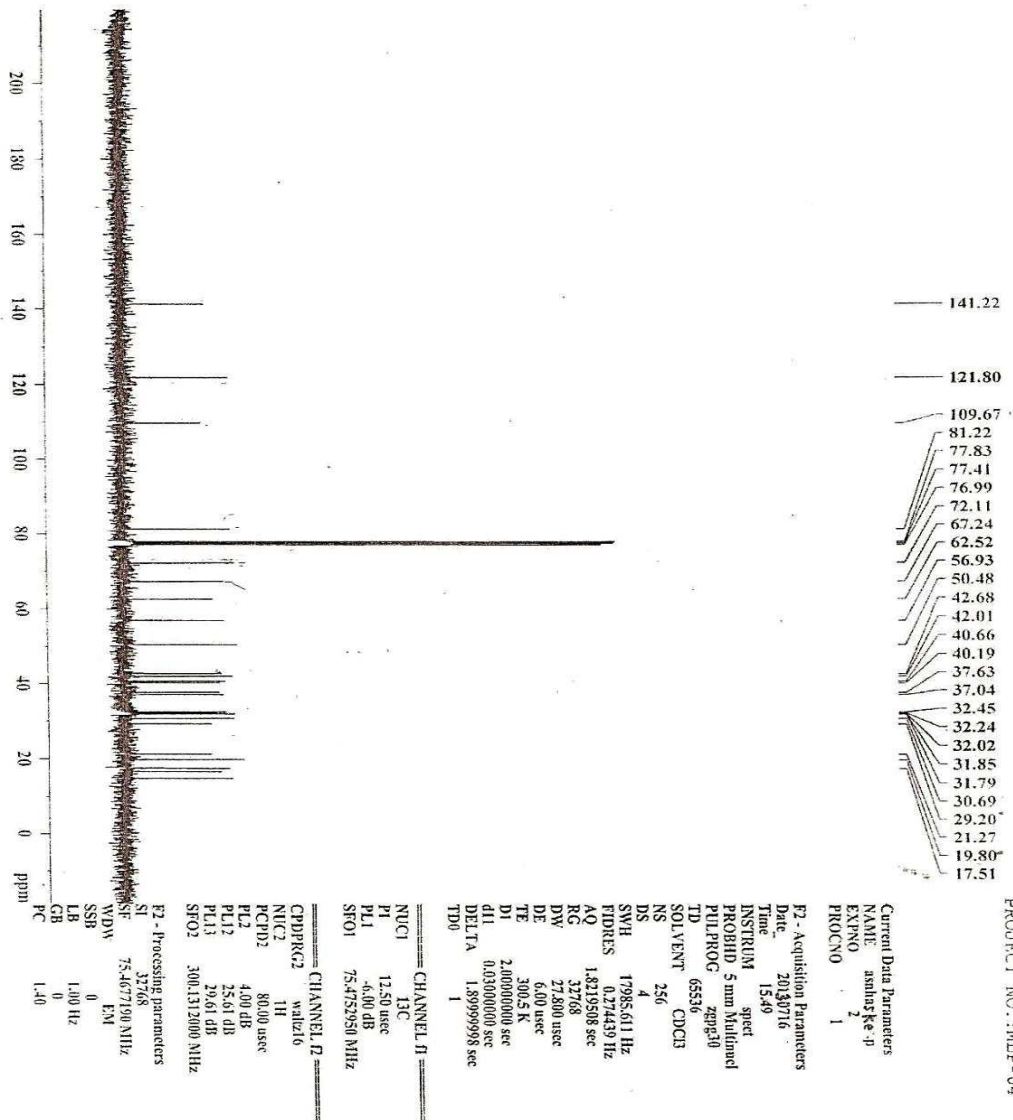


Fig. 4.49 <sup>13</sup>C NMR spectrum of Haske-9 in CDCl<sub>3</sub>



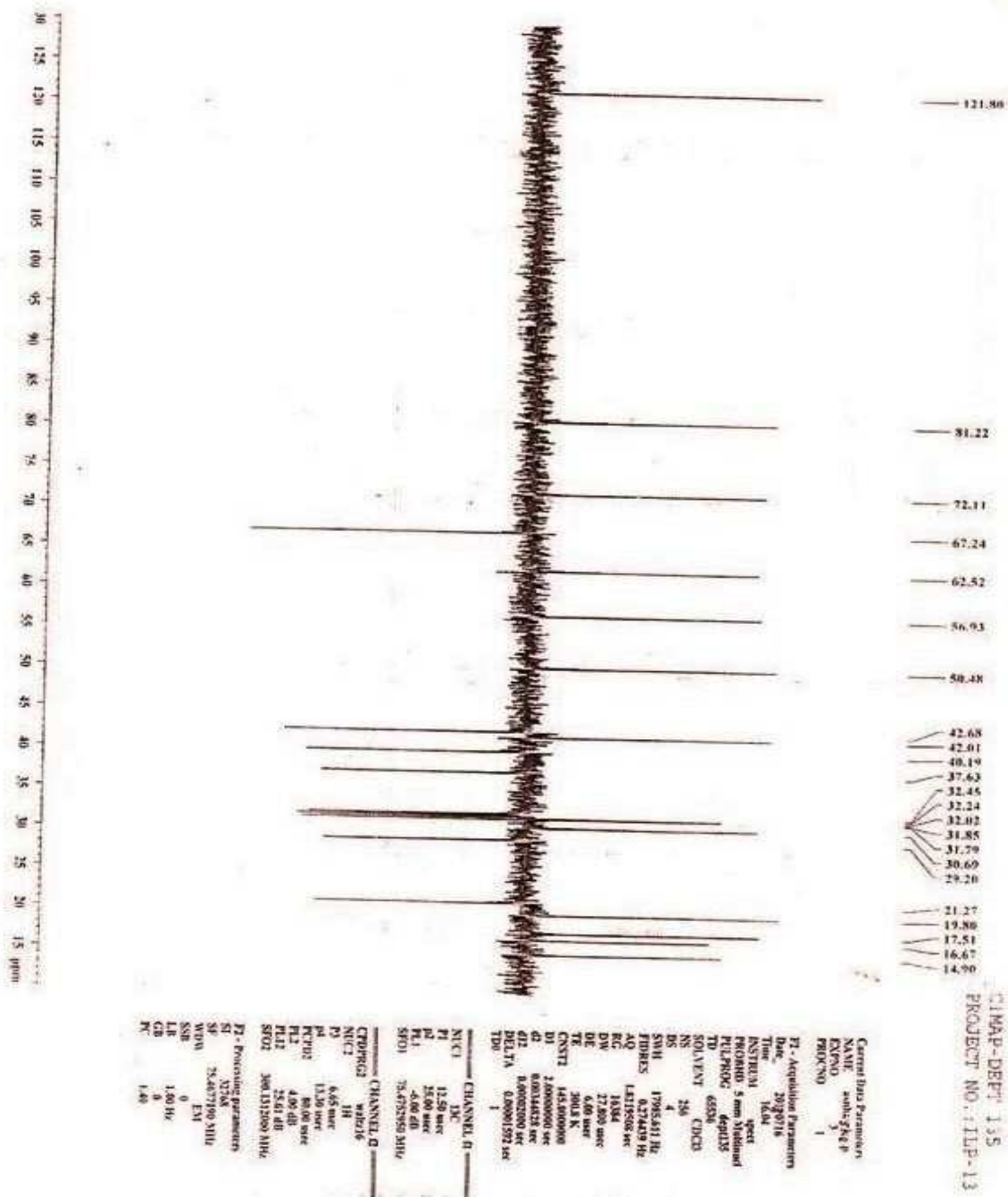


Fig. 4.50 DEPT spectrum of Haske-9 in CDCl<sub>3</sub>

#### 4.6 Column chromatography of methanol extract of *S.kraussiana* (aerial parts)

The methanol extract (8.5 g) of *S. kraussiana* (aerial parts) was subjected to column chromatography (silica gel) and eluted with hexane: ethyl acetate to obtain 80 fractions. The fractions were pooled together using TLC analysis to 9 sub-fractions, SKM (1-9). SKM-2 was chromatographed on silica gel and further purified with preparative TLC using appropriate solvent ratios as described in section 3.8 to give a white crystalline compound coded Haskm-1 (26.0 mg) and cream solid, Haskm-2 (17.0 mg). The chromatographic isolation and recrystallisation of fraction SKM-4 and SKM-6 yielded a white crystalline compound, Haskm-3 (15.0 mg) and a light yellow gelly-like solid coded Haskm-4 (25.0 mg). SKM-8 was also purified with column chromatography on silica gel and recrystallised with  $\text{CHCl}_3$  and hexane to give a pure white powdered solid coded Haskm-5 (22.0 mg).

##### 4.6.1 Characterisation of Haskm-1

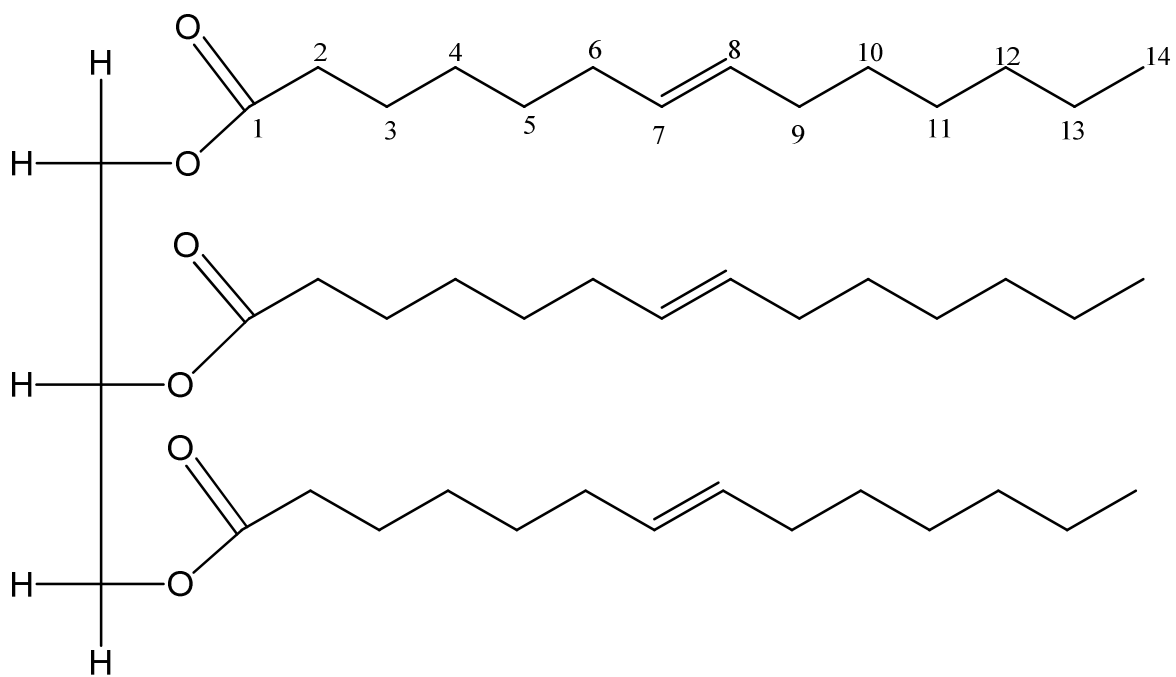
Compound Haskm-1 (26.0 mg) is a white crystalline compound which has a melting point of 84 - 86°C. The MS fragment ions 615  $[\text{M}-2\text{K}-\text{Na}]^-$  calculated for molecular formula  $\text{C}_{45}\text{H}_{80}\text{O}_6$  (716). The IR  $\bar{\nu}$  ( $\text{cm}^{-1}$ ) vibrational absorptions of O-H, C-H, C=O and C=C functions appeared at 3750, 2854, 1744 and 1544  $\text{cm}^{-1}$  respectively. The  $^1\text{H}$  NMR signals at  $\delta_{\text{H}}$  0.87-0.89 (3 x 3H, t, 3 x  $\text{CH}_3$ ,  $\text{H}_{-14}$ ), 1.25-1.42 (3 x 14H, m, 3 x  $7\text{CH}_2$ ), 1.60 (3 x 2H, m,  $\text{H}_6$ ), 4.13 and 4.28 are characteristics of methyl, methylene and oxymethylene protons of fatty triglycerides. The peaks at  $\delta_{\text{H}}$  5.20 (s) and 5.35 (t) correspond to oxymethine proton of fatty triester and olefinic protons at C-7 and C-8 respectively.  $^{13}\text{C}$  NMR spectrum also indicates resonances consistent with glycerides of fatty acid skeleton. The identified carbon skeleton in each chain were one methyl carbon, ten methylene carbons, two olefinic methine carbons, carbonyl quaternary carbon, and one oxymethine and two oxymethylene carbon  $\delta_{\text{C}}$  62.49 (2 x  $\text{OCH}_2$ ) and 69.29 ( $\text{OCH}$ ) resonances. The spectroscopic data of Haskm-1 [Table 4.54] was identical to that of 1,2,3-Propanetriyl (7Z, 7'Z, 7''Z)tris(-7-tetradecenoate) reported in the literature (Lie Ken Jie and Lam 1995). Hence, the structure of Haskm-1 was identified as 1,2,3-Propanetriyl (7Z, 7'Z, 7''Z)tris(-7-tetradecenoate) (**112**).

**Table 4.54:**  $^{13}\text{C}$  and  $^1\text{H}$  NMR ( $\text{CDCl}_3$ ) spectra data of Haskm-1 and 1,2,3-Propanetriyl (7Z, 7'Z, 7''Z)tris(-7-tetradecenoate)

Assignment	$^{13}\text{C}$ , Multiplicity	$^1\text{H}$ , Multiplicity	* $^{13}\text{C}$	* $^1\text{H}$
1	173.24		173.27,	
	173.68 (Q)	-	172.88	-
2	34.45 ( $\text{CH}_2$ )	2.33, t, 2H	34.07	2.31
3	23.03 ( $\text{CH}_2$ )	1.25-1.42, m, 2H	24.91	1.23
4	29.67 ( $\text{CH}_2$ )	1.25-1.42, m, 2H	29.16	1.23
5	29.52 ( $\text{CH}_2$ )	1.25-1.42, m, 2H	29.32	1.23
6	27.62 ( $\text{CH}_2$ )	1.60, m, 2H	27.52	1.63
7	130.09 (CH)	5.35, t, 1H	130.20	5.37
8	130.41 (CH)	5.35, t, 1H	130.45	5.37
9	29.72 ( $\text{CH}_2$ )	2.12, m, 2H	29.72	2.32
10	30.09 ( $\text{CH}_2$ )	1.25-1.42, m, 2H	29.64	1.23
11	29.75 ( $\text{CH}_2$ )	1.25-1.42, m, 2H	29.72	1.23
12	30.09 ( $\text{CH}_2$ )	1.25-1.42, m, 2H	29.42	1.23
13	32.32 ( $\text{CH}_2$ )	1.25-1.42, m, 2H	31.98	1.23
14	14.42 ( $\text{CH}_3$ )	0.87-0.89, t, 3H	14.11	0.89

Implied multiplicities of the carbons were determined from the DEPT experiment.

\* Lie Ken Jie and Lam 1995



1,2,3-Propanetriyl (7Z, 7'Z, 7''Z)tris(-7-tetradecenoate) (112)

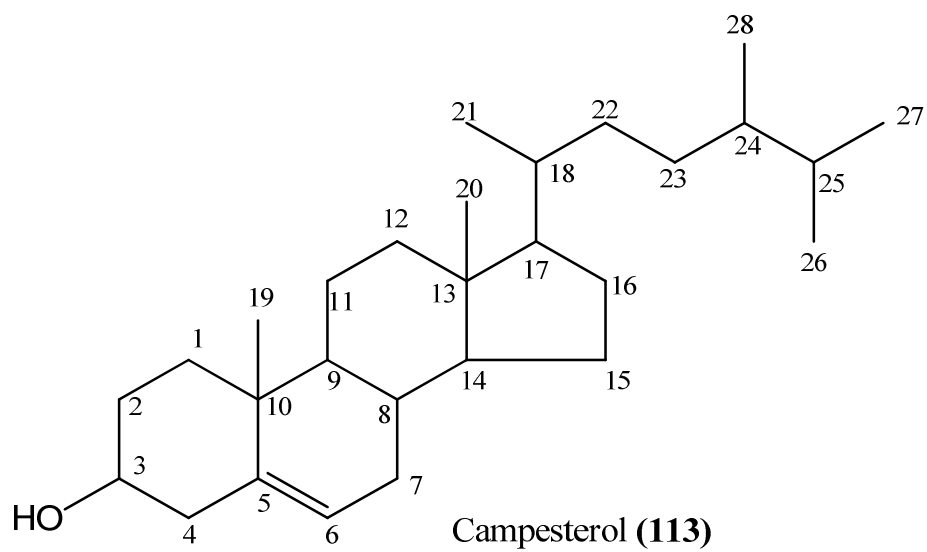
#### 4.6.2 Characterisation of Haskm-2

Compound Haskm-2 (17.0 mg) was obtained as a cream solid (melting point 135 - 138°C). The MS fragment ions 447  $[M+2Na+H]^+$ , 685  $[2M-5Na]^-$  correspond to a molecular formula  $C_{28}H_{48}O$  (400.12) [Fig. 4.51]. The IR  $\bar{\nu}$  ( $cm^{-1}$ ) absorptions at 3433, 2939 and 1646  $cm^{-1}$  indicated the presence of O-H, C-H and C=C functional groups respectively [Fig. 4.52]. The  $^1H$  NMR signals at  $\delta_H$  0.68-0.85 (18H, m, 6 x  $CH_3$ ), 0.87-1.32 (16H, m, 8 x  $CH_2$ ) and 1.33-1.81 (14H, m, 7 x CH) are characteristics of methyl, methylene and methine protons of oleanane steroids. The signals at  $\delta_H$  3.53 (m) and 5.36 (t) were assigned to oxymethine proton at C-3 and olefinic proton at C-6 respectively [Fig. 4.53].  $^{13}C$  NMR spectrum also showed resonances consistent with twenty eight carbon member-steroid skeleton [Fig. 4.54 and 4.55]. The identified carbons were sorted by DEPT experiment [Fig. 4.56] into six methyl carbons, ten methylene carbons, nine methine carbons and three quaternary carbons. The chemical shifts  $\delta_c$  72.21 (m), 141.17 (s) and 122.11 (t) were attributable to oxymethine carbon at C-3 and olefinic carbons at C-5 and C-6.  $^1H$ - $^1H$  COSY spectrum [Fig. 4.57] revealed the correlation of oxymethine proton at C-3 with methylene protons at C-4, while olefinic methine proton at C-6 was correlated with methylene protons at C-7. The HSQC spectrum (Fig. 4.58) showed that methine protons at  $\delta_H$  3.53 (1H, m,  $H_3$ ) and 5.36 (1H, t,  $H_6$ ) were bonded to carbons at  $\delta_c$  72.21 (C-3), 122.11 (C-6) respectively. In  $^1H$ - $^{13}C$  HMBC experiment [Fig. 4.59], there was correlation of methine proton at C-6 with C-4, C-7 and C-8. Methylene protons at C-1, C-2, C-4 and C-7 showed correlations with oxymethine carbon at C-3, while methylene protons at C-7 were also correlated with olefinic carbons C-5 and C-6. Further, methylene protons at C-4 also revealed correlation with C-5 and C-6. The spectroscopic data of Haskm-2 [Table 4.55] was similar to campesterol reported by Jain and Bari, (2010). Hence, Haskm-2 was elucidated to be Campesterol (**113**).

**Table 4.55:**  $^{13}\text{C}$  and  $^1\text{H}$  NMR ( $\text{CDCl}_3$ ) spectra data of Haskm-2 and Campesterol

Assignment	$^{13}\text{C}$	Multiplicity	$^1\text{H}$ , multiplicity
1	21.61	$\text{CH}_2$	0.87-1.32, m, 2H
2	37.67	$\text{CH}_2$	0.87-1.32, m, 2H
3	72.21	CH	3.53, m, 1H
4	42.72	$\text{CH}_2$	2.28, d, 2H
5	141.17	Q	-
6	122.11	CH	5.36, t, 1H
7	32.32	$\text{CH}_2$	1.98, t, 2H
8	40.19	CH	1.33-1.81, m, 1H
9	56.48	CH	1.33-1.81, m, 1H
10	34.37	Q	-
11	23.48	$\text{CH}_2$	0.87-1.32, m, 2H
12	24.70	$\text{CH}_2$	0.87-1.32, m, 2H
13	36.91	Q	-
14	46.26	CH	1.33-1.81, m, 1H
15	30.09	$\text{CH}_2$	0.87-1.32, m, 2H
16	32.07	$\text{CH}_2$	0.87-1.32, m, 2H
17	57.18	CH	1.33-1.81, m, 1H
18	50.56	CH	1.33-1.81, m, 1H
19	12.25	$\text{CH}_3$	0.68-0.85, m, 3H
20	12.38	$\text{CH}_3$	0.68-0.85, m, 3H
21	19.18	$\text{CH}_3$	0.68-0.85, m, 3H
22	26.52	$\text{CH}_2$	0.87-1.32, m, 2H
23	28.64	$\text{CH}_2$	0.87-1.32, m, 2H
24	29.50	CH	1.33-1.81, m, 1H
25	36.54	CH	1.33-1.81, m, 1H
26	19.44	$\text{CH}_3$	0.68-0.85, m, 3H
27	19.79	$\text{CH}_3$	0.68-0.85, m, 3H
28	20.20	$\text{CH}_3$	0.68-0.85, m, 3H

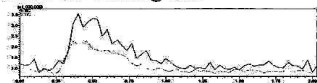
Implied multiplicities of the carbons were determined from the DEPT experiment.



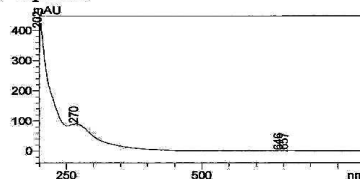
ANALYTICAL TEST REPORT

Sample Information for Direct Mass Analysis of Isolates/synthetic molecule  
Sample Code : ASN-HASKM-8  
Solubility : MeOH  
Name of the Scientist : Dr.A S Negi  
Project Code: MLP-02  
Mass Range: 100-800

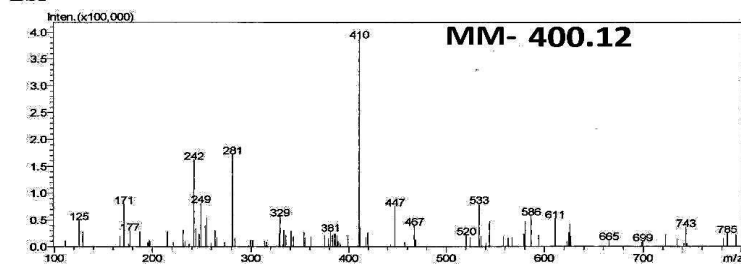
Mass chromatogram



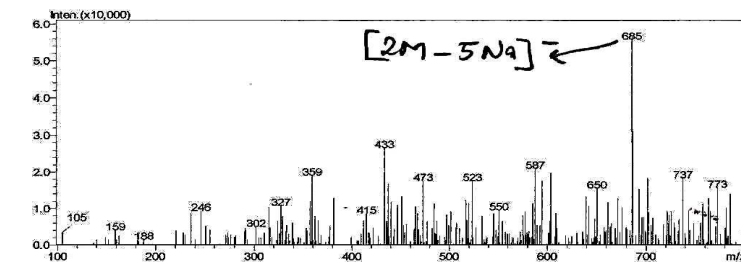
UV-Spectra



ESI+



ESI-



File Path-D:\Direct Mass report- Aug 2010\ASN-HASKM-8.doc

Oct 14, 2013

[Dr. Karuna Shanker]

Fig. 4.51 Mass spectrum of Haskm-2 in MeOH



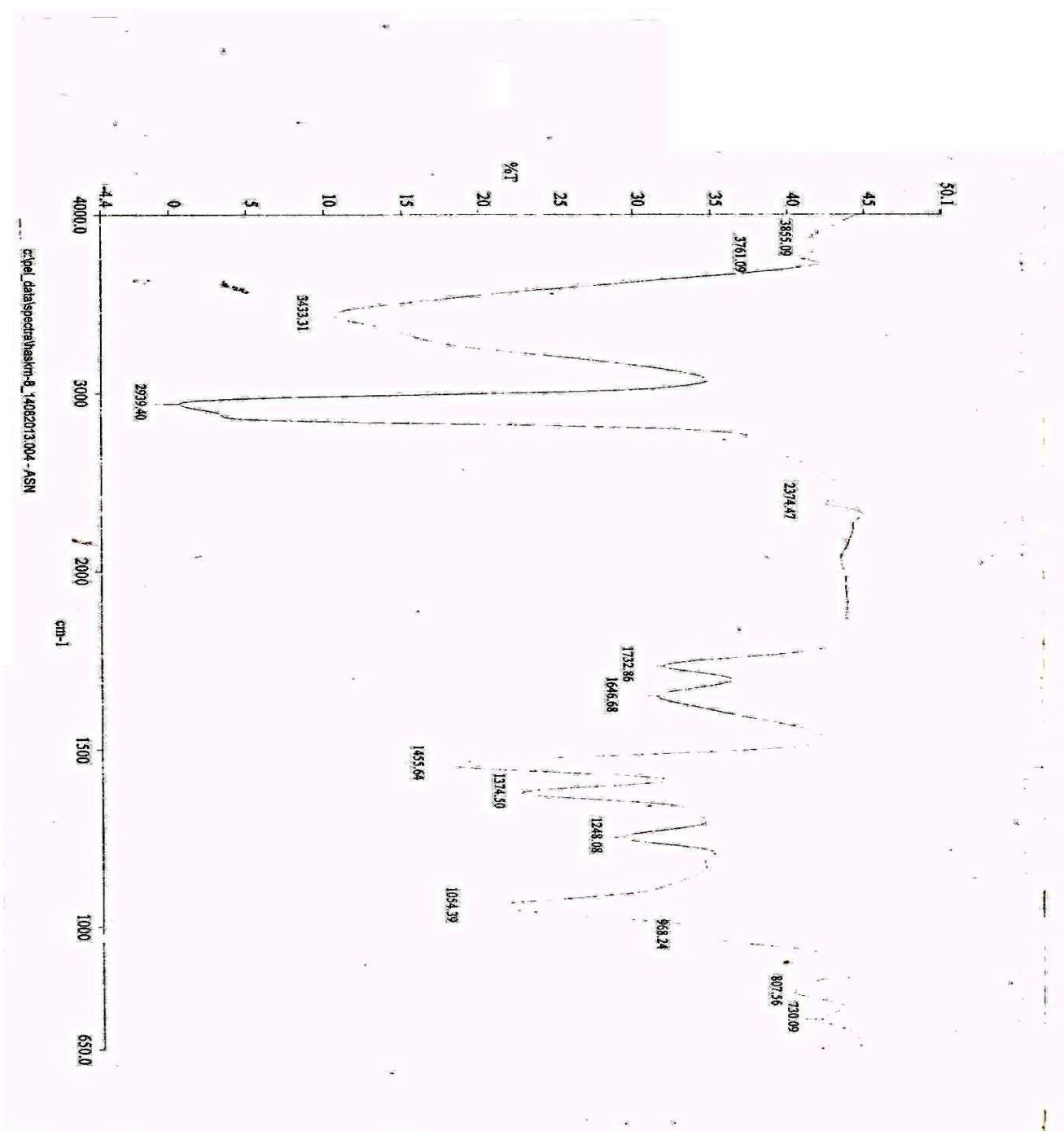


Fig. 4.52 IR spectrum of Haskm-2 in CCl<sub>4</sub> and KBr

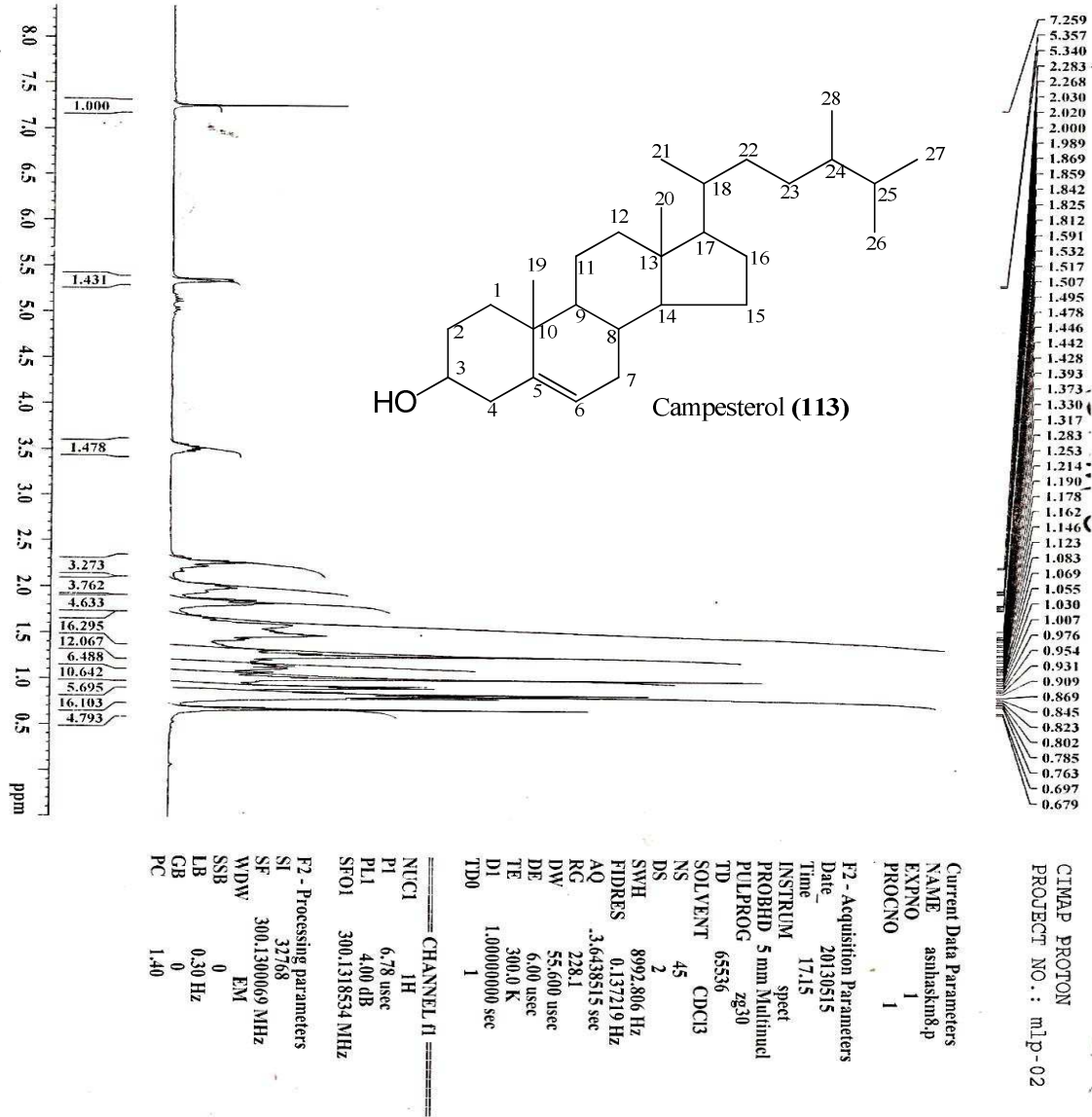


Fig. 4.53  $^1\text{H}$  NMR spectrum of Haskm-2 in  $\text{CDCl}_3$

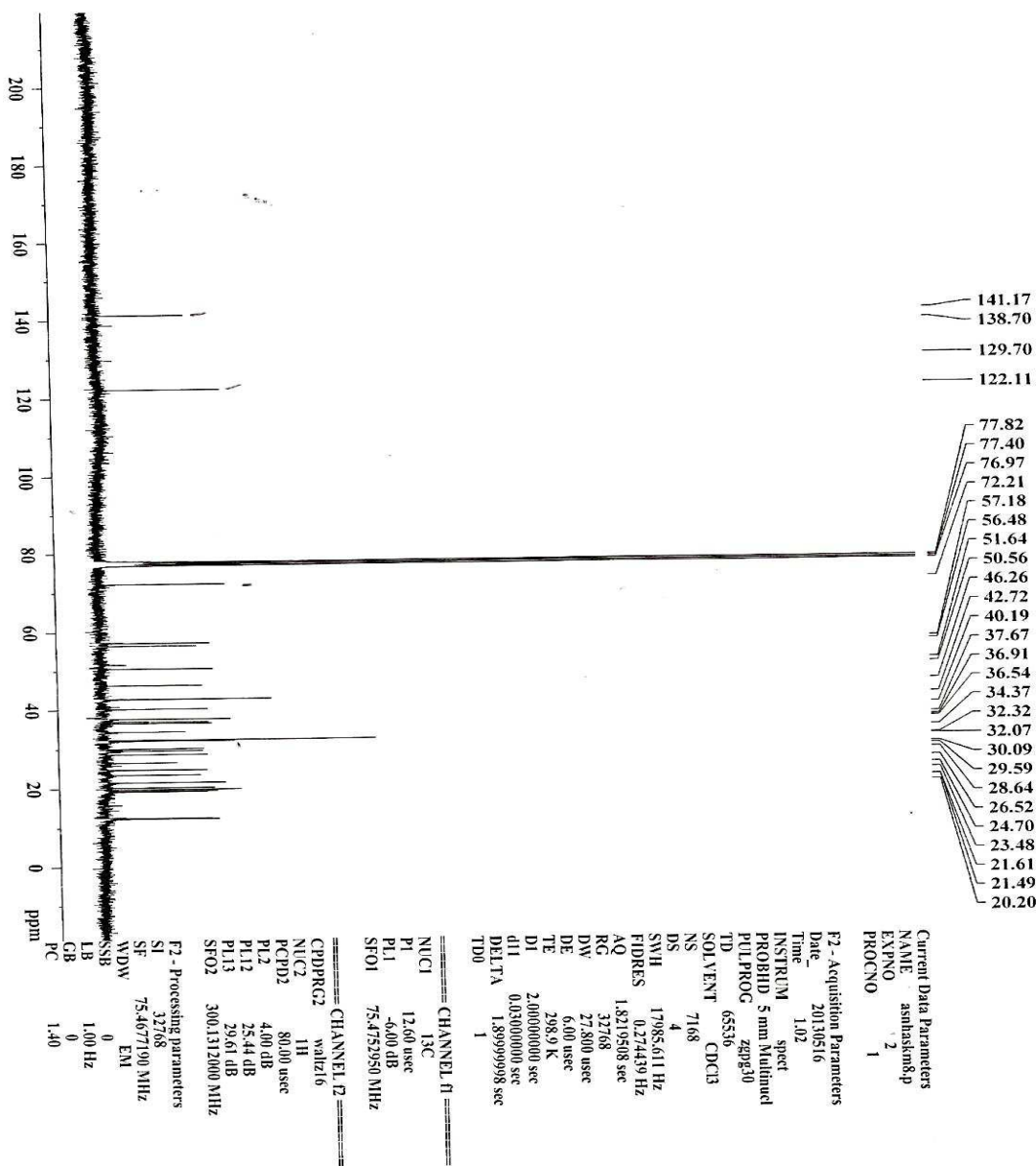


Fig. 4.54  $^{13}\text{C}$  NMR spectrum of Haskm-2 in  $\text{CDCl}_3$

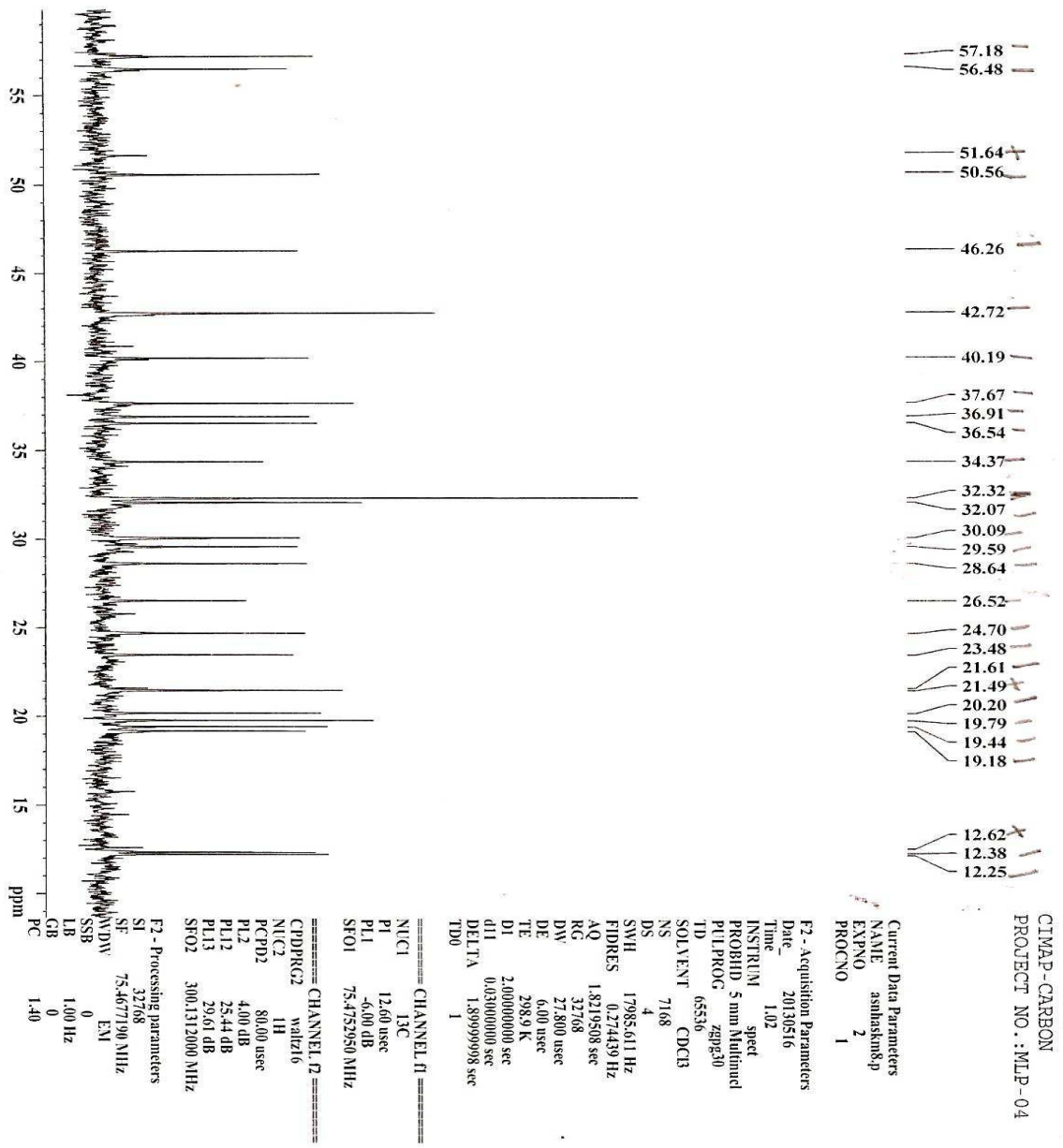
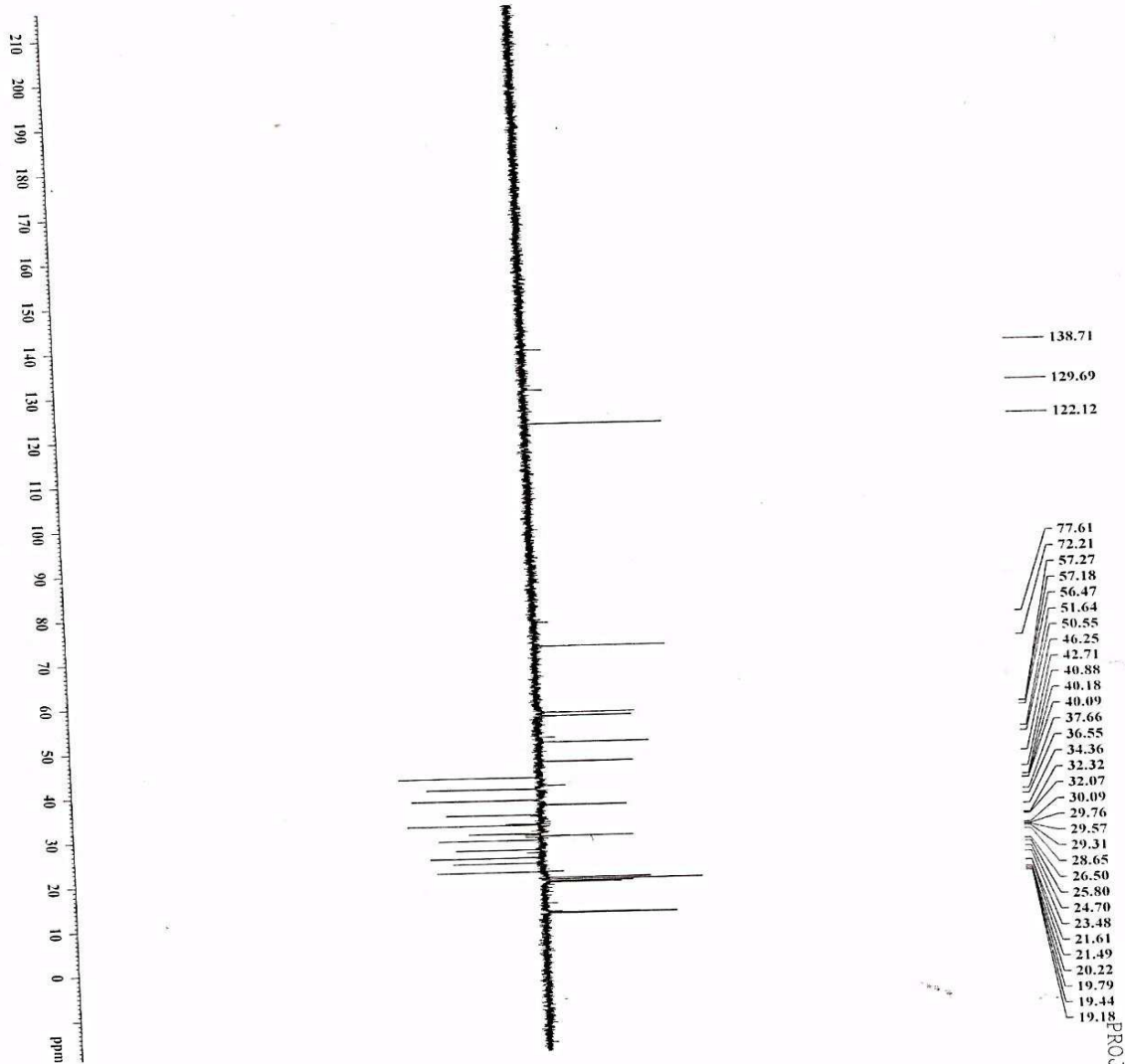


Fig. 4.55 Expanded <sup>13</sup>C NMR spectrum of Haskm-2 in CDCl<sub>3</sub>



CIMAP-DEPT 135  
PROJECT NO.: ILP-13

```

Current Data Parameters
NAME: haskm2amp
EXPNO: 3
PROCNO: 1

F2 - Acquisition Parameters
Date_   : 20130516
Time    : 6:33
INSTRUM : spect
PROBHD  : 5mm ddzlxnd
PULPROG : zgpg30
TD       : 65536
SOLVENT : DCl3
NS       : 5120
DS       : 4
SWH      : 17985.611 Hz
FIDRES   : 0.274439 Hz
AQ       : 1.8219508 sec
RG       : 16384
DW       : 27.800 usec
DE       : 6.00 usec
TE       : 298.0 K
CNS1     : 145.000000
D1       : 2.00000000 sec
d12      : 0.00000200 sec
DELTA    : 0.00001004 sec
T100     : 1

===== CHANNEL f1 =====
NUC1      : 13C
P1        : 12.60 usec
PL1       : 25.20 usec
PL12      : -6.00 dB
SFO1      : 75.4752950 MHz

===== CHANNEL f2 =====
CPDPRG2   : walz16
NUC2       : 1H
P2         : 6.78 usec
PL2        : 13.50 usec
RCPRP2    : 80.00 usec
PL12       : 6.00 dB
PL12       : 35.44 dB
SFO2       : 300.1312000 MHz

F2 - Processing parameters
SI         : 32768
SF         : 75.4677190 MHz
WDW        : EM
SSB        : 0
LB         : 1.00 Hz
GB         : 0
PC         : 1.40
  
```

Fig. 4.56 DEPT spectrum of Haskm-2 in CDCl<sub>3</sub>

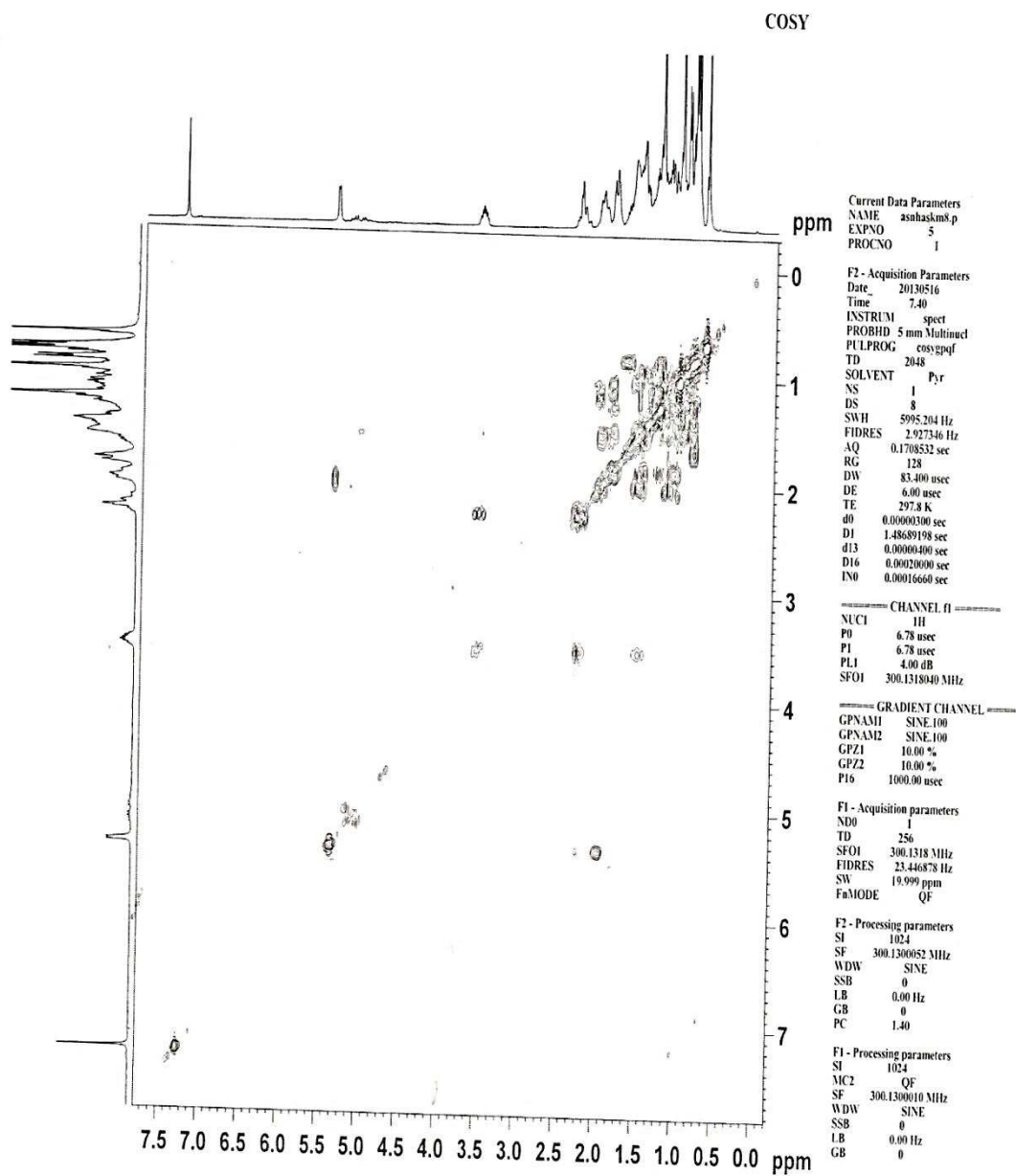


Fig. 4.57  $^1\text{H}$ - $^1\text{H}$  COSY spectrum of Haskm-2 in  $\text{CDCl}_3$

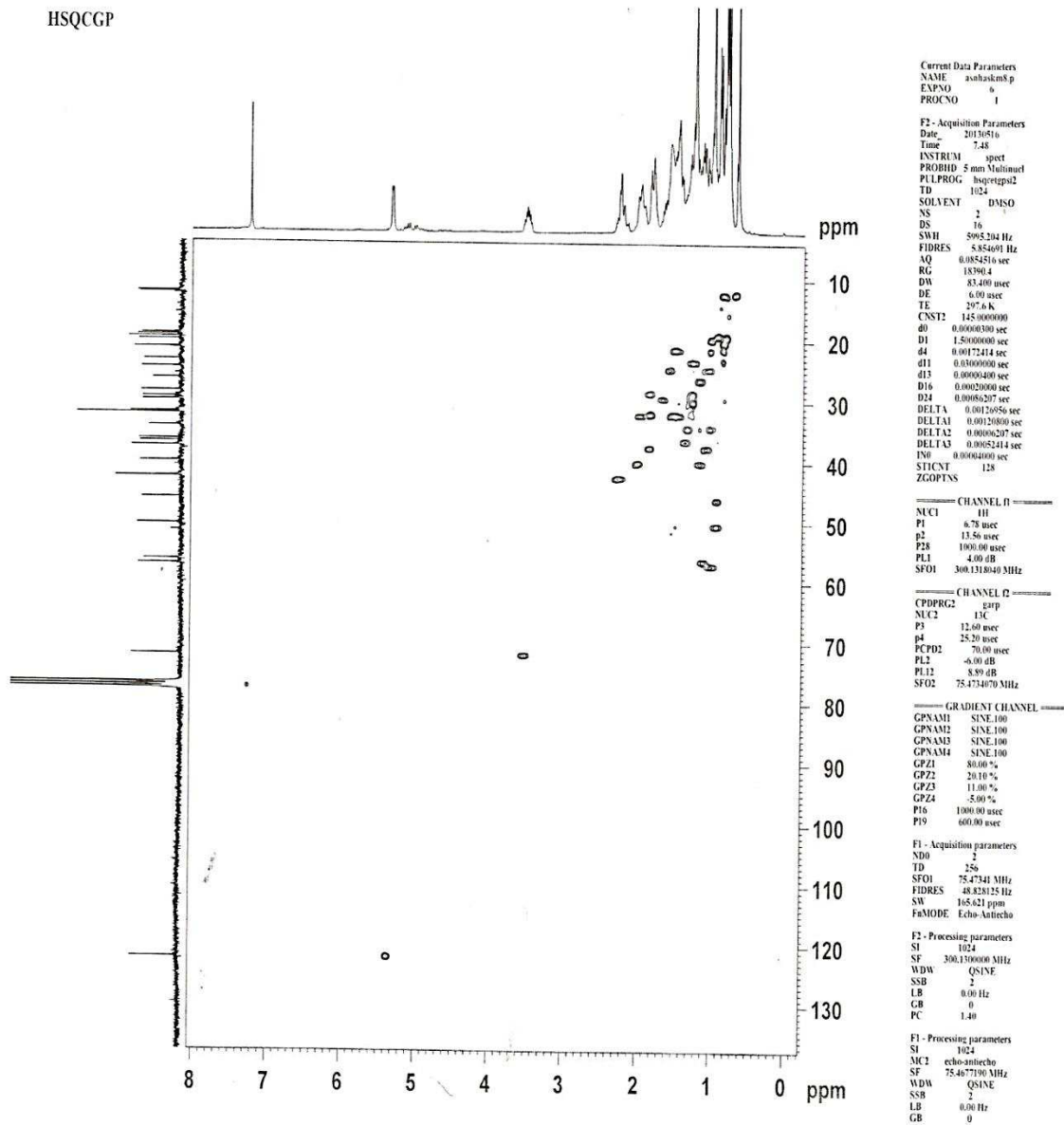


Fig. 4.58 HSQC spectrum of Haskm-2 in  $\text{CDCl}_3$

HMBC

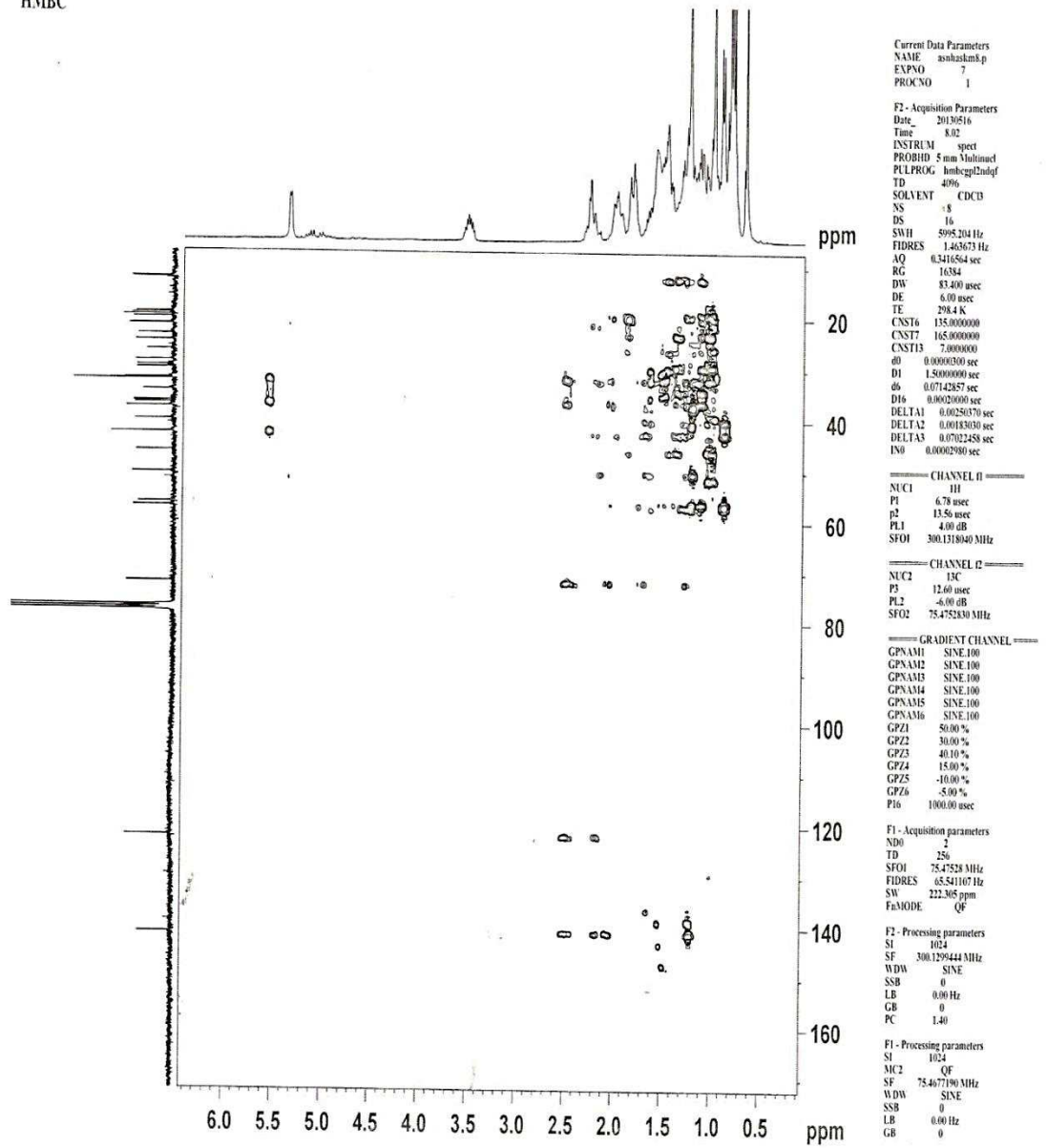


Fig. 4.59  $^1\text{H}$ - $^{13}\text{C}$  HMBC spectrum of Haskm2 in  $\text{CDCl}_3$



### 4.6.3 Characterisation of Haskm-3

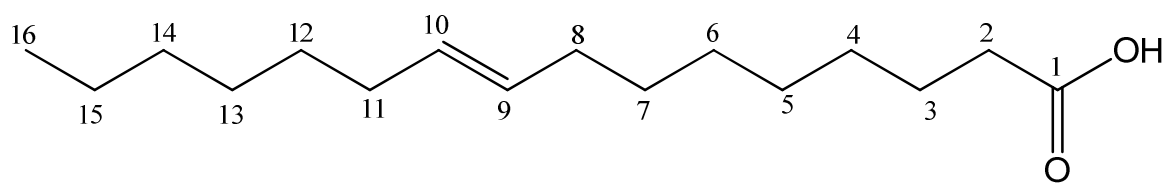
Compound Haskm-3 (15.0 mg) is a white crystalline solid which has a melting point of 51 - 52°C. The MS fragment ions 255 [M+H]<sup>+</sup>, 508 [2M]<sup>-</sup> calculated for molecular formula C<sub>16</sub>H<sub>30</sub>O<sub>2</sub> (254). The IR  $\bar{\nu}$  (cm<sup>-1</sup>) vibrational absorptions at 3760, 2854, 1703 and 1453 cm<sup>-1</sup> indicated the presence of O-H, C-H, C=O and C=C functions respectively. The <sup>1</sup>H NMR signals at  $\delta_{\text{H}}$  0.86-0.88 (3H, t, H<sub>16</sub>) and 1.26-1.43 (18H, s, 9 x CH<sub>2</sub>) are characteristics of methyl and cluster of methylene protons of fatty acid. The peaks at  $\delta_{\text{H}}$  2.37 (t) and 5.34 (t) correspond to methylene protons at C-2 and olefinic methine protons at C-9 and C-10. <sup>13</sup>C NMR spectrum also showed characteristics of fatty acid resonances, which are consistent with hexadec-9-enoic acid skeleton. The DEPT experiment classified the carbon resonances into one methyl carbon, twelve methylene carbons, two methine carbons and one quaternary carbon resonances. The spectroscopic data of Haskm-3 [Table 4.56] was similar to that of cis-hexadec-9-enoic acid previously reported in the literature (Gunstone 1993, Mannina *et al.* 1999, Bus *et al.* 1976, Joshi *et al.*, 2009, Syed *et al.*, 2006). Hence, the structure of Haskm-3 was identified as cis-hexadec-9-enoic acid (**114**).

**Table 4.56:**  $^{13}\text{C}$  and  $^1\text{H}$  NMR ( $\text{CDCl}_3$ ) spectra data of Haskm-3 and Hexadec-9-enoic acid

Assignment	$^{13}\text{C}$	Multiplicity	$^1\text{H}$ , multiplicity	$^{13}\text{C}$	$^1\text{H}$
1	180.65	Q	-	179.85	-
2	34.21	$\text{CH}_2$	2.37, t, 2H	34.03	2.34
3	30.08	$\text{CH}_2$	1.26-1.43, s, 2H	24.69	1.63
4	30.08	$\text{CH}_2$	1.26-1.43, s, 2H	29.35	1.27
5	29.83	$\text{CH}_2$	1.26-1.43, s, 2H	29.46	1.27
6	29.75	$\text{CH}_2$	1.26-1.43, s, 2H	29.61	1.27
7	29.98	$\text{CH}_2$	1.26-1.43, s, 2H	29.26	1.27
8	25.07	$\text{CH}_2$	1.61, m, 2H	25.82	
9	130.11	CH	5.34, t, 1H	130.21	5.28
10	130.40	CH	5.34, t, 1H	130.85	5.28
11	27.61	$\text{CH}_2$	2.02, m, 2H	27.71	
12	29.46	$\text{CH}_2$	1.26-1.43, s, 2H	29.72	1.27
13	29.63	$\text{CH}_2$	1.26-1.43, s, 2H	29.07	1.27
14	32.32	$\text{CH}_2$	1.26-1.43, s, 2H	31.95	1.27
15	23.74	$\text{CH}_2$	1.26-1.43, s, 2H	22.72	1.27
16	14.49	$\text{CH}_3$	0.86-0.88, t, 3H	14.15	0.88

Implied multiplicities of the carbons were determined from the DEPT experiment.

\*Gundstone, 1994, Joshi *et al.*, 2009, Syed *et al.*, 2006



**cis-hexadec-9-enoic acid (114)**

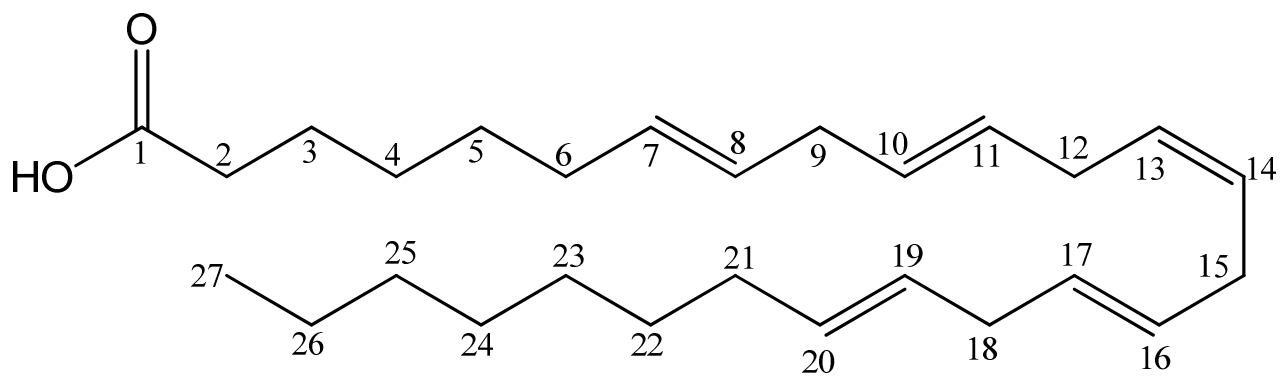
#### 4.6.4 Characterisation of Haskm-4

Compound Haskm-4 (25.0 mg) was obtained as light yellow gelly-like solid. It has a melting point of 85 - 88°C. The MS signals at 299 [M-2K-Na]<sup>+</sup>, 776 [2M-Na-H]<sup>+</sup> correspond to a molecular formula C<sub>27</sub>H<sub>44</sub>O<sub>2</sub> (400). The IR  $\bar{\nu}$  (cm<sup>-1</sup>) vibrations at 3750, 2852, 1707 and 1664 cm<sup>-1</sup> revealed the presence of O-H, C-H, C=O and C=C moieties respectively. The <sup>1</sup>H NMR signals at  $\delta_{\text{H}}$  0.84-0.86 (3H, t, H<sub>27</sub>), 1.18-1.38 (18H, d, 9 x CH<sub>2</sub>) and 5.29 (t) are characteristics of methyl, methylene and olefinic methine protons of fatty acid. <sup>13</sup>C NMR spectrum indicates resonances consistent with polyunsaturated fatty acid skeleton. The identified carbon skeleton were sorted by DEPT experiment into one methyl carbon, fifteen methylene carbons, ten olefinic methine carbons and one quaternary carbon resonances. The <sup>1</sup>H-<sup>1</sup>H COSY spectra data showed correlation of olefinic methine proton at C-7 with methylene protons at C-6 and C-9. Methylene protons at C-2 were correlated with methylene protons at C-3 and C-4, while terminal methyl protons at C-27 also showed correlation with methylene protons at C-24, C-25 and C-26. The correlation of methine proton at C-7 with C-5 and C-9 was shown by <sup>1</sup>H-<sup>13</sup>C HMBC spectrum, while methylene protons at C-9, C-12 and C-21 were correlated with C-11, C-8 and C-19 respectively. Further, methylene protons at C-2 showed correlation with carbonyl C-1. The spectroscopic data of Haskm-4 [Table 4.59] correlated with the reported data from the literature (Gundstone, 1993, Spitzer *et al.*, 1996, Blaise *et al.*, 1997) resulting in elucidation of Haskm-4 to be Z-7,10,13,16,19-heptaicos-pentaenoic acid (**115**).

**Table 4.57:**  $^{13}\text{C}$  and  $^1\text{H}$  NMR ( $\text{CDCl}_3$ ) spectra data of Haskm-4

Assignment	$^{13}\text{C}$	Multiplicity	$^1\text{H}$ , multiplicity
1	180.29	Q	-
2	34.21	$\text{CH}_2$	2.34, t, 2H
3	30.08	$\text{CH}_2$	1.12-1.29, d, 2H
4	30.08	$\text{CH}_2$	1.12-1.29, d, 2H
5	30.08	$\text{CH}_2$	1.12-1.29, d, 2H
6	28.36	$\text{CH}_2$	1.53, bs, 2H
7	127.51	CH	5.33, bs, 1H
8	128.14	CH	5.33, bs, 1H
9	29.45	$\text{CH}_2$	2.75, t, 2H
10	128.30	CH	5.33, bs, 1H
11	128.46	CH	5.33, bs, 1H
12	30.59	$\text{CH}_2$	2.75, t, 2H
13	128.63	CH	5.33, bs, 1H
14	130.10	CH	5.33, bs, 1H
15	31.81	$\text{CH}_2$	2.75, t, 2H
16	130.39	CH	5.33, bs, 1H
17	130.58	CH	5.33, bs, 1H
18	29.52	$\text{CH}_2$	2.75, t, 2H
19	130.61	CH	5.33, bs, 1H
20	132.32	CH	5.33, bs, 1H
21	25.07	$\text{CH}_2$	2.02, bs, 2H
22	29.97	$\text{CH}_2$	1.12-1.29, d, 2H
23	29.82	$\text{CH}_2$	1.12-1.29, d, 2H
24	29.62	$\text{CH}_2$	1.12-1.29, d, 2H
25	32.31	$\text{CH}_2$	1.12-1.29, d, 2H
26	23.06	$\text{CH}_2$	1.12-1.29, d, 2H
27	14.42	$\text{CH}_3$	0.84-0.86, t, 3H

Implied multiplicities of the carbons were determined from the DEPT experiment.



Z-7,10,13,16,19-heptaecos-pentaenoic acid (**115**)

#### 4.6.5 Characterisation of Haskm-5

Haskm-5 (22.0 mg) is a white powdered solid (melting point 51 - 53°C). The ESI MS fragment ions 309.2 [M+H]<sup>+</sup>, 331.4 [M+Na]<sup>+</sup> correspond to molecular formula C<sub>20</sub>H<sub>36</sub>O<sub>2</sub> (308). The IR  $\bar{\nu}$  (cm<sup>-1</sup>) absorptions of O-H, C-H, C=O and C=C functions appeared at 3753, 2925, 1725 and 1464 cm<sup>-1</sup> respectively. The <sup>1</sup>H NMR signals at  $\delta_H$  0.89 (3H, t, H<sub>20</sub>) and 1.18-1.38 (20H, m, 10 x CH<sub>2</sub>) are characteristics of methyl and accumulated methylene protons of fatty acid, while the peak at  $\delta_H$  5.29 (t) correspond to olefinic protons of fatty acid. <sup>13</sup>C NMR spectra data revealed resonances consistent with di-unsaturated fatty acid skeleton. The carbon skeletons were classified by DEPT spectrum into one methyl carbon, fourteen methylene carbons, four methine carbons and one quaternary carbon resonances. The spectroscopic data of Haskm-5 [Table 4.58] was correlated to cis-eicos-5,8-dienoic acid (Gunstone and Seth, 1994, Gunstone *et al.*, 1995, Lie ken jie *et al.*, 1996). The structure of Haskm-5 was identified as Z5, 8-eicosdienoic acid (**116**).

All these isolated compounds from *S. kraussiana* are being characterized and reported for the first time from *Smilax kraussiana*.

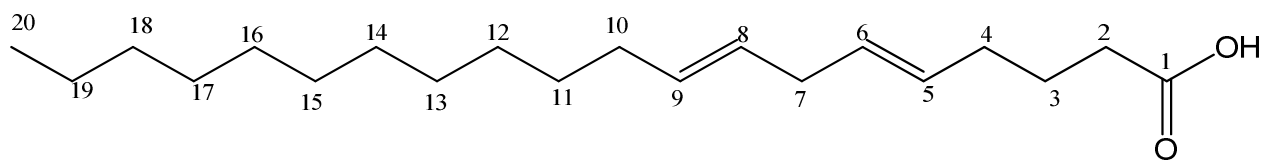
**Table 4.58:**  $^{13}\text{C}$  and  $^1\text{H}$  NMR ( $\text{CDCl}_3$ ) spectra data of Haskm-5 and Z5,8-eicosdienoic acid

Assignment	$^{13}\text{C}$	Multiplicity	$^1\text{H}$ , multiplicity	$^{13}\text{C}$
1	180.45	Q	-	180.36
2	34.26	$\text{CH}_2$	1.18-1.38, d, 2H	33.48
3	29.47	$\text{CH}_2$	3.58, m, 1H	24.51
4	25.07	$\text{CH}_2$	1.56, bs, 2H	26.48
5	127.52	CH	5.29, t, 1H	129.09
6	128.15	CH	5.29, t, 1H	128.77
7	26.02	$\text{CH}_2$	2.74, s, 2H	25.63
8	128.69	CH	5.29, t, 1H	127.88
9	130.65	CH	5.29, t, 1H	130.52
10	27.60	$\text{CH}_2$	1.98-2.11, s, 2H	27.26
11	29.53	$\text{CH}_2$	1.18-1.38, d, 2H	29.37
12	29.75	$\text{CH}_2$	1.18-1.38, d, 2H	29.37
13	29.96	$\text{CH}_2$	1.18-1.38, d, 2H	29.37
14	30.09	$\text{CH}_2$	1.18-1.38, d, 2H	29.98
15	30.69	$\text{CH}_2$	1.18-1.38, d, 2H	29.98
16	30.09	$\text{CH}_2$	1.18-1.38, d, 2H	29.98
17	30.09	$\text{CH}_2$	1.18-1.38, d, 2H	29.98
18	32.32	$\text{CH}_2$	1.18-1.38, d, 2H	31.57
19	23.09	$\text{CH}_2$	1.18-1.38, d, 2H	22.63
20	14.51	$\text{CH}_3$	0.89, t, 3H	14.12

Implied multiplicities of the carbons were determined from the DEPT experiment.

\*Lie ken jie *et al.*, 1996





**Z5, 8-icosdienoic acid (116)**

#### 4.7 Antiproliferative activity of isolated compounds obtained from *Smilax kraussiana* (Aerial parts)

The isolated compounds from extracts of *S. kraussiana* were tested for *in-vitro* antiproliferative activities against four human cancer cell lines; leukaemia carcinoma (K562), hepatic liver (WRL) cell lines, breast carcinoma (MCF-7) and colorectal carcinoma (COLO) at 100 and 50  $\mu\text{M}$  concentrations.

Eighteen compounds isolated from aerial parts of *S. kraussiana* inhibited the growth of tested cancer cell lines at different concentrations. Octadecane (Haskh-1) and Ursa-12,20-dien-19-ol-3-one (Haskh-4) showed antiproliferative activities against K-562 and WRL with  $\text{IC}_{50}$  values of 32.0 and 114.2  $\mu\text{M}$ , and 75.20 and 256  $\mu\text{M}$  respectively. Oleane-9(11),12-dien-3-ol coded Haske-1, Lup-5,11,20-trien-23-ol (Haske-2) and Ethylheptadec-17-oic-9-enoate (Haske-6) obtained from ethyl acetate extract of *S. kraussiana* aerial parts inhibited the growth of COLO, K-562 and WRL with  $\text{IC}_{50}$  values of 125.3, 90.2 and 125.5  $\mu\text{M}$  respectively. Further, fatty acids Haske-7 and Haske-8 possess high cytotoxic activities against all tested cell lines except MCF-7. The most active and prominent compound isolated from *S. kraussiana*, diosgenin (Haske-9) exhibited significant antiproliferative activity against all the cell lines: K-562, WRL, MCF-7 and COLO with corresponding  $\text{IC}_{50}$  values of 6.25, 14.34, 38.0 and 12.4  $\mu\text{M}$ . The isolated compounds from methanol extract of *S. kraussiana* aerial parts, campesterol (Haskm-2), showed inhibition of K-562 and WRL cells with  $\text{IC}_{50}$  values of 432.1 and 85.2, while cis-hexadec-9-enoic acid (Haskm-3) exhibited anticancer activities against K-562 and WRL cell lines with  $\text{IC}_{50}$  values of 50.66 and 30.10  $\mu\text{M}$ . Meanwhile polyunsaturated fatty acid, Haskm-4 and Z5,8-eicosdienoic acid coded Haskm-5 also exhibited antiproliferative properties against K-562, MCF-7 and K-562, COLO with the corresponding  $\text{IC}_{50}$  values between 23.23 and 86.36; and 13.13 and 141.5  $\mu\text{M}$ . The antiproliferative activities of all isolated compounds with their respective  $\text{IC}_{50}$  values were shown in Table 4.59

**Table 4.59:** Antiproliferative activities of isolated compounds from extracts of *S. kraussiana* (aerial parts)

S/No.	Compound codes from hexane extract	Cell lines/IC <sub>50</sub> ( $\mu$ M)			
		K562	WRL	MCF-7	COLO
1.	Haskh-1	32.00	114.20	***	***
2.	Haskh-2	***	***	***	***
3.	Haskh-3	140.20	195.40	***	***
4.	Haskh-4	75.20	256.00	450.10	225.00
	<b>Compound codes from ethyl acetate extract</b>				
5.	Haske-1	***	482.30	***	125.30
6.	Haske-2	90.20	282.20	282.20	301.00
7.	Haske-3	***	295.00	***	216.50
8.	Haske-4	***	248.50	***	410.00
9.	Haske-5	322.00	420.00	***	233.00
10.	Haske-6	483.10	125.50	***	182.00
11.	Haske-7	75.92	104.60	***	145.00
12.	Haske-8	50.72	35.20	***	282.2
13.	Haske-9	12.25	14.34	35.50	12.40
	<b>Compound codes from methanol extract</b>				
14.	Haskm-1	***	392.20	***	280.00
15.	Haskm-2	432.10	85.20	481.30	365.10
16.	Haskm-3	50.66	30.10	***	283.00
17.	Haskm-4	23.23	495.30	82.36	65.30
18.	Haskm-5	13.13	462.10	104.30	141.50
	Tamoxifen	7.26	12.25	8.54	10.08

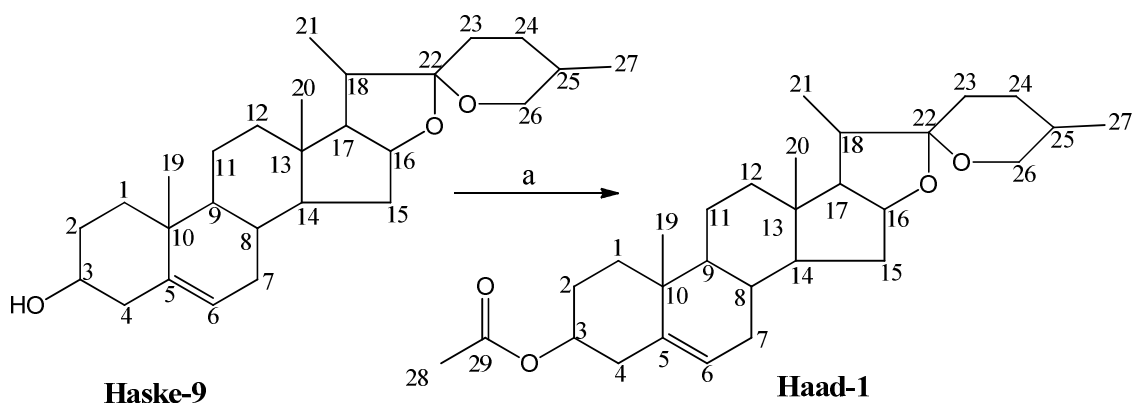
\*\*\* IC<sub>50</sub> (ug/mL) >500; K562 - leukaemia carcinoma; WRL - hepatic liver cell lines; MCF-7 – breast carcinoma; COLO – colorectal carcinoma.

## 4.8 Synthetic modification of diosgenin (First reaction scheme)

3 $\beta$ -hydroxy-5-spirostene (diosgenin) is a spiroacetal steroid which has been isolated from *Smilax spp.*, and other plant families. It was the most abundant and anticancer-active pure molecule isolated from ethyl acetate extract of aerial parts of *S. kraussiana*. Diosgenin was modified synthetically to obtain new derivatives. Two reaction schemes were proposed. The first scheme involved synthetic modification of diosgenin to form diosgenin acetate. The reductive cleavage of ring F of spiroketal linkage of diosgenin acetate was done by using sodium cyanoborohydride in ethanoic acid (CH<sub>3</sub>COOH) at room temperature to get the alcohol, Haad-2a that possesses furostenic system at spiroketal position (C-22). The first reaction scheme eventually yielded fifteen different furostane analogues. The second scheme involved oxidation and condensation reactions at C-7 position and protection of spiroketal linkage of diosgenin to give twelve analogues. Nineteen out of the twenty seven compounds from the two schemes are being synthesized for the first time.

### 4.8.1. Synthesis and characterization of (22 $\beta$ ,25R)-spirost-5-en-3 $\beta$ -yl-3-acetate (Haad-1)

Acetylation of diosgenin (Haske-9) was done using acetic anhydride in pyridine (Chaosuancharoen *et al.*, 2004) in the presence of chloroform as a solvent to yield the acetate as a creamy white crystalline compound, Haad-1 (Chaosuancharoen *et al.*, 2004).



**agents and conditions:** a) Acetic anhydride (Ac<sub>2</sub>O), chloroform, dry pyridine, RT, 6 hrs

Haad-1 (1.01 g, 91%) has a melting point of 193 - 196°C (195-196°C, Rosado-Abon *et al.*, 2013). The ESI-MS fragment ions 457.3 [M+H]<sup>+</sup>, 479.3 [M+Na]<sup>+</sup>, 495.4 [M+K]<sup>+</sup> correspond to a molecular formula C<sub>29</sub>H<sub>44</sub>O<sub>4</sub> (456) [Fig. 4.60]. The <sup>1</sup>H NMR [Fig. 4.61], <sup>13</sup>C NMR [Fig. 4.62] and DEPT spectra of Haad-1 [Fig. 4.63] are similar to that of diosgenin except the formation of acetate at C-3 [Table 4.60]. Hence, Haad-1 is (22β,25R)-spirost-5-en-3β-yl-3-acetate (Rosado-Abon *et al.*, 2013). The differences in <sup>1</sup>H and <sup>13</sup>C NMR of Haad-1 and diosgenin are listed below.

<sup>1</sup>H NMR (CDCl<sub>3</sub>): 2.01 (s, 3H, H<sub>28</sub>, CH<sub>3</sub>COO, Acetate);

<sup>13</sup>C NMR (CDCl<sub>3</sub>): 170.82 (C-29) and 30.12 (C-28) [Table 4.60; Figs: 4.61 - 4.63]

IR (KBr, cm<sup>-1</sup>): 2907 (C-H), 1724 (C=O), 1651 (C=C), 1231 (C-O)

**Table 4.60:** Comparison of  $^{13}\text{C}$  and  $^1\text{H}$  NMR data of Diosgenin and Haad-1

Assignment	$^{13}\text{C}$	Multiplicity	$^1\text{H}$ , multiplicity	$^{13}\text{C}$	$^1\text{H}$
1	21.23	$\text{CH}_2$	1.44-2.03, m, 2H	21.74	1.44-1.96, m, 2H
2	37.63	$\text{CH}_2$	1.44-2.03, m, 2H	37.34	1.44-1.96, m, 2H
3	72.11	CH	3.58, m, 1H	74.26	4.35, s, 1H
4	42.68	$\text{CH}_2$	1.44-2.03, m, 2H	42.00	1.44-1.96, m, 2H
5	141.22	Q	-	140.05	-
6	121.80	CH	5.35, t, 1H	122.72	5.36, t, 1H
7	32.45	$\text{CH}_2$	2.30, t, 2H	32.42	2.32, t, 2H
8	31.79	CH	1.44-2.03, m, 1H	31.80	1.44-1.96, m, 2H
9	50.48	CH	1.44-2.03, m, 1H	50.35	1.44-1.96, m, 2H
10	37.04	Q	-	37.10	-
11	32.24	$\text{CH}_2$	1.44-2.03, m, 2H	32.24	1.44-1.96, m, 2H
12	29.20	$\text{CH}_2$	1.44-2.03, m, 2H	29.19	1.44-1.96, m, 2H
13	40.66	Q	-	40.66	-
14	40.19	CH	1.44-2.03, m, 1H	40.19	1.44-1.96, m, 2H
15	30.69	$\text{CH}_2$	1.44-2.03, m, 2H	30.66	1.44-1.96, m, 2H
16	81.22	CH	4.41, m, 1H	81.16	4.59, m, 1H
17	62.52	CH	1.44-2.03, m, 1H	62.52	1.44-1.96, m, 2H
18	56.93	CH	1.44-2.03, m, 1H	56.82	1.44-1.96, m, 2H
19	14.90	$\text{CH}_3$	0.97-1.31, m, 3H	14.89	0.96-1.32, m, 3H
20	16.67	$\text{CH}_3$	0.97-1.31, m, 3H	16.64	0.96-1.32, m, 3H
21	17.51	$\text{CH}_3$	0.79-0.81, m, 3H	17.51	0.78-0.86, m, 3H
22	109.67	Q	-	109.60	-
23	32.02	$\text{CH}_2$	1.44-2.03, m, 2H	32.21	1.44-1.96, m, 2H
24	28.13	$\text{CH}_2$	1.44-2.03, m, 2H	28.12	1.44-1.96, m, 2H
25	42.68	CH	1.44-2.03, m, 1H	42.00	1.44-1.96, m, 2H
26	67.24	$\text{CH}_2$	3.38, d, 3H	67.19	3.38, d, 3H
27	19.80	$\text{CH}_3$	0.97-1.31, m, 3H	19.69	0.96-1.32, m, 3H
28	-	$\text{CH}_3$	-	<b>30.07</b>	<b>2.01, s, 3H</b>
29	-	Q	-	<b>170.82</b>	-

Implied multiplicities of the carbons were determined from the DEPT experiment.

\*Haske-9

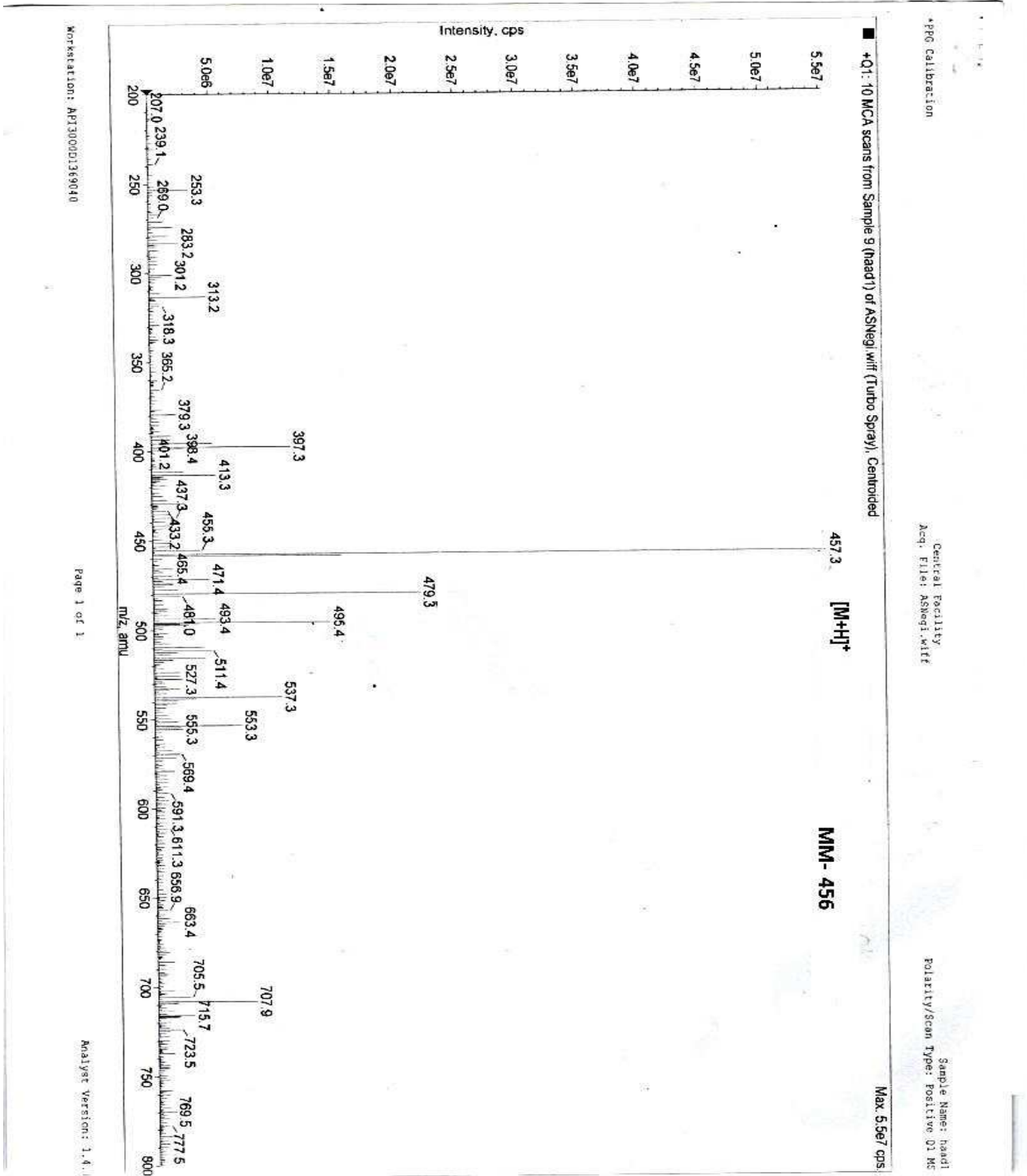
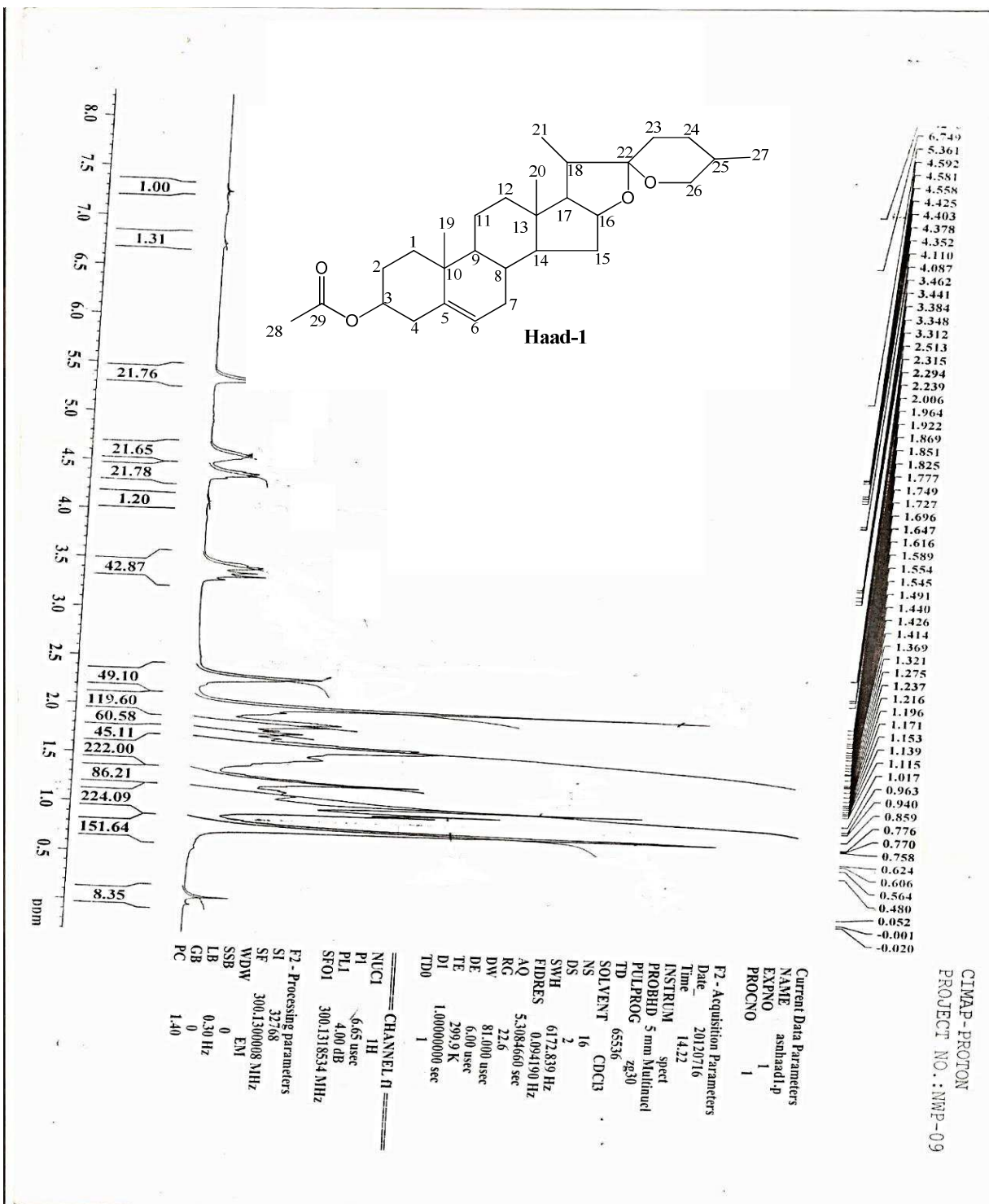


Fig. 4.60: ESI-MS spectrum of Haad-1 in MeOH



CIMAP-PROTON  
PROJECT NO.: NMP-09

Fig. 4.61: <sup>1</sup>H NMR spectrum of Haad-1 in CDCl<sub>3</sub>



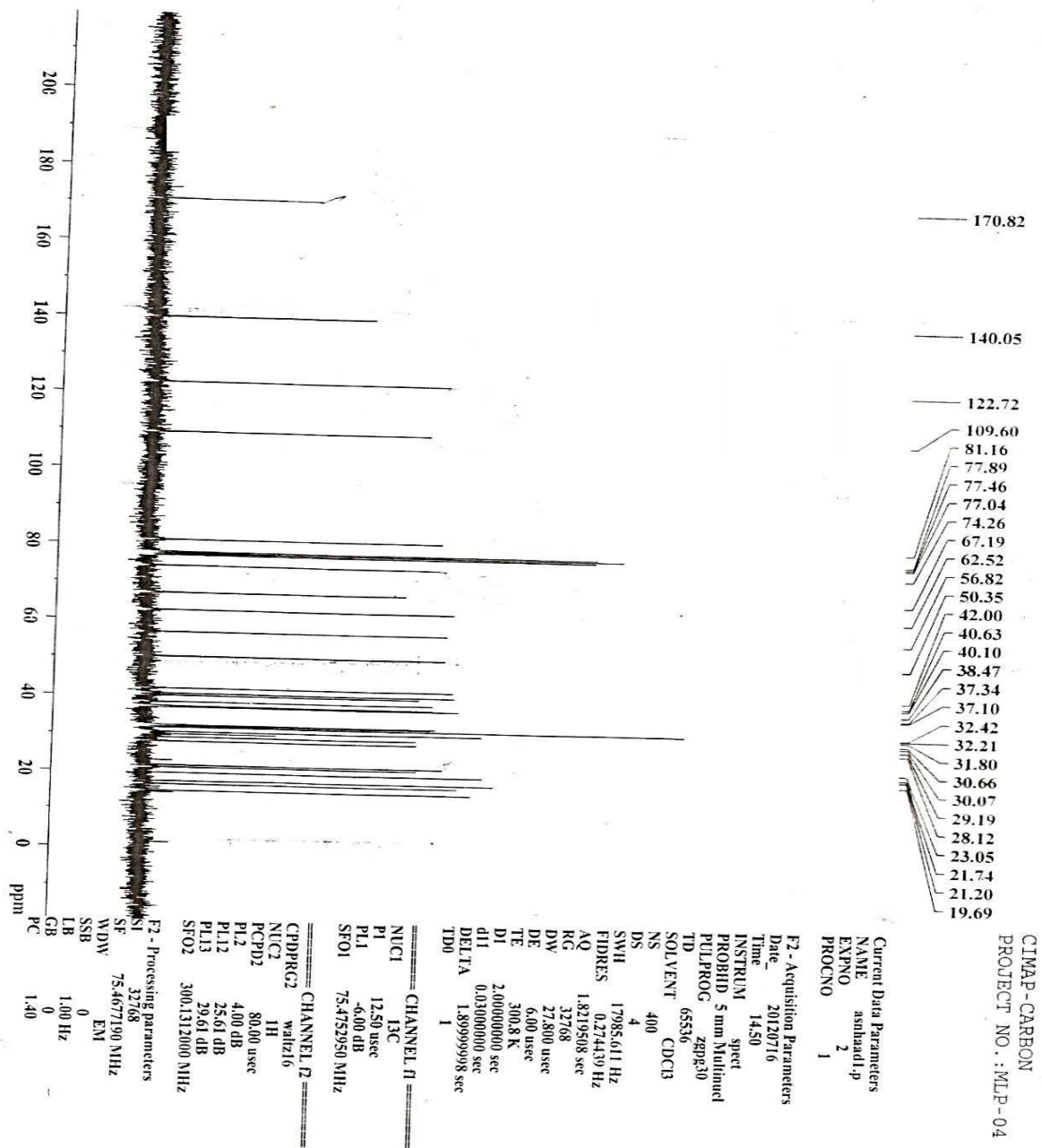
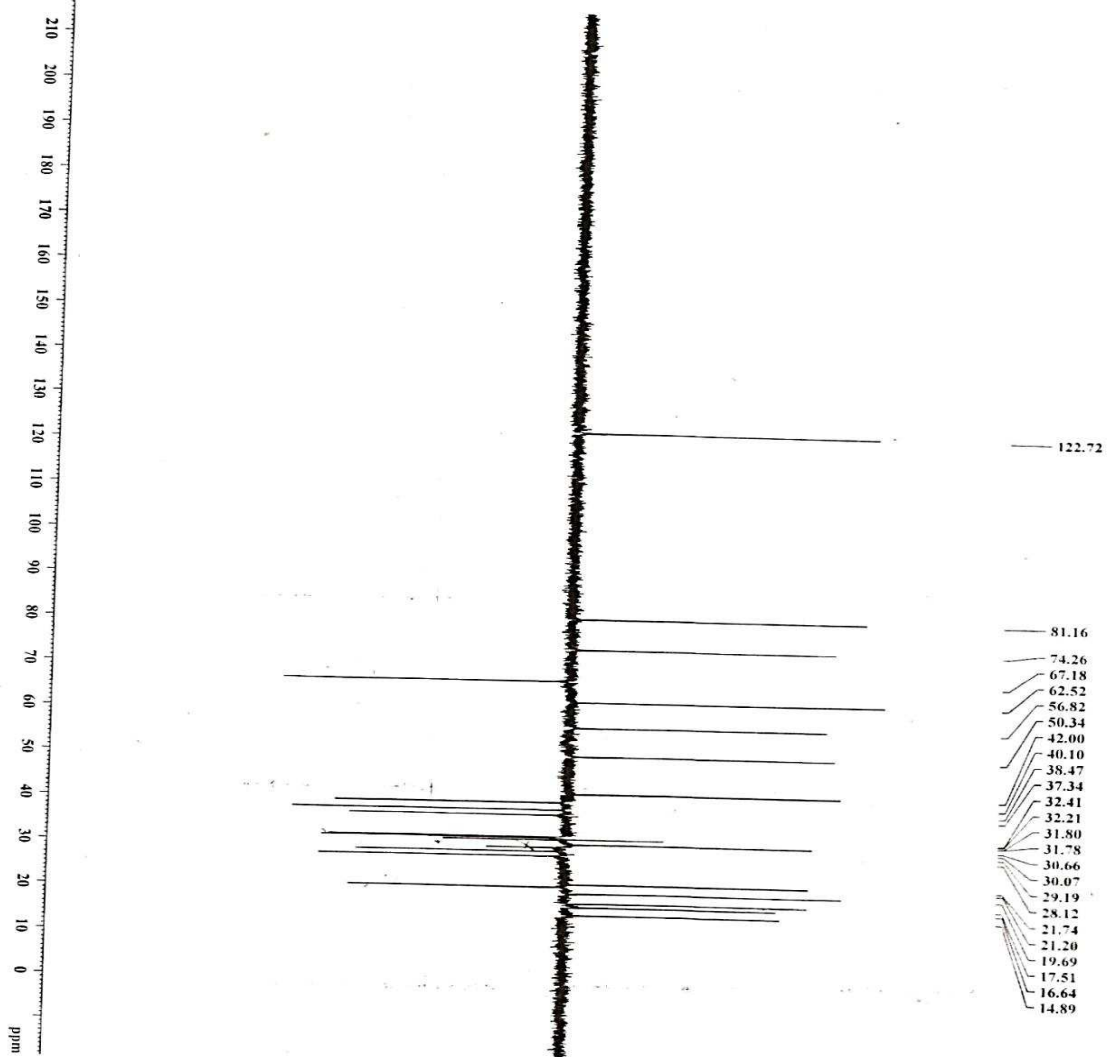


Fig. 4.62:  $^{13}\text{C}$  NMR spectrum of Haad-1 in  $\text{CDCl}_3$



CIMAP-DEPT 135  
PROJECT NO.: ILP-13

```

Current Data Parameters
NAME      amhad1.p
EXPNO     3
PROCNO    1

F2 - Acquisition Parameters
Date_     20120716
Time      14:59
INSTRUM   spect
PROBHD    5 mm MSL5mm
PULPROG   zgpg30
TD         65536
SOLVENT   DCl3
NS         261
DS         4
SWH        17985.611 Hz
FIDRES     0.274439 Hz
AQ         1.8219508 sec
RG         16384
DM         27.800 usec
DE         6.00 usec
TE         300.8 K
D1         2.00000000 sec
d12        0.00000000 sec
DELTA     0.000015912 sec
TD0        1

===== CHANNEL f1 =====
NUC1       13C
P1         12.50 usec
P2         25.00 usec
PL1        -6.00 dB
SFO1       75.475950 MHz

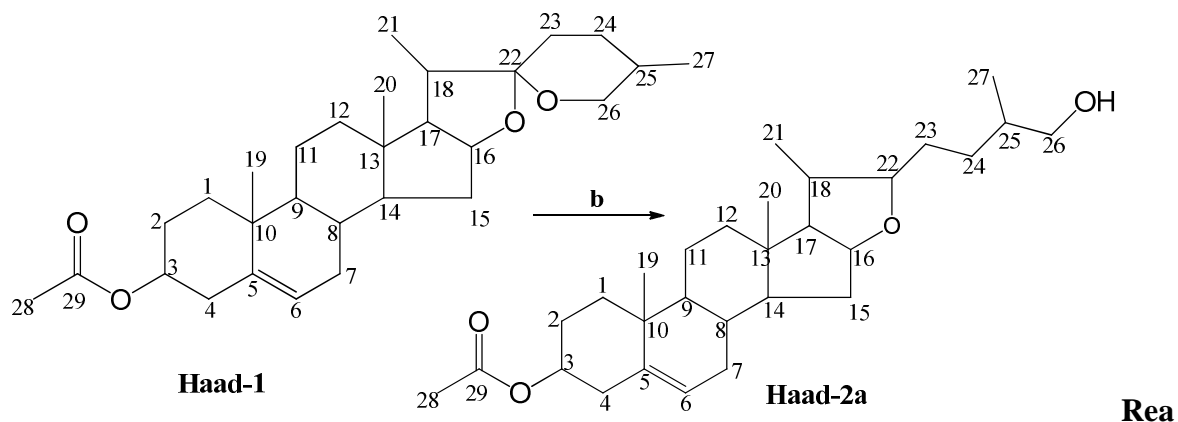
===== CHANNEL f2 =====
CPDPRG2   waltz16
NUC2       1H
P3         6.65 usec
P4         13.30 usec
PCPD2     80.00 usec
PL2        4.00 dB
PL12      25.61 dB
SFO2       300.1312000 MHz

F2 - Processing parameters
SI         32768
SF         75467190 MHz
WDW        EM
SSB        0
GB         1.00 Hz
PC         1.40
  
```

Fig. 4.63: DEPT spectrum of Haad-1 in CDCl<sub>3</sub>

#### 4.8.2. Synthesis and characterization of (22 $\beta$ ,25R)-26-hydroxyfurost-5-en-3 $\beta$ -acetate (Haad-2a)

The reduction of Haad-1 at spiroketal ring in the presence of Sodium cyanoboro hydride (NaCNBH<sub>4</sub>) in glacial acetic acid gave 26-hydroxy analogue coded Haad-2a (Chaosuancharoen *et al.*, 2004).



**agents and conditions:** b) AcOH, NaCNBH<sub>3</sub>, RT, 2hrs

Haad-2a (164 mg, 81%) has a melting point of 121 - 122°C. The ESI-MS fragment ions 459.4 [M+H]<sup>+</sup>, 481.3 [M+Na]<sup>+</sup>, 497.4 [M+K]<sup>+</sup> calculated for molecular formula C<sub>29</sub>H<sub>46</sub>O<sub>4</sub> (458) [Fig. 4.64]. The <sup>1</sup>H NMR signal at  $\delta_H$  3.36 (bs) and 3.48 (m) were due to the presence of oxymethine proton at C-22 and oxymethylene protons of alcohol at C-26 [Fig. 4.65]. <sup>13</sup>C NMR [Fig. 4.66] and DEPT experiment [Fig. 4.67] of Haad-2a are characteristics of diogenin acetate except the formation of methine and methylene Carbons at 22 and 26 positions by breakage of spiroketal bond [Table 4.61]. Therefore, Haad-2a is (22 $\beta$ ,25R)-26-hydroxyfurost-5-en-3 $\beta$ -acetate. The differences in <sup>1</sup>H and <sup>13</sup>C NMR of Haad-2a and Haad-1 are shown below.

<sup>1</sup>H NMR (CDCl<sub>3</sub>): 3.36 (bs, 1H, H<sub>22</sub>), 3.48 (m, 2H, 26-CH<sub>2</sub>OH);

<sup>13</sup>C NMR (CDCl<sub>3</sub>): 90.71 (C-22), 68.27 (C-26) [Table 4.61; Figs: 4.65 - 4.67]

IR (KBr, cm<sup>-1</sup>): 3423 (O-H), 2934 (C-H), 1731 (C=O), 1664 (C=C), 1376 (C-O)

**Table 4.61:** Comparison of  $^{13}\text{C}$  and  $^1\text{H}$  NMR data of Haad-1 and Haad-2a

Assignment	* $^{13}\text{C}$	Multiplicity	* $^1\text{H}$	$^{13}\text{C}$	$^1\text{H}$
1	21.74	CH <sub>2</sub>	1.44-1.96, m, 2H	21.03	1.34-1.90, m, 2H
2	37.34	CH <sub>2</sub>	1.44-1.96, m, 2H	37.37	1.34-1.90, m, 2H
3	74.26	CH	4.35, m, 1H	74.26	4.34, m, 1H
4	42.00	CH <sub>2</sub>	1.44-1.96, m, 2H	38.46	1.34-1.90, m, 2H
5	140.05	Q	-	140.04	-
6	122.72	CH	5.36, t, 1H	122.74	5.40, t, 1H
7	32.42	CH <sub>2</sub>	2.32, t, 2H	32.36	2.36, t, 2H
8	31.80	CH	1.44-1.96, m, 1H	31.94	1.34-1.90, m, 2H
9	50.35	CH	1.44-1.96, m, 1H	50.39	1.34-1.90, m, 2H
10	37.10	Q	-	37.07	-
11	32.24	CH <sub>2</sub>	1.44-1.96, m, 2H	30.46	1.34-1.90, m, 2H
12	29.19	CH <sub>2</sub>	1.44-1.96, m, 2H	30.06	1.34-1.90, m, 2H
13	40.66	Q	-	39.78	-
14	40.19	CH	1.44-1.96, m, 1H	38.28	1.34-1.90, m, 2H
15	30.66	CH <sub>2</sub>	1.44-1.96, m, 2H	32.59	1.34-1.90, m, 2H
16	81.16	CH	4.59, m, 1H	83.57	4.63, m, 1H
17	62.52	CH	1.44-1.96, m, 1H	65.48	1.34-1.90, m, 2H
18	56.82	CH	1.44-1.96, m, 1H	57.28	1.34-1.90, m, 2H
19	14.89	CH <sub>3</sub>	0.96-1.32, m, 3H	19.69	0.83-1.29, m, 3H
20	16.64	CH <sub>3</sub>	0.96-1.32, m, 3H	17.00	0.83-1.29, m, 3H
21	17.51	CH <sub>3</sub>	0.78-0.86, m, 3H	16.80	0.83-1.29, m, 3H
22	109.60	Q	-	<b>90.71</b>	<b>3.36, s, 1H</b>
23	32.21	CH <sub>2</sub>	1.44-1.96, m, 2H	32.21	1.34-1.90, m, 2H
24	28.12	CH <sub>2</sub>	1.44-1.96, m, 2H	28.12	1.34-1.90, m, 2H
25	42.00	CH	1.44-1.96, m, 1H	42.00	1.34-1.90, m, 1H
26	67.19	CH <sub>2</sub>	3.38, d, 2H	68.27	<b>3.48, m, 2H</b>
27	19.69	CH <sub>3</sub>	0.96-1.32, m, 3H	19.69	0.83-1.29, m, 3H
28	30.07	CH <sub>3</sub>	2.01, s, 3H	30.82	2.05, s, 3H
29	170.82	Q	-	<b>170.91</b>	-

Implied multiplicities of the carbons were determined from the DEPT experiment.  
\* Haad-1

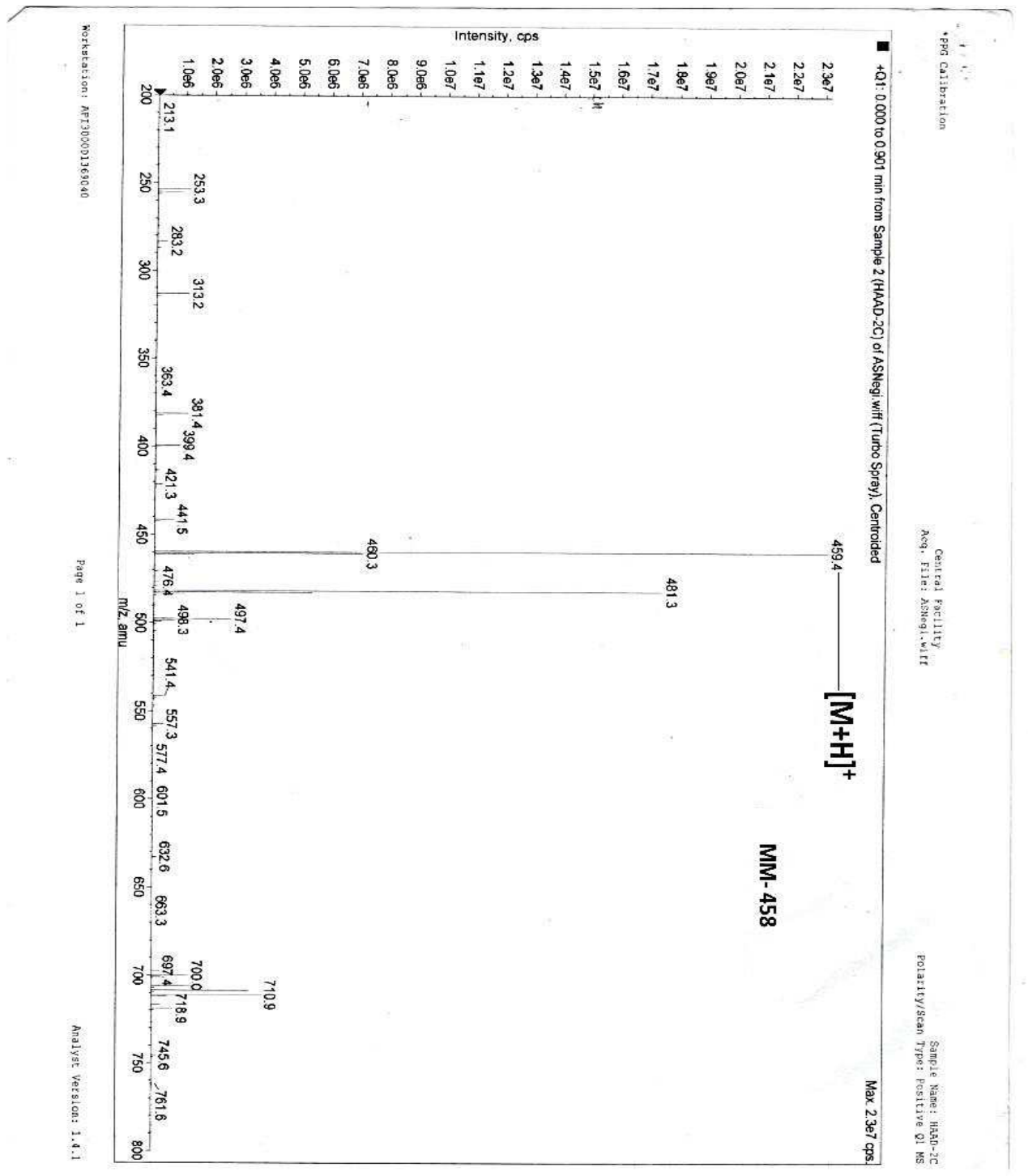


Fig. 4.64: ESI-MS spectrum of Haad-2a in MeOH

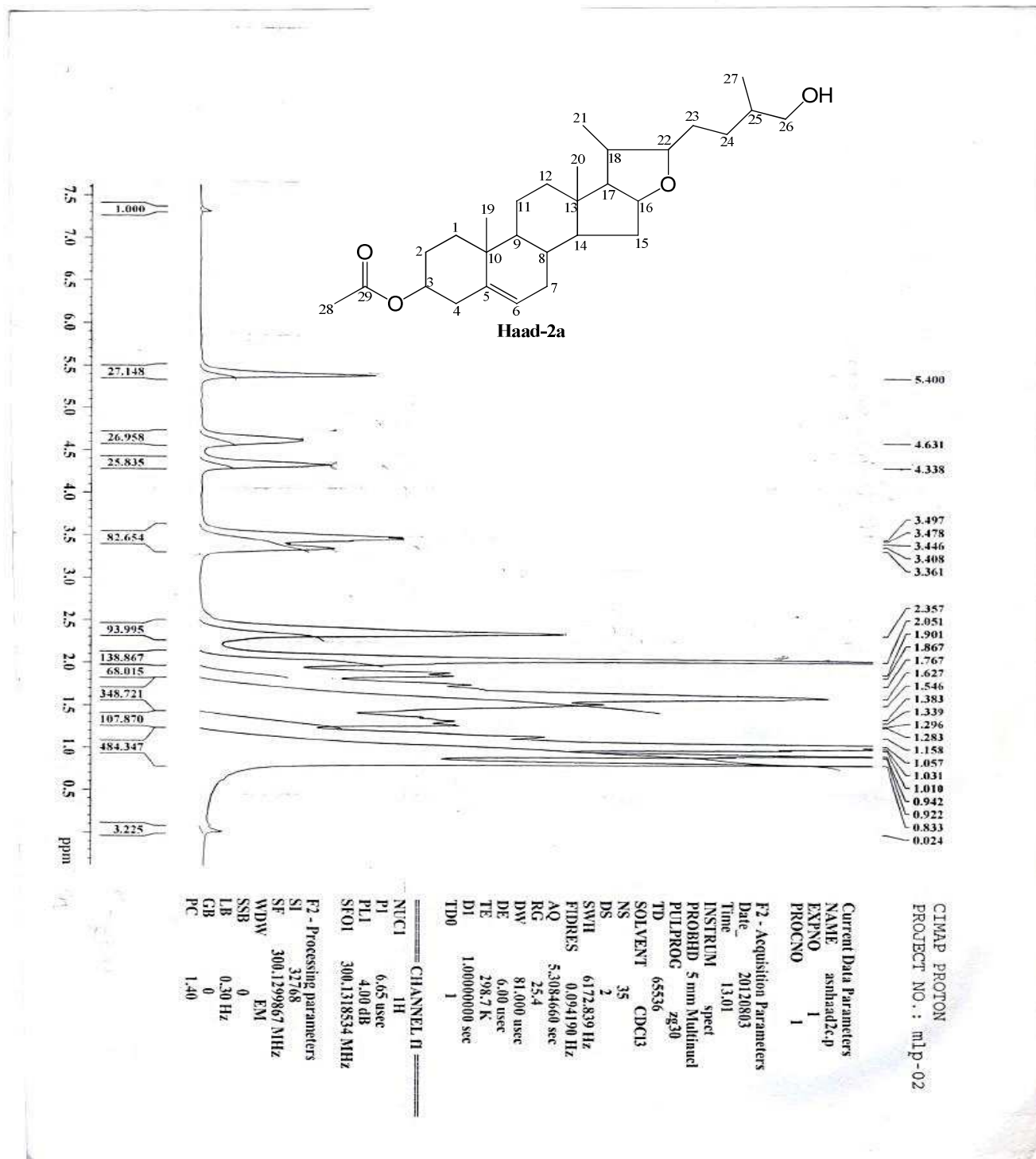
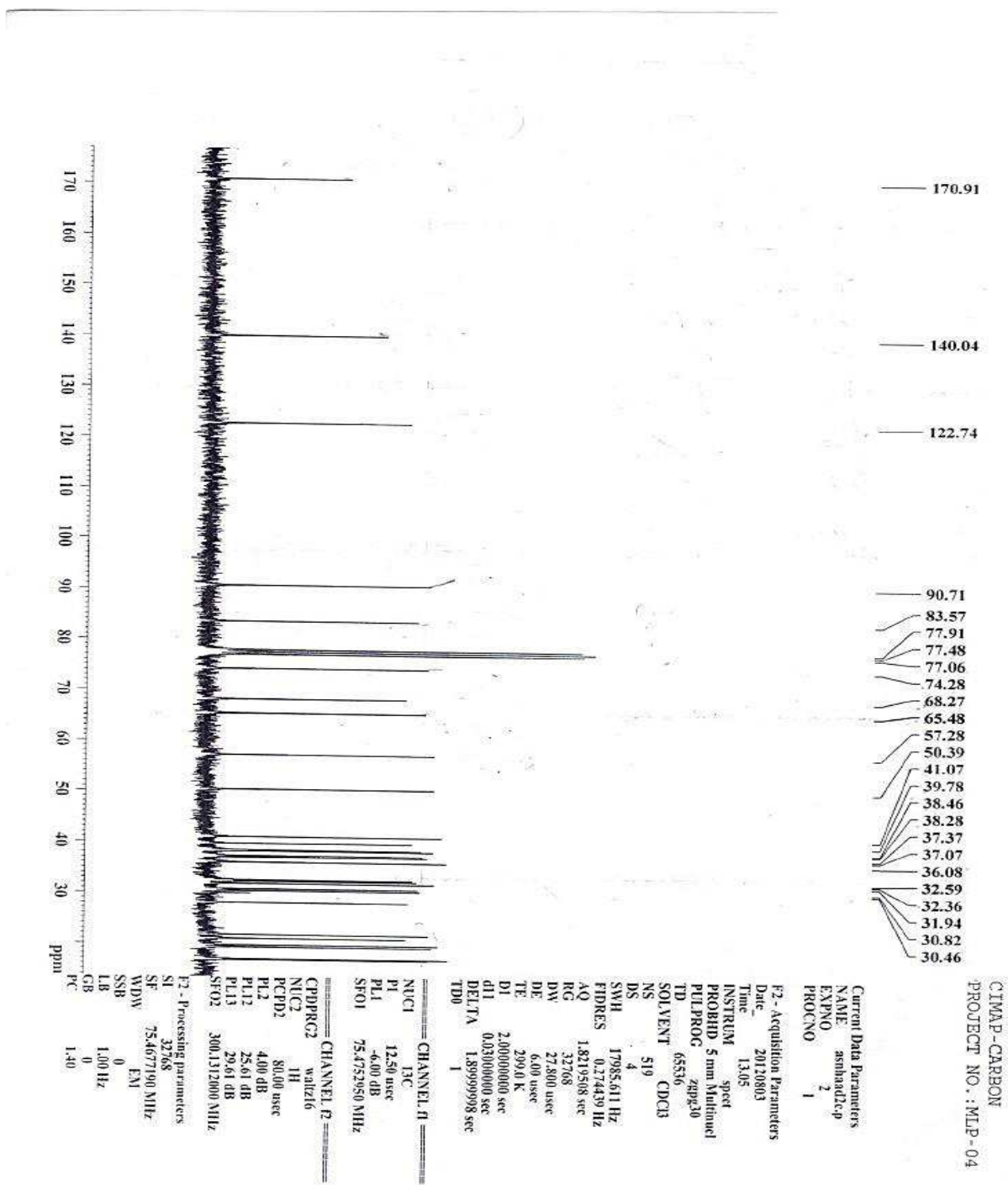
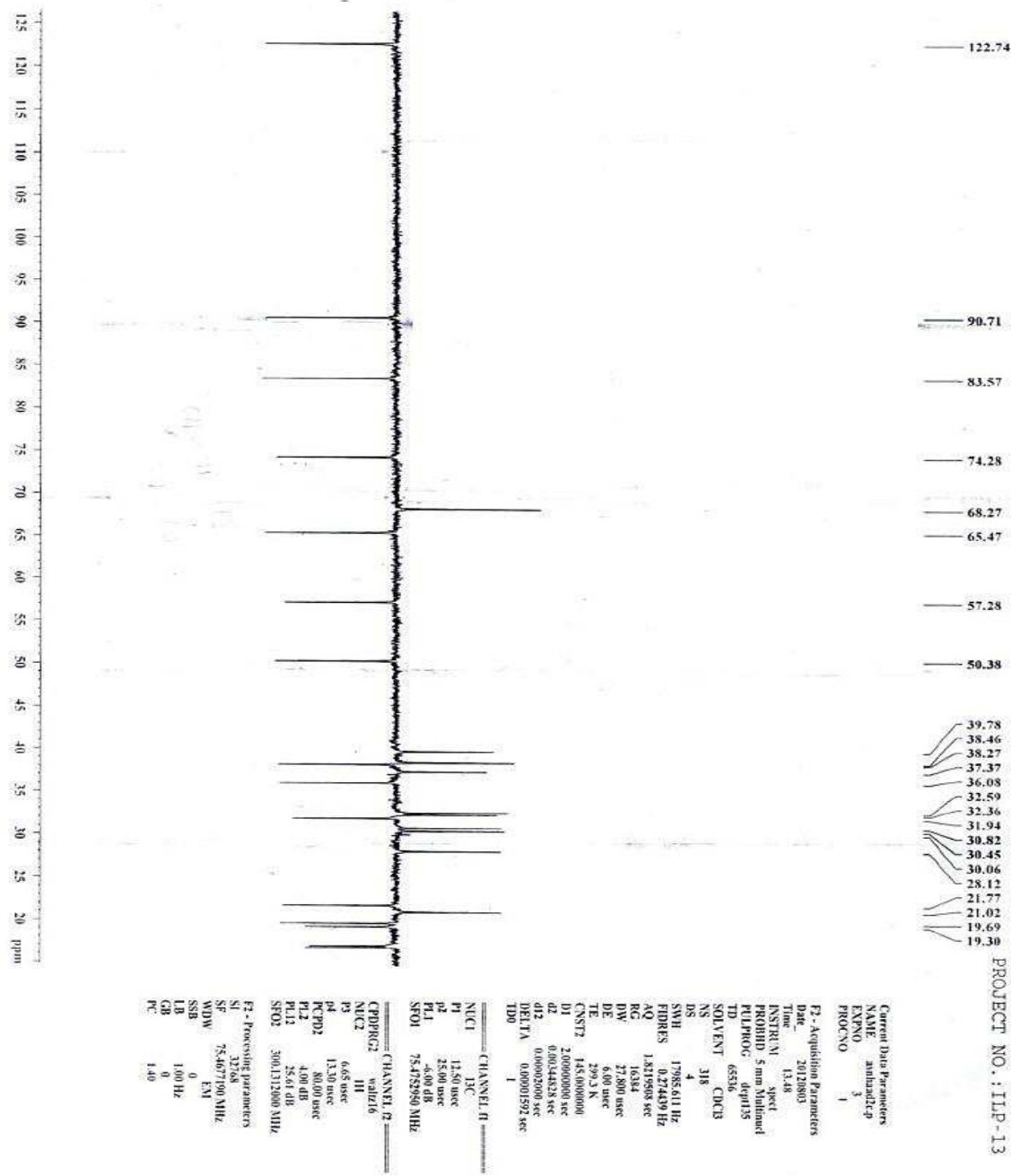


Fig. 4.65:  $^1\text{H}$  NMR spectrum of Haad-2a in  $\text{CDCl}_3$



**Fig. 4.66:**  $^{13}\text{C}$  NMR spectrum of Haad-2a in  $\text{CDCl}_3$



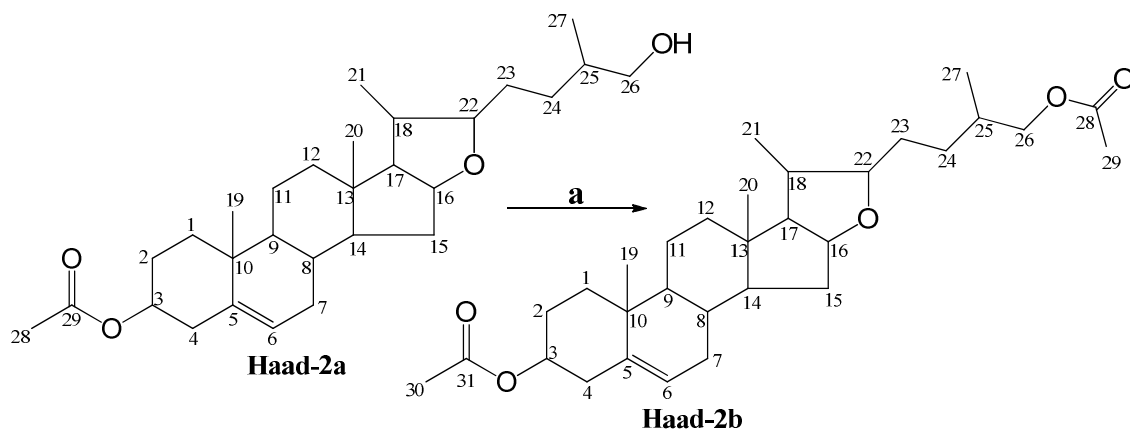
CIMAP-DEPT 135  
 PROJECT NO.: ILP-13

Fig. 4.67: DEPT spectrum of Haad-2a in CDCl<sub>3</sub>



### 4.8.3. Synthesis and characterisation of (22 $\beta$ ,25R)-furost-5-en-3 $\beta$ ,26-diacetate (Haad-2b)

Acetylation of Haad-2a using acetic anhydride in pyridine and chloroform as a solvent afforded 3,26-diacetyl analogue, Haad-2b (Chaosuancharoen *et al.*, 2004).



Re

**agents and conditions:** a) Ac<sub>2</sub>O, chloroform, dry pyridine, RT, 5 hrs

Haad-2b (100 mg, 35%) was obtained as a cream solid with a melting point of 167 - 169°C. The fragment ions 501.4 [M+H]<sup>+</sup>, 523.4 [M+Na]<sup>+</sup> and 539.4 [M+K]<sup>+</sup> obtained from ESI-MS correspond to a molecular formula C<sub>31</sub>H<sub>48</sub>O<sub>5</sub> (500) [Fig. 4.68]. The <sup>1</sup>H NMR signals at  $\delta_{\text{H}}$  3.36 (bs) and 3.98 (dd) were attributed to oxymethine proton at C-22 and oxymethylene protons at C-26 [Fig. 4.69], while 2.05(s) and 2.07(s) were assigned to methyl protons of acetate at C-29 and C-30 respectively. <sup>13</sup>C NMR [Fig. 4.70] and DEPT spectra data [Fig. 4.71] of Haad-2b were similar to Haad-2a spectroscopic data except the formation of an acetyl group at positions 28 and 29 [Table 4.62]. Haad-2b is identified as (22 $\beta$ ,25R)-furost-5-en-3 $\beta$ ,26-diacetate. The differences in its spectroscopic data and Haad-2a are given below.

<sup>1</sup>H NMR (CDCl<sub>3</sub>): 2.07 (s, 3H, H<sub>29</sub>, CH<sub>3</sub>COO, Acetate)

<sup>13</sup>C NMR (CDCl<sub>3</sub>): 171.56 (C-28), 21.29 (C-29) [Table 4.62; Figs: 4.69 - 4.71]

IR (KBr, cm<sup>-1</sup>): 2934 (C-H), 1731 (C=O), 1656 (C=C), 1248 (C-O)

**Table 4.62:** Comparison of  $^{13}\text{C}$  and  $^1\text{H}$  NMR data of Haad-2a and Haad-2b

Assignment	* $^{13}\text{C}$	Multiplicity	* $^1\text{H}$	$^{13}\text{C}$	$^1\text{H}$
1	21.03	$\text{CH}_2$	1.34-1.90, m, 2H	21.03	1.34-1.90, m, 2H
2	37.37	$\text{CH}_2$	1.34-1.90, m, 2H	37.37	1.34-1.90, m, 2H
3	74.26	CH	4.34, m, 1H	74.26	4.34, m, 1H
4	38.46	$\text{CH}_2$	1.34-1.90, m, 2H	38.46	1.34-1.90, m, 2H
5	140.04	Q	-	140.04	-
6	122.74	CH	5.40, t, 1H	122.74	5.40, t, 1H
7	32.36	$\text{CH}_2$	2.36, t, 2H	32.36	2.36, t, 2H
8	31.94	CH	1.34-1.90, m, 1H	31.94	1.34-1.90, m, 2H
9	50.39	CH	1.34-1.90, m, 1H	50.39	1.34-1.90, m, 2H
10	37.07	Q	-	37.07	-
11	30.46	$\text{CH}_2$	1.34-1.90, m, 2H	30.46	1.34-1.90, m, 2H
12	30.06	$\text{CH}_2$	1.34-1.90, m, 2H	30.06	1.34-1.90, m, 2H
13	39.78	Q	-	39.78	-
14	38.28	CH	1.34-1.90, m, 1H	38.28	1.34-1.90, m, 2H
15	32.59	$\text{CH}_2$	1.34-1.90, m, 2H	32.59	1.34-1.90, m, 2H
16	83.57	CH	4.63, m, 1H	83.57	4.63, m, 1H
17	65.48	CH	1.34-1.90, m, 1H	65.48	1.34-1.90, m, 2H
18	57.28	CH	1.34-1.90, m, 1H	57.28	1.34-1.90, m, 2H
19	19.69	$\text{CH}_3$	0.83-1.29, m, 3H	19.69	0.83-1.29, m, 3H
20	17.00	$\text{CH}_3$	0.83-1.29, m, 3H	17.00	0.83-1.29, m, 3H
21	16.80	$\text{CH}_3$	0.83-1.29, m, 3H	16.80	0.83-1.29, m, 3H
22	90.71	CH	3.36, s, 1H	<b>90.52</b>	<b>3.36, s, 1H</b>
23	32.21	$\text{CH}_2$	1.34-1.90, m, 2H	32.21	1.34-1.90, m, 2H
24	28.12	$\text{CH}_2$	1.34-1.90, m, 2H	28.12	1.34-1.90, m, 2H
25	42.00	CH	1.34-1.90, m, 1H	42.00	1.34-1.90, m, 1H
26	67.19	$\text{CH}_2$	3.48, m, 2H	69.71	3.48, m, 2H
27	19.69	$\text{CH}_3$	0.83-1.29, m, 3H	19.69	0.83-1.29, m, 3H
28	30.82	$\text{CH}_3$	2.05, s, 3H	<b>171.56</b>	-
29	170.91	Q		<b>21.29</b>	<b>2.07, s, 3H</b>
				21.74	2.05, s, 3H
				171.56	-

Implied multiplicities of the carbons were determined from the DEPT experiment.  
\* Haad-2a

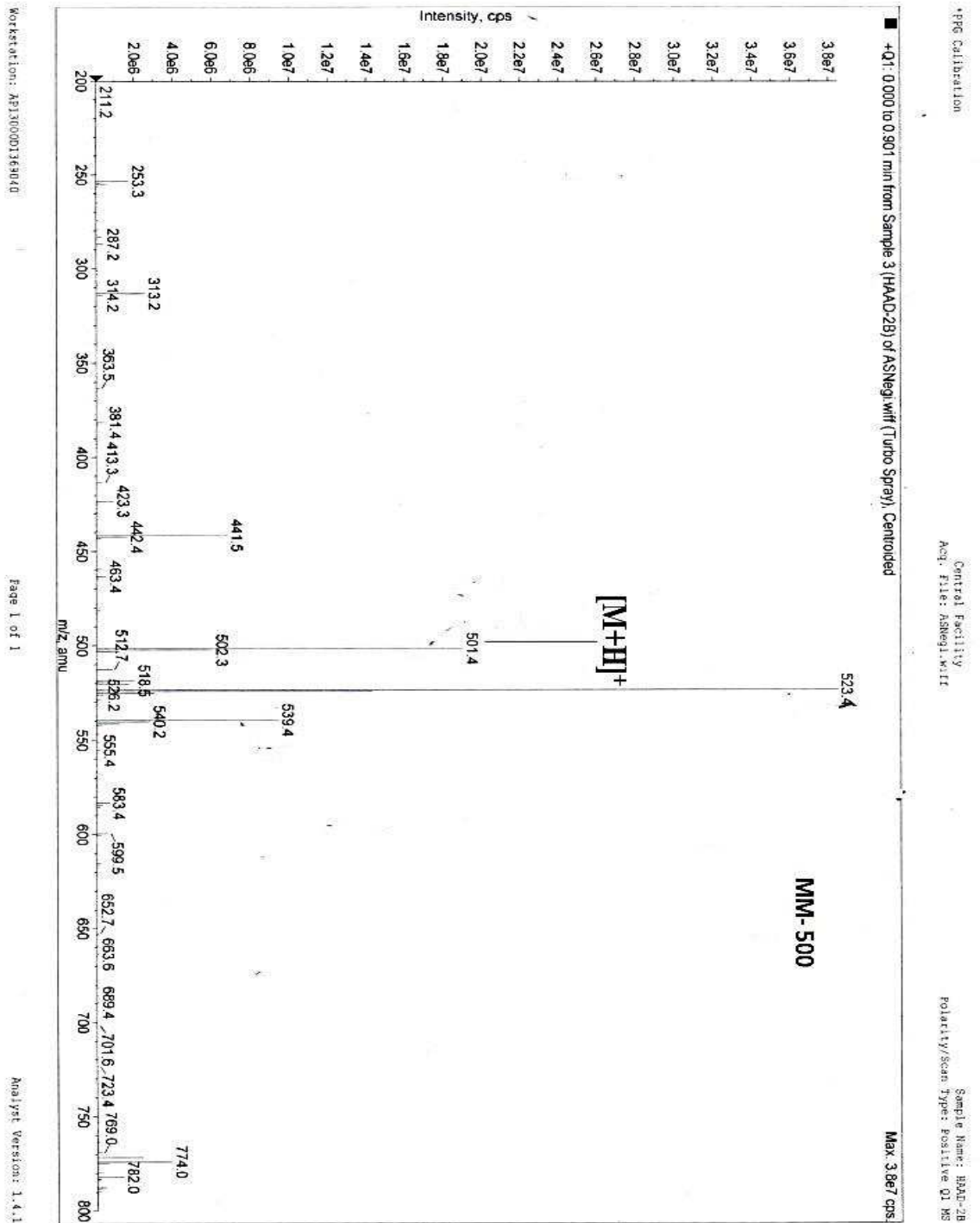


Fig. 4.68: ESI-MS spectrum of Haad-2b in MeOH

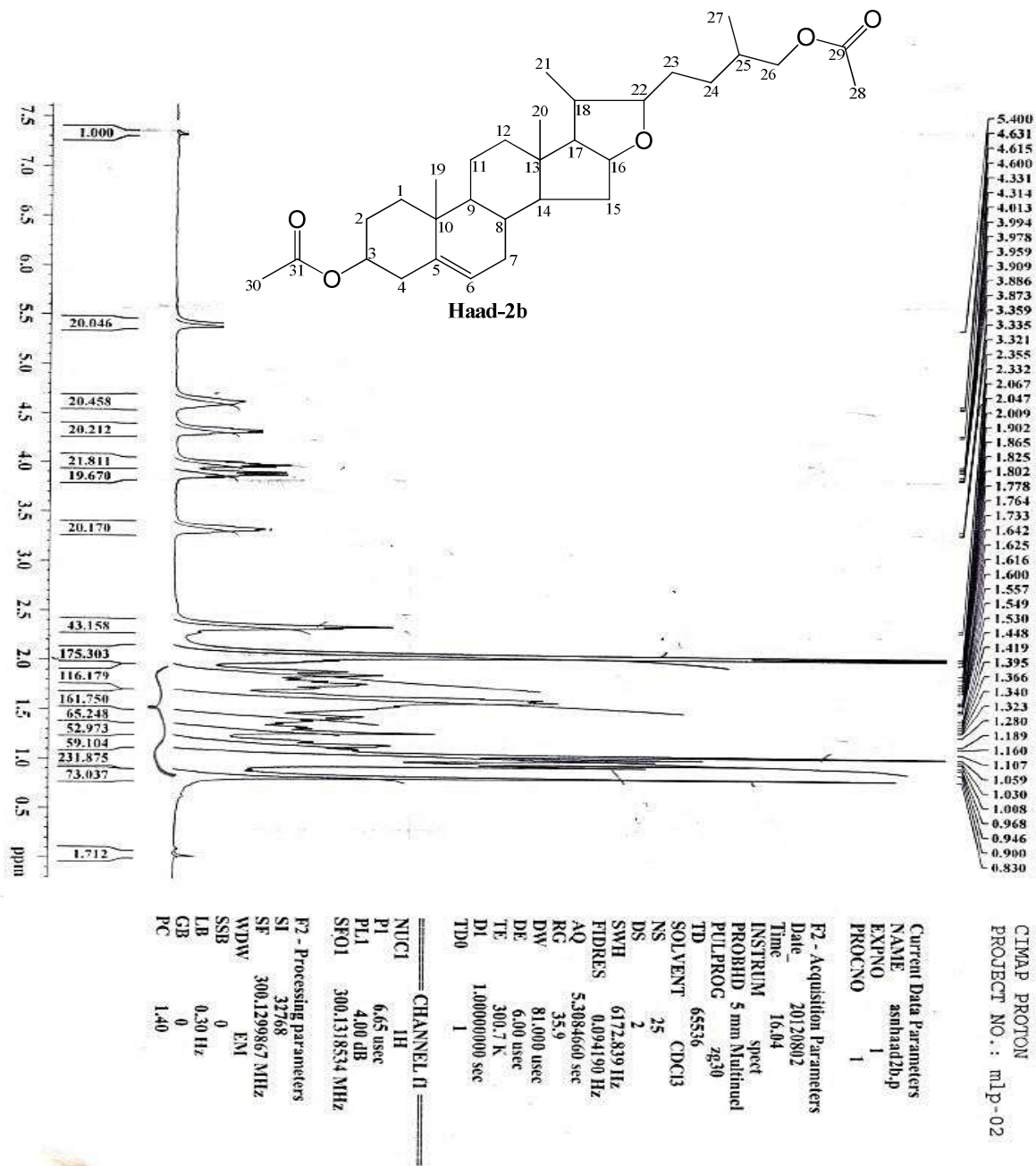


Fig. 4.69:  $^1\text{H}$  NMR spectrum of Haad-2b in  $\text{CDCl}_3$

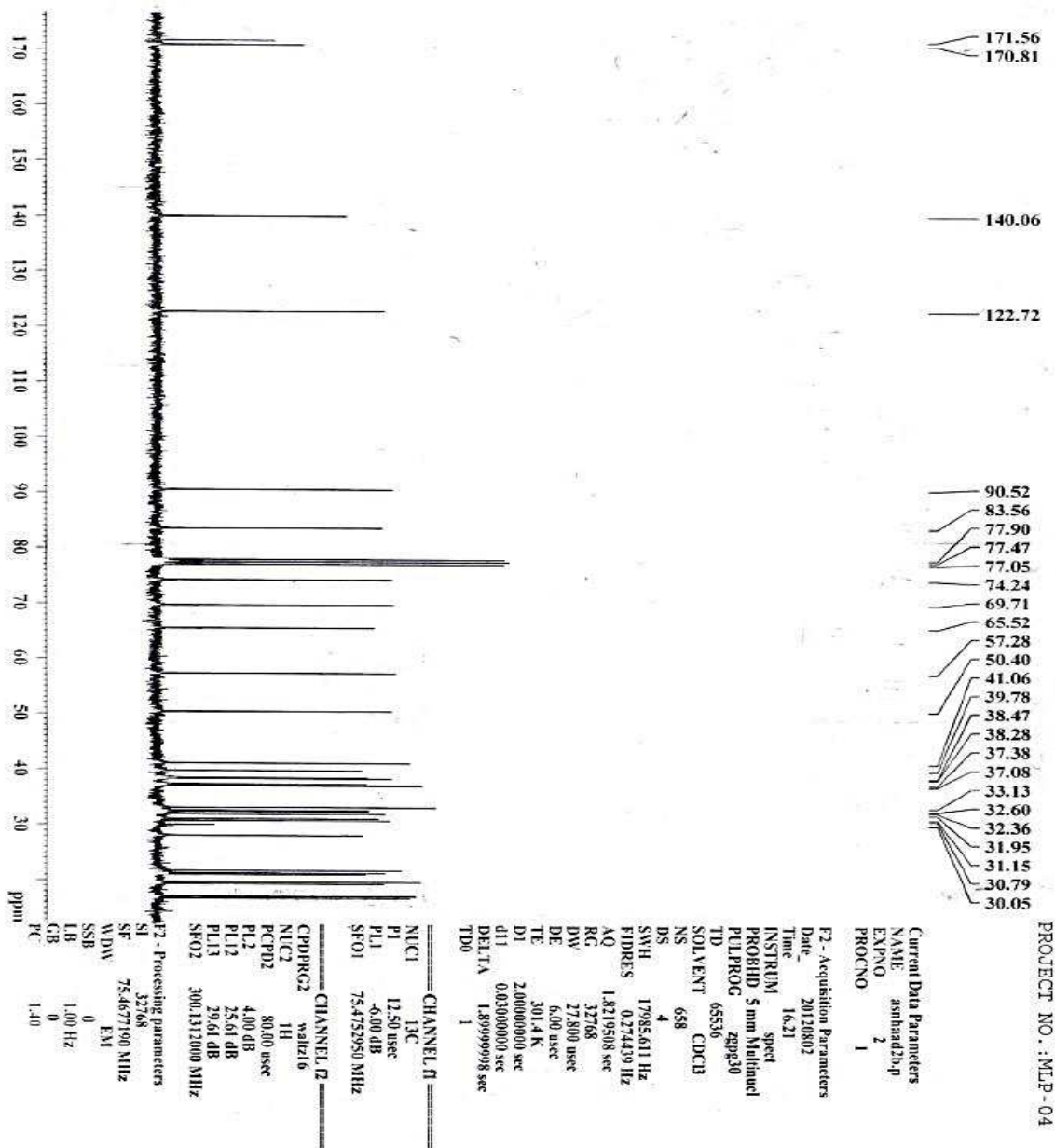


Fig. 4.70:  $^{13}\text{C}$  NMR spectrum of Haad-2b in  $\text{CDCl}_3$

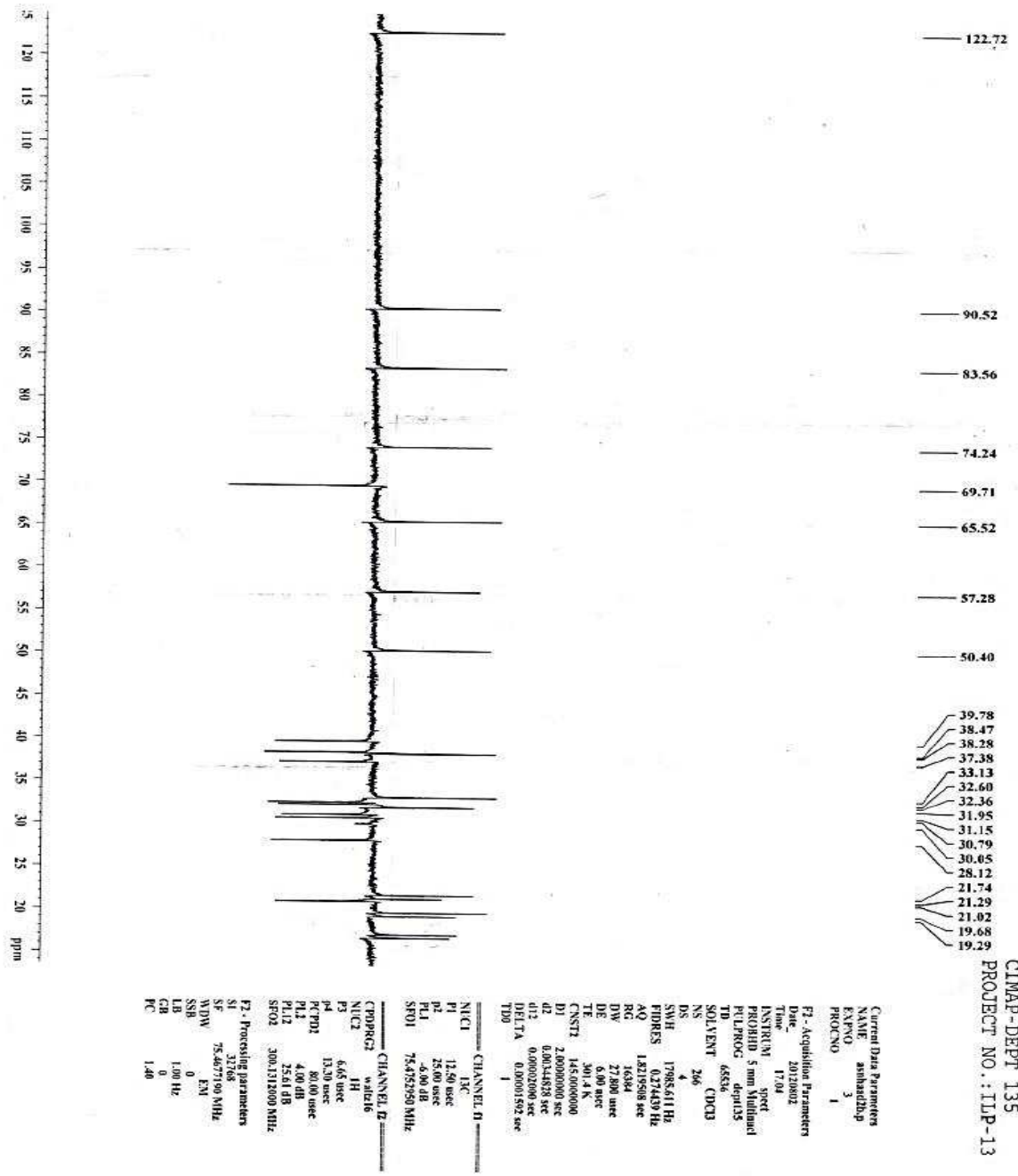
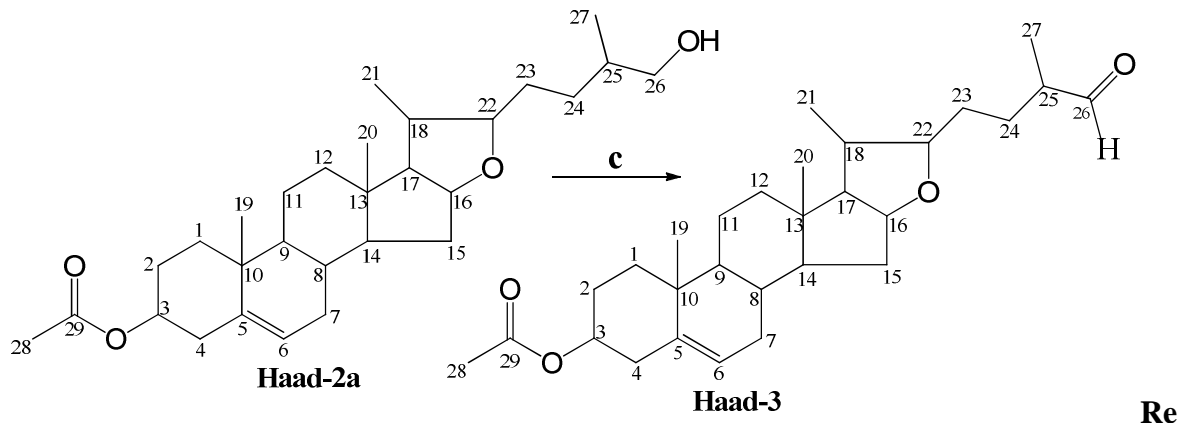


Fig. 4.71: DEPT spectrum of Haad-2b in CDCl<sub>3</sub>

#### 4.8.4. Synthesis and characterization of (22 $\beta$ ,25R)-3 $\beta$ -hydroxy,26-formyl-furost-5-en-3 $\beta$ -acetate (Haad-3)

Haad-2a was oxidized to aldehyde analogue Haad-3 using pyridinium chlorochromate (PCC) in dichloromethane (DCM).



**agents and conditions:** c) Pyridinium chlorochromate (PCC), DCM, RT, 1 hr

Haad-3 (182 mg, 91%) was obtained as a brown crystalline solid, which has a melting point of 122 - 125°C (123-125°C, Shawakfeh *et al.*, 2010). The fragment ions 457.3 [M+H]<sup>+</sup>, 479.3 [M+Na]<sup>+</sup> and 495.4 [M+K]<sup>+</sup> obtained from ESI-MS correspond to a molecular formula C<sub>29</sub>H<sub>42</sub>O<sub>4</sub> (456) [Fig. 4.72]. The <sup>1</sup>H NMR spectra data at  $\delta_H$  3.45 (bs) and 9.75 (s) indicated the presence of oxymethine proton at C-22 and methine proton at C-26 [Fig. 4.73], while 2.16(s) was assigned to methyl protons of acetate at C-28. <sup>13</sup>C NMR spectrum [Fig. 4.74] showed twenty nine carbon resonances and DEPT experiment [Fig. 4.75] of Haad-3 sorted the carbons into five methyl, nine methylene, ten methine and five quaternary carbons present in the compound. The spectroscopic data of Haad-3 was similar to Haad-2a data except at position 26 where the hydroxyl was converted to aldehyde moiety [Table 4.63]. Hence, Haad-3 was elucidated as (22 $\beta$ ,25R)-26-formyl-furost-5-en-3 $\beta$ -acetate (Shawakfeh *et al.*, 2010). The differences in its spectroscopic data and Haad-2a are outlined below.

<sup>1</sup>H NMR (CDCl<sub>3</sub>): 9.75 (s, 1H, 26-CHO);

<sup>13</sup>C NMR (CDCl<sub>3</sub>): 205.54 (C-26) and 170.91 (C-29) [Table 4.63; Figs: 4.73 - 4.75]

IR (KBr, cm<sup>-1</sup>): 2833 (C-H), 1739 (C=O), 1254 (C-O)

**Table 4.63:** Comparison of <sup>13</sup>C and <sup>1</sup>H NMR data of Haad-2a and Haad-3

Assignment	* <sup>13</sup> C	Muultiplicity	* <sup>1</sup> H	<sup>13</sup> C	<sup>1</sup> H
1	21.03	CH <sub>2</sub>	1.34-1.90, m, 2H	21.03	1.34-1.90, m, 2H
2	37.37	CH <sub>2</sub>	1.34-1.90, m, 2H	37.39	1.34-1.90, m, 2H
3	74.26	CH	4.34, m, 1H	74.28	4.34, m, 1H
4	38.46	CH <sub>2</sub>	1.34-1.90, m, 2H	38.48	1.34-1.90, m, 2H
5	140.04	Q	-	140.09	-
6	122.74	CH	5.40, t, 1H	122.73	5.40, t, 1H
7	32.36	CH <sub>2</sub>	2.36, t, 2H	32.37	2.36, t, 2H
8	31.94	CH	1.34-1.90, m, 1H	38.28	1.34-1.90, m, 2H
9	50.39	CH	1.34-1.90, m, 1H	50.41	1.34-1.90, m, 2H
10	37.07	Q	-	37.09	-
11	30.46	CH <sub>2</sub>	1.34-1.90, m, 2H	30.07	1.34-1.90, m, 2H
12	30.06	CH <sub>2</sub>	1.34-1.90, m, 2H	31.96	1.34-1.90, m, 2H
13	39.78	Q	-	39.77	-
14	38.28	CH	1.34-1.90, m, 1H	41.08	1.34-1.90, m, 2H
15	32.59	CH <sub>2</sub>	1.34-1.90, m, 2H	32.59	1.34-1.90, m, 2H
16	83.57	CH	4.63, m, 1H	83.28	4.63, m, 1H
17	65.48	CH	1.34-1.90, m, 1H	65.44	1.34-1.90, m, 2H
18	57.28	CH	1.34-1.90, m, 1H	57.29	1.34-1.90, m, 2H
19	19.69	CH <sub>3</sub>	0.83-1.29, m, 3H	19.22	0.83-1.29, m, 3H
20	17.00	CH <sub>3</sub>	0.83-1.29, m, 3H	16.79	0.83-1.29, m, 3H
21	16.80	CH <sub>3</sub>	0.83-1.29, m, 3H	13.78	0.83-1.29, m, 3H
22	90.71	CH	3.36, s, 1H	<b>90.11</b>	<b>3.45, s, 1H</b>
23	32.21	CH <sub>2</sub>	1.34-1.90, m, 2H	31.11	1.34-1.90, m, 2H
24	28.12	CH <sub>2</sub>	1.34-1.90, m, 2H	28.15	1.34-1.90, m, 2H
25	42.00	CH	1.34-1.90, m, 1H	46.72	1.34-1.90, m, 1H
26	67.19	CH <sub>2</sub>	3.48, m, 2H	<b>205.54</b>	<b>9.75, s, 1H</b>
27	19.69	CH <sub>3</sub>	0.83-1.29, m, 3H	19.71	0.83-1.29, m, 3H
28	30.82	CH <sub>3</sub>	2.05, s, 3H	<b>21.77</b>	<b>2.16, s, 3H</b> -
29	170.91	Q		<b>170.91</b>	<b>2.07, s, 3H</b>



Implied multiplicities of the carbons were determined from the DEPT experiment.  
\* Haad-2a

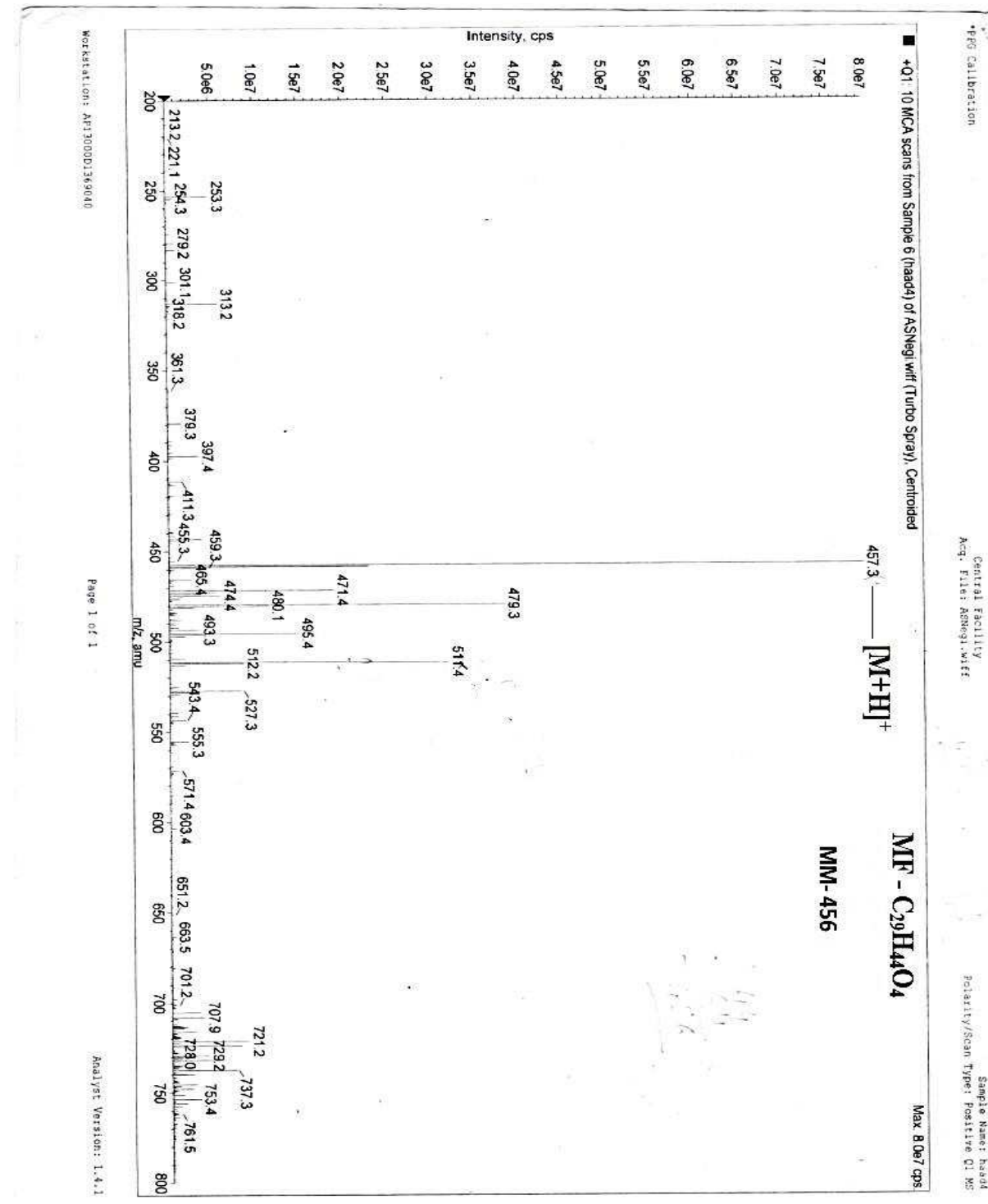


Fig. 4.72: ESI-MS spectrum of Haad-3 in MeOH

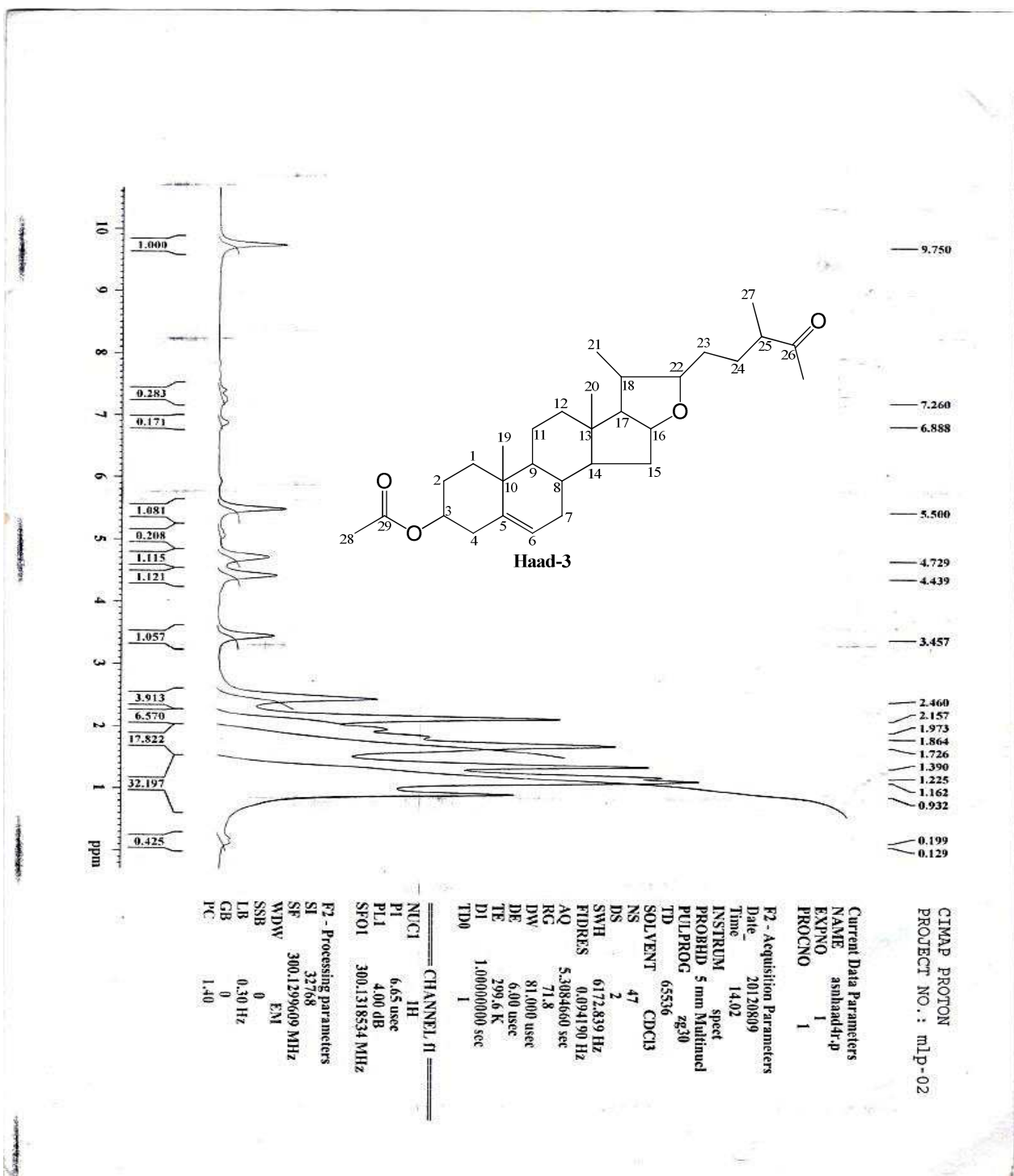


Fig. 4.73:  $^1\text{H}$  NMR spectrum of Haad-3 in  $\text{CDCl}_3$

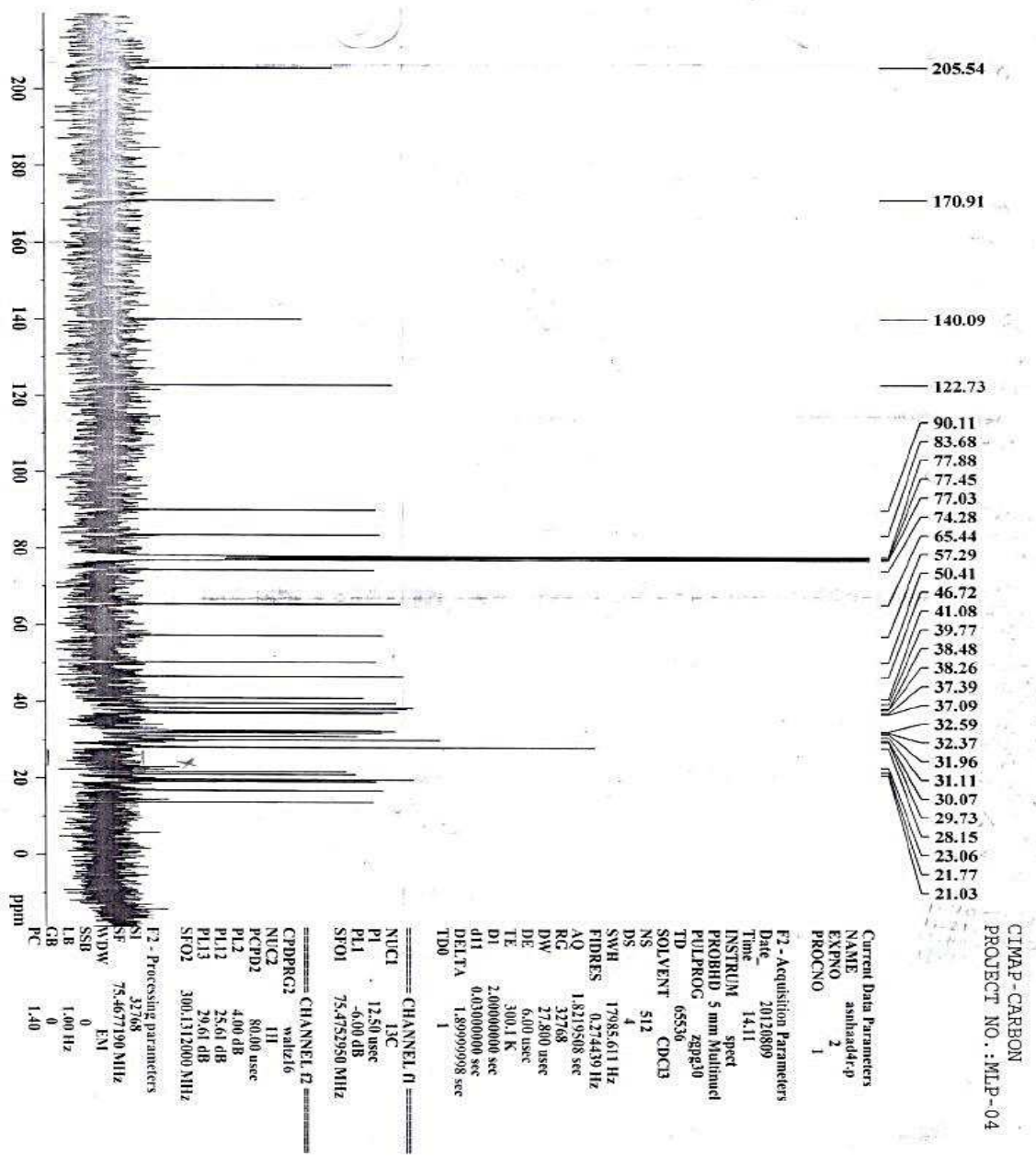
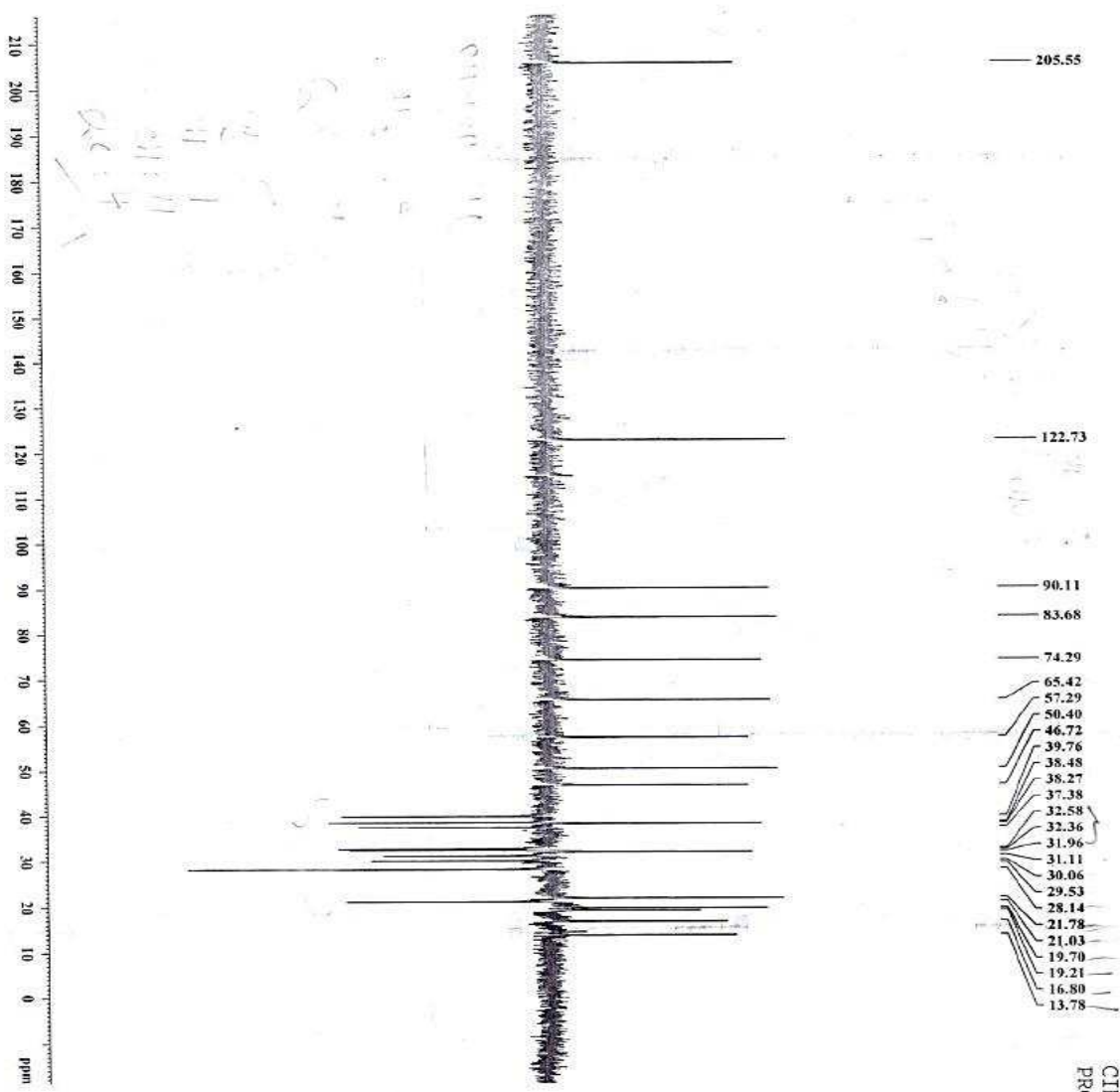


Fig. 4.74: <sup>13</sup>C NMR spectrum of Haad-3 in CDCl<sub>3</sub>



CIMAP-DEPT 135  
PROJECT NO.: ILP-13

Current Data Parameters  
NAME anhadtr.p  
EXPNO 5  
PROCNO 1

F2 - Acquisition Parameters  
Date\_ 20120809  
Time 14.39  
INSTRUM spect  
PROBHD 5 mm Hyperind  
PULPROG zgpg30  
TD 65536  
SOLVENT CDCl3  
NS 574  
DS 4  
SWH 17985.611 Hz  
FIDRES 0.274439 Hz  
AQ 1.8219588 sec  
RG 16384  
DW 27.800 sec  
DE 6.00 usec  
TE 300.3 K  
CNSF2 145.000000  
D1 2.0000000 sec  
d11 0.0000000 sec  
d12 0.0000000 sec  
DELTA 0.00001592 sec  
TD0 1

CHANNEL F1  
NUC1 13C  
P1 12.50 usec  
P2 25.00 usec  
PL1 -6.09 dB  
SFO1 75.4752950 MHz

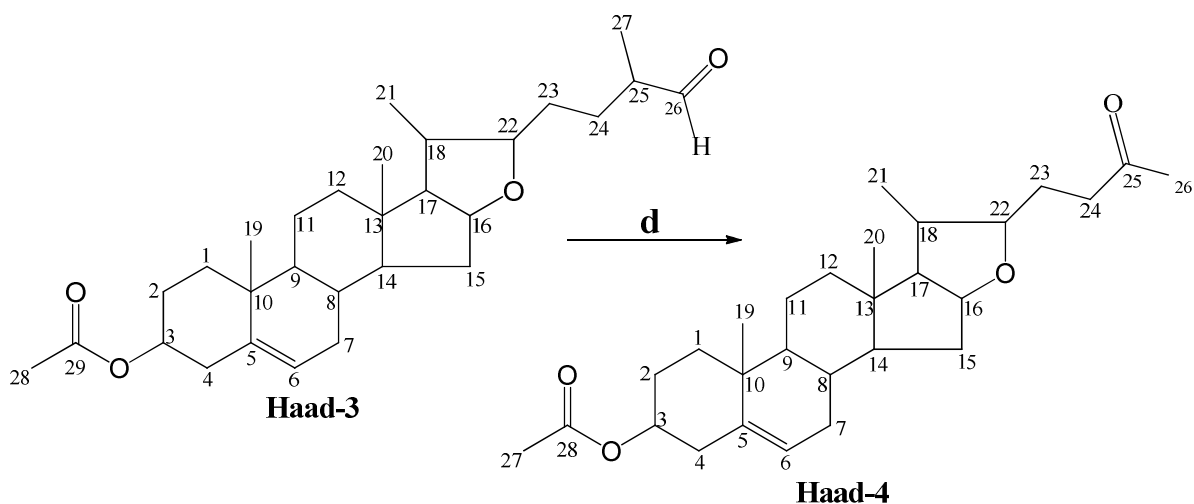
CHANNEL D2  
CPDPRG2 waltz16  
NUC2 1H  
P3 6.65 usec  
P4 13.50 usec  
PCPD2 13.50 usec  
PL2 -6.09 dB  
PL12 15.61 dB  
SFO2 300.1372000 MHz

F3 - Processing parameters  
SI 32768  
SF 75.4677196 MHz  
WDW EM  
SSB 0  
LB 1.00 Hz  
GB 0  
PC 1.40

Fig. 4.75: DEPT spectrum of Haad-3 in CDCl<sub>3</sub>

#### 4.8.5. Synthesis and characterization of (22 $\beta$ )-25-oxo-27-nor-furost-5-en-3 $\beta$ -acetate (Haad-4)

A new analogue, C<sub>28</sub> ketone derivative Haad-4 was formed while trying to synthesize Schiff's bases from C<sub>29</sub> aldehyde analogue, Haad-3. Compound Haad-3 reacts with aromatic amine (3,4,5-trimethoxyaniline) in ethanol at 30 - 35°C to give a creamy white solid. Various aromatic amines (3,4-dimethoxyaniline, 3,4,5-trimethoxyaniline and 3,4-methylenedioxyaniline) were employed and the same product, Haad-4 was obtained in varied yields (66 - 84%). The reaction of aldehyde, Haad-3 with aliphatic amines (MeNH<sub>2</sub> and EtNH<sub>2</sub>) and even with ammonia was unsuccessful. Benzyl amines (BnNH<sub>2</sub> and 3,4-methylenedioxybenzylamine) also did not yield the product Haad-4 [Table 4.64]. The effect of various solvents was also observed, as shown in Table 4.65. Ethanol was found to be the best solvent. However, methanol was equally good. In case of less polar solvents like THF, dichloromethane and toluene, the yield of the product was relatively low. It will be worth mentioning that without aromatic amine this transformation does not take place. Aldehyde Haad-3 did not form Schiff's base with any of these amines. The structure of the ketone Haad-4 was confirmed by 1D NMR (<sup>1</sup>H & <sup>13</sup>C), 2D NMR (COSY, HSQC, HMBC), Mass and IR spectroscopy, and X-ray.



**Reagents and conditions:** d) Aromatic amine, DCM, pyridine, reflux, 3 hrs

A plausible mechanism of the reaction is given in Fig. 4.76

Compound Haad-4 (163 mg, 84%) was obtained as a creamy white solid (melting point 138-140°C). The ESI-MS fragment ions 443.3 [M+H]<sup>+</sup>, 465.4 [M+Na]<sup>+</sup> and 481.3 [M+K]<sup>+</sup> gave molecular formula C<sub>28</sub>H<sub>42</sub>O<sub>4</sub> (442) [Fig. 4.77]. The IR  $\bar{\nu}$  (cm<sup>-1</sup>) absorptions of C-H, C=O and C=C functional groups appeared at 2927, 1724 and 1453 cm<sup>-1</sup> respectively. The <sup>1</sup>H NMR signals at  $\delta_{\text{H}}$  0.79-0.98 (9H, s, 3 x CH<sub>3</sub>), 1.02-1.87 (20H, m, 8 x CH<sub>2</sub> & 4 x CH) and 2.32 (2H, d, H<sub>7</sub>) are similar to methyl, methylene and methine protons of diosgenin, while the signals at  $\delta_{\text{H}}$  3.27 (bs) and 4.26 (bs) correspond to oxymethylene and oxymethine protons at C-22 and C-16 of furostane skeleton [Fig. 4.78]. <sup>13</sup>C NMR spectrum also showed resonances consistent with twenty eight-carbon member skeleton [Fig. 4.79]. The identified carbons were sorted by DEPT experiment [Fig. 4.80] into five methyl carbons, nine methylene carbons, nine methine carbons and five quaternary carbon resonances. The chemical shifts  $\delta_{\text{C}}$  89.53 (d), 170.95 (s) and 209.24 (s) were attributed to oxymethine carbon at C-22 and quaternary carbonyl carbons of acetate and ketone moieties at C-28 and C-25 respectively.

<sup>1</sup>H-<sup>1</sup>H COSY spectrum [Fig. 4.81 & 4.84] revealed the correlation of oxymethine protons at C-16 and C-22 with methylene protons at C-15 and C-23 respectively, while olefinic methine proton at C-6 was correlated with methylene protons at C-7. The HSQC spectrum (Fig. 4.82) showed that methine protons at  $\delta_{\text{H}}$  3.27 (bs) and 4.26 (bs) were bonded to carbons at  $\delta_{\text{C}}$  89.53 (C-22) and 83.69 (C-16) respectively. In <sup>1</sup>H-<sup>13</sup>C HMBC experiment [Fig. 4.83 & 4.84], there was correlation of methylene protons at C-23 with C-22, C-24 and C-25. Methyl protons at C-26 also showed correlations with C-24 and C-25, which confirm the presence of ketonic carbon at position 25. Furthermore, methylene protons at C-24 were also correlated with C-23 and C-26 while methyl protons at C-27 revealed correlation with carbonyl C-28 and olefinic carbons C-5 and C-6. Therefore, the new derivative, Haad-4 [Table 4.66] was elucidated as (22 $\beta$ )-25-oxo-27-nor-furost-5-en-3 $\beta$ -acetate. The difference in NMR of Haad-3 and Haad-4 are:

<sup>1</sup>H NMR (CDCl<sub>3</sub>): 2.13 (s, 3H, H-26, CH<sub>3</sub>CO);

<sup>13</sup>C NMR (CDCl<sub>3</sub>): 30.33 (C26) and 209.24 (C25) [Table 4.66; Figs: 4.78 - 4.80]

IR (KBR, cm<sup>-1</sup>): 2927 (C-H), 1724 (C=O), 1653 (C=C), 1241 (C-O)

Further, the molecular conformation of compound Haad-4 in crystals is depicted in Figure 4.85. All the bond lengths and bond angles are within the accepted range. The crystal packing is stabilized by van der Waals interactions, in the absence of strong hydrogen bond donors in this molecule. However, the ketonic O atom and the methylene group (C24) adjacent to the ketone functionality of symmetry-related molecules are at 3.22Å apart, suggesting a weak C-H...O interaction ( $O3...H = 2.55\text{\AA}$ ,  $C24...O3 = 3.22\text{\AA}$ ,  $\angle C24-H...O3 = 125.8^\circ$ ). The ring conformations of compound Haad-4 are very similar to that observed in other diosgenin derivatives and solvates:

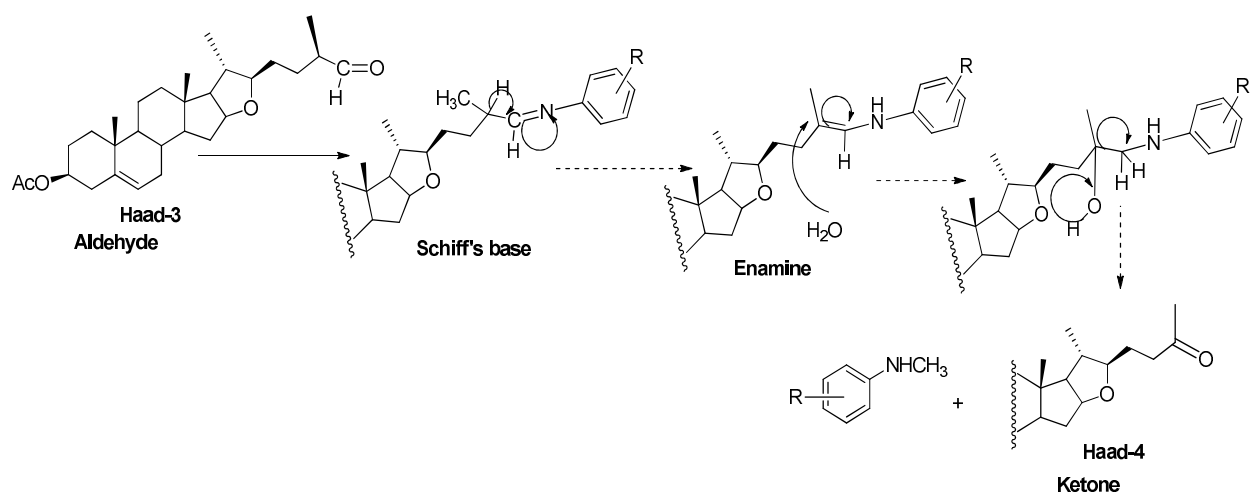


**Fig. 4.76:** Plausible mechanism of conversion of aldehyde (Haad-3) to ketone (Haad-4).



**Table 4.64:** Effect of various amines on transformation of Haad-3 to Haad-4

Entry	Aldehyde	Amine	solvent	Reaction Time	% Yield of Haad-4
1.	Haad-3	No amine	EtOH	16h	No reaction
2.	Haad-3	3,4,-Dimethoxyaniline	EtOH	2h	66
3.	Haad-3	3,4,5-Trimethoxyaniline	EtOH	2h	84
4.	Haad-3	3,4-Methylenedioxyaniline	EtOH	2h	72
5.	Haad-3	Benzyl amine	EtOH	16h	No reaction
6.	Haad-3	3,4-Methylenedioxybenzyl amine	EtOH	16h	No reaction
7.	Haad-3	Ammonia	EtOH	16h	No reaction
8.	Haad-3	Methylamine	EtOH	16h	No reaction
9.	Haad-3	Ethylamine	EtOH	16h	No reaction

**Table 4.65:** Effect of solvent polarity on transformation of compound Haad-3 to Haad-4.

Entry	aldehyde	Amine	Solvent	Reaction Time	% Yield of Haad-4
1.	Haad-3	3,4,5-trimethoxyaniline	EtOH	2h	84
2.	Haad-3	3,4,5-trimethoxyaniline	MeOH	2h	73
3.	Haad-3	3,4,5-trimethoxyaniline	THF	2h	44
4.	Haad-3	3,4,5-trimethoxyaniline	Dichloromethane	2h	49
5.	Haad-3	3,4,5-trimethoxyaniline	Toluene	2h	28

**Table 4.66:** Comparison of  $^{13}\text{C}$  and  $^1\text{H}$  NMR data of Haad-3 and Haad-4

Assignment	* $^{13}\text{C}$	Multiplicity	* $^1\text{H}$	$^{13}\text{C}$	$^1\text{H}$
1	21.03	$\text{CH}_2$	1.34-1.90, m, 2H	21.02	1.32-1.90, m, 2H
2	37.37	$\text{CH}_2$	1.34-1.90, m, 2H	37.38	1.32-1.90, m, 2H
3	74.26	CH	4.34, m, 1H	74.28	4.57, m, 1H
4	38.46	$\text{CH}_2$	1.34-1.90, m, 2H	39.75	1.32-1.90, m, 2H
5	140.04	Q	-	140.12	-
6	122.74	CH	5.40, t, 1H	122.72	5.35, t, 1H
7	32.36	$\text{CH}_2$	2.36, t, 2H	32.37	2.32, t, 2H
8	31.94	CH	1.34-1.90, m, 1H	31.95	1.32-1.90, m, 2H
9	50.39	CH	1.34-1.90, m, 1H	50.38	1.32-1.90, m, 2H
10	37.07	Q	-	37.10	-
11	30.46	$\text{CH}_2$	1.34-1.90, m, 2H	28.13	1.32-1.90, m, 2H
12	30.06	$\text{CH}_2$	1.34-1.90, m, 2H	38.48	1.32-1.90, m, 2H
13	39.78	Q	-	41.09	-
14	38.28	CH	1.34-1.90, m, 1H	38.24	1.32-1.90, m, 2H
15	32.59	$\text{CH}_2$	1.34-1.90, m, 2H	32.55	1.32-1.90, m, 2H
16	83.57	CH	4.63, m, 1H	83.69	4.29, m, 1H
17	65.48	CH	1.34-1.90, m, 1H	65.39	1.32-1.90, m, 2H
18	57.28	CH	1.34-1.90, m, 1H	57.27	1.32-1.90, m, 2H
19	19.69	$\text{CH}_3$	0.83-1.29, m, 3H	19.01	0.83-1.29, m, 3H
20	17.00	$\text{CH}_3$	0.83-1.29, m, 3H	16.80	0.83-1.29, m, 3H
21	16.80	$\text{CH}_3$	0.83-1.29, m, 3H	19.71	0.83-1.29, m, 3H
22	90.11	CH	3.45, s, 1H	<b>89.53</b>	<b>3.27, s, 1H</b>
23	32.21	$\text{CH}_2$	1.34-1.90, m, 2H	27.44	1.32-1.90, m, 2H
24	28.12	$\text{CH}_2$	1.34-1.90, m, 2H	<b>41.28</b>	<b>2.51, d, 2H</b>
25	42.00	CH	1.34-1.90, m, 1H	<b>209.24</b>	-
26	205.54	CH	9.75, s, 1H	<b>30.33</b>	<b>2.13, s, 3H</b>
27	19.71	$\text{CH}_3$	0.83-1.29, m, 3H	<b>21.80</b>	<b>1.95, s, 3H</b>
28	21.77	$\text{CH}_3$	2.05, s, 3H	<b>170.95</b>	-
29	170.91	Q			

Implied multiplicities of the carbons were determined from the DEPT experiment.

\* Haad-3

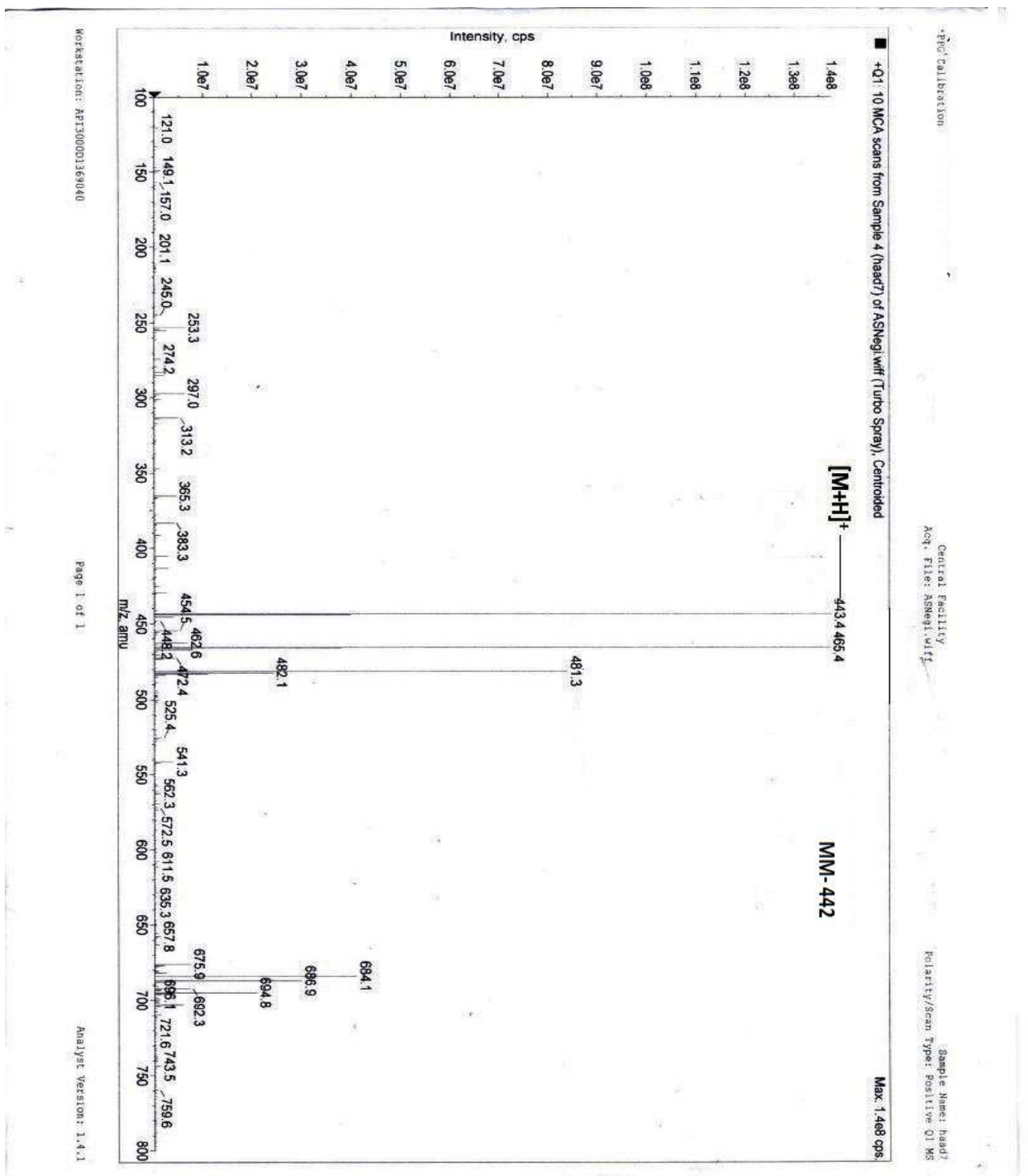


Fig. 4.77: ESI-MS spectrum of Haad-4 in MeOH

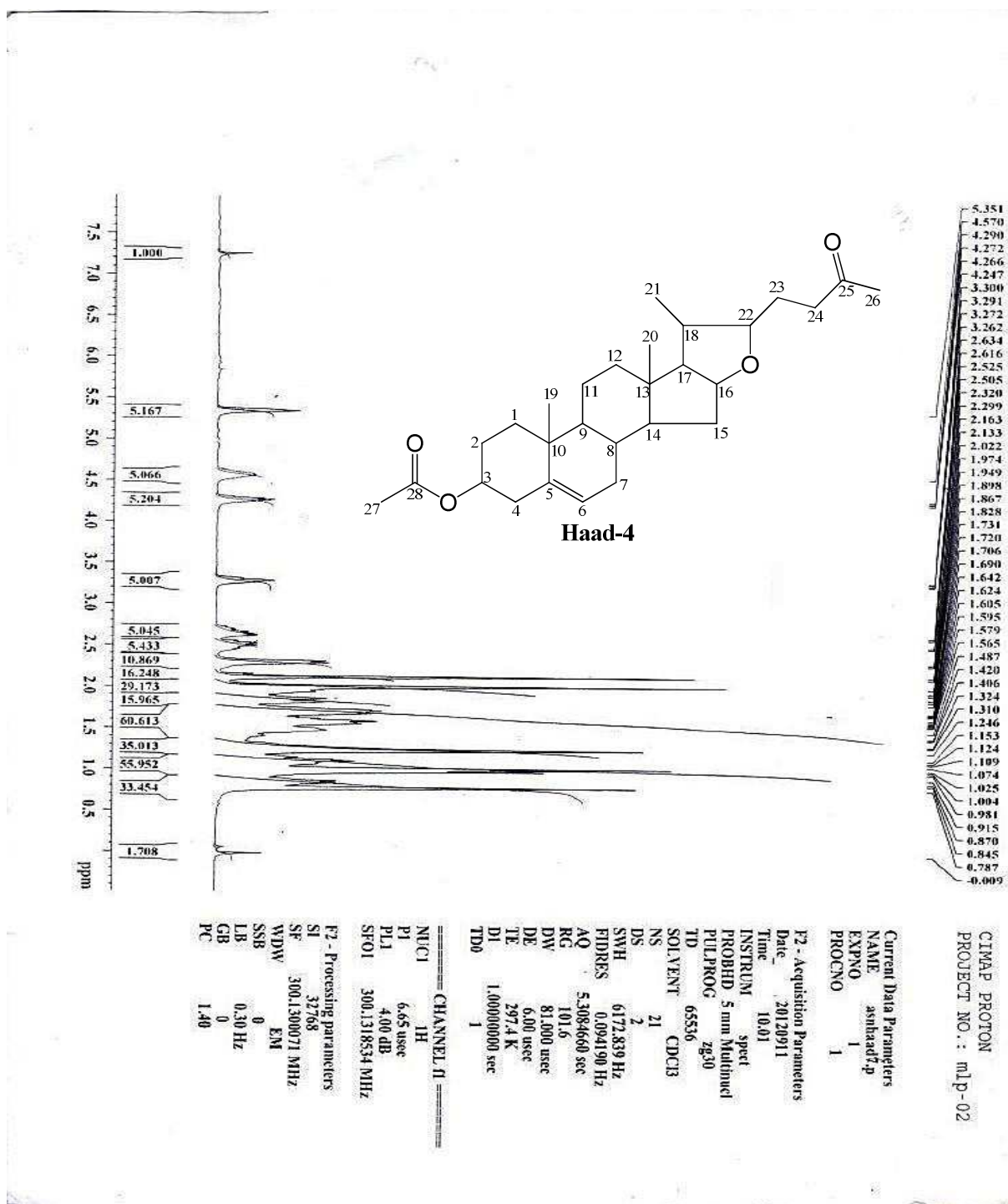


Fig. 4.78:  $^1\text{H}$  NMR spectrum of Haad-4 in  $\text{CDCl}_3$

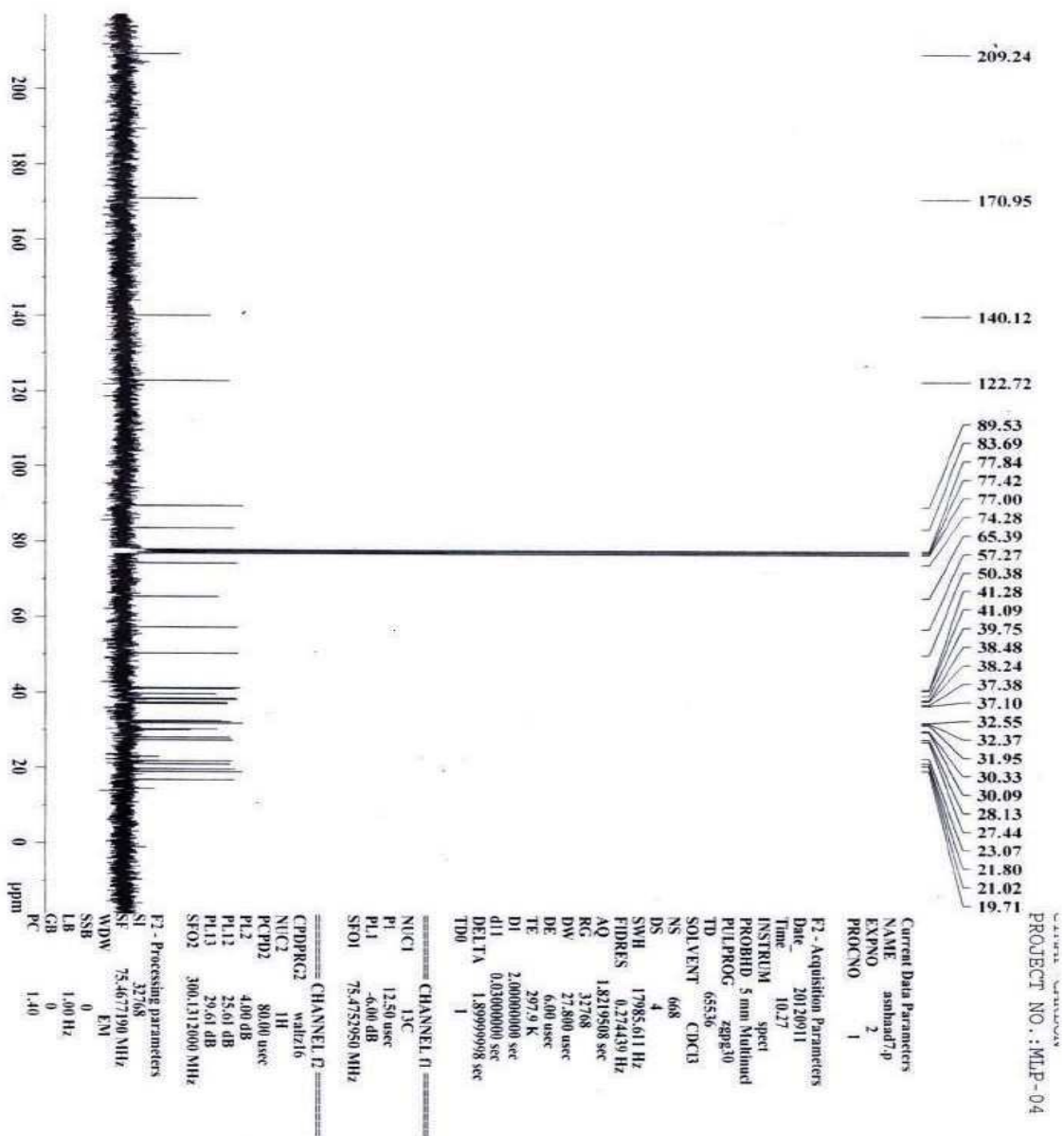
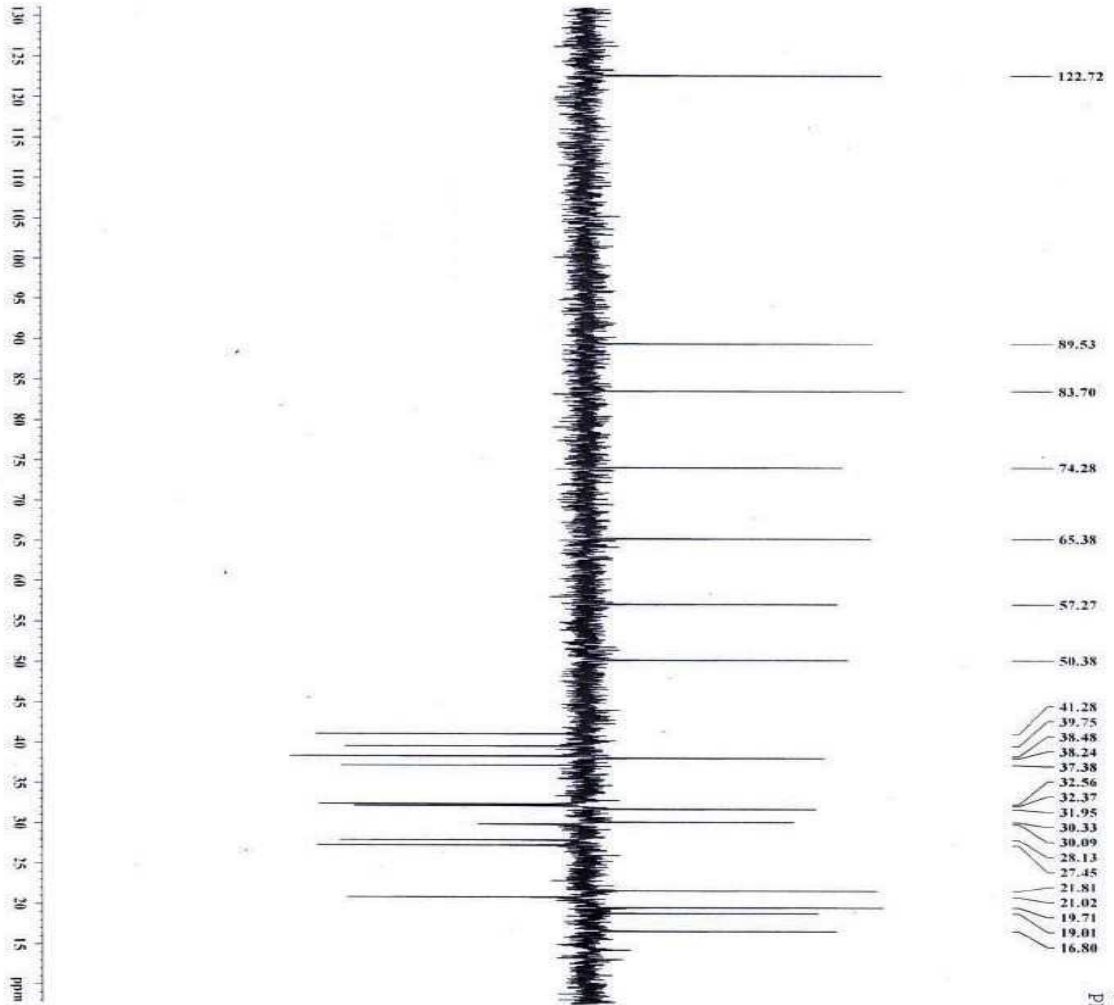


Fig. 4.79:  $^{13}\text{C}$  NMR spectrum of Haad-4 in  $\text{CDCl}_3$



CIMAP-DEPT 135  
PROJECT NO.: IIP-13

```

Current Data Parameters
NAME      amhdia7.p
EXPNO     3
PROCNO    1

F1-Acquisition Parameters
Date_     20120111
Time      10:41
INSTRUM   spect
PROBHD    5 mm,Multiband
PULPROG   zgpg30
TD         65536
SOLVENT   CDCl3
NS         512
DS         4
SWH        17985.611 Hz
FIDRES     0.274439 Hz
AQ         1.8219508 sec
RG         16384
DW         27.800 nsec
DE         6.000 nsec
TE         297.73 K
CNS2       145.0000000
NUC1       13C
NUC2       1H
PC         1.40

===== CHANNEL f1 =====
NUC1      13C
P1         12.50 nsec
PL1        25.00 nsec
PL12       -6.00 dB
SFO1       75.4752950 MHz

===== CHANNEL f2 =====
CPDPRG2   waltz16
NUC1      13C
NUC2      1H
P2         6.05 nsec
PL2        13.20 nsec
PL12       4.00 dB
PL13       15.00 dB
SFO2       200.1312000 MHz

F2 - Processing parameters
SI         32768
SF         75.4677190 MHz
WDW        EM
SSB        0
LB         1.00 Hz
GB         0
PC         1.40
  
```

Fig. 4.80: DEPT spectrum of Haad-4 in CDCl<sub>3</sub>

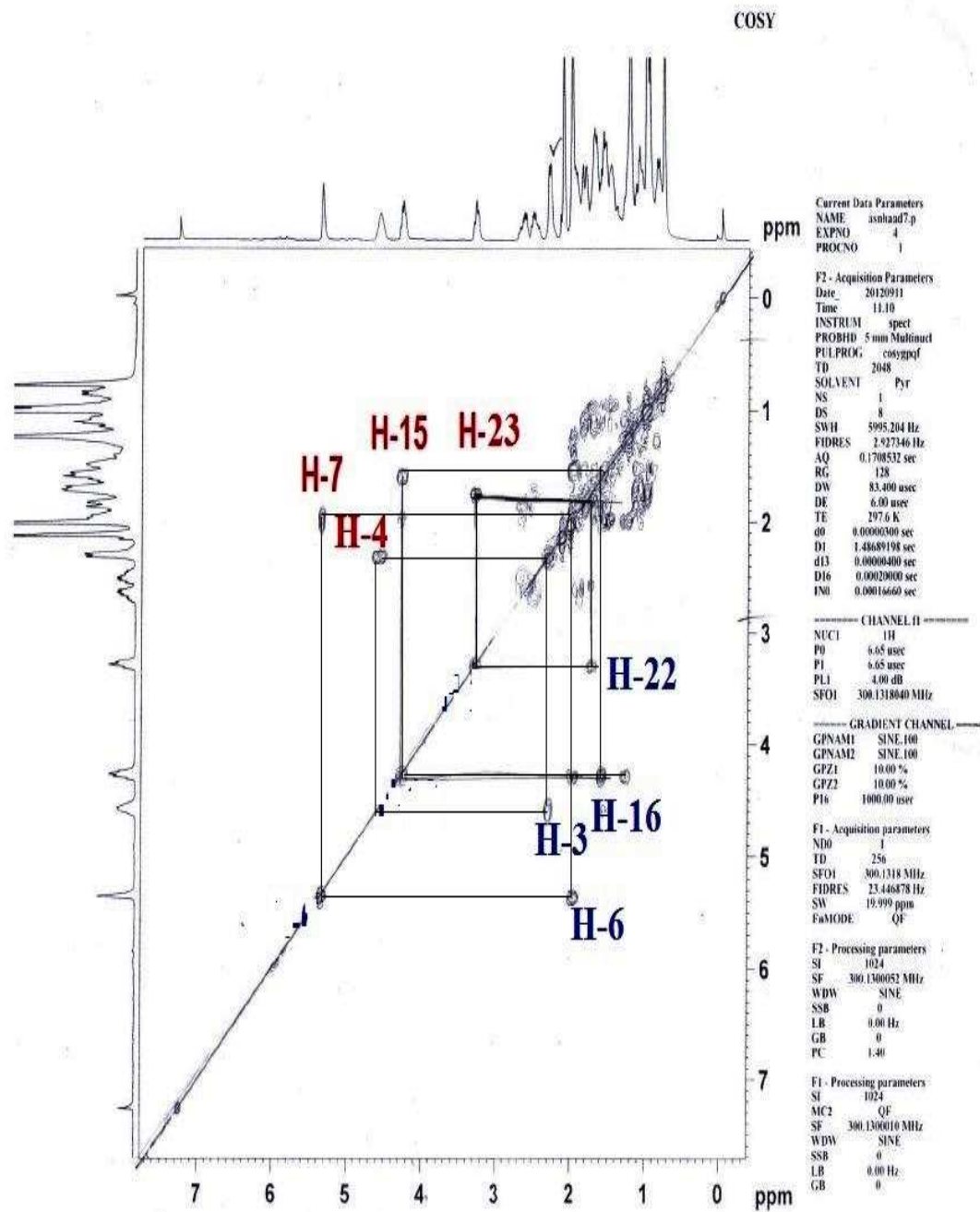
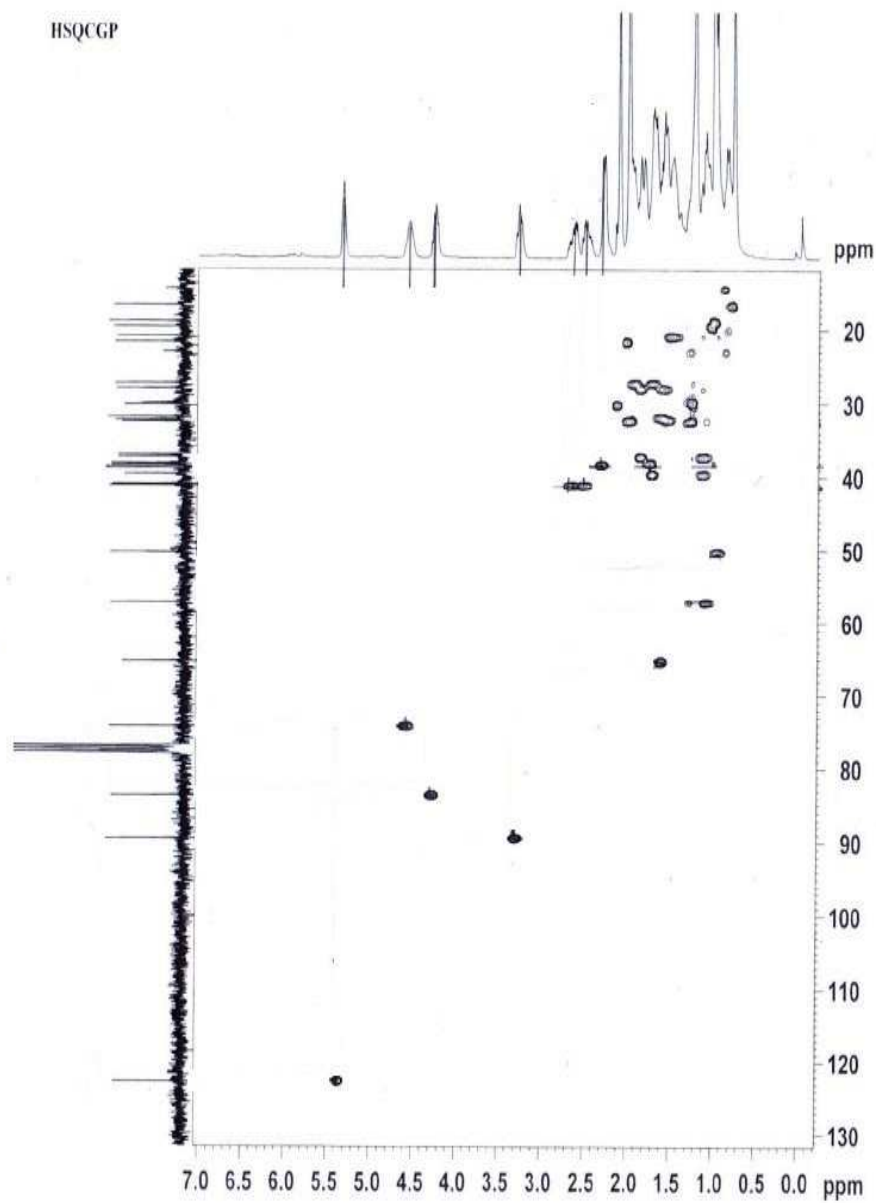


Fig. 4.81:  $^1\text{H}$ - $^1\text{H}$  COSY spectrum of Haad-4 in  $\text{CDCl}_3$

HSQCGP



Current Data Parameters  
 NAME: haad47.p  
 EXPNO: 5  
 PROCNO: 1

F1 - Acquisition Parameters  
 Date\_: 2012011  
 Time: 11:18  
 INSTRUM: spect  
 PROBHD: 5 mm Maltinnal  
 PULPROG: zgpg30  
 TD: 1024  
 SOLVENT: DMSO  
 NS: 2  
 DS: 16  
 SWH: 8995.284 Hz  
 FIDRES: 0.0045416 Hz  
 AQ: 0.0854516 sec  
 RG: 13390.4  
 DW: 83.400 usec  
 DE: 4.00 usec  
 TE: 297.4 K  
 CNST2: 145.000000  
 d0: 0.0000000 sec  
 D1: 1.5000000 sec  
 d11: 0.0017214 sec  
 d12: 0.0300000 sec  
 d13: 0.0000000 sec  
 D14: 0.0002000 sec  
 DELTA: 0.0012690 sec  
 DELTA1: 0.0012060 sec  
 DELTA2: 0.0006207 sec  
 DELTA3: 0.0005214 sec  
 EN0: 0.0004000 sec  
 ST1CNT: 328  
 ZGPG30:

----- CHANNEL f1 -----  
 NUCL1: 1H  
 P1: 6.65 usec  
 p2: 13.30 usec  
 P2: 1000.00 usec  
 PL1: 4.00 dB  
 SFO1: 300.131040 MHz

----- CHANNEL f2 -----  
 CPDPRG2: zgpg  
 NUCL2: 13C  
 P3: 12.50 usec  
 p4: 25.00 usec  
 PCPD2: 70.00 usec  
 PL2: -8.00 dB  
 PL12: 4.00 dB  
 SFO2: 75.473470 MHz

----- GRADIENT CHANNEL -----  
 GPNAM1: SINE.100  
 GPNAM2: SINE.100  
 GPNAM3: SINE.100  
 GPNAM4: SINE.100  
 GPZ1: 80.00 %  
 GPZ2: 30.10 %  
 GPZ3: 11.00 %  
 GPZ4: 5.00 %  
 P1a: 1000.00 usec  
 P11: 600.00 usec

F1 - Acquisition parameters  
 TD: 256  
 SFO1: 75.47341 MHz  
 FIDRES: 40.828125 Hz  
 SW: 165.621 ppm  
 F0MODE: Echo-Antiecho

F2 - Processing parameters  
 SI: 1024  
 SF: 300.130000 MHz  
 WDW: QSINE  
 SSB: 2  
 LB: 0.00 Hz  
 GB: 0  
 PC: 1.40

F1 - Processing parameters  
 SI: 1024  
 M2: echo-antiecho  
 SF: 75.467190 MHz  
 WDW: QSINE  
 SSB: 2  
 LB: 0.00 Hz  
 GB: 0

Fig. 4.82: HSQC spectrum of Haad-4 in CDCl<sub>3</sub>



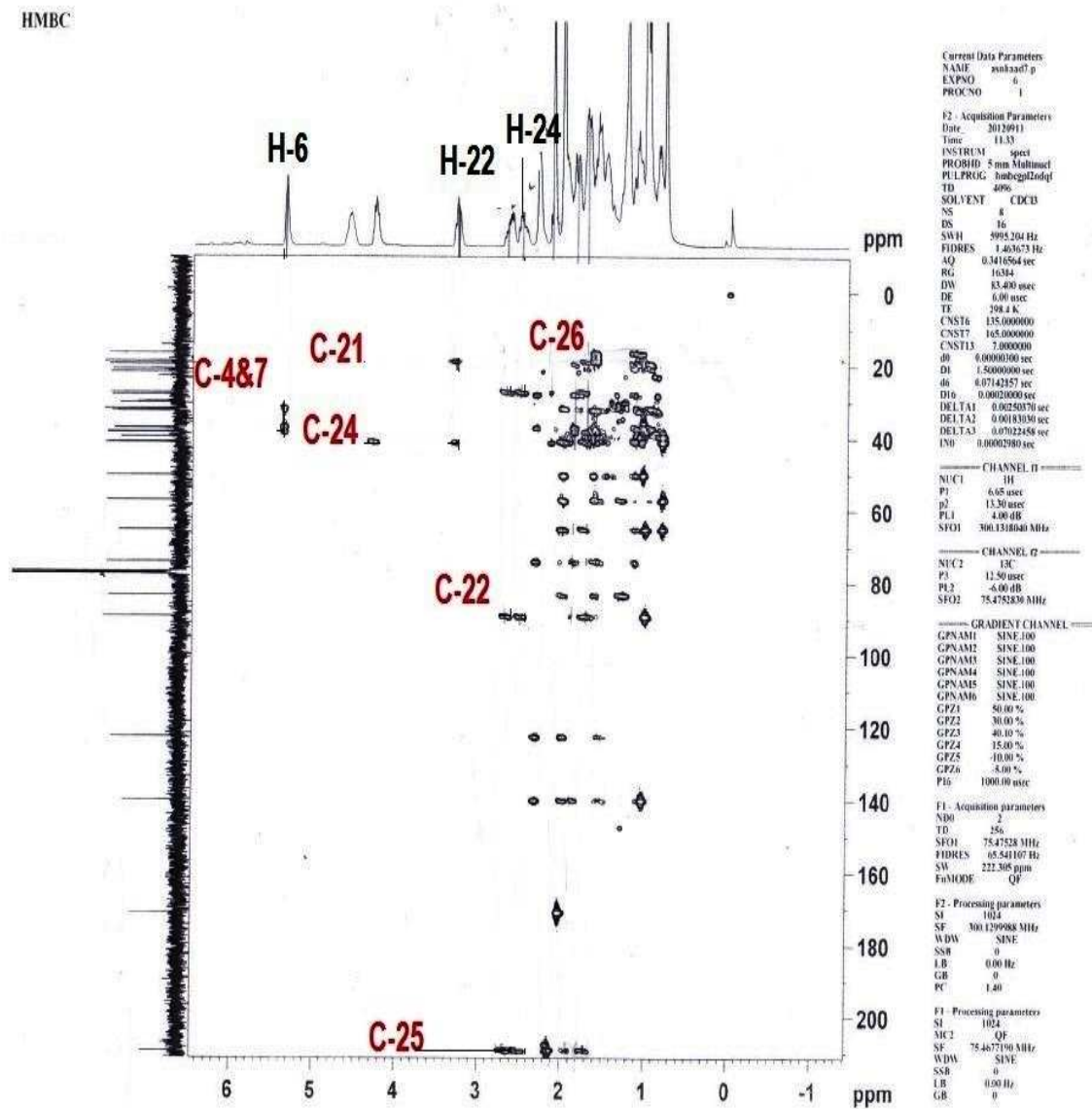
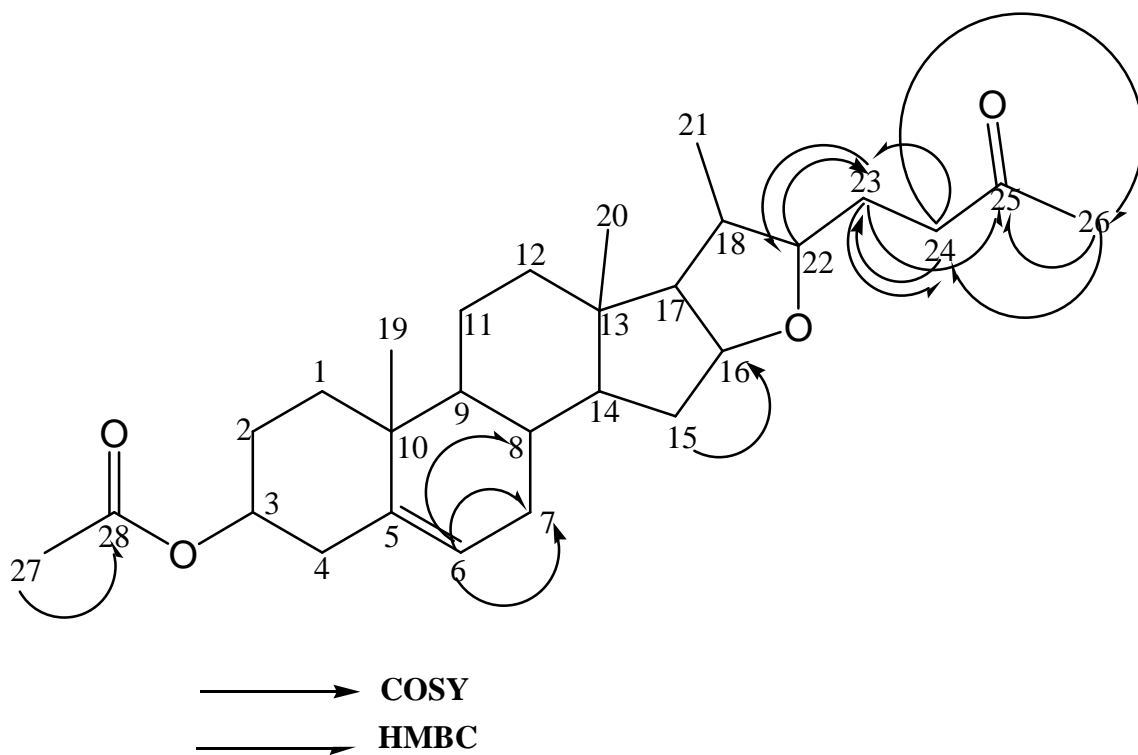
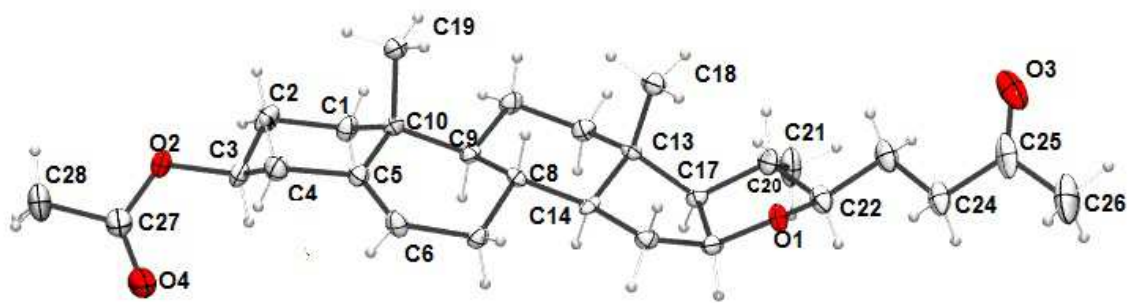


Fig. 4.83:  $^1\text{H}$ - $^{13}\text{C}$  HMBC spectrum of Haad-4 in  $\text{CDCl}_3$



**Fig. 4.84:** COSY and HMBC correlations of Haad-4

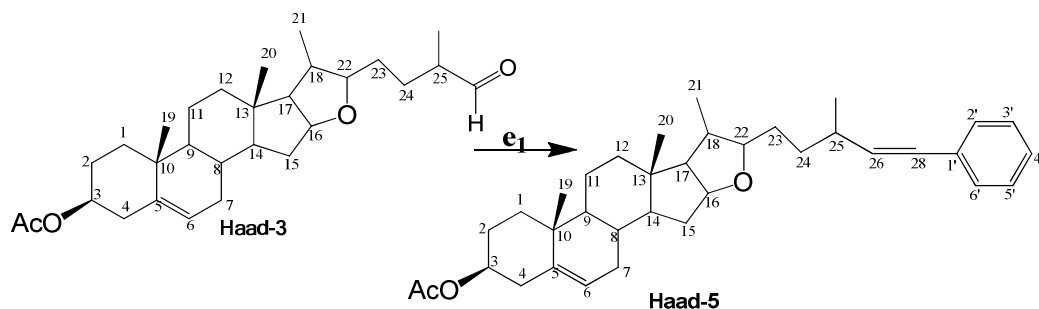


**Fig. 4.85:** Molecular conformation (X-ray) of Haad-4 in crystals. Thermal ellipsoids are shown at 50% probability level.

#### 4.8.6. Synthesis and characterisation of (22 $\beta$ )-(E)-26-Benzylidene-3 $\beta$ -yl-furost-5-en-

### 3-acetate (Haad-5)

Several novel styrene derivatives (Haad-5, Haad-6, Haad-7a and Haad-7b) were prepared from aldehyde Haad-3 using Wittig reaction. Various Wittig salts (Benzylidenetriphenylphosphonium bromides) were prepared using triphenylphosphine ( $\text{Ph}_3\text{P}$ ) and corresponding benzylbromides in toluene. Finally the styrene derivatives of diosgenin were obtained by treating Wittig salts with Haad-3 in sodium hydride in the presence of toluene under reflux conditions at 110 - 130°C. The formation of Haad-5 by Wittig reaction involves the use of Benzylidenetriphenylphosphonium bromide as Wittig salt.



**Reagents and conditions:**  $e_1$ ) Wittig salt (benzylidenetriphenylphosphonium bromide), NaH, Toluene, Reflux 110 - 130°C, 4 hrs.

Haad-5 (158 mg, 68%) was obtained as yellowish viscous liquid. The ESI-MS fragment ions 531.5  $[\text{M}+\text{H}]^+$ , 553.5  $[\text{M}+\text{Na}]^+$  and 569.6  $[\text{M}+\text{K}]^+$  correspond to a molecular formula  $\text{C}_{36}\text{H}_{50}\text{O}_3$  (530) [Fig. 4.86]. The  $^1\text{H}$  NMR chemical shifts at  $\delta_{\text{H}}$  5.96 (dd) and 6.29 (d) were attributed to olefinic methine protons at C-26 and C-28, while the signals of aromatic protons at C-2' to C-6' appeared at  $\delta_{\text{H}}$  7.12 (m) [Fig. 4.87]. The peaks at 3.23 (bd) and 4.22 (bs) were assigned to methine protons at C-22 and C-16 respectively.  $^{13}\text{C}$  NMR [Fig. 4.88] and DEPT spectra [Fig. 4.89] of Haad-5 were identical to Haad-3 spectroscopic data except the at the side chain where the wittig condensation reaction of benzylidenetriphenyl group with Haad-3 occur (26, 28 and 2'-6' positions) [Table 4.67]. Therefore, Haad-5 was identified as (22 $\beta$ )-(E)-26-Benzylidene-3 $\beta$ -yl-furost-5-en-3-acetate. The differences in its spectral data and Haad-3 are given below.

$^1\text{H}$  NMR ( $\text{CDCl}_3$ ): 5.96 (t, 1H, H-26), 6.29 (s, 1H, H-28), 7.12 (m, 5H, H-2' - H-6');

$^{13}\text{C}$  NMR ( $\text{CDCl}_3$ ): 127.15, 128.83 (C-26 & 28), 127.15 (C-6' of phenyl ring), 137.05 (C-4' of phenyl ring), 128.73 (C-2' & C-6' of phenyl ring), 126.39 (C-3' & 5' of phenyl ring) and 138.33 (C-1' of phenyl ring). [Table 4.67; Figs: 4.87 - 4.89]

IR (KBR,  $\text{cm}^{-1}$ ): 2946 (C-H), 1734 (C=O), 1656 (C=C), 1372 (C-O)

**Table 4.67:** Comparison of  $^{13}\text{C}$  and  $^1\text{H}$  NMR data of Haad-3 and Haad-5

Assignment	* <sup>13</sup> C	Multiplicity	* <sup>1</sup> H, multiplicity	<sup>13</sup> C	<sup>1</sup> H
1	21.03	CH <sub>2</sub>	1.34-1.90, m, 2H	28.16	1.42-1.95, m, 2H
2	37.39	CH <sub>2</sub>	1.34-1.90, m, 2H	37.41	1.42-1.95, m, 2H
3	74.28	CH	4.34, m, 1H	74.33	4.24, m, 1H
4	38.48	CH <sub>2</sub>	1.34-1.90, m, 2H	39.82	1.42-1.95, m, 2H
5	141.09	Q	-	140.09	-
6	122.73	CH	5.49, t, 1H	122.77	5.29, t, 1H
7	32.37	CH <sub>2</sub>	2.36, t, 2H	32.40	2.26, t, 2H
8	38.28	CH	1.34-1.90, m, 1H	31.94	1.42-1.95, m, 1H
9	50.41	CH	1.34-1.90, m, 1H	50.44	1.42-1.95, m, 1H
10	37.09	Q	-	37.12	-
11	30.07	CH <sub>2</sub>	1.34-1.90, m, 2H	21.06	1.42-1.95, m, 2H
12	31.96	CH <sub>2</sub>	1.34-1.90, m, 2H	38.51	1.42-1.95, m, 2H
13	39.77	Q	-	39.78	-
14	41.08	CH	1.34-1.90, m, 1H	38.31	1.42-1.95, m, 1H
15	32.59	CH <sub>2</sub>	1.34-1.90, m, 2H	32.66	1.42-1.95, m, 2H
16	83.28	CH	4.63, m, 1H	83.58	4.51, m, 1H
17	65.44	CH	1.34-1.90, m, 1H	65.60	1.42-1.95, m, 1H
18	57.29	CH	1.34-1.90, m, 1H	57.31	1.42-1.95, m, 1H
19	19.22	CH <sub>3</sub>	0.83-1.29, m, 3H	19.39	0.78-1.24, m, 3H
20	16.79	CH <sub>3</sub>	0.83-1.29, m, 3H	16.83	0.78-1.24, m, 3H
21	13.78	CH <sub>3</sub>	0.79-0.81, m, 3H	19.72	0.78-1.24, m, 3H
22	90.11	CH <sub>2</sub>	3.45, s, 2H	90.82	3.23, bd, 1H
23	31.11	CH <sub>2</sub>	1.34-1.90, m, 2H	32.21	1.42-1.95, m, 2H
24	28.15	CH <sub>2</sub>	1.34-1.90, m, 2H	34.48	1.42-1.95, m, 2H
25	46.72	CH	1.34-1.90, m, 1H	42.00	1.42-1.95, m, 1H
26	205.54	Q	9.75, 2, 1H	<b>127.15</b>	<b>5.96, dd, 1H</b>
27	19.71	CH <sub>3</sub>	0.83-1.29, m, 3H	19.69	0.78-1.24, m, 3H
28	21.77	CH <sub>3</sub>	2.16, s, 3H	<b>128.83</b>	<b>6.29, d, 1H</b>
29	170.91	Q	-	<b>21.79</b>	<b>1.99, s, 3H</b>
30				<b>170.97</b>	-
1'				<b>138.33</b>	-
2'				<b>128.73</b>	<b>7.12,m,1H</b>
3'				<b>128.83</b>	<b>7.12,m,1H</b>
4'				<b>137.05</b>	-
5'				<b>128.83</b>	<b>7.12,m,1H</b>
6'				<b>128.73</b>	<b>7.12,m,1H</b>

Implied multiplicities of the carbons were determined from the DEPT experiment.

\*Haad-3

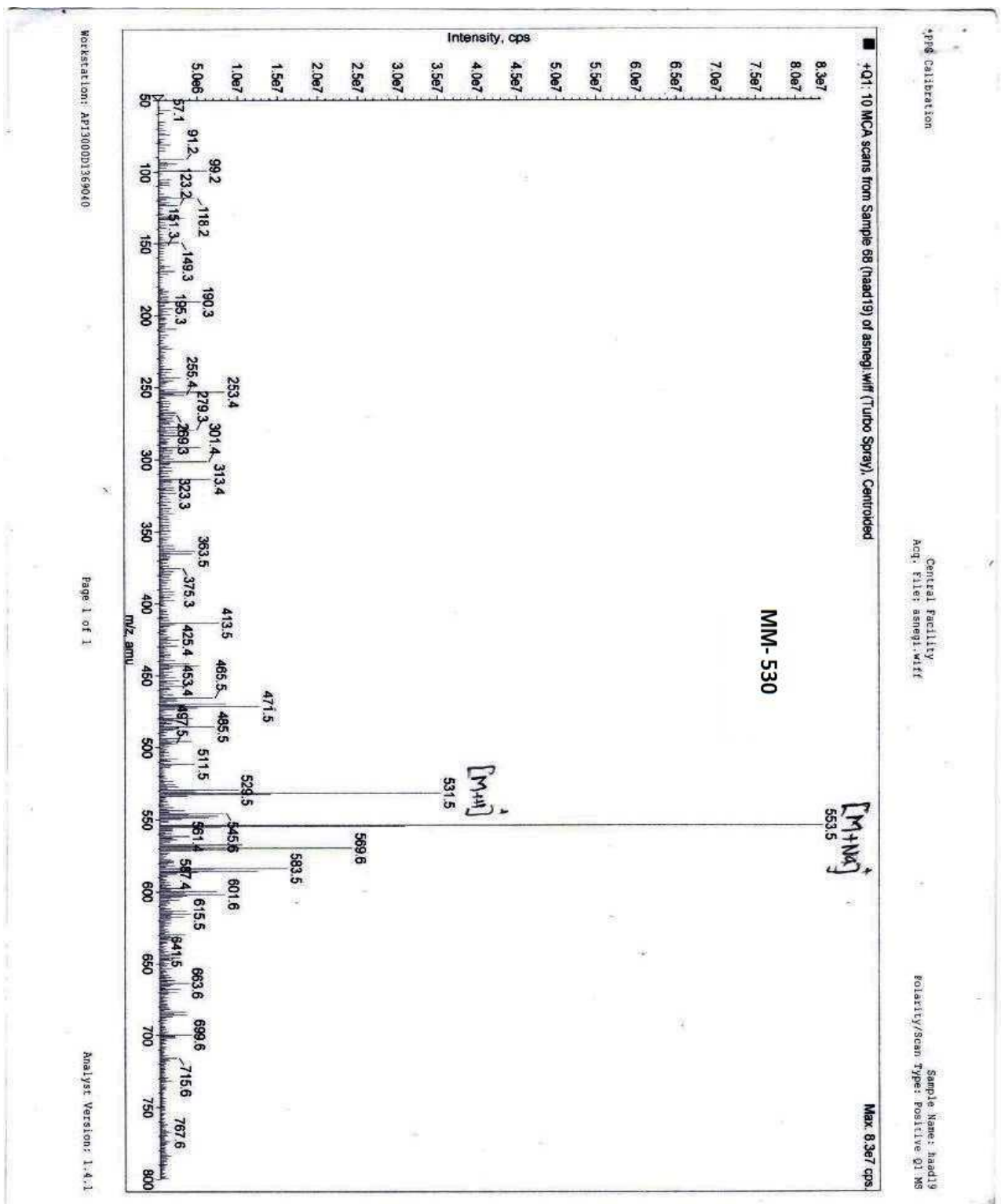


Fig. 4.86: ESI-MS spectrum of Haad-5 in MeOH

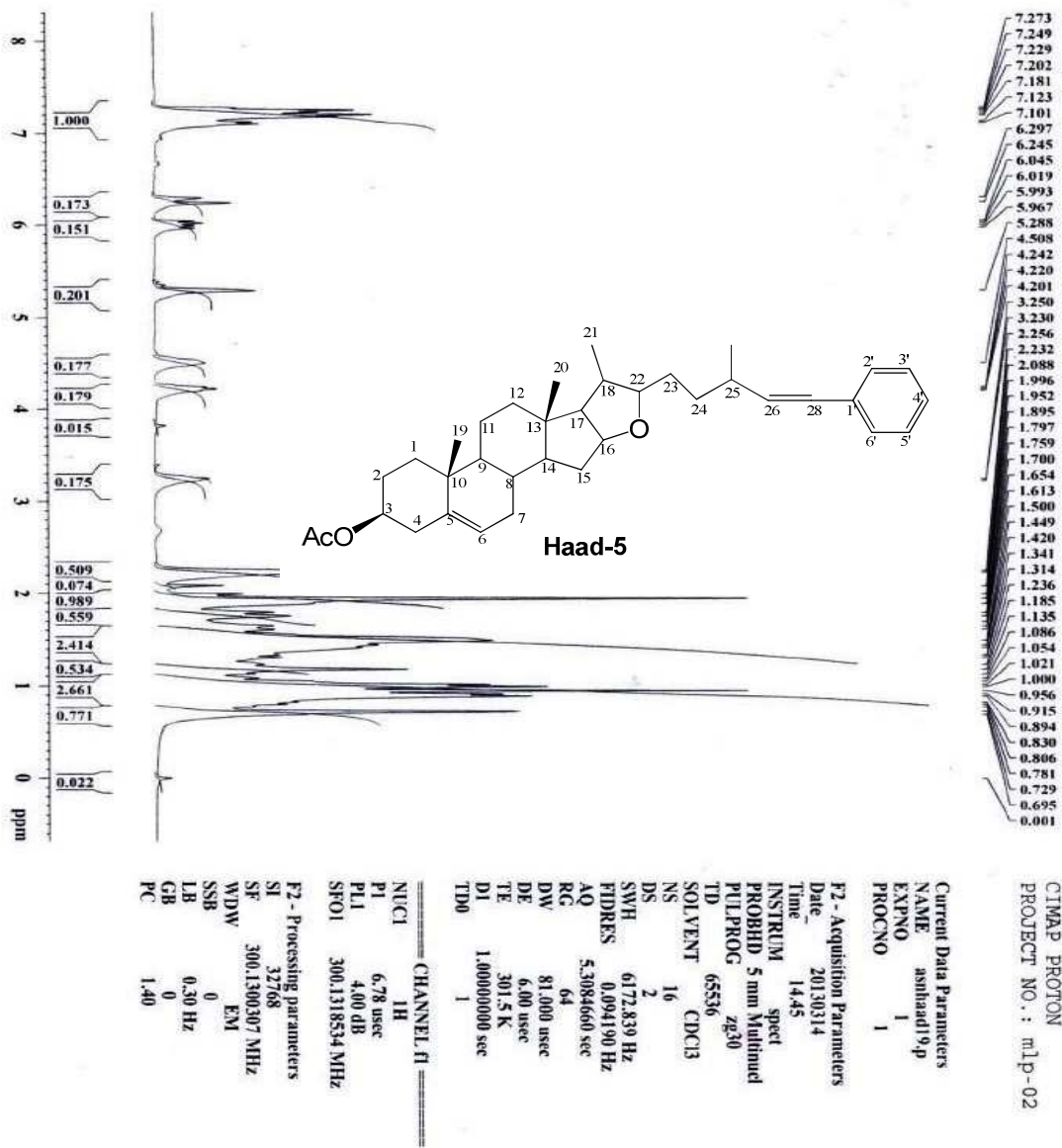


Fig. 4.87: <sup>1</sup>H NMR spectrum of Haad-5 in CDCl<sub>3</sub>

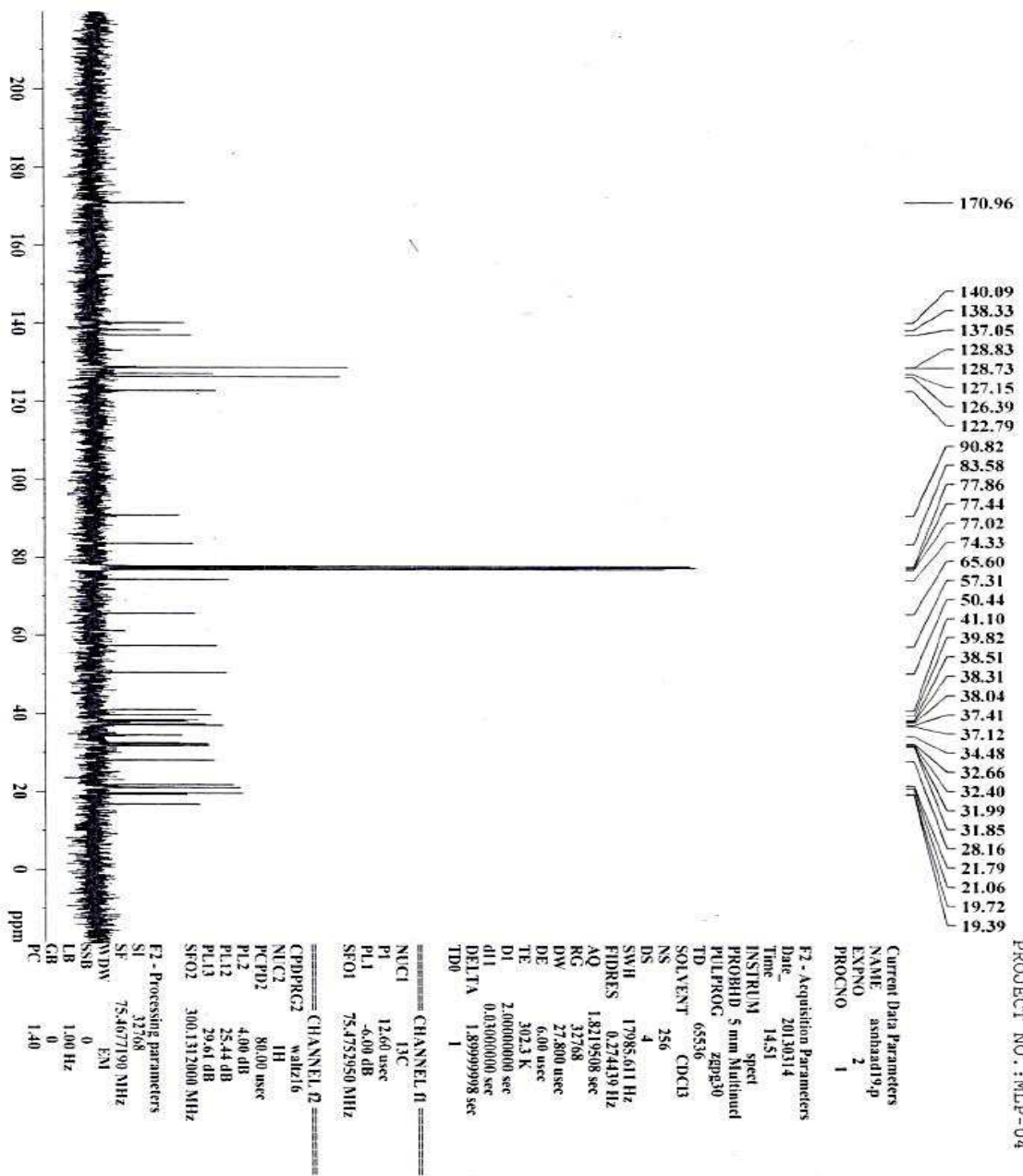


Fig. 4.88:  $^{13}\text{C}$  NMR spectrum of Haad-5 in  $\text{CDCl}_3$

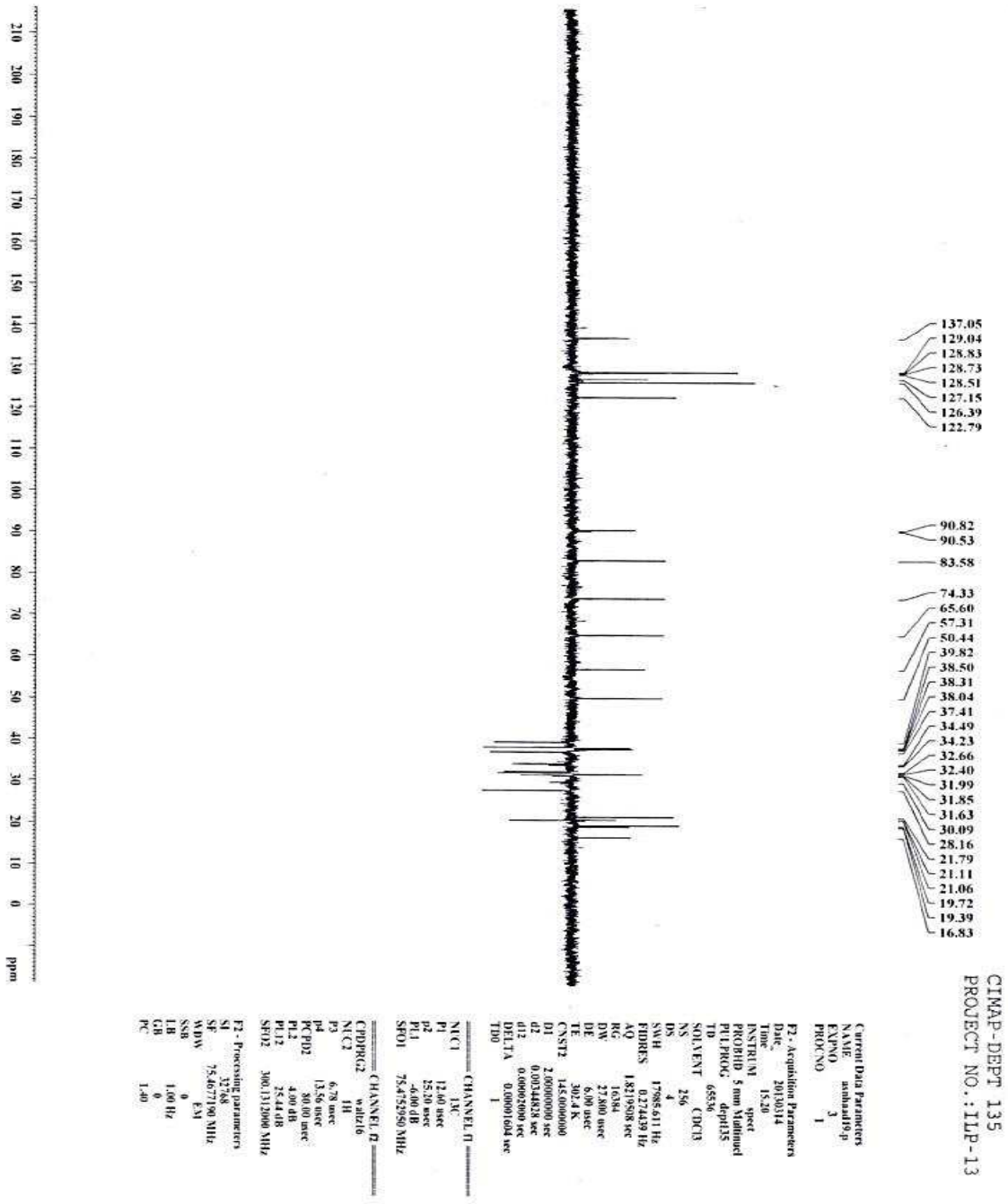


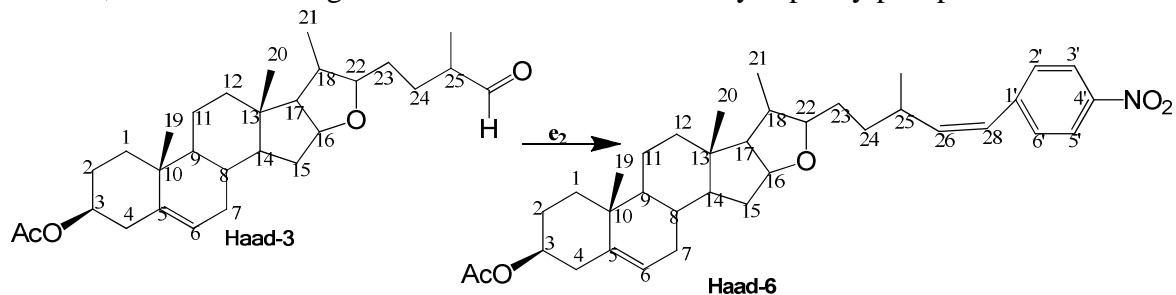
Fig. 4.89: DEPT spectrum of Haad-5 in CDCl<sub>3</sub>

#### 4.8.7. Synthesis and characterisation of (22 $\beta$ )-(Z)-26-(4'-Nitrobenzylidene)-3 $\beta$ -yl-



### furost-5-en-3-acetate (Haad-6)

The formation of Haad-6 by Wittig reaction followed the same reaction procedure as for Haad-5, but the Wittig salt used was 4-nitrobenzyltriphenylphosphonium bromide



**Reagents and conditions:**  $e_2$ ) Wittig salt (4-nitrobenzyltriphenylphosphonium bromide), NaH, Toluene, Reflux 110-130°C, 4 hrs

Haad-6 (157 mg, 62%) also appeared as yellowish viscous liquid. The fragment ions 576.6  $[M+H]^+$ , 598.6  $[M+Na]^+$  and 614.5  $[M+K]^+$  of ESI-MS gave molecular formula  $C_{36}H_{49}NO_5$  (575) [Fig. 4.90]. The  $^1H$  NMR signals at  $\delta_H$  6.29 (dd) and 6.79 (d) correspond to olefinic methine protons at C-26 and C-28, while the chemical shifts of aromatic protons at C-C-2', C-3', C-5' & C-6' appeared at  $\delta_H$  7.33-8.05 (m) [Fig. 4.91]. The peaks at 3.20 (bd) and 4.20 (bs) were assigned to methine protons at C-22 and C-16 respectively.  $^{13}C$  NMR [Fig. 4.92] and DEPT carbon resonances [Fig. 4.93] of Haad-6 were similar to Haad-3 spectroscopic data except at the side chain where the wittig condensation reaction of 4-nitrobenzyltriphenyl group with Haad-3 occur (26, 28 and 2'-6' positions) [Table 4.70]. Hence, Haad-6 was elucidated to be (22 $\beta$ )-(Z)-26-(4'-Nitrobenzylidene)-3 $\beta$ -yl-furost-5-en-3-acetate. The main differences in the spectroscopic data of Haad-6 and Haad-3 are given below.

$^1H$  NMR ( $CDCl_3$ ): 6.29 (t, 1H, H-26), 6.79 (d, 1H, H-28), 7.33 (m, 2H, H-3' & H-5'), 8.05 (t, 2H, 2H, H-2' & H-6')

$^{13}C$  NMR ( $CDCl_3$ ): 134.03, 130.53 (C-26 & 28), 142.28 (C-2' & C-6' of phenyl ring), 143.26 (C-3' & C-5' of phenyl ring) and 162.83 (C-4') [Table 4.68; Figs: 4.91 - 4.93]

IR (KBR,  $cm^{-1}$ ): 2940 (C-H), 1728 (C=O), 1595 (C=C), 1340 (C-O)

**Table 4.68:** Comparison of  $^{13}C$  and  $^1H$  NMR data of Haad-3 and Haad-6

Assignment	* <sup>13</sup> C	Multiplicity	* <sup>1</sup> H, multiplicity	<sup>13</sup> C	<sup>1</sup> H
1	21.03	CH <sub>2</sub>	1.34-1.90, m, 2H	28.11	1.42-1.95, m, 2H
2	37.39	CH <sub>2</sub>	1.34-1.90, m, 2H	37.36	1.42-1.95, m, 2H
3	74.28	CH	4.34, m, 1H	74.50	4.51, m, 1H
4	38.48	CH <sub>2</sub>	1.34-1.90, m, 2H	39.74	1.42-1.95, m, 2H
5	141.09	Q	-	140.09	-
6	122.73	CH	5.49, t, 1H	122.77	5.29, t, 1H
7	32.37	CH <sub>2</sub>	2.36, t, 2H	32.40	2.26, t, 2H
8	38.28	CH	1.34-1.90, m, 1H	31.94	1.42-1.95, m, 1H
9	50.41	CH	1.34-1.90, m, 1H	50.37	1.42-1.95, m, 1H
10	37.09	Q	-	37.09	-
11	30.07	CH <sub>2</sub>	1.34-1.90, m, 2H	21.01	1.42-1.95, m, 2H
12	31.96	CH <sub>2</sub>	1.34-1.90, m, 2H	38.51	1.42-1.95, m, 2H
13	39.77	Q	-	39.78	-
14	41.08	CH	1.34-1.90, m, 1H	41.10	1.42-1.95, m, 1H
15	32.59	CH <sub>2</sub>	1.34-1.90, m, 2H	32.66	1.42-1.95, m, 2H
16	83.28	CH	4.63, m, 1H	83.58	4.24, m, 1H
17	65.44	CH	1.34-1.90, m, 1H	65.40	1.42-1.95, m, 1H
18	57.29	CH	1.34-1.90, m, 1H	57.27	1.42-1.95, m, 1H
19	19.22	CH <sub>3</sub>	0.83-1.29, m, 3H	19.39	0.78-1.24, m, 3H
20	16.79	CH <sub>3</sub>	0.83-1.29, m, 3H	16.83	0.78-1.24, m, 3H
21	13.78	CH <sub>3</sub>	0.79-0.81, m, 3H	19.72	0.78-1.24, m, 3H
22	90.11	CH <sub>2</sub>	3.45, s, 2H	90.54	3.20, bd, 1H
23	31.11	CH <sub>2</sub>	1.34-1.90, m, 2H	32.21	1.42-1.95, m, 2H
24	28.15	CH <sub>2</sub>	1.34-1.90, m, 2H	34.48	1.42-1.95, m, 2H
25	46.72	CH	1.34-1.90, m, 1H	42.00	1.42-1.95, m, 1H
26	205.54	Q	9.75, 2, 1H	<b>143.03</b>	<b>6.29, dd, 1H</b>
27	19.71	CH <sub>3</sub>	0.83-1.29, m, 3H	19.69	0.78-1.24, m, 3H
28	21.77	CH <sub>3</sub>	2.16, s, 3H	<b>130.53</b>	<b>6.79, d, 1H</b>
29	170.91	Q	-	<b>21.81</b>	<b>2.02, s, 3H</b>
30				<b>171.85</b>	-
1'				<b>144.83</b>	-
2'				<b>142.28</b>	<b>8.05,m,1H</b>
3'				<b>143.26</b>	<b>7.33,m,1H</b>
4'				<b>162.83</b>	-
5'				<b>143.26</b>	<b>7.33,m,1H</b>
6'				<b>142.28</b>	<b>8.05,m,1H</b>

Implied multiplicities of the carbons were determined from the DEPT experiment.

\*Haad-3

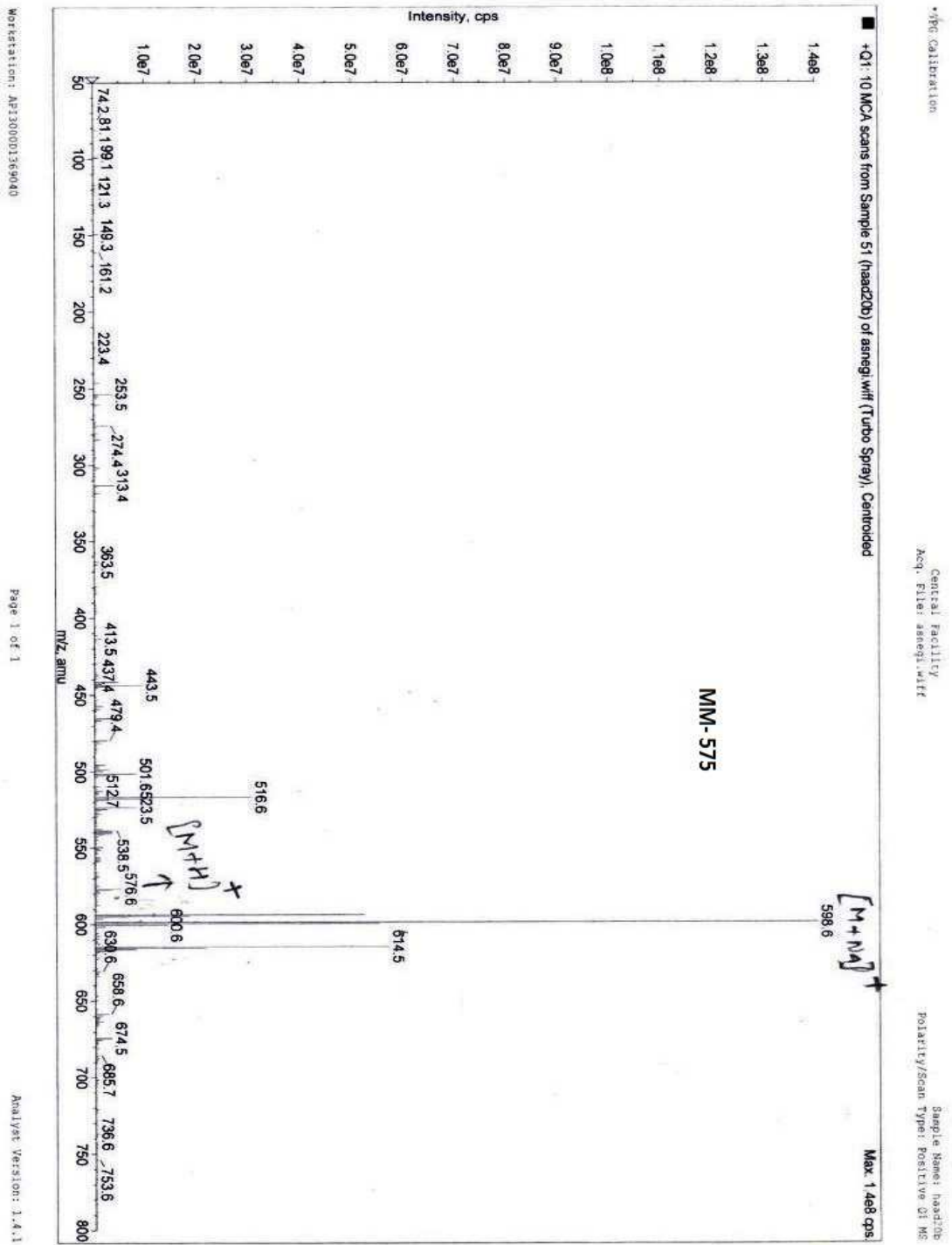
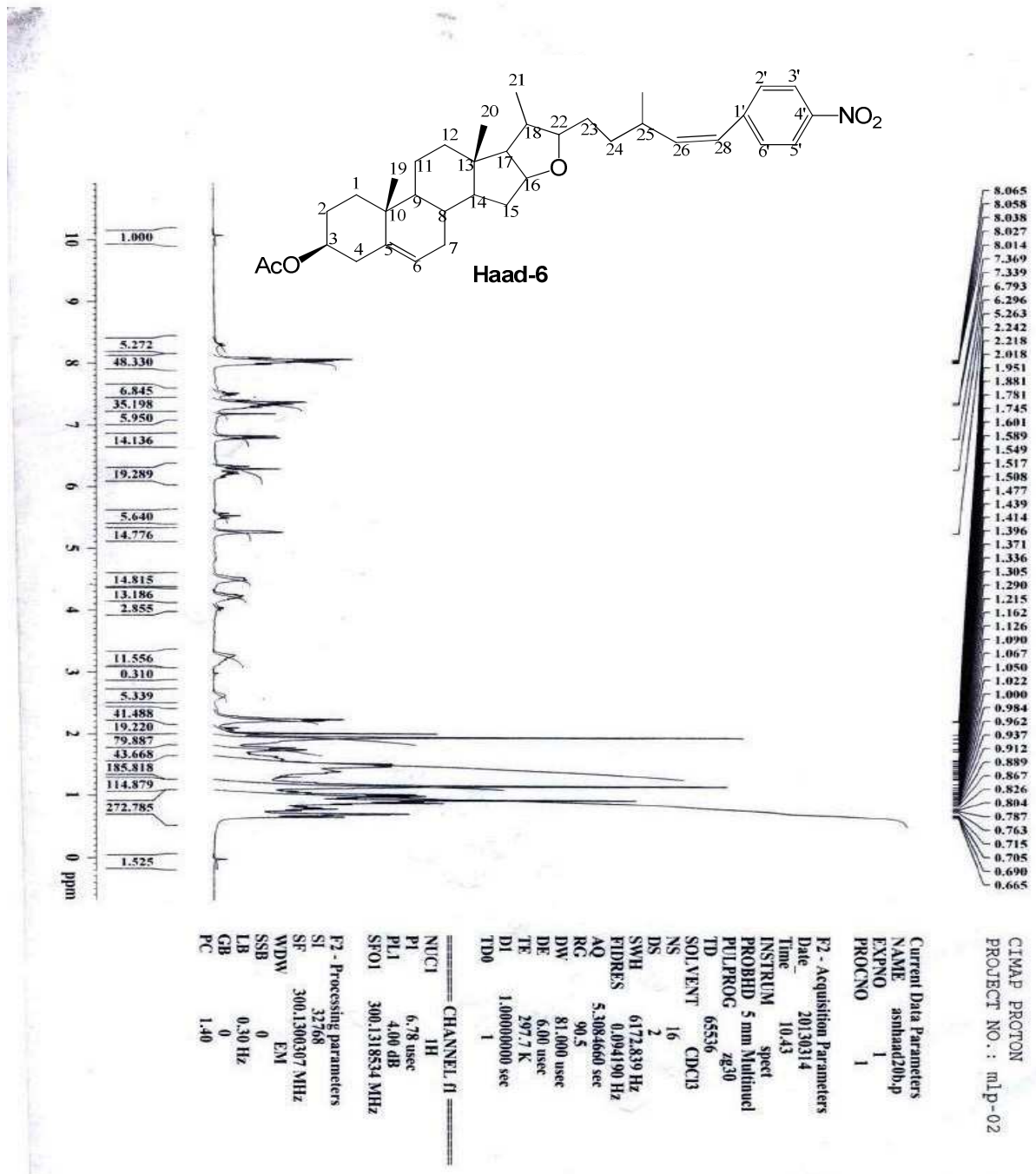


Fig. 4.90: ESI-MS spectrum of Haad-6 in MeOH



**Fig. 4.91:**  $^1\text{H}$  NMR spectrum of Haad-6 in  $\text{CDCl}_3$

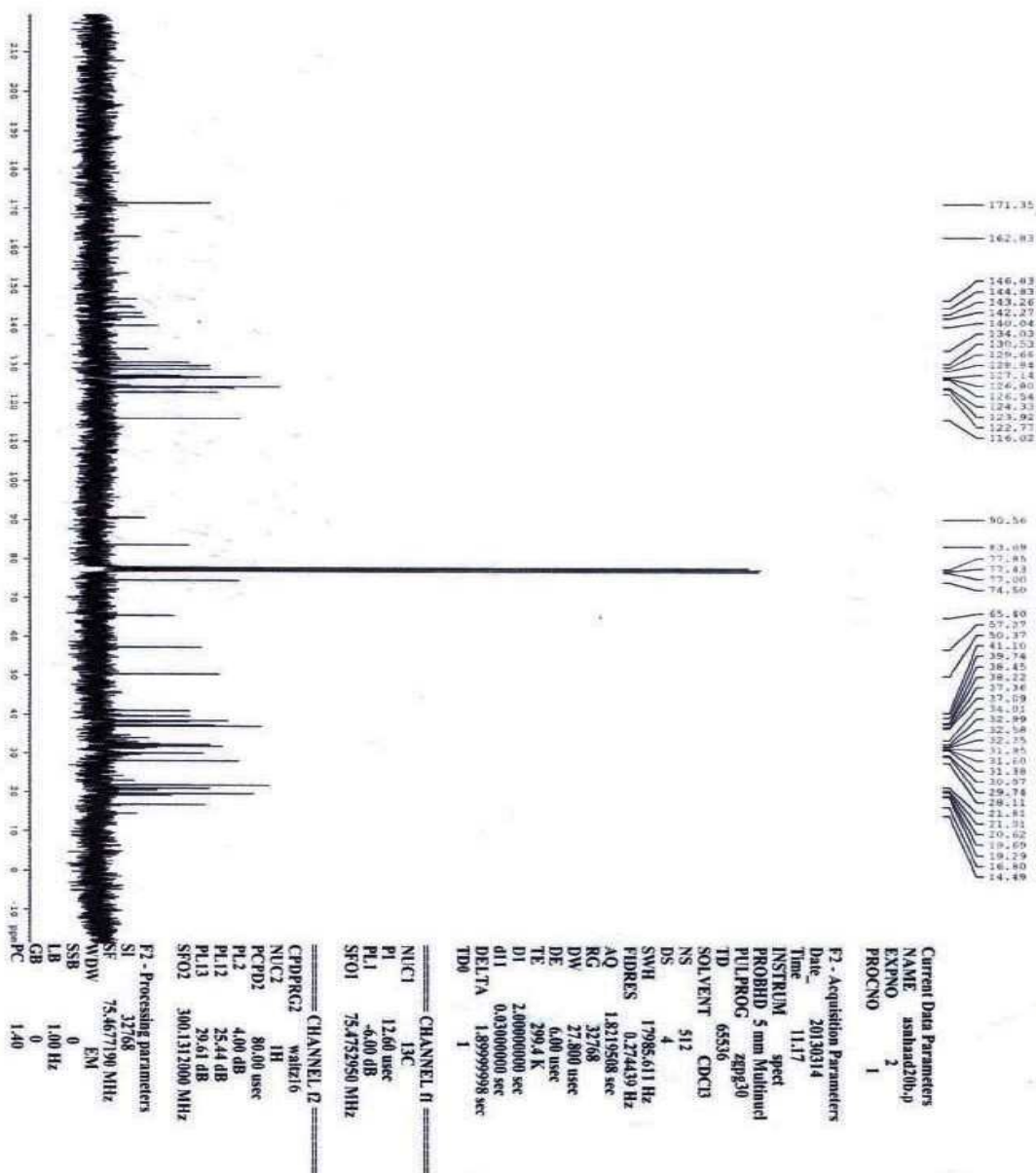


Fig. 4.92:  $^{13}\text{C}$  NMR spectrum of Haad-6 in  $\text{CDCl}_3$

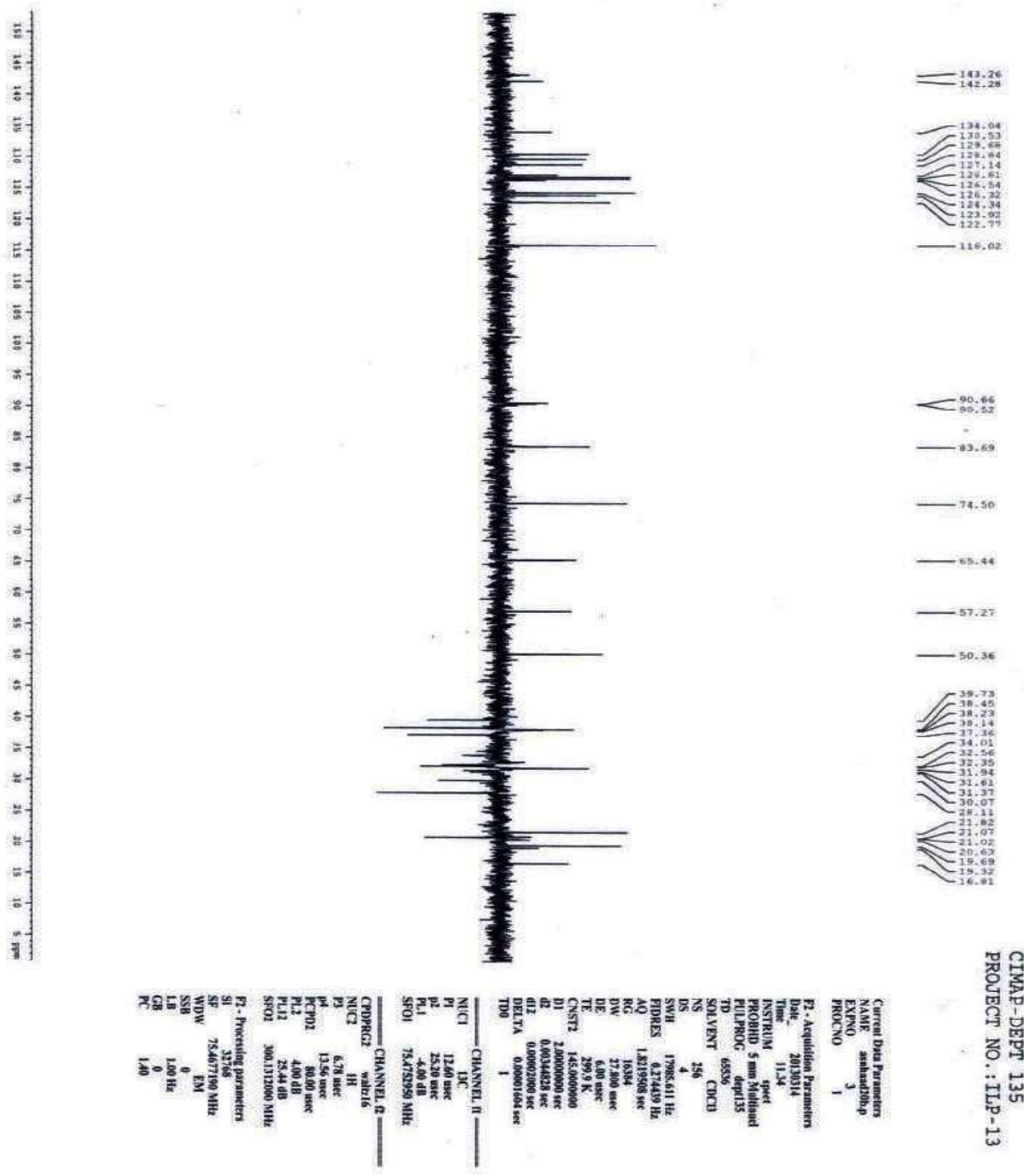
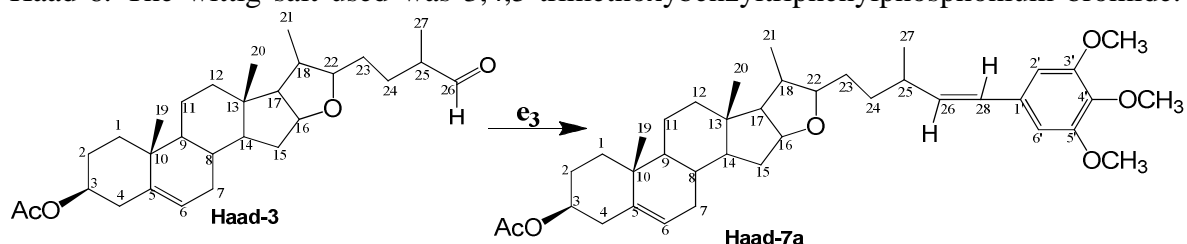


Fig. 4.93: DEPT spectrum of Haad-6 in CDCl<sub>3</sub>

#### 4.8.8. Synthesis and characterisation of (22 $\beta$ )-(E)-26-(3',4',5'-Trimethoxybenzylidene)-3 $\beta$ -yl-furost-5-en-3-acetate (Haad-7a)

Haad-7a was also obtained by wittig reaction with the same reaction procedure as for Haad-6. The wittig salt used was 3,4,5-trimethoxybenzyltriphenylphosphonium bromide.



**Reagents and conditions:**  $e_3$ ) Wittig salt (3,4,5-trimethoxybenzyltriphenylphosphonium bromide), NaH, Toluene, Reflux 110-130°C, 3 hrs.

Haad-7a (142 mg, 52%) obtained as a yellowish oily compound. The fragment ions 621.5  $[M+H]^+$ , 643.5  $[M+Na]^+$  and 659.4  $[M+K]^+$  of ESI-MS gave molecular formula  $C_{39}H_{56}O_6$  (620) [Fig. 4.94]. The  $^1H$  NMR spectrum showed signals at  $\delta_H$  5.98 (dd) and 6.22 (d) correspond to olefinic methine protons at C-26 and C-28, which is a characteristic of trans-product, while the signals of aromatic protons at C-2' & C-6' appeared at  $\delta_H$  6.54 (s) [Fig. 4.95]. The signals at 3.30 (bd) and 4.27 (bs) were attributable to methine protons at C-22 and C-16 respectively.  $^{13}C$  NMR [Fig. 4.96] and DEPT carbon resonances [Fig. 4.97] of the analogue were also similar to Haad-3 spectroscopic data except the coupling of 3,4,5-trimethoxybenzyltriphenyl group to the side chain of wittig product Haad-7a [Table 4.69]. Haad-7a was elucidated to be (22 $\beta$ )-(E)-26-(3',4',5'-Trimethoxybenzylidene)-3 $\beta$ -yl-furost-5-en-3-acetate. The differences in the spectroscopic data of the compound and Haad-3 are given below.

$^1H$  NMR ( $CDCl_3$ ): 5.98 (t, 1H, H-26), 6.22 (d, 1H, H-28), 6.54 (s, 2H, H-2' & H-6')

$^{13}C$  NMR ( $CDCl_3$ ): 134.05, 128.64 (C-26 & 28), 136.50, 128.64 (C-2' & C-6' of phenyl ring), 153.63 (C-3' & C-5' of phenyl ring) and 137.61 (C-4') [Table 4.69; Figs: 4.95-4.97]

IR (KBR,  $cm^{-1}$ ): 2943 (C-H), 1732 (C=O), 1588 (C=C), 1337 (C-O)

**Table 4.69:** Comparison of  $^{13}\text{C}$  and  $^1\text{H}$  NMR data of Haad-3 and Haad-7a

Assignment	* $^{13}\text{C}$	Multiplicity	* $^1\text{H}$ , multiplicity	$^{13}\text{C}$	$^1\text{H}$
1	21.03	$\text{CH}_2$	1.34-1.90, m, 2H	28.11	1.42-1.95, m, 2H
2	37.39	$\text{CH}_2$	1.34-1.90, m, 2H	37.36	1.42-1.95, m, 2H
3	74.28	CH	4.34, m, 1H	74.50	4.51, m, 1H
4	38.48	$\text{CH}_2$	1.34-1.90, m, 2H	39.74	1.42-1.95, m, 2H
5	141.09	Q	-	140.09	-
6	122.73	CH	5.49, t, 1H	122.77	5.29, t, 1H
7	32.37	$\text{CH}_2$	2.36, t, 2H	32.40	2.26, t, 2H
8	38.28	CH	1.34-1.90, m, 1H	31.94	1.42-1.95, m, 1H
9	50.41	CH	1.34-1.90, m, 1H	50.37	1.42-1.95, m, 1H
10	37.09	Q	-	37.09	-
11	30.07	$\text{CH}_2$	1.34-1.90, m, 2H	21.01	1.42-1.95, m, 2H
12	31.96	$\text{CH}_2$	1.34-1.90, m, 2H	38.51	1.42-1.95, m, 2H
13	39.77	Q	-	39.78	-
14	41.08	CH	1.34-1.90, m, 1H	41.10	1.42-1.95, m, 1H
15	32.59	$\text{CH}_2$	1.34-1.90, m, 2H	32.66	1.42-1.95, m, 2H
16	83.28	CH	4.63, m, 1H	83.58	4.27, m, 1H
17	65.44	CH	1.34-1.90, m, 1H	65.40	1.42-1.95, m, 1H
18	57.29	CH	1.34-1.90, m, 1H	57.27	1.42-1.95, m, 1H
19	19.22	$\text{CH}_3$	0.83-1.29, m, 3H	19.39	0.78-1.24, m, 3H
20	16.79	$\text{CH}_3$	0.83-1.29, m, 3H	16.83	0.78-1.24, m, 3H
21	13.78	$\text{CH}_3$	0.79-0.81, m, 3H	19.72	0.78-1.24, m, 3H
22	90.11	$\text{CH}_2$	3.45, s, 2H	90.72	3.30, bd, 1H
23	31.11	$\text{CH}_2$	1.34-1.90, m, 2H	32.21	1.42-1.95, m, 2H
24	28.15	$\text{CH}_2$	1.34-1.90, m, 2H	34.48	1.42-1.95, m, 2H
25	46.72	CH	1.34-1.90, m, 1H	42.00	1.42-1.95, m, 1H
26	205.54	Q	9.75, 2, 1H	<b>136.50</b>	<b>5.98, dd, 1H</b>
27	19.71	$\text{CH}_3$	0.83-1.29, m, 3H	19.69	0.78-1.24, m, 3H
28	21.77	$\text{CH}_3$	2.16, s, 3H	<b>128.64</b>	<b>6.22, d, 1H</b>
29	170.91	Q	-	<b>21.77</b>	<b>1.99, s, 3H</b>
30				<b>170.85</b>	-
1'				<b>144.83</b>	-
2'				<b>134.05</b>	<b>6.54, s, 1H</b>
3'				<b>153.63</b>	-
4'				<b>137.61</b>	-
5'				<b>153.63</b>	-
6'				<b>134.05</b>	<b>6.54, s, 1H</b>
3 X $\text{OCH}_3$				<b>60.73</b>	<b>3.84, s, 1H</b>
				<b>61.26</b>	<b>3.84, s, 1H</b>
				<b>57.26</b>	<b>3.84, s, 1H</b>

Implied multiplicities of the carbons were determined from the DEPT experiment. \*Haad-3



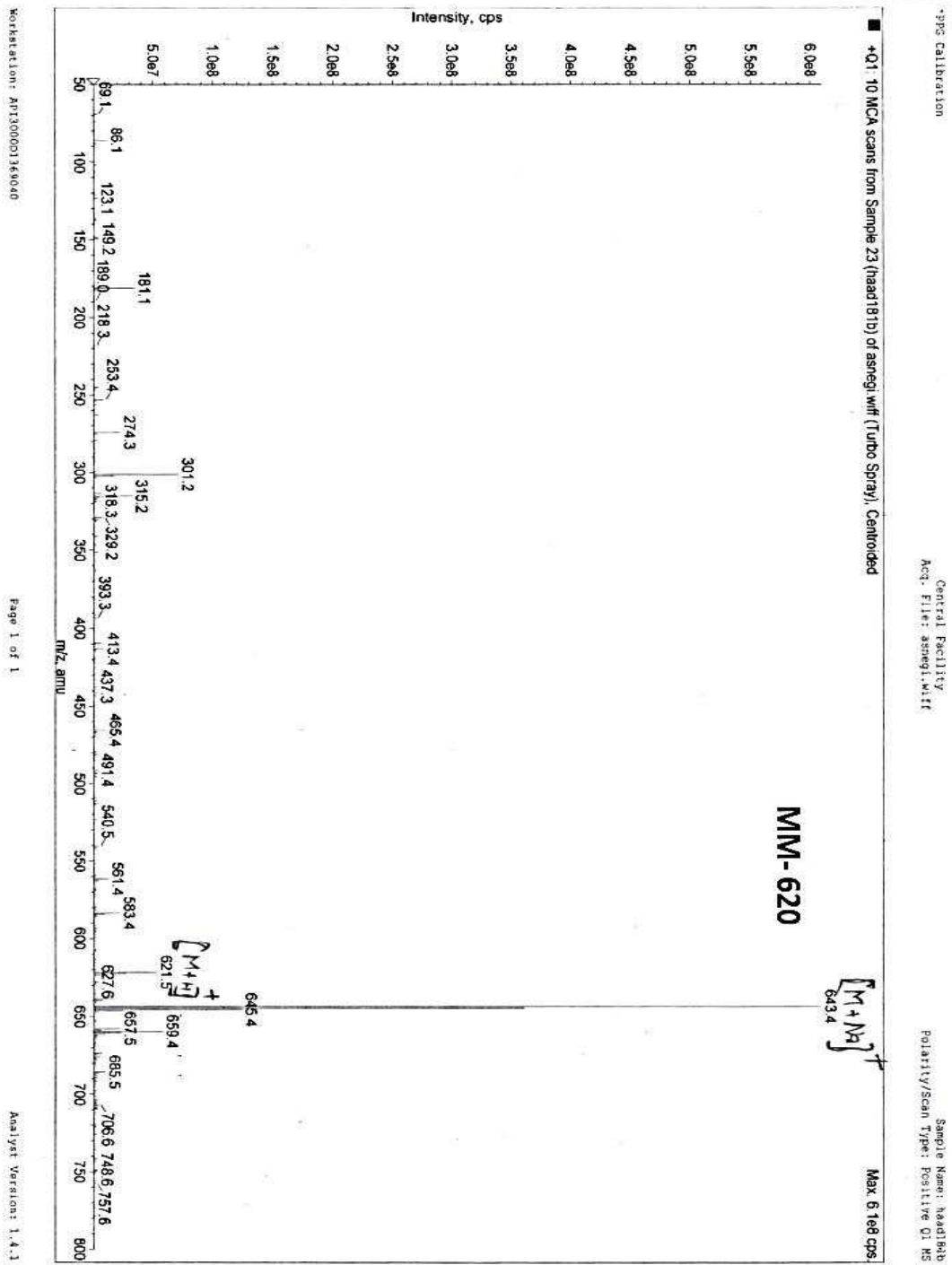


Fig. 4.94: ESI-MS spectrum of Haad-7a in MeOH

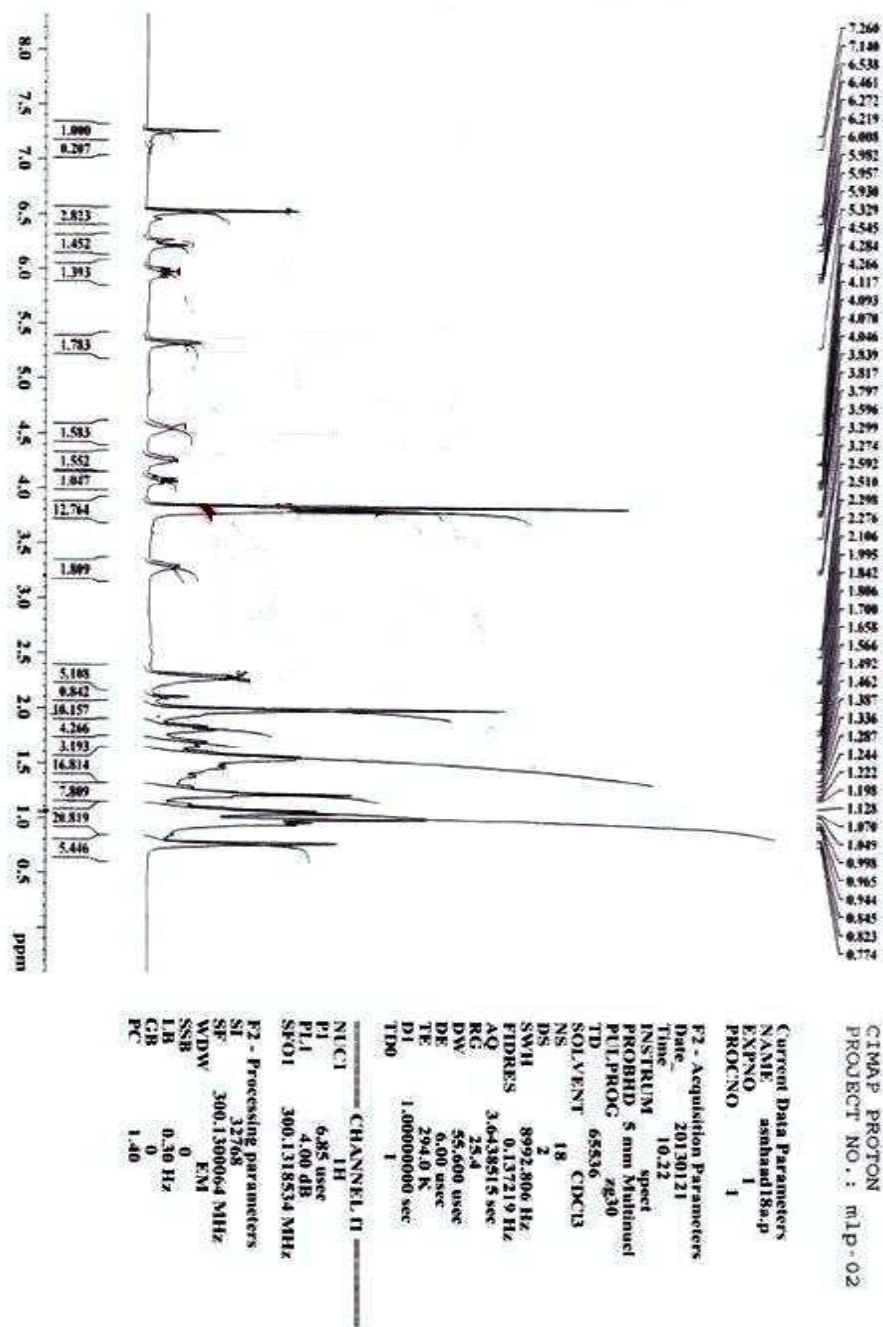


Fig. 4.95:  $^1\text{H}$  NMR spectrum of Haad-7a in  $\text{CDCl}_3$

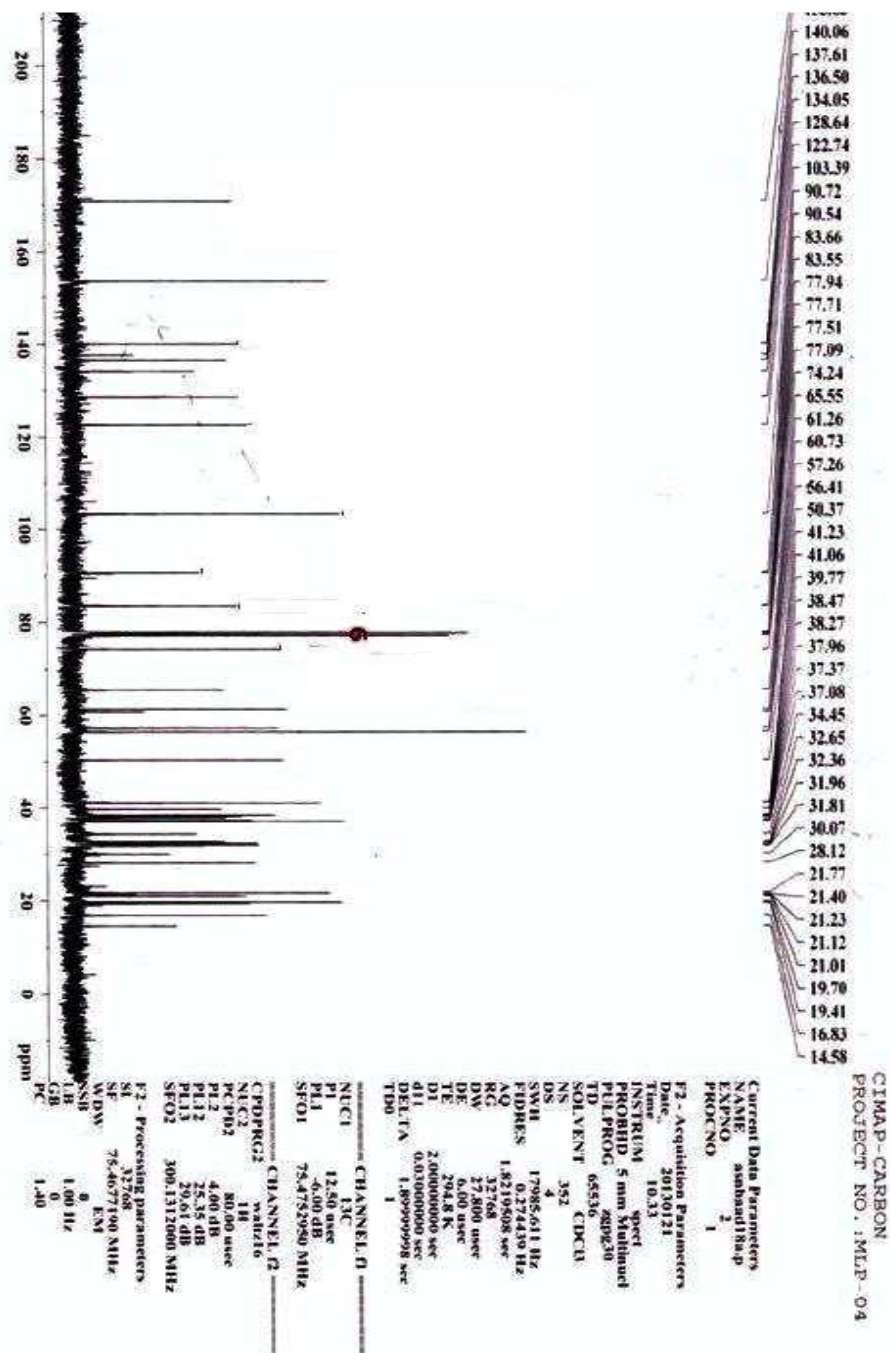


Fig. 4.96:  $^{13}\text{C}$  NMR spectrum of Haad-7a in  $\text{CDCl}_3$

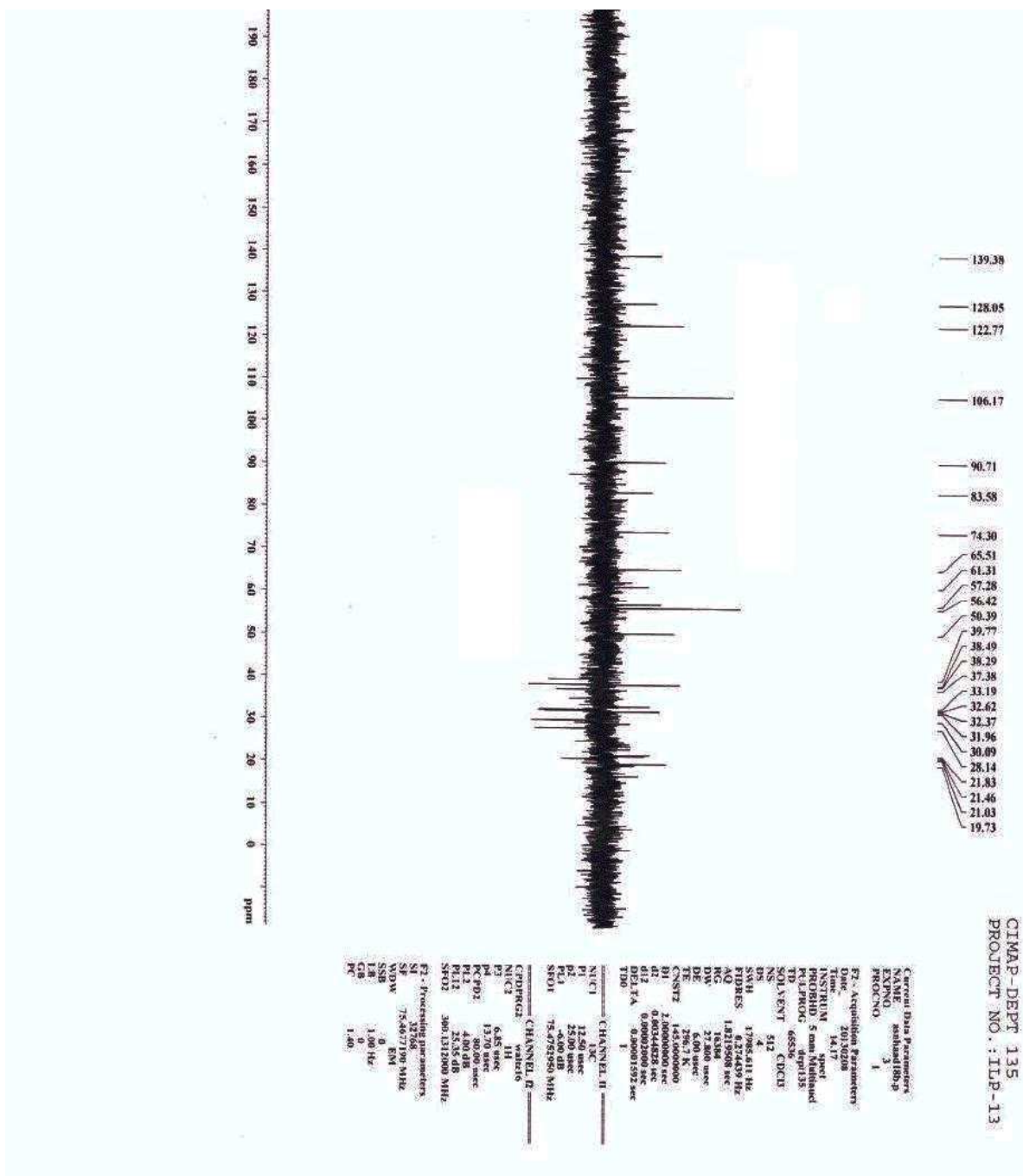
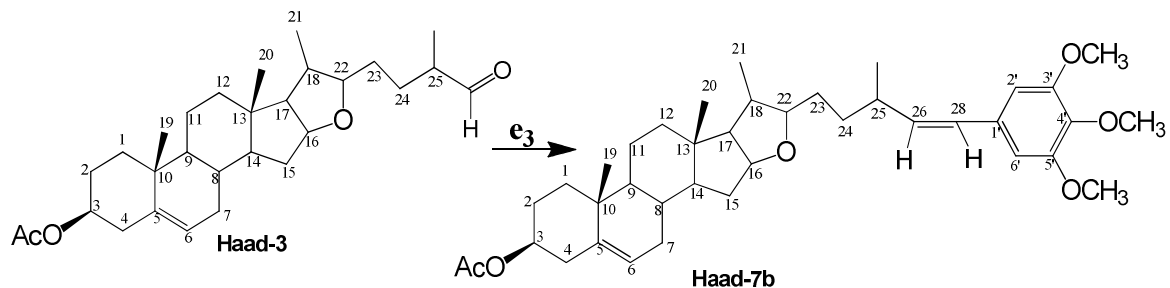


Fig. 4.97: DEPT spectrum of Haad-7a in CDCl<sub>3</sub>

#### 4.8.9. Synthesis and characterisation of (22 $\beta$ )-(Z)-26-(3',4',5'-Trimethoxybenzylidene)-3 $\beta$ -yl-furost-5-en-3-acetate (Haad-7b)

Haad-7b was formed by Wittig reaction with the same reaction procedure as for Haad-7a. The wittig salt used was also 3,4,5-trimethoxybenzyltriphenylphosphonium bromide



**Reagents and conditions:** e) Wittig salt (3,4,5-trimethoxybenzyltriphenylphosphonium bromide), NaH, Toluene, Reflux 110-130°C, 3 hrs

Haad-7b has a low yield (79 mg, 29%) and also gave a yellowish oily compound. The ESI-MS fragment ions 620.5 [M+H]<sup>+</sup>, 643.5 [M+Na]<sup>+</sup> and 659.4 [M+K]<sup>+</sup> calculated for a molecular formula C<sub>39</sub>H<sub>56</sub>O<sub>6</sub> (620) [Fig. 4.98]. The <sup>1</sup>H NMR spectrum showed signals at  $\delta_H$  6.28 (dd) and 6.32 (d) correspond to olefinic methine protons at C-26 and C-28, which is a characteristic of cis-product, while the chemical shifts of aromatic protons at C-2' & C-6' appeared at  $\delta_H$  6.50 (s) [Fig. 4.99]. The proton peaks at 3.27 (bd) and 4.28 (bs) were assigned to methine protons at C-22 and C-16 respectively. <sup>13</sup>C NMR [Fig. 5.00] and DEPT carbon resonances [Fig. 5.01] of the analogue were also identical to Haad-7a spectroscopic data except the olefinic methine protons at 26 and 28 positions which distinguished cis- and trans-derivatives. The compound was also similar to aldehyde, Haad-3 except the coupling of 3,4,5-trimethoxybenzyltriphenyl group to the side chain of wittig product Haad-7b [Table 4.70]. Therefore, Haad-7b was elucidated to be (22 $\beta$ )-(Z)-26-(3',4',5'-Trimethoxybenzylidene)-3 $\beta$ -yl-furost-5-en-3-acetate. The main differences in the spectroscopic data of Haad-7b with that of Haad-3 are given below.

<sup>1</sup>H NMR (CDCl<sub>3</sub>): 6.28 (t, 1H, H-26), 6.32 (d, 1H, H-28), 6.50 (s, 2H, H-2' & H-6')

<sup>13</sup>C NMR (CDCl<sub>3</sub>): 139.38, 128.05 (C-26 & 28), 106.17 (C-2' & C-6' of phenyl ring), 153.27 (C-3' & C-5' of phenyl ring) and 133.94 (C-4') [Table 4.70; Figs: 4.99 - 5.01]

IR (KBR, cm<sup>-1</sup>): 2945 (C-H), 1733 (C=O), 1582 (C=C), 1243 (C-O)

**Table 4.70:** Comparison of  $^{13}\text{C}$  and  $^1\text{H}$  NMR data of Haad-3 and Haad-7b

Assignment	* $^{13}\text{C}$	Multiplicity	* $^1\text{H}$ , multiplicity	$^{13}\text{C}$	$^1\text{H}$
1	21.03	CH <sub>2</sub>	1.34-1.90, m, 2H	28.11	1.42-1.95, m, 2H
2	37.39	CH <sub>2</sub>	1.34-1.90, m, 2H	37.36	1.42-1.95, m, 2H
3	74.28	CH	4.34, m, 1H	74.50	4.61, m, 1H
4	38.48	CH <sub>2</sub>	1.34-1.90, m, 2H	39.74	1.42-1.95, m, 2H
5	141.09	Q	-	140.09	-
6	122.73	CH	5.49, t, 1H	122.77	5.29, t, 1H
7	32.37	CH <sub>2</sub>	2.36, t, 2H	32.40	2.26, t, 2H
8	38.28	CH	1.34-1.90, m, 1H	31.94	1.42-1.95, m, 1H
9	50.41	CH	1.34-1.90, m, 1H	50.37	1.42-1.95, m, 1H
10	37.09	Q	-	37.09	-
11	30.07	CH <sub>2</sub>	1.34-1.90, m, 2H	21.01	1.42-1.95, m, 2H
12	31.96	CH <sub>2</sub>	1.34-1.90, m, 2H	38.51	1.42-1.95, m, 2H
13	39.77	Q	-	39.78	-
14	41.08	CH	1.34-1.90, m, 1H	41.10	1.42-1.95, m, 1H
15	32.59	CH <sub>2</sub>	1.34-1.90, m, 2H	32.66	1.42-1.95, m, 2H
16	83.28	CH	4.63, m, 1H	83.58	4.28, m, 1H
17	65.44	CH	1.34-1.90, m, 1H	65.40	1.42-1.95, m, 1H
18	57.29	CH	1.34-1.90, m, 1H	56.41	1.42-1.95, m, 1H
19	19.22	CH <sub>3</sub>	0.83-1.29, m, 3H	19.39	0.78-1.24, m, 3H
20	16.79	CH <sub>3</sub>	0.83-1.29, m, 3H	16.83	0.78-1.24, m, 3H
21	13.78	CH <sub>3</sub>	0.79-0.81, m, 3H	19.72	0.78-1.24, m, 3H
22	90.11	CH <sub>2</sub>	3.45, s, 2H	90.71	3.27, bd, 1H
23	31.11	CH <sub>2</sub>	1.34-1.90, m, 2H	32.21	1.42-1.95, m, 2H
24	28.15	CH <sub>2</sub>	1.34-1.90, m, 2H	34.48	1.42-1.95, m, 2H
25	46.72	CH	1.34-1.90, m, 1H	42.00	1.42-1.95, m, 1H
26	205.54	Q	9.75, 2, 1H	<b>139.38</b>	<b>6.28, dd, 1H</b>
27	19.71	CH <sub>3</sub>	0.83-1.29, m, 3H	19.69	0.78-1.24, m, 3H
28	21.77	CH <sub>3</sub>	2.16, s, 3H	<b>128.05</b>	<b>6.32, d, 1H</b>
29	170.91	Q	-	<b>21.77</b>	<b>2.02, s, 3H</b>
30				<b>170.97</b>	-
1'				<b>144.89</b>	-
2'				<b>106.17</b>	<b>6.50, s, 1H</b>
3'				<b>153.27</b>	-
4'				<b>133.94</b>	-
5'				<b>153.27</b>	-
6'				<b>106.17</b>	<b>6.50, s, 1H</b>
3 X OCH <sub>3</sub>				<b>60.71</b>	<b>3.85, s, 1H</b>
				<b>61.30</b>	<b>3.85, s, 1H</b>
				<b>57.28</b>	<b>3.85, s, 1H</b>

Implied multiplicities of the carbons were determined from the DEPT experiment. \*Haad-3

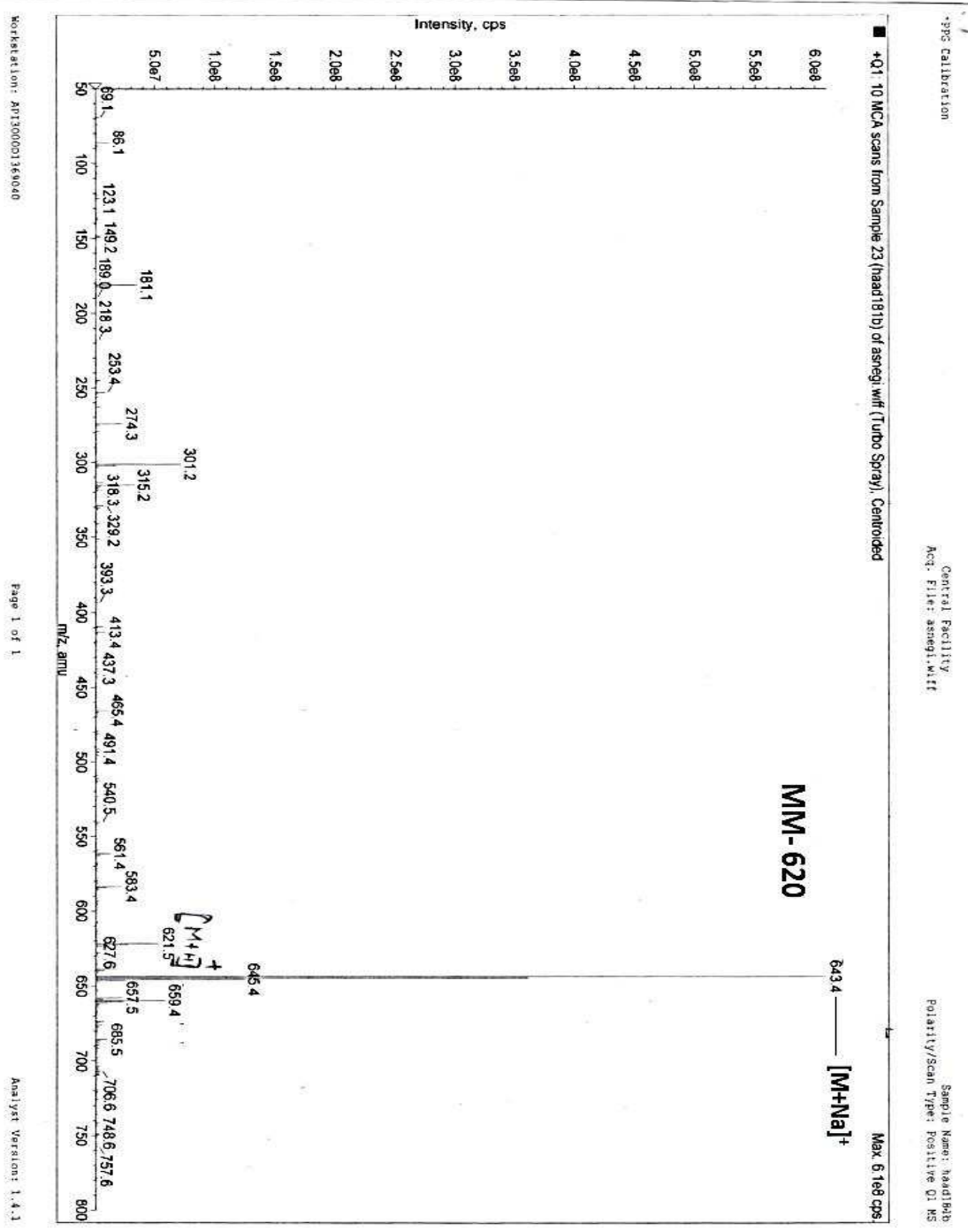


Fig. 4.98: ESI-MS spectrum of Haad-7b in MeOH

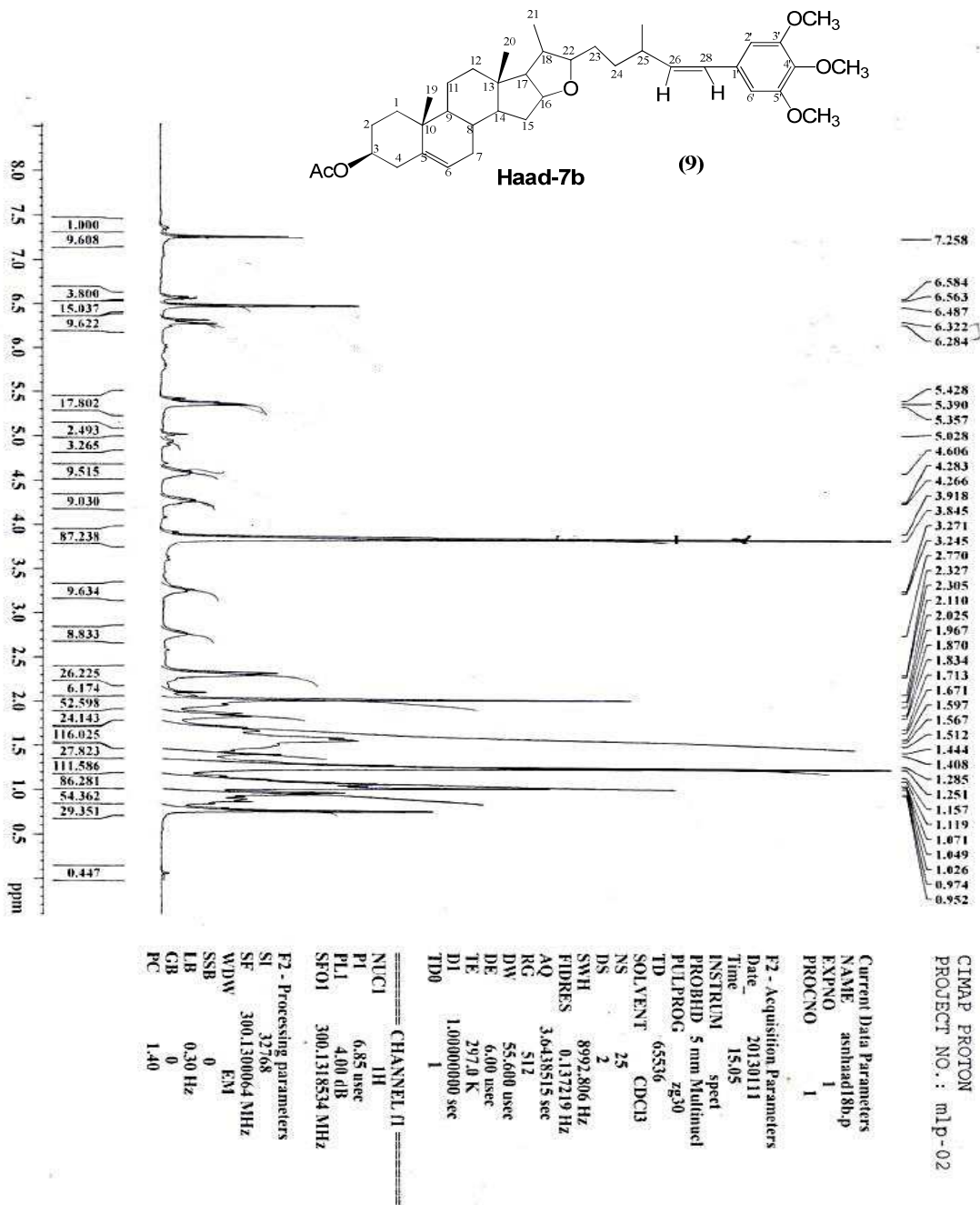


Fig. 4.99: <sup>1</sup>H NMR spectrum of Haad-7b in CDCl<sub>3</sub>



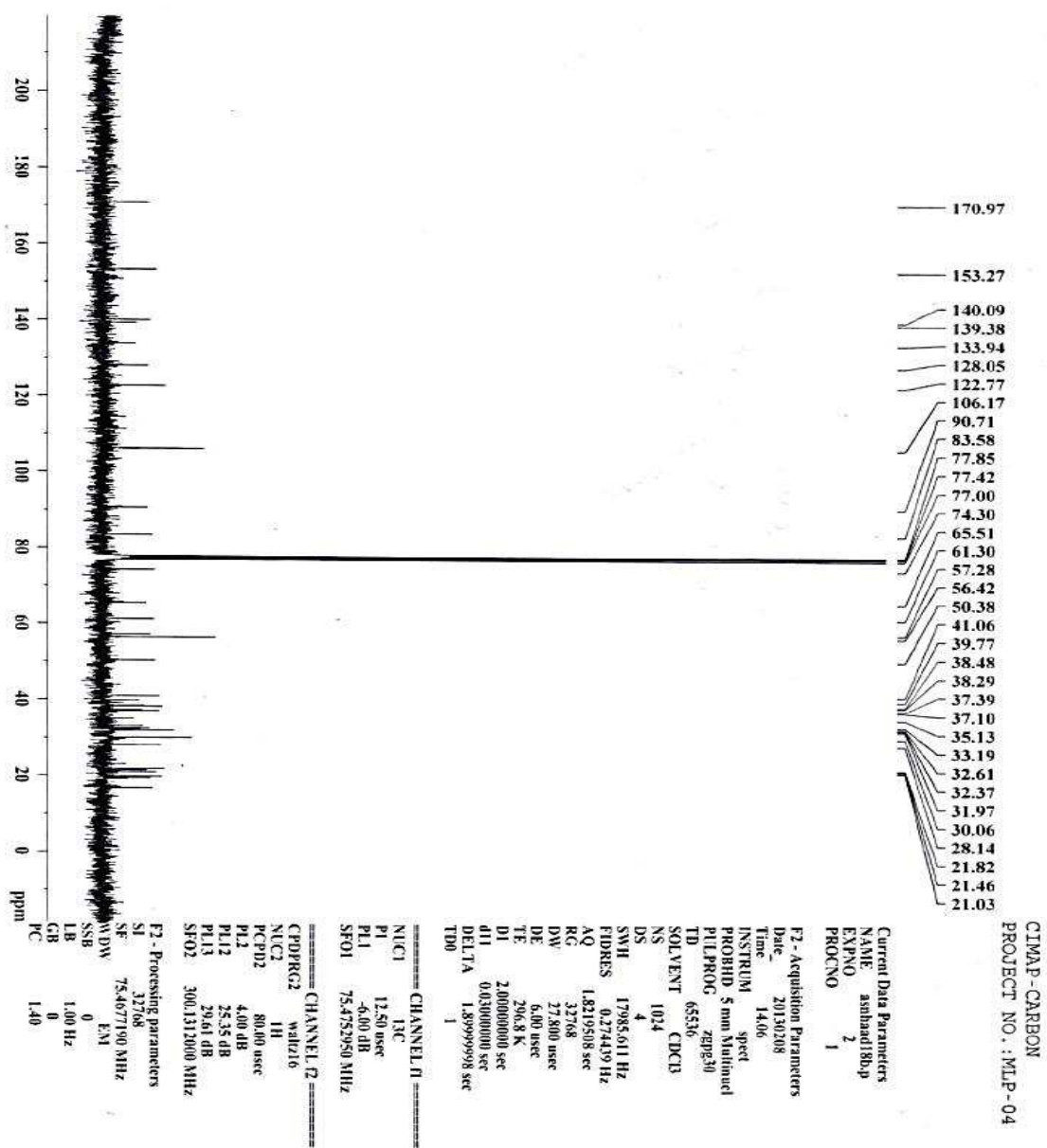
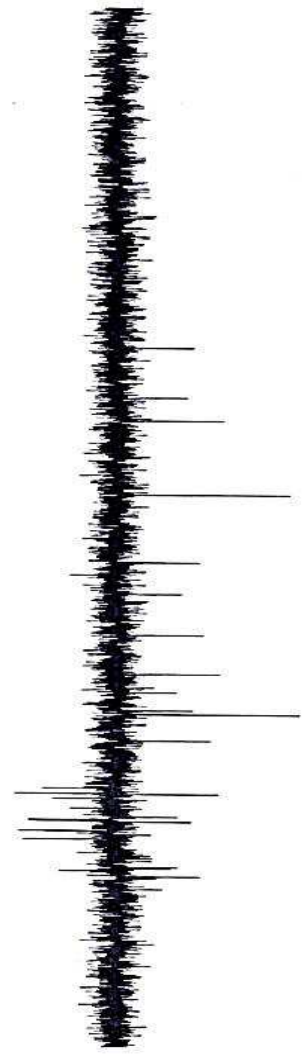


Fig. 5.00:  $^{13}\text{C}$  NMR spectrum of Haad-7b in  $\text{CDCl}_3$

210 200 190 180 170 160 150 140 130 120 110 100 90 80 70 60 50 40 30 20 10 0 ppm



139.38  
128.05  
122.77  
106.17  
90.71  
83.58  
74.30  
65.51  
61.31  
57.28  
56.42  
50.39  
39.77  
38.49  
38.29  
37.38  
33.19  
32.62  
32.37  
31.96  
30.09  
28.14  
21.83  
21.46  
21.03  
19.73

CIMAP-DEPT 135  
PROJECT NO.: ILP-13

```

Current Data Parameters
NAME      anthracilb.p
EXPNO     3
PROCNO    1

F2 - Acquisition Parameters
Date_     20130308
Time      14:17:04
INSTRUM   spect
PROBHD    5 mm/1H/13
PULPROG   zgpg30
TD         65536
SOLVENT   CDCl3
NS         512
DS         4
SWH        17982.611 Hz
FIDRES     0.1274289 Hz
AQ         1.4841498 sec
RG         65384
DVS        27.800 usec
DE         6.90 usec
TE         298.7 K
CNS12     145.0000000
HI         2.0000000 usec
DI         0.002524818 usec
DELTA     0.009015925 usec
TD0        1

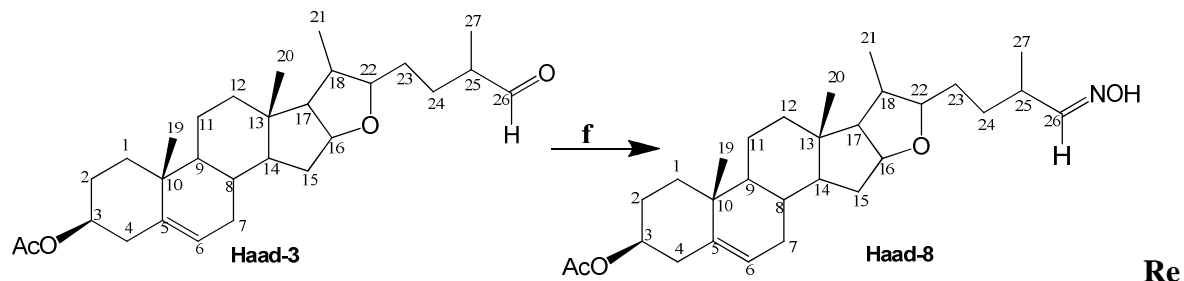
===== CHANNEL f1 =====
NUC1       13C
P1         12.50 usec
PL1        2.50 usec
PC1        200.131200 MHz
NUC2       1H
P2         6.85 usec
PL2        1.70 usec
PC2        400.146000 MHz
===== CHANNEL f2 =====
C1PROBHD2  waltz16
NUC2       1H
P2         6.85 usec
PL2        1.70 usec
PC2        400.146000 MHz
===== CHANNEL f3 =====
C1PROBHD3  waltz16
NUC2       1H
P2         6.85 usec
PL2        1.70 usec
PC2        400.146000 MHz

F2 - Processing parameters
SI         32768
SF         75467190 MHz
WDW        EM
SSB        0
GB         0
PC         1.40
  
```

Fig. 5.01: DEPT spectrum of Haad-7b in CDCl<sub>3</sub>

#### 4.8.10. Synthesis and characterisation of (22 $\beta$ )-3 $\beta$ -Acetoxy-furost-5-en-26-aldoxime (Haad-8)

Aldoxime Haad-8 was also formed from the reaction of aldehyde Haad-3 with hydroxyl ammonium hydrochloride (NH<sub>4</sub>OH.HCl) and dry pyridine in ethanol.



**agents and conditions:** f) NH<sub>4</sub>OH.HCl, Ethanol, pyridine, reflux, 2 hrs

Haad-8 (73 mg, 70%) was obtained as a creamy white solid. The fragment ions 472.4 [M+H]<sup>+</sup>, 494.5 [M+Na]<sup>+</sup> and 510.3 [M+K]<sup>+</sup> of ESI-MS gave molecular formula C<sub>29</sub>H<sub>45</sub>NO<sub>4</sub> (471) [Fig. 5.02]. The <sup>1</sup>H NMR spectrum showed signals at  $\delta_H$  3.29 (m) and 4.29 (m) correspond to methine protons at C-22 and C-16, while the signals at  $\delta_H$  4.59 (m) and 5.36 (s) indicated the presence of oxymethine proton at C-3 and olefinic methine proton at C-6 [Fig. 5.03]. The signals at 7.29 (bd) was attributed to methine proton alpha to oxime carbon at 26 position. <sup>13</sup>C NMR [Fig. 5.04] and DEPT carbon resonances [Fig. 5.05] of the analogue were also similar to Haad-3 data except the oxime carbon at position 26 [Table 4.71]. Haad-8 was identified as (22 $\beta$ )-3 $\beta$ -acetoxy-furost-5-en-26-aldoxime. Some slight differences in the spectroscopic data of Haad-8 and Haad-3 are given below.

<sup>1</sup>H NMR (CDCl<sub>3</sub>): 7.29 (bd, 1H, 26-CH);

<sup>13</sup>C NMR (CDCl<sub>3</sub>): 156.46 (C-26) [Table 4.71; Figs: 5.03 - 5.05]

IR (KBR, cm<sup>-1</sup>): 2945 (C-H), 1733 (C=O), 1582 (C=C), 1243 (C-O)

**Table 4.71:** Comparison of  $^{13}\text{C}$  and  $^1\text{H}$  NMR data of Haad-3 and Haad-8

Assignment	* $^{13}\text{C}$	Multiplicity	* $^1\text{H}$ , multiplicity	$^{13}\text{C}$	$^1\text{H}$
1	21.03	$\text{CH}_2$	1.34-1.90, m, 2H	28.12	1.42-1.95, m, 2H
2	37.39	$\text{CH}_2$	1.34-1.90, m, 2H	37.38	1.42-1.95, m, 2H
3	74.28	CH	4.34, m, 1H	73.32	4.59, m, 1H
4	38.48	$\text{CH}_2$	1.34-1.90, m, 2H	39.78	1.42-1.95, m, 2H
5	141.09	Q	-	140.06	-
6	122.73	CH	5.49, t, 1H	122.75	5.36, t, 1H
7	32.37	$\text{CH}_2$	2.36, t, 2H	32.36	2.26, t, 2H
8	38.28	CH	1.34-1.90, m, 1H	38.24	1.42-1.95, m, 1H
9	50.41	CH	1.34-1.90, m, 1H	50.39	1.42-1.95, m, 1H
10	37.09	Q	-	37.08	-
11	30.07	$\text{CH}_2$	1.34-1.90, m, 2H	21.03	1.42-1.95, m, 2H
12	31.96	$\text{CH}_2$	1.34-1.90, m, 2H	31.95	1.42-1.95, m, 2H
13	39.77	Q	-	41.07	-
14	41.08	CH	1.34-1.90, m, 1H	38.47	1.42-1.95, m, 1H
15	32.59	$\text{CH}_2$	1.34-1.90, m, 2H	32.56	1.42-1.95, m, 2H
16	83.28	CH	4.63, m, 1H	83.62	4.29, m, 1H
17	65.44	CH	1.34-1.90, m, 1H	65.46	1.42-1.95, m, 1H
18	57.29	CH	1.34-1.90, m, 1H	57.28	1.42-1.95, m, 1H
19	19.22	$\text{CH}_3$	0.83-1.29, m, 3H	19.26	0.78-1.24, m, 3H
20	16.79	$\text{CH}_3$	0.83-1.29, m, 3H	16.81	0.78-1.24, m, 3H
21	13.78	$\text{CH}_3$	0.79-0.81, m, 3H	18.44	0.78-1.24, m, 3H
22	90.11	$\text{CH}_2$	3.45, s, 2H	90.39	3.29, m, 1H
23	31.11	$\text{CH}_2$	1.34-1.90, m, 2H	31.32	1.42-1.95, m, 2H
24	28.15	$\text{CH}_2$	1.34-1.90, m, 2H	30.06	1.42-1.95, m, 2H
25	46.72	CH	1.34-1.90, m, 1H	42.00	1.42-1.95, m, 1H
26	205.54	Q	9.75, 2, 1H	<b>156.46</b>	<b>7.29, bd, 1H</b>
27	19.71	$\text{CH}_3$	0.83-1.29, m, 3H	19.70	0.78-1.24, m, 3H
28	21.77	$\text{CH}_3$	2.16, s, 3H	21.78	2.01, s, 3H
29	170.91	Q	-	171.01	-

---

Implied multiplicities of the carbons were determined from the DEPT experiment. \*Haad-3

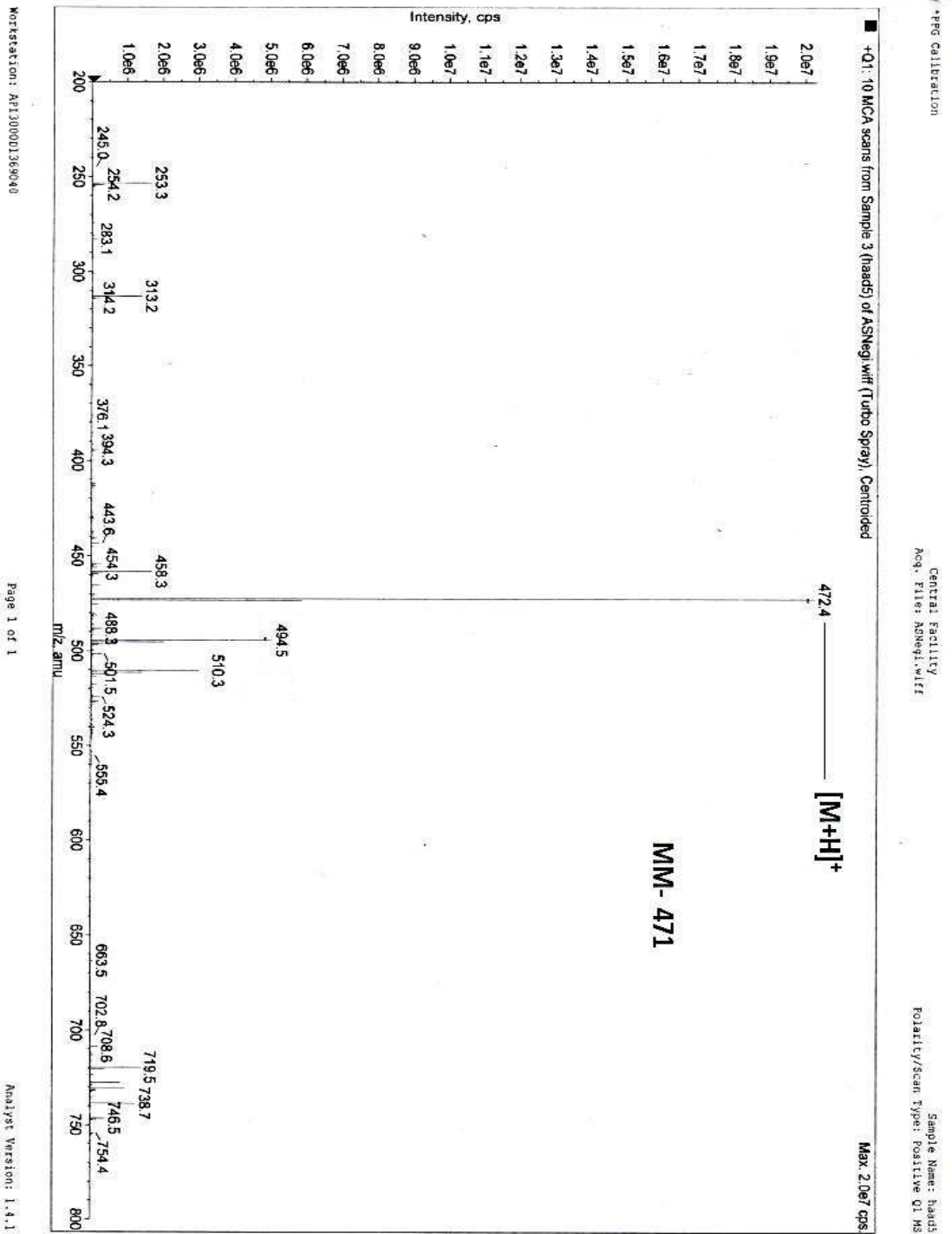


Fig. 5.02: ESI-MS spectrum of Haad-8 in MeOH

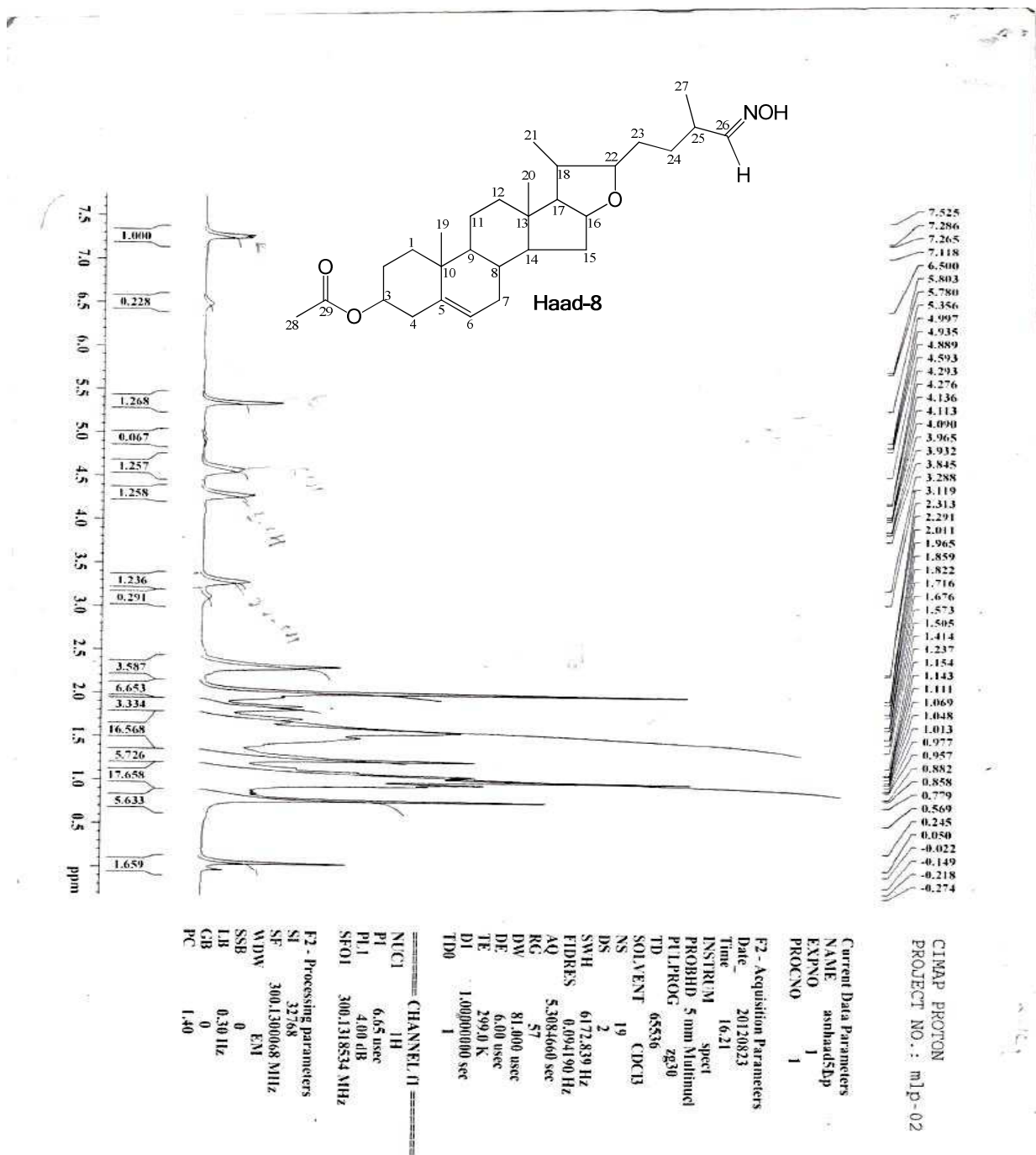


Fig. 5.03: <sup>1</sup>H NMR spectrum of Haad-8 in CDCl<sub>3</sub>

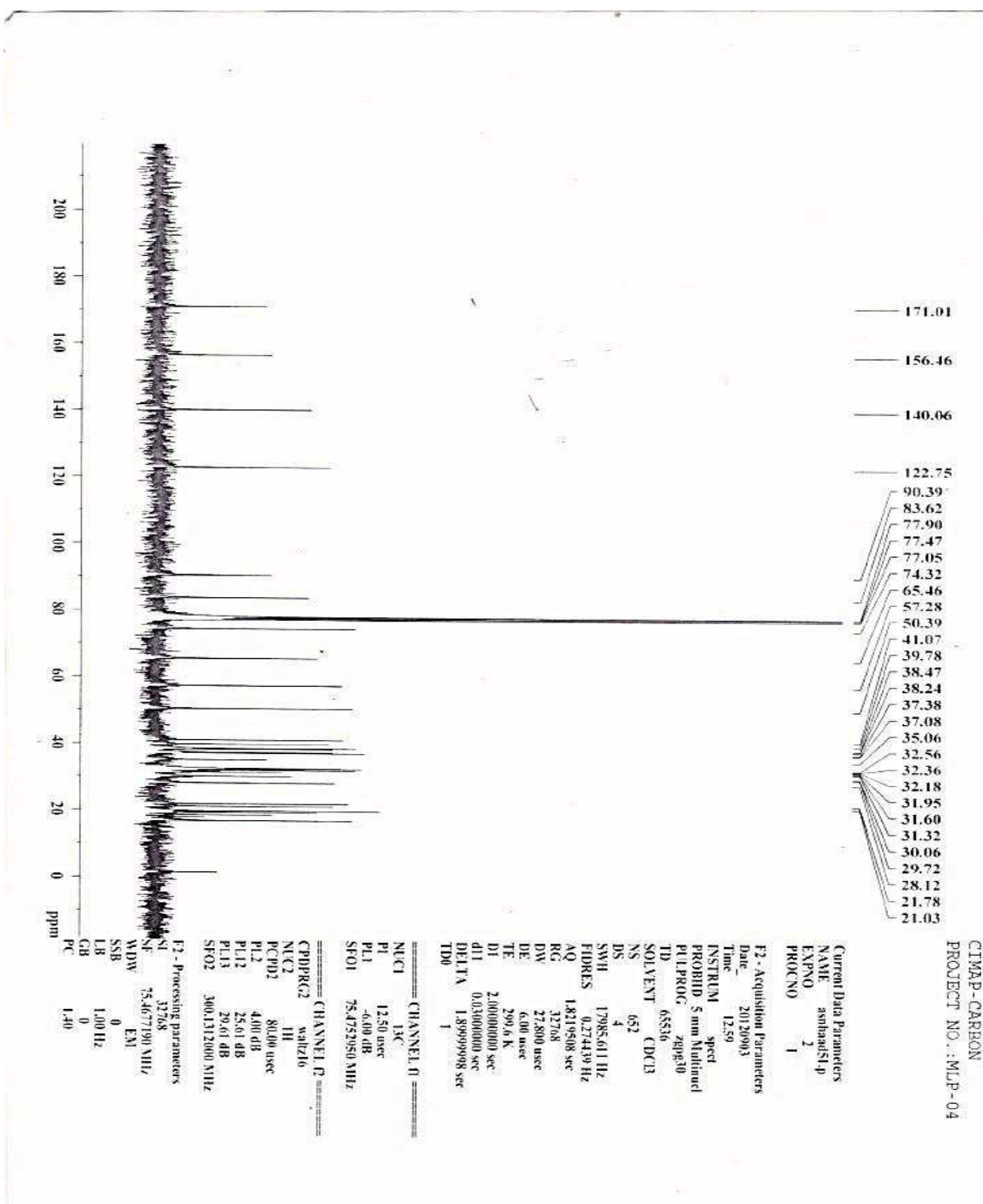


Fig. 5.04:  $^{13}\text{C}$  NMR spectrum of Haad-8 in  $\text{CDCl}_3$

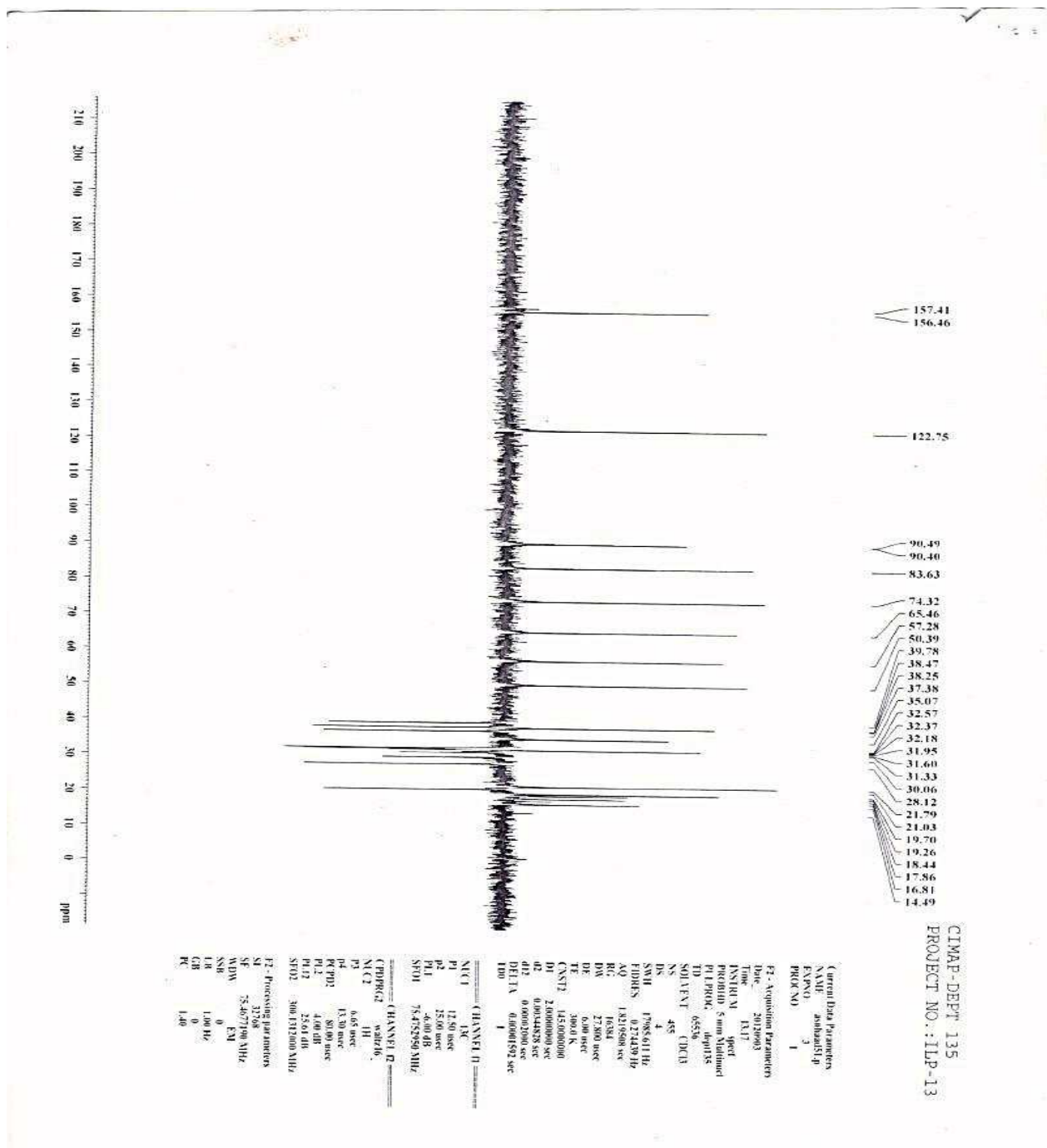
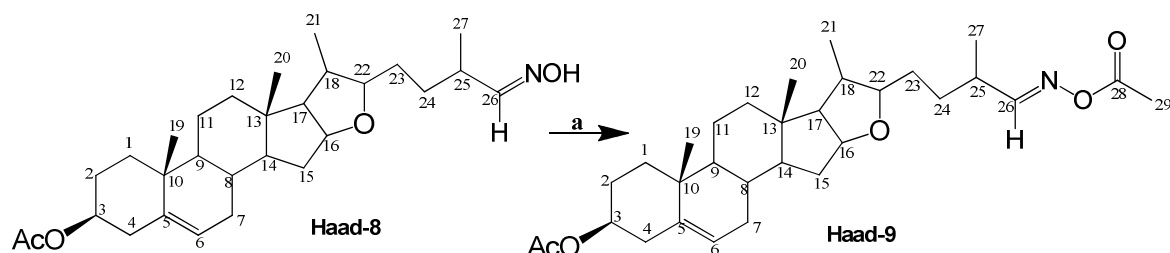


Fig. 5.05: DEPT spectrum of Haad-8 in CDCl<sub>3</sub>



#### 4.8.11. Synthesis and characterisation of (22 $\beta$ )-3 $\beta$ -Acetoxy-furost-5-en-26-aldoxime acetate (Haad-9)

Aldoxime acetate, Haad-9 was also formed from acetylation of aldoxime Haad-8, which was done using acetic anhydride and pyridine (Chaosuancharoen *et al.*, 2004) in the presence of chloroform as a solvent to yield a creamy compound.



**Reagents and conditions:** a) Ac<sub>2</sub>O, chloroform, dry pyridine, RT, 5 hrs

Haad-9 (1.0 g, 92%) was obtained as a cream solid. The ESI-MS fragment ions 511.4 [M-2H]<sup>+</sup> and 551.4 [M+K-H]<sup>+</sup> gave molecular formula C<sub>31</sub>H<sub>47</sub>NO<sub>5</sub> (513) [Fig. 5.06]. The <sup>1</sup>H NMR spectrum revealed signals at  $\delta_{\text{H}}$  2.02 (s) correspond to methoxyl protons at C-29 and C-30. The chemical shifts at 3.29 (bs) and 4.29 (m) were attributed to oxymethine protons at C-22 and C-16, while the signals at  $\delta_{\text{H}}$  4.60 (m) and 5.36 (t) indicated the presence of oxymethine proton at C-3 and olefinic methine proton at C-6 [Fig. 5.07]. The signal at 7.50 (d) showed the presence of methine proton of oxime carbon at C-26. <sup>13</sup>C NMR [Fig. 5.08] and DEPT spectra data [Fig. 5.09] of the analogue were also similar to Haad-8 data except the carbonyl moiety at positions 28 and 29 [Table 4.72]. Hence, Haad-9 was elucidated to be (22 $\beta$ )-3 $\beta$ -Acetoxy-furost-5-en-26-aldoxime acetate. The differences in the spectroscopic data of Haad-9 and that of Haad-8 are given below.

<sup>1</sup>H NMR (CDCl<sub>3</sub>): 2.02 (s, 3H, H-29, CH<sub>3</sub>COO)

<sup>13</sup>C NMR (CDCl<sub>3</sub>): 26.33 (C-29), and 170.95 (C-28) [Table 4.72; Figs: 5.07 - 5.09]

IR (KBR, cm<sup>-1</sup>): 2934 (C-H), 1734 (C=O), 1582 (C=C), 1244 (C-O)

**Table 4.72:** Comparison of  $^{13}\text{C}$  and  $^1\text{H}$  NMR data of Haad-8 and Haad-9

Assignment	* $^{13}\text{C}$	Multiplicity	* $^1\text{H}$ , multiplicity	$^{13}\text{C}$	$^1\text{H}$
1	28.12	$\text{CH}_2$	1.34-1.90, m, 2H	28.14	1.42-1.95, m, 2H
2	37.38	$\text{CH}_2$	1.34-1.90, m, 2H	37.39	1.42-1.95, m, 2H
3	73.32	CH	4.34, m, 1H	74.29	4.60, m, 1H
4	39.78	$\text{CH}_2$	1.34-1.90, m, 2H	39.77	1.42-1.95, m, 2H
5	141.06	Q	-	140.12	-
6	122.75	CH	5.49, t, 1H	122.74	5.36, t, 1H
7	32.36	$\text{CH}_2$	2.36, t, 2H	32.38	2.26, t, 2H
8	38.24	CH	1.34-1.90, m, 1H	38.28	1.42-1.95, m, 1H
9	50.39	CH	1.34-1.90, m, 1H	50.40	1.42-1.95, m, 1H
10	37.08	Q	-	37.11	-
11	21.03	$\text{CH}_2$	1.34-1.90, m, 2H	21.03	1.42-1.95, m, 2H
12	31.95	$\text{CH}_2$	1.34-1.90, m, 2H	31.52	1.42-1.95, m, 2H
13	41.07	Q	-	41.09	-
14	38.47	CH	1.34-1.90, m, 1H	38.49	1.42-1.95, m, 1H
15	32.56	$\text{CH}_2$	1.34-1.90, m, 2H	32.59	1.42-1.95, m, 2H
16	83.62	CH	4.63, m, 1H	83.83	4.29, m, 1H
17	65.46	CH	1.34-1.90, m, 1H	65.32	1.42-1.95, m, 1H
18	57.28	CH	1.34-1.90, m, 1H	57.29	1.42-1.95, m, 1H
19	19.26	$\text{CH}_3$	0.83-1.29, m, 3H	19.20	0.78-1.24, m, 3H
20	16.81	$\text{CH}_3$	0.83-1.29, m, 3H	16.81	0.78-1.24, m, 3H
21	18.44	$\text{CH}_3$	0.79-0.81, m, 3H	19.91	0.78-1.24, m, 3H
22	90.39	CH	3.45, s, 2H	90.14	3.29, bs, 1H
23	31.32	$\text{CH}_2$	1.34-1.90, m, 2H	30.08	1.42-1.95, m, 2H
24	30.06	$\text{CH}_2$	1.34-1.90, m, 2H	31.96	1.42-1.95, m, 2H
25	42.00	CH	1.34-1.90, m, 1H	38.06	1.42-1.95, m, 1H
26	156.46	CH	7.29, d, 1H	163.46	7.50, d, 1H
27	19.70	$\text{CH}_3$	0.78-1.24, m, 3H	19.72	0.78-1.24, m, 3H
28	21.78	$\text{CH}_3$	2.01, s, 3H	<b>170.85</b>	-
29	171.01	Q	-	<b>21.81</b>	<b>2.02, s, 3H</b>
				<b>21.81</b>	<b>2.01, s, 3H</b>
				<b>169.16</b>	-

---

Implied multiplicities of the carbons were determined from the DEPT experiment.

\*Haad-8

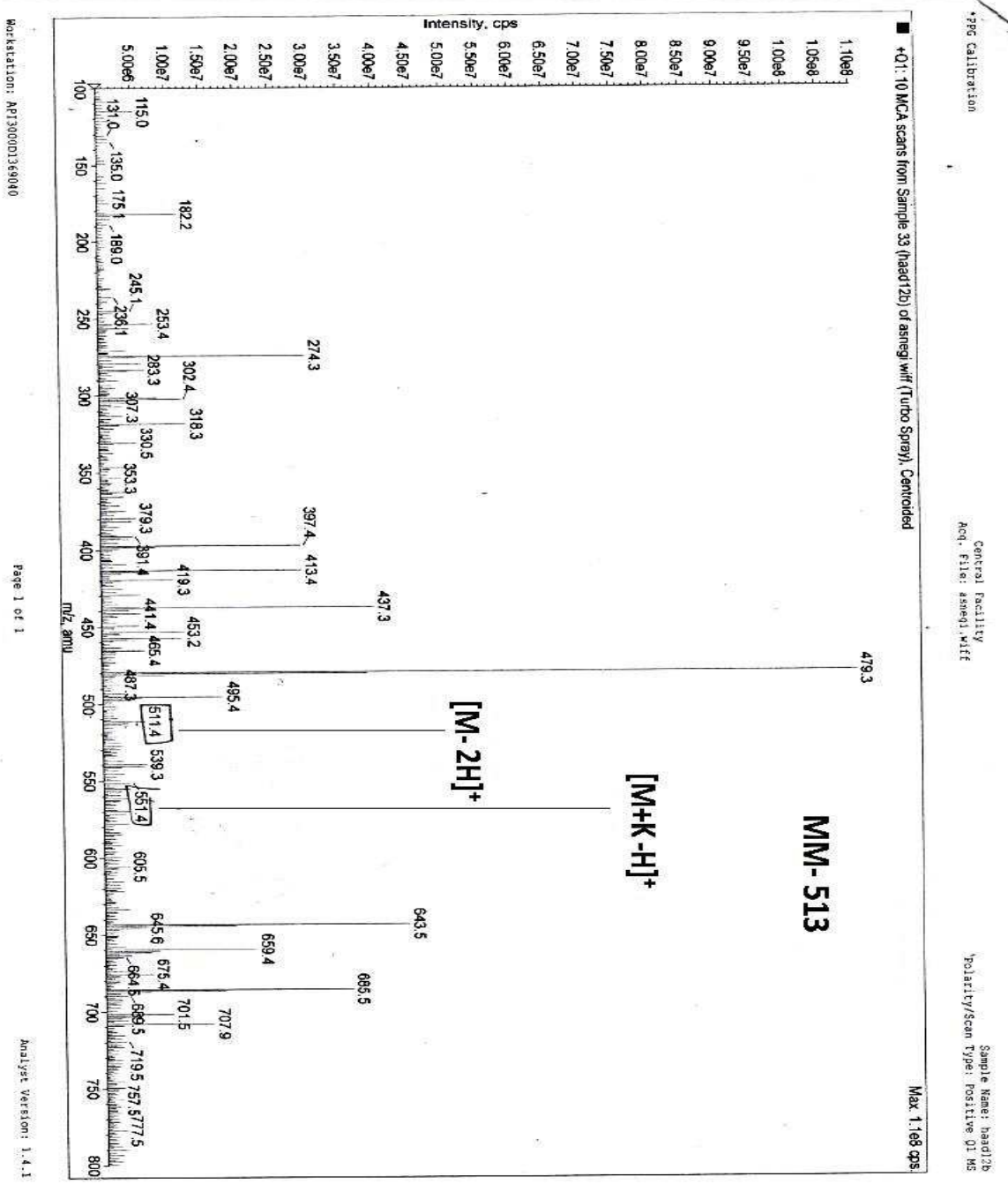
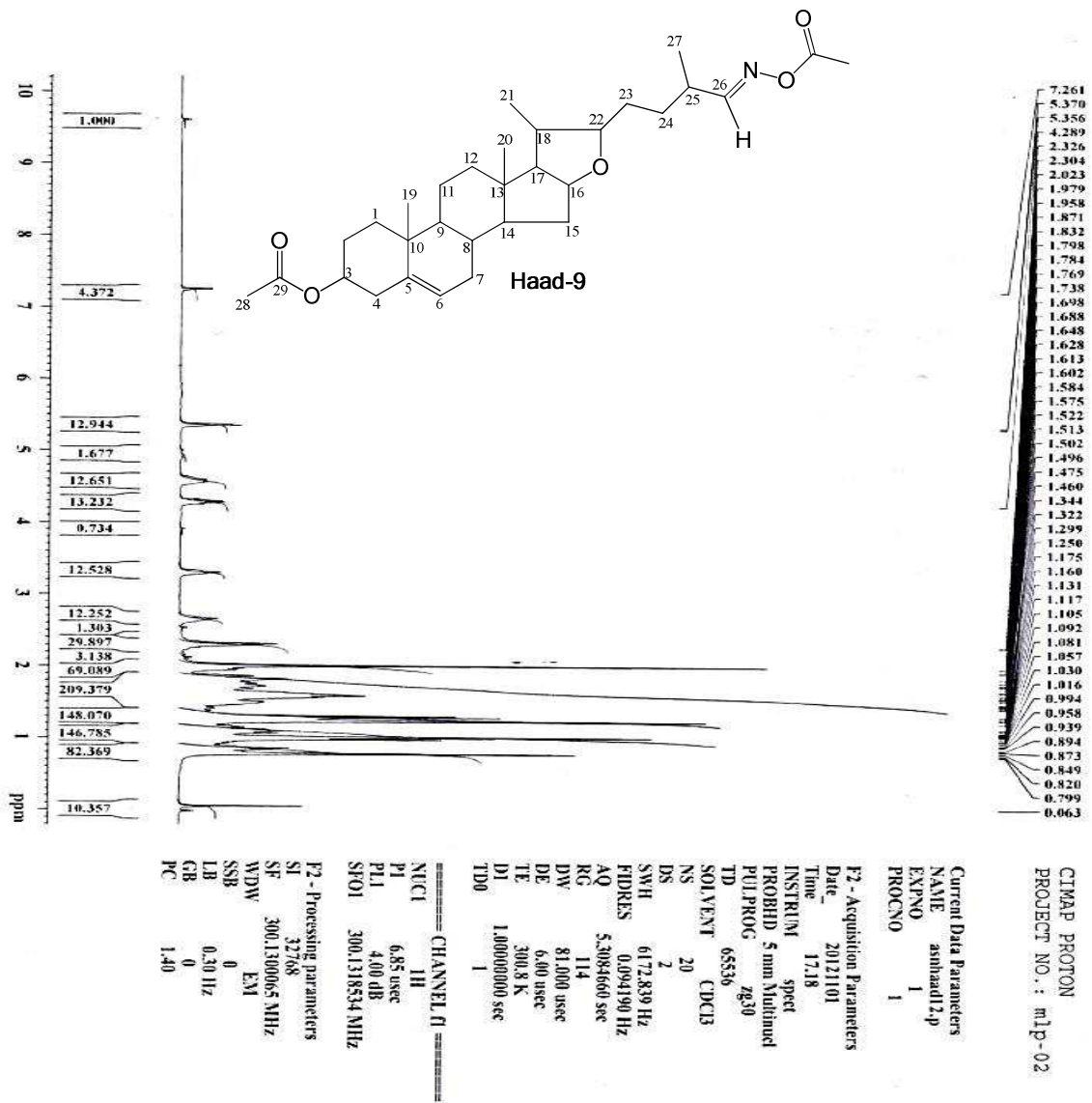


Fig. 5.06: ESI-MS spectrum of Haad-9 in MeOH



**Fig. 5.07:** <sup>1</sup>H NMR spectrum of Haad-9 in CDCl<sub>3</sub>

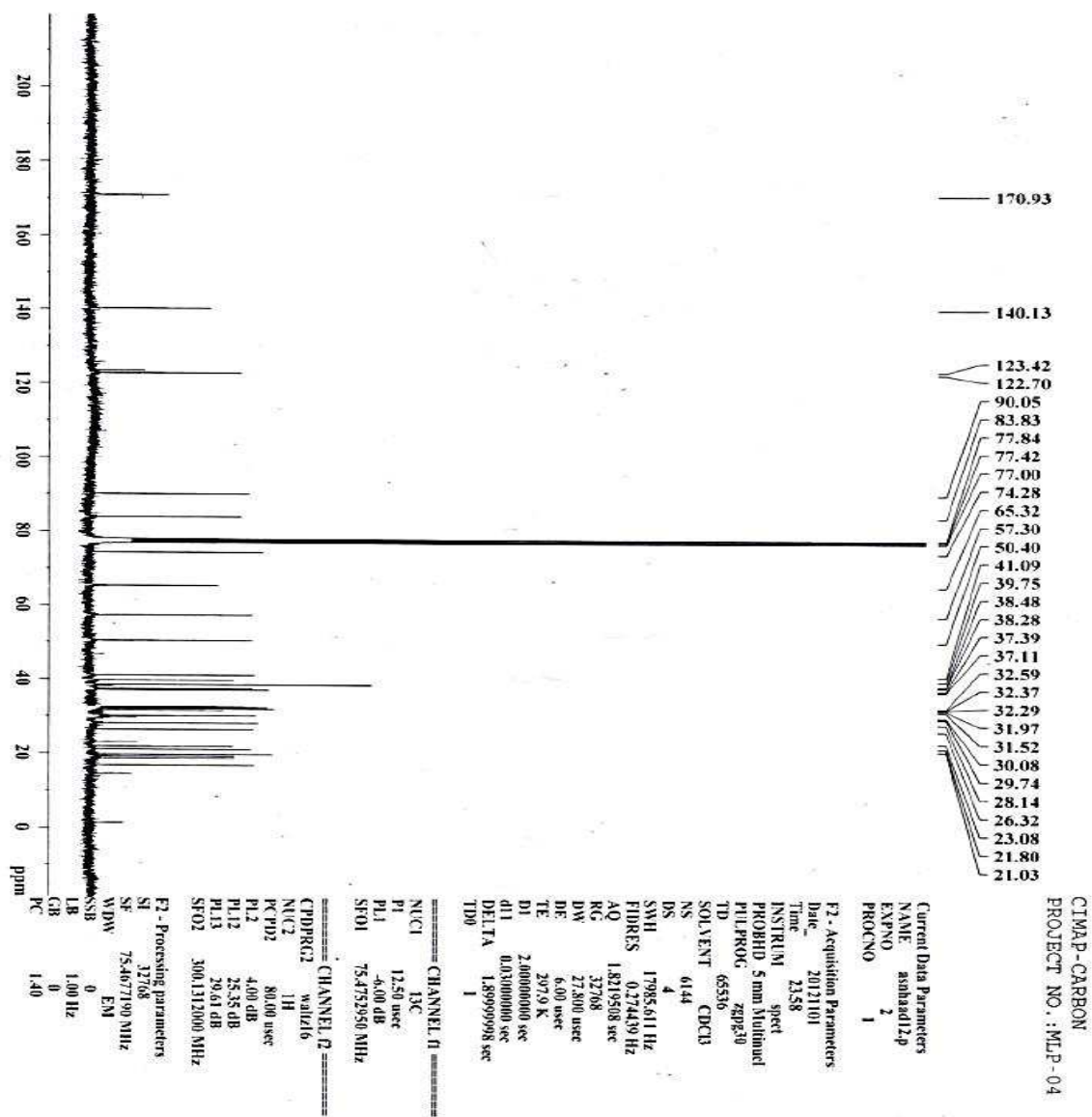


Fig. 5.08:  $^{13}\text{C}$  NMR spectrum of Haad-9 in  $\text{CDCl}_3$

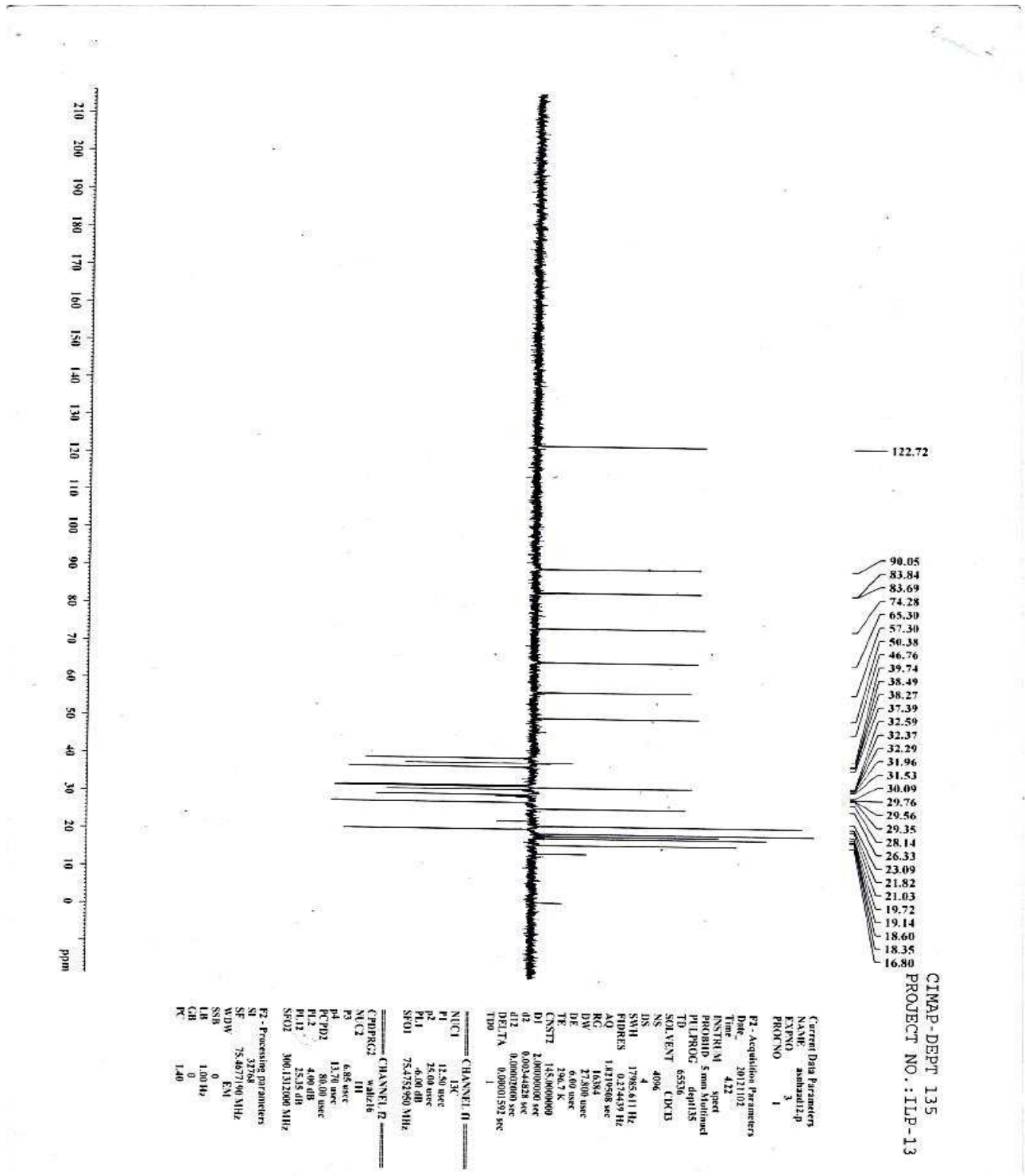
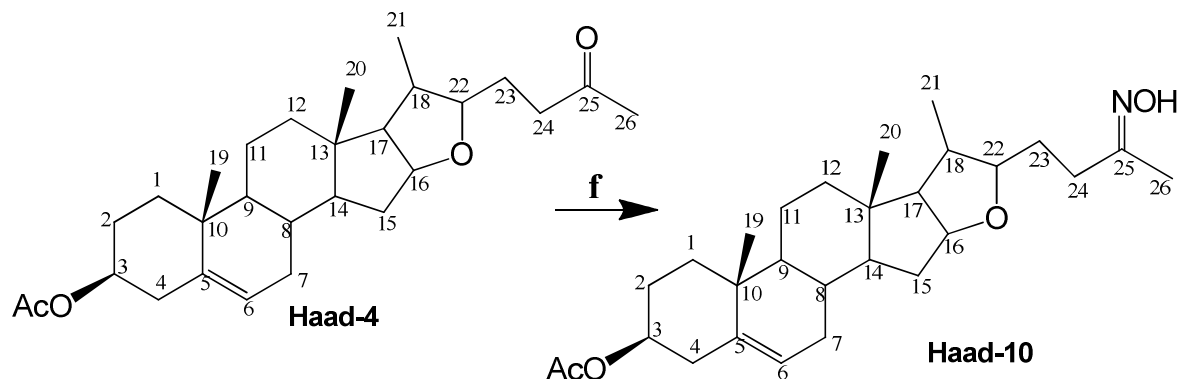


Fig. 5.09: DEPT spectrum of Haad-9 in CDCl<sub>3</sub>

#### 4.8.12. Synthesis and characterisation of (22 $\beta$ )-3 $\beta$ -Acetoxy-27-nor-furost-5-en-25-ketoxime (Haad-10)

Ketoxime Haad-10 was also prepared from the reaction of ketone Haad-4 with hydroxyl ammonium hydrochloride (NH<sub>4</sub>OH.HCl) and dry pyridine in the presence of ethanol (same method as for Haad-8).



**Reagents and conditions:** f) NH<sub>4</sub>OH.HCl, Ethanol, pyridine, reflux, 2 hrs

Haad-10 (87 mg, 84%) appeared as a cream solid. The fragment ions 458.3 [M+H]<sup>+</sup>, 480.3 [M+Na]<sup>+</sup> and 496.4 [M+K]<sup>+</sup> of ESI-MS correspond to a molecular formula C<sub>28</sub>H<sub>43</sub>NO<sub>4</sub> (457) [Fig. 5.10]. The <sup>1</sup>H NMR spectrum showed signals at  $\delta_H$  1.97 (s) and 2.03 (s) were attributable to methoxy protons of acetate at C-27 and methyl protons of C-26 attached to carbonyl of ketoxime. Chemical shifts at  $\delta_H$  3.33 (m) and 4.29 (m) correspond to methine protons at C-22 and C-16, while the signals at  $\delta_H$  4.53 (m) and 5.36 (t) showed the presence of oxymethine proton at C-3 and olefinic methine proton at C-6 [Fig. 5.11]. <sup>13</sup>C NMR [Fig. 5.12] and DEPT carbon resonances [Fig. 5.13] of the compound were identical to Haad-4 data except the oxime carbon at position 25 [Table 4.73]. Therefore, Haad-10 was identified as (22 $\beta$ )-3 $\beta$ -Acetoxy-27-nor-furost-5-en-25-ketoxime. The major spectroscopic data difference between Haad-10 and Haad-4 are:

<sup>1</sup>H NMR (CDCl<sub>3</sub>): 2.03 (s, 3H, 26-CH<sub>3</sub>, CH<sub>3</sub>C=N-O)

<sup>13</sup>C NMR (CDCl<sub>3</sub>): 21.81 (C-26 & 27) and 158.98 (C-25) [Table 4.73; Figs: 5.11 - 5.13]

IR (KBR, cm<sup>-1</sup>): 3382 (O-H), 2941 (C-H), 1721 (C=O), 1648 (C=C), 1248 (C-O)

**Table 4.73:** Comparison of  $^{13}\text{C}$  and  $^1\text{H}$  NMR data of Haad-4 and Haad-10

Assignment	$^{13}\text{C}$	Multiplicity	$^1\text{H}$ , Multiplicity	$^{13}\text{C}$	$^1\text{H}$
1	21.02	$\text{CH}_2$	1.34-1.90, m, 2H	28.14	1.34-1.90, m, 2H
2	37.38	$\text{CH}_2$	1.34-1.90, m, 2H	37.39	1.34-1.90, m, 2H
3	74.28	CH	4.34, m, 1H	74.30	4.53, m, 1H
4	38.75	$\text{CH}_2$	1.34-1.90, m, 2H	39.77	1.34-1.90, m, 2H
5	140.12	Q	-	140.09	-
6	122.72	CH	5.40, t, 1H	122.76	5.36, t, 1H
7	32.37	$\text{CH}_2$	2.36, t, 2H	32.38	2.36, t, 2H
8	31.95	CH	1.34-1.90, m, 1H	38.20	1.34-1.90, m, 2H
9	50.38	CH	1.34-1.90, m, 1H	50.39	1.34-1.90, m, 2H
10	37.10	Q	-	37.10	-
11	28.13	$\text{CH}_2$	1.34-1.90, m, 2H	21.04	1.34-1.90, m, 2H
12	38.48	$\text{CH}_2$	1.34-1.90, m, 2H	31.96	1.34-1.90, m, 2H
13	41.09	Q	-	41.10	-
14	38.24	CH	1.34-1.90, m, 1H	38.48	1.34-1.90, m, 2H
15	32.55	$\text{CH}_2$	1.34-1.90, m, 2H	32.59	1.34-1.90, m, 2H
16	83.69	CH	4.63, m, 1H	83.70	4.29, m, 1H
17	65.39	CH	1.34-1.90, m, 1H	65.49	1.34-1.90, m, 2H
18	57.27	CH	1.34-1.90, m, 1H	57.29	1.34-1.90, m, 2H
19	19.01	$\text{CH}_3$	0.83-1.29, m, 3H	19.20	0.83-1.29, m, 3H
20	16.80	$\text{CH}_3$	0.83-1.29, m, 3H	16.80	0.83-1.29, m, 3H
21	19.71	$\text{CH}_3$	0.83-1.29, m, 3H	19.72	0.83-1.29, m, 3H
22	89.53	CH	3.27, s, 1H	<b>89.70</b>	<b>3.33, s, 1H</b>
23	27.44	$\text{CH}_2$	1.34-1.90, m, 2H	30.19	1.34-1.90, m, 2H
24	41.28	$\text{CH}_2$	2.51, d, 2H	<b>42.02</b>	<b>2.51, d, 2H</b>
25	209.24	Q	-	<b>158.98</b>	-
26	30.33	$\text{CH}_3$	2.13, s, 3H	<b>30.08</b>	<b>2.03, s, 3H</b>
27	21.80	$\text{CH}_3$	1.95, s, 3H	<b>21.81</b>	<b>1.97, s, 3H</b>
28	170.95	Q	-	<b>170.97</b>	-

Implied multiplicities of the carbons were determined from the DEPT experiment.

\* Haad-4



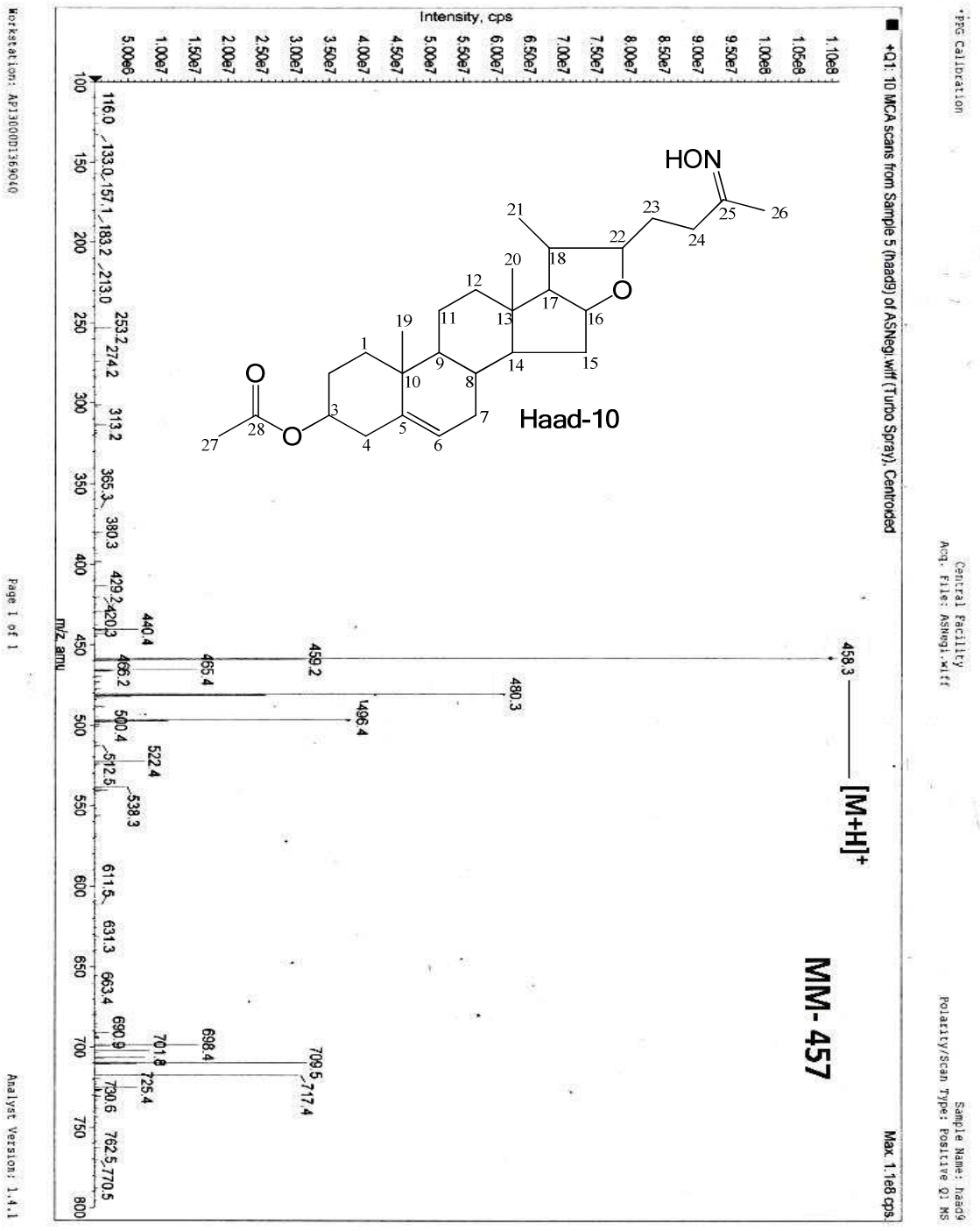


Fig. 5.10: ESI-MS spectrum of Haad-10 in MeOH

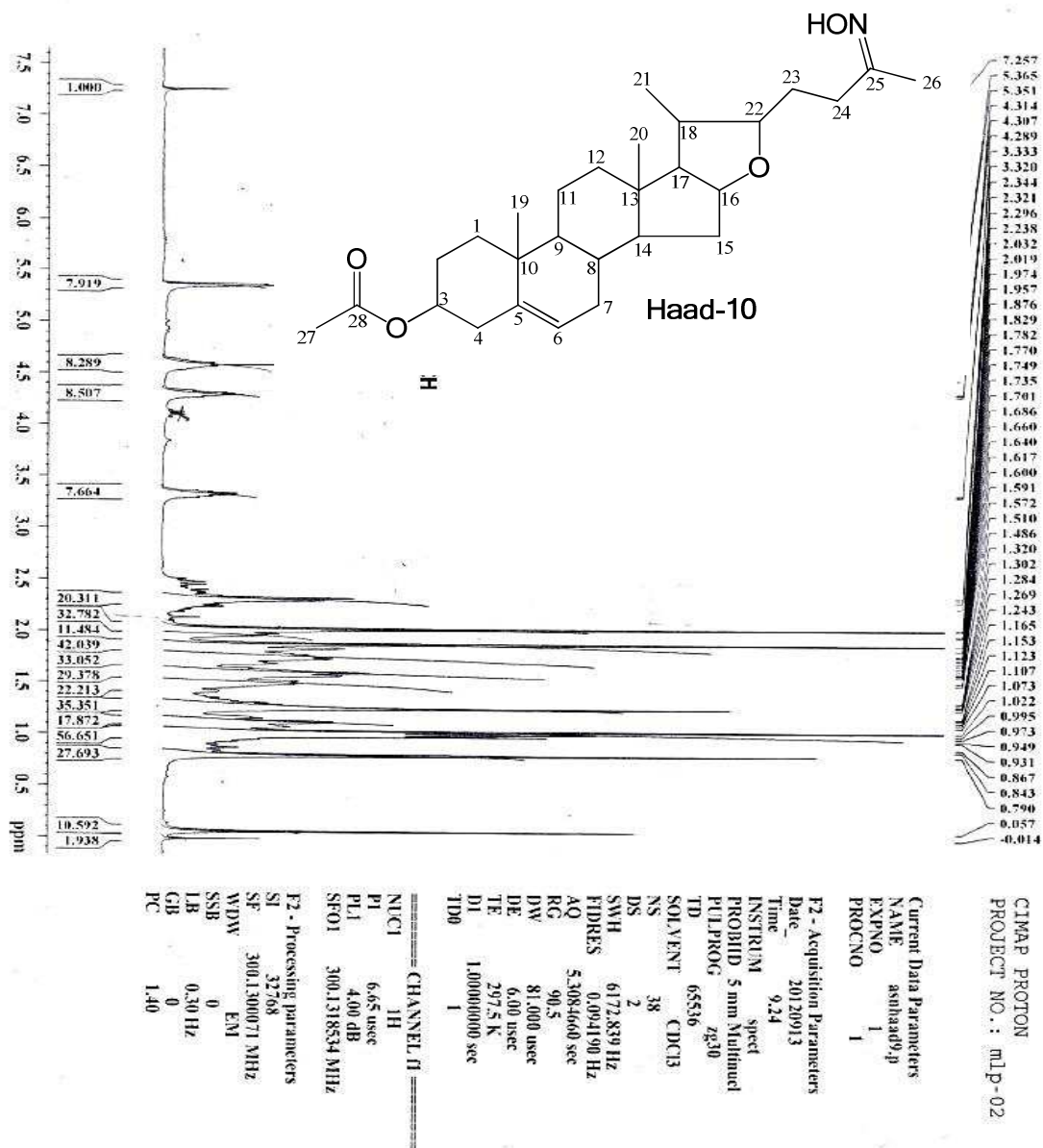


Fig. 5.11: <sup>1</sup>H NMR spectrum of Haad-10 in CDCl<sub>3</sub>

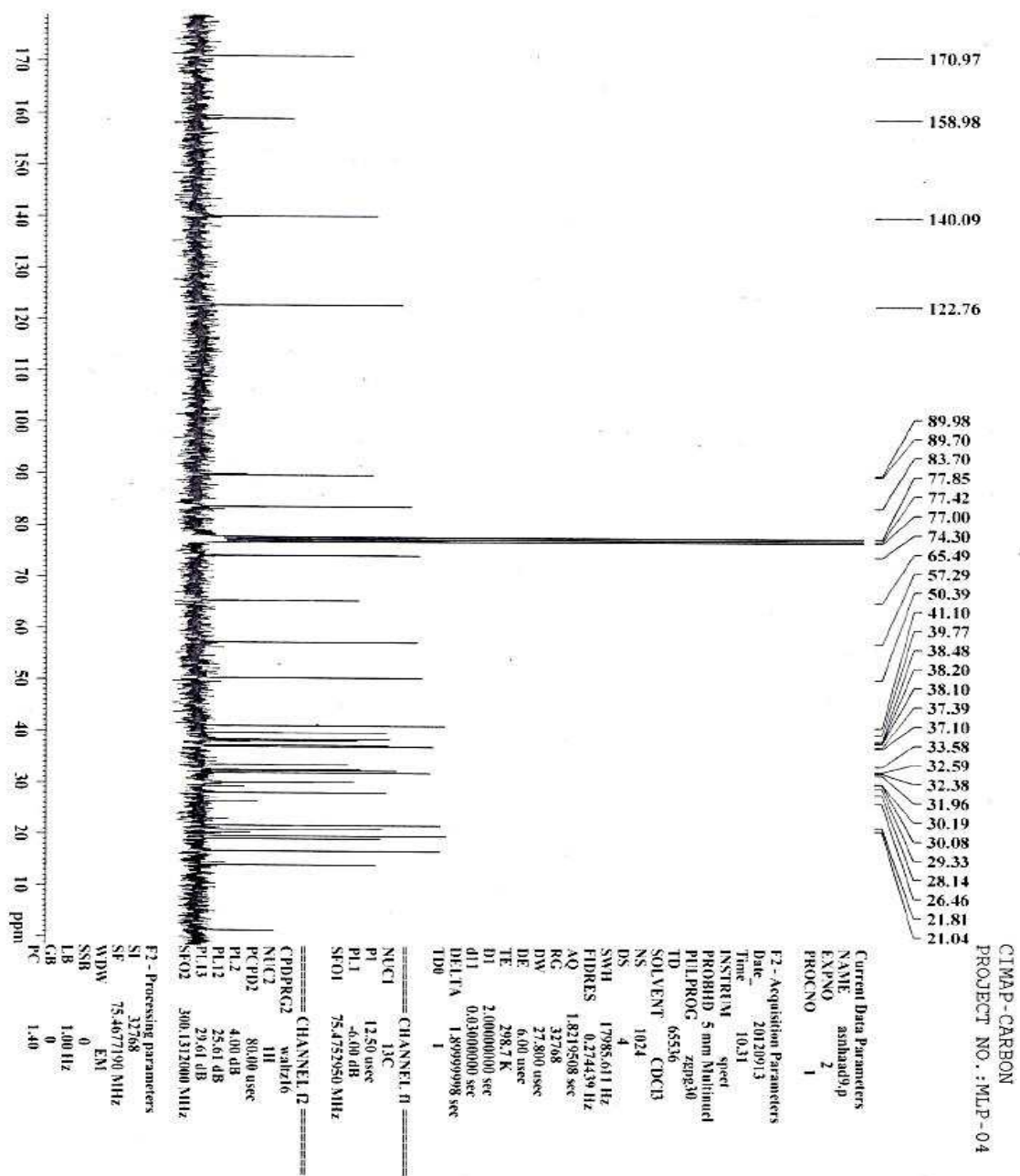


Fig. 5.12:  $^{13}\text{C}$  NMR spectrum of Haad-10 in  $\text{CDCl}_3$

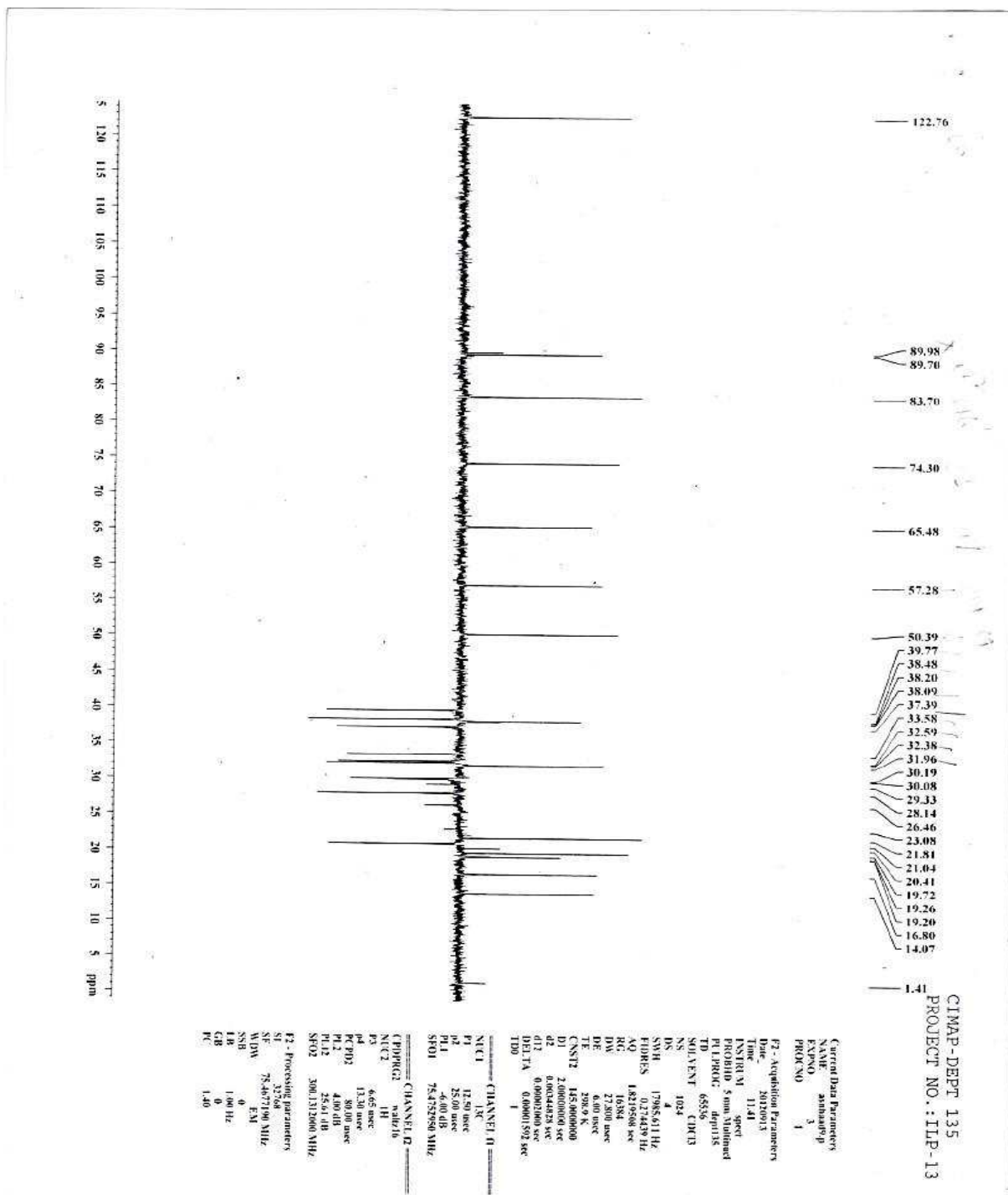
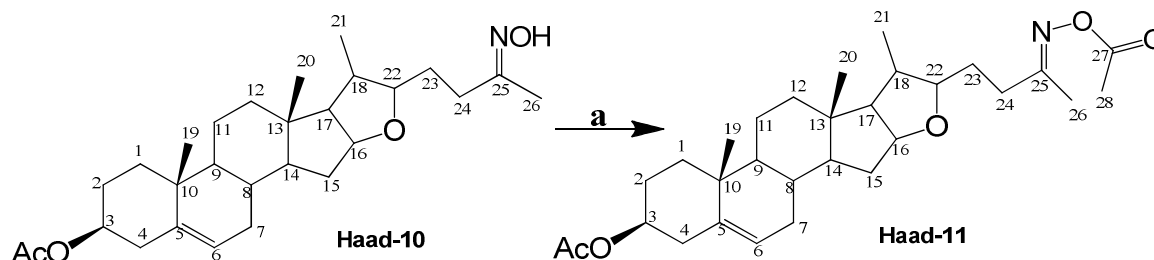


Fig. 5.13: DEPT spectrum of Haad-10 in  $CDCl_3$

#### 4.8.13. Synthesis and characterisation of (22 $\beta$ )-27-nor-furost-5-en-25-ketoxime-3 $\beta$ -yl-3 $\beta$ ,26-diacetate (Haad-11)

Ketoxime acetate, Haad-11 was also prepared from acetylation of ketoxime, Haad-10 using the same procedure as for Haad-9.



**Reagents and conditions:** a) Ac<sub>2</sub>O, dry pyridine, Chloroform, RT, 5 hrs

Haad-11 (57 mg, 52%) was obtained as creamy white solid. The ESI-MS ions 500.4 [M+H]<sup>+</sup> and 538.3 [M+K]<sup>+</sup> gave molecular formula C<sub>30</sub>H<sub>45</sub>NO<sub>5</sub> (499) [Fig. 5.14]. The <sup>1</sup>H NMR signals at  $\delta_H$  1.98 (s) and 2.03 (s) correspond to methyl protons at C-28 and C-29. The chemical shifts at 3.30 (m) and 4.32 (m) were attributed to oxymethine protons at C-22 and C-16, while the signals at  $\delta_H$  4.60 (m) and 5.38 (t) were assigned to oxymethine proton at C-3 and olefinic methine proton at C-6, [Fig. 5.15]. Chemical shift at 2.16 (s) showed the presence of methyl protons at C-26 attached to ketoxime carbon at C-25. <sup>13</sup>C NMR [Fig. 5.16] and DEPT spectra data [Fig. 5.17] of the analogue were also similar to its ketoxime analogue, Haad-10 data except at C-28 and C-27 (acetate), and also similar to diosgenin skeleton except at C-22, and terminal oxime acetates at C-25, C-27 and C-30 [Table 4.74]. Haad-11 was identified as (22 $\beta$ )-27-nor-furost-5-en-25-ketoxime-3 $\beta$ -yl-3 $\beta$ ,26-diacetate. Some main spectroscopic data differences of Haad-11 and Haad-10 are given below.

<sup>1</sup>H NMR (CDCl<sub>3</sub>): 1.98 (s, 3H, H-28, CH<sub>3</sub>COO), 2.16 (s, 3H, H-26, CH<sub>3</sub>CO).

<sup>13</sup>C NMR (CDCl<sub>3</sub>): 21.80 (C-28), 29.89 (C-26) and 170.90 (C-27) [Table 4.74; Figs: 5.15 - 5.17];

IR (KBR, cm<sup>-1</sup>): 2924 (C-H), 1735 (C=O), 1658 (C=C), 1245 (C-O)

**Table 4.74:** Comparison of  $^{13}\text{C}$  and  $^1\text{H}$  NMR data of Haad-10 and Haad-11

Assignment	$^{13}\text{C}$	Multiplicity	$^1\text{H}$ , Multiplicity	$^{13}\text{C}$	$^1\text{H}$
1	28.14	$\text{CH}_2$	1.34-1.90, m, 2H	28.04	1.34-1.90, m, 2H
2	37.39	$\text{CH}_2$	1.34-1.90, m, 2H	37.39	1.34-1.90, m, 2H
3	74.30	CH	4.53, m, 1H	74.27	4.60, m, 1H
4	39.77	$\text{CH}_2$	1.34-1.90, m, 2H	39.36	1.34-1.90, m, 2H
5	140.12	Q	-	140.09	-
6	122.76	CH	5.36, t, 1H	122.71	5.38, t, 1H
7	32.38	$\text{CH}_2$	2.36, t, 2H	32.37	2.36, t, 2H
8	38.20	CH	1.34-1.90, m, 1H	38.07	1.34-1.90, m, 2H
9	50.39	CH	1.34-1.90, m, 1H	50.40	1.34-1.90, m, 2H
10	37.10	Q	-	37.10	-
11	28.04	$\text{CH}_2$	1.34-1.90, m, 2H	21.03	1.34-1.90, m, 2H
12	31.96	$\text{CH}_2$	1.34-1.90, m, 2H	31.97	1.34-1.90, m, 2H
13	41.10	Q	-	41.12	-
14	38.48	CH	1.34-1.90, m, 1H	38.48	1.34-1.90, m, 2H
15	32.59	$\text{CH}_2$	1.34-1.90, m, 2H	32.57	1.34-1.90, m, 2H
16	83.70	CH	4.29, m, 1H	83.73	4.32, m, 1H
17	65.49	CH	1.34-1.90, m, 1H	65.46	1.34-1.90, m, 2H
18	57.29	CH	1.34-1.90, m, 1H	57.28	1.34-1.90, m, 2H
19	19.20	$\text{CH}_3$	0.83-1.29, m, 3H	19.13	0.83-1.29, m, 3H
20	16.80	$\text{CH}_3$	0.83-1.29, m, 3H	16.82	0.83-1.29, m, 3H
21	19.72	$\text{CH}_3$	0.83-1.29, m, 3H	19.72	0.83-1.29, m, 3H
22	89.70	CH	3.30, s, 1H	89.61	3.30, m, 1H
23	30.19	$\text{CH}_2$	1.34-1.90, m, 2H	30.08	1.34-1.90, m, 2H
24	42.02	$\text{CH}_2$	2.51, d, 2H	33.76	2.51, d, 2H
25	158.98	Q	-	<b>166.81</b>	-
26	30.08	$\text{CH}_3$	2.13, s, 3H	<b>29.89</b>	<b>2.16, s, 3H</b>
27	21.81	$\text{CH}_3$	1.95, s, 3H	<b>170.90</b>	-
28	170.97	Q		21.80	1.98, s, 3H
				<b>21.80</b>	<b>2.03, s, 3H</b>
				<b>169.26</b>	-

Implied multiplicities of the carbons were determined from the DEPT experiment.

\* Haad-10

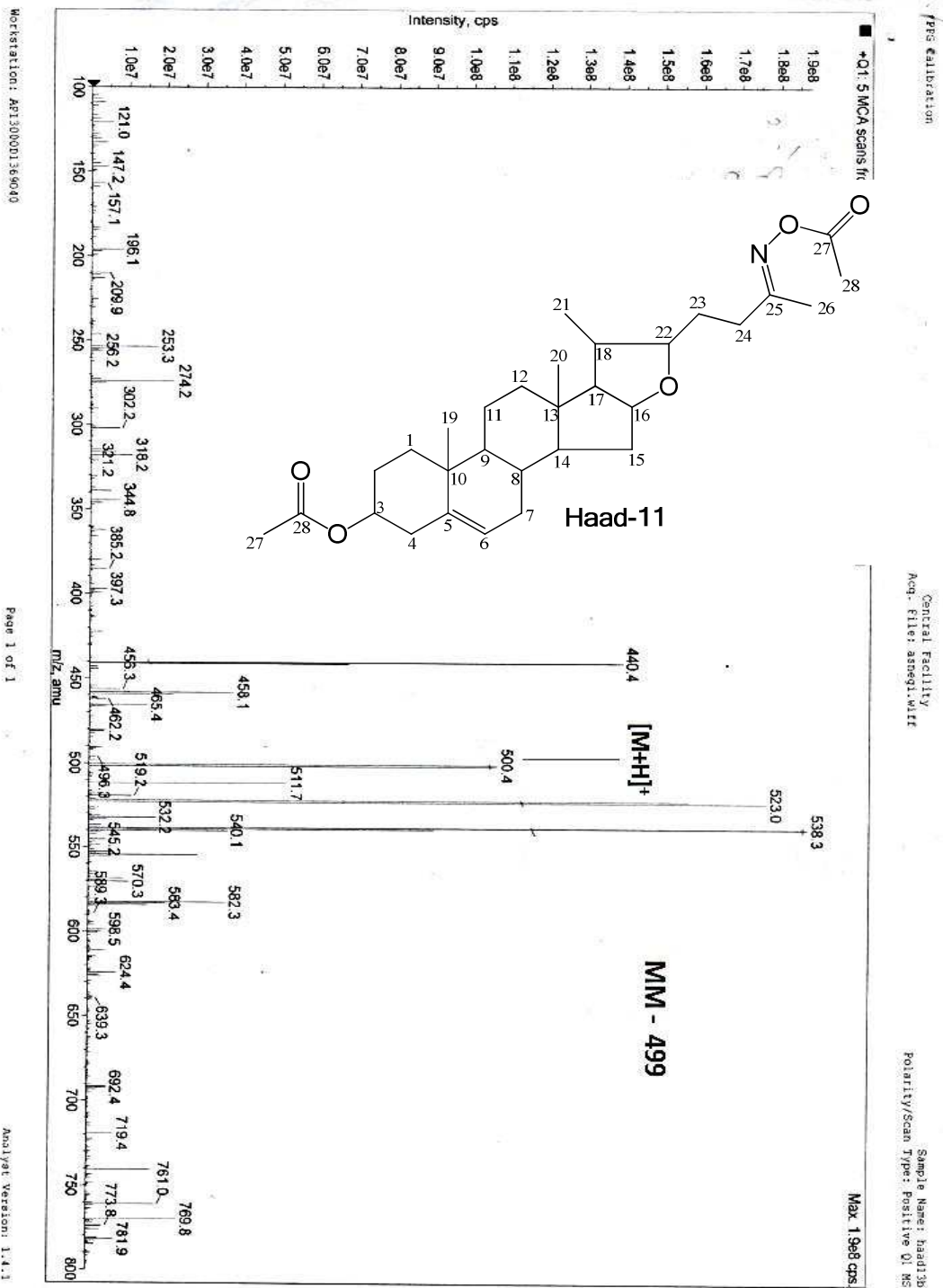


**Fig. 5.14:** ESI-MS spectrum of Haad-11 in MeOH

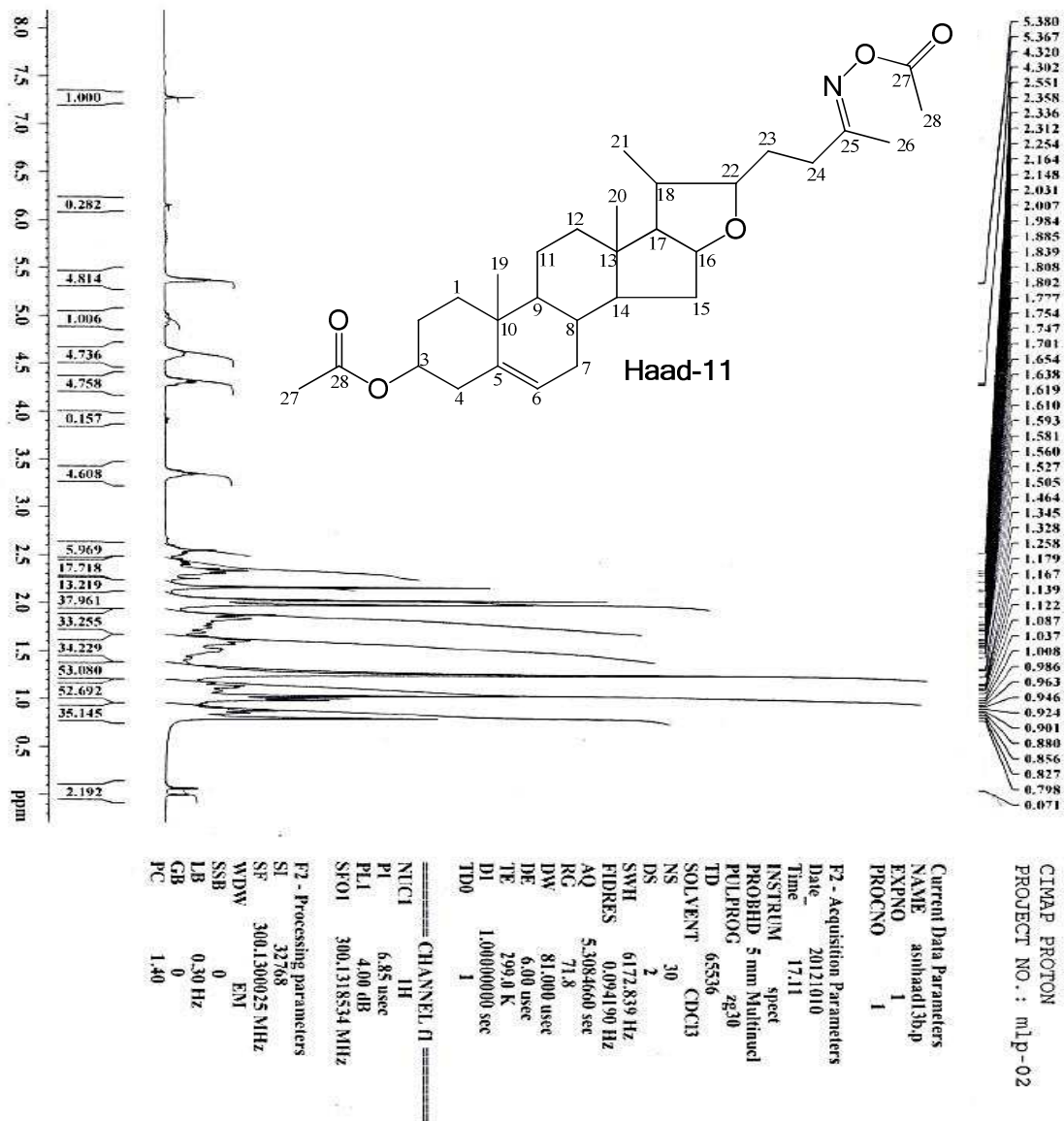
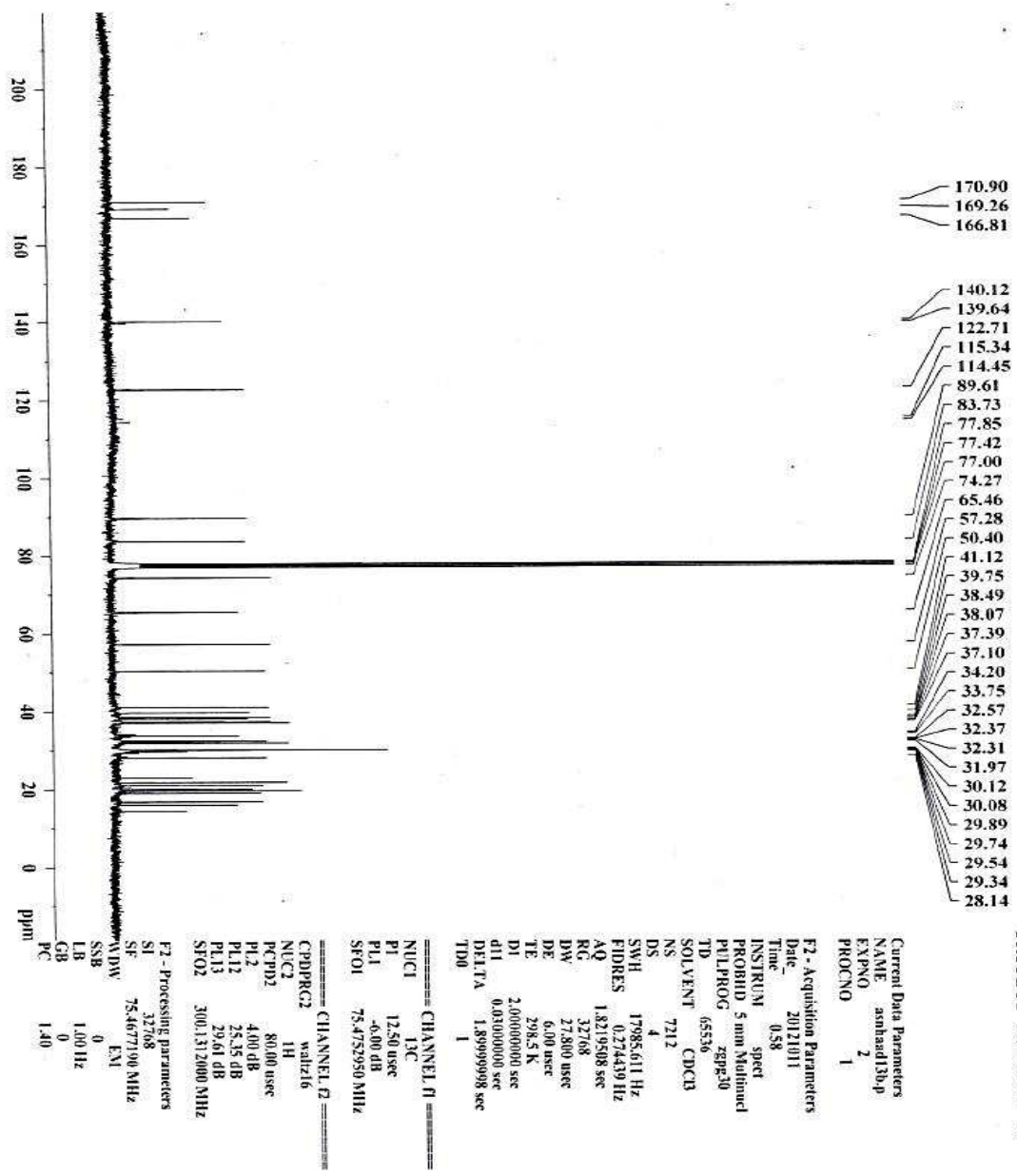


**Fig. 5.15:**  $^1\text{H}$  NMR spectrum of Haad-11 in  $\text{CDCl}_3$





CIMAP-CARBON  
PROJECT NO.: MLP-04

Fig. 5.16: <sup>13</sup>C NMR spectrum of Haad-11 in CDCl<sub>3</sub>

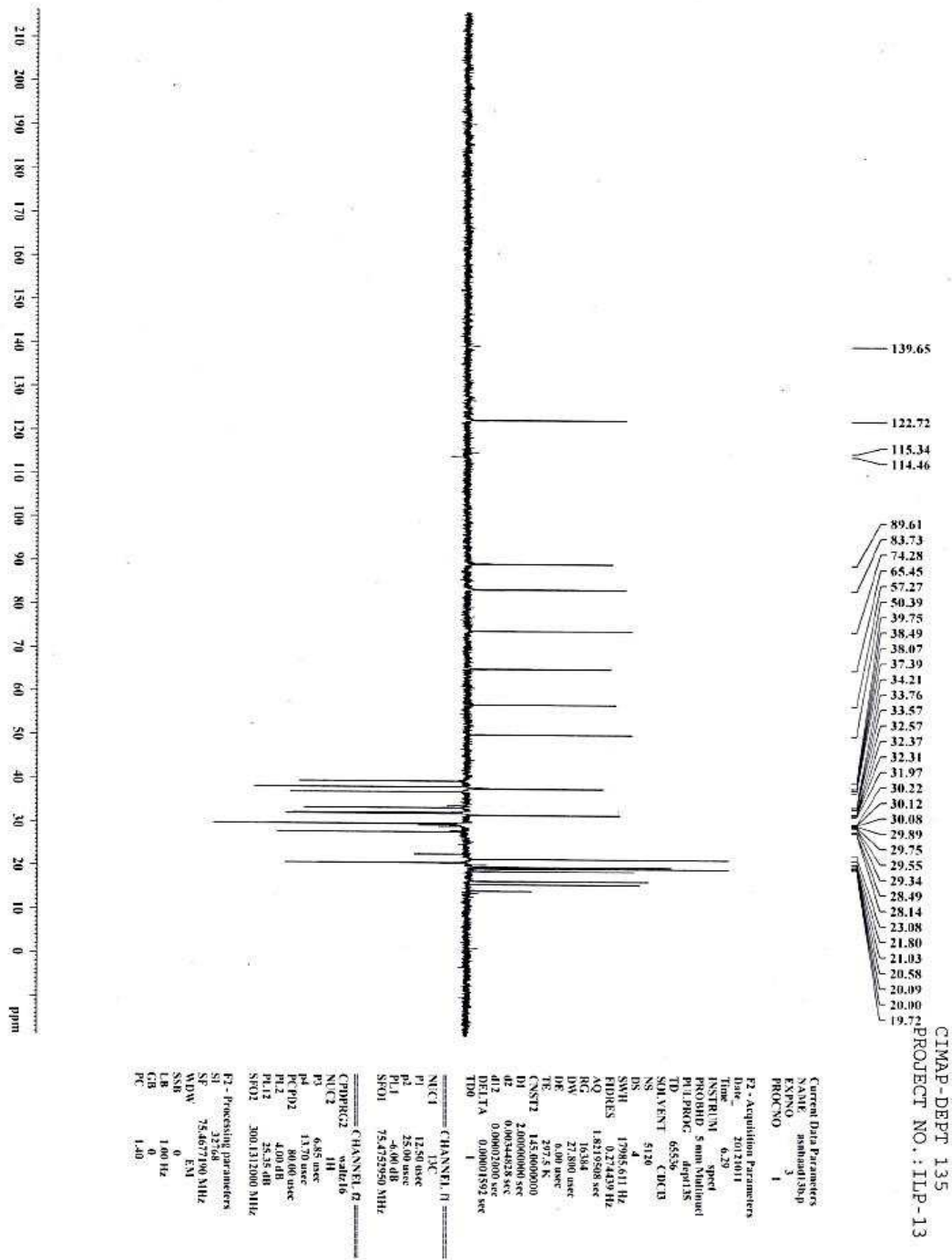
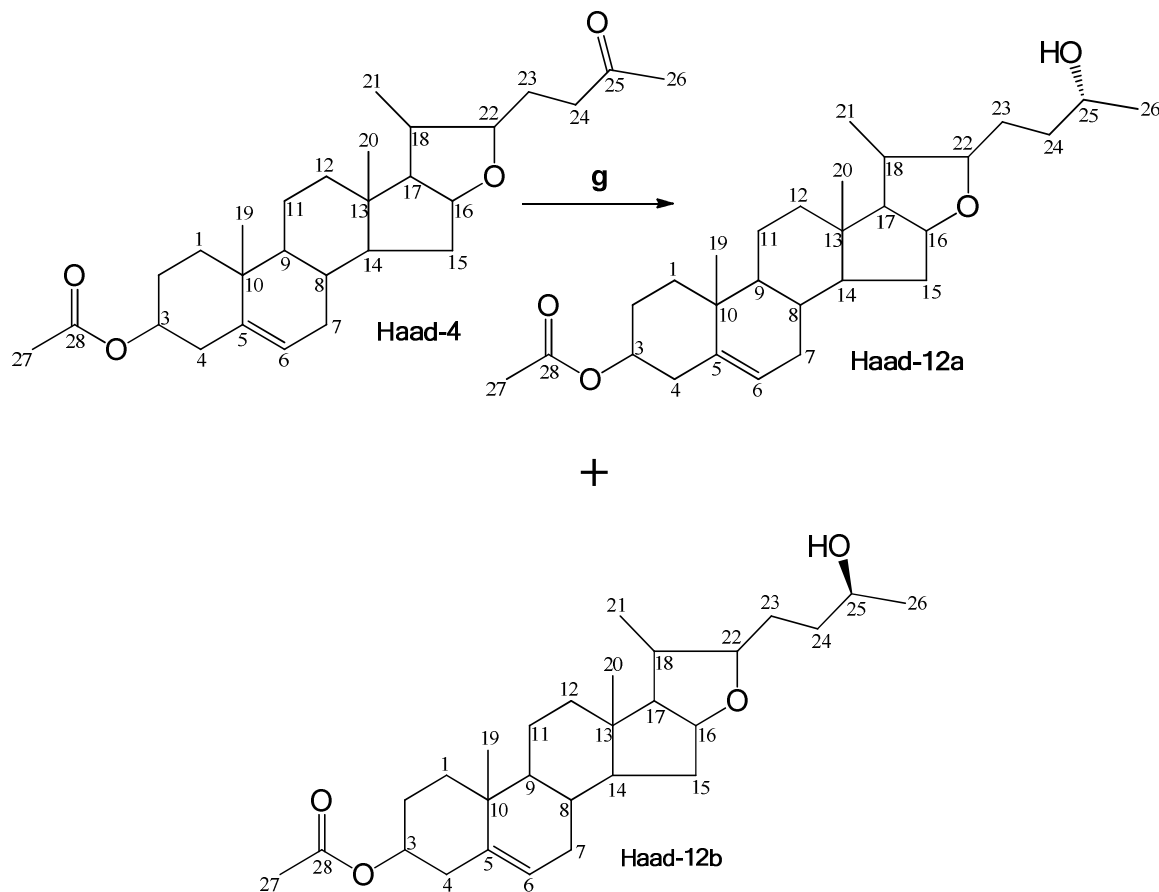


Fig. 5.17: DEPT spectrum of Haad-11 in CDCl<sub>3</sub>

#### 4.8.14. Synthesis and characterisation of (22 $\beta$ )-25 $\alpha$ -Hydroxy-3 $\beta$ -yl-27-nor-furost-5-en-3-acetate and (22 $\beta$ )-25 $\beta$ -Hydroxy-3 $\beta$ -yl-27-nor-furost-5-en-3-acetate (Haad-12a and Haad-12b)

Haad-12 $\alpha$ - and  $\beta$ - products were synthesised via the reduction of ketone (Haad-4) with sodium borohydride (NaBH<sub>4</sub>) in methanol at room temperature.



**Reagents and conditions:** g) NaBH<sub>4</sub>, MeOH, RT, 1 hr.

Haad-12 $\alpha$  and 12 $\beta$  (21 mg, 21%; and 86 mg, 86%) appeared as creamy crystalline and brown solid. The ESI-MS fragment ions 445.3 [M+H]<sup>+</sup>, 467.4 [M+Na]<sup>+</sup> and 483.2 [M+K]<sup>+</sup> correspond to a molecular formula C<sub>28</sub>H<sub>44</sub>O<sub>4</sub> (444) [Fig. 5.18]. The <sup>1</sup>H NMR chemical shifts at  $\delta_H$  2.03 (s) and 2.30 (d) were assigned to methyl protons of acetate at C-27 and methyl protons at C-26 attached to oxymethine carbon (alcohol) at C-25. The proton signals at  $\delta_H$  3.35 (bs) and 3.80 (m) correspond to methine protons at C-22 and C-25, while the chemical shifts  $\delta_H$  4.33 (bs) and 5.36 (s) showed the presence of oxymethine proton at

C-16 and olefinic methine proton at C-6 [Fig. 5.19].  $^{13}\text{C}$  NMR [Fig. 5.20] and DEPT spectra [Fig. 5.21] of the analogues were identical to Haad-4 data except at hydroxyl carbon at position 25 where both  $\alpha$  (67.91, C-25a) and  $\beta$  (68.75, C-25b) products were confirmed, while the spectroscopic data of the compounds were also similar to diosgenin data except at the acetate, C-22 and C-25.  $^1\text{H}$  and  $^{13}\text{C}$  NMR spectroscopic data of the derivatives and ketone Haad-4 were shown in Table 4.75. Hence, Haad-12a & 12b were identified as (22 $\beta$ )-25 $\alpha$ -Hydroxy-3 $\beta$ -yl-27-nor-furost-5-en-3-acetate and (22 $\beta$ )-25 $\beta$ -hydroxy-3 $\beta$ -yl-27-nor-furost-5-en-3-acetate.

$^1\text{H}$  NMR: 3.80 (m, 1H, H-25, alcohol)

$^{13}\text{C}$  NMR: 67.91 (C-25 $\alpha$ ) and 68.75 (C-25 $\beta$ ) [Table 4.75; Figs: 5.19 - 5.21];

IR (KBR,  $\text{cm}^{-1}$ ): 3423 (O-H), 2935 (C-H), 1732 (C=O), 1245 (C-O)

**Table 4.75:** Comparison of  $^{13}\text{C}$  and  $^1\text{H}$  NMR data of Haad-4 and Haad-12 ( $\alpha$  and  $\beta$ )

Assignment	$^{13}\text{C}$	Multiplicity	$^1\text{H}$ , Multiplicity	$^{13}\text{C}$	$^1\text{H}$
1	21.02	$\text{CH}_2$	1.34-1.90, m, 2H	28.14	1.34-1.90, m, 2H
2	37.38	$\text{CH}_2$	1.34-1.90, m, 2H	37.38	1.34-1.90, m, 2H
3	74.28	CH	4.34, m, 1H	74.28	4.57, m, 1H
4	38.75	$\text{CH}_2$	1.34-1.90, m, 2H	39.81	1.34-1.90, m, 2H
5	140.12	Q	-	140.08	-
6	122.72	CH	5.40, t, 1H	122.75	5.36, t, 1H
7	32.37	$\text{CH}_2$	2.36, t, 2H	32.36	2.36, t, 2H
8	31.95	CH	1.34-1.90, m, 1H	36.69	1.34-1.90, m, 2H
9	50.38	CH	1.34-1.90, m, 1H	50.38	1.34-1.90, m, 2H
10	37.10	Q	-	37.10	-
11	28.13	$\text{CH}_2$	1.34-1.90, m, 2H	21.03	1.34-1.90, m, 2H
12	38.48	$\text{CH}_2$	1.34-1.90, m, 2H	31.93	1.34-1.90, m, 2H
13	41.09	Q	-	41.10	-
14	38.24	CH	1.34-1.90, m, 1H	38.47	1.34-1.90, m, 2H
15	32.55	$\text{CH}_2$	1.34-1.90, m, 2H	32.49	1.34-1.90, m, 2H
16	83.69	CH	4.63, m, 1H	83.80	4.33, m, 1H
17	65.39	CH	1.34-1.90, m, 1H	65.17	1.34-1.90, m, 2H
18	57.27	CH	1.34-1.90, m, 1H	57.38	1.34-1.90, m, 2H
19	19.01	$\text{CH}_3$	0.83-1.29, m, 3H	19.08	0.83-1.29, m, 3H
20	16.80	$\text{CH}_3$	0.83-1.29, m, 3H	16.80	0.83-1.29, m, 3H
21	19.71	$\text{CH}_3$	0.83-1.29, m, 3H	19.71	0.83-1.29, m, 3H
22	89.53	CH	3.27, s, 1H	90.60	3.35, s, 1H
23	27.44	$\text{CH}_2$	1.34-1.90, m, 2H	30.08	1.34-1.90, m, 2H
24	41.28	$\text{CH}_2$	2.51, d, 2H	38.28	2.51, d, 2H
25	209.24	Q	-	<b>67.91(<math>\alpha</math>), 68.75(<math>\beta</math>)</b>	<b>3.80, m, 1H</b>
26	30.33	$\text{CH}_3$	2.13, s, 3H	30.08	2.30, s, 3H
27	21.80	$\text{CH}_3$	1.95, s, 3H	21.81	2.03, s, 3H
28	170.95	Q	-	170.94	-

Implied multiplicities of the carbons were determined from the DEPT experiment.

\* Haad-4

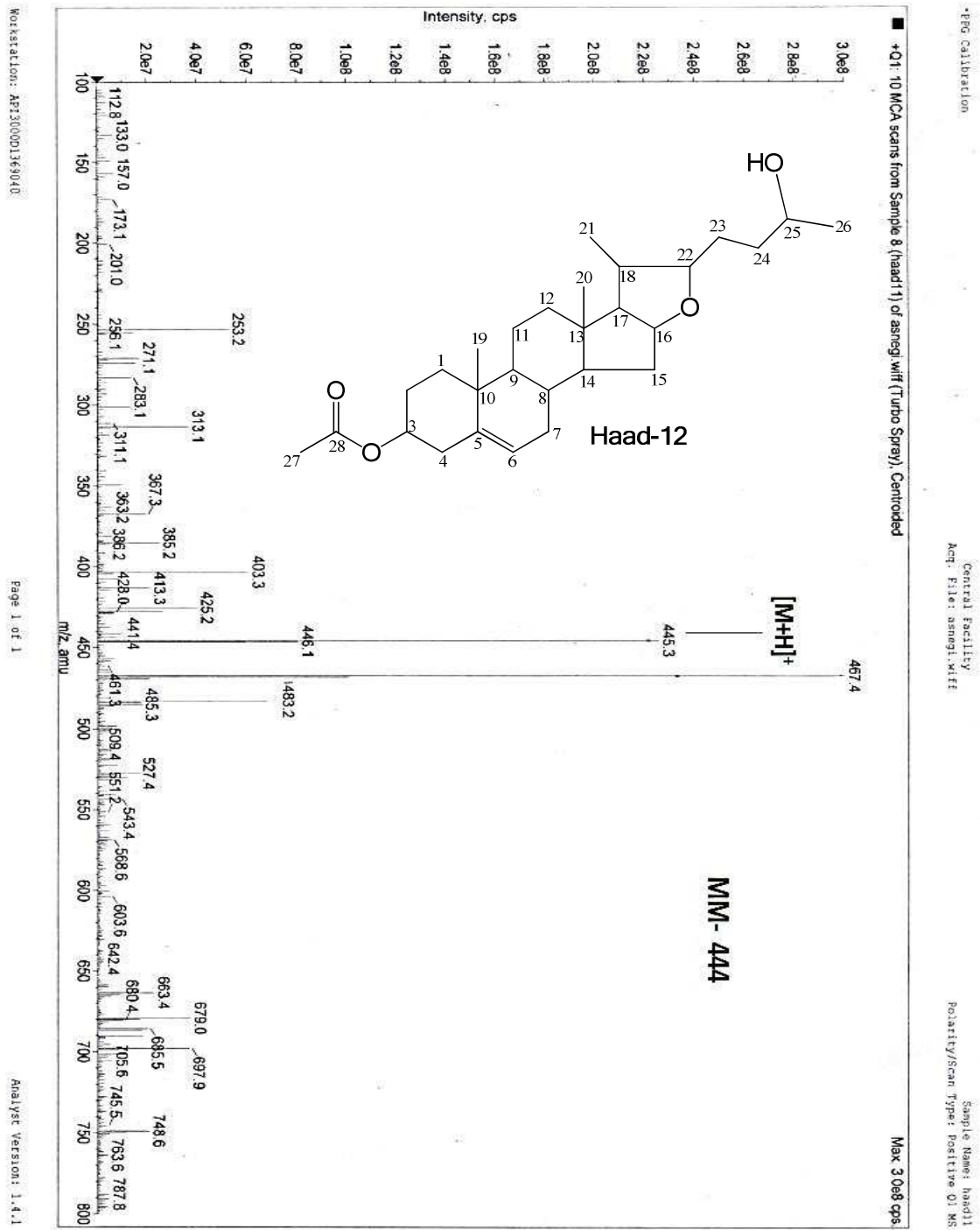


Fig. 5.18: ESI-MS spectrum of Haad-12 in MeOH

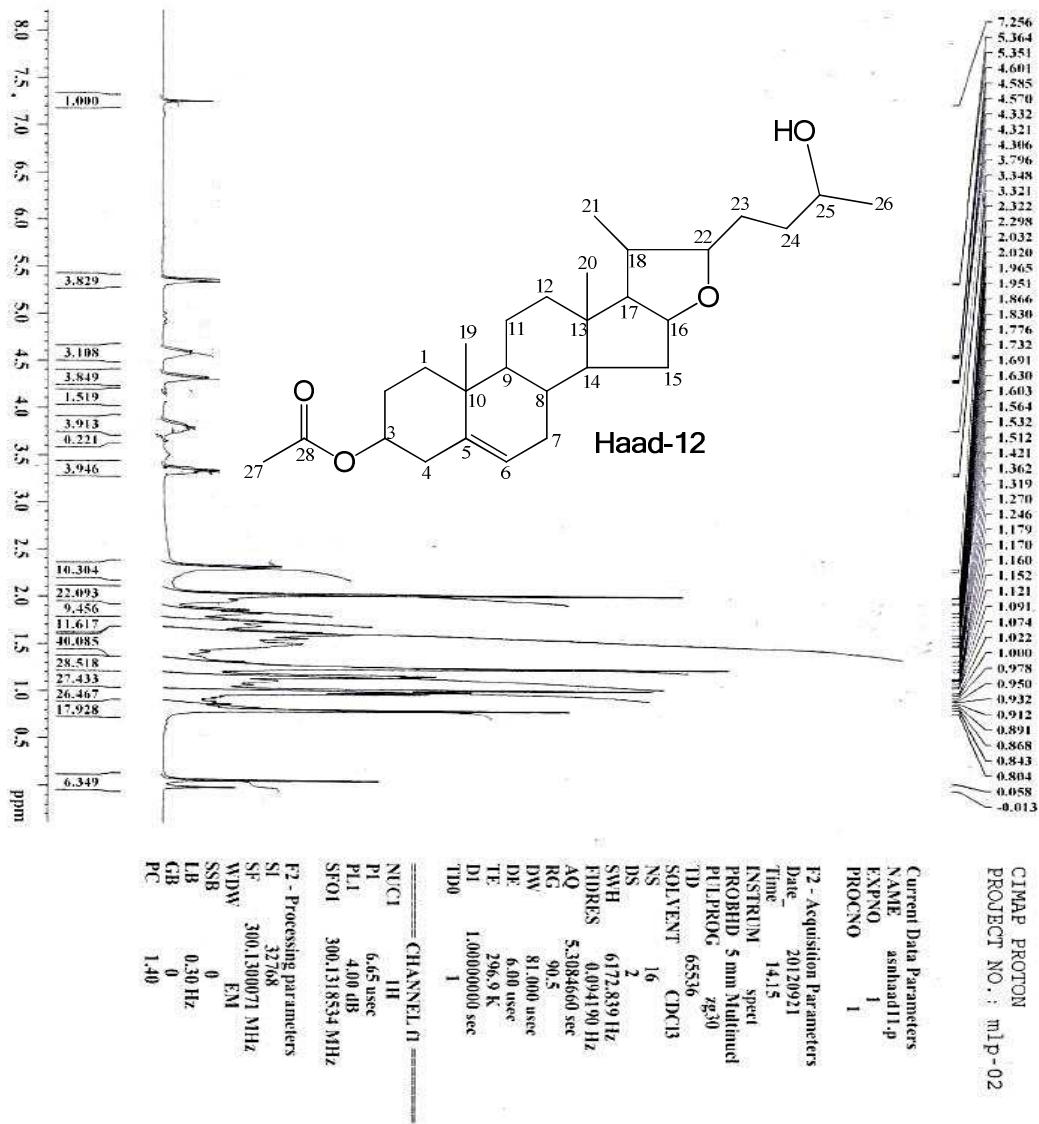


Fig. 5.19:  $^1\text{H}$  NMR spectrum of Haad-12 in  $\text{CDCl}_3$

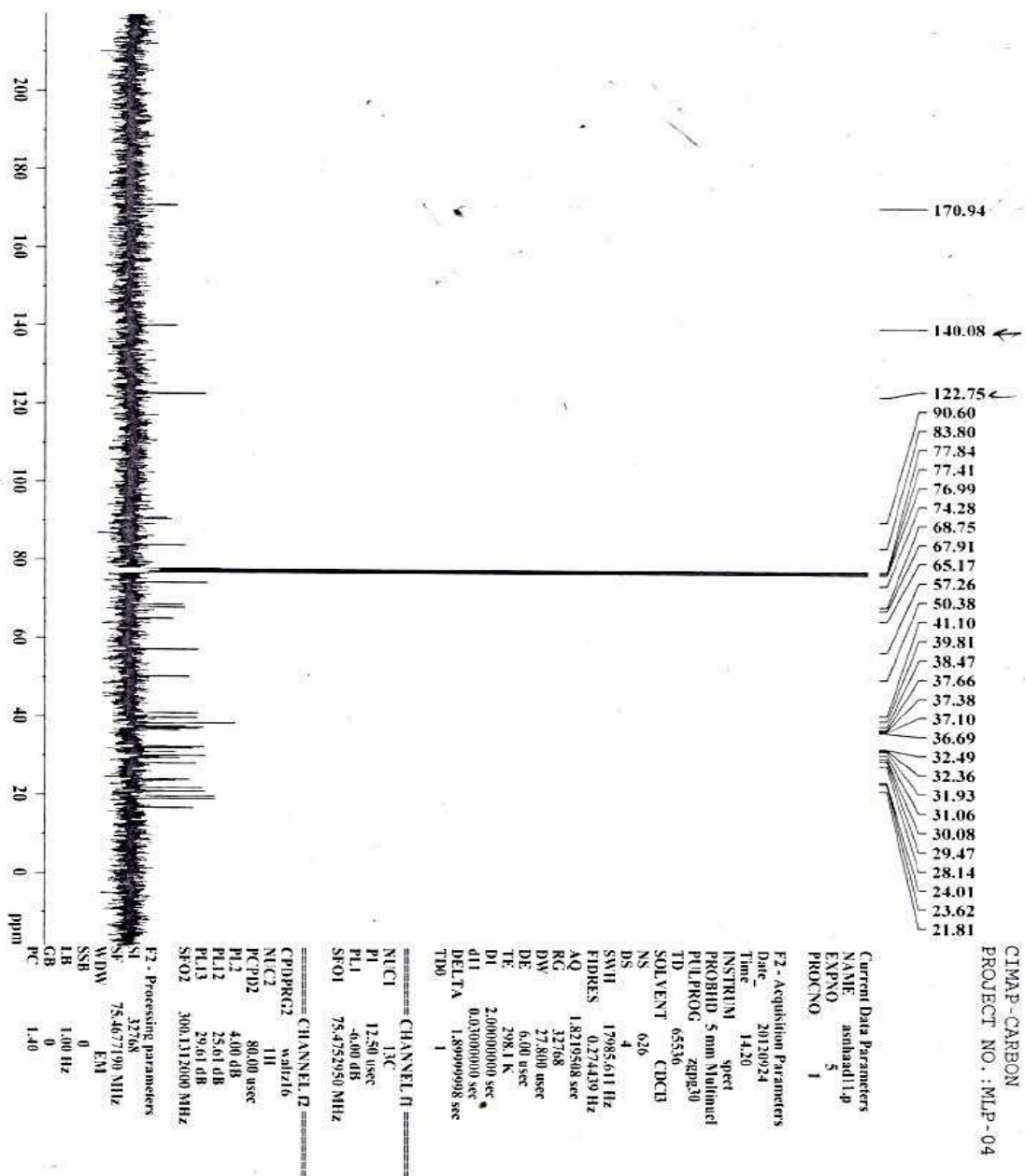
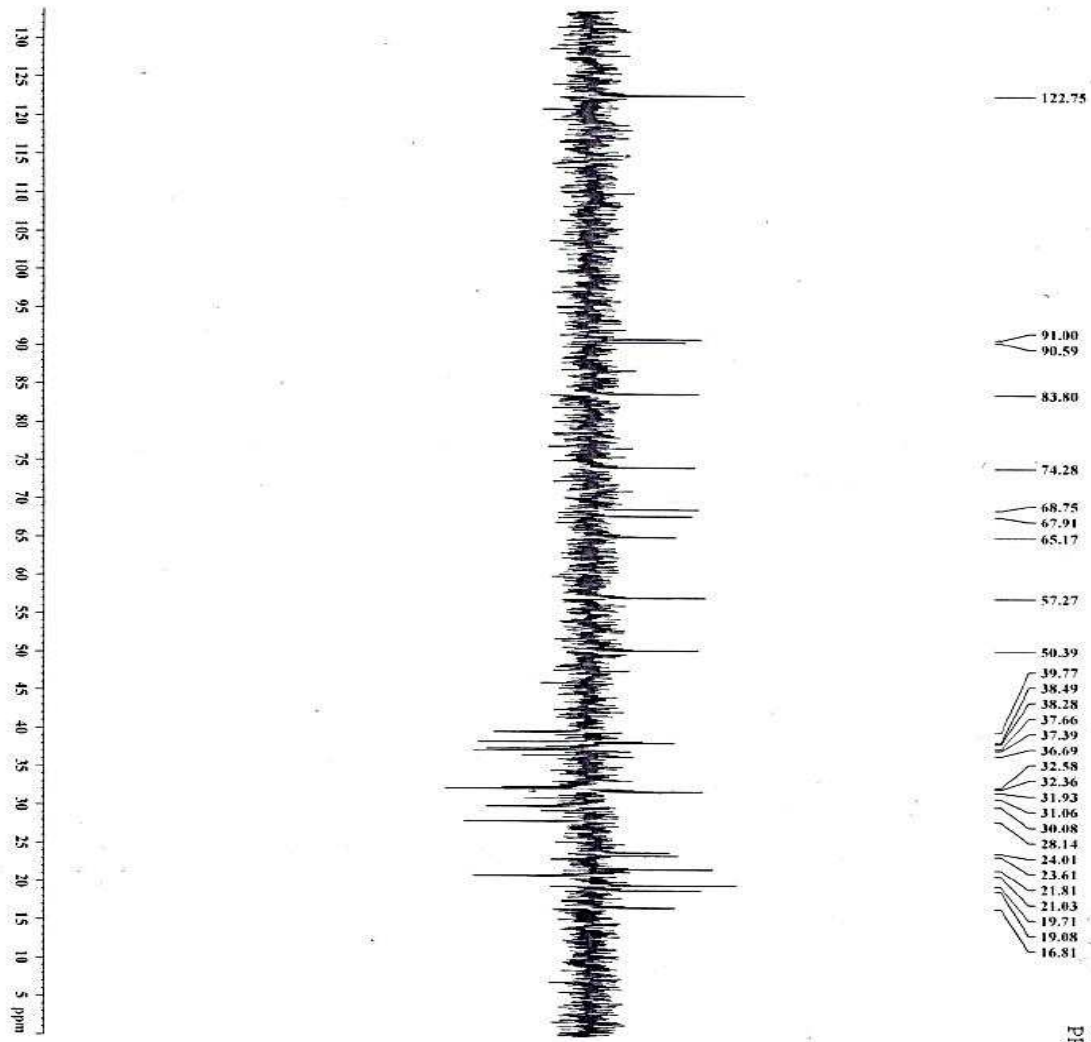


Fig. 5.20:  $^{13}\text{C}$  NMR spectrum of Haad-12 in  $\text{CDCl}_3$





CIMAP-DEPT 135  
PROJECT NO.: ILP-13

```

Current Data Parameters
NAME      sanhad11.p
EXPNO     6
PROCNO    1

F2-Acquisition Parameters
Date_     20120924
Time      15:04
INSTRUM   spect
PROBHD    5 mm Multinuc
PULPROG   zgpg30
TD         65536
SOLVENT   CDCl3
NS         300
DS         4
SWH        17985.611 Hz
FIDRES     0.274439 Hz
AQ         1.8219508 sec
RG         16384
DNW        2.2809 sec
DE         20.3 Hz
TE         300.2 K
CONST1    146.000000
D1         2.0000000 sec
d2         0.20344823 sec
d12        0.00002000 sec
DELTA     0.00001592 sec
TD0        1

===== CHANNEL f1 =====
NUC1       13C
P1         12.50 usec
P2         25.00 usec
SFO1       40.00 MHz
SFO2       75.473250 MHz

===== CHANNEL f2 =====
CPDPRG2   waltz16
NUC2       1H
P3         6.65 usec
P4         13.30 usec
PCPD2     80.00 usec
P12       4.00 dB
P13       25.01 dB
SFO2      300.137900 MHz

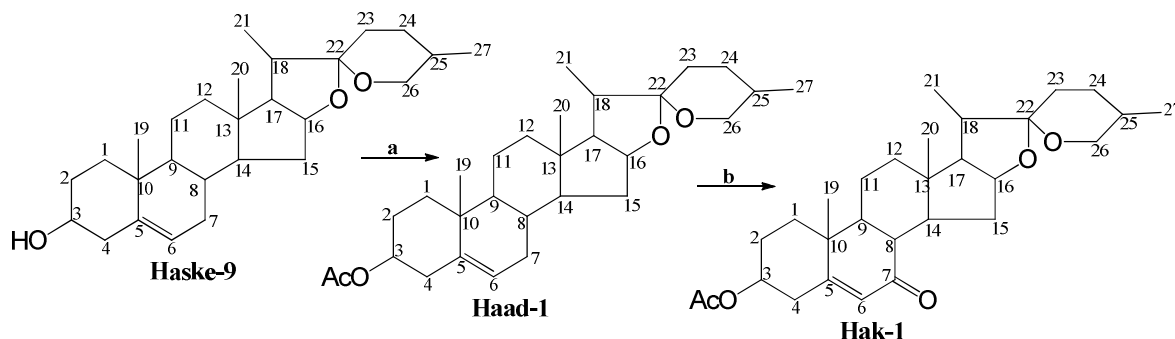
F2-Processing parameters
SI         32768
SF         75.467709 MHz
WDW        EM
SSB        0
LB         1.00 Hz
GB         0
PC         1.40
  
```

Fig. 5.21: DEPT spectrum of Haad-12 in CDCl<sub>3</sub>

## 4.9 Synthetic modification of diosgenin (Second reaction scheme)

### 4.9.1. Synthesis and characterisation of (22 $\beta$ ,25R)-7-oxo-spirost-5-en-3 $\beta$ -yl-3-acetate (Hak-1)

7-Ketone analogue, Hak-1 was prepared when diosgenin acetate (Haad-1) in dichloromethane (DCM) reacts with chromium VI oxide (CrO<sub>3</sub>) and pyridine in the presence of (DCM) in ice bath, and later at room temperature for 10 hrs.



**Reagents and conditions:** a) Ac<sub>2</sub>O, dry pyridine, Chloroform, RT, 6 hrs  
b) CrO<sub>3</sub>-Pyridine-DCM system, RT, 10 hrs

Hak-1 (106 mg, 53%) was obtained as white solid. The ESI-MS ions 471.4 [M+H]<sup>+</sup>, 493.5 [M+Na]<sup>+</sup> and 509.4 [M+K]<sup>+</sup> correspond to molecular formula C<sub>29</sub>H<sub>42</sub>O<sub>5</sub> (470) [Fig. 5.22]. The <sup>1</sup>H NMR signals at  $\delta_H$  0.77-1.82 (m) are similar to cluster of methyl, methylene and methine protons chemical shifts of diosgenin. Chemical shifts  $\delta_H$  2.01 (s) and 4.43 (bs) were attributed to methyl protons of acetate at C-28 and methine proton at C-3, while 3.39 (m) and 2.84 (t) were assigned to methylene protons at C-26 and methine proton at C-8. The proton signals at  $\delta_H$  4.67 (bd) and 5.67 (s) correspond to methine proton at C-16 and olefinic methine proton at C-6 respectively [Fig. 5.23]. <sup>13</sup>C NMR [Fig. 5.24] and DEPT spectra data [Fig. 5.25] of the analogue were identical to that of diosgenin acetate except at keto (C-7) position. <sup>1</sup>H and <sup>13</sup>C NMR spectroscopic data of the derivative and Haad-1 were shown in Table 4.76. Hence, Hak-1 was elucidated to be (22 $\beta$ ,25R)-7-oxo-spirost-5-en-3 $\beta$ -yl-3-acetate. The main differences in spectra data of Hak-1 and Haad-1 were listed below

<sup>1</sup>H NMR (CDCl<sub>3</sub>): 2.01 (s, 3H, H-28, CH<sub>3</sub>COO, Acetate), 2.84 (t, 1H, H-8).

<sup>13</sup>C NMR (CDCl<sub>3</sub>): 164.46 (C-5) and 201.66 (C-7) [Table 4.76; Figs: 5.23 - 5.25];

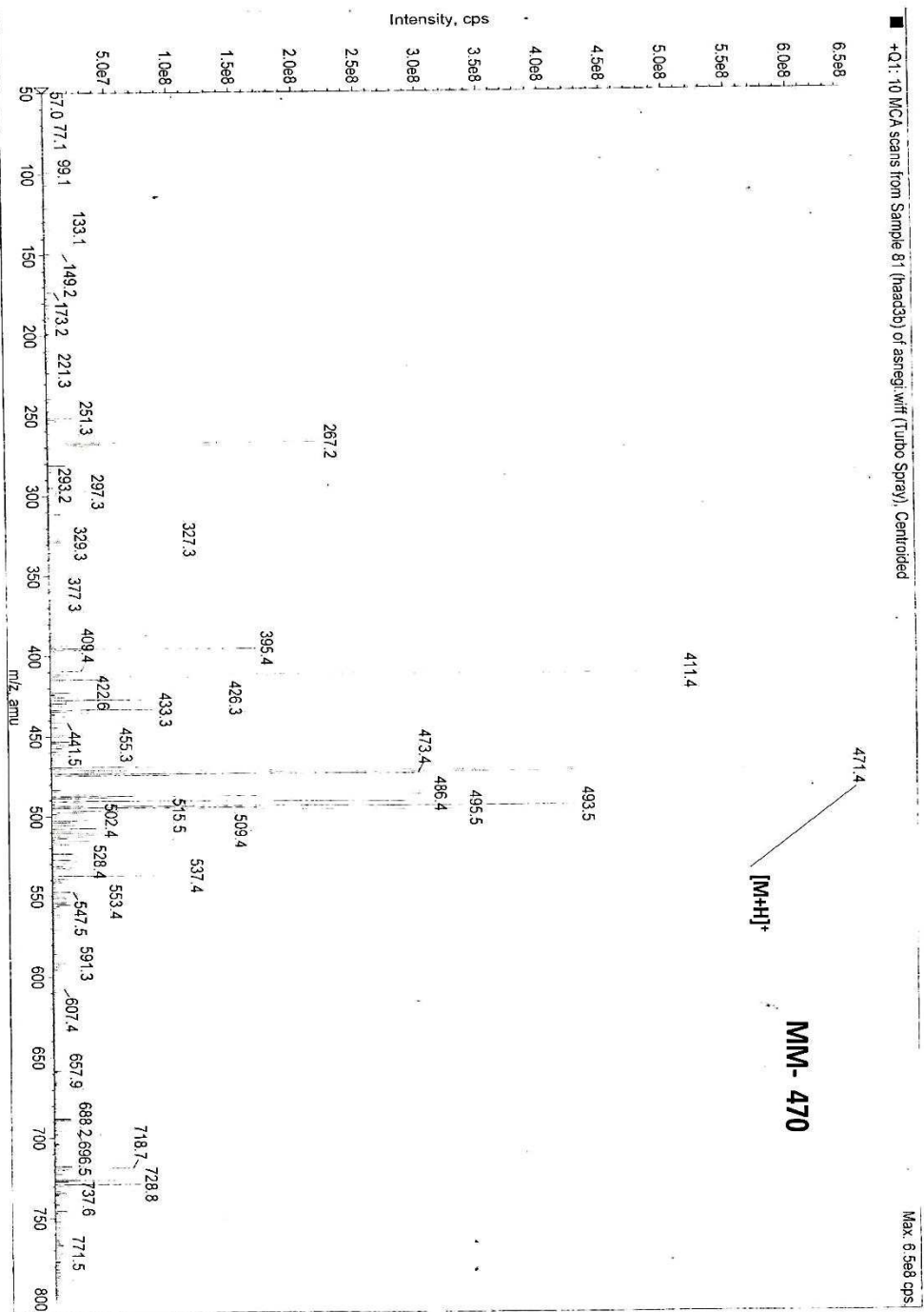
IR (KBR, cm<sup>-1</sup>): 2907 (C-H), 1724 (C=O), 1709 (C=C), 1231 (C-O)

**Table 4.76:** Comparison of  $^{13}\text{C}$  and  $^1\text{H}$  NMR data of Haad-1 and Hak-1

Assignment	$^{13}\text{C}$	Multiplicity	$^1\text{H}$ , Multiplicity	$^{13}\text{C}$	$^1\text{H}$
1	21.74	$\text{CH}_2$	1.44-1.96, m, 2H	29.18	1.40-1.97, m, 2H
2	37.34	$\text{CH}_2$	1.44-1.96, m, 2H	36.37	1.40-1.97, m, 2H
3	74.26	CH	4.35, m, 1H	72.51	4.39, m, 1H
4	42.00	$\text{CH}_2$	1.44-1.96, m, 2H	40.15	1.40-1.97, m, 2H
5	140.05	Q	-	<b>164.46</b>	-
6	122.72	CH	5.35, t, 1H	126.85	5.67, t, 1H
7	32.42	$\text{CH}_2$	2.32, t, 2H	<b>201.66</b>	-
8	31.80	CH	1.44-1.96, m, 1H	45.26	2.50, t, 2H
9	50.35	CH	1.44-1.96, m, 1H	50.04	1.40-1.97, m, 2H
10	37.10	Q	-	35.55	-
11	32.24	$\text{CH}_2$	1.44-1.96, m, 2H	21.28	1.40-1.97, m, 2H
12	29.19	$\text{CH}_2$	1.44-1.96, m, 2H	30.06	1.40-1.97, m, 2H
13	40.66	Q	-	41.34	-
14	40.19	CH	1.44-1.96, m, 1H	41.46	1.40-1.97, m, 1H
15	30.66	$\text{CH}_2$	1.44-1.96, m, 2H	32.29	1.40-1.97, m, 2H
16	81.16	CH	4.59, m, 1H	81.30	4.67, m, 1H
17	62.52	CH	1.44-1.96, m, 1H	62.45	1.40-1.97, m, 2H
18	56.82	CH	1.44-1.96, m, 1H	61.50	1.40-1.97, m, 2H
19	14.89	$\text{CH}_3$	0.96-1.32, m, 3H	17.67	0.93-1.22, m, 3H
20	16.64	$\text{CH}_3$	0.96-1.32, m, 3H	16.78	0.93-1.22, m, 3H
21	17.51	$\text{CH}_3$	0.79-0.81, m, 3H	14.86	0.93-1.22, m, 3H
22	109.60	Q	-	109.67	-
23	32.21	$\text{CH}_2$	1.44-1.96, m, 2H	30.68	1.40-1.97, m, 2H
24	28.12	$\text{CH}_2$	2.51, d, 2H	27.70	1.40-1.97, m, 2H
25	42.00	$\text{CH}_2$	1.44-1.96, m, 2H	38.47	1.44-1.96, m, 2H
26	67.19	$\text{CH}_3$	3.38, d, 2H	67.15	3.43, d, 2H
27	19.69	$\text{CH}_3$	0.96-1.32, m, 3H	17.50	0.93-1.22, m, 3H
28	30.07	$\text{CH}_3$	2.01, s, 3H	21.59	2.03, s, 3H
29	170.82	Q	-	170.61	-

Implied multiplicities of the carbons were determined from the DEPT experiment.

\* Haad-1



Workstation: API300D1569040

Page 1 of 1

Analyst Version: 1.4.1

Fig. 5.22: ESI-MS spectrum of Hak-1 in MeOH

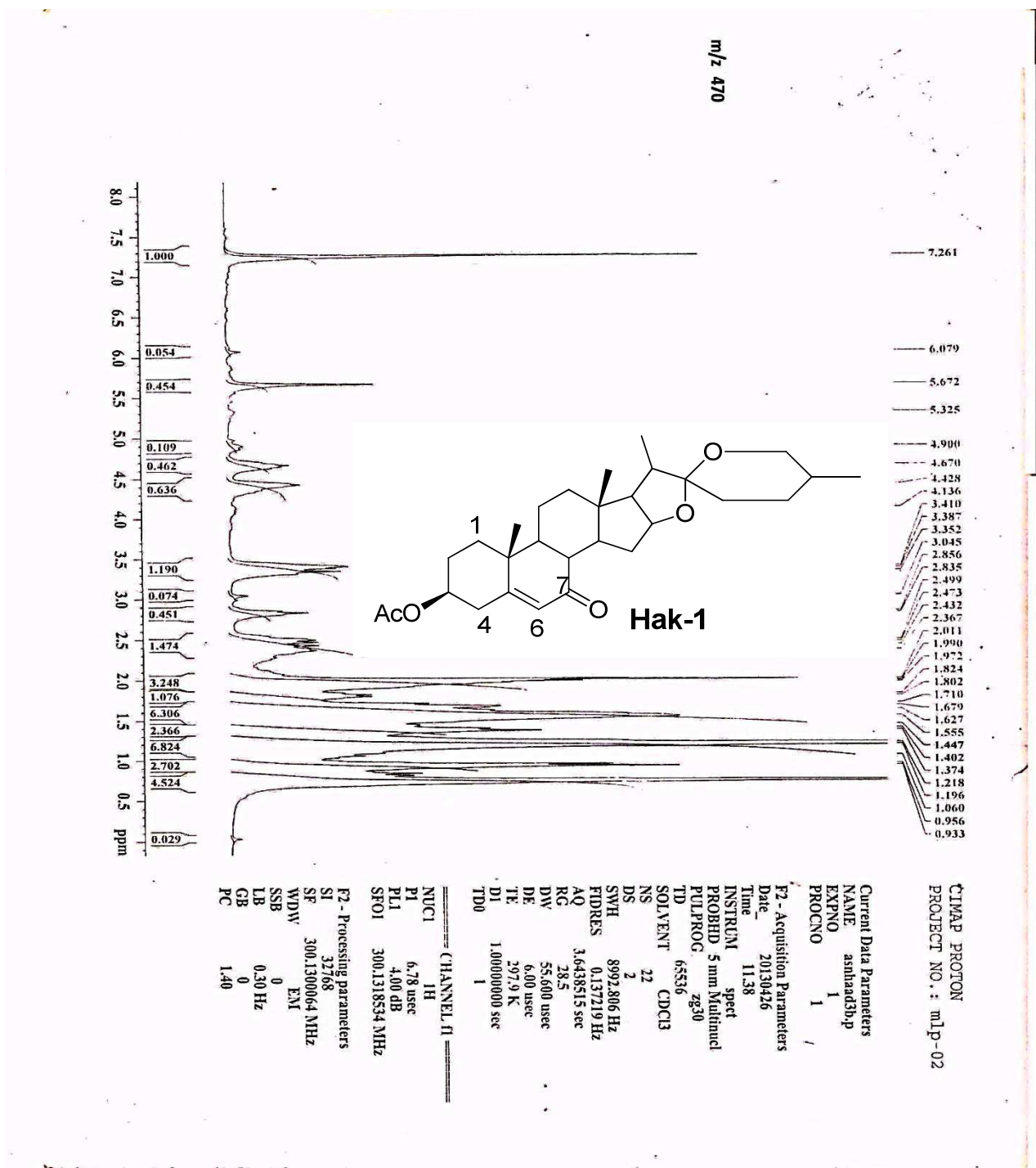


Fig. 5.23: <sup>1</sup>H NMR spectrum of Hak-1 in CDCl<sub>3</sub>

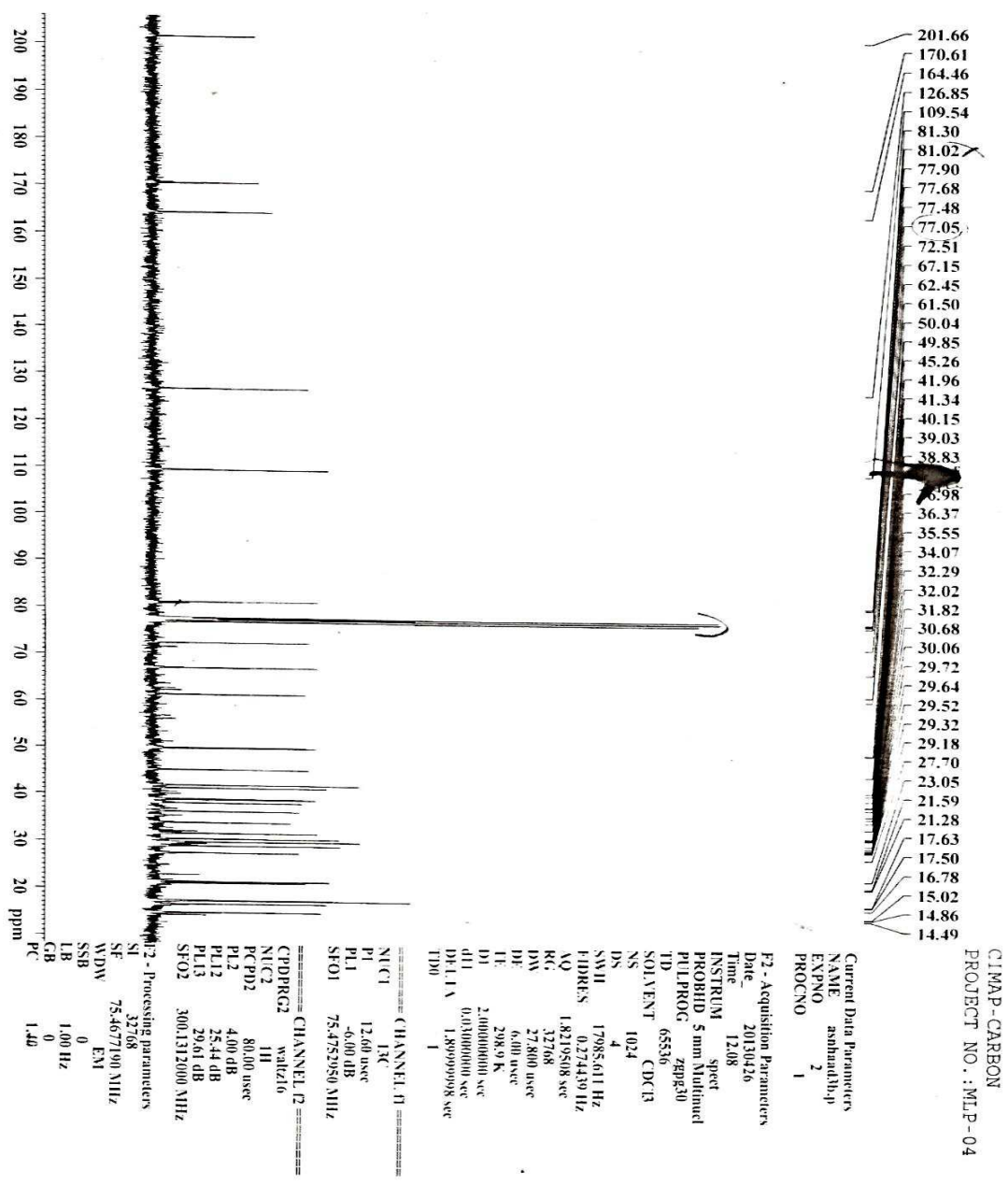


Fig. 5.24:  $^{13}\text{C}$  NMR spectrum of Hak-1 in  $\text{CDCl}_3$

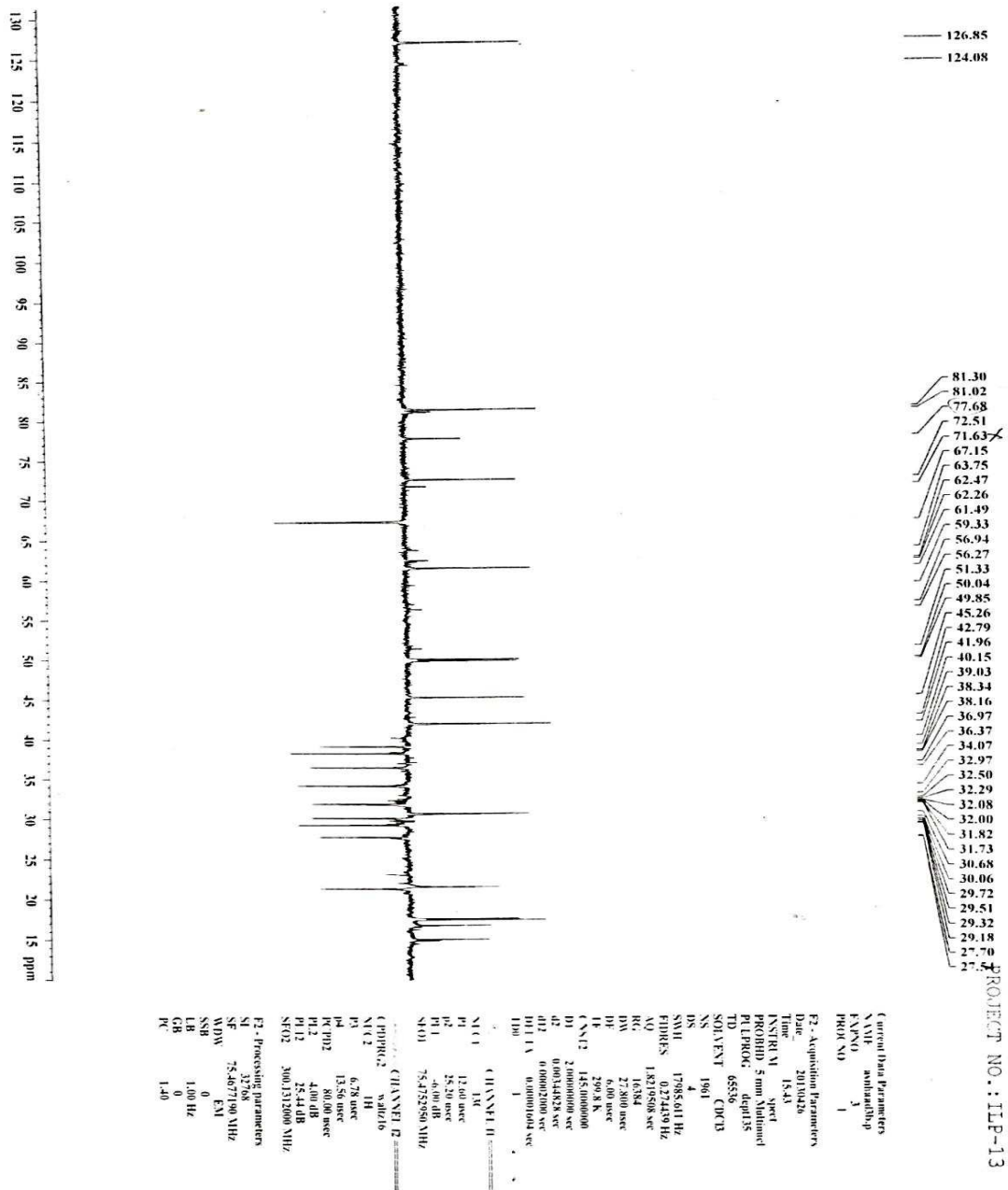
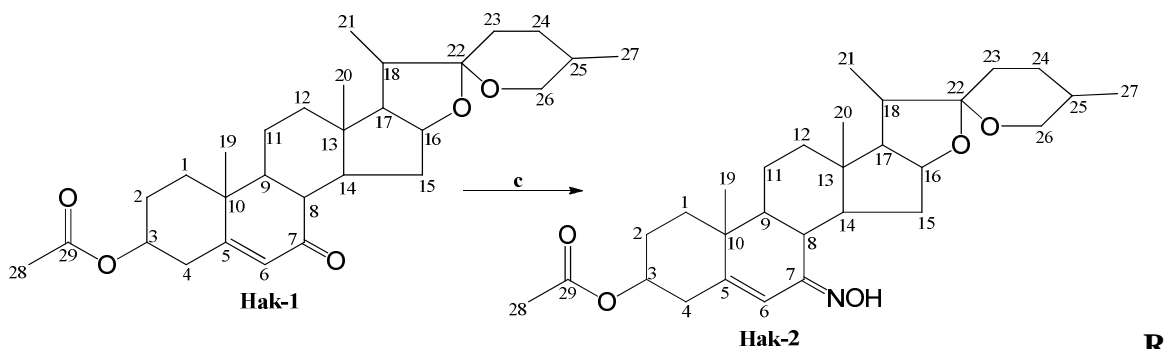


Fig. 5.25: DEPT spectrum of Hak-1 in CDCl<sub>3</sub>

#### 4.9.2. Synthesis and characterisation of (22 $\beta$ ,25R)-3 $\beta$ -Acetoxy-spirost-5-en-3 $\beta$ -yl-7-ketoxime (Hak-2)

7-Ketone (Hak-1) was transformed to 7-ketoxime, Hak-2 when Hak-1 reacts with hydroxyl ammonium hydrochloride (NH<sub>4</sub>OH.HCl) and dry pyridine in the presence of ethanol as a solvent.



**agents and conditions:** c) NH<sub>4</sub>OH.HCl, pyridine, Ethanol, 2 hrs

Hak-2 (90 mg, 90%) was obtained as brown oily liquid. The ESI-MS fragment ions 486.4 [M+H]<sup>+</sup>, 508.3 [M+Na]<sup>+</sup> and 524.4 [M+K]<sup>+</sup> gave molecular formula C<sub>29</sub>H<sub>43</sub>NO<sub>5</sub> (485) [Fig. 5.26]. The <sup>1</sup>H NMR signals at  $\delta_H$  2.02 (s) and 2.82 (s) were attributed to methyl protons of acetate at C-28 and methine proton at C-8. The chemical shifts at  $\delta_H$  3.46 (m) and 4.55 (bs) correspond to oxymethylene and oxymethine protons at C-26 and C-3 respectively, while the signals at  $\delta_H$  4.65 (bd) and 6.57 (s) indicated the presence of oxymethine proton at C-16 and olefinic methine proton at C-6 [Fig. 5.27]. <sup>13</sup>C NMR [Fig. 5.28] and DEPT carbon resonances [Fig. 5.29] of the compound were identical to 7-keto derivative (Hak-1) data except at C-7 [Table 4.77]. Therefore, the structure of Hak-2 was elucidated to be (22 $\beta$ ,25R)-3 $\beta$ -Acetoxy-spirost-5-en-3 $\beta$ -yl-7-ketoxime. The difference in spectroscopic data of Hak-2 and Hak-1 are:

<sup>1</sup>H NMR: 2.82 (t, 1H, 8-CH), 6.57 (s, 1H, 6-CH)

<sup>13</sup>C NMR: 56.86 (C-7) [Table 4.77; Figs: 5.27-5.29];

IR (KBR, cm<sup>-1</sup>): 3452 (O-H), 2932 (C-H), 1723 (C=O), 1643 (C=C), 1211 (C-O)



**Table 4.77:** Comparison of  $^{13}\text{C}$  and  $^1\text{H}$  NMR data of Hak-1 and Hak-2

Assignment	$^{13}\text{C}$	Multiplicity	$^1\text{H}$ , Multiplicity	$^{13}\text{C}$	$^1\text{H}$
1	29.18	$\text{CH}_2$	1.40-1.97, m, 2H	29.10	1.39-1.90, m, 2H
2	37.37	$\text{CH}_2$	1.40-1.97, m, 2H	36.58	1.39-1.90, m, 2H
3	72.51	CH	4.35, m, 1H	73.36	4.55, m, 1H
4	40.15	$\text{CH}_2$	1.40-1.97, m, 2H	39.00	1.39-1.90, m, 2H
5	164.46	Q	-	<b>151.75</b>	-
6	126.85	CH	5.67, s, 1H	114.96	6.57, s, 1H
7	201.66	$\text{CH}_2$	-	<b>156.86</b>	-
8	45.26	CH	2.50, t, 1H	<b>38.89</b>	<b>2.82, t, 1H</b>
9	50.04	CH	1.40-1.97, m, 1H	49.81	1.39-1.90, m, 1H
10	35.55	Q	-	36.67	-
11	21.28	$\text{CH}_2$	1.40-1.97, m, 2H	20.88	1.39-1.90, m, 2H
12	30.06	$\text{CH}_2$	1.40-1.97, m, 2H	38.45	1.39-1.90, m, 2H
13	41.34	Q	-	41.04	-
14	41.46	CH	1.40-1.97, m, 1H	41.97	1.39-1.90, m, 1H
15	32.29	$\text{CH}_2$	1.40-1.97, m, 2H	34.89	1.39-1.90, m, 2H
16	81.30	CH	4.67, m, 1H	81.26	4.65, m, 1H
17	62.45	CH	1.40-1.97, m, 1H	61.01	1.39-1.90, m, 2H
18	61.50	CH	1.40-1.97, m, 1H	50.24	1.39-1.90, m, 2H
19	17.67	$\text{CH}_3$	0.93-1.22, m, 3H	18.29	0.78-1.36, m, 3H
20	16.78	$\text{CH}_3$	0.93-1.22, m, 3H	16.78	0.78-1.36, m, 3H
21	14.86	$\text{CH}_3$	0.93-1.22, m, 3H	14.86	0.78-1.36, m, 3H
22	109.67	Q	-	109.96	-
23	30.68	$\text{CH}_2$	1.40-1.97, m, 2H	30.67	1.39-1.90, m, 2H
24	27.70	$\text{CH}_2$	1.40-1.97, m, 2H	27.87	1.39-1.90, m, 2H
25	38.47	$\text{CH}_2$	1.40-1.97, m, 2H	30.67	1.39-1.90, m, 2H
26	67.15	$\text{CH}_3$	3.43, d, 2H	67.13	3.46, d, 2H
27	17.50	$\text{CH}_3$	0.93-1.22, m, 3H	19.81	0.78-1.36, m, 3H
28	21.59	$\text{CH}_3$	2.03, s, 3H	21.68	2.02, s, 3H
29	170.61	Q	-	170.69	-

Implied multiplicities of the carbons were determined from the DEPT experiment.

\* Hak-1

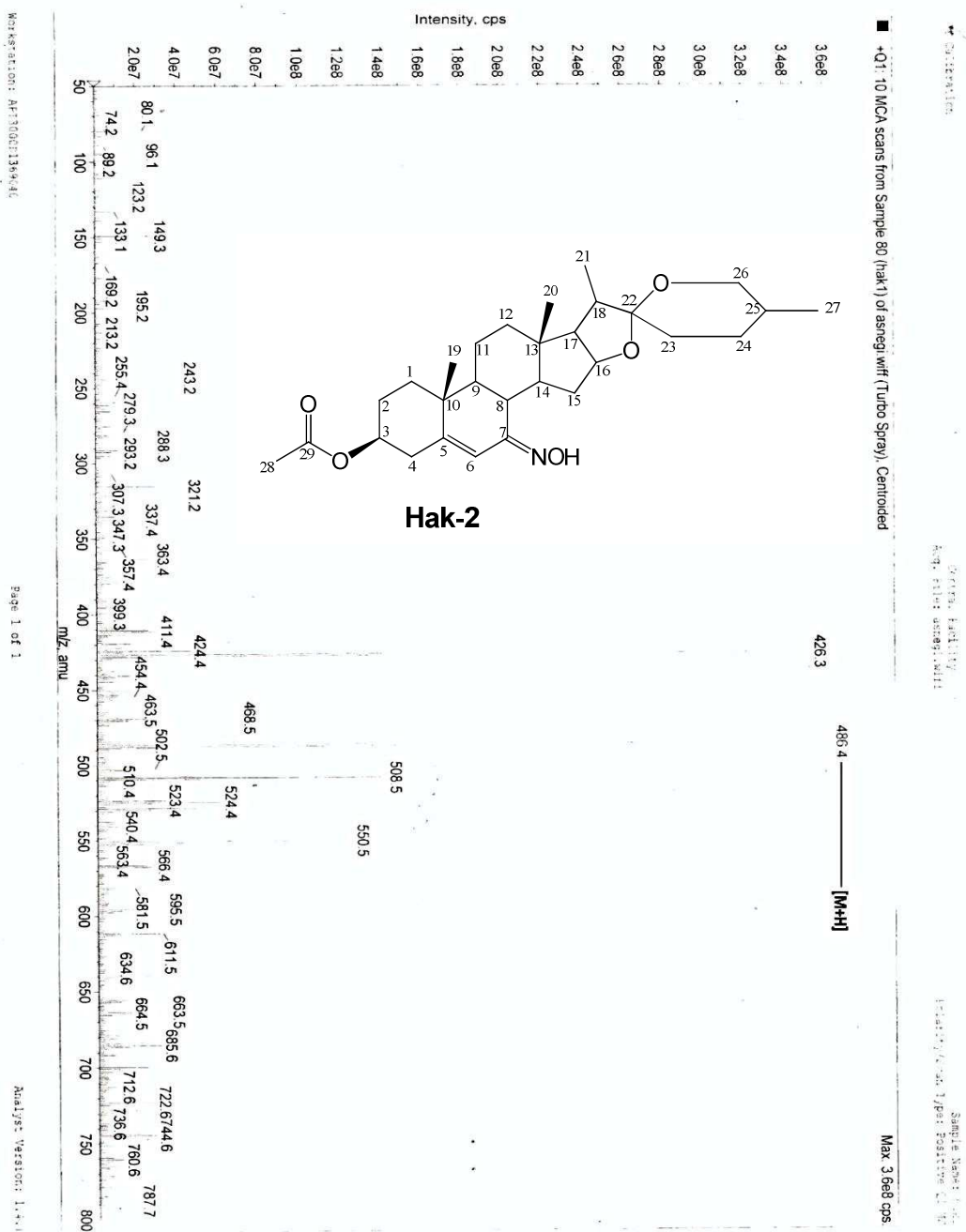


Fig. 5.26: ESI-MS spectrum of Hak-2 in MeOH

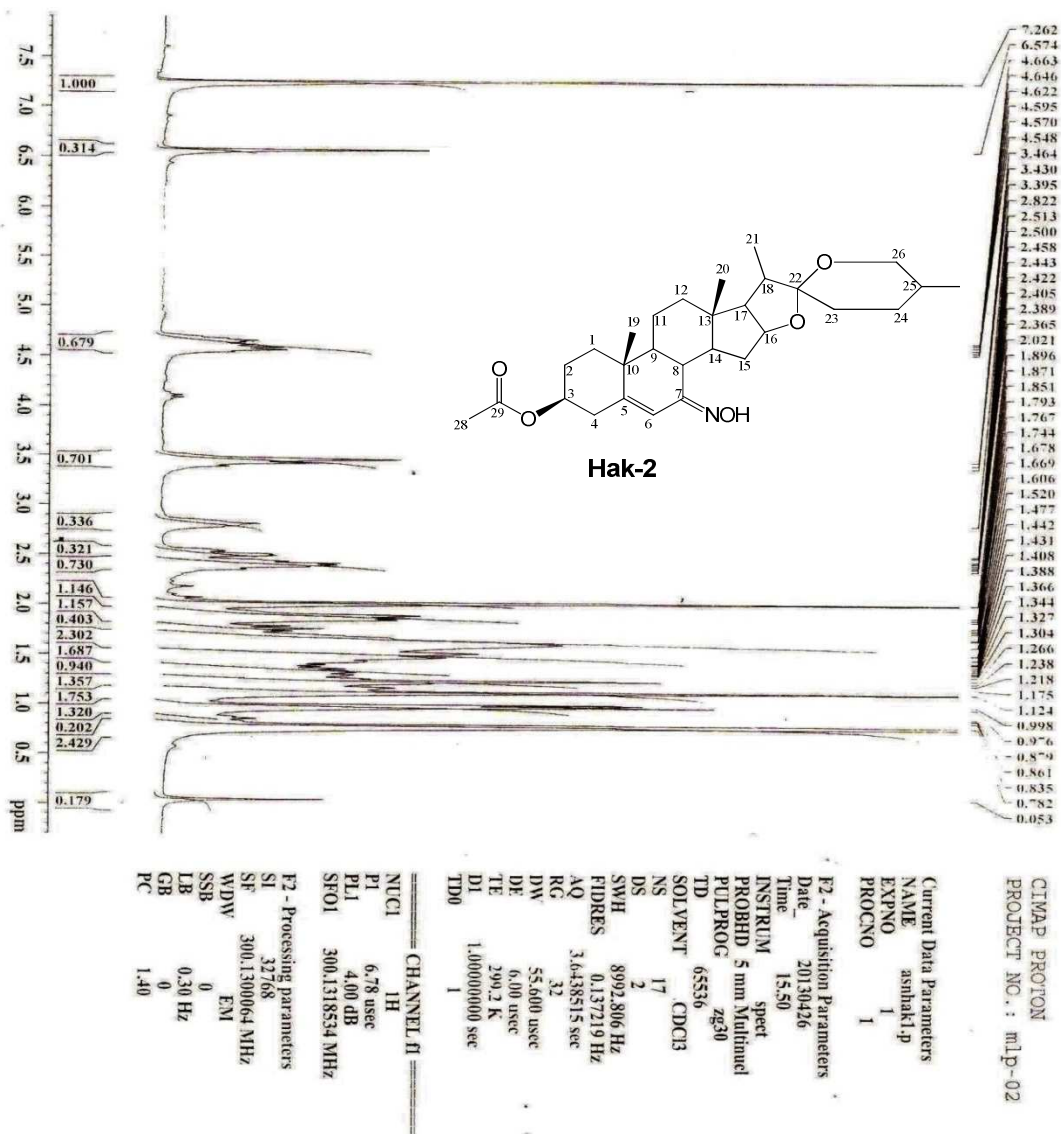


Fig. 5.27:  $^1\text{H}$  NMR spectrum of Hak-2 in  $\text{CDCl}_3$

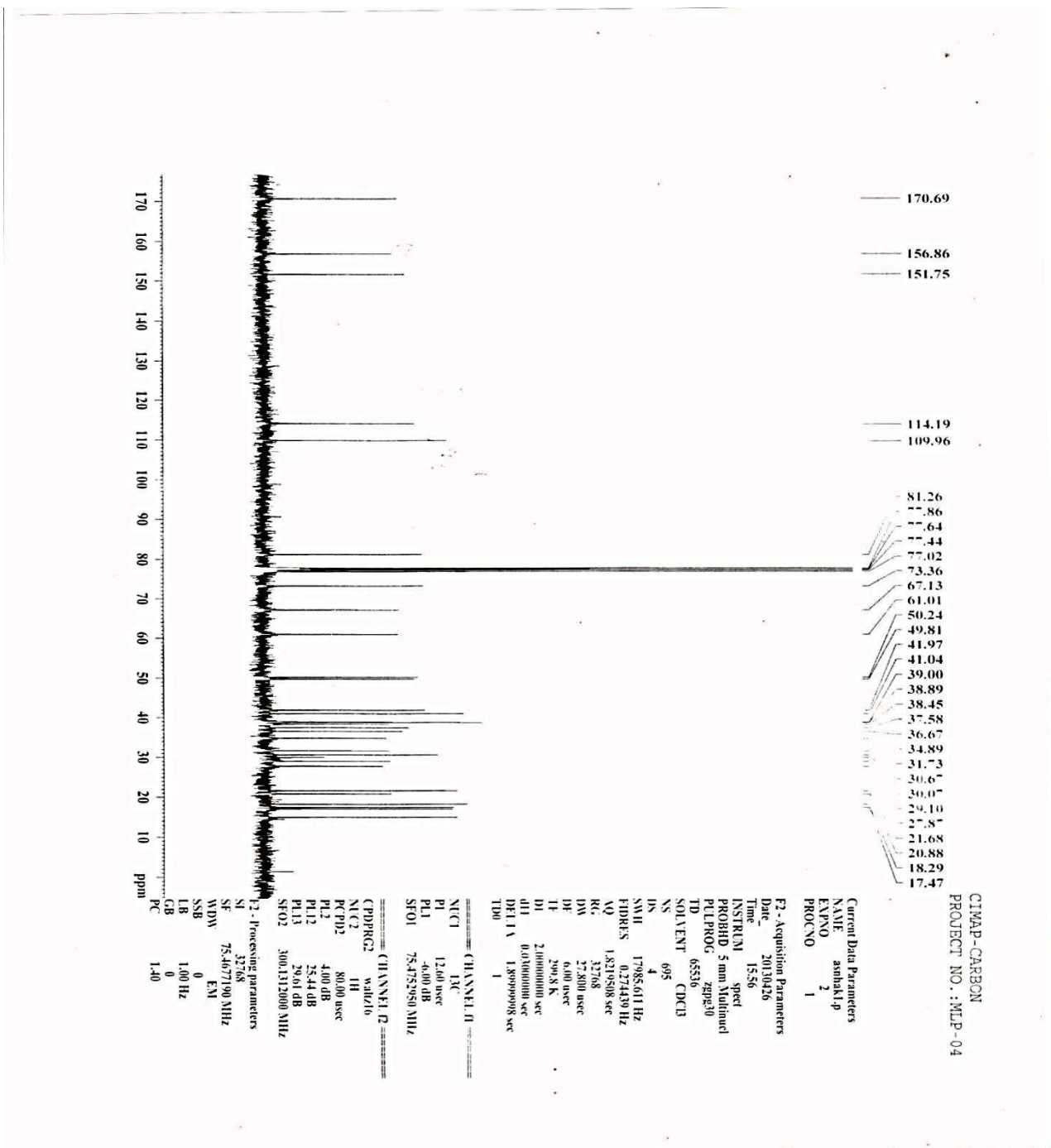


Fig. 5.28:  $^{13}\text{C}$  NMR spectrum of Hak-2 in  $\text{CDCl}_3$

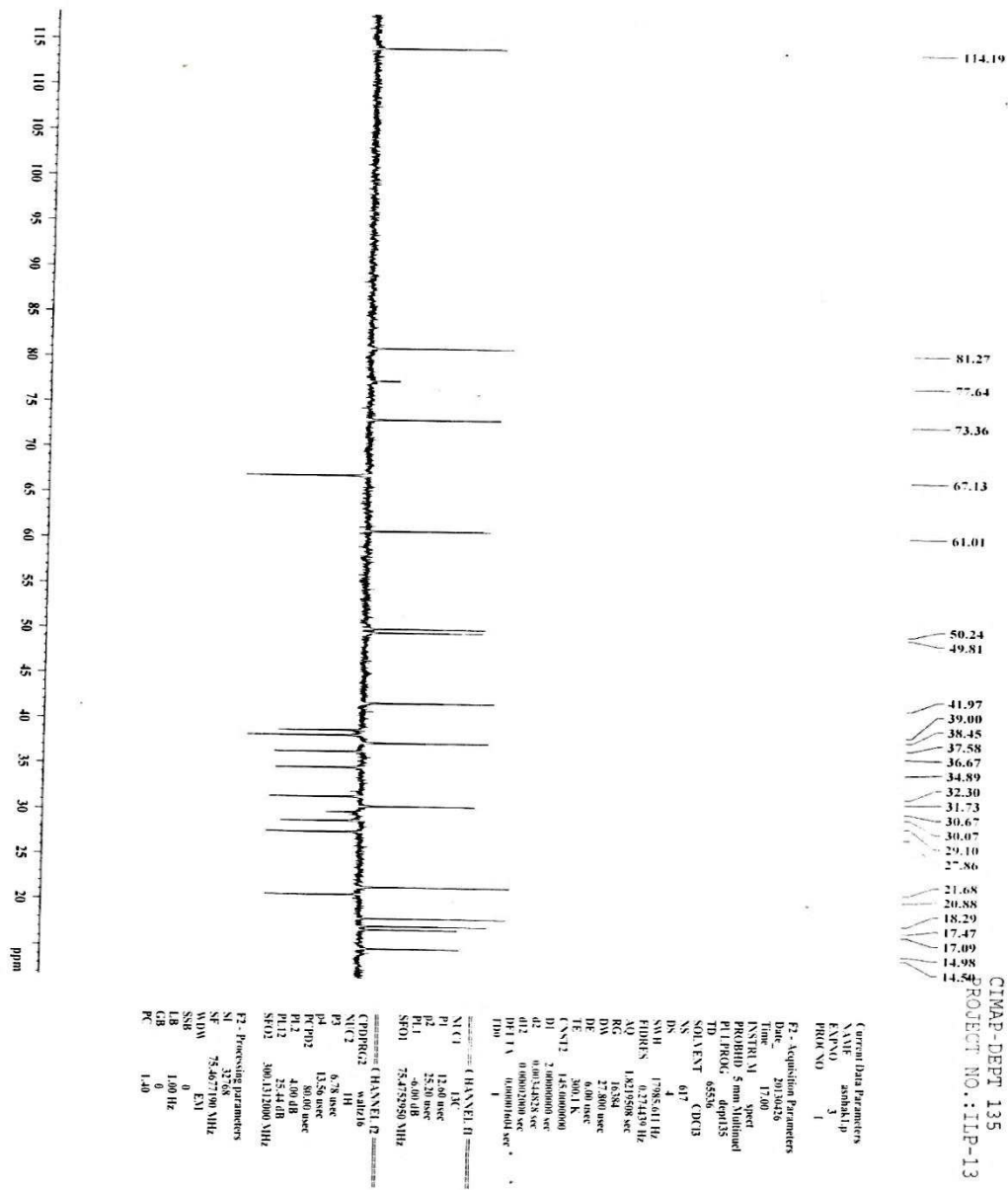
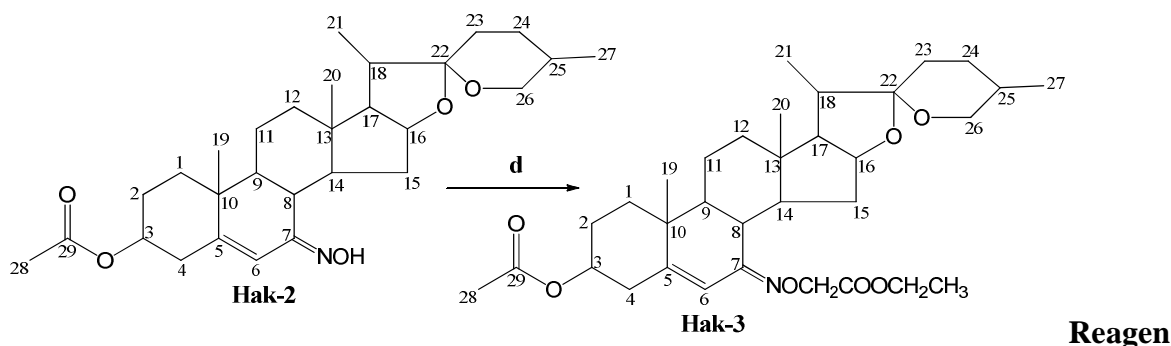


Fig. 5.29: DEPT spectrum of Hak-2 in CDCl<sub>3</sub>

### 4.9.3. Synthesis and characterisation of (22 $\beta$ ,25R)-3 $\beta$ -Acetoxy-spirost-5-en-3 $\beta$ -yl-7-(ethyl-2'-acetate)-ketoxime (Hak-3)

Several new 7-oxime esters of diosgenin were prepared from the reaction of Hak-2 with iodo/bromoester chains and benzy bromide using potassium carbonate ( $K_2CO_3$ ) in dried acetone. The new analogues prepared included Hak-3, Hak-4, Hak-5, Hak-6, Hak-7, Hak-8 and Hak-9.



**ts and conditions:** d)  $K_2CO_3$ , dried Acetone, Ethyl-2-iodoethanoate, reflux at 80 - 100°C, 2hrs

Hak-3 (82 mg, 82%) was obtained as white crystals (melting point 143 - 146°C). The ESI-MS fragment ions 572.3  $[M+H]^+$ , 594.4  $[M+Na]^+$  confirm the molecular formula  $C_{33}H_{49}NO_7$  (571). The  $^1H$  NMR signals at  $\delta_H$  2.03 (s) and 2.51 (t) were assigned to methyl protons of acetate at C-28 and methine proton at C-8, chemical shifts at  $\delta_H$  3.36 (m, 2H,  $OCH_2$ ) and 4.24 (d, 2H,  $OCH_2$  in 2'- $CH_2$ ) correspond to oxymethylene protons of ester and C-2' respectively, while the signals at  $\delta_H$  3.45 (m) and 4.43 (bs) indicated the presence of oxymethylene protons at C-26 and oxymethine proton at C-3 [Fig. 5.30].  $^{13}C$  NMR [Fig. 5.31] and DEPT carbon resonances [Fig. 5.32] of the compound were similar to 7-ketoxime, Hak-2. The changes were signals at  $\delta_C$  157.70 (C-7), 60.86 ( $OCH_2$  of ester) and 61.51 (C-2'), ester chain [Table 4.78]. Hence, the structure of Hak-3 was elucidated to be (22 $\beta$ ,25R)-3 $\beta$ -Acetoxy-spirost-5-en-3 $\beta$ -yl-7-(ethyl-2'-acetate)-ketoxime. The spectroscopic data below highlight the difference between Hak-3 and Hak-2

$^1H$  NMR ( $CDCl_3$ ): 3.36 (m, 2H,  $OCH_2$  of ester), 4.24 (d, 2H,  $OCH_2$ , 2'- $CH_2$ )

$^{13}C$  NMR ( $CDCl_3$ ): 60.86 ( $OCH_2$  of ester), 61.51 (C-2') and 170.69 (ester) [Table 4.77;

Figs: 5.30 -5.32]; IR (KBR,  $cm^{-1}$ ): 2931 (C-H), 1723 (C=O), 1643 (C=C), 1341 (C-O)

**Table 4.78:** Comparison of  $^{13}\text{C}$  and  $^1\text{H}$  NMR data of Hak-2 and Hak-3

Assignment	$^{13}\text{C}$	Multiplicity	$^1\text{H}$ , Multiplicity	$^{13}\text{C}$	$^1\text{H}$
1	29.10	$\text{CH}_2$	1.39-1.90, m, 2H	29.21	1.39-1.90, m, 2H
2	36.58	$\text{CH}_2$	1.39-1.90, m, 2H	37.57	1.39-1.90, m, 2H
3	73.36	CH	4.55, m, 1H	73.20	4.43, m, 1H
4	39.00	$\text{CH}_2$	1.39-1.90, m, 2H	39.11	1.39-1.90, m, 2H
5	151.75	Q	-	153.33	-
6	114.96	CH	6.57, s, 1H	114.48	6.54, s, 1H
7	156.86	$\text{CH}_2$	-	157.70	-
8	38.89	CH	2.82, t, 1H	38.81	2.51, t, 1H
9	49.81	CH	1.39-1.90, m, 1H	49.85	1.39-1.90, m, 1H
10	36.67	Q	-	36.61	-
11	20.88	$\text{CH}_2$	1.39-1.90, m, 2H	20.94	1.39-1.90, m, 2H
12	38.45	$\text{CH}_2$	1.39-1.90, m, 2H	38.42	1.39-1.90, m, 2H
13	41.04	Q	-	41.11	-
14	41.97	CH	1.39-1.90, m, 1H	41.96	1.39-1.90, m, 1H
15	34.89	$\text{CH}_2$	1.39-1.90, m, 2H	34.92	1.39-1.90, m, 2H
16	81.26	CH	4.66, m, 1H	81.08	4.56, m, 1H
17	61.01	CH	1.39-1.90, m, 1H	61.13	1.39-1.90, m, 1H
18	50.24	CH	1.39-1.90, m, 1H	50.50	1.39-1.90, m, 1H
19	18.29	$\text{CH}_3$	0.78-1.36, m, 3H	18.28	0.78-1.36, m, 3H
20	16.78	$\text{CH}_3$	0.78-1.36, m, 3H	16.78	0.78-1.36, m, 3H
21	14.86	$\text{CH}_3$	0.78-1.36, m, 3H	14.86	0.78-1.36, m, 3H
22	109.96	Q	-	109.58	-
23	30.67	$\text{CH}_2$	1.39-1.90, m, 2H	30.70	1.39-1.90, m, 2H
24	27.87	$\text{CH}_2$	1.39-1.90, m, 2H	27.82	1.39-1.90, m, 2H
25	30.67	CH	1.39-1.90, m, 2H	30.07	1.39-1.90, m, 2H
26	67.13	$\text{CH}_3$	3.46, d, 2H	67.18	3.45, d, 2H
27	19.81	$\text{CH}_3$	0.78-1.36, m, 3H	17.47	0.78-1.36, m, 3H
28	21.68	$\text{CH}_3$	2.03, s, 3H	21.68	2.03, s, 3H
29	170.69	Q	-	170.66	-
1', ester				<b>170.66</b>	-
2'				<b>61.51</b>	<b>4.24, d, 2H</b>
$\text{OCH}_2$ of ester				<b>60.86</b>	<b>3.36, m, 2H</b>

Implied multiplicities of the carbons were determined from the DEPT experiment. \* Hak-2

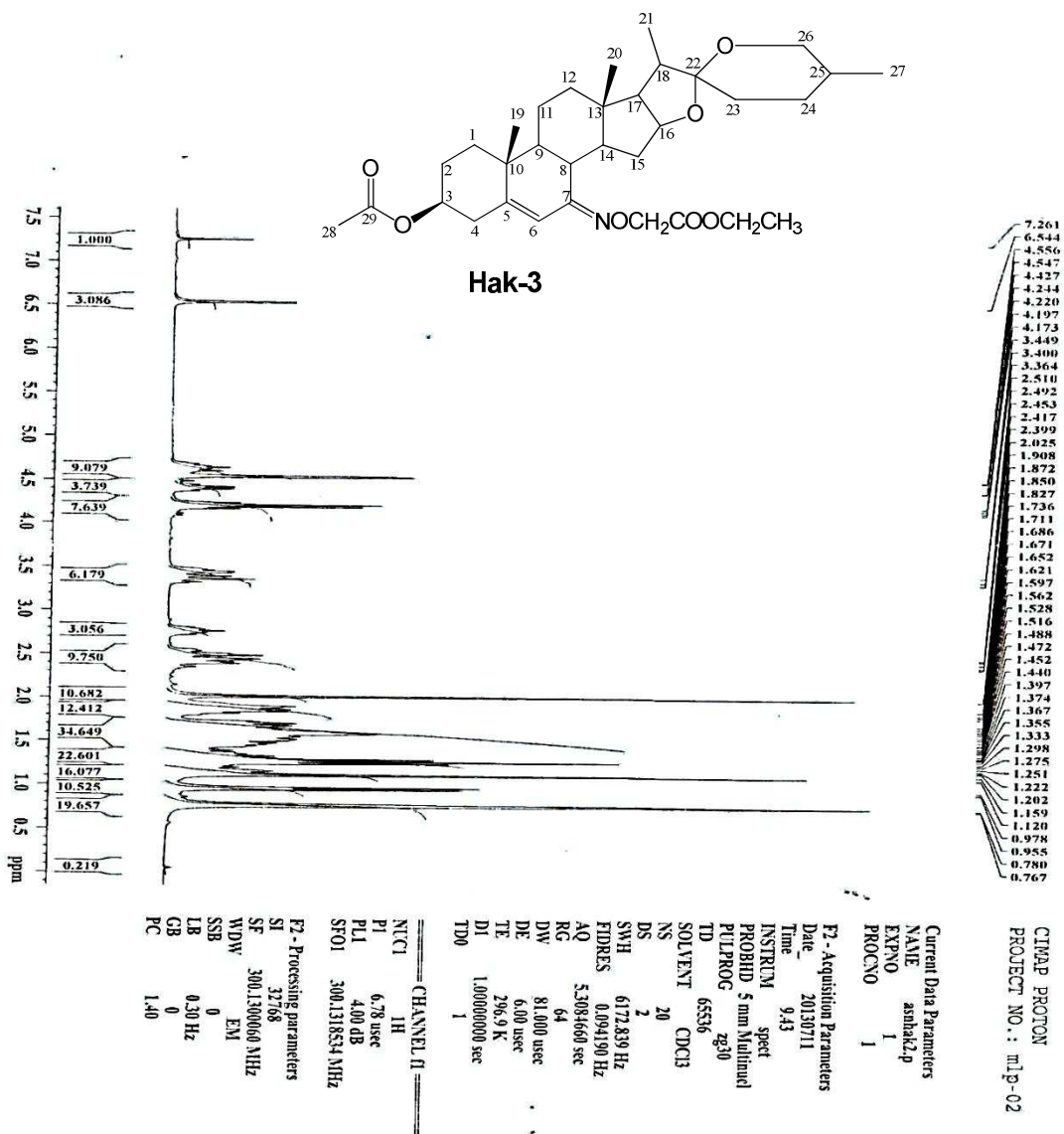
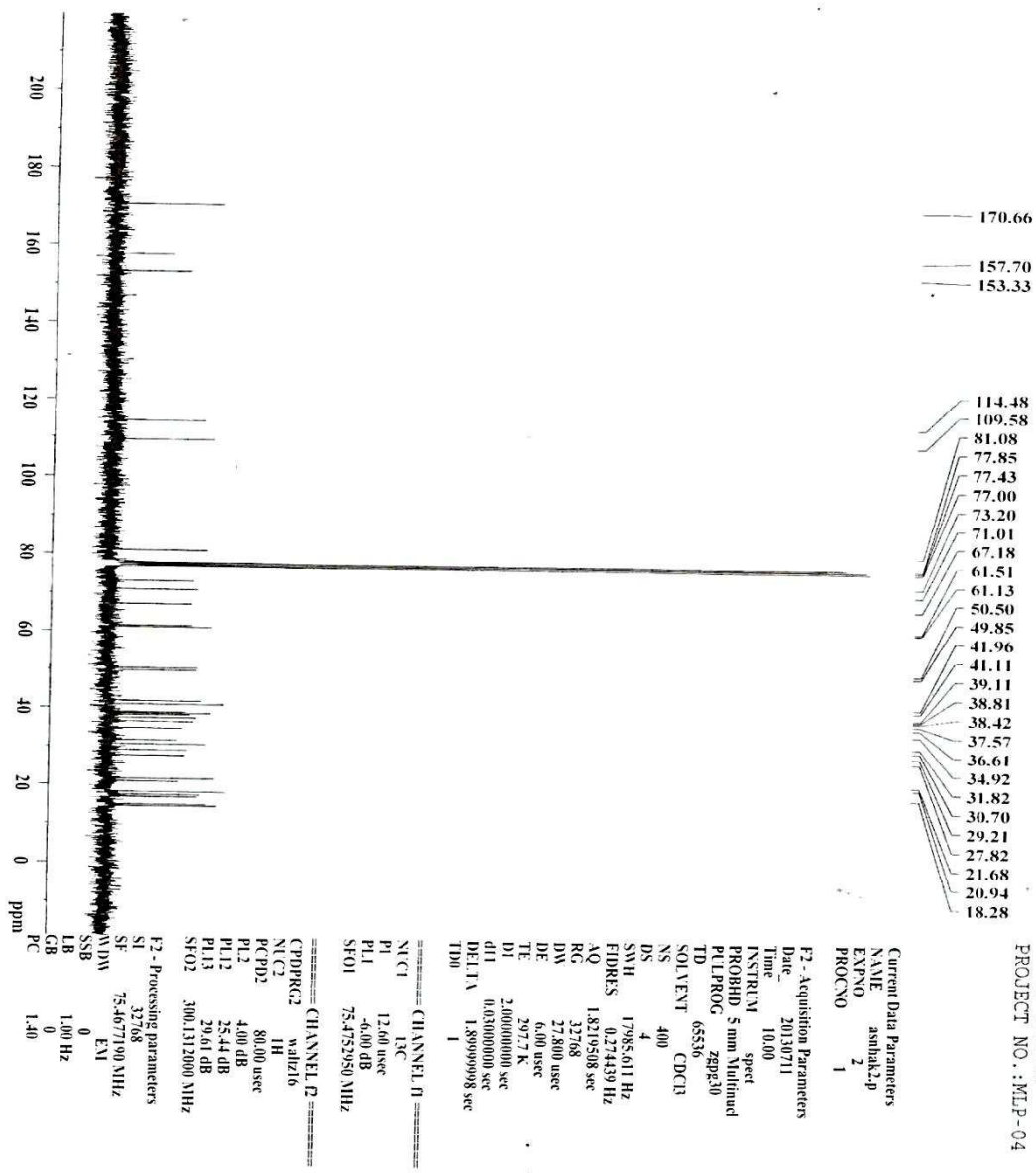


**Fig. 5.30:**  $^1\text{H}$  NMR spectrum of Hak-3 in  $\text{CDCl}_3$





CIMAP-CARBON  
 PROJECT NO.: MLP-04

Fig. 5.31: <sup>13</sup>C NMR spectrum of Hak-3 in CDCl<sub>3</sub>

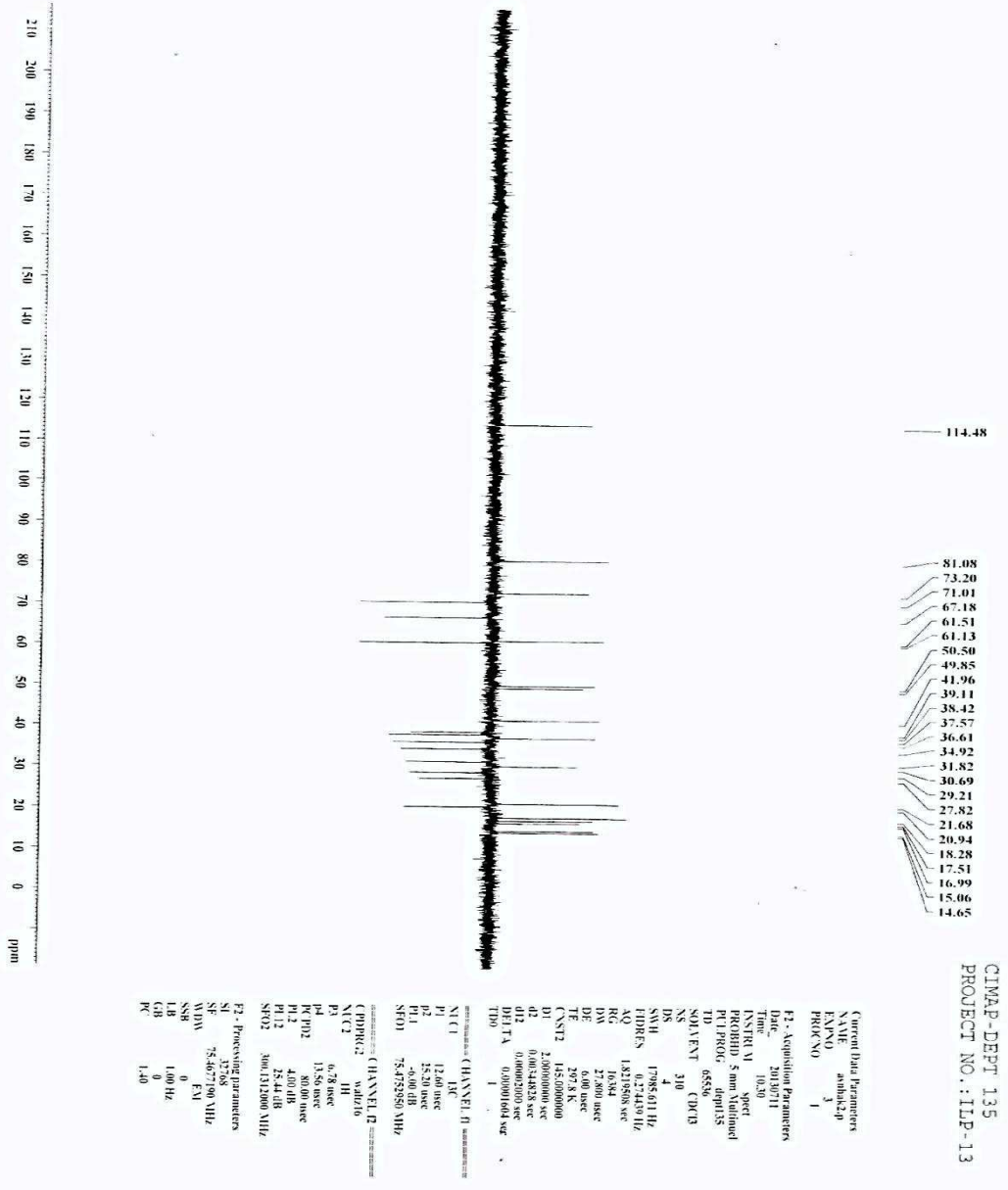
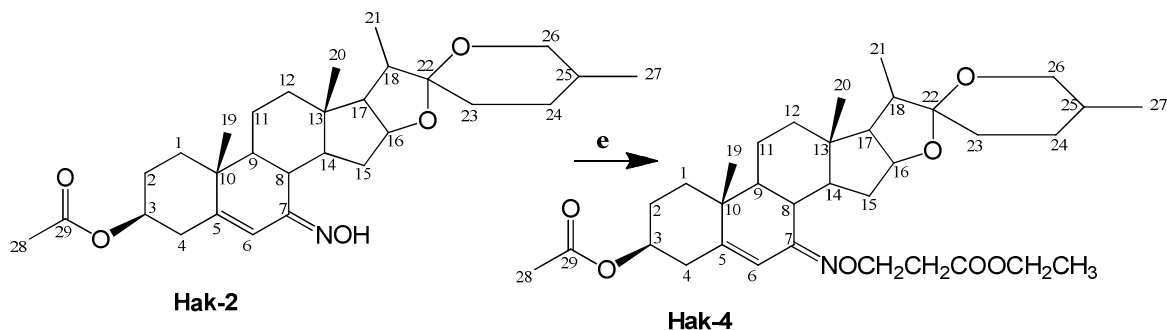


Fig. 5.32: DEPT spectrum of Hak-3 in CDCl<sub>3</sub>

#### 4.9.4. Synthesis and characterisation of (22 $\beta$ ,25R)-3 $\beta$ -Acetoxy-spirost-5-en-3 $\beta$ -yl-7-(ethyl-3'-propanoate)-ketoxime (Hak-4)

Hak-4 was also prepared by using the same method as for Hak-3. The ester chain used was ethyl-3-bromopropanoate.



**Reagents and conditions:** e)  $K_2CO_3$ , dried Acetone, Ethyl-3-bromopropanoate, reflux at 80 - 100°C, 2 hrs

Hak-4 (90 mg, 90%) is a creamy white crystalline solid (melting point 139 - 142°C). The ESI-MS fragmentation peaks at 586  $[M+H]^-$ , 608  $[M+Na]^-$ , 625  $[M+K+H]^+$  gave molecular formula  $C_{34}H_{51}NO_7$  (585) [Fig. 5.33]. The  $^1H$  NMR signals at  $\delta_H$  2.01 (s) and 2.41 (t) correspond to methyl protons of acetate and esters, and methine proton at C-8, while the proton signals at  $\delta_H$  3.34 (m, 2H,  $OCH_2$ ) and 4.15 (m, 2H,  $OCH_2$ ) showed the presence of oxymethylene protons of ester and oxime at C-3 $^1$  respectively. Methylene and methine protons of oxygenated carbons at C-26 and C-3 appeared at  $\delta_H$  3.42 (d) and 4.20 (m) respectively [Fig. 5.34].  $^{13}C$  NMR spectrum [Fig. 5.35] revealed thirty four carbon resonances and the carbons were sorted by DEPT spectra [Fig. 5.36] into six methyl, twelve methylene, nine methine and seven quaternary carbon resonances. The spectroscopic data of Hak-4 were also identical to its 7-keto derivative except the coupling of ester chain at position 7 [ $\delta_C$  36.55 (C-2'), 61.57 ( $OCH_2$  of ester), 61.57 (C-3') and 173.31 (C-1', ester)]. The  $^{13}C$  and  $^1H$  NMR data of Hak-4 and Hak-2 were shown in Table 4.79. Therefore, the structure of Hak-4 was confirmed to be (22 $\beta$ ,25R)-3 $\beta$ -Acetoxy-spirost-5-en-3 $\beta$ -yl-7-(ethyl-3'-propanoate)-ketoxime.

**Table 4.79:** Comparison of  $^{13}\text{C}$  and  $^1\text{H}$  NMR data of Hak-2 and Hak-4

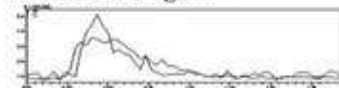
Assignment	* $^{13}\text{C}$	Multiplicity	* $^1\text{H}$ , Multiplicity	$^{13}\text{C}$	$^1\text{H}$
1	29.10	$\text{CH}_2$	1.39-1.90, m, 2H	29.21	1.39-1.86, m, 2H
2	36.58	$\text{CH}_2$	1.39-1.90, m, 2H	37.57	1.39-1.86, m, 2H
3	73.36	CH	4.55, m, 1H	73.24	4.20, m, 1H
4	39.00	$\text{CH}_2$	1.39-1.90, m, 2H	38.09	1.39-1.86, m, 2H
5	151.75	Q	-	153.08	-
6	114.96	CH	6.57, s, 1H	114.74	6.52, s, 1H
7	156.86	$\text{CH}_2$	-	156.90	-
8	38.89	CH	2.82, t, 1H	38.83	2.41, t, 1H
9	49.81	CH	1.39-1.90, m, 1H	49.92	1.39-1.86, m, 1H
10	36.67	Q	-	36.61	-
11	20.88	$\text{CH}_2$	1.39-1.90, m, 2H	20.91	1.39-1.86, m, 2H
12	38.45	$\text{CH}_2$	1.39-1.90, m, 2H	38.40	1.39-1.86, m, 2H
13	41.04	Q	-	40.02	-
14	41.97	CH	1.39-1.90, m, 1H	41.92	1.39-1.86, m, 1H
15	34.89	$\text{CH}_2$	1.39-1.90, m, 2H	34.76	1.39-1.86, m, 2H
16	81.26	CH	4.66, m, 1H	81.09	4.56, m, 1H
17	61.01	CH	1.39-1.90, m, 1H	60.03	1.39-1.86, m, 1H
18	50.24	CH	1.39-1.90, m, 1H	50.92	1.39-1.86, m, 1H
19	18.29	$\text{CH}_3$	0.78-1.36, m, 3H	18.26	0.74-1.33, m, 3H
20	16.78	$\text{CH}_3$	0.78-1.36, m, 3H	16.95	0.74-1.33, m, 3H
21	14.86	$\text{CH}_3$	0.78-1.36, m, 3H	14.69	0.74-1.33, m, 3H
22	109.96	Q	-	109.48	-
23	30.67	$\text{CH}_2$	1.39-1.90, m, 2H	34.98	1.39-1.86, m, 2H
24	27.87	$\text{CH}_2$	1.39-1.90, m, 2H	27.81	1.39-1.86, m, 2H
25	30.67	$\text{CH}_2$	1.39-1.86, m, 2H	30.67	1.39-1.86, m, 2H
26	67.13	$\text{CH}_3$	3.46, d, 2H	67.13	3.42, d, 2H
27	19.81	$\text{CH}_3$	0.78-1.36, m, 3H	17.50	0.74-1.33, m, 3H
28	21.68	$\text{CH}_3$	2.03, s, 3H	21.64	2.01, s, 3H
29	170.69	Q	-	170.91	-
1', ester				<b>173.31</b>	-
2'				<b>36.55</b>	<b>1.18-2.41, m, 2H</b>
3'				<b>61.57</b>	<b>4.15, d, 2H</b>
$\text{OCH}_2$ of ester				<b>61.57</b>	<b>3.34, m, 2H</b>

Implied multiplicities of the carbons were determined from the DEPT experiment. \* Hak-2

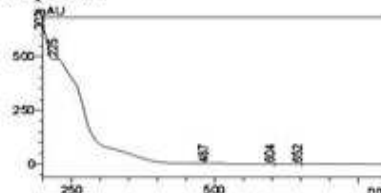
ANALYTICAL TEST REPORT

Sample Information for Direct Mass Analysis of Isolates/synthetic molecule  
Sample Code : ASN-HAK-5  
Solubility : MeOH  
Name of the Scientist : Dr.A S Negi  
Project Code: MLP-02  
Mass Range: 100-800

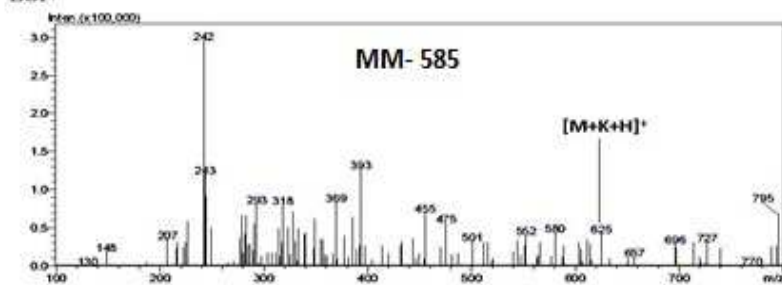
Mass chromatogram



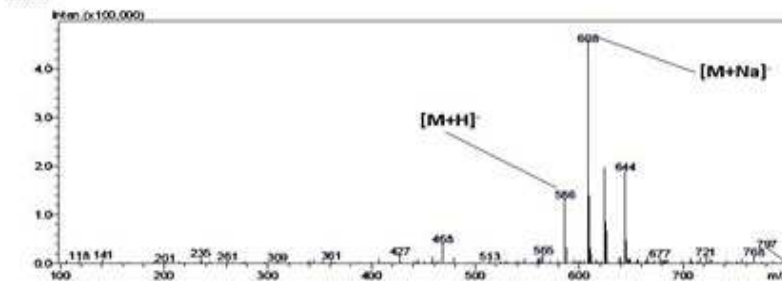
UV-Spectra



ESI+



ESI-



File Path-D:\Direct Mass report- Aug 2010\ASN-HAK-5.doc

Oct 14, 2013

[Dr. Karuna Shanker]

Fig. 5.33: Mass spectrum of Hak-4 in MeOH

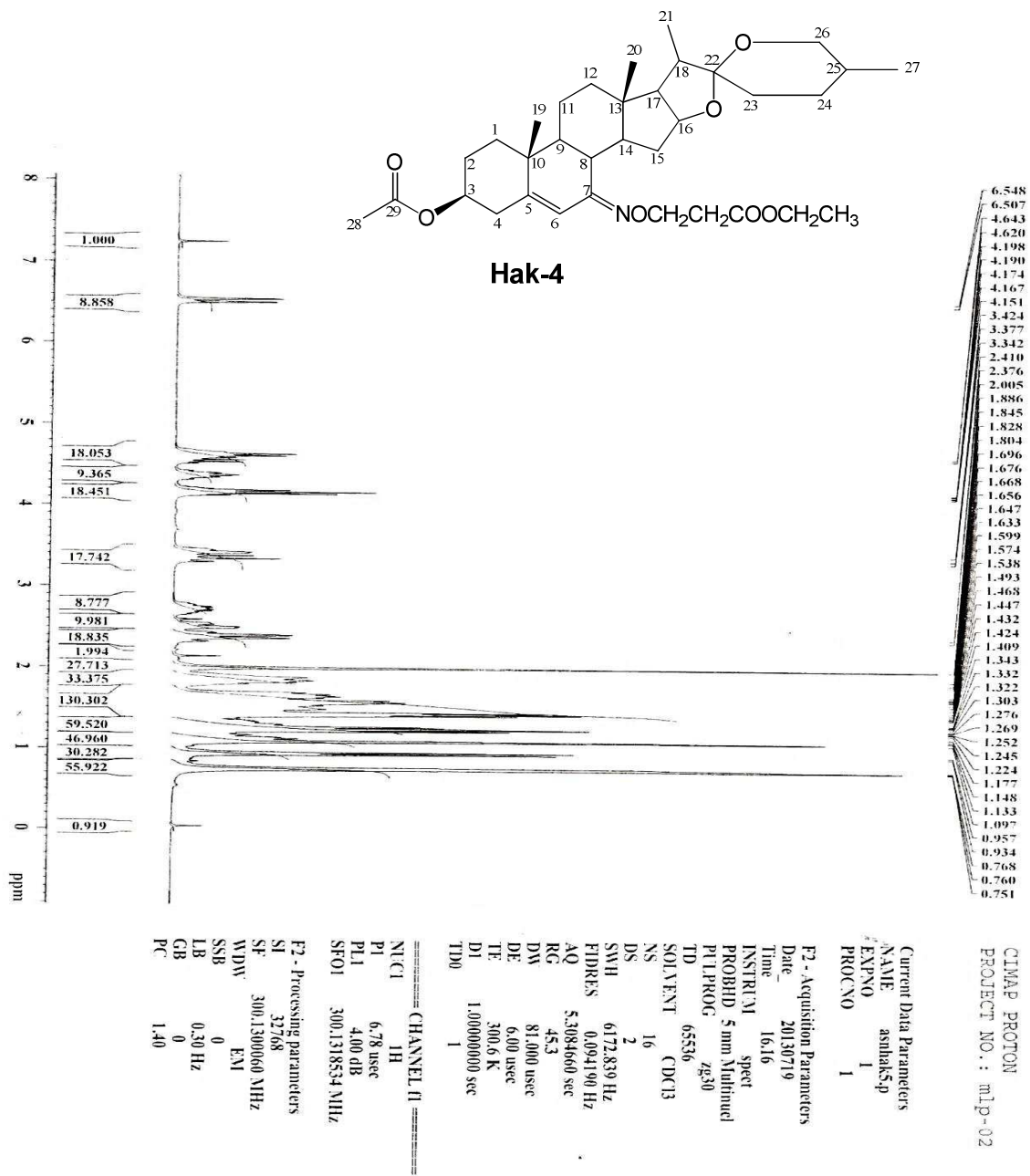


**Fig. 5.34:**  $^1\text{H}$  NMR spectrum of Hak-4 in  $\text{CDCl}_3$

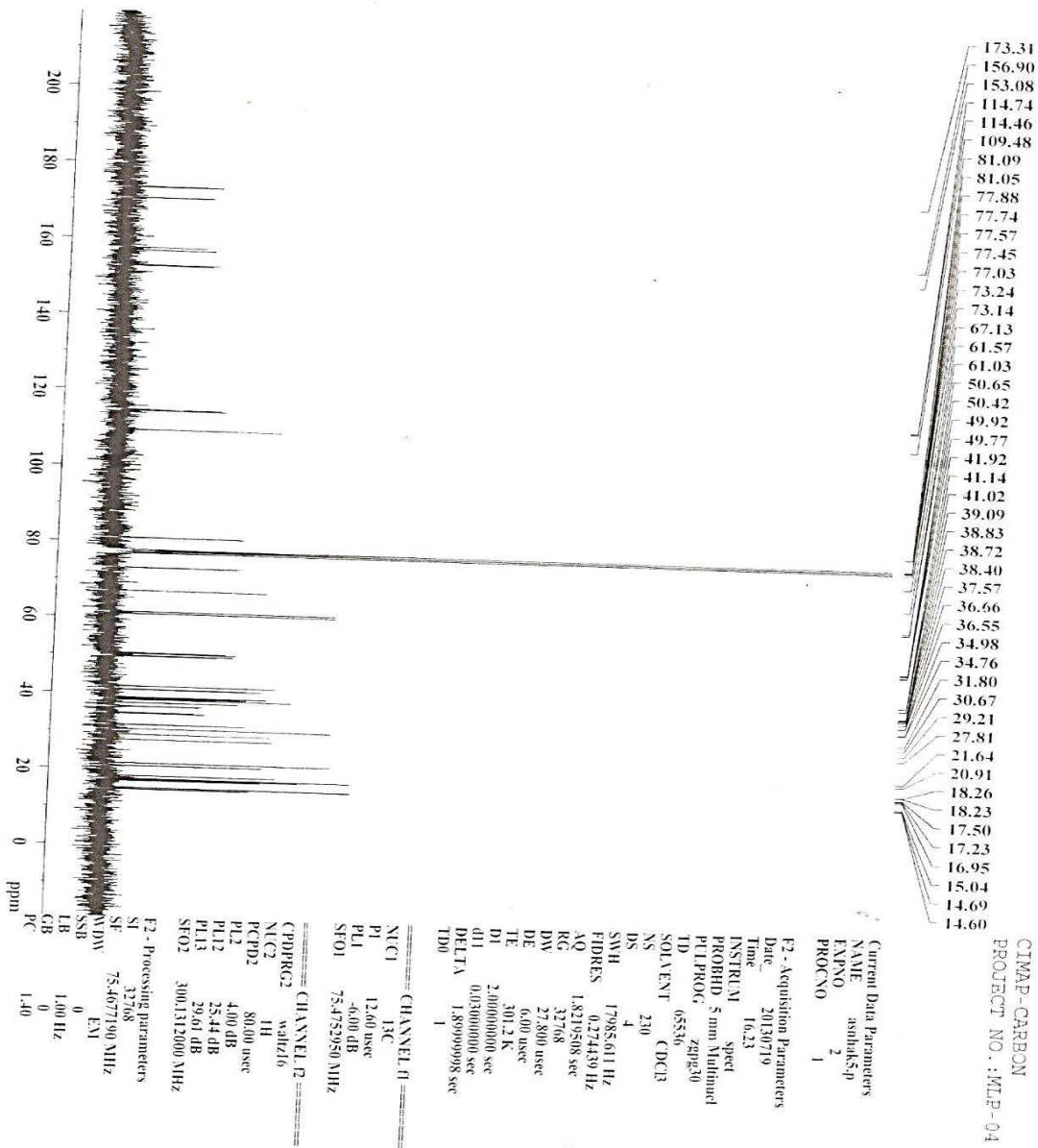
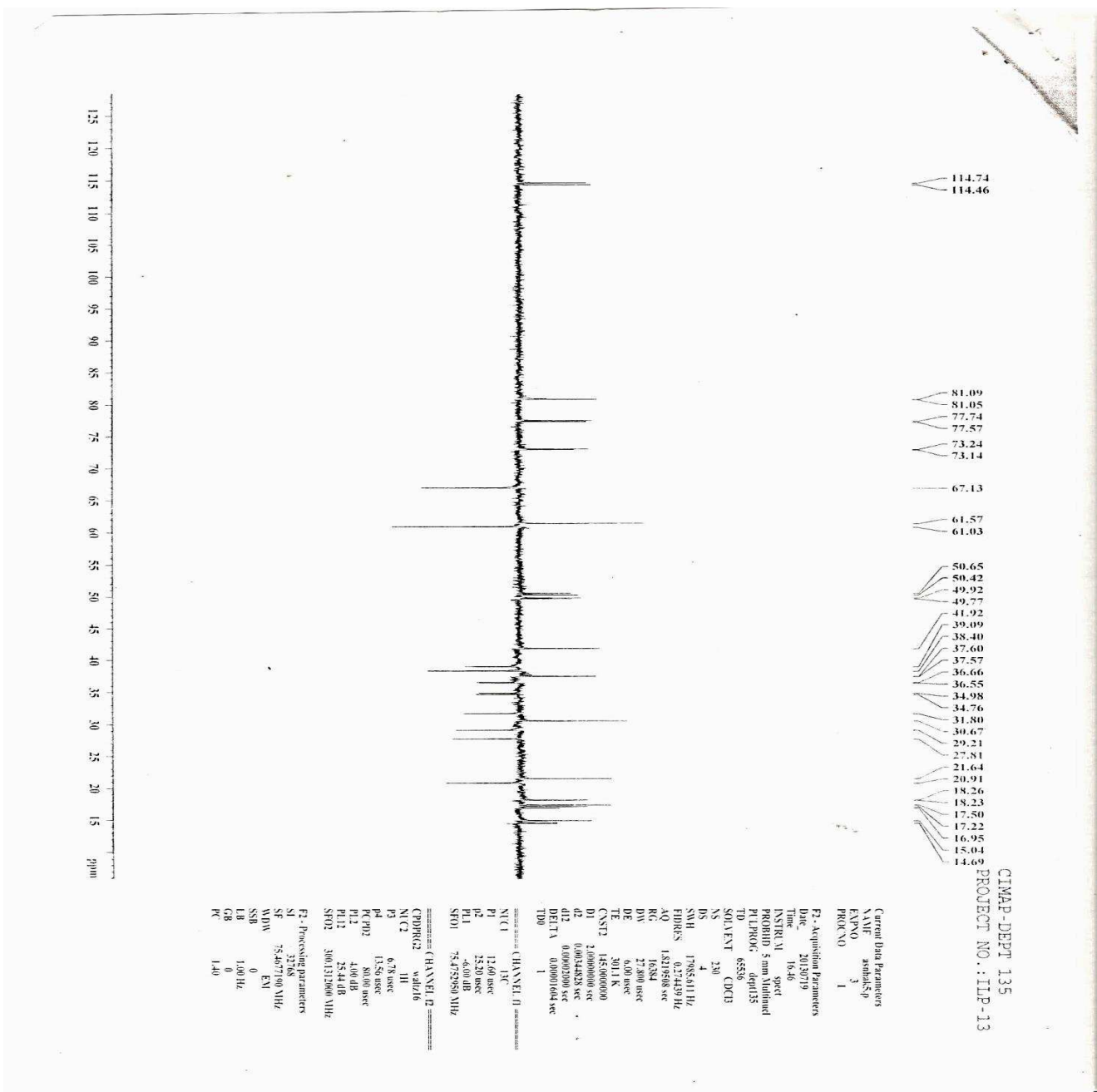


Fig. 5.35: <sup>13</sup>C NMR spectrum of Hak-4 in CDCl<sub>3</sub>

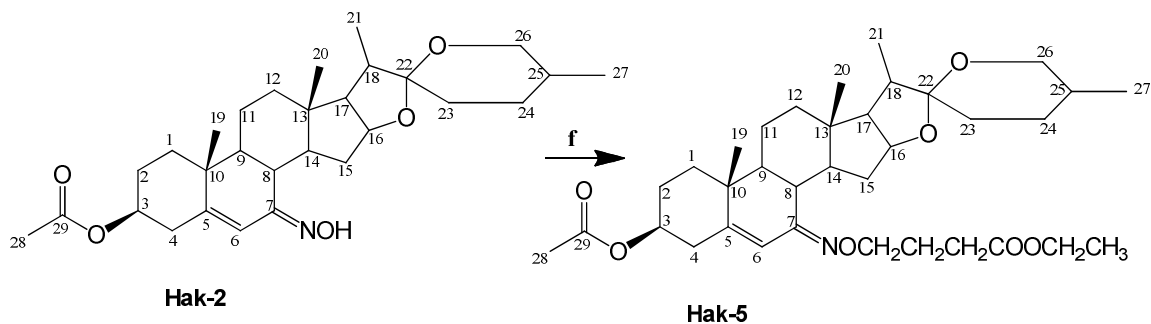


**Fig. 5.36:** DEPT spectrum of Hak-4 in CDCl<sub>3</sub>



#### 4.9.5. Synthesis and characterisation of (22 $\beta$ ,25R)-3 $\beta$ -Acetoxy-spirost-5-en-3 $\beta$ -yl-7-(ethyl-4'-butyrate)-ketoxime (Hak-5)

Hak-5 was also prepared by using long ester chain, ethyl-4-bromobutyrate. The same method was employed as for Hak-3.



**Reagents and conditions:** f)  $K_2CO_3$ , dried Acetone, Ethyl-4-bromobutyrate, reflux at 80 - 100°C, 3 hrs

Hak-5 (82 mg, 82%) was obtained as a white crystalline solid which has a melting point of 145 - 148°C. The ESI-MS fragment ions at 242, 599  $[M]^+$ , 623  $[M+Na+H]^+$ , 640  $[M+K+2H]^+$  confirm the molecular formula  $C_{35}H_{53}NO_7$  (599) [Fig. 5.37]. The  $^1H$  NMR chemical shifts at  $\delta_H$  0.78-1.13 and 2.03 (s) are characteristics of angular methyl protons, and methyl protons of acetate and esters, while the proton signals at  $\delta_H$  3.34 (m, 2H,  $OCH_2$ ) and 4.05 (m, 2H,  $OCH_2$ ) indicated the presence of oxymethylene protons of ester and oxime at C-4' respectively. Methine proton at C-16 appeared at 4.64 (bd), while the proton signals at  $\delta_H$  3.45 (d) and 4.14 (m) were assigned to methylene and methine protons of oxygenated carbons at C-26 and C-3 respectively [Fig. 5.38].  $^{13}C$  NMR spectrum [Fig. 5.39] revealed thirty five carbon resonances which were sorted by DEPT spectra [Fig. 5.40] into six methyl, thirteen methylene, nine methine and seven quaternary carbon resonances. The spectroscopic data of Hak-5 were similar to spirostene skeleton except at position 7 where the condensation of ester chain to C-7 occurred [ $\delta_C$  25.23 (C-3'), 31.85 (C-2'), 61.56 ( $OCH_2$  of ester), 61.56 (C-4') and 173.31 (C-1', ester)]. The  $^{13}C$  and  $^1H$  NMR data of Hak-5 and Hak-2 were shown in Table 4.80. The spectroscopic data of Hak-5, compared with its 7-ketoxime analogue led to structural elucidation of Hak-5 to be (22 $\beta$ ,25R)-3 $\beta$ -Acetoxy-spirost-5-en-3 $\beta$ -yl-7-(ethyl-4'-butyrate)-ketoxime.

**Table 4.80:** Comparison of  $^{13}\text{C}$  and  $^1\text{H}$  NMR data of Hak-2 and Hak-5

Assignment	$^{13}\text{C}$	Multiplicity	$^1\text{H}$ , Multiplicity	$^{13}\text{C}$	$^1\text{H}$
1	29.10	$\text{CH}_2$	1.39-1.90, m, 2H	29.23	1.41-1.87, m, 2H
2	36.58	$\text{CH}_2$	1.39-1.90, m, 2H	37.61	1.41-1.87, m, 2H
3	73.36	CH	4.55, m, 1H	73.30	4.14, m, 1H
4	39.00	$\text{CH}_2$	1.39-1.90, m, 2H	39.17	1.41-1.87, m, 2H
5	151.75	Q	-	152.40	-
6	114.96	CH	6.57, s, 1H	114.51	6.45, s, 1H
7	156.86	$\text{CH}_2$	-	156.90	-
8	38.89	CH	2.82, t, 1H	38.80	2.40, t, 1H
9	49.81	CH	1.39-1.90, m, 1H	49.97	1.41-1.87, m, 1H
10	36.67	Q	-	36.67	-
11	20.88	$\text{CH}_2$	1.39-1.90, m, 2H	20.91	1.41-1.87, m, 2H
12	38.45	$\text{CH}_2$	1.39-1.90, m, 2H	38.46	1.41-1.87, m, 2H
13	41.04	Q	-	41.12	-
14	41.97	CH	1.39-1.90, m, 1H	41.99	1.41-1.87, m, 1H
15	34.89	$\text{CH}_2$	1.39-1.90, m, 2H	35.04	1.41-1.87, m, 2H
16	81.26	CH	4.66, m, 1H	81.14	4.64, m, 1H
17	61.01	CH	1.39-1.90, m, 1H	60.69	1.41-1.87, m, 1H
18	50.24	CH	1.39-1.90, m, 1H	50.63	1.41-1.87, m, 1H
19	18.29	$\text{CH}_3$	0.78-1.36, m, 3H	18.33	0.78-1.36, m, 3H
20	16.78	$\text{CH}_3$	0.78-1.36, m, 3H	16.95	0.78-1.36, m, 3H
21	14.86	$\text{CH}_3$	0.78-1.36, m, 3H	14.69	0.78-1.36, m, 3H
22	109.96	Q	-	109.48	-
23	30.67	$\text{CH}_2$	1.39-1.90, m, 2H	35.04	1.41-1.87, m, 2H
24	27.87	$\text{CH}_2$	1.39-1.90, m, 2H	27.85	1.41-1.87, m, 2H
25	30.67	CH	1.39-1.90, m, 2H	31.43	1.41-1.87, m, 2H
26	67.13	$\text{CH}_3$	3.46, d, 2H	67.20	3.45, d, 2H
27	19.81	$\text{CH}_3$	0.78-1.36, m, 3H	17.50	0.78-1.36, m, 3H
28	21.68	$\text{CH}_3$	2.03, s, 3H	21.67	2.03, s, 3H
29	170.69	Q	-	170.91	-
1', ester				<b>173.31</b>	
2'				<b>31.85</b>	<b>1.18-2.40, m, 2H</b>
3'				<b>25.23</b>	<b>1.18-2.40, m, 2H</b>
4'				<b>61.56</b>	<b>4.05, d, 2H</b>
$\text{OCH}_2$ of ester				<b>61.56</b>	<b>3.34, m, 2H</b>

Implied multiplicities of the carbons were determined from the DEPT experiment. \* Hak-2

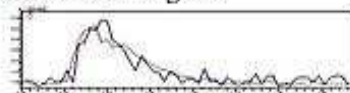
ANALYTICAL TEST REPORT

Sample Information for Direct Mass Analysis of Isolates/synthetic molecule

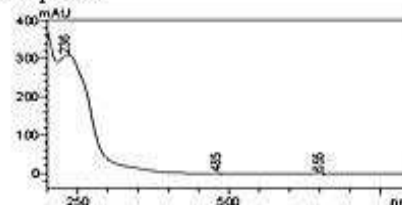
Sample Code : ASN-HAK-7.1  
Solubility : MeOH  
Name of the Scientist : Dr. A S Negi

Project Code: MLP-02  
Mass Range: 100-800

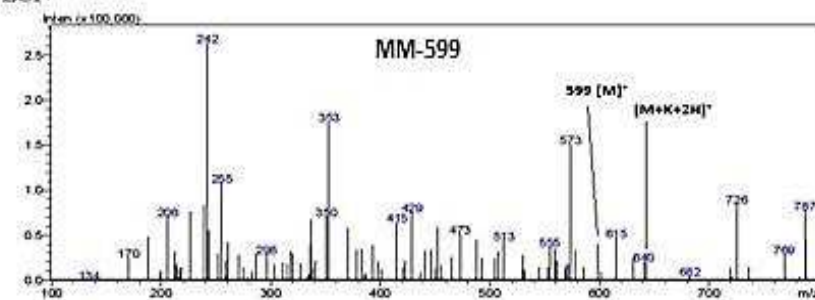
Mass chromatogram



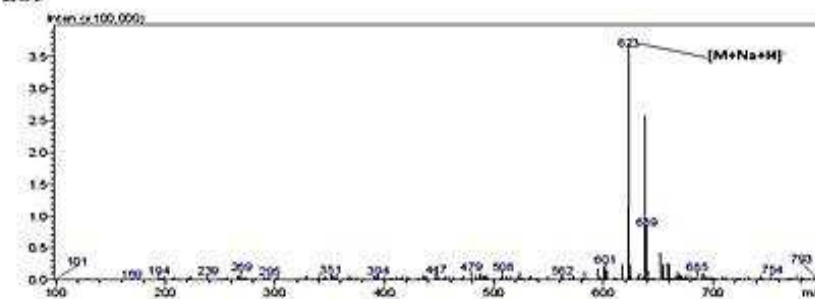
UV-Spectra



ESI+



ESI-



File Path:D:\Direct Mass report- Aug 2010\ASN-HAK-7.1.doc

Oct 14, 2013

[Dr. Karuna Shanker]

Fig. 5.37: Mass spectrum of Hak-5 in MeOH

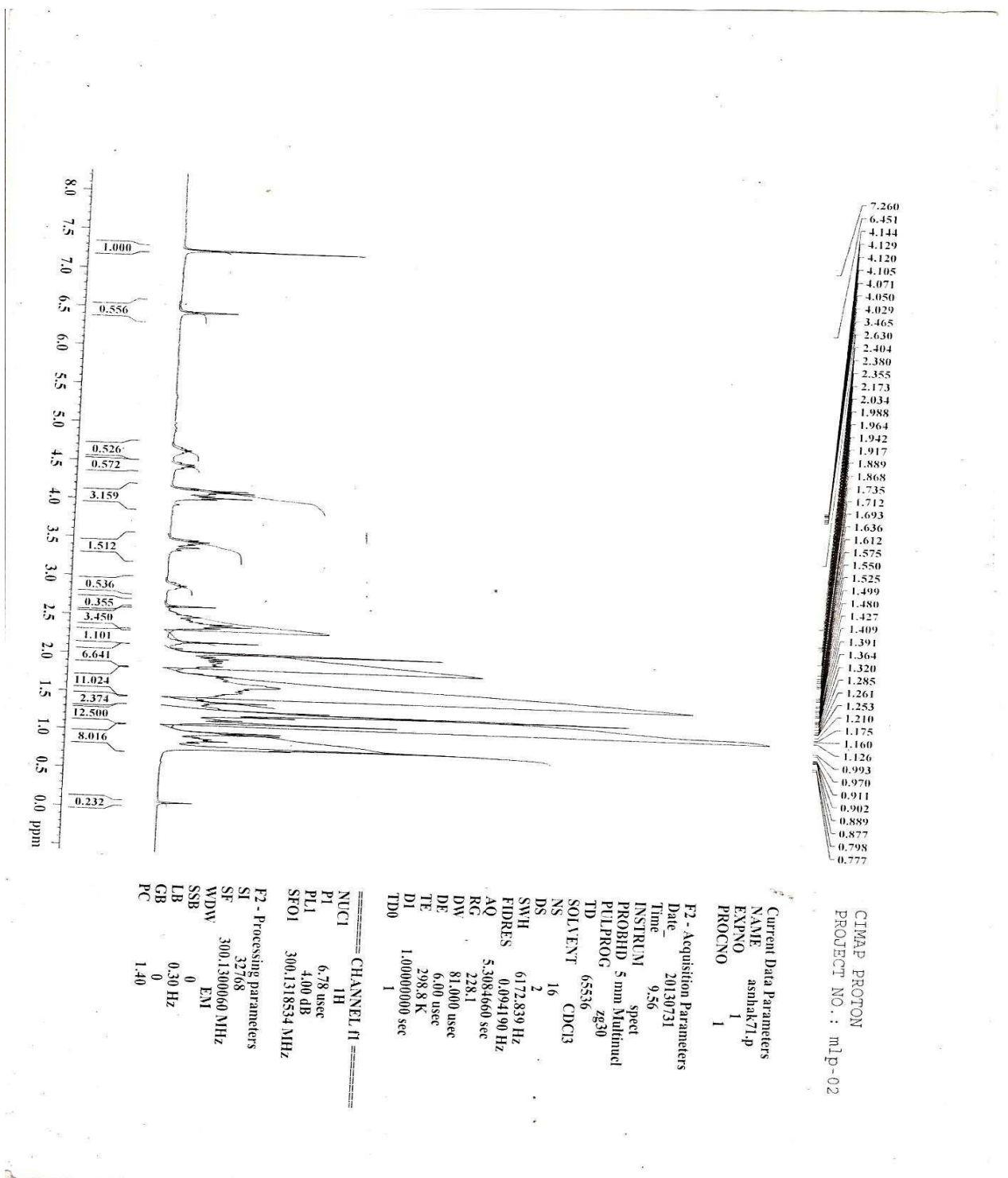


Fig. 5.38:  $^1\text{H}$  NMR spectrum of Hak-5 in  $\text{CDCl}_3$

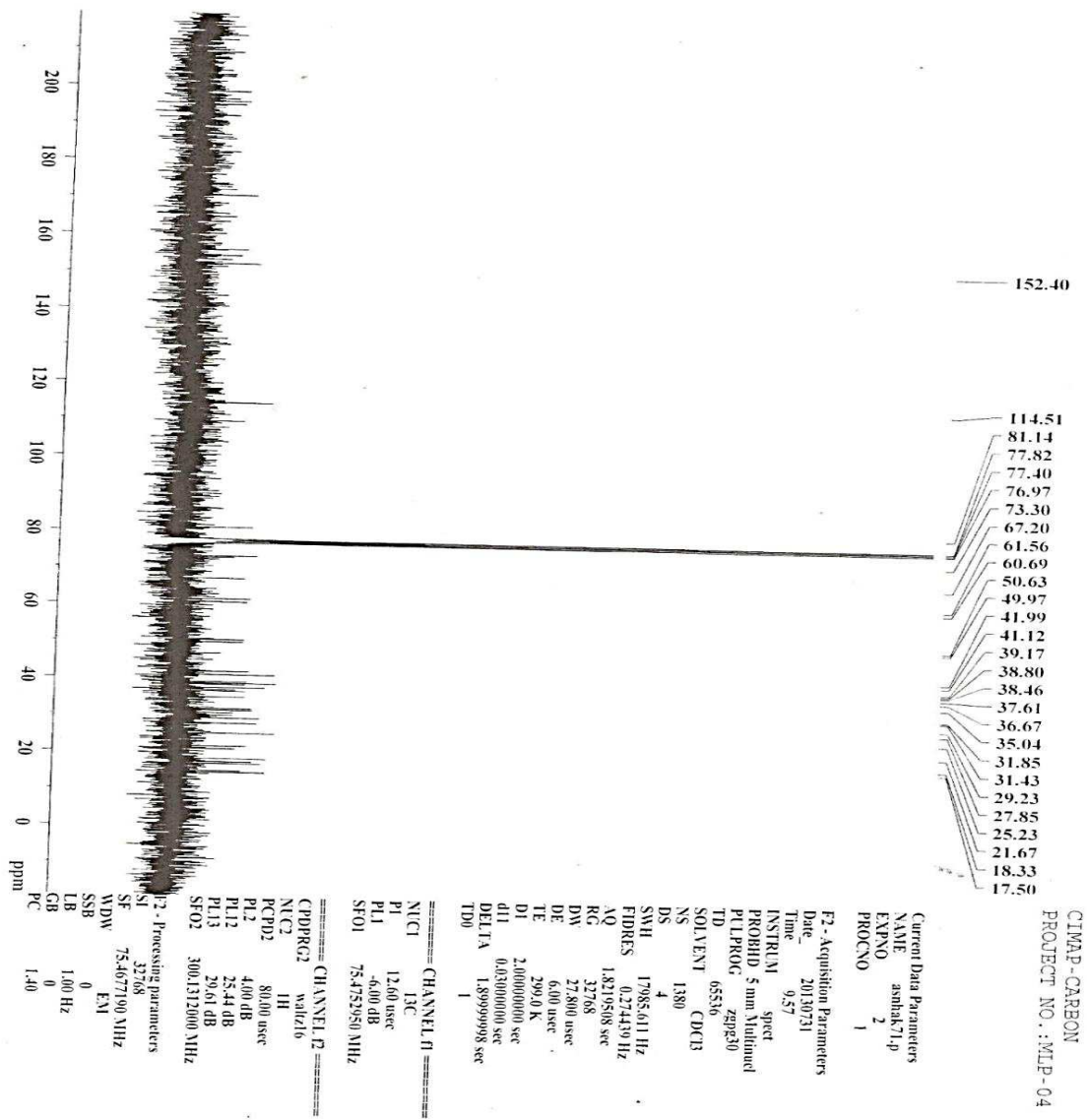


Fig. 5.39:  $^{13}\text{C}$  NMR spectrum of Hak-5 in  $\text{CDCl}_3$

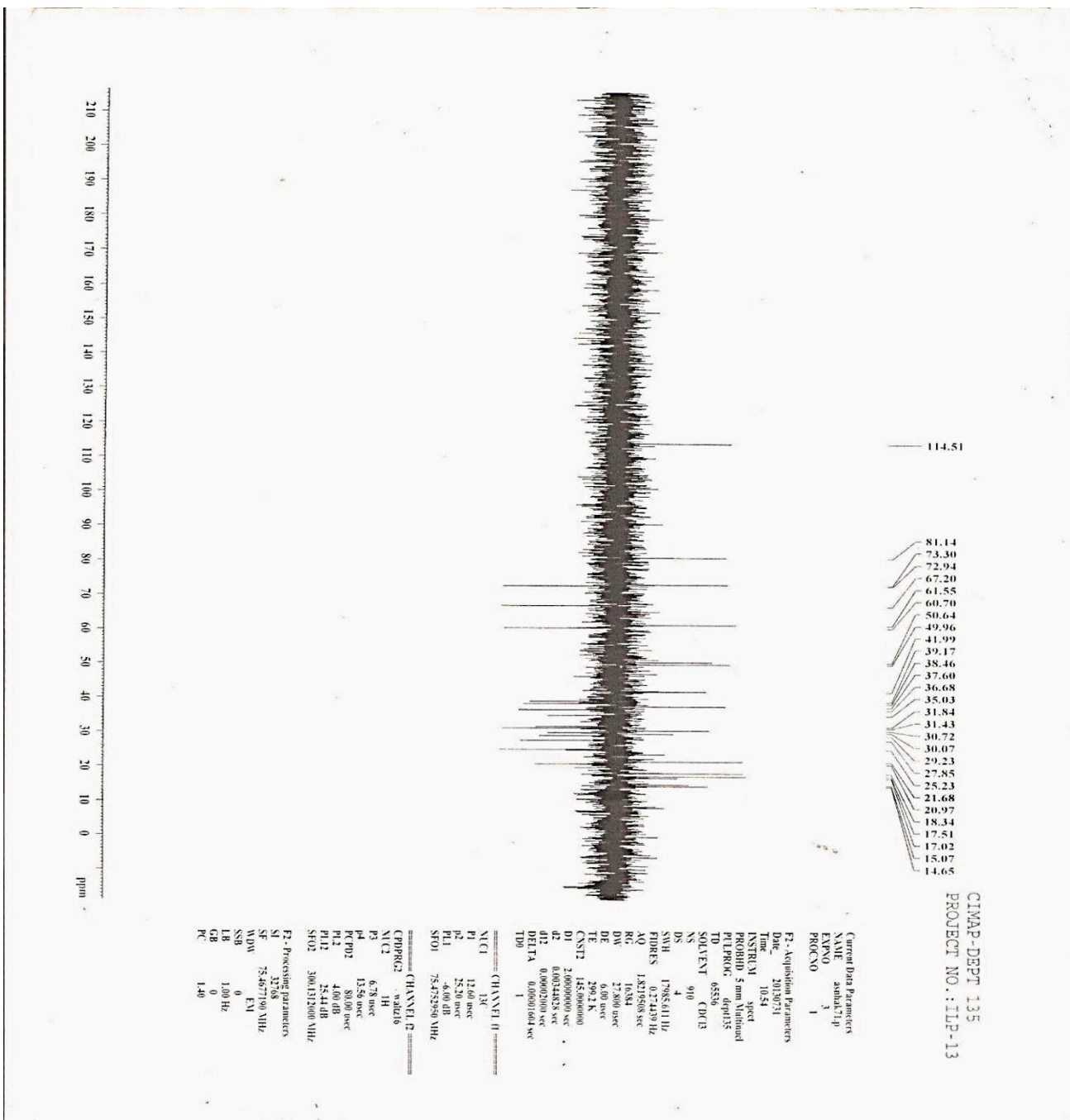
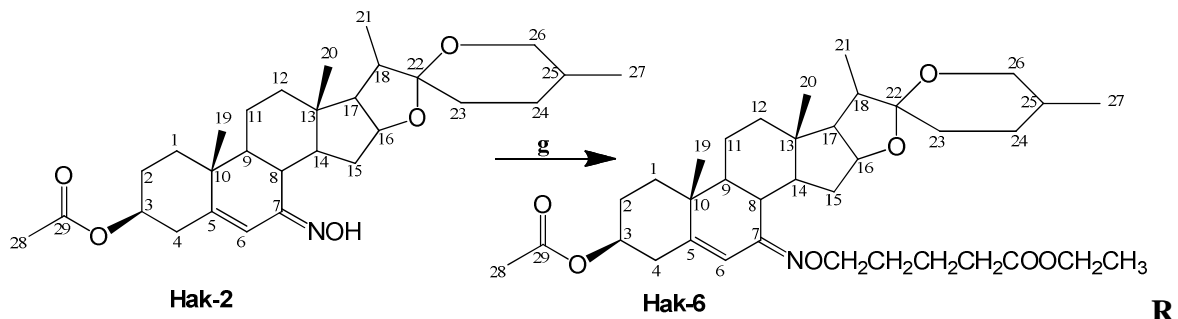


Fig. 5.40: DEPT spectrum of Hak-5 in CDCl<sub>3</sub>

#### 4.9.6. Synthesis and characterisation of (22 $\beta$ ,25R)-3 $\beta$ -Acetoxy-spirost-5-en-3 $\beta$ -yl-7-(ethyl-5'-pentanoate)-ketoxime (Hak-6)

Hak-6 was also obtained in the presence of ethyl-5-bromopentanoate as the ester chain. The same method was used as for Hak-3.



**agents and conditions:** g)  $K_2CO_3$ , dried Acetone, Ethyl-5-bromopentanoate, reflux at 80 - 100°C, 3 hrs

Hak-6 (92 mg, 92%) yielded a white crystalline solid (melting point 198 - 201°C). The ESI-MS fragment ions at 566  $[M-2Na-H]^-$ , 567  $[M-2Na]^-$ , 636  $[M+Na]^+$ , 660  $[M+2Na+H]^+$  gave molecular formula  $C_{36}H_{55}NO_7$  (613) [Fig. 5.41]. The  $^1H$  NMR signals at  $\delta_H$  2.02 (s) and 2.44 (t) indicated the presence of methyl protons of acetate and esters, and methine proton at C-8, while the proton signals at  $\delta_H$  3.41 (m, 2H,  $OCH_2$ ) and 4.06 (m, 2H,  $OCH_2$ ) correspond to the presence of oxymethylene protons of ester and oxime at C-5'. Methylene and methine protons of oxygenated carbons at C-26 and C-3 also appeared at  $\delta_H$  3.46 (d) and 4.46 (m) respectively [Fig. 5.42].  $^{13}C$  NMR experiment [Fig. 5.43] revealed thirty six carbon resonances. The carbons were sorted by DEPT spectrum [Fig. 5.44] into six methyl, fourteen methylene, nine methine and seven quaternary carbon resonances. The spectra data of Hak-6 were similar to Hak-2 except the condensation of ester chain at position 7 [ $\delta_C$  29.12 (C-3'), 31.75 (C-4'), 32.01 (C-2'), 60.76 ( $OCH_2$  of ester), 61.16 (C-5') and 171.54 (C-1', ester)]. The  $^{13}C$  and  $^1H$  NMR data of Hak-6 and Hak-2 were shown in Table 4.81. Hence, the structure of Hak-6 was elucidated to be (22 $\beta$ ,25R)-3 $\beta$ -Acetoxy-spirost-5-en-3 $\beta$ -yl-7-(ethyl-5'-pentanoate)-ketoxime.

**Table 4.81:** Comparison of  $^{13}\text{C}$  and  $^1\text{H}$  NMR data of Hak-2 and Hak-6

Assignment	* $^{13}\text{C}$	Multiplicity	* $^1\text{H}$ , Multiplicity	$^{13}\text{C}$	$^1\text{H}$
1	29.10	$\text{CH}_2$	1.39-1.90, m, 2H	29.12	1.39-1.86, m, 2H
2	36.58	$\text{CH}_2$	1.39-1.90, m, 2H	37.57	1.39-1.86, m, 2H
3	73.36	CH	4.55, m, 1H	73.35	4.46, m, 1H
4	39.00	$\text{CH}_2$	1.39-1.90, m, 2H	39.02	1.39-1.86, m, 2H
5	151.75	Q	-	151.85	-
6	114.96	CH	6.57, s, 1H	114.08	6.52, s, 1H
7	156.86	$\text{CH}_2$	-	156.99	-
8	38.89	CH	2.82, t, 1H	38.87	2.44, t, 1H
9	49.81	CH	1.39-1.90, m, 1H	49.85	1.39-1.86, m, 1H
10	36.67	Q	-	36.67	-
11	20.88	$\text{CH}_2$	1.39-1.90, m, 2H	20.88	1.39-1.86, m, 2H
12	38.45	$\text{CH}_2$	1.39-1.90, m, 2H	38.45	1.39-1.86, m, 2H
13	41.04	Q	-	41.04	-
14	41.97	CH	1.39-1.90, m, 1H	41.96	1.39-1.86, m, 1H
15	34.89	$\text{CH}_2$	1.39-1.90, m, 2H	34.88	1.39-1.86, m, 2H
16	81.26	CH	4.66, m, 1H	81.22	4.56, m, 1H
17	61.01	CH	1.39-1.90, m, 1H	60.76	1.39-1.86, m, 1H
18	50.24	CH	1.39-1.90, m, 1H	50.30	1.39-1.86, m, 1H
19	18.29	$\text{CH}_3$	0.78-1.36, m, 3H	18.28	0.74-1.33, m, 3H
20	16.78	$\text{CH}_3$	0.78-1.36, m, 3H	16.78	0.74-1.33, m, 3H
21	14.86	$\text{CH}_3$	0.78-1.36, m, 3H	14.86	0.74-1.33, m, 3H
22	109.96	Q	-	109.84	-
23	30.67	$\text{CH}_2$	1.39-1.90, m, 2H	30.66	1.39-1.86, m, 2H
24	27.87	$\text{CH}_2$	1.39-1.90, m, 2H	27.85	1.39-1.86, m, 2H
25	30.67	$\text{CH}_2$	1.39-1.90, m, 2H	30.00	1.39-1.90, m, 2H
26	67.13	$\text{CH}_3$	3.46, d, 2H	67.13	3.46, d, 2H
27	19.81	$\text{CH}_3$	0.78-1.36, m, 3H	17.47	0.74-1.33, m, 3H
28	21.68	$\text{CH}_3$	2.03, s, 3H	21.65	2.02, s, 3H
29	170.69	Q	-	170.67	-
1', ester				<b>171.54</b>	
2'				<b>32.01</b>	<b>1.17-2.40, m, 2H</b>
3'				<b>29.12</b>	<b>1.17-2.40, m, 2H</b>
4'				<b>31.75</b>	<b>1.17-2.40, m, 2H</b>
5'				<b>61.16</b>	<b>4.06, d, 2H</b>
$\text{OCH}_2$ of ester				<b>61.57</b>	<b>3.41, m, 2H</b>

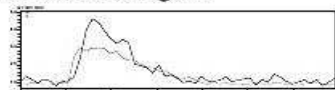
Implied multiplicities of the carbons were determined from the DEPT experiment. \* Hak-2



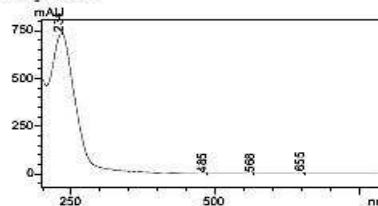
ANALYTICAL TEST REPORT

Sample Information for Direct Mass Analysis of Isolates/synthetic molecule  
Sample Code : ASN-HAK-6  
Solubility : MeOH  
Name of the Scientist : Dr.A S Negi  
Project Code: MLP-02  
Mass Range: 100-800

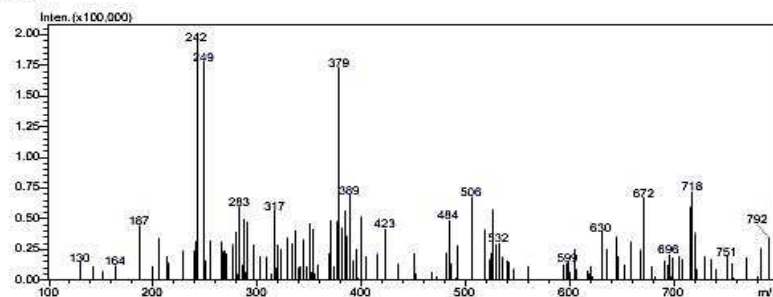
Mass chromatogram



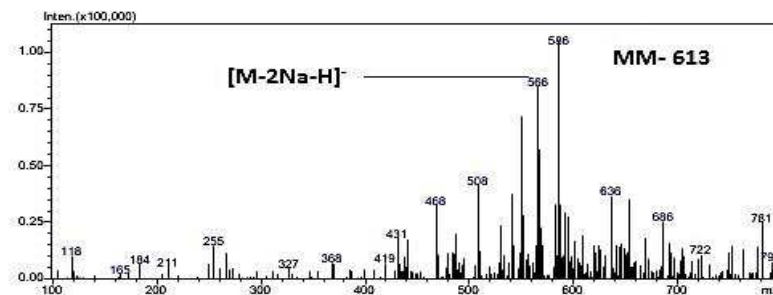
UV-Spectra



ESI+



ESI-



File Path-D:\Direct Mass report- Aug 2010\ASN-HAK-6.doc

Oct 14, 2013

[Dr. Karuna Shanker]

Fig. 5.41: Mass spectrum of Hak-6 in MeOH

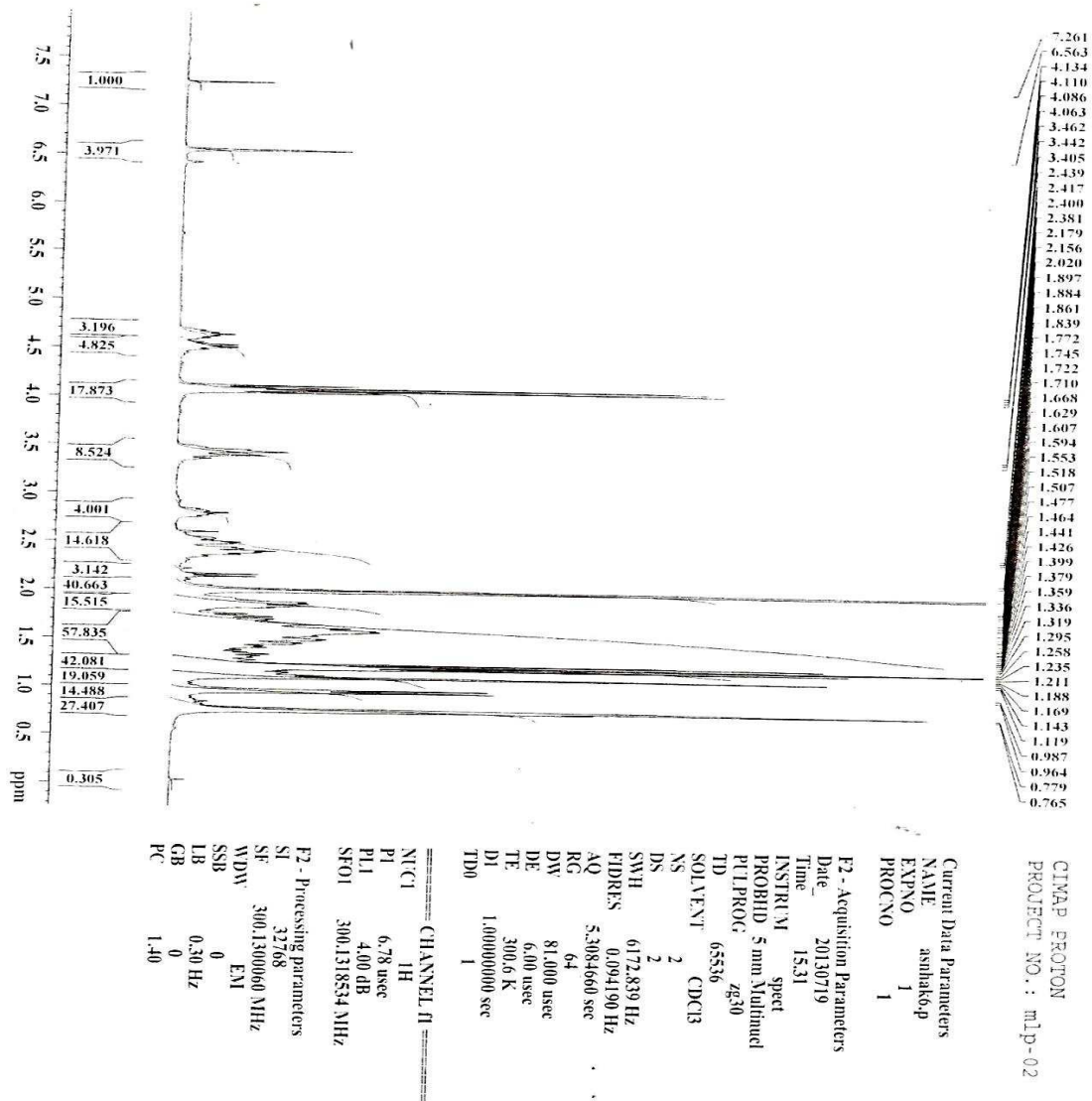
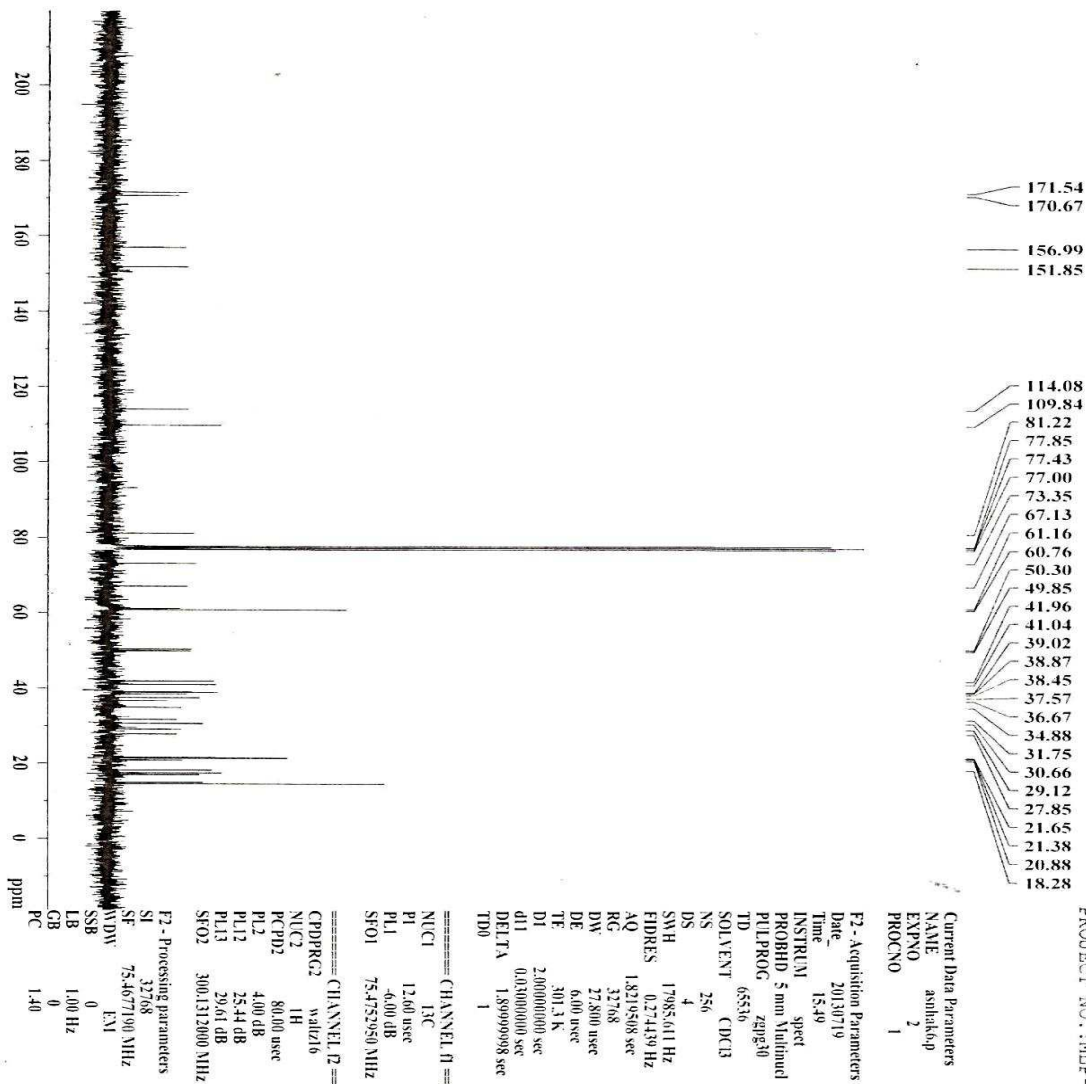
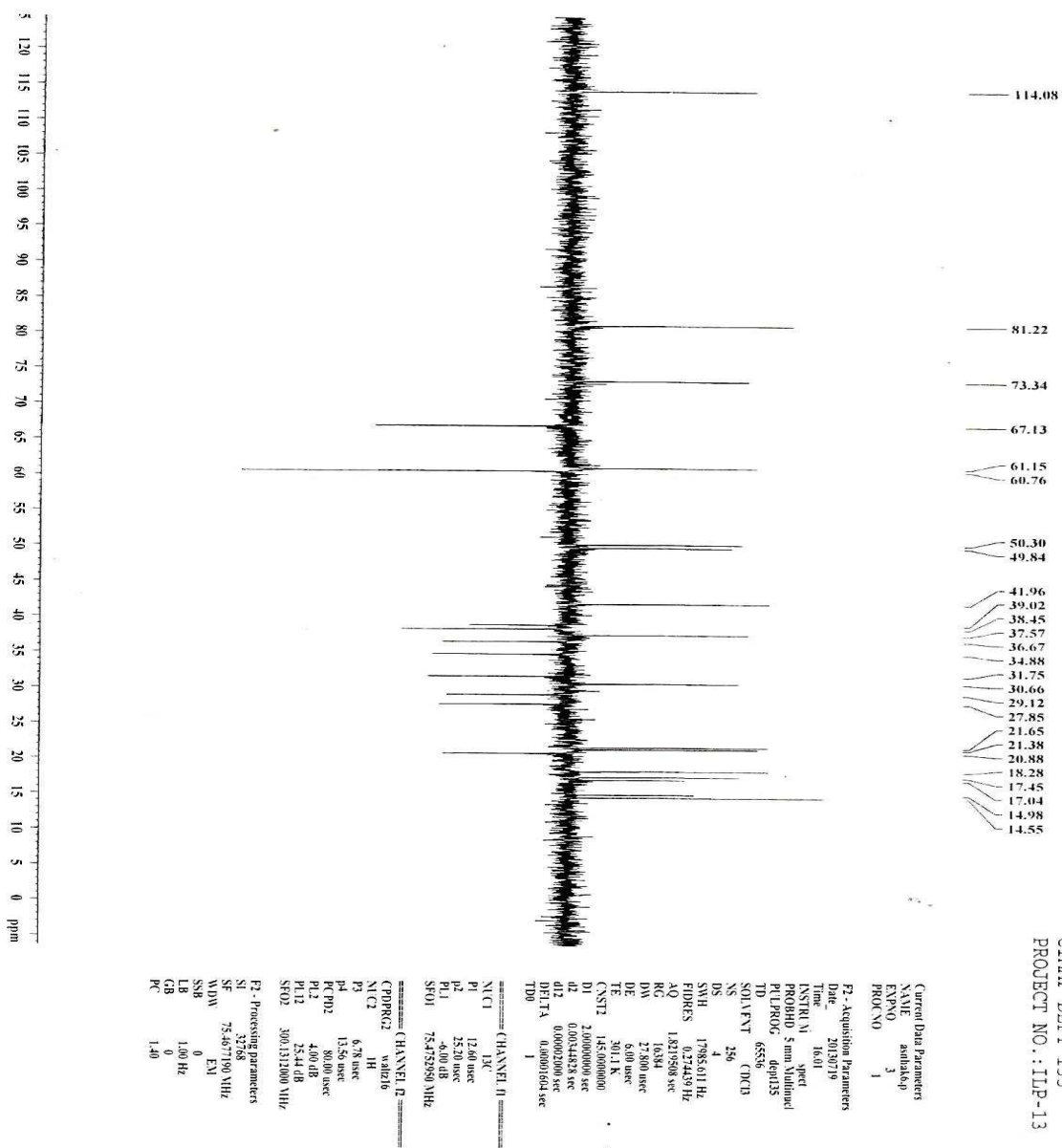


Fig. 5.42:  $^1\text{H}$  NMR spectrum of Hak-6 in  $\text{CDCl}_3$



CIMAP-CARBON  
PROJECT NO.: MLP-04

Fig. 5.43:  $^{13}\text{C}$  NMR spectrum of Hak-6 in  $\text{CDCl}_3$

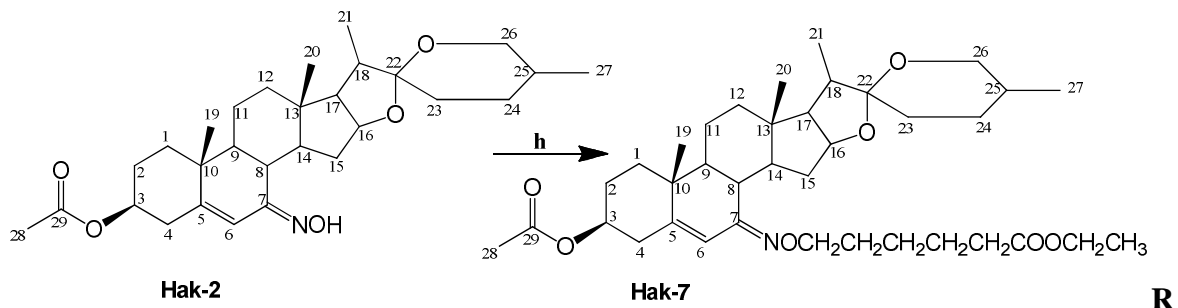


CIMAP-DEPT 135  
 PROJECT NO.: ILP-13

Fig. 5.44: DEPT spectrum of Hak-6 in CDCl<sub>3</sub>

#### 4.9.7. Synthesis and characterisation of (22 $\beta$ ,25R)-3 $\beta$ -Acetoxy-spirost-5-en-3 $\beta$ -yl-7-(ethyl-6'-hexanoate)-ketoxime (Hak-7)

Hak-7 was obtained using the same procedure as for Hak-3, but ethyl-6-bromohexanoate was employed as bromoester chain.



**agents and conditions:** h)  $K_2CO_3$ , dried Acetone, Ethyl-6-bromohexanoate, reflux at 80 -100 $^{\circ}C$ , 4 hrs

Hak-7 (90 mg, 90%) was a creamy white crystalline solid. It has a melting point of 87 - 90 $^{\circ}C$ . The ESI-MS fragmentation peaks at 509  $[M-3K-H]^-$ , 687  $[M+K+Na-2H]^+$  calculated for a molecular formula  $C_{37}H_{57}NO_7$  (627) [Fig. 5.45]. The  $^1H$  NMR chemical shifts at  $\delta_H$  2.02 (s) and 2.59 (t) were attributed to methyl protons of acetate and esters, and methine proton at C-8, while the signals at  $\delta_H$  3.35 (m, 2H,  $OCH_2$ ) and 4.04 (m, 2H,  $OCH_2$ ) correspond to oxymethylene protons of ester and oxime at C-6' respectively. Oxymethylene protons at C-26 and oxymethine proton at C-3 appeared at  $\delta_H$  3.43 (m) and 4.41 (bs) respectively [Fig. 5.46].  $^{13}C$  NMR spectrum [Fig. 5.47] revealed thirty seven carbon resonances. These carbons were sorted by DEPT experiment [Fig. 5.48] into six methyl, fifteen methylene, nine methine and seven quaternary carbon resonances. NMR spectroscopic data of the compound were identical to 7-keto diosgenin acetate data except the coupling of long ester chain at position 7 [ $\delta_C$  29.44 (C-4'), 31.67 (C-5'), 32.01 (C-3'), 32.10 (C-2'), 171.80 (C-1', ester), 60.84 ( $OCH_2$  of ester) and 61.15 (C-6')]. The  $^{13}C$  and  $^1H$  NMR data of Hak-7 and Hak-2 were shown in Table 4.82. Therefore, the structure of Hak-4 was confirmed to be (22 $\beta$ ,25R)-3 $\beta$ -Acetoxy-spirost-5-en-3 $\beta$ -yl-7-(ethyl-6'-hexanoate)-ketoxime.

**Table 4.82:** Comparison of  $^{13}\text{C}$  and  $^1\text{H}$  NMR data of Hak-2 and Hak-7

Assignment	* $^{13}\text{C}$	Multiplicity	* $^1\text{H}$ , Multiplicity	$^{13}\text{C}$	$^1\text{H}$
1	29.10	CH <sub>2</sub>	1.39-1.90, m, 2H	29.05	1.39-1.86, m, 2H
2	36.58	CH <sub>2</sub>	1.39-1.90, m, 2H	37.62	1.39-1.86, m, 2H
3	73.36	CH	4.55, m, 1H	73.40	4.41, m, 1H
4	39.00	CH <sub>2</sub>	1.39-1.90, m, 2H	38.95	1.39-1.86, m, 2H
5	151.75	Q	-	152.32	-
6	114.96	CH	6.57, s, 1H	163.70	6.52, s, 1H
7	156.86	CH <sub>2</sub>	-	157.16	-
8	38.89	CH	2.82, t, 1H	38.88	2.59, t, 1H
9	49.81	CH	1.39-1.90, m, 1H	49.88	1.39-1.86, m, 1H
10	36.67	Q	-	36.61	-
11	20.88	CH <sub>2</sub>	1.39-1.90, m, 2H	20.94	1.39-1.86, m, 2H
12	38.45	CH <sub>2</sub>	1.39-1.90, m, 2H	38.40	1.39-1.86, m, 2H
13	41.04	Q	-	40.96	-
14	41.97	CH	1.39-1.90, m, 1H	41.89	1.39-1.86, m, 1H
15	34.89	CH <sub>2</sub>	1.39-1.90, m, 2H	34.62	1.39-1.86, m, 2H
16	81.26	CH	4.66, m, 1H	81.08	4.56, m, 1H
17	61.01	CH	1.39-1.90, m, 1H	60.84	1.39-1.86, m, 1H
18	50.24	CH	1.39-1.90, m, 1H	54.12	1.39-1.86, m, 1H
19	18.29	CH <sub>3</sub>	0.78-1.36, m, 3H	18.28	0.74-1.33, m, 3H
20	16.78	CH <sub>3</sub>	0.78-1.36, m, 3H	16.78	0.74-1.33, m, 3H
21	14.86	CH <sub>3</sub>	0.78-1.36, m, 3H	14.86	0.74-1.33, m, 3H
22	109.96	Q	-	109.89	-
23	30.67	CH <sub>2</sub>	1.39-1.90, m, 2H	30.57	1.39-1.86, m, 2H
24	27.87	CH <sub>2</sub>	1.39-1.90, m, 2H	27.76	1.39-1.86, m, 2H
25	30.67	CH <sub>2</sub>	1.39-1.90, m, 2H	30.00	1.39-1.86, m, 2H
26	67.13	CH <sub>3</sub>	3.46, d, 2H	67.11	3.43, d, 2H
27	19.81	CH <sub>3</sub>	0.78-1.36, m, 3H	17.47	0.74-1.33, m, 3H
28	21.68	CH <sub>3</sub>	2.03, s, 3H	21.68	2.02, s, 3H
29	170.69	Q	-	170.91	-
1', ester				<b>170.66</b>	-
2'				<b>32.10</b>	<b>1.17-2.40, m, 2H</b>
3'				<b>32.01</b>	<b>1.17-2.40, m, 2H</b>
4'				<b>29.44</b>	<b>1.17-2.40, m, 2H</b>
5'				<b>31.67</b>	<b>1.17-2.40, m, 2H</b>
6'				<b>61.15</b>	<b>4.04, m, 2H</b>
OCH <sub>2</sub> of ester				<b>60.84</b>	<b>3.35, m, 2H</b>

Implied multiplicities of the carbons were determined from the DEPT experiment. \* Hak-2

ANALYTICAL TEST REPORT

Sample Information for Direct Mass Analysis of Isolates/synthetic molecule

Sample Code : ASN-HAK-4

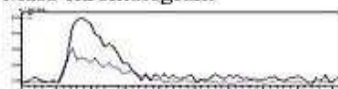
Solubility : MeOH

Name of the Scientist : Dr. A S Negi

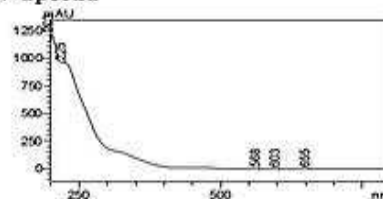
Project Code: MLP-02

Mass Range: 100-800

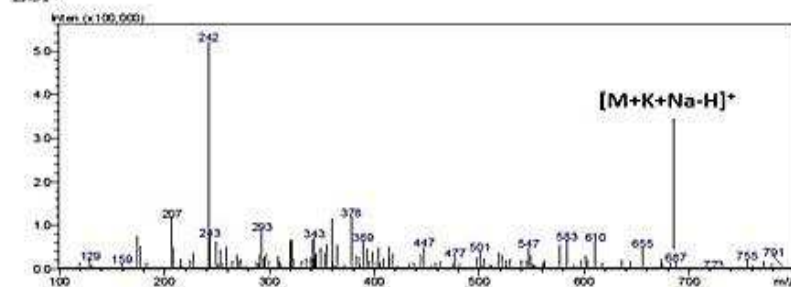
Mass chromatogram



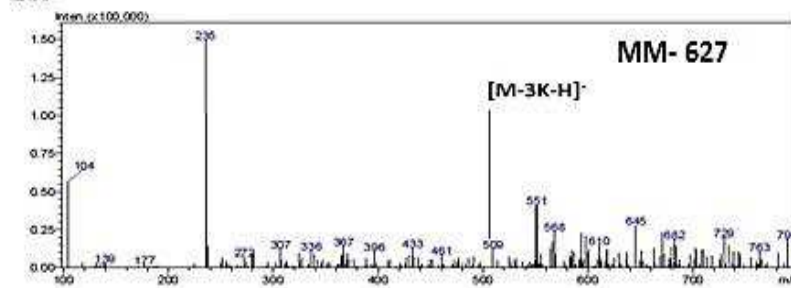
UV-Spectra



ESI+



ESI-



File Path: D:\Direct Mass report- Aug 2010\ASN-HAK-4.doc

Oct 14, 2013

[Dr. Karuna Shanker]

Fig. 5.45: Mass spectrum of Hak-7 in MeOH

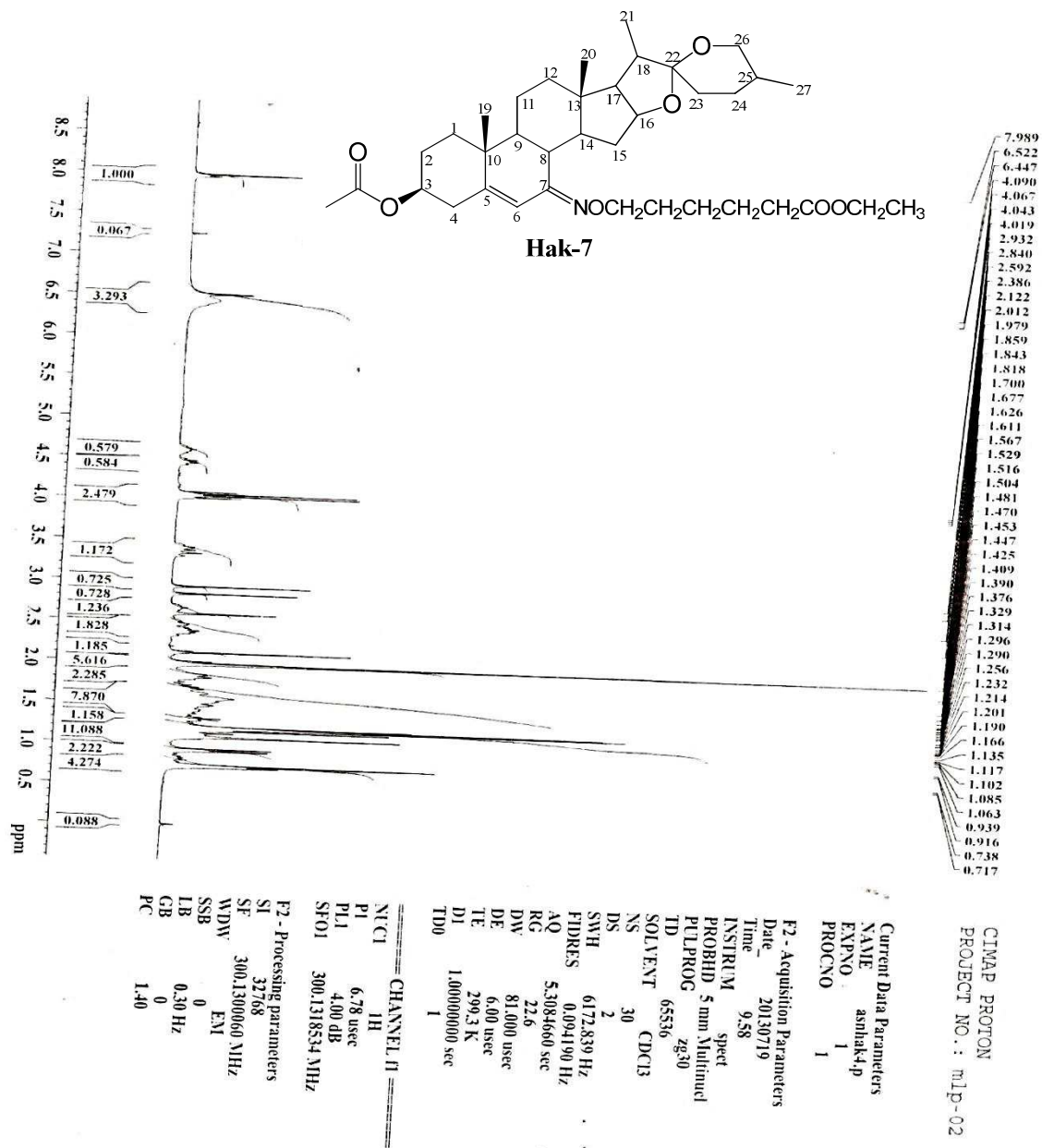


Fig. 5.46: <sup>1</sup>H NMR spectrum of Hak-7 in CDCl<sub>3</sub>



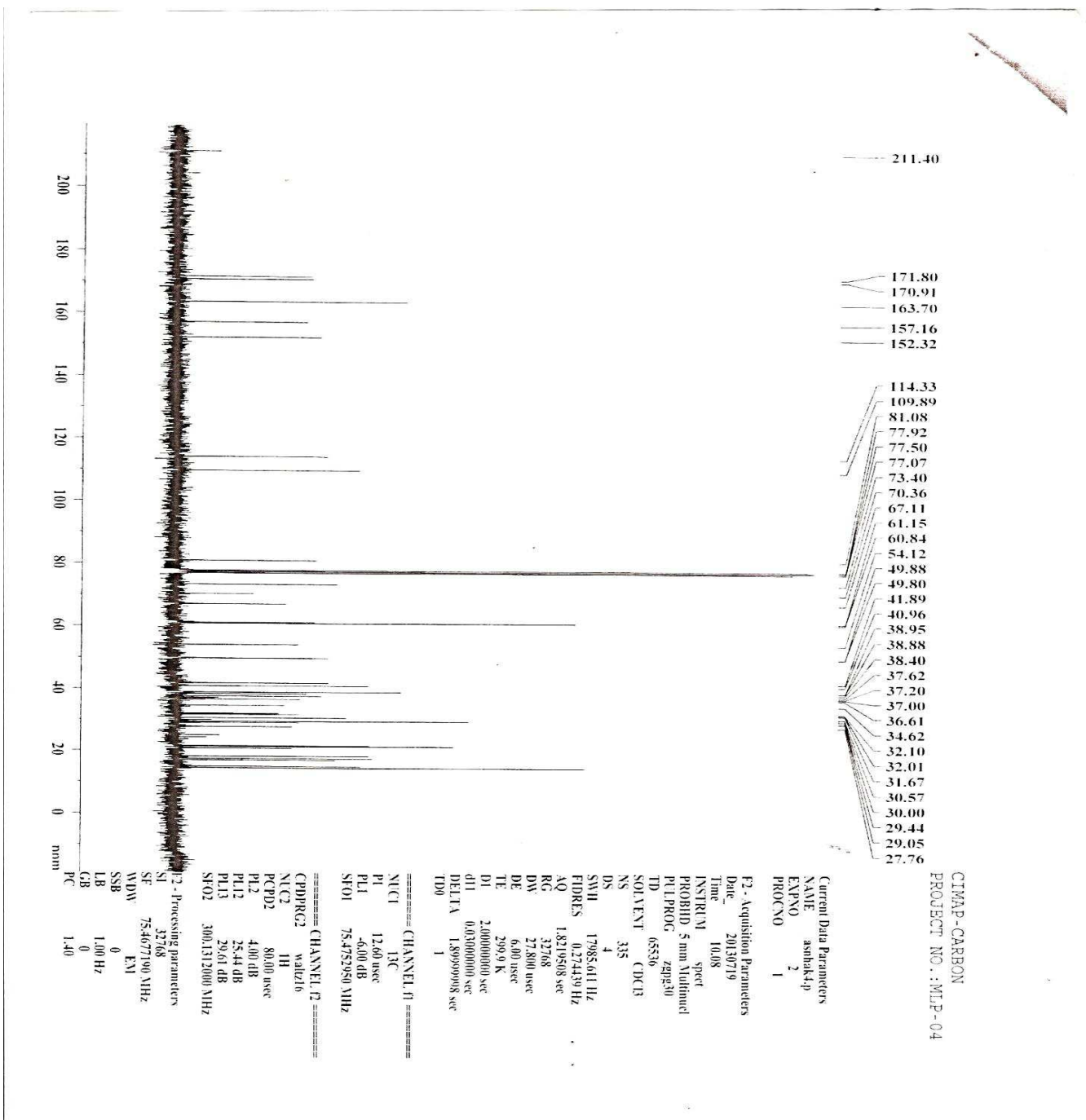


Fig. 5.47:  $^{13}\text{C}$  NMR spectrum of Hak-7 in  $\text{CDCl}_3$

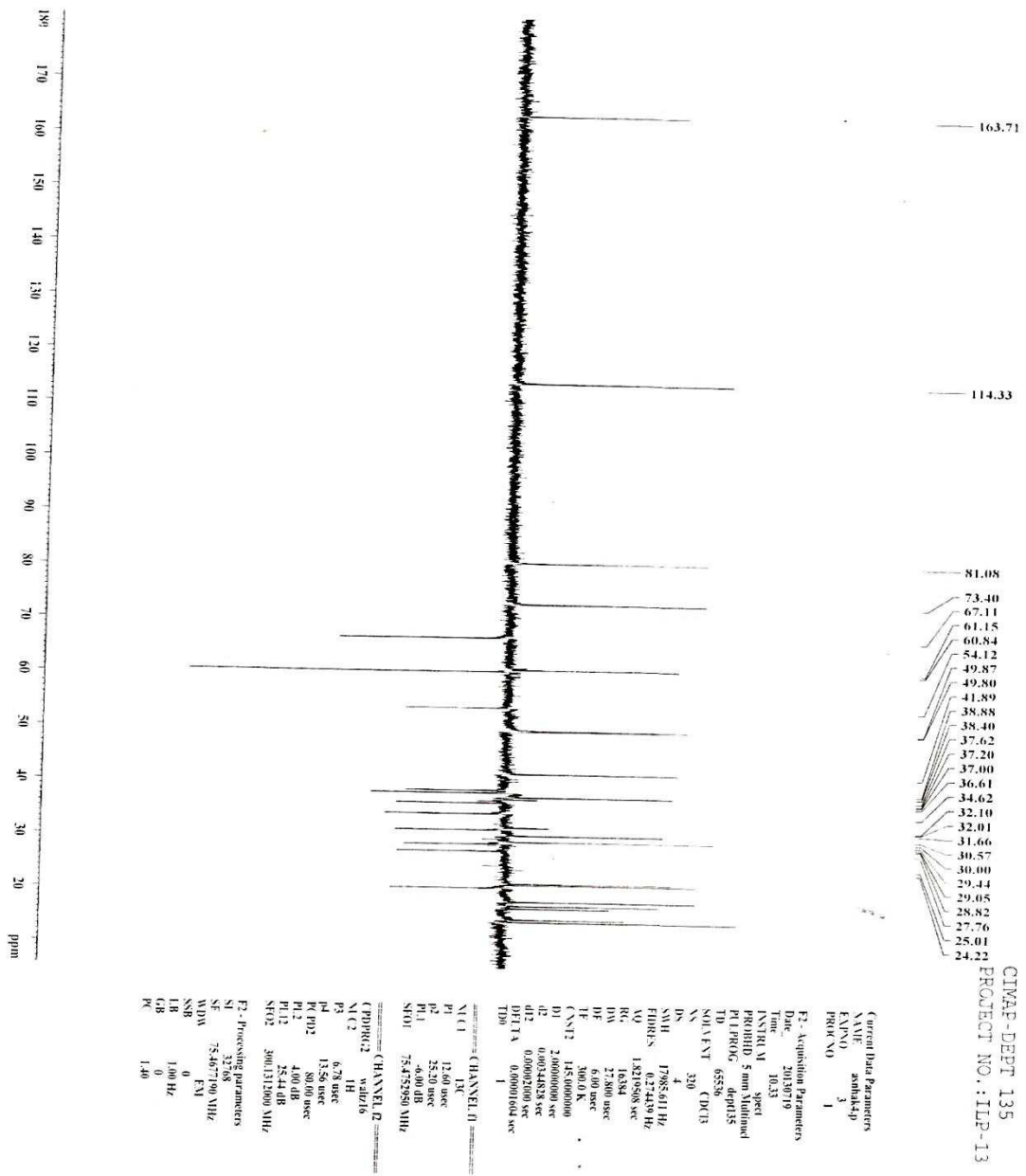
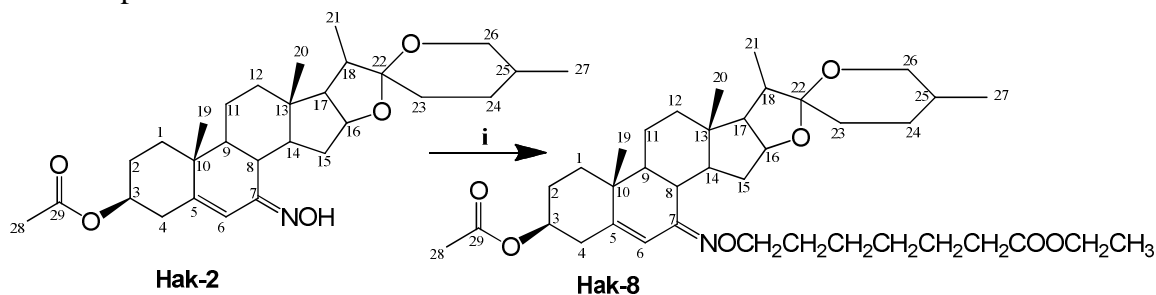


Fig. 5.48: DEPT spectrum of Hak-7 in CDCl<sub>3</sub>

#### 4.9.8. Synthesis and characterisation of (22 $\beta$ ,25R)-3 $\beta$ -Acetoxy-spirost-5-en-3 $\beta$ -yl-7-(ethyl-7'-heptanoate)-ketoxime (Hak-8).

The ester chain used for the preparation of Hak-8 was ethyl-7-bromoheptanoate.



**Reagents and conditions:** n)  $K_2CO_3$ , dried Acetone, Ethyl-7-bromoheptanoate, reflux at 80 - 100°C, 4 hrs

Hak-8 (82 mg, 82%) was obtained as white crystalline solid (melting point 115 - 118°C). The ESI-MS fragment ions at 577  $[M-K-Na]^+$ , 685  $[M+2Na]^+$ , 740  $[M+2K+Na]^+$  gave molecular formula  $C_{38}H_{59}NO_7$  (639) [Fig. 5.49]. The  $^1H$  NMR chemical shifts at  $\delta_H$  0.78-1.41 and 1.90 (s) are characteristics of angular methyl protons, and methyl protons of esters, while the signals at  $\delta_H$  3.38 (m, 2H,  $OCH_2$ ) and 4.05 (m, 2H,  $OCH_2$ ) revealed the presence of oxymethylene protons of ester and oxime at C-7' respectively. Methine protons at C-16 and C-6 appeared at 4.45 (m) and 6.45 (s), while the peaks at  $\delta_H$  3.40 (d) and 4.12 (bs) correspond to methylene and methine protons of oxygenated carbons at C-26 and C-3 respectively [Fig. 5.50].  $^{13}C$  NMR spectrum [Fig. 5.51] revealed thirty eight carbon resonances. The multiplicities of the carbons were showed by DEPT spectrum [Fig. 5.52]. They are: six methyl, sixteen methylene, nine methine and seven quaternary carbon resonances. The spectra data of Hak-8 were also similar to spirostene skeleton of its 7-ketoxime derivative except the coupling of a long ester chain at position 7 [ $\delta_C$  28.17 (C-5'), 28.85 (C-4'), 29.72 (C-6'), 31.80 (C-3'), 35.24 (C-2'), 60.62 ( $OCH_2$  of ester), 64.68 (C-7') and 173.31 (C-1', ester)]. The  $^{13}C$  and  $^1H$  NMR data of Hak-8 and Hak-2 were shown in Table 4.83. The spectroscopic data of Hak-8, compared with its 7-ketoxime analogue, Hak-2 led to characterization of Hak-8 to be (22 $\beta$ ,25R)-3 $\beta$ -Acetoxy-spirost-5-en-3 $\beta$ -yl-7-(ethyl-7'-heptanoate)-ketoxime.

**Table 4.83:** Comparison of  $^{13}\text{C}$  and  $^1\text{H}$  NMR data of Hak-2 and Hak-8

Assignment	* $^{13}\text{C}$	Multiplicity	* $^1\text{H}$ , Multiplicity	$^{13}\text{C}$	$^1\text{H}$
1	29.10	$\text{CH}_2$	1.39-1.90, m, 2H	29.12	1.45-1.88, m, 2H
2	36.58	$\text{CH}_2$	1.39-1.90, m, 2H	37.04	1.45-1.88, m, 2H
3	73.36	CH	4.55, m, 1H	73.30	4.12, m, 1H
4	39.00	$\text{CH}_2$	1.39-1.90, m, 2H	39.35	1.45-1.88, m, 2H
5	151.75	Q	-	152.40	-
6	114.96	CH	6.57, s, 1H	112.02	6.45, s, 1H
7	156.86	$\text{CH}_2$	-	156.90	-
8	38.89	CH	2.82, t, 1H	38.80	2.40, t, 1H
9	49.81	CH	1.39-1.90, m, 1H	51.41	1.45-1.88, m, 1H
10	36.67	Q	-	36.67	-
11	20.88	$\text{CH}_2$	1.39-1.90, m, 2H	20.91	1.45-1.88, m, 2H
12	38.45	$\text{CH}_2$	1.39-1.90, m, 2H	38.46	1.45-1.88, m, 2H
13	41.04	Q	-	41.56	-
14	41.97	CH	1.39-1.90, m, 1H	42.00	1.45-1.88, m, 1H
15	34.89	$\text{CH}_2$	1.39-1.90, m, 2H	34.07	1.45-1.88, m, 2H
16	81.26	CH	4.66, m, 1H	81.23	4.45, m, 1H
17	61.01	CH	1.39-1.90, m, 1H	60.62	1.45-1.88, m, 1H
18	50.24	CH	1.39-1.90, m, 1H	51.41	1.45-1.88, m, 1H
19	18.29	$\text{CH}_3$	0.78-1.36, m, 3H	18.33	0.78-1.41, m, 3H
20	16.78	$\text{CH}_3$	0.78-1.36, m, 3H	16.95	0.78-1.41, m, 3H
21	14.86	$\text{CH}_3$	0.78-1.36, m, 3H	14.69	0.78-1.41, m, 3H
22	109.96	Q	-	109.70	-
23	30.67	$\text{CH}_2$	1.39-1.90, m, 2H	25.14	1.45-1.88, m, 2H
24	27.87	$\text{CH}_2$	1.39-1.90, m, 2H	26.09	1.45-1.88, m, 2H
25	30.67	$\text{CH}_2$	1.39-1.90, m, 2H	30.70	1.45-1.88, m, 2H
26	67.13	$\text{CH}_3$	3.46, d, 2H	67.18	3.40, d, 2H
27	19.81	$\text{CH}_3$	0.78-1.36, m, 3H	17.50	0.78-1.41, m, 3H
28	21.68	$\text{CH}_3$	2.03, s, 3H	21.67	1.99, s, 3H
29	170.69	Q	-	170.91	-
1', ester				<b>173.31</b>	-
2'				<b>32.24</b>	<b>1.21-2.40, m, 2H</b>
3'				<b>31.80</b>	<b>1.21-2.40, m, 2H</b>
4'				<b>28.85</b>	<b>1.21-2.40, m, 2H</b>
5'				<b>28.18</b>	<b>1.21-2.40, m, 2H</b>
6'				<b>29.72</b>	<b>1.21-2.40, m, 2H</b>
7'				<b>61.68</b>	<b>4.05, m, 2H</b>
$\text{OCH}_2$ of ester				<b>60.62</b>	<b>3.38, m, 2H</b>

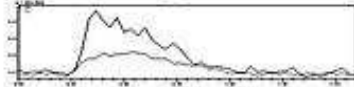
Implied multiplicities of the carbons were determined from the DEPT experiment. \*Hak-2

ANALYTICAL TEST REPORT

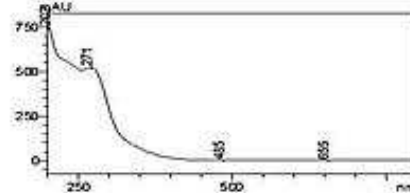
Sample Information for Direct Mass Analysis of Isolates/synthetic molecule

Sample Code	: ASN-HAK-9.1	Project Code: MLP-02
Solubility	: MeOH	Mass Range: 100-800
Name of the Scientist	: Dr.A S Negi	

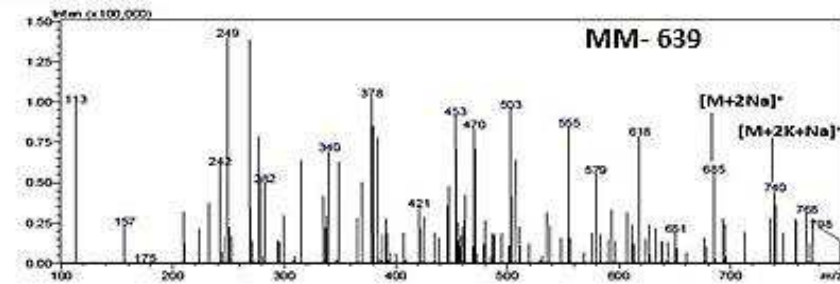
Mass chromatogram



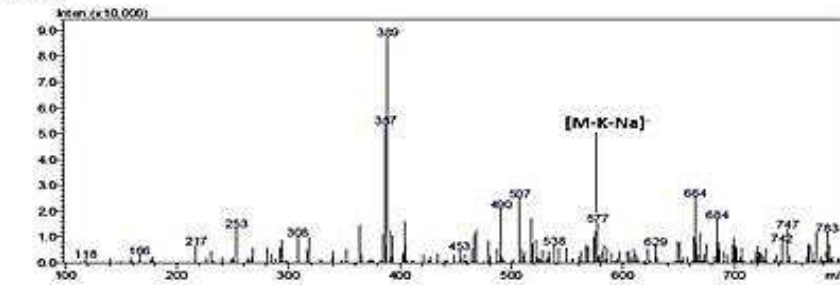
UV-Spectra



ESI+



ESI-



File Path-D:\Direct Mass report- Aug 2010\ASN-HAK-9.1.doc

Oct 14, 2013

[Dr. Karuna Shanker]

**Fig. 5.49:** Mass spectrum of Hak-8 in MeOH

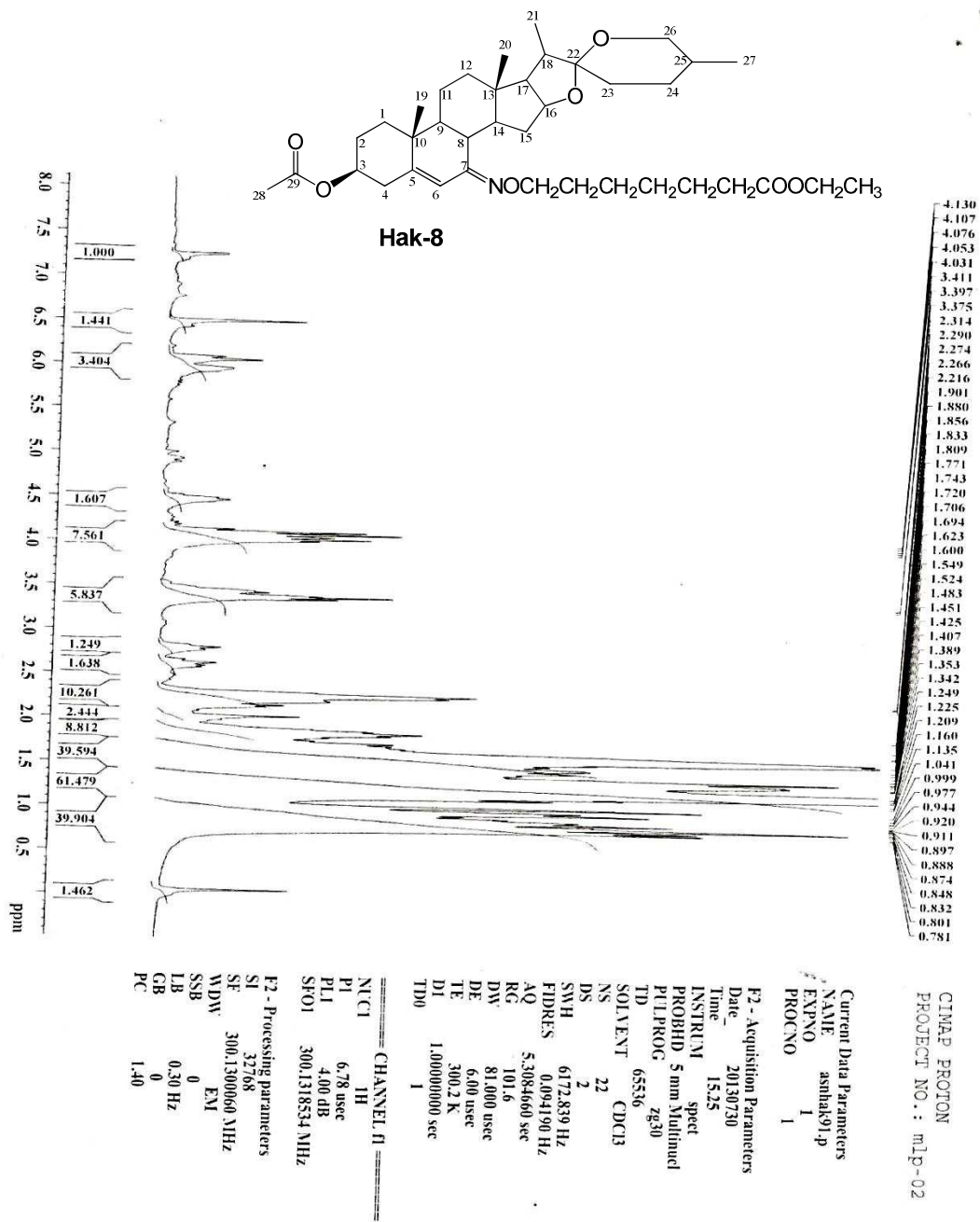


**Fig. 5.50:**  $^1\text{H}$  NMR spectrum of Hak-8 in  $\text{CDCl}_3$

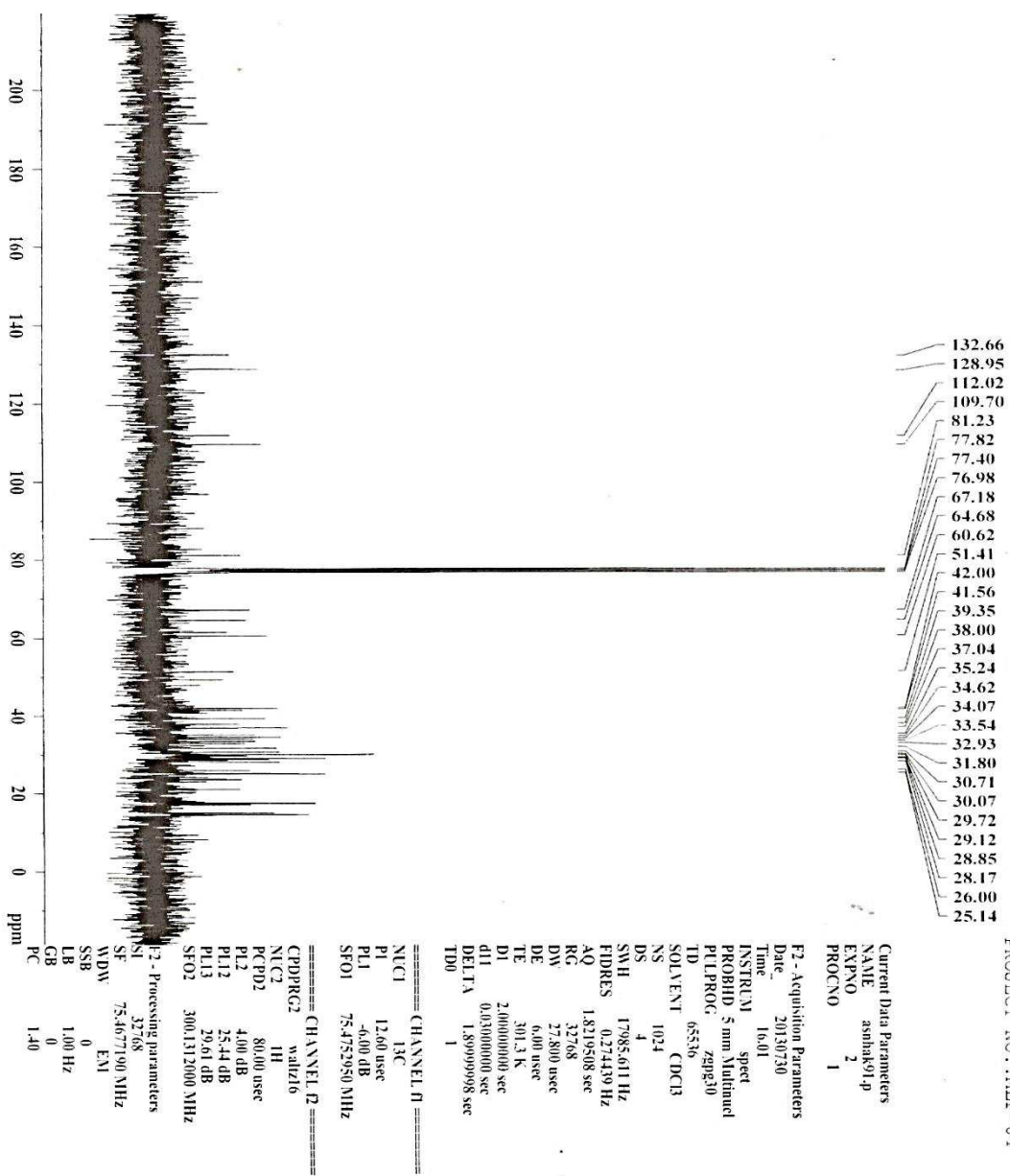


Fig. 5.51: <sup>13</sup>C NMR spectrum of Hak-8 in CDCl<sub>3</sub>

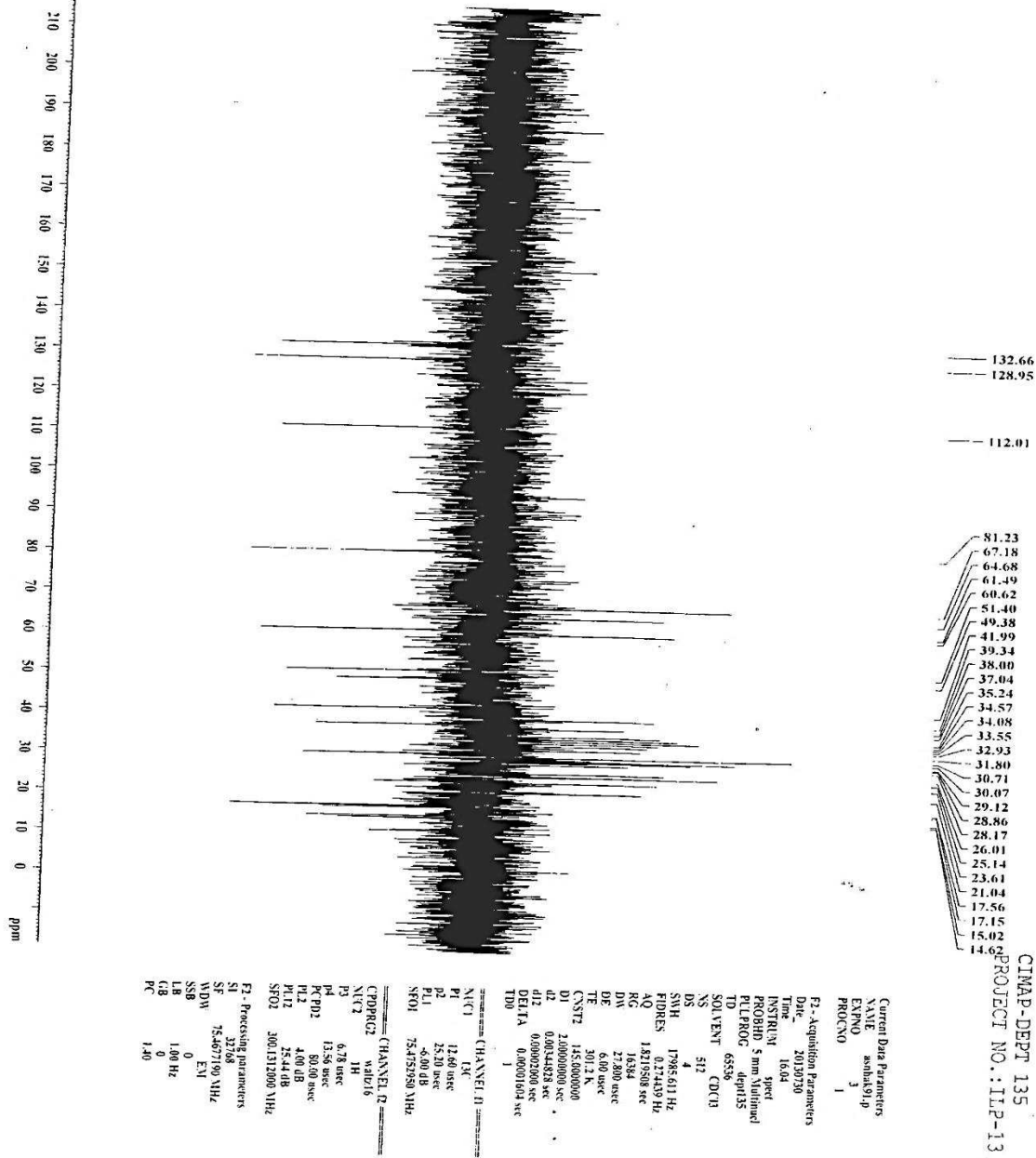
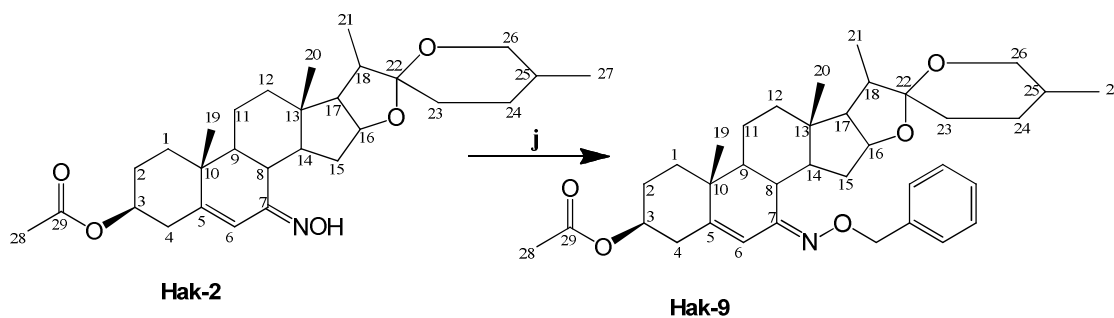


Fig. 5.52: DEPT spectrum of Hak-8 in CDCl<sub>3</sub>



#### 4.9.9. Synthesis and characterisation of (22 $\beta$ ,25R)-3 $\beta$ -Acetoxy-spirost-5-en-3 $\beta$ -yl-7-benzyloxime (Hak-9)

Aromatic analogue of 7-ketoxime, Hak-9 was also prepared by using benzy bromide. The same method was employed as for Hak-3.



**agents and conditions:** j)  $K_2CO_3$ , dried Acetone, Benzy bromide, reflux at 80 - 100°C, 4 hrs

Hak-9 (95 mg, 95%) was obtained as brownish yellow solid which has a melting point of 107 - 110°C. The Mass fragment ions at 576  $[M+H]^+$ , 608  $[M+Na]^+$  gave molecular formula  $C_{36}H_{49}NO_5$  (575) [Fig. 5.53]. The assigned  $^1H$  NMR signals at  $\delta_H$  2.00 (s) and 2.75 (t) were due to the presence of methyl protons of acetate and methine proton at C-8, while the proton signals at  $\delta_H$  3.35 (m, 2H,  $OCH_2$ ) and 4.98 (d, 1H,  $OCH$ ) were attributed to oxymethylene and oxymethine protons at C-26 and C-16 respectively. Methine proton at C-3 and methylene protons at C-1' appeared at 4.58 (m) and 4.03 (m). Further, the chemical shift at  $\delta_H$  6.42 (s) correspond to olefinic methine proton at C-6 while the aromatic protons ( $CH-3'-7'$ ) appeared at  $\delta_H$  8.52 (s) [Fig. 5.54].  $^{13}C$  NMR spectrum [Fig. 5.55] showed thirty six carbon resonances which were sorted by DEPT experiment [Fig. 5.56] into five methyl, ten methylene, fourteen methine and seven quaternary carbon resonances. The spectroscopic data of Hak-9 were similar to that of Hak-2 skeleton. The difference was the coupling of benzy group at position 7 which was also shown by  $^{13}C$  chemical shifts [ $\delta_C$  61.32 (C-1'), 127.40 (C-6'), 127.89 (C-4'), 128.54 (C-3'), 128.70 (C-7'), 128.82 (C-5') and 138.63 (C-2')]. The  $^{13}C$  and  $^1H$  NMR data of Hak-9 and Hak-2 were shown in Table 4.84. The spectra data of Hak-9, which were compared with its 7-ketoxime

analogue, Hak-2 led to its structural elucidation to be (22 $\beta$ ,25R)-3 $\beta$ -Acetoxy-spirost-5-en-3 $\beta$ -yl-7-benzyketoxime.

**Table 4.84:** Comparison of  $^{13}\text{C}$  and  $^1\text{H}$  NMR data of Hak-2 and Hak-9

Assignment	* $^{13}\text{C}$	Multiplicity	* $^1\text{H}$ , Multiplicity	$^{13}\text{C}$	$^1\text{H}$
1	29.10	CH <sub>2</sub>	1.39-1.90, m, 2H	29.95	1.45-1.88, m, 2H
2	36.58	CH <sub>2</sub>	1.39-1.90, m, 2H	37.51	1.45-1.88, m, 2H
3	73.36	CH	4.55, m, 1H	73.56	4.58, m, 1H
4	39.00	CH <sub>2</sub>	1.39-1.90, m, 2H	38.99	1.45-1.88, m, 2H
5	151.75	Q	-	152.35	-
6	114.96	CH	6.57, s, 1H	114.61	6.42, s, 1H
7	156.86	CH <sub>2</sub>	-	156.43	-
8	38.89	CH	2.82, t, 1H	38.68	2.75, t, 1H
9	49.81	CH	1.39-1.90, m, 1H	49.87	1.45-1.88, m, 1H
10	36.67	Q	-	36.51	-
11	20.88	CH <sub>2</sub>	1.39-1.90, m, 2H	20.81	1.45-1.88, m, 2H
12	38.45	CH <sub>2</sub>	1.39-1.90, m, 2H	38.23	1.45-1.88, m, 2H
13	41.04	Q	-	40.98	-
14	41.97	CH	1.39-1.90, m, 1H	41.89	1.45-1.88, m, 1H
15	34.89	CH <sub>2</sub>	1.39-1.90, m, 2H	31.59	1.45-1.88, m, 2H
16	81.26	CH	4.66, m, 1H	81.23	4.98, d, 1H
17	61.01	CH	1.39-1.90, m, 1H	61.00	1.45-1.88, m, 1H
18	50.24	CH	1.39-1.90, m, 1H	50.45	1.45-1.88, m, 1H
19	18.29	CH <sub>3</sub>	0.78-1.36, m, 3H	18.07	0.78-1.41, m, 3H
20	16.78	CH <sub>3</sub>	0.78-1.36, m, 3H	16.79	0.78-1.41, m, 3H
21	14.86	CH <sub>3</sub>	0.78-1.36, m, 3H	14.80	0.78-1.41, m, 3H
22	109.96	Q	-	109.84	-
23	30.67	CH <sub>2</sub>	1.39-1.90, m, 2H	34.69	1.45-1.88, m, 2H
24	27.87	CH <sub>2</sub>	1.39-1.90, m, 2H	27.66	1.45-1.88, m, 2H
25	30.67	CH <sub>2</sub>	1.39-1.90, m, 2H	30.46	1.45-1.88, m, 2H
26	67.13	CH <sub>3</sub>	3.46, d, 2H	67.02	3.35, m, 2H
27	19.81	CH <sub>3</sub>	0.78-1.36, m, 3H	17.25	0.78-1.41, m, 3H
28	21.68	CH <sub>3</sub>	2.03, s, 3H	21.07	2.00, s, 3H
29	170.69	Q	-	177.02	-
1'				<b>61.32</b>	<b>4.03, m, 2H</b>
2'				<b>138.63</b>	-
3'				<b>128.54</b>	<b>8.52, s, 2H</b>
4'				<b>127.89</b>	<b>8.52, s, 2H</b>
5'				<b>128.82</b>	<b>8.52, s, 2H</b>
6'				<b>127.40</b>	<b>8.52, s, 2H</b>
7'				<b>128.70</b>	<b>8.52, s, 2H</b>

Implied multiplicities of the carbons were determined from the DEPT experiment. \*Hak-2

Central Institute of Medicinal and Aromatic Plants  
(Analytical Chemistry Division)  
Lucknow-226015

ANALYTICAL TEST REPORT

Sample Information for Direct Mass Analysis of Isolates/synthetic molecule

Sample Code : ASN-HAK-10

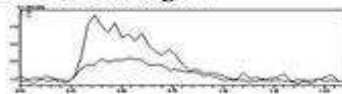
Solubility : MeOH

Name of the Scientist : Dr. A S Negi

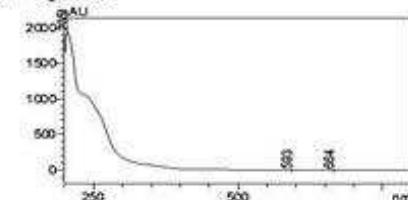
Project Code: MLP-02

Mass Range: 100-800

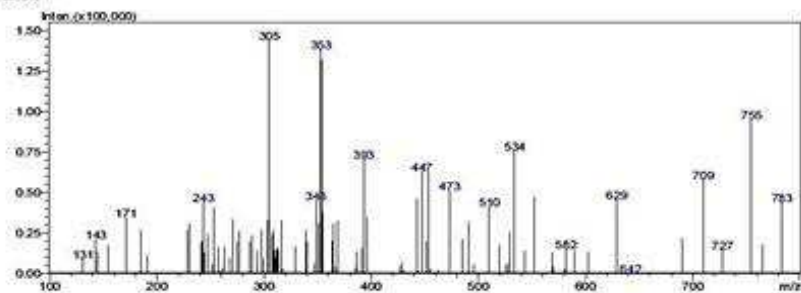
Mass chromatogram



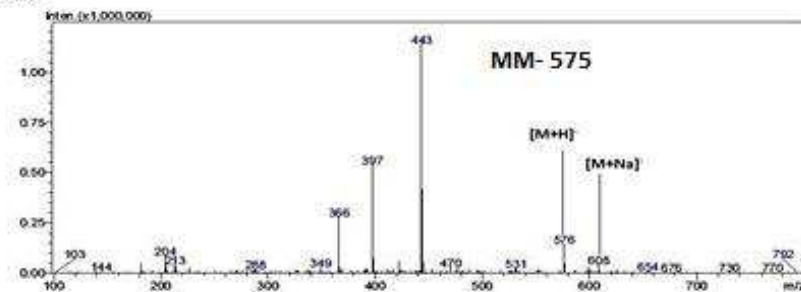
UV-Spectra



ESI+



ESI-



File Path: D:\Direct Mass report- Aug 2010\ASN-HAK-9.L.doc

Oct 14, 2013

[Dr. Karuna Shanker]

Fig. 5.53: Mass spectrum of Hak-9 in MeOH

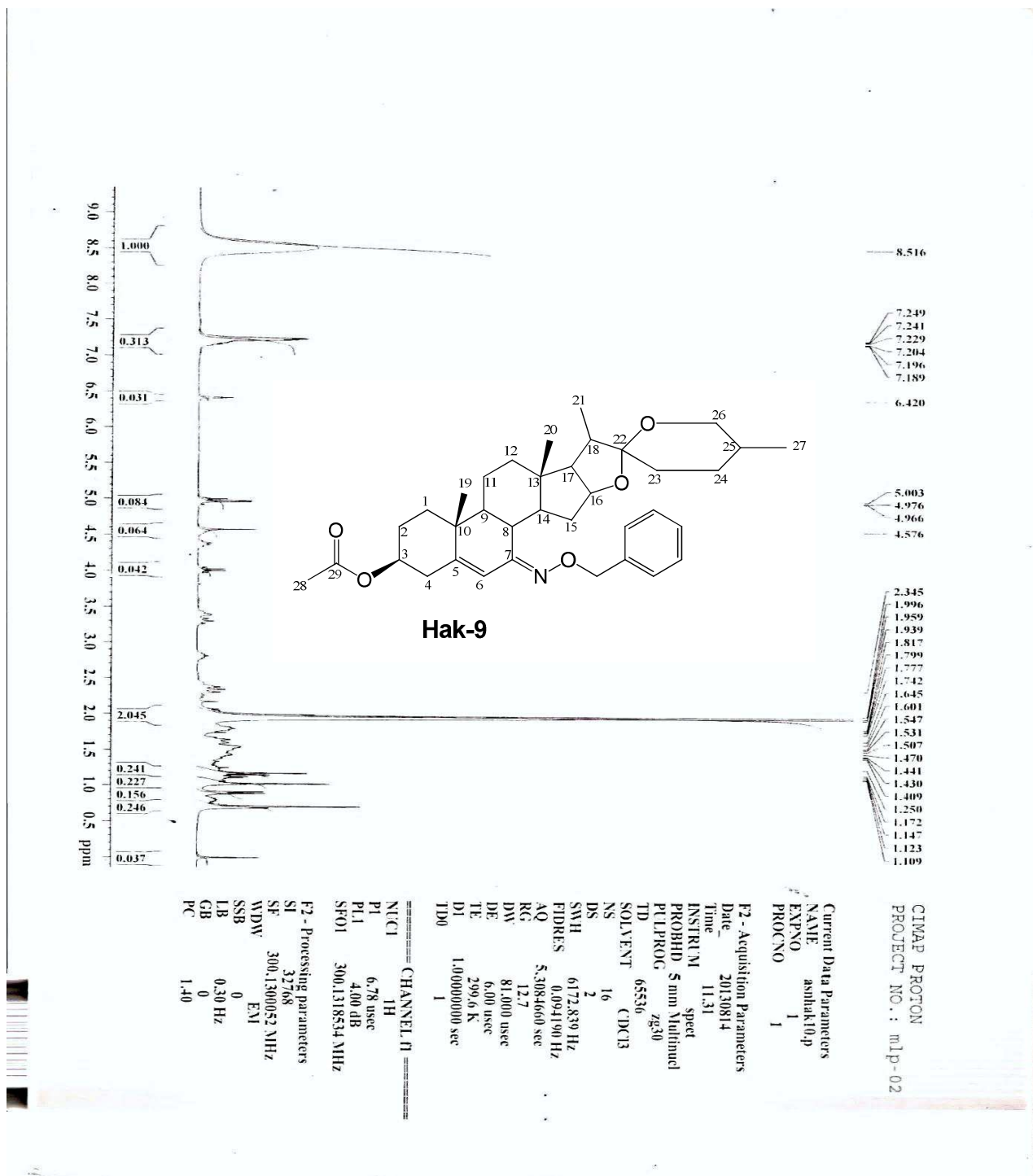


Fig. 5.54: <sup>1</sup>H NMR spectrum of Hak-9 in CDCl<sub>3</sub>

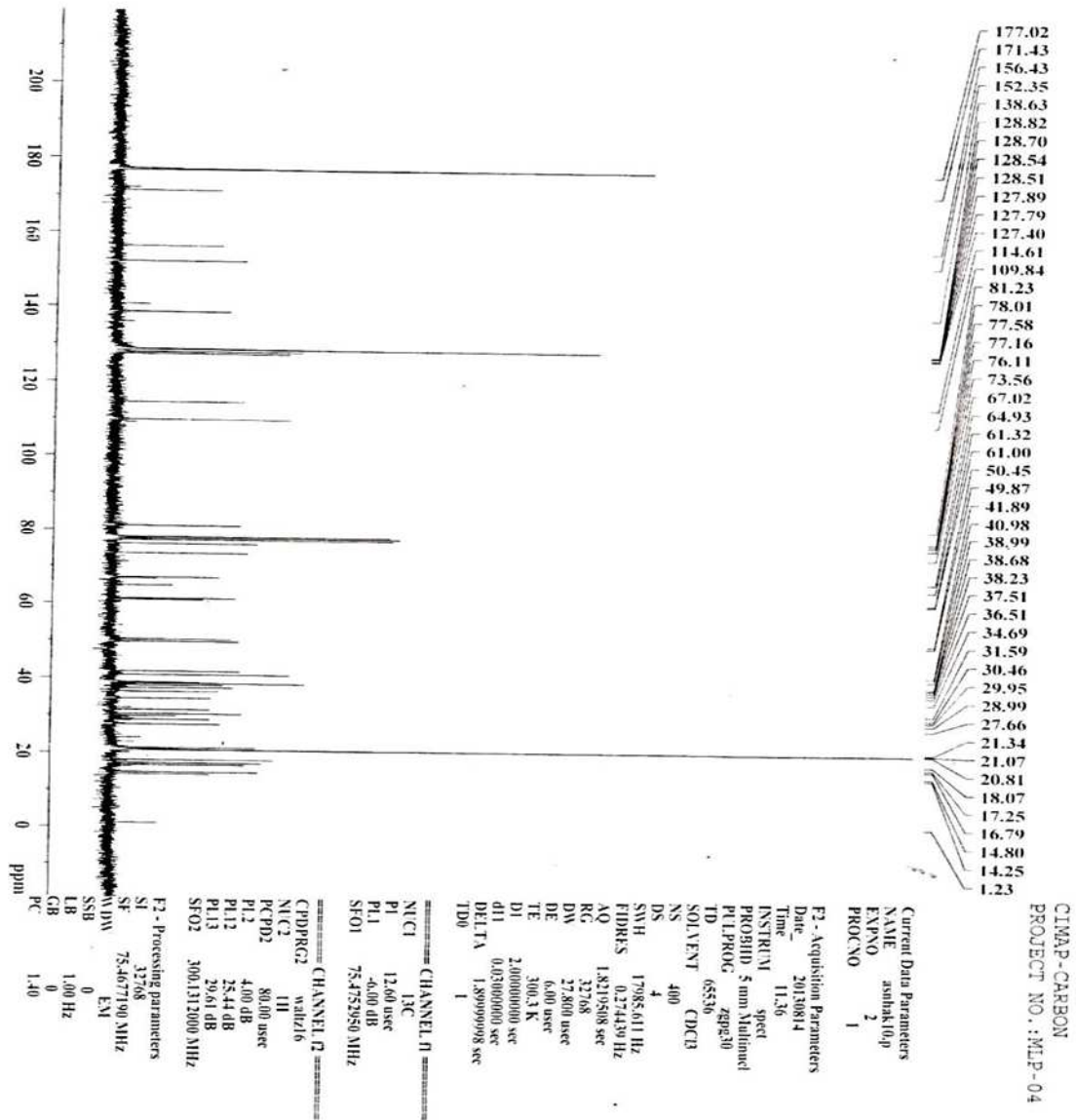


Fig. 5.55:  $^{13}\text{C}$  NMR spectrum of Hak-9 in  $\text{CDCl}_3$



CIMAP-DEPT 135  
PROJECT NO.: ILP-13

```

Current Data Parameters
NAME      aminkdup
EXPNO     1
PROCNO    1

F2 - Acquisition Parameters
Date_     20130814
Time      12.34
INSTRUM   spect
PROBHD    5 mm Multiband
PULPROG   dept135
TD         65536
SOLVENT   CDCl3
NS         562
DS         4
SOLSH     1706.641 Hz
FIDRES    0.27149 Hz
AQ         1.821958 sec
RG         16384
DW         27.800 usec
DE         6.00 usec
TE         301.0 K
(CSST2    HS(000000)
d1         2.00000000 sec
d12        0.00344828 sec
d13        0.00002000 sec
DELTA     0.00016084 sec
TD0        1

===== CHANNEL f1 =====
NUC1       13C
P1         12.60 usec
PL1        25.20 usec
PL2        -6.00 dB
SFO1       75.475950 MHz

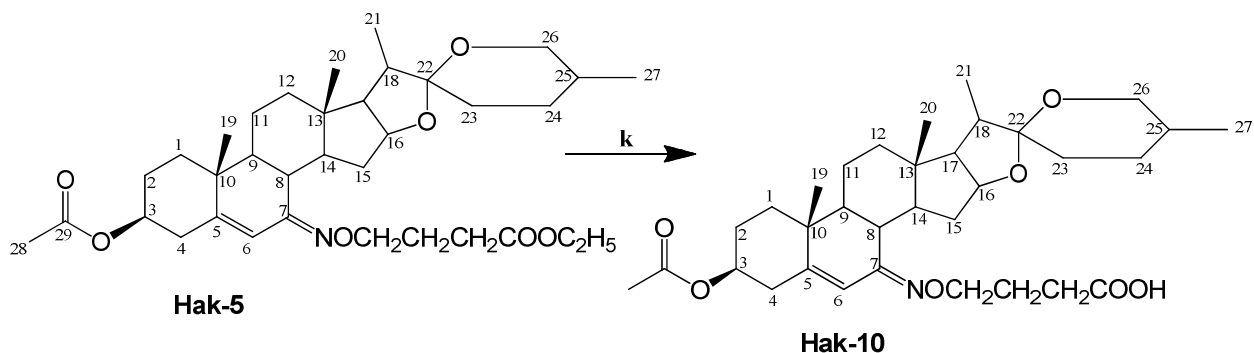
===== CHANNEL f2 =====
CPDPRG2    waltz16
NUC2       1H
P2         6.78 usec
PL2        13.50 usec
PL3        4.00 usec
PL4        25.44 dB
SFO2       300.131200 MHz

F2 - Processing parameters
SI         32768
SF         75.467190 MHz
WDW        EM
SSB        0
LB         1.00 Hz
GB         0
PC         1.40
  
```

Fig. 5.56: DEPT spectrum of Hak-9 in  $\text{CDCl}_3$

#### 4.9.10. Synthesis and characterisation of (22 $\beta$ ,25R)-3 $\beta$ -Acetoxy-spirost-5-en-3 $\beta$ -yl-7-(4'-butanoic)-ketoxime (Hak-10).

Hak-10 was prepared by dissolving Hak-5 in sodium or potassium hydroxide (NaOH/KOH) in the presence of 90% methanol (MeOH) at room temperature.



**Reagents and conditions:** k) NaOH/KOH, 90%MeOH, RT, 1 hr

Hak-10 (82 mg, 82%) is a light brown crystals (melting point 158 - 162°C). The Mass fragmentation peaks at 571 [M]<sup>+</sup>, 619 [M+2Na+2H]<sup>+</sup> correspond to molecular formula C<sub>33</sub>H<sub>49</sub>NO<sub>7</sub> (571) [Fig. 5.57]. IR  $\bar{\nu}$  (cm<sup>-1</sup>) absorptions of O-H, C-H, C=O and C=C functions appeared at 3428, 2365, 1629 and 1443. The <sup>1</sup>H NMR chemical shifts at  $\delta_H$  2.09 (s) and 2.40 (t) are characteristics of methyl protons of acetate, and methine proton at C-8, while the proton signals at  $\delta_H$  3.35 (m) and 3.55 (m) indicated the presence of oxymethylene protons at C-4' and C-26 respectively. Methine protons at C-16 and C-3 appeared at 4.23-4.28 (m), while the proton signal at  $\delta_H$  6.40 (s) was attributed to olefinic methine proton at C-6 [Fig. 5.58]. <sup>13</sup>C NMR spectrum [Fig. 5.59] revealed thirty three carbon resonances which were confirmed by DEPT spectra data [Fig. 5.60]. The multiplicities of carbons are: five methyl, twelve methylene, nine methine and seven quaternary carbon resonances. The NMR data of Hak-10 were also compared with its 7-oxime ester analogue data in Table 4.85. The spectroscopic data of Hak-10, compared with its 7-oxime ester analogue, Hak-5 led to its structural elucidation to be (22 $\beta$ ,25R)-3 $\beta$ -Acetoxy-spirost-5-en-3 $\beta$ -yl-7-(4'-butanoic)-ketoxime.

**Table 4.85:** Comparison of  $^{13}\text{C}$  and  $^1\text{H}$  NMR data of Hak-5 and Hak-10

Assignment	* $^{13}\text{C}$	Multiplicity	* $^1\text{H}$ , Muultiplicity	$^{13}\text{C}$	$^1\text{H}$
1	29.23	$\text{CH}_2$	1.41-1.87, m, 2H	29.06	1.38-1.79, m, 2H
2	37.61	$\text{CH}_2$	1.41-1.87, m, 2H	37.57	1.38-1.79, m, 2H
3	73.30	CH	4.55, m, 1H	71.14	4.28, m, 1H
4	39.17	$\text{CH}_2$	1.41-1.87, m, 2H	38.97	1.38-1.79, m, 2H
5	152.40	Q	-	153.91	-
6	114.51	CH	6.57, s, 1H	114.46	6.45, s, 1H
7	156.90	$\text{CH}_2$	-	157.38	-
8	38.80	CH	2.82, t, 1H	38.84	2.40, t, 1H
9	49.97	CH	1.41-1.87, m, 1H	49.97	1.38-1.79, m, 1H
10	36.67	Q	-	36.97	-
11	20.91	$\text{CH}_2$	1.41-1.87, m, 2H	20.85	1.38-1.79, m, 2H
12	38.46	$\text{CH}_2$	1.41-1.87, m, 2H	31.37	1.38-1.79, m, 2H
13	41.12	Q	-	40.97	-
14	41.99	CH	1.41-1.87, m, 1H	41.84	1.38-1.79, m, 1H
15	35.04	$\text{CH}_2$	1.41-1.87, m, 2H	34.73	1.38-1.79, m, 2H
16	81.14	CH	4.66, m, 1H	81.11	4.23, m, 1H
17	60.69	CH	1.41-1.87, m, 1H	60.76	1.38-1.79, m, 1H
18	50.63	CH	1.41-1.87, m, 1H	50.61	1.38-1.79, m, 1H
19	18.33	$\text{CH}_3$	0.78-1.36, m, 3H	18.27	0.68-1.30, m, 3H
20	16.95	$\text{CH}_3$	0.78-1.36, m, 3H	16.92	0.68-1.30, m, 3H
21	14.69	$\text{CH}_3$	0.78-1.36, m, 3H	14.47	0.68-1.30, m, 3H
22	109.48	Q	-	109.74	-
23	35.04	$\text{CH}_2$	1.41-1.87, m, 2H	30.56	1.38-1.79, m, 2H
24	27.85	$\text{CH}_2$	1.41-1.87, m, 2H	22.45	1.38-1.79, m, 2H
25	31.43	$\text{CH}_2$	1.41-1.87, m, 2H	29.96	1.38-1.79, m, 2H
26	67.20	$\text{CH}_3$	3.46, d, 2H	67.07	3.55, d, 2H
27	17.50	$\text{CH}_3$	0.78-1.36, m, 3H	17.42	0.68-1.30, m, 3H
28	21.67	$\text{CH}_3$	2.03, s, 3H	21.01	2.09, s, 3H
29	170.91	Q	-	174.81	-
1', acid	173.31	Q	-	<b>178.47</b>	-
2'	31.85	$\text{CH}_2$	1.18-2.40, m, 2H	42.43	1.12-2.31, m, 2H
3'	25.23	$\text{CH}_2$	1.18-2.40, m, 2H	28.85	1.12-2.31, m, 2H
4'	61.56	$\text{CH}_2$	4.05, m, 2H	69.00	3.35, m, 2H
$\text{OCH}_2$ of ester	61.56	$\text{CH}_2$	3.34, m, 2H		

Implied multiplicities of the carbons were determined from the DEPT experiment. \* Hak-5



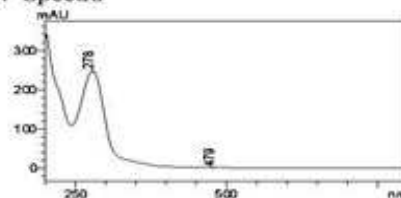
ANALYTICAL TEST REPORT

Sample Information for Direct Mass Analysis of Isolates/synthetic molecule  
Sample Code : ASN-HAK-7.4  
Solubility : MeOH  
Name of the Scientist : Dr.A S Negi  
Project Code: MLP-02  
Mass Range: 100-800

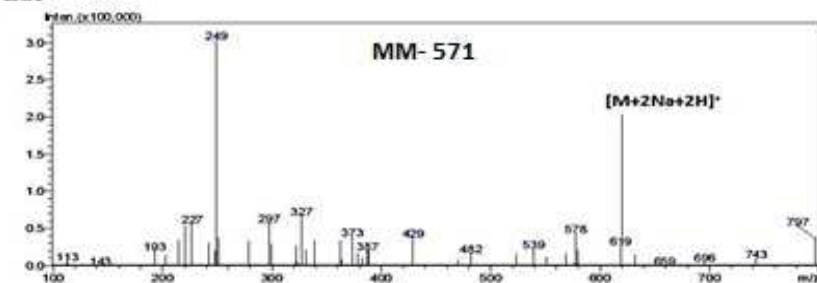
Mass chromatogram



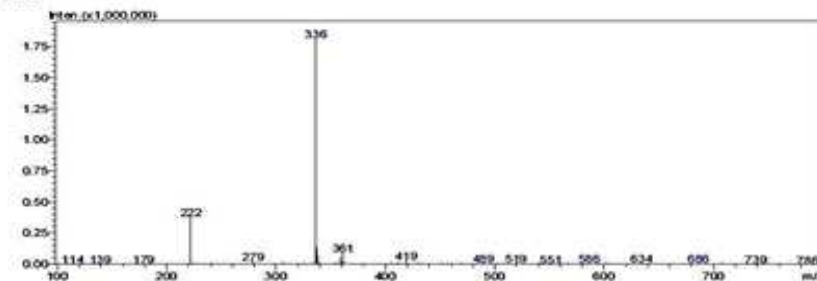
UV-Spectra



ESI+



ESI-



File Path-D:\Direct Mass report- Aug 2010\ASN-HAK-6.5.doc

Oct 14, 2013

[Dr. Karuna Shanker]

Fig. 5.57: Mass spectrum of Hak-10 in MeOH

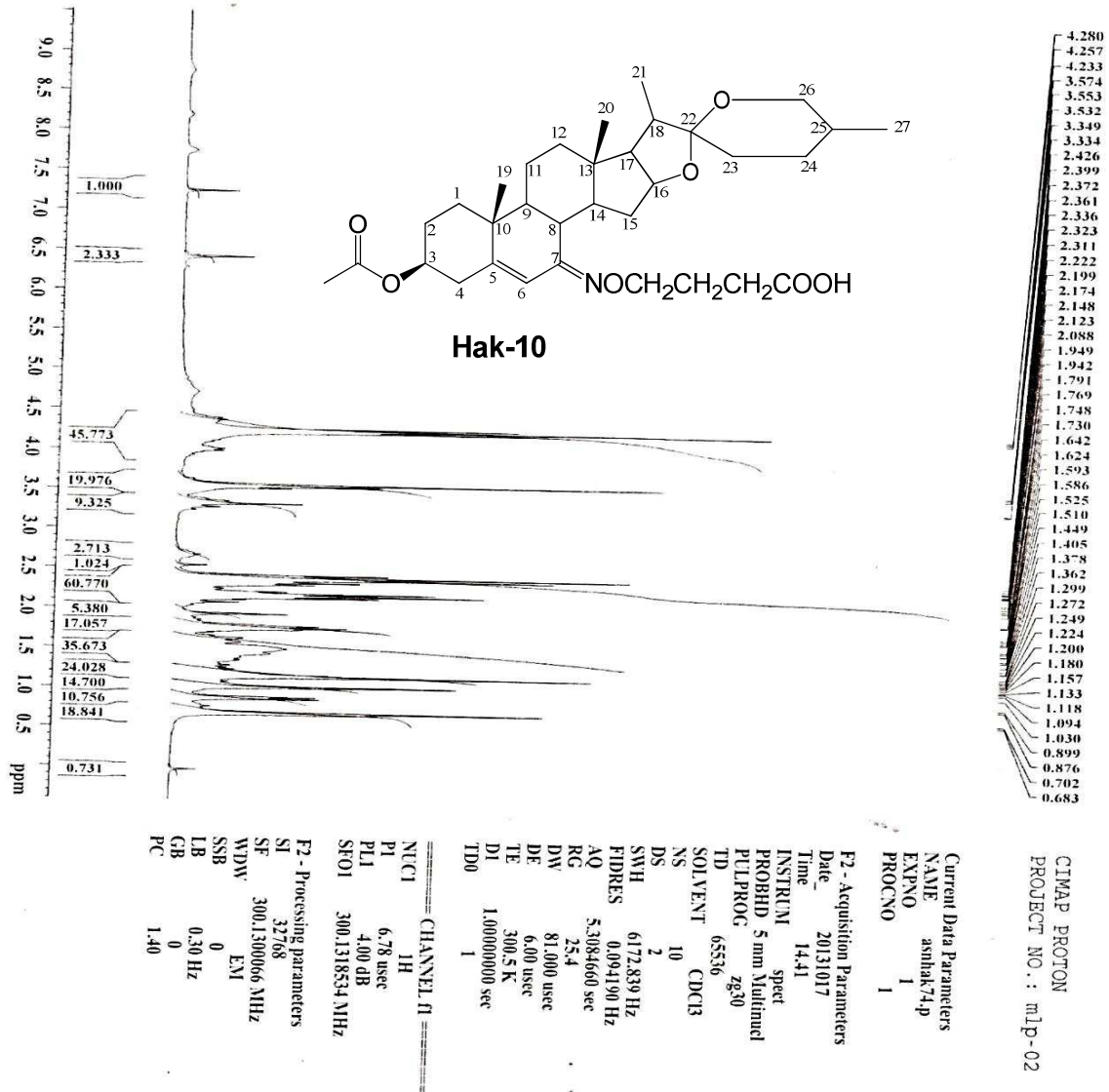


**Fig. 5.58:**  $^1\text{H}$  NMR spectrum of Hak-10 in  $\text{CDCl}_3$

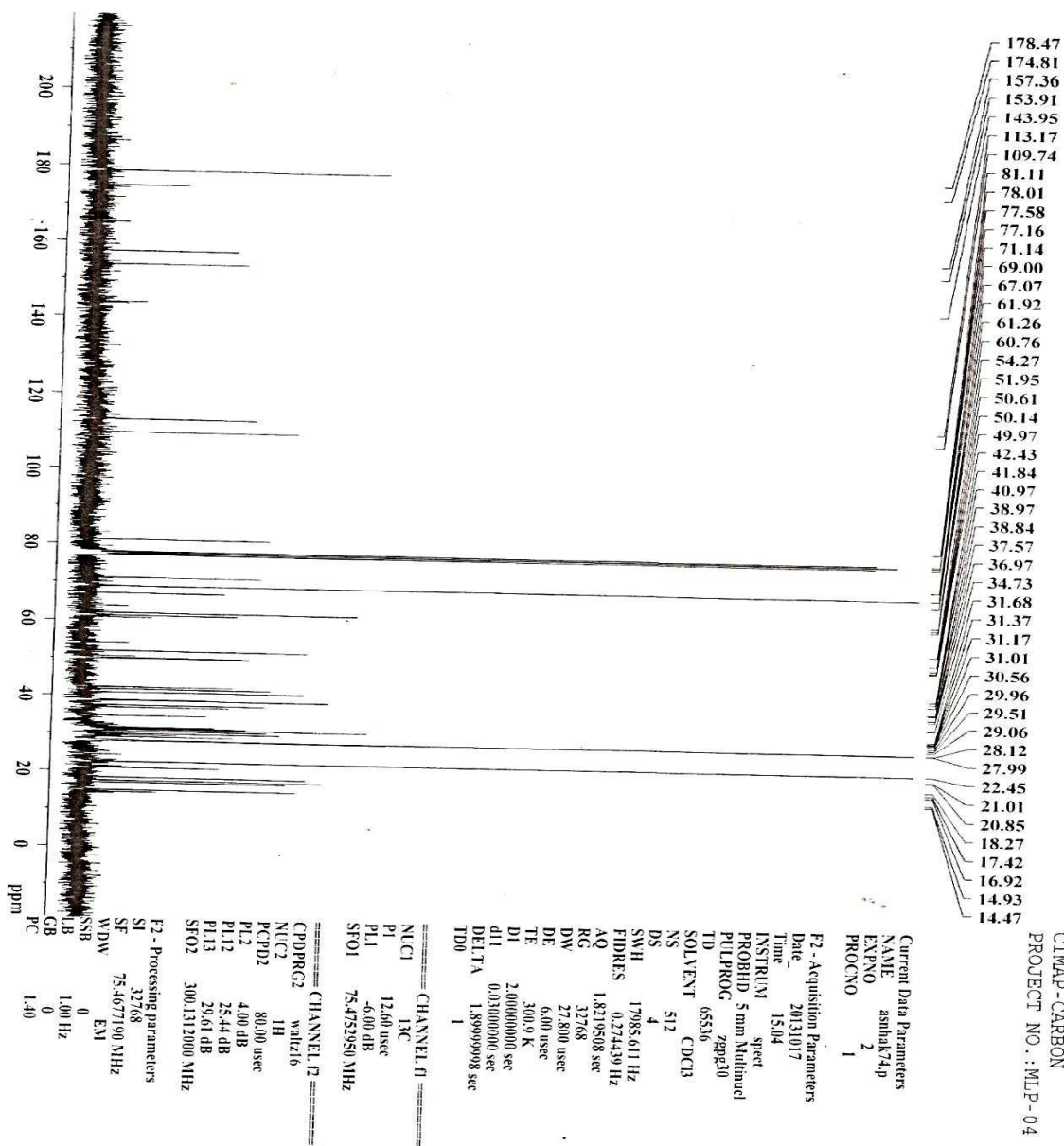


Fig. 5.59:  $^{13}\text{C}$  NMR spectrum of Hak-10 in  $\text{CDCl}_3$

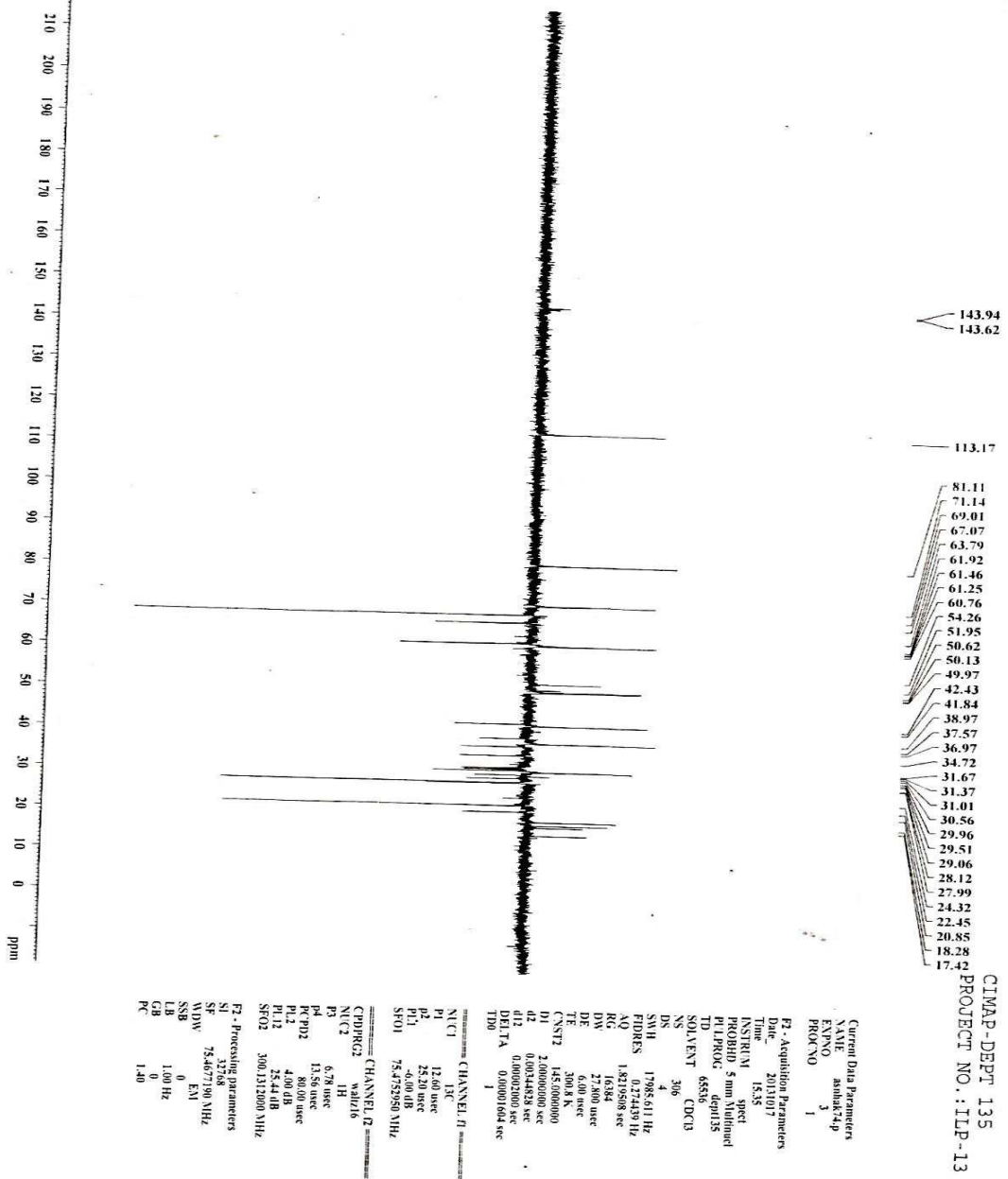
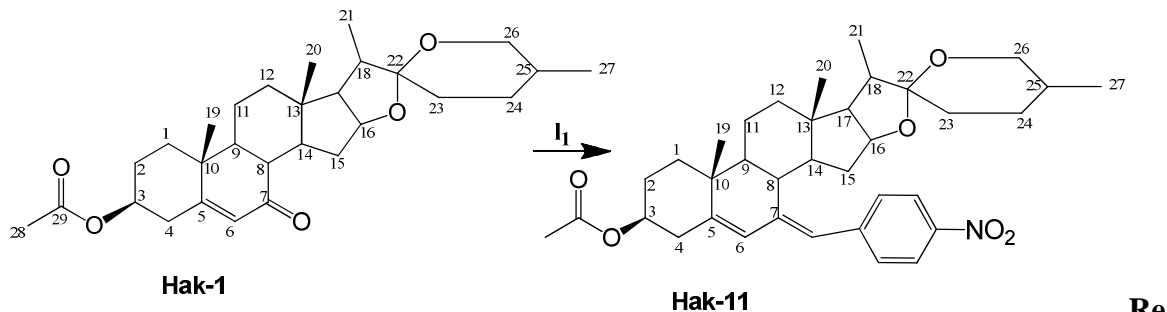


Fig. 5.60: DEPT spectrum of Hak-10 in  $CDCl_3$

#### 4.9.11. Synthesis and characterisation of (22 $\beta$ ,25R)-3 $\beta$ -Acetoxy-7-(4'-nitrobenzylidene)-spirost-5-en-3 $\beta$ -yl (Hak-11)

Wittig analogue Hak-11 was also prepared from Hak-1 following the same procedure as for Haad-6. The Wittig salt used was 4-nitrobenzyltriphenylphosphonium bromide



**agents and conditions:** I<sub>1</sub>) Wittig salt (4-nitrobenzyltriphenylphosphonium bromide), NaH, Toluene, Reflux at 110 - 130°C, 4 hrs

Hak-11 (65 mg, 65%) was obtained as orange solid with a melting point of 150 - 153°C. The Mass fragment ions at 549 [M-K-H]<sup>-</sup>, 691 [M+2K+Na+H]<sup>+</sup> gave molecular formula C<sub>36</sub>H<sub>47</sub>NO<sub>6</sub> (589) [Fig. 5.61]. The <sup>1</sup>H NMR signals at  $\delta_H$  1.95 (s) and 2.96 (t) correspond to methyl protons of acetate and methine proton at C-8, while the proton signals at  $\delta_H$  3.26 (m, 2H, OCH<sub>2</sub>) and 4.30 (m, 1H, OCH) were attributed to oxymethylene and oxymethine protons at C-26 and C-16 respectively. Methine protons at C-3 and C-1' also appeared at 4.03 (m) and 5.99 (bd). The chemical shift at  $\delta_H$  5.50 (s) was due to the presence of olefinic methine proton at C-6 while the aromatic protons (CH-3', 4', 6' & 7') appeared at  $\delta_H$  8.02 (t) [Fig. 5.62]. <sup>13</sup>C NMR spectrum [Fig. 5.63] revealed the resonance of spirostene skeleton of thirty six carbons, which were sorted by DEPT experiment [Fig. 5.64] into five methyl, nine methylene, fourteen methine and eight quaternary carbon resonances. The NMR data of Hak-11 were identical to 7-keto diosgenin skeleton, Hak-1. The difference was coupling of benzy group at position 7 which was also indicated by <sup>13</sup>C chemical shifts [ $\delta_C$  127.97 (C-1'), 124.09 (C-3'), 124.18 (C-7'), 129.66 (C-4') and 130.04 (C-6')]. The <sup>13</sup>C and <sup>1</sup>H NMR data of Hak-11 and Hak-1 were shown in Table 4.86. The spectroscopic data of Hak-11 and Hak-1 led to the confirmation of its structure to be (22 $\beta$ ,25R)-3 $\beta$ -Acetoxy-7-(4'-nitrobenzylidene)-spirost-5-en-3 $\beta$ -yl.

**Table 4.86:** Comparison of  $^{13}\text{C}$  and  $^1\text{H}$  NMR data of Hak-1 and Hak-11

Assignment	* $^{13}\text{C}$	Multiplicity	* $^1\text{H}$ , Multiplicity	$^{13}\text{C}$	$^1\text{H}$
1	29.18	CH <sub>2</sub>	1.40-1.97, m, 2H	30.01	1.39-1.90, m, 2H
2	37.37	CH <sub>2</sub>	1.40-1.97, m, 2H	36.79	1.39-1.90, m, 2H
3	72.51	CH	4.35, m, 1H	61.47	4.03, m, 1H
4	40.15	CH <sub>2</sub>	1.40-1.97, m, 2H	39.25	1.39-1.90, m, 2H
5	164.46	Q	-	162.27	-
6	126.85	CH	5.67, s, 1H	137.51	5.50, s, 1H
7	201.66	CH <sub>2</sub>	-	171.85	-
8	45.26	CH	2.50, t, 1H	45.90	2.40, t, 1H
9	50.04	CH	1.40-1.97, m, 1H	49.91	1.39-1.90, m, 1H
10	35.55	Q	-	34.14	-
11	21.28	CH <sub>2</sub>	1.40-1.97, m, 2H	21.28	1.39-1.90, m, 2H
12	30.06	CH <sub>2</sub>	1.40-1.97, m, 2H	37.20	1.39-1.90, m, 2H
13	41.34	Q	-	41.80	-
14	41.46	CH	1.40-1.97, m, 1H	41.99	1.39-1.90, m, 1H
15	32.29	CH <sub>2</sub>	1.40-1.97, m, 2H	31.71	1.39-1.90, m, 2H
16	81.30	CH	4.67, m, 1H	81.43	4.30, m, 1H
17	62.45	CH	1.40-1.97, m, 1H	61.47	1.39-1.90, m, 2H
18	61.50	CH	1.40-1.97, m, 1H	50.54	1.39-1.90, m, 2H
19	17.67	CH <sub>3</sub>	0.93-1.22, m, 3H	21.04	0.78-1.36, m, 3H
20	16.78	CH <sub>3</sub>	0.93-1.22, m, 3H	16.86	0.78-1.36, m, 3H
21	14.86	CH <sub>3</sub>	0.93-1.22, m, 3H	14.45	0.78-1.36, m, 3H
22	109.67	Q	-	109.67	-
23	30.68	CH <sub>2</sub>	1.40-1.97, m, 2H	33.13	1.39-1.90, m, 2H
24	27.70	CH <sub>2</sub>	1.40-1.97, m, 2H	29.08	1.39-1.90, m, 2H
25	38.47	CH <sub>2</sub>	1.40-1.97, m, 2H	30.59	1.39-1.90, m, 2H
26	67.15	CH <sub>3</sub>	3.43, d, 2H	67.11	3.26, d, 2H
27	17.50	CH <sub>3</sub>	0.93-1.22, m, 3H	17.40	0.78-1.36, m, 3H
28	21.59	CH <sub>3</sub>	2.03, s, 3H	23.73	1.95, s, 3H
29	170.61	Q	-	176.90	-
1'				<b>127.97</b>	<b>5.99, d, 1H</b>
2'				<b>148.50</b>	-
3'				<b>124.09</b>	<b>8.02, s, 1H</b>
4'				<b>129.66</b>	<b>8.02, s, 1H</b>
5'				<b>176.90</b>	-
6'				<b>130.04</b>	<b>8.02, s, 1H</b>
7'				<b>124.18</b>	<b>8.02, s, 1H</b>

Implied multiplicities of the carbons were determined from the DEPT experiment. \* Hak-1

ANALYTICAL TEST REPORT

Sample Information for Direct Mass Analysis of Isolates/synthetic molecule

Sample Code : ASN-HAK-12

Solubility : MeOH

Name of the Scientist : Dr.A S Negi

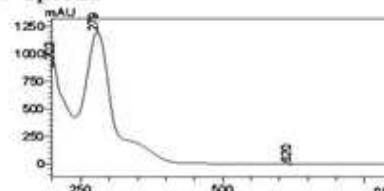
Project Code: MLP-02

Mass Range: 100-800

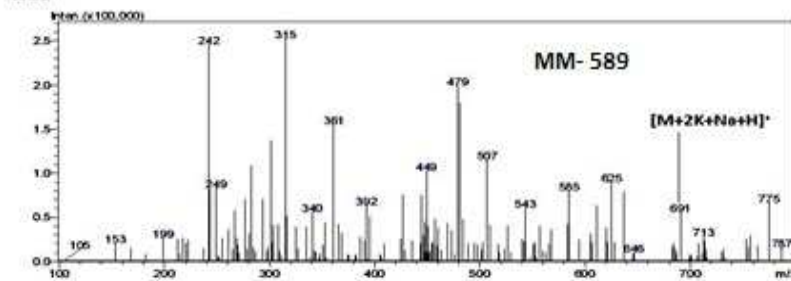
Mass chromatogram



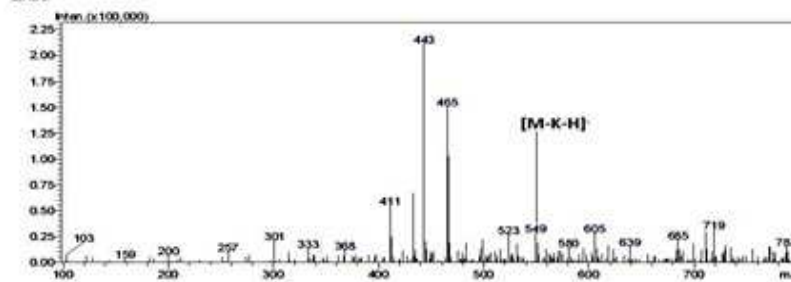
UV-Spectra



ESI+



ESI-



File Path-D:\Direct Mass report- Aug 2010\ASN-HAK-12.doc

Oct 14, 2013

[Dr. Karuna Shanker]

Fig. 5.61: Mass spectrum of Hak-11 in MeOH

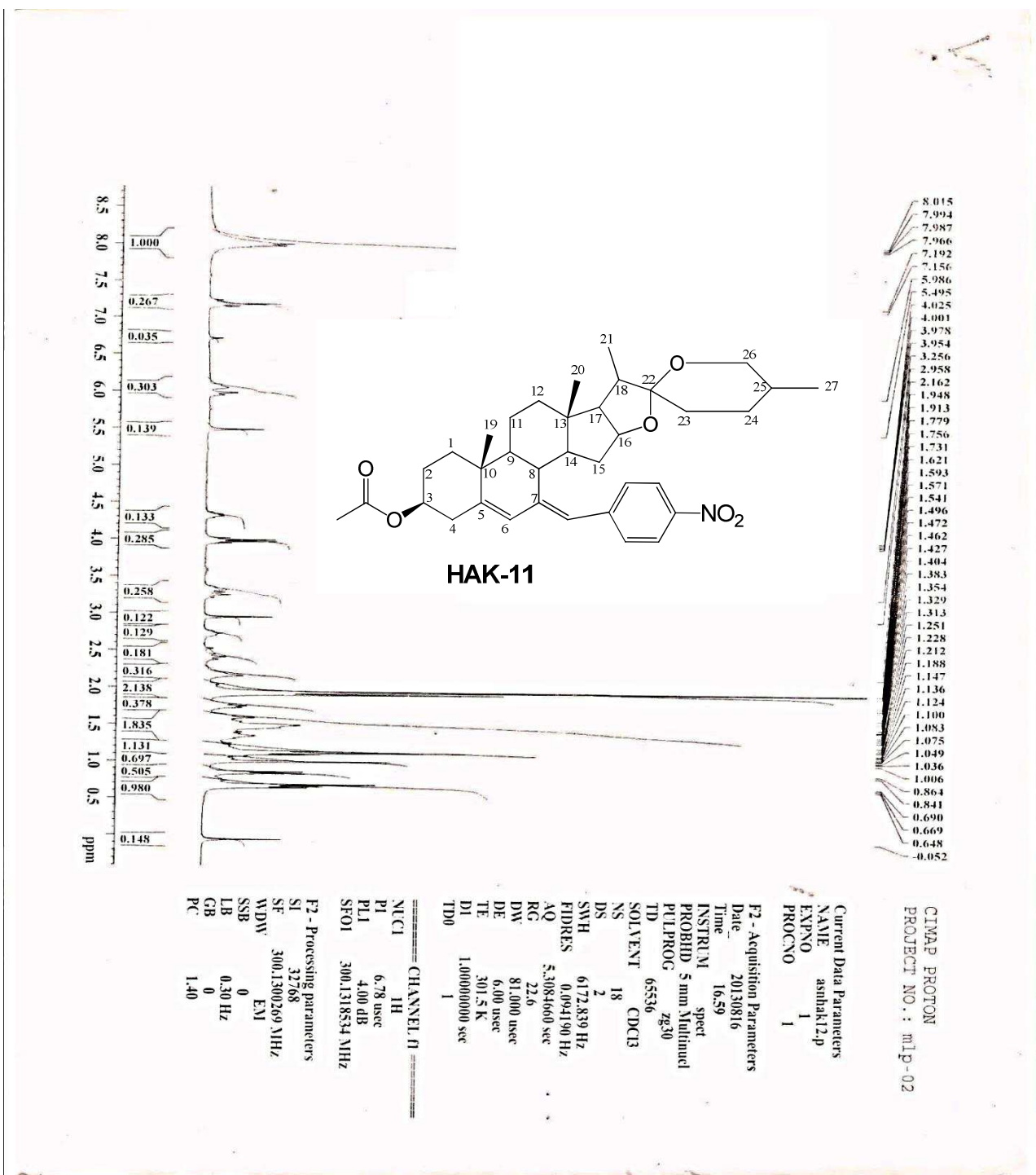


**Fig. 5.62:**  $^1\text{H}$  NMR spectrum of Hak-11 in  $\text{CDCl}_3$



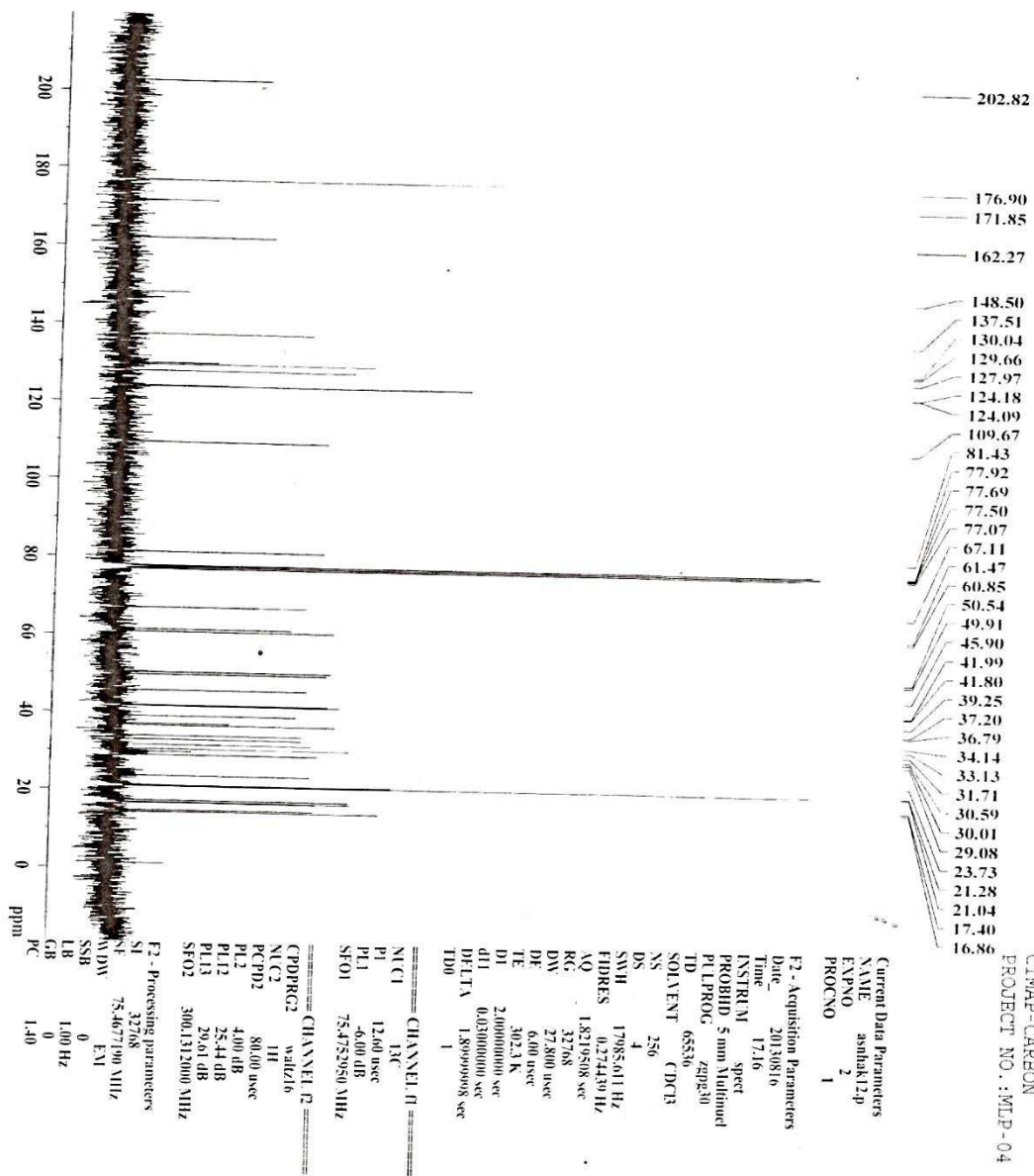
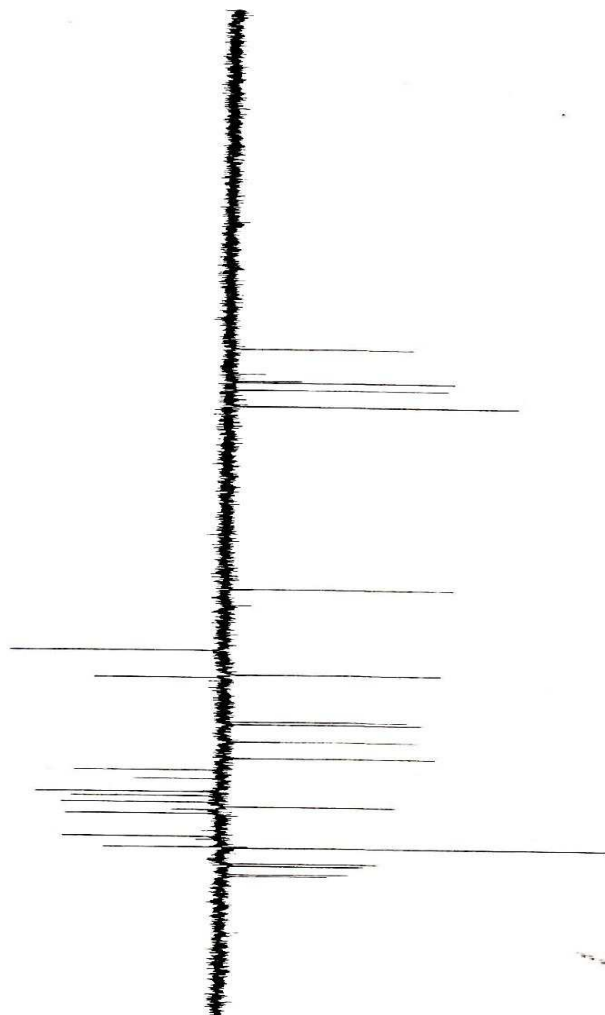


Fig. 5.63: <sup>13</sup>C NMR spectrum of Hak-11 in CDCl<sub>3</sub>

210 200 190 180 170 160 150 140 130 120 110 100 90 80 70 60 50 40 30 20 10 0 ppm

137.51  
131.72  
130.04  
129.66  
127.97  
124.18  
124.09

81.43  
77.70  
67.11  
61.46  
60.86  
50.54  
49.91  
45.90  
41.99  
39.25  
37.20  
34.14  
33.13  
31.71  
30.59  
30.01  
29.08  
23.72  
22.99  
21.26  
21.04  
17.40  
16.86  
16.76  
14.90  
14.45



CIMAP-DEPT 135  
PROJECT NO.: ILLP-13

```

Current Data Parameters
NAME      anah12.p
EXPNO     3
PROCNO    1

F2 - Acquisition Parameters
Date_     20190816
Time      17:21
INSTRUM   spect
PROBHD    5mm VNP1H
PULPROG   zgpg30
TD         65536
SOLVENT   CDCl3
NS         200
DS         4
SWH        17985.611 Hz
FIDRES     0.274439 Hz
AQ         1.8219568 sec
RG         16.84
DM         27.800 usec
DE         6.00 usec
TE         302.1 K
CA12      1.65900000
D1         2.00000000 usec
d12        0.00000000 usec
DEFTV     0.00001004 usec
100

===== CHANNEL f1 =====
NUC1       13C
P1         12.00 usec
PC         25.20 usec
PL1        -8.00 dB
SFO1       75.475250 MHz

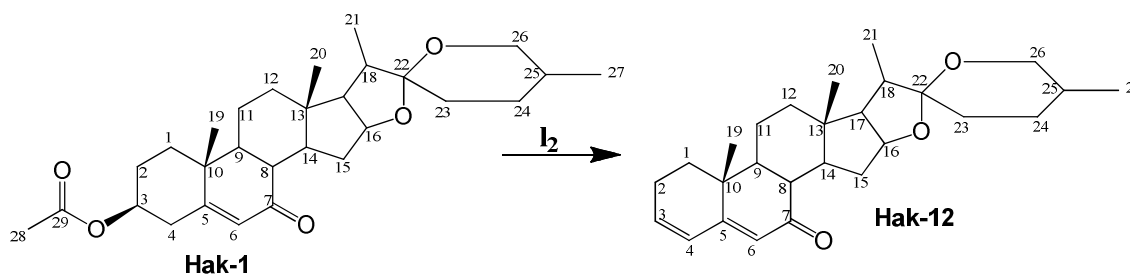
===== CHANNEL f2 =====
CPDPRG2    waltz16
NUC2       1H
P2         6.78 usec
PC         13.56 usec
PL2        80.00 usec
PL12       4.00 dB
PL12       28.44 dB
SFO2       300.137200 MHz

F2 - Processing parameters
SI         32768
SF         75.467190 MHz
SSB        0
LB         1.00 Hz
GB         0
PC         1.40
  
```

Fig. 5.64: DEPT spectrum of Hak-11 in CDCl<sub>3</sub>

#### 4.9.12 Synthesis and characterisation of (22 $\beta$ ,25R)-7-oxo-spirost-3,5-diene (Hak-12)

Hak-12 was formed while trying to obtain Wittig analogues from 7-keto derivative Hak-1 by using other electron withdrawing-substituent Wittig salts (Benzyltriphenylphosphonium bromide, 3,4,5-trimethoxybenzyltriphenylphosphonium bromide and 3,4-methylenedioxybenzyltriphenylphosphonium bromide). The same procedure was also used as for Haad-6.



**Reagents and conditions:**  $I_2$ ) Wittig salts (Benzyltriphenylphosphonium bromide, 3,4,5-trimethoxybenzyltriphenylphosphonium bromide and 3,4-methylenedioxybenzyltriphenylphosphonium bromide), NaH, Toluene, Reflux at 110 - 130°C, 3 hrs

Hak-12 (90 mg, 90%) is an orange solid (melting point 181 - 184°C). The Mass fragment peaks at 412  $[M+2H]^-$ , 433  $[M+Na]^+$ , 449  $[M+K]^-$  gave molecular formula  $C_{27}H_{38}O_3$  (410) [Fig. 5.65]. The  $^1H$  NMR chemical shifts at  $\delta_H$  2.86 (t) and 3.40 (m) correspond to methine and oxymethylene protons at C-8 and C-26, while the proton signals at  $\delta_H$  4.44 (m,) and 5.56 (s) were assignable to oxymethine and olefinic methine protons at C-16 and C-6 respectively. The chemical shift at  $\delta_H$  6.13 (m) indicated the presence of olefinic methine protons at C-3 and C-4 [Fig. 5.66].  $^{13}C$  NMR and DEPT spectra [Fig. 5.67 & 5.68] also revealed carbon resonances similar to spirostene skeleton. There were twenty seven carbons which were sorted into four methyl, eight methylene, ten methine and five quaternary carbon resonances. The NMR data of Hak-12 were identical to its 7-keto analogue skeleton, Hak-1 except the presence of olefinic carbons at 3 and 4 positions [ $\delta_C$  124.32 (C-3) and 137.13 (C-4)]. The  $^{13}C$  and  $^1H$  NMR data of Hak-12 and Hak-1 were shown in Table 4.87. Hence, the structure of Hak-12 was identified as (22 $\beta$ ,25R)-7-oxo-spirost-3,5-diene.

**Table 4.87:** Comparison of  $^{13}\text{C}$  and  $^1\text{H}$  NMR data of Hak-1 and Hak-12

Assignment	* $^{13}\text{C}$	Multiplicity	* $^1\text{H}$ , Multiplicity	$^{13}\text{C}$	$^1\text{H}$
1	29.18	$\text{CH}_2$	1.40-1.97, m, 2H	29.19	1.40-1.86, m, 2H
2	37.37	$\text{CH}_2$	1.40-1.97, m, 2H	33.20	2.50, m, 2H
3	72.51	CH	4.35, m, 1H	<b>124.32</b>	<b>6.13, m, 1H</b>
4	40.15	$\text{CH}_2$	1.40-1.97, m, 2H	<b>137.13</b>	<b>6.13, m, 1H</b>
5	164.46	Q	-	161.59	-
6	126.85	CH	5.67, s, 1H	128.05	5.56, s, 1H
7	201.66	$\text{CH}_2$	-	202.14	-
8	45.26	CH	2.50, t, 1H	45.95	2.86, t, 1H
9	50.04	CH	1.40-1.97, m, 1H	49.94	2.25, d, 1H
10	35.55	Q	-	36.80	-
11	21.28	$\text{CH}_2$	1.40-1.97, m, 2H	21.31	1.40-1.86, m, 2H
12	30.06	$\text{CH}_2$	1.40-1.97, m, 2H	34.27	1.40-1.86, m, 2H
13	41.34	Q	-	41.79	-
14	41.46	CH	1.40-1.97, m, 1H	42.01	1.40-1.86, m, 1H
15	32.29	$\text{CH}_2$	1.40-1.97, m, 2H	32.28	1.40-1.86, m, 2H
16	81.30	CH	4.67, m, 1H	81.41	4.44, m, 1H
17	62.45	CH	1.40-1.97, m, 1H	61.60	1.40-1.86, m, 2H
18	61.50	CH	1.40-1.97, m, 1H	50.61	1.40-1.86, m, 1H
19	17.67	$\text{CH}_3$	0.93-1.22, m, 3H	17.50	0.75-1.32, m, 3H
20	16.78	$\text{CH}_3$	0.93-1.22, m, 3H	16.85	0.75-1.32, m, 3H
21	14.86	$\text{CH}_3$	0.93-1.22, m, 3H	15.02	0.75-1.32, m, 3H
22	109.67	Q	-	109.51	-
23	30.68	$\text{CH}_2$	1.40-1.97, m, 2H	30.69	1.40-1.86, m, 2H
24	27.70	$\text{CH}_2$	1.40-1.97, m, 2H	23.76	1.40-1.86, m, 2H
25	38.47	$\text{CH}_2$	1.40-1.97, m, 2H	30.06	1.40-1.86, m, 2H
26	67.15	$\text{CH}_3$	3.43, d, 2H	67.15	3.40, d, 2H
27	17.50	$\text{CH}_3$	0.93-1.22, m, 3H	16.97	0.75-1.32, m, 3H
28	21.59	$\text{CH}_3$	2.03, s, 3H		
29	170.61	Q			

Implied multiplicities of the carbons were determined from the DEPT experiment. \* Hak-1

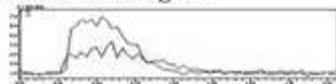
ANALYTICAL TEST REPORT

Sample Information for Direct Mass Analysis of Isolates/synthetic molecule

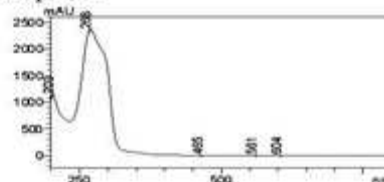
Sample Code : ASN-HAK-17  
Solubility : MeOH  
Name of the Scientist : Dr. A S Negi

Project Code: MLP-02  
Mass Range: 100-800

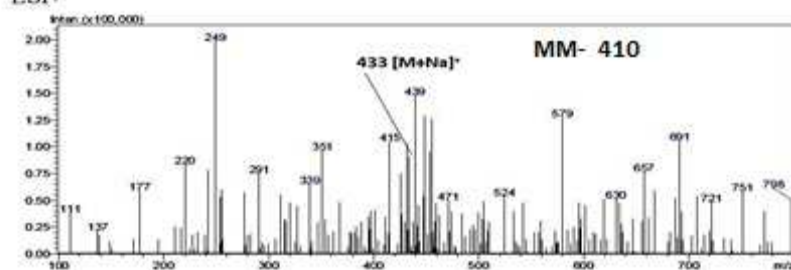
Mass chromatogram



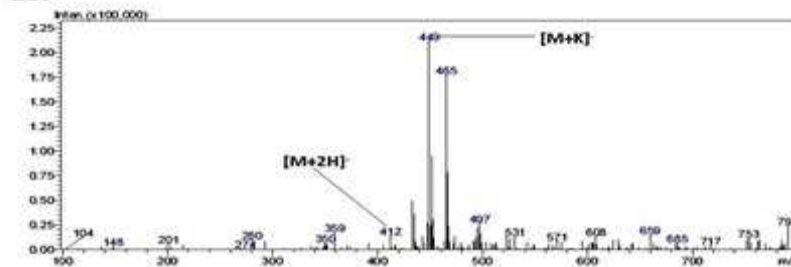
UV-Spectra



ESI+



ESI-



File Path-D:\Direct Mass report- Aug 2010\ASN-HAK-17.doc

Oct 14, 2013

[Dr. Karuna Shanker]

Fig. 5.65: Mass spectrum of Hak-12 in MeOH

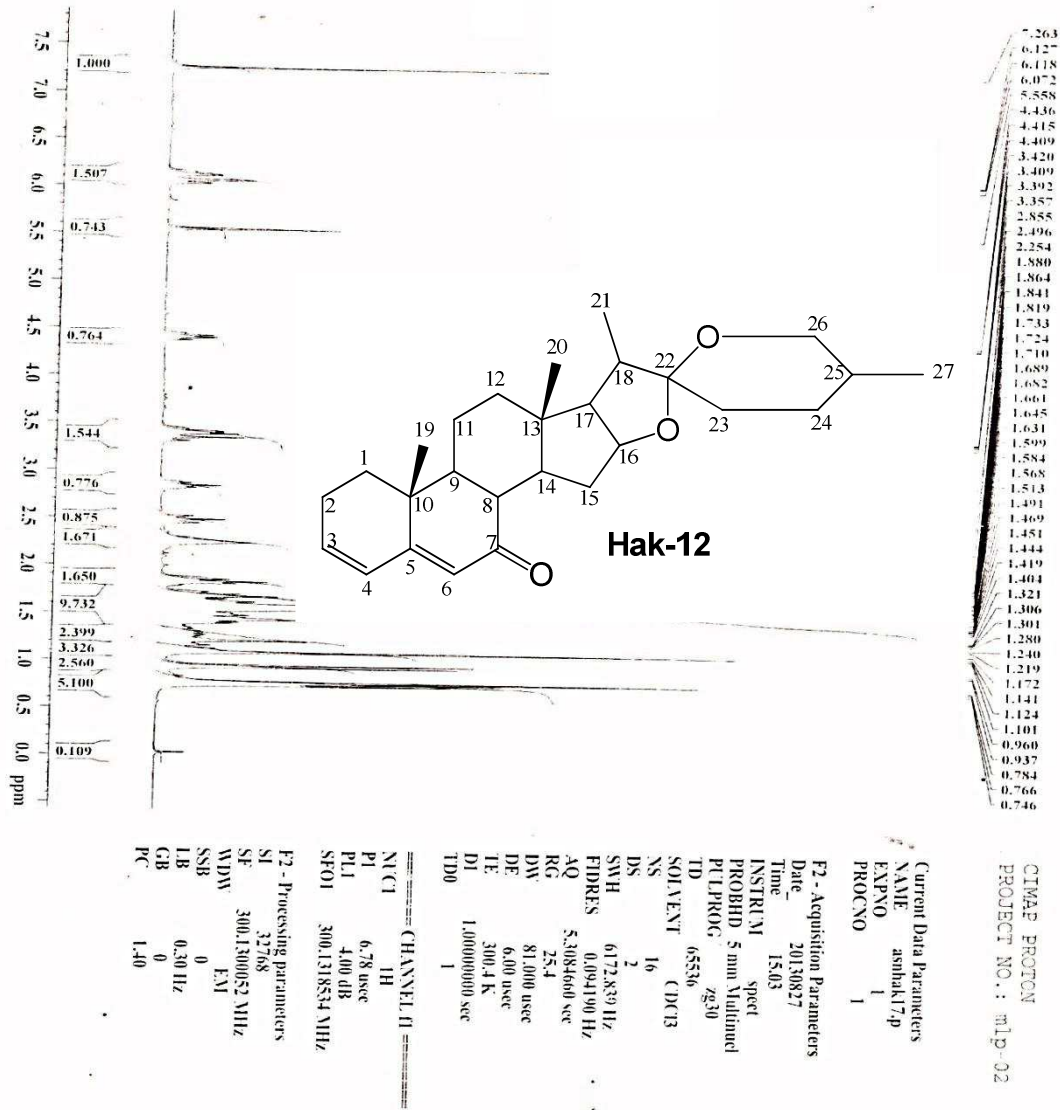


Fig. 5.66: <sup>1</sup>H NMR spectrum of Hak-12 in CDCl<sub>3</sub>

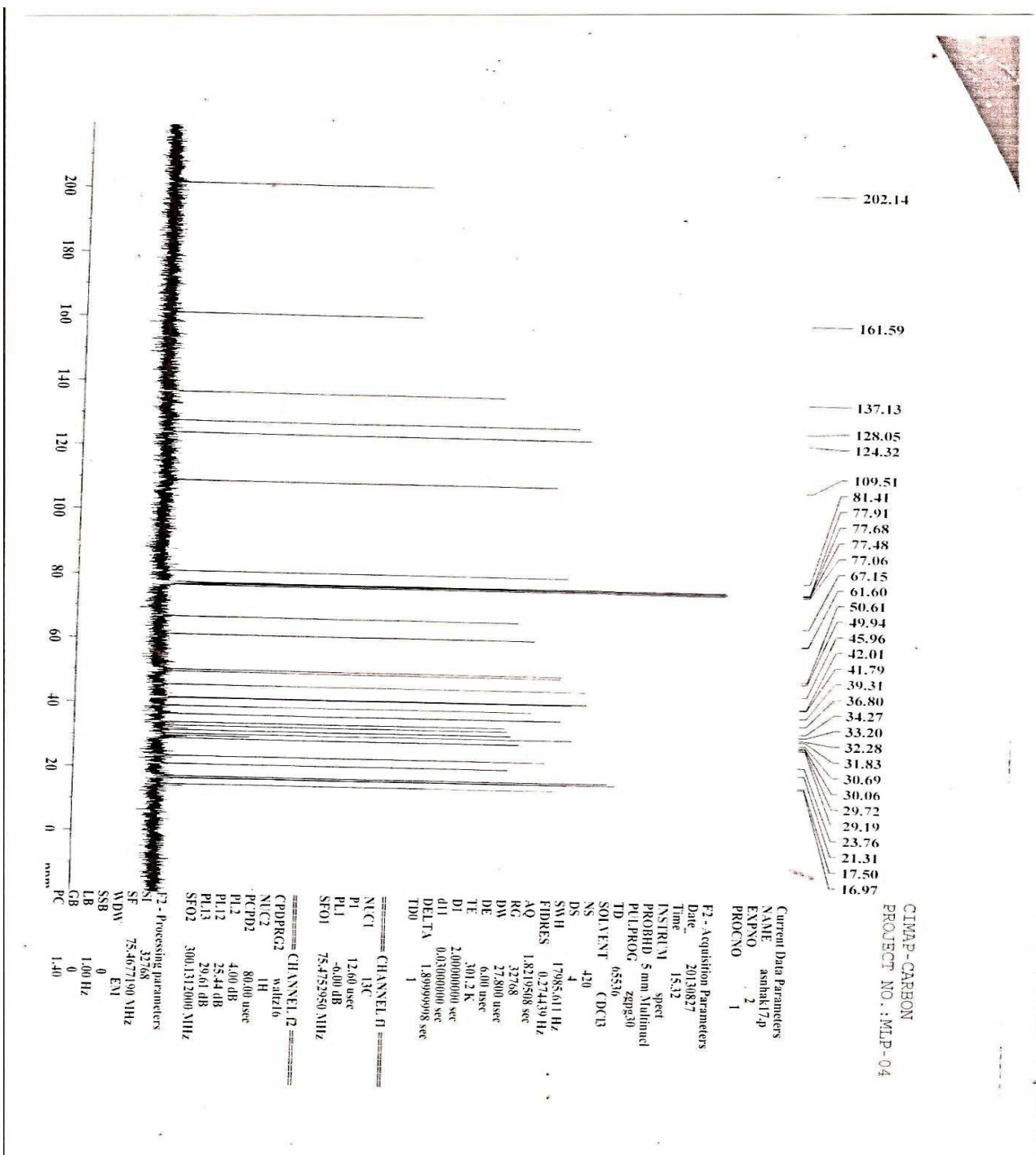


Fig. 5.67:  $^{13}\text{C}$  NMR spectrum of Hak-12 in  $\text{CDCl}_3$

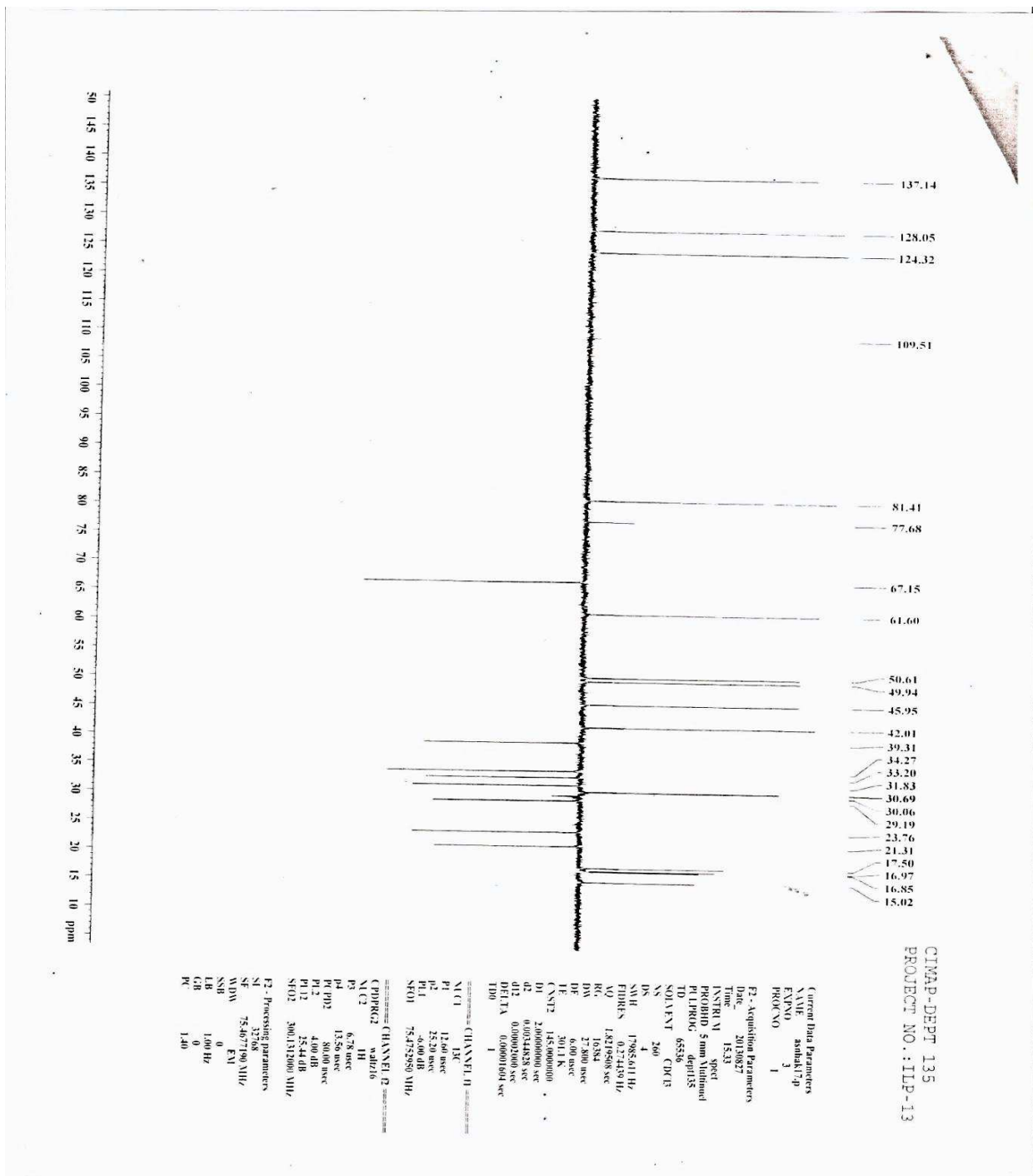


Fig. 5.68: DEPT spectrum of Hak-12 in CDCl<sub>3</sub>



#### 4.10 Antiproliferative activity of synthesized compounds

Fifteen and twelve diogenin derivatives from scheme 5 and scheme 6 respectively were tested for antiproliferative activities. All synthesized compounds were evaluated against C33A (Cervical carcinoma), A549 (Lung carcinoma), KB (HeLa contaminant of mouth epidermal carcinoma), MCF-7 (Breast adenocarcinoma), DU145 (prostate carcinoma), COLO (colorectal adenocarcinoma) and FaDu (hypopharyngeal carcinoma) human cancer cell lines by Sulphorhodamine assay. The synthesized compounds possess higher antiproliferative properties than diosgenin. Five of the analogues from scheme 5; (22 $\beta$ ,25R)-26-hydroxyfurost-5-en-3 $\beta$ -acetate (Haad-2a), (22 $\beta$ )-25-oxo-27-nor-furost-5-en-3 $\beta$ -acetate (Haad-4), (22 $\beta$ )-3 $\beta$ -acetoxy-furost-5-en-26-aldoxime (Haad-8), (22 $\beta$ )-3 $\beta$ -Acetoxy-furost-5-en-26-aldoxime acetate (Haad-9) and (22 $\beta$ )-25-oxo-27-nor-furost-5-en-25-ketoxime-3 $\beta$ ,26-diacetate (Haad-11) exhibited significant anticancer activities at a very low concentration of 20  $\mu$ M. Compound Haad-2a inhibited the growth of KB, C-33A and MCF-7 with IC<sub>50</sub> of 11.43, 7.54 and 10.95  $\mu$ M respectively, the activities being comparable with that of the standard drug, Tamoxifen. (22 $\beta$ )-25-oxo-27-nor-furost-5-en-3 $\beta$ -acetate (Haad-4) exhibited cytotoxic activity against KB, C-33A, DU145 and MCF-7 with IC<sub>50</sub> of 17.55, 11.54, 16.83 and 15.17  $\mu$ M but showed no activity against A549 cell line below concentration of 20  $\mu$ M [Table 4.88]. Aldoxime and ketoxime derivatives, Haad-8, Haad-9 and Haad-11 showed antiproliferative activities against KB, C-33A, DU145, A549 and MCF-7 cell lines with IC<sub>50</sub> below 20  $\mu$ M, except Haad-11 which exhibited no anticancer activity against DU145 cell line below IC<sub>50</sub> of 20  $\mu$ M.

Four analogues from scheme 6 exhibited cytotoxic activities against FaDU, A549, COLO, MCF-7 and DU145 cell lines. The compounds are: (22 $\beta$ ,25R)-3 $\beta$ -Acetoxy-spirost-5-en-3 $\beta$ -yl-7-(ethyl-3<sup>1</sup>-propanoate)-ketoxime (Hak-4), (22 $\beta$ ,25R)-3 $\beta$ -Acetoxy-spirost-5-en-3 $\beta$ -yl-7-(ethyl-7<sup>1</sup>-heptanoate)-ketoxime (Hak-8), (22 $\beta$ ,25R)-3 $\beta$ -Acetoxy-spirost-5-en-3 $\beta$ -yl-7-(4<sup>1</sup>-butanoic)-ketoxime (Hak-10) and (22 $\beta$ ,25R)-3 $\beta$ -Acetoxy-7-(4-nitrobenzylidene)-spirost-5-en-3 $\beta$ -yl (Hak-11). The results of antiproliferative activities of the derivatives are shown in Table 4.89. Compounds Hak-4 and Hak-8 inhibited the growth of FaDU, A549, COLO,

MCF-7 and DU145 cancer cell lines with with  $IC_{50}$  less than 50  $\mu$ M, except Hak-4 which showed low inhibition of A549 cell line with with  $IC_{50}$  above 50  $\mu$ M. Butanoic and nitrobenzylidene ketoxime derivatives, Hak-10 and Hak-11 exhibited significant antiproliferative activities against five cell lines (FaDU, A549, COLO, MCF-7 and DU145) with  $IC_{50}$  of 16.56 and 15.21; 17.05 and 15.77; 16.01 and 14.55; 15.59 and 15.77; and 14.67 and 12.82  $\mu$ M respectively. The activities of the two derivatives were comparable to that of anticancer drug, Tamoxifen ( $IC_{50}$  of 10.25, 6.94, 12.24, 10.07 and 8.54  $\mu$ M). Other analogues showed <50% growth inhibition at 50  $\mu$ M concentrations.

**Table 4.88:** Antiproliferative activities of synthesized compounds from the first reaction scheme

S/No	Compound code/Standard	Cell lines/IC <sub>50</sub> (uM)				
		KB	C-33A	DU145	A549	MCF-7
1.	<b>Haad-1</b>	>20	>20	>20	>20	>20
2.	<b>Haad-2a</b>	11.43	7.54	>20	>20	10.95
3.	<b>Haad-2b</b>	>20	>20	>20	>20	>20
4.	<b>Haad-3</b>	>20	>20	>20	>20	>20
5.	<b>Haad-4</b>	17.55	11.54	16.83	>20	15.17
6.	<b>Haad-5</b>	>20	>20	>20	>20	>20
7.	<b>Haad-6</b>	>20	>20	>20	>20	>20
8.	<b>Haad-7a</b>	>20	>20	>20	>20	>20
9.	<b>Haad-7b</b>	>20	>20	>20	>20	>20
10.	<b>Haad-8</b>	15.97	11.18	17.08	15.27	14.53
11.	<b>Haad-9</b>	13.96	12.27	13.27	12.56	14.28
12.	<b>Haad-10</b>	>20	>20	>20	>20	>20
13.	<b>Haad-11</b>	17.52	13.15	>20	16.29	18.67
14.	<b>Haad-12a</b>	>20	>20	>20	>20	>20
15.	<b>Haad-12b</b>	>20	>20	>20	>20	>20
16.	Tamoxifen	10.25	6.94	12.24	10.07	8.54

**KB** - HeLa contaminant of mouth epidermal carcinoma; **C33A** - Cervical carcinoma  
**DU145** - prostate carcinoma; **A549** - Lung carcinoma; **MCF-7** - Breast adenocarcinoma

**Table 4.89:** Antiproliferative activities of synthesized compounds from the second reaction scheme

S/No	Compound code/Standard	Cell lines/IC <sub>50</sub> (uM)				
		FaDu	A549	COLO	MCF-7	DU145
1.	<b>Hak-1</b>	>50	>50	>50	>50	>50
2.	<b>Hak-2</b>	>50	>50	>50	>50	>50
3.	<b>Hak-3</b>	>50	>50	>50	>50	>50
4.	<b>Hak-4</b>	33.30	>50	35.49	35.10	31.52
5.	<b>Hak-5</b>	>50	>50	>50	>50	>50
6.	<b>Hak-6</b>	>50	>50	>50	>50	>50
7.	<b>Hak-7</b>	>50	>50	>50	>50	>50
8.	<b>Hak-8</b>	26.95	21.92	40.20	29.43	35.43
9.	<b>Hak-9</b>	>50	>50	>50	>50	>50
10.	<b>Hak-10</b>	16.56	17.05	16.01	15.59	14.67
11.	<b>Hak-11</b>	15.21	15.77	14.55	15.77	12.82
12.	<b>Hak-12</b>	>50	>50	>50	>50	>50
13.	Tamoxifen	10.25	6.94	12.24	10.07	8.54

**FaDu** – hypopharyngeal; **A549** - Lung carcinoma, carcinoma;

**COLO** - colorectal adenocarcinoma; **MCF-7** - Breast adenocarcinoma;

**DU145** - prostate carcinoma

#### 4.11 Conclusion and Recommendations

*Smilax kraussiana* is used traditionally for the treatment of fever, venereal diseases, skin diseases, tumor and infertility. The findings of this research showed that the aerial parts of *S. kraussiana* possess antiproliferative properties. Nineteen compounds were isolated from the plant, and exhibited anticancer activities against tested cancer cell lines. These compounds are being reported for the first time from *Smilax kraussiana*. Furthermore, synthetic modification of the most bioactive isolated compound, diosgenin via two different schemes afforded twenty seven compounds. Nineteen of these compounds are new, and have not been previously reported in the chemical literature. Some of these synthesized compounds exhibited higher antiproliferative activities than diosgenin at low concentration of 20  $\mu$ M. The phytochemical constituents of extracts of *S. kraussiana* justify its use in ethnomedicine.

The synthesized diosgenin derivatives could serve as lead compounds in drug discovery.

## References

- Aburjai, T., Hudaib, M., Tayyem, R., Yousef, M., Qishawi. 2007. Ethnopharmacological survey of medicinal herbs in Jordan, the Ajloun Heights region. *Journal of Ethnopharmacology*, 110(2), 294-304.
- Adaramoye, O.A., Sarkar, J., Singh, N., Meena, S., Changkija, B., Yadav, P.P., Kanojiya, S., Sinha, S. 2011. Antiproliferative action of *Xylopiya aethiopica* fruit extract on human cervical cancer cells. *Phytotherapy Research*, 25 (10):1558-1563.
- Ageel, A.M., Mossa, J.S., Al-Yahya, M.A., Al-Said, M.S., Tariq, M. 1989. Experimental studies on antirheumatic crude drugs used in Saudi traditional medicine. *Drugs under Experimental and Clinical Research*, 15(8): 369-372.
- Akita, C., Kawaguchi, T., Kaneko, F., Yamamoto, H. 2004. Solid-state  $^{13}\text{C}$ -NMR study on order disorder phase transition in oleic acid. *The Journal of Physical Chemistry B*, 2, 108: 4862-4868.
- Aniszewski, T. 2007. Alkaloids - Secrets of life: alkaloid chemistry, biological significance, applications and ecological role. UK: Elsevier, Pp. 72-73
- Bedford, S.B., Quarteman, C.P., Rathbone, D.L., Slack, J.A. 1996. Synthesis of water-soluble prodrugs of the cytotoxic agent combretastatin A-4, *Bioorganic and Medicinal Chemistry Letters*, 6: 157-160.
- Bishop, J.M., Weinberg, R.A., 1996. eds. Molecular Oncology, New York: Scientific American Inc.
- Blaise, P., Wolff, R., Farines, M. 1997. Regiospecific study of vegetable oil triacylglycerols by chemical cleavage and high-resolution  $^{13}\text{C}$  NMR. *Oil seeds, fats, lipids*, 4 (2): 135-141
- Breitmaier, E. 2006. Terpenes: flavors, fragrances, pharmaca, pheromones. Germany: Wiley-vch Verlag GmbH & Co. KGaA, Weinheim ISBN: 3- 527-31786-4.
- Brown, R.T., Fox, B.W., Hadfield, J.A., McGown, A.T., Mayalarp, S.P., Pettit, R., Wood, J.A. 1995. Synthesis of water-soluble sugar derivatives of combretastatin A-4, *Journal of American Chemical Society, Perkin Trans*, 1 (5): 577-581.

- Brummitt, R.K. 1992. *Vascular Plant Families and Genera*, Kew: Royal Botanical Gardens.
- Bruneton, J. 1995. Pharmacognosy, phytochemistry, medicinal Plants. Paris: Lavoisier Publishing. Pp. 538–544.
- Burkill, H.M., 1985. The useful plants of West Tropical Africa. 2nd Edition. Volume 1, Families A–D. Royal Botanic Gardens, Kew, Richmond, United Kingdom. Pp. 960.
- Butler, M.S. 2004. The Role of Natural Product Chemistry in Drug Discovery. *Journal of Natural Products*. 67: 2141-2153.
- Carter, C.W.Jr. 1997. Response surface methods for optimizing and improving reproductivity of crystal growth. *Methods in Enzymology*, 277: 74-99.
- Cassady, J. M., Douros, J. D. 1980. Jardin, I. In Podophyllotoxins. In Anticancer agents based on natural product models; Eds.; Academic Press: New York, Pp. 319–351.
- Chaosuancharoen, N., Kongkathip, N., Kongkathip, B. 2004. Novel synthetic approach from diosgenin to a 17 $\alpha$ -hydroxy orthoester via a region- and stereo specific rearrangement of an epoxy ester. *Synthetic Communications*, 34: 961-983.
- Chandrasekharan, N.V. 2002. COX-3, a cyclooxygenase-1 variant inhibited by acetaminophen and other analgesic/antipyretic drugs:cloning, structure and expression. *Proceeding of National Academy of Science*. 99: 13926-13931.
- Chaturvedula, V.S.P., Prakash, I. 2012. Isolation of Stigmasterol and  $\beta$ -Sitosterol from the dichloromethane extract of *Rubus suavissimus*, *International current pharmaceutical journal*, 1(9):239-242.
- Chen, W., Tang, S., Qin, N., Zhai, H., Duan, H. 2012. Antioxidant constituents from *Smilax riparia*, *China Journal of Chinese Materia Medica*, 37(6): 806-810.
- Chhabra, S.C., Mahunnah, R.L.A., Mshu, E.N. 1993. Plants used in traditional medicine in Eastern Tanzania VI. Angiosperms (Sapotaceae to Zingiberaceae). *Journal of Ethnopharmacology*., 39: 83-103.

- Chin, Y.N., Balunas, M.J., Chai, H.B., Kighorn, A.D. 2006. Drug discover from Natural Sources. *American Association of Pharmaceuticals Scientists Journal*. 8:2-6.
- Cragg, G.M., Newman, D.J. 2005. Biodiversity: A continuing source of novel drug leads, *Pure and Applied Chemistry*. 77(1): 7-24.
- Croteau, R., Kutchan, T. M., Lewis. N. G. 2000. Natural products (secondary metabolites). *Biochemistry and Molecular Biology of Plants*. 1250-1318.
- Cushman, M., He, H.M., Lin, C.M., Hamel, E. 1993. Synthesis and evaluation of a series of benzylaniline hydrochlorides as potential cytotoxic and antimetabolic agents by acting by inhibition of tubulin polymerization, *Journal of Medicinal Chemistry*, 36: 2817-2821.
- Cushman, M., Nagarathnam, D., Gopal, D., Chakraborti, A.K., Lin, C.M., Hamel, E. 1991. Synthesis and evaluation of stilbene and dihydrostilbene derivatives as potential anticancer agents that inhibit tubulin polymerization, *Journal of Medicinal Chemistry*, 34: 2579-2588.
- Da Orta, G. 1895. *Colloquies of Simples and Drugs of India*. Trans Sir Clement Markham, London: H. Sotheran and Co; 1913. p. 378.
- Dalziel, J.M., 1937. The useful plants of West Tropical Africa. Crown Agents for Overseas Governments and Administrations, London, United Kingdom. Pp 612.
- Demo, A., Petrakis, C., Kefalas, P., Boskou, D. 1998. Nutrient antioxidants in some herbs and mediterranean plant leaves. *Food Research International*, 31(5): 351-354.
- Devon, T. K., Scott, A. I. 1972. Handbook of Naturally occurring compounds, vol. 2, The Terpenes, Academic press, London.
- Dixon, R. 2001. Natural products and plant disease resistance. *Nature* 411: 843–847.
- Dorr, R.T., Dvorakova, K., Snead, K., Alberts, D., Salmon, S.E., Petit, G.R. 1996. Antitumor activity of combretastatin A-4 phosphate, a natural tubulin inhibitor, *Investigational New Drugs*, 14:131-137.



- Ducki, S., Mackenzie, G., Lawrence, N. J., Snyder, J.P. 2005. Quantitative structure-activity relationship (5D-QSAR) study of combretastatin-like analogues as inhibitors of tubulin assembly, *Journal of Medicinal Chemistry*, 48: 457-465.
- Edeoga, H.O., Okwu, D.E., Mbaebie, B.O. 2005. Phytochemical constituents of some Nigerian medicinal plants. *African Journal of Biotechnology* 4(7): 685-688.
- Emerson, D.L., Besterman, J.M., Brown, H.R., Evans, M.G., Leitner, P.P., Luzzio, M.J., Shaffer, J.E., Sternbach, D.D., Uehling, D., Vuong, A. 1995. *In vivo* antitumor activity of two new seven-substituted water-soluble camptothecin analogues, *Cancer Research*, 55(3): 603-609.
- Engel, C., Mifflin, H. 2002. Wild health: How animals keep themselves well and what we can learn from them. Published by Houghton Mifflin Harcourt: 1<sup>st</sup> edition , ISBN-10: 0618071784.
- Estrada, A., Katselis, G. S., Laarveld, B., Barl, B. 2000. Isolation and evaluation of immunologicaladjuvant activities of saponins from *Polygala senega* L. *Comparative Immunology microbiology and infectious diseases* 23: 27-43.
- Ferguson, L.R. 2001. Role of plant polyphenols in genomic stability. *Mutation Research*, 475: 89 -111.
- Filippos, V. F; Emmanouil, T.; Carl, D.; Guenter, V.; Georg, K.; Nickolas, P. 2007. Biotechnology of flavonoids and other phenylpropanoid-derived natural products. Part I: Chemical diversity, impacts on plant biology and human health". *Biotechnology Journal* 2 (10): 1214-34.
- Fujioka, T., Iwamoto, M., Iwase, Y., Hachiyama, S., Okabe, H., Yamuchi, T., Mihashi, K. 1989. Studies on the constituents of *Actinostemma lobatum* Maxim V: structures of lobatosides B,E,F, and G, the dicrotalic acid esters of bayogenin bisdesmosides isolated from the herb, *Chemical and Pharmaceutical Bulletin*, 37(9): 2355-2360.
- Fukunaga, T., Miura, T., Furuta, K., Kato, A. 1997. Hypoglycemic effect of the rhizome of *Smilax glabra* in normal and diabetic mice. *Biological and Pharmaceutical Bulletin*, 20(1): 44-46.

- Gore, M., ten Bokkel Huinink, W., Carmichael, J., Gordon, A., Davidson, N., Coleman, R., Spaczynski, M., Heron, J.F., Bolis, G., Malmstrom, H., Malfetano, J., Acarabelli, C., Vennin, P., Ross, G., Fields, S. Z. 2001. *Journal of Clinical Oncology*, 19: 1893.
- Gunstone, F.D. 1993. High resolution  $^{13}\text{C}$ -NMR spectroscopy of lipids. In: *Advances in Lipid Methodology-Two*, pp. 1-68 (Ed. W.W. Christie, Oily Press, Dundee).
- Gunstone, F.D., Seth, S. 1994. A study of the distribution of eicosapentaenoic acid and docosahexaenoic acid between the  $\alpha$  and  $\beta$  glycerol chains in fish oils by  $^{13}\text{C}$ -NMR spectroscopy. *Chemistry and Physics of Lipids*, 72: 119-126.
- Gunstone, F.D., Seth, S. and Wolff, R.L. 1995. The distribution of  $\Delta 5$  polyene acids in some pine seed oils between the  $\alpha$ - and  $\beta$ -chains by  $^{13}\text{C}$ -NMR spectroscopy. *Chemistry and Physics of Lipids*, 78: 89-96.
- Gupta, A., Kumar, B.S., Negi, A.S. 2013. Current status on development of steroids as anticancer agents. *Journal of Steroid Biochemistry and Molecular Biology*, 137: 242–70 and reference no. 90, 91, 137 and 149 cited therein
- Gurib-Fakim, A. 2006. Medicinal plants: Tradition of yesterday and drugs of tomorrow, Review article. *Molecular Aspects of Medicine*, 27(1):1-93.
- Gwaltney II, S.L., Imade, H.M., Barr, K.J., Li, Q., Gehrke, L., Credo, R.D., Warner, R., Lee, J.Y., Kovar, P., Wang, J., Nukkala, M.A., Zielinski, N.A., Frost, D., Ng, S.C., Sham, H.L. 2001. Novel sulfonate analogues of combretastatin A-4: Potent antimetabolic agents, *Bioorganic and Medicinal Chemistry Letters*, 11(7): 871-874
- Habib, M.R., Nikkon, F., Rahman, M., Haque, M.E., Karim, M.R. 2007. Isolation of Stigmasterol and  $\beta$ -Sitosterol from Methanolic Extract of Root Bark of *Calotropis gigantea* (Linn), *Pakistan Journal of Biological Sciences*, 10: 4174-4176.
- Hamel, E., Lin, C. M. 1983. Interactions of combretastatin, a new plant-derived antimetabolic agent, with tubulin, *Biochemical Pharmacology*, 32: 3864.
- Hamid, A.A., Aiyelaagbe, O.O. 2011. The Screening of Phytoconstituents, Antibacterial and Antifungal, Properties of *Smilax kraussiana* Leaves, *Der Pharmacia Sinica*, Pelagia Research Library, 2(4):267-273.

- Harborne J. B. 1998. *Phytochemical methods: A guide to modern technique of plants analysis*, London: Chapman and Hall.
- Harvey, A. 2001. The continuing value of natural products to drug discovery. *GIT Lab. J.*, 5(6): 284–285.
- Haslam, E. 1981. Vegetable tannins. *The biochemistry of plants*, Vol. 7. New York, Academic press. 527-554.
- Heim, K.E., Tagliaferro, A.R., Bobilya, D. J. 2002. Flavonoid antioxidants: chemistry, metabolism and structure-activity relationships. *Journal of Nutritional Biochemistry* 13: 572–584.
- Heinrich, M., Barnes, J., Gibbons, S., Williamson, E.M. 2004. *Fundamentals of Pharmacognosy and Phytotherapy*. Churchill Livingstone, Elsevier Science Ltd; UK.
- Hertzberg, R.P., Caranfa, M.J., Holden, K.G., Jakas, D.R., Gallagher, G., Mattern, M.R., Mong, S.M., Bartus, J.O., Johnson, R.K., Kingsbury, W.D. 1989. Modification of the hydroxy lactone ring of camptothecin: inhibition of mammalian topoisomerase 1 and biological activity, *Journal of Medicinal Chemistry*, 32(3): 715-720.
- Herzog T.J., Pothuri B. 2006. Ovarian cancer: a focus on management of recurrent disease, *Nature Clinical Practice Oncology*, 3: 604-611.
- Hodek, P., Trefil, P. and Stiborova, M. 2002. Flavonoids-potent and versatile biologically active compounds interacting with cytochromes. *Chemico-Biological interactions* 139: 1–21.
- Hoffman, E., Stroobank, V. 2002. *Mass spectroscopy: principle and applications* 2<sup>nd</sup> edition. UK: John Wiley and Sons Inc.
- Hostettmann, K., Marston, A. 2005. *Saponins: chemistry and pharmacology of natural products*. UK: Cambridge University Press, Cambridge.
- Hutchings, M.R., Athanasiadou, S., Kyriazakis, I., Gordon, I.J. 2003. Can animals use foraging behaviour to combat parasites? *Proceedings of the Nutrition Society*, 62(2): 361. doi:10.1079/PNS2003243., PMID 14506883.

- Inyang, E. 2000. Forests our divine treasure. Uyo, Nigeria. Dorand Publishers, Pp. 155-181.
- Inyang, E. 2003. Ethnobotany conventional and Traditional uses of plants. The Verdict Press, Uyo, Nigeria, Pp.124.
- Irvine, R.F. 1961. *Woody plants of Ghana*, With special references to their uses, Oxford University Press, London.
- Ishola, I.O., Agbaje, E.O., Adeyemi, O.O, Shukla, R. 2014. Analgesic and anti-inflammatory effects of the methanol root extracts of some selected Nigerian medicinal plants, *Pharmaceutical Biology*, 52(9): 1208-1216.
- Ivanova, A., Mikhova, B., Batsalova, T., Dzhambazov, B., Kostova, I. 2011. New furostanol saponins from *Smilax aspera* L. and their in vitro cytotoxicity, *Fitoterapia* 82: 282–287.
- Iwu, M.M., Anyanwu, B.N. 1982. Phytotherapeutic profile of Nigerian herbs 1. Antiinflammatory and anti-arthritic agents, *Journal of Ethnopharmacology*, 63: 263-274.
- Jagessar, R.C., Mars, A., Gomes, G. 2009. Leaf extract of *Smilax schomburgkiana* exhibit selective antimicrobial properties against pathogenic microorganisms, *Life Science Journal*, 6(1): 76-83.
- Jain, P.S., Bari, S.B. 2010. Isolation of Lupeol, Stigmasterol and Campesterol from Petroleum Ether Extract of Woody Stem of *Wrightia tinctoria*. *Asian Journal of Plant Sciences*, 9: 163-167.
- Jamal, A. K., Yaacob, W. A., Din, L. B. 2009. A Chemical Study on *Phyllanthus columnaris*, *European Journal of Scientific Research*, 28: 76-81.
- James A. 2001. *Duke Handbook of phytochemical constituents of GRAS herbs and other economic plants*. Boca Raton: CRC Press; Pp. 5622.
- Jan, T., Wey, S., Kuan, C., Liao, M., Wu, H. 2007. Diosgenin, a steroidal sapogenin, enhances antigen-specific IgG<sub>2a</sub> and interferon- $\gamma$  expression in ovalbumin-sensitized BALB/AC Mice, *Planta Medical*, 73(5): 421-426.

- Jaxel, C., Kohn, K.W., Wani, M.C., Wall, M.E., Pommier, Y.C. 1989. Structure-activity study of the actions of camptothecin derivatives on mammalian topoisomerase I: evidence for a specific receptor site and a relation to antitumor activity, *Cancer Research*, 49(6): 1465-1469
- Jean-Paul, V., Heng, L., Groot, A., Gruppen, H. 2007. Saponins, classification and occurrence in the plant kingdom. *Phytochemistry*, 68: 275–297.
- Joshi, H., Joshi, A.B., Sati, H., Gururaja, M.P., Shetty, P.R., Subrahmanyam, E.V.S., Satyanaryana, D. 2009. Fatty acids from *Memecylon umbellatum* (Burm.). *Asian Journal of Research Chemistry*, 2: 178-180.
- Kalsi, P. S. 2004. Spectroscopy of organic compounds 6<sup>th</sup> edition. New Delhi: New Age International Ltd, Pp. 25-42.
- Khare, C.P. 2004. Indian herbal remedies: rational Western therapy. New York: Springer. Pp. 428.
- Kelly, M. G., Hartwell, J. L. 1954. The biological effects and chemical composition of podophyllin. A review. *Journal of National Cancer Institute*, 14: 967.
- Kimura, T., But, P. P. H. 1996. *Northeast Asia Unesco*. Singapore: World Scientific Publishing Co; Pp. 181.
- Kingsbury, W.D., Boehm, J.C., Jakas, D.R., Holden, K.G., Hecht, S.M., Gallagher, G., Caranfa, M.J., McCabe, F.L., Faucette, L.F., Johnson, R.K., Hertzberg, R.P. 1991. Synthesis of water-soluble (aminoalkyl)camptothecin analogues: inhibition of topoisomerase I and antitumor activity, *Journal of Medicinal Chemistry*, 34 (1): 98-107.
- Kobayashi Y., Takeda T., Ogihara Y. 1981. New triterpenoid glycosides from the leaves of *Bupleurum rotundifolium* L., *Chemical and Pharmaceutical Bulletin*, 29: 2222-2229.
- Kojima, H., Tominaga, H., Sato, S., Ogura, H. 1987. Pentacyclic triterpenoids from *Prunellavulgaris*, *Phytochemistry*, 26(4): 1107-1111.
- Kubo, S., Mimaki, Y., Sashida, Y., Nikaido, T., Ohmoto, T. 1992. Steroidal saponins from *Smilax riparia* and *S. china*. *Phytochemistry*, 31: 2439-2443.

- Kumar, S., Baker, K., Seger, D. 2002. Dinitrophenol–induced hyperthermia resolving with dantrolene administration. Abstract of North American Congress of Clinical Toxicology. *Clinical Toxicology*, 40: 599 – 673.
- Kumar, A., Ilavarasn, R., Jayachandran, T., Qaisar, M. 2011. Phytochemical investigation on a tropical plant. *Pakistan Journal of Nutrition* 8: 83-85.
- Kuo, Y.H., Hsu, Y.W., Liaw, C.C., Lee, J.K., Huang, H.C., Kuo, L.M. 2005. Cytotoxic phenylpropanoid glycosides from the stems of *Smilax china*. *Journal of Natural Product*, 68(10): 1475-1478.
- Lackey, K., Besterman, J.M., Fletcher, W., Leitner, P., Morton, B., Sternbach, D.D. 1995. Rigid analogues of camptothecin as DNA topoisomerase 1 inhibitors. *Journal of Medicinal Chemistry*, 38: 906.
- Lai, P.K., Roy, J. 2004. Antimicrobial and chemopreventive properties of herbs and spices. *Current Medicinal Chemistry*, 11 (11): 1451-1460. PMID 15180577.
- Lamber, J. B., Mazzola, E. P. 2002. NMR spectroscopy: an introduction to principle, application and experimental methods. New Jersey: Pearson Educational Inc.
- Lawrence, N.J., Hepworth, L.A., Rennison, D., McGown, A.T.; Hadfield, J.A. 2003. Synthesis and anticancer activity of fluorinated analogues of combretastatin A-4, *Journal of Fluorine Chemistry*, 123(1): 101–108.
- Lasztity, R., Hidvegi, M., Bata, A. 1998. Saponins in food. *Food Review International*, 14(4): 371–390.
- Lie Ken Jie, M.S.F., Lam, C.C. 1995. <sup>1</sup>H-Nuclear magnetic resonance spectroscopic studies of saturated, acetylenic and ethylene triacylglycerols. *Chemistry and Physics of Lipids*, 77: 155-171.
- Lie Ken Jie, M.S.F., Lam, C.C., Pasha, M.K. 1996. <sup>13</sup>C nuclear magnetic resonance spectroscopic analysis of the triacylglycerol composition of *Biota orientalis* and carrot seed oil. *Journal of the American Oil Chemists' Society*, 73: 557-562.

- Lin, C.M., Ho, H.H., Pettit, G.R., Hamel, E. 1989. Antimitotic natural products combretastatin A-4 and combretastatin A-2: studies on the mechanism of their inhibition of the binding of colchicine to tubulin. *Biochemistry*, 28(17): 6984-6991.
- Longo, L., Vasapollo, G. 2006. Extraction and identification of anthocyanins from *Smilax aspera* L. berry, *Food Chemistry*, 94(2): 226-231.
- Luzzio, M. J., Besterman, J. M., Emerson, D.L., Evans, G., Lackey, K., Leitner, P.L., McIntyere, G., Morton B., Myers, P.L., Peel, M., Sisco, J.M., Sternbach, D.D., Tong, W.Q., Truesdale, A., Uehling, D.E., Vuong, A., Yates, J. 1995. Synthesis and antitumor activity of novel water soluble derivatives of camptothecin as specific inhibitors of topoisomerase 1. *Journal of Medicinal Chemistry*, 38(3): 395-401.
- Mabberley, D.J. 1987. The plant-book, A portable dictionary of higher plants, Cambridge: Cambridge university press.
- Macomber, R. S. 1998. A complete introduction to modern NMR spectroscopy. Canada: John Wiley and Sons Inc, Pp. 165-182.
- Melero, C.P., Maya, A.B.S., Rey, B.D., Peláez, R., Caballero, E., Medarde, M. 2004. A new family of quinoline and quinoxaline analogues of combretastatins, *Bioorganic and Medicinal Chemistry Letters*, 14 (14): 3771-3774.
- Merril, E.D. 1935. A Commentary on Loureiro's "Flora Cochinchinensis" Transactions, American Philosophical Society) Philadelphia. *The American Philosophical Society*, 24(2): 111.
- Mifsud, S. 2002. Wild plants of Malta and Gozo-mediterranean *Smilax*, Retrieved 2011
- Mitchell, J., Rook, A. 1979. *Botanical Dermatology*, Greengrass, Vancouver, pp.647.
- Moertel, C.G., Schutt, A.J., Reitemeier, R. J., Hahn, R.G. 1972. Phase II study of camptothecin (NSC-100880) in the treatment of advanced gastrointestinal cancer, *Cancer Chemotherapy Reports*, 56(1): 95-101.

- Muggia, F.M., Creaven, P.J., Hansen, H.H., Cohen, M.H., Selawry, O.S. 1972. Phase I clinical trial of weekly and daily treatment with camptothecin (NSC-100880): correlation with preclinical studies. *Cancer Chemotherapy Reports*, 56: 515–521.
- Newman, D.J., Cragg, G.M., Snader, K.M. 2000. The influence of National Products upon drug discovery. *Natural Product Report*. 171: 215-234.
- Newman, D.J., Cragg, G.M., Snader, K.M. 2003. National Products as sources of new drugs over period 1981-2002. *Journal of Natural Products*. 66: 1022-1037.
- Ng, T.B., Yu, Y.L. 2001. Isolation of a novel heterodimeric agglutinin from rhizomes of *Smilax glabra*, the Chinese medicinal material tufuling. *International Journal of Biochemistry and Cell Biology*, 33: 269-277.
- Numata, A., Takahashi, C., Miyamoto, T., Yoneda, M., Yang, P. 1990. New triterpenes from a Chinese medicine, *Goreishi*, *Chemical and Pharmaceutical Bulletin, Bull.* 38:942.
- Nwafor, P.A., Ekpo, M., Udezi, T.W., Okokon, J., Bassey, A.L. 2006. Acute toxicity potential of methanolic extract of *Smilax kraussiana* leaves in rats. *International Journal of Pharmacology*, 2(4): 463-466.
- Nwafor, P.A., Nwajiobi, N., Uko, I.E., Obot, J.E. 2010. Analgesic and antiinflammatory activities of ethanol extract of *Smilax kraussiana* leaf in mice. *African Journal of Biomedical Research*, 13: 141-148.
- Nwafor, P.A., Ekpo, E., Udofia, E.E., Smith M.E. 2012. Effects of methanol extract of *Piper umbellatum* leaves on contraceptive and sexual behaviour in rodents. *Nigerian Journal of Pharmaceutical and Applied Science Research*, 1:1-14.
- Nwafor, P. A., Idiong, O. J., Davies, K. 2013. Contraceptive and sexual behavioural effects of methanol extract of *Smilax kraussiana* root in rodents, *African Journal of Pharmacology and Therapeutics*, 2(3): 94-100.
- Odugbemi, T., Akinsulire, O. 2008. Medicinal plants species, family names and uses. In: A Text book of medicinal plants from Nigeria. Ed. Tolu Odugbemi., University of Lagos Press, Nigeria. Pg. 61.



- O'Dwyer, P.J., Leyland-Jones, B., Alonso, M.T., Marsoni, S., Wittes, R.E.N. 1985. Etoposide (VP-16-213). Current status of an active anticancer drug, *The New England Journal of Medicine*, 312: 692.
- Ohsumi, K., Nakagawa, R., Fukuda, Y., Hatanaka, T., Morinaga, Y., Nihei, Y., Ohishi, K., Suga, Y., Akiyama, Y., Tsuji, T. 1998. Novel combretastatin analogues effective against murine solid tumors: design and structure-activity relationship, *Journal of Medicinal Chemistry*, 41: 3022-3032.
- Okokon, J.E., Ndehekedehe, I., Akpan, E.J. 2012. *In vivo* antiplasmodial and antipyretic activities of *Smilax kraussiana*. *Phytopharmacology*, 3: 376-385.
- Oleszek, W.A. 2002. Chromatographic determination of plant saponins. *Journal of Chromatography*, 967, 147-162.
- Ormrod, D.; Spencer, C. M. 1999. Topotecan: a review of its efficacy in small cell lung cancer. *Drugs*, 58(3): 533-551.
- Pavia, D. L., Lampman, G. M., Kriz, G. S. 2001. Introduction to spectroscopy 3<sup>rd</sup> edition. USA: Thompson Learning Inc. Pp. 18-45.
- Pettit, G.R., Cragg, G.M., Herald, D.L., Schmidt, J.M., Lohavanijaya, P. 1982. Isolation and structure of combretastatin, *Canadian Journal of Chemistry*, 60: 1374-1376.
- Pettit, G. R., Singh, S. B., Cragg, G. M. 1985. Synthesis of natural (-) combretastatin, *Journal of Organic Chemistry*, 50: 3404-3406.
- Pettit, G.R., Cragg, G.M., Singh, S.B. 1987a. Antineoplastic agents 122, Constituents of *Combretum caffrum*, *Journal of Natural Products*, 50, 386-391.
- Pettit, G.R., Singh, S.B., Niven, M.L., Hamel, E., Schmit, M.J. 1987b. Isolation, structure and synthesis of combretastatins A-1 and B-1, Potent new inhibitors of microtubule assembly, *Journal of Natural Products*, 50: 119-131.
- Pettit, G.R., Singh, S.B. 1987c. Isolation, structure and synthesis of combretastatins A-2, A-3 and B-2, *Canadian Journal of Chemistry*. 65, 2390-2396.

- Pettit, G.R., Singh, S.B., Hamel, E., Lin, C.M., Alberts, D.S., Garcia-Kendal, D. 1989. Isolation and structure of the strong cell growth and tubulin inhibitor combretastatin A-4. *Experientia*, 45:209.
- Pettit, G.R., Singh, S.B., Boyd, M.R., Hamel, E., Pettit, R.K., Schmit, J.M., Hogan, F. 1995a. Antineoplastic agents 291, Isolation and synthesis of combretastatins A-4, A-5, and A-6(1a), *Journal of Medicinal Chemistry*, 38: 1666.
- Pettit, G.R., Temple, C. Jr., Narayanan, V.L., Varma, R., Simpson, M.J., Boyd, M.R., Rener, G.A., Bansal, N. 1995b. Antineoplastic agents 322, synthesis of combretastatin A-4 prodrugs, *Journal of Medicinal Chemistry*, 43: 2731.
- Pettit, G.R., Lippert, J.W., Herald, D.L., Hamel, E., Pettit, R.K. 2000. Antineoplastic agent 440. Asymmetric synthesis and evaluation of the combretastatin A-1 SAR probes (1S,2S)- and (1R,2R)- 1,2-dihydroxy-1-(2',3'-dihydroxy-4'-methoxyphenyl)-2-(3'',4'',5''-trimethoxyphenyl)-ethane, *Journal of Natural Products*, 63(7): 969-974.
- Pignatti, S. 1982. Flora d'Italia, Bologna, Edagricole, 3: 401.
- Pinney, K.G., Mejia, M.P., Villalobos, V.M., Rosen-quist, B.E., Pettit, G.R., Verdier-Pinard, P., Hamel, H. E. 2000. Synthesis and Biological Evaluation of Aryl Azide Derivatives of Combretastatin A-4 as Molecular Probes for Tubulin, *Bioorganic and Medicinal Chemistry*, 8(10): 2417-2425.
- Podwysstozki, V. 1880. Pharmakologische Studien uber Podophyllum peltatum, *Archiv for Experimentelle Pathologie und Pharmakologie*, 13(1-2): 29-52.
- Pommier, Y., Kohlhagen, G., Kohn, K.W., Leteurtre, F., Wani, M.C., Wall, M.E. 1995. Interaction of an alkylating camptothecin derivative with a DNA base at topoisomerase I-DNA cleavage sites. *Proceedings of the National Academy of Sciences*, 92: 8861-8865.
- Potmesil, M., Giovanella, B.C., Liu, L.F., Wall, M.E., Silber, R., Stehlin, J.S. Jr., Hsiang, Y.H., Wani, M.C. 1991. Preclinical studies of DNA topoisomerase 1-targeted 9-amino and 10,11-methylenedioxy camptothecins, In: Potmesil, M, Kohn, K.W., eds. *DNA Topoisomerases in Cancer*, New York: Oxford University: New York, pg. 299.

- Raju, J., Bird, R.P. 2007. Diosgenin, a naturally occurring steroid [corrected] saponin suppresses 3-hydroxy-3-methylglutaryl CoA reductase expression and induces apoptosis in HCT-116 human colon carcinoma cells, *Cancer Letters*, 255(2): 194-204.
- Rang, H.P., Dale, M.M., Ritter, J.M., Moore, P.K. 2007. *Pharmacology*, 6th ed. Churchill Livingstone. Edinburgh.
- Raymond, E., Campone, M., Stupp, R., Menten, J., Chollet, P., Lesimple, T., Fety-Deporte, R., Lacombe, D., Paoletti, X., Fumoleau, P. 2002. EORTC Early Clinical Studies Group (ECSG); Brain Tumor Studies Group (BTSG); New Drug Development Program (NDDP). Multicentre phase II and pharmacokinetic study of RFS2000 (9-nitro-camptothecin) administered orally 5 days a week in patients with glioblastoma multiforme, *European Journal of Cancer*, 38(10): 1348-1350.
- Raven, P., Zhengyi, W. 2000. 11. *Smilax*. In: *Flora of China* (Vol. 24: Flagellariaceae-Marantaceae): 96. Missouri Botanical Garden Press. ISBN 0-915279-83-5.
- Redinbo, M.R., Stewart, L., Kuhn, P., Champoux, J.J., Hol, W.G. 1998. Crystal structures of human topoisomerase 1 in covalent and noncovalent complexes with DNA. *Journal of Science*, 279(5356): 1504-1513.
- Reynolds, W.F., McLean, S., Poplawski, J., Enriquez, R.G., Escobar, L.I., Leon, I. 1986. Total assignment of  $^{13}\text{C}$  and  $^1\text{H}$  spectra of three isomeric triterpenol derivatives by 2D NMR: An investigation of the potential utility of  $^1\text{H}$  chemical shifts in structural investigations, *Tetrahedron*, 42: 3419.
- Rhodes, G. 1993. *Crystallography Made Crystal Clear*. USA: Academic Press, San Diego.
- Rosado-Abon, A., Esturau-Escofet, N., Flores-A'lamo, M., Moreno-Esparza, R., Iglesias-Arteaga, M.A. 2013. The crystal structure of diosgenin acetate and its 23-oxygenated derivatives. *Journal of Chemical Crystallography*, 43: 187-196.
- Rose, M.E., Johnstone, R.A.W. 2001. *Mass spectroscopy for Chemists and Biochemists* 2<sup>nd</sup> edition. Editors Benkovic, S.J., Elmone, D.T. and Schofield, K. UK: Cambridge University Press.
- Rothwell, G.W., Scheckler, S.E., Gillespie, W.H. 1989. *Elkinsia* gen. nov., a late Devonian gymnosperm with cupulate ovules. *Botanical Gazette*, 150(2):170-189.

- Saltz, L.B., Cox, J.V., Blanke, C., Rosen, L.S., Fehrenbacher, L., Moore, M.J., Maroun, J.A., Ackland, S.P., Locker, P.K., Pirota, N., Elfring, G.L., Miller, L. 2000. Irinotecan plus fluorouracil and leucovorin for metastatic colorectal cancer, Irinotecan Study Group. *The New England Journal of Medicine*, 343: 905-914.
- Savithramma, N., Linga, M., Rao, J., Suhurulatha, D. 2011. Screening of medicinal plants for secondary metabolites. *Middle-East Journal of Scientific Research*, 8(3): 579-584.
- Schofield, D. M., Mbugua, A. N., Pell, M. 2001. Analysis of condensed tannins: a review. *Animal feed science and Technology*. 91: 21-40.
- Schoffski, P., Herr, A., Vermorken, J.B., Vanden Brande, J., Beijnen, J.H., Rosing, H., Volk, J., Ganser, A., Adank, S., Botma, H.J., Wanders, J. 2002. Clinical phase II study and pharmacological evaluation of rubitecan in non-pretreated patients with metastatic colorectal cancer-significant effect of food intake on the bioavailability of the oral camptothecin analogue, *European Journal of Cancer*, 38: 807-813.
- Schram, J., Bellama, J. M. 1988. Two dimensional NMR spectroscopy. New York: John Wiley and Sons Inc.
- Shao, B., Guo, H.Z., Cui, Y.J., Liu, A.H., Yu, H.L., Guo, H., Xu, M., Guo, D.A. 2007. Simultaneous determination of six major stilbenes and flavonoids in *Smilax china* by high performance liquid chromatography. *Journal of Pharmaceutical and Biomedical Analysis*, 44(3): 737-742.
- Shawakfeh, K.Q., Al-Said, N.H., Abboushi, E.K. 2010. Synthesis of new di- and triamine diosgenin dimers, *Tetrahedron* 66: 1420–1423.
- Shu, X.S., Gao, Z.H., Yang, X.L. 2006. Anti-inflammatory and anti-nociceptive activities of *Smilax china* L. aqueous extract. *Journal of Ethnopharmacology*, 103(3): 327-332.
- Shu, Y. 1998. Recent natural products based drug development: a pharmaceutical industry perspective. *Journal of Natural Products*, 61: 1053–1071.
- Siddiqui, B.S., Rasheed, M., Ilyas, F., Gulzar, T., Tariq, R.M., Naqvi, S.N. 2004. Analysis of insecticidal *Azadirachta indica* A. Juss fractions. *Z Naturforsch C*, 59: 104-112.

- Silanikove, N., Perevolotsky, A., Provenza, F.D. 2001. Use of tannin-binding chemicals to assay for tannins and their negative postingestive effect in ruminants. *Animal feed science and technology*. 91(2): 69-81.
- Smith, B. 1996. Fundamentals of Fourier Transform Infrared Spectroscopy. Washington D.C., CRC Press.
- Sofowora E.A. 1982a. Medicinal Plant and Traditional Medicine In Africa. Spectrum Books Limited, Ibadan Nigeria. pp. 6 and 154.
- Sofowora E.A. 1982b. Problems and prospect of their standardization in the state of medicinal plant research in Nigeria edi. IUP –pp 65-75.
- Snyder, L. R., Kirkland, J. J. and Glajch, J. L. 1997. Practical HPLC method development. UK: John wiley and son Inc.
- Sparg, S.G., Light, M. E., Staden, V. J. 2004. Biological activities and distribution of plant saponins. *Journal of Ethnopharmacology* 94: 219-243.
- Spitzer, V., Tomberg, W. and Zucolotto, M. 1996. Identification of  $\alpha$ -parinaric acid in the seed oil of *Sebastiania brasiliensis* Sprengel (Euphorbiaceae). *Journal of the American Oil Chemists' Society*, 73: 569-573.
- Srivastava, V., Negi, A.S., Kumar, J.K., Gupta, M. M., Khanuja, S.P.S. 2005. Plant based anticancer molecules: A chemical and biological profile of some important leads. *Bioorganic and Medicinal Chemistry*, 13 (21), 5892-5908
- Staker, B.L., Hjerrild, K., Feese, M.D., Behnke, C.A., Burgin, A.B. Jr., Stewart, L. 2002. The mechanism of topoisomerase 1 poisoning by a camptothecin analogue, *Proceedings of the National Academy of Sciences*, U.S.A., 99: 15387.
- Subrahmanyam, D., Renuka, B., Rao, C.B., Sagar, P.S., Deevi, D.S., Babu, J.M., Vyas, K. 1998. Novel D-ring analogues of podophyllotoxin as potent anticancer agents, *Bioorganic and Medicinal Chemistry Letter*, 8: 1391-1396.
- Suffness, M. 1995. Taxolreg, Science and applications. CRC Press, Boca, Raton, F.L.

- Sun, L., Vasilevich, N.I., Fuselier, J.A., Hocart, S.J., Coy, D.H. 2004. Examination of the 1,4-disubstituted azetidinone ring system as a template for combretastatin A-4 conformationally restricted analogue design, *Bioorganic and Medicinal Chemistry Letter*, 14(9): 2041-2046.
- Talvitie, A., Mannila, E., Kolehmainen, E. 1992. Synthesis of some biologically active compounds from stilbenes isolated from the bark of *Picea abies*, *Liebigs Annalen der chemi.*, 4:399-401.
- Tapsell, L.C., Hemphill, I., Cobiac, L. 2006. "Health benefits of herbs and spices: the past, the present, the future.". *Medical Journal of Australia*, 185 (4 Suppl): S4: PMID 17022438.
- Tesemma, M., Adane, L., Tariku, Y., Muleta, D., Demise, S. 2013. Isolation of compounds from Acetone extract of root wood of *Moringa stenopetala* and evaluation of their antibacterial activities, *Research Journal of Medicinal Plant*, 7(1): 32-47.
- Thirugnanasampandan, R., Mutharaian, V.N., Narmatha Bai, V. 2009. *In vitro* propagation and free radical studies of *Smilax zeylanica* Vent. *African Journal of Biotechnology*, 8 (3): 395-400.
- Thomas, S. C. Li. 2002. *Chinese & Related North American Herbs*. Boca Raton: CRC Press, pp. 135.
- Tolstoy, V.P., Chernyshova, V.A., Skryshersky, V.A. 2003. *Handbook of Infrared Spectroscopy of ultrathin films*. Canada: John Wiley and Sons Inc.
- Toyota, M., Msonthi, J.D., Hostettman, K. 1990. A molluscicidal and antifungal triterpenoid saponin from the roots of *Clerodendron wildii*, *Phytochemistry*, 29: 2849-2851.
- Trease, G. E., Evans, W. C. 1989. *Pharmacognosy*. 13<sup>th</sup> Ed. UK: London: Bailliere Tindall Ltd. 101-104.
- Utsugi, T., Shibata, J., Sugimoto, Y., Aoyagi, K., Wierzba, K., Kobunani, T., Terada, T., Oh-hara, T., Tsuruo, T., Yamada, Y. 1996. Antitumor activity of a novel podophyllotoxin derivative (TOP-53) against lung cancer and lung metastatic cancer, *Cancer Research*, 56(12): 2809-2814.

- Van Acker, S.A., Plemper van Balen, G.P., Van den Berg, D.J., Bast, A., Van der Vijgh, W.J.F. 1998. Influence of iron chelation on the antioxidant activity of flavonoids, *Biochemistry Pharmacology* 56: 935-943.
- Vermani, K., Garg, S. 2002. Herbal medicines transmitted diseases and AIDs. *Journal of Ethnopharmacology*, 80 (1): 4966.
- Vijayalakshmi, A., Ravichandiran, V., Malarkodi, V., Nirmala, S., Jayakumari, S. 2012. Screening of flavonoid “quercetin” from the rhizome of *Smilax china* Linn. for anti-psoriatic activity, *Asian Pacific Journal of Tropical Biomedicine*, 2(4): 269-275.
- Wall, M.E., Wani, M.C., Cook, C.E., Palmer, K.H., McPhail, H.T., Sim, G.A. 1996. Plant antitumor agents I. The isolation and structure of camptothecin, a novel alkaloidal leukemia and tumor inhibitor from *Camptotheca acuminata*. *Journal of American Chemical Society*, 88: 3888-3890.
- Wall, M.E. 1998. Camptothecin and Taxol: Discovery to Clinic. *Medicinal Research Reviews*, 18: 299-314.
- Wang, W., Qian, J., Wang, X., Jiang, A., Jia, A. 2014. Anti-HIV-1 activities of extracts and phenolics from *Smilax china* L. *Pakistan Journal of Pharmaceutical Science*, 27 (1): 147-151.
- Warjeet, S., Laitonjam, I., Rajkumar, S., Yumnam, B., Kongbrailatpam, D. 2011. Study on Isolation and Comparison of the Chemical Compositions of *Cissus adnata* Roxb. leaves and *Smilax lanceaefolia* Roxb. roots and their Free Radical Scavenging Activities. *International Research Journal of Pure & Applied Chemistry*, 1(1): 1-13.
- Warrier, P.K., Nambiar, V.P.K., Ramankutty, C., Vasudevan Nair, R. 1994. *Indian medicinal plants: a compendium of 500 species*. 5. Chennai: Orient Longmans, p. 143.
- Weil, V.P., Cirigliano, M.D., Battistini, M. 2000. Herbal treatments for symptoms of menopause. *Clinical perspectives in Complementary Medicine*, Hospital Physician, 35-44

- Wenkert, E., Baddeley, G.V., Burfitt, I.R., Moreno, L.N., 1978. Carbon-13 nuclear magnetic resonance spectroscopy of naturally-occurring substances. *Organic Magnetic Resonance*, 11: 337–342.
- Wilson, I. D., Plumb, R., Granger, J., Major, H. and Lenz, E. M. 2005. HPLC-MS-based methods for the study of metabonomics. *Journal of Chromatography B*, 817(1): 67-76
- Woerdenbag, H.J., Moskal, T.A., Pras, N., Malingr'e, T.M., Farouk. S., El-Ferally, F.S., Kampinga, H.H., Konings, A.W. 1993. Cytotoxicity of Artemisinin-related endoperoxides to ehrlich ascites tumor cells. *Journal of Natural Products*, 56(6): 849–56.
- Xu, Y., Liang, J.Y., Zou, Z.M. 2008. Studies on chemical constituents of rhizomes of *Smilax china*. *Journal of Chinese materia medica*, 33(21): 2497-2499.
- Xu, S., Shang, M., Liu, G., Xu, F., Wang, X., Shou, C., Cai, S. 2013. Chemical constituents from the Rhizomes of *Smilax glabra* and their antimicrobial activity, *Molecules*, 18: 5265-5287.
- You, Y.J., Kim, Y., Nam, N.H., Bang, S.C., Ahn, B.Z. 2004. Alkyl and carboxylalkyl esters of 4'-demethyl-4-deoxypodophyllotoxin: synthesis, cytotoxic, and antitumor activity, *European Journal of Medicinal Chemistry*, 39(2): 189-193.
- Zubair, M.F., Oladosu, I.A., Olawore, N.O., Usman, L.A., Fakunle, C.O., Hamid, A.A., Ali, M.S. 2011. Bioactive Steroid from the Root Bark of *Psorospermum Corymbiferum*. *Chinese Journal of Natural Medicine*, 9(4): 264-266.





## Synthesis of novel anticancer agents through opening of spiroacetal ring of diosgenin



A.A. Hamid<sup>a,c</sup>, Mohammad Hasanain<sup>b</sup>, Arjun Singh<sup>a</sup>, Balakishan Bhukya<sup>a</sup>, Omprakash<sup>a</sup>, Prema G. Vasudev<sup>a</sup>, Jayanta Sarkar<sup>b</sup>, Debabrata Chanda<sup>a</sup>, Feroz Khan<sup>a</sup>, O.O. Aiyelaagbe<sup>d</sup>, Arvind S. Negi<sup>a,\*</sup>

<sup>a</sup> CSIR-Central Institute of Medicinal and Aromatic Plants (CSIR-CIMAP), Kukrail Picnic Spot Road, P.O. CIMAP, Lucknow 226015, India

<sup>b</sup> CSIR-Central Drug Research Institute (CSIR-CDRI), B.S. 10/1, Sector 10, Jankipuram Extension, Sitapur Road, Lucknow 226031, India

<sup>c</sup> Department of Chemistry, University of Ilorin, Ilorin, Nigeria

<sup>d</sup> Organic Chemistry Unit, Department of Chemistry, University of Ibadan, Ibadan, Nigeria

### ARTICLE INFO

#### Article history:

Received 10 December 2013

Received in revised form 26 May 2014

Accepted 29 May 2014

Available online 12 June 2014

#### Keywords:

Diosgenin

X-ray crystallography

Anticancer

Cell cycle

Caspase

Acute oral toxicity

### ABSTRACT

Diosgenin has been modified to furostane derivatives after opening the F-spiroacetal ring. The aldehyde group at C26 in derivative **8** was unexpectedly transformed to the ketone **9**. The structure of ketone **9** was confirmed by spectroscopy and finally by X-ray crystallography. Five of the diosgenin derivatives showed significant anticancer activity against human cancer cell lines. The most potent molecule of this series i.e. compound **7**, inhibited cellular growth by arresting the population at G<sub>0</sub>/G<sub>1</sub> phase of cell division cycle. Cells undergo apoptosis after exposure to the derivative **7** which was evident by increase in sub G<sub>0</sub> population in cell cycle analysis. Docking experiments showed caspase-3 and caspase-9 as possible molecular targets for these compounds. This was further validated by cleavage of PARP, a caspase target in apoptotic pathway. Compound **7** was found non-toxic up to 1000 mg/kg dose in acute oral toxicity in Swiss albino mice.

© 2014 Elsevier Inc. All rights reserved.

### 1. Introduction

Cancer is a major health menace. Over the period, cancer has become a challenge to public healthcare system. The morbidity and mortality of cancer is so high that it is an economic concern to the society nowadays. There are more than 100 types of cancers. Worldwide lung, stomach, liver, colon and breast cancer cause the most deaths each year. About 70% of all cancer deaths occur in low- and middle-income countries. Tobacco use is the single largest preventable cause of cancer in the world causing 20% of cancer deaths. Cancers of major public health relevance such as breast, cervical and colorectal cancer can be cured if detected early and treated adequately. One fifth of all cancers worldwide are caused by a chronic infection, for example human papillomavirus (HPV) causes cervical cancer and hepatitis B virus (HBV) causes liver cancer [1]. Despite continued efforts of researchers to combat cancer, this disease presents about 13% of total deaths.

Development of cancer therapeutics from steroids has been an attractive choice for medicinal chemists and many active molecules have emerged. Steroids have been developed either as anti-proliferative or cytotoxic agents. Withaferin A (**1**), Gymnasterol (**2**), 24-hydroxyperoxide desmosterol (**3**), timosaponin A-III (**4**) etc. are some of the notable plant based cytotoxic steroidal leads [2,3]. Semisynthetic modification of some of these natural products have yielded better cytotoxic analogs. Several synthetic analogs of withaferin are much better cytotoxic compounds [2].

Diosgenin (**5**) is a C<sub>27</sub> spiroacetal steroidal sapogenin abundantly available in nature. It is obtained mainly in saponin form from *Smilax* spp., *Dioscorea* spp., *Costus speciosus* etc. The molecule exhibits significant activity against colon and leukemia cells by inducing apoptosis [4a–c]. In the present communication, we modified diosgenin at spiroketal position to get few anticancer analogs. While transforming C<sub>29</sub> aldehyde to Schiff's bases a C<sub>28</sub> ketone was formed which was confirmed by spectroscopy. All the derivatives were evaluated for cytotoxicity by Sulphorhodamine assay against five human cancer cell lines. The best analog of the series was further evaluated for cell cycle analysis and *in-vivo* acute oral toxicity in Swiss-albino mice.

\* Corresponding author. Tel.: +91 522 2718583; fax: +91 522 2342666.

E-mail address: [arvindcimap@rediffmail.com](mailto:arvindcimap@rediffmail.com) (A.S. Negi).

## 2. Experimental

### 2.1. General

Melting points were determined in open capillaries using E-Z Melt automated melting point apparatus, Stanford Research System, USA and were uncorrected. The starting substrate diosgenin was procured for Sigma, USA. Dry solvents were prepared as per standard methods. Reactions were monitored on aluminium thin layer chromatography (TLC, UV<sub>254nm</sub> plates), E. Merck Germany. Further, visualization was accomplished by spraying with a solution of 2% ceric sulfate in 10% aqueous sulfuric acid and charring at 80–100 °C. Column chromatography was carried out on silica gel (100–200 mesh, Avra Chemicals, India). NMR spectra were obtained on Bruker Avance-300 MHz instrument with tetramethylsilane (TMS, chemical shifts in  $\delta$  ppm) as an internal standard. ESI mass spectra were recorded on API 3000 LC-MS-MS, Applied Biosystem, USA after dissolving the compounds in methanol or acetonitrile. The best compound **7** was analyzed for high resolution mass (ESI-HRMS) also in Agilent 6520 Q-TOF. FT-IR spectra were recorded on Perkin-Elmer SpectrumBX. X-ray diffraction data were collected on a Bruker AXS SMART APEX CCD diffractometer using MoK $\alpha$  radiation ( $\lambda = 0.71073 \text{ \AA}$ ). Nomenclature of steroid derivatives has been given as per the recommendations published by the Joint Commission on the Biochemical Nomenclature (JCBN) of IUPAC [5].

### 2.2. Chemical synthesis

#### 2.2.1. Synthesis of (22 $\beta$ ,25R)-spirost-5-en-3 $\beta$ -yl-3-acetate (**6**)

Acetylation of diosgenin (**5**) was done as per reported method [6a] with a little modification using dry chloroform as a co-solvent.

**6**: Yield = 1.01 g (91%), mp = 193–96 °C [195 °C, 6b]; <sup>1</sup>H NMR (CDCl<sub>3</sub>),  $\delta$  0.77 (s, 3H, 18-CH<sub>3</sub>), 0.96 (d, 3H, 27-CH<sub>3</sub>), 1.02 (s, 3H, 19-CH<sub>3</sub>), 1.11–2.31 (m, 25H, rest of the 1  $\times$  CH<sub>3</sub>, 8  $\times$  CH<sub>2</sub> and 6  $\times$  CH of steroidal ring), 2.01 (s, 3H, CH<sub>3</sub>COO, Acetate), 2.24–2.31 (bd, 2H, 7-CH<sub>2</sub>), 3.38 (m, 2H, 26-CH<sub>2</sub>), 4.37 (bs, 1H, 3-CH), 4.42 (bd, 1H, 16-CH), 5.36 (s, 1H, 6-CH). <sup>13</sup>C NMR (CDCl<sub>3</sub>, 75 MHz):  $\delta$  14.89 (C21), 16.64 (C18), 17.51 (C11), 19.69 (C19), 21.20 (C11), 21.74 (acetate CH<sub>3</sub>), 28.12 (C24), 29.19 (C2), 30.66 (C25), 31.78 (C23), 31.80 (C8), 32.21 (C7), 32.41 (C15), 37.10 (C10), 37.34 (C1), 38.47 (C12), 40.10 (C4), 40.63 (C13), 42.00 (C20), 42.68, 50.35 (C9), 56.82 (C14), 62.52 (C17), 67.19 (C26), 74.26 (C3), 81.16 (C16), 109.60 (C22), 122.72 (C6), 140.05 (C5), 170.82 (acetate ester). ESI Mass (MeOH): 457.3 [M+H]<sup>+</sup>, 479.3 [M+Na]<sup>+</sup>, 495.4 [M+K]<sup>+</sup>. IR (KBr, cm<sup>-1</sup>): 2907, 1724, 1451, 1231.

#### 2.2.2. Synthesis of (22 $\beta$ ,25R)-3 $\beta$ ,26-dihydroxyfurost-5-en-3 $\beta$ -acetate (**7**)

Compound **7** was synthesized as per reported method [6a].

**7**: Yield = 164 mg (81%), mp = 108–110 °C [6a]. <sup>1</sup>H NMR (CDCl<sub>3</sub>):  $\delta$  0.83 (s, 3H, 18-CH<sub>3</sub>), 0.94 (s, 3H, 19-CH<sub>3</sub>), 1.03–1.90 (m, 28H, rest of the 2  $\times$  CH<sub>3</sub>, 8  $\times$  CH<sub>2</sub> and 6  $\times$  CH of steroidal ring), 2.05 (s, 3H, CH<sub>3</sub>COO, acetate), 2.35 (bd, 2H, 7-CH<sub>2</sub>), 3.36 (bs, 1H, 22-CH), 3.48 (m, 2H, 27-CH<sub>2</sub>OH), 4.34 (bs, 1H, 3-CH), 4.63 (bs, 1H, 16-CH), 5.40 (s, 1H, 6-CH). <sup>13</sup>C NMR (CDCl<sub>3</sub>, 75 MHz):  $\delta$  16.80 (C18), 17.00 (C20), 19.30 (C27), 19.69 (C19), 21.03 (C11), 21.77 (acetate CH<sub>3</sub>), 28.13 (C24), 30.46 (C2), 30.82 (C25), 31.94 (C8), 32.36 (C7), 32.59 (C15), 36.08 (C23), 37.07 (C10), 37.37 (C1), 38.28 (C4), 38.46 (C12), 39.78 (C13), 41.07 (C20), 50.39 (C9), 57.28 (C14), 65.48 (C17), 68.27 (C26), 74.28 (C3), 83.57 (C16), 90.71 (C22), 122.74 (C6), 140.04 (C5), 170.91 (acetate ester); ESI Mass (MeOH): 459.4 [M+H]<sup>+</sup>, 481.3 [M+Na]<sup>+</sup>, 497.4 [M+K]<sup>+</sup>; ESI-HRMS: 459.3467 for C<sub>29</sub>H<sub>47</sub>O<sub>4</sub>, cal: 459.3474; 481.3282 for C<sub>29</sub>H<sub>46</sub>O<sub>6</sub>Na, cal:

481.3294; IR (KBr, cm<sup>-1</sup>): 3423, 2934, 1731, 1456, 1376, 1248, 1035.

#### 2.2.3. Synthesis of (22 $\beta$ ,25R)-3 $\beta$ -hydroxy,26-formyl-furost-5-en-3 $\beta$ -acetate (**8**)

Aldehyde **7** (200 mg, 0.43 mmol) was dissolved in dry dichloromethane (10 mL) and stirred at room temperature. To this pyridinium chlorochromate (PCC) (200 mg, 0.93 mmol) was added and further stirred for an hour. Solvent was evaporated and residue was dissolved in ethyl acetate (30 mL). It was acidified with dil. HCl (5%, 10 mL) and washed with water. The organic layer was dried over anhydrous sodium sulfate and dried *in vacuo*. The crude mass was recrystallised with chloroform-hexane (1:3) to get aldehyde **8** as brown crystalline solid.

**8**: Yield = 182 mg (91%), mp = 119–123 °C; <sup>1</sup>H NMR (CDCl<sub>3</sub>):  $\delta$  0.80 (s, 3H, 18-CH<sub>3</sub>), 0.93 (s, 3H, 19-CH<sub>3</sub>), 1.16–1.97 (m, 28H, rest of the 2  $\times$  CH<sub>3</sub>, 8  $\times$  CH<sub>2</sub> and 6  $\times$  CH of steroidal ring), 2.16 (s, 3H, CH<sub>3</sub>COO, Acetate), 2.46 (bd, 2H, 7-CH<sub>2</sub>), 3.45 (bs, 1H, 22-CH), 4.44 (bs, 1H, 3-CH), 4.73 (bd, 1H, 16-CH), 5.50 (s, 1H, 6-CH), 9.75 (s, 1H, 26-CHO). <sup>13</sup>C NMR (CDCl<sub>3</sub>, 75 MHz):  $\delta$  13.78 (C21), 16.79 (C18), 19.22 (C19), 19.71 (C27), 21.03 (C11), 21.77 (acetate CH<sub>3</sub>), 28.15 (C24), 30.07 (C2), 31.11 (C23), 31.96 (C20), 32.37 (C7), 32.59 (C15), 37.09 (C10), 37.39 (C1), 38.26 (CH), 38.48 (C12), 39.77 (C4), 41.08 (C13), 46.72 (C25), 50.41 (C9), 57.29 (C14), 65.44 (C17), 74.28 (C3), 83.28 (C16), 90.11 (C22), 122.73 (C6), 140.09 (C5), 170.91 (acetate ester), 205.54 (C26); ESI Mass (MeOH): 457.3 [M+H]<sup>+</sup>, 479.3 [M+Na]<sup>+</sup>, 495.4 [M+K]<sup>+</sup>; IR (KBr, cm<sup>-1</sup>): 2833, 1739, 1254.

#### 2.2.4. Synthesis of (22 $\beta$ )-3 $\beta$ -hydroxy,25-oxo-27-nor-furost-5-en-3 $\beta$ -acetate (**9**)

Aldehyde **8** (200 mg, 0.44 mmol) was taken in ethanol (10 mL) and stirred at ambient temperature (30–35 °C). To this 3,4,5-trimethoxyaniline (200 mg, 1.09 mmol) was added and further stirred for 2 h. The solvent was evaporated, residue was dissolved in ethyl acetate (30 mL) and washed with water. The organic phase was dried over anhydrous sodium sulfate and dried *in vacuo*. The crude mass was purified through silica gel column eluting with ethyl acetate:hexane. The ketone **9** was obtained at 8–10% ethyl acetate hexane as creamish white solid.

**9**: Yield = 163 mg (84%), mp = 138–40 °C; <sup>1</sup>H NMR (CDCl<sub>3</sub>):  $\delta$  0.79 (s, 3H, 18-CH<sub>3</sub>), 0.98 (s, 3H, 19-CH<sub>3</sub>), 1.02–1.87 (m, 23H, rest of the 1  $\times$  CH<sub>3</sub>, 8  $\times$  CH<sub>2</sub> and 4  $\times$  CH of steroidal ring), 1.95 (s, 3H, CH<sub>3</sub>COO, acetate), 2.13 (s, 3H, 26-CH<sub>3</sub>CO), 2.32 (d, 1H, 7-CH<sub>2</sub>, J = 6.3 Hz), 2.51–2.63 (bd, 2H, 24-CH<sub>2</sub>), 3.26–3.29 (bs, 1H, 22-CH), 4.24–4.29 (bs, 1H, 16-CH), 4.57 (bd, 1H, 3-CH), 5.35 (s, 1H, 6-CH). <sup>13</sup>C NMR (CDCl<sub>3</sub>, 75 MHz):  $\delta$  16.80 (C18), 19.01 (C19), 19.71 (C21), 21.02 (C11), 21.80 (acetate CH<sub>3</sub>), 27.44 (C23), 28.13 (C1), 30.33 (C26), 31.95 (C8), 32.37 (C7), 32.55 (C15), 37.10 (C10), 37.38 (C2), 38.24 (C20), 38.48 (C12), 39.75 (C4), 41.09 (C13), 41.28 (C24), 50.38 (C9), 57.27 (C14), 65.39 (C17), 74.28 (C3), 83.69 (C16), 89.53 (C22), 122.72 (C6), 140.12 (C5), 170.95 (Acetate ester), 209.24 (C25); ESI Mass (MeOH): 443.3 [M+H]<sup>+</sup>, 465.4 [M+Na]<sup>+</sup>, 481.3 [M+K]<sup>+</sup>; IR (KBr, cm<sup>-1</sup>): 2927, 1724, 1453, 1372, 1241.

#### 2.2.5. Wittig reaction on aldehyde **8**

Synthesis of (22 $\beta$ )-(E)-26-Benzylidene-3 $\beta$ -yl-furost-5-en-3-acetate (**10**): Benzyltriphenylphosphonium bromide (Wittig salt, 200 mg) was taken in dry toluene (10 mL). To this stirred solution pre-washed sodium hydride (200 mg, 8.33 mmol) added and stirred for 20 min. Aldehyde **8** (100 mg, 0.22 mmol) was added and the reaction mixture was further stirred for 2 h. Toluene was evaporated under vacuum and residue was taken in ethyl acetate

(20 mL × 3), washed with water and dried over anhydrous sodium sulfate. The organic layer was dried *in vacuo* to get a crude mass, which was purified through silica gel column eluting with ethyl acetate-hexane. The desired product was obtained as yellowish viscous liquid.

**10:** Yield = 158 mg (68%), oil; <sup>1</sup>H NMR (CDCl<sub>3</sub>): δ 0.73 (s, 3H, 18-CH<sub>3</sub>), 0.95 (s, 3H, 19-CH<sub>3</sub>), 1.02–1.95 (m, 26H, rest of the 2 × CH<sub>3</sub>, 7 × CH<sub>2</sub> and 6 × CH of steroidal ring), 1.99 (s, 3H, CH<sub>3</sub>COO, acetate), 2.23 (d, 2H, 4-CH<sub>2</sub>, J = 5.4 Hz), 2.30 (bd, 2H, 7-CH<sub>2</sub>), 3.23 (bd, 1H, 22-CH), 4.22 (bs, 1H, 16-CH), 4.51 (bs, 1H, 3-CH), 5.28 (s, 1H, 6-CH), 5.96 (dd, 1H, 26-CH, J = 15.6 Hz and 7.8 Hz), 6.26 (d, 1H, 28-CH, J = 15.6 Hz), 7.12 (m, 5H, aromatic protons of phenyl ring). <sup>13</sup>C NMR (CDCl<sub>3</sub>, 75 MHz): δ 16.83 (C18), 19.39 (C19), 19.72 (C21), 21.06 (C11), 21.79 (acetate CH<sub>3</sub>), 28.16 (C1), 30.06 (C28), 31.85, 31.99, 32.40 (C7), 32.66 (C15), 34.48 (C24), 37.12 (C10), 37.41 (C2), 38.04, 38.31 (C20), 38.51 (C12), 39.82 (C4), 41.10, 50.44 (C9), 57.31 (C14), 65.60 (C17), 74.33 (C3), 83.58 (C16), 90.82 (C22), 122.77 (C6), 126.39 (C3' & C5' of Phenyl ring), 127.15 (C26), 128.73 (C2' & C6' of phenyl ring), 128.83 (C27), 137.05 (C4' of phenyl ring), 138.33 (C1' of phenyl ring), 140.09 (C5), 170.97 (acetate ester); ESI Mass (MeOH): 531.5 [M+H]<sup>+</sup>, 553.5 [M+K]<sup>+</sup>, 569.6 [M+K]<sup>+</sup>; IR (KBr, cm<sup>-1</sup>): 2946, 1734, 1456, 1372, 1244.

**2.2.6. (22β)-(Z)-26-(4'-Nitrobenzylidene)-3β-yl-furost-5-en-3-acetate (11):** procedure same as for **10**, Wittig salt (200mg) was 4-nitrobenzyltriphenylphosphonium bromide

Yield = 157 mg (62%), oil; <sup>1</sup>H NMR (CDCl<sub>3</sub>): δ 0.71 (s, 3H, 18-CH<sub>3</sub>), 0.96 (s, 3H, 19-CH<sub>3</sub>), 1.05–1.88 (m, 26H, rest of the 2 × CH<sub>3</sub>, 7 × CH<sub>2</sub> and 6 × CH of steroidal ring), 2.02 (s, 3H, CH<sub>3</sub>COO, acetate), 2.21 (bs, 2H, 4-CH<sub>2</sub>), 2.30 (bd, 2H, 7-CH<sub>2</sub>), 3.20 (bd, 1H, 22-CH), 4.20 (bs, 1H, 16-CH), 4.50 (bs, 1H, 3-CH), 5.26 (bs, 1H, 6-CH), 6.29 (m, 1H, 26-CH), 6.79 (d, 1H, 28-CH, J = 9.0 Hz), 7.33–8.05 (m, 4H, aromatic protons of phenyl ring). <sup>13</sup>C NMR (CDCl<sub>3</sub>, 75 MHz): δ 16.80 (C18), 19.29 (C19), 19.69 (C21), 20.62, 21.01 (C11), 21.81 (acetate CH<sub>3</sub>), 28.11 (C1), 29.74, 31.38, 31.95, 32.35 (C7), 32.99 (C15), 34.01 (C23), 37.09, 37.36 (C2), 38.22, 38.45 (C12), 39.74 (C4), 41.10, 50.37 (C9), 57.27 (C14), 65.40 (C17), 74.50 (C3), 83.69 (C16), 90.54 (C22), 122.77 (C6), 123.92, 124.33, 126.80, 130.53 (C27), 134.03 (C26), 140.04 (C5), 142.28 (2' & 6' of phenyl ring), 143.26 (3' & 5' of phenyl ring), 162.83 (4' of phenyl ring), 171.85 (acetate ester); ESI Mass (MeOH): 576.6 [M+H]<sup>+</sup>, 574.6 [M-H]<sup>+</sup>, 598.6 [M+Na]<sup>+</sup>, 614.5 [M+K]<sup>+</sup>; IR (KBr, cm<sup>-1</sup>): 2940, 1728, 1595, 1516, 1340, 1246.

**2.2.7. (22β)-(Z)-26-(3',4',5'-Trimethoxybenzylidene)-3β-yl-furost-5-en-3-acetate (12):** procedure same as for **10** Wittig salt was 4-nitrobenzyltriphenylphosphonium bromide (200 mg) to get **12** and **13**

Yield = 79 mg (29%), oil; <sup>1</sup>H NMR (CDCl<sub>3</sub>): δ 0.79 (s, 3H, 18-CH<sub>3</sub>), 0.95 (s, 3H, 19-CH<sub>3</sub>), 1.04–1.87 (m, 29H, rest of the 2 × CH<sub>3</sub>, 8 × CH<sub>2</sub> and 7 × CH of steroidal ring), 2.02 (s, 3H, CH<sub>3</sub>COO, acetate), 2.29 (bd, 2H, 7-CH<sub>2</sub>), 3.85 (s, 9H, 3XOCH<sub>3</sub>), 4.28 (bd, 1H, 22-CH), 4.61 (bs, 1H, 3-CH), 5.39 (t, 1H, 6-CH), 6.28 (d, 1H, 27-CH, J = 11.4 Hz), 6.32 (bd, 1H, 26-CH), 6.50 (d, 2H, 2' & 6'-CH of phenyl ring). <sup>13</sup>C NMR (CDCl<sub>3</sub>, 75 MHz): δ 16.83 (C18), 19.41 (C19), 19.71 (C21), 21.03 (C11), 21.82 (acetate CH<sub>3</sub>), 28.14 (C1), 30.06, 31.97, 32.37 (C7), 32.61 (C15), 33.39, 35.13, 37.10, 37.39 (C2), 38.29, 38.48 (C12), 39.77 (C4), 41.06, 50.38 (C9), 56.42, 57.28 (C14), 61.30, 65.51 (C17), 74.30 (C3), 83.58 (C16), 90.71 (C22), 106.17 (2' & 6' of phenyl ring), 122.77 (C6), 128.05 (C27), 133.94 (4' of phenyl ring), 139.38 (C26), 140.09 (C5), 153.27 (3' & 5' of phenyl ring), 170.97 (acetate ester); ESI Mass (MeOH): 621.5 [M+H]<sup>+</sup>, 643.4 [M+K]<sup>+</sup>, 659.4 [M+K]<sup>+</sup>; IR (KBr, cm<sup>-1</sup>): 2945, 1733, 1582, 1504, 1456, 1243.

**2.2.8. (22β)-(E)-26-(3',4',5'-Trimethoxybenzylidene)-3β-yl-furost-5-en-3-acetate (13)**

Yield = 142 mg (52%), oil; <sup>1</sup>H NMR (CDCl<sub>3</sub>): δ 0.77 (s, 3H, 18-CH<sub>3</sub>), 0.94 (s, 3H, 19-CH<sub>3</sub>), 1.04–1.84 (m, 30H, rest of the 2 × CH<sub>3</sub>, 9 × CH<sub>2</sub> and 6 × CH of steroidal ring), 1.99 (s, 3H, CH<sub>3</sub>COO, acetate), 2.29 (bd, 2H, 7-CH<sub>2</sub>), 3.84 (s, 9H, 3XOCH<sub>3</sub>), 4.10 (bd, 1H, 22-CH, J = 7.1 Hz), 4.27 (bs, 1H, 16-CH), 4.54 (bs, 1H, 3-CH), 5.33 (s, 1H, 6-CH), 5.98 (dd, 1H, 26-CH, J = 15.6 Hz & 7.8 Hz), 6.22 (d, 1H, 27-CH, J = 15.9 Hz), 6.54 (s, 2H, 2' & 6'-CH of phenyl ring). <sup>13</sup>C NMR (CDCl<sub>3</sub>, 75 MHz): δ 16.83 (C18), 19.41 (C19), 19.70 (C21), 21.01 (C11), 21.77 (acetate CH<sub>3</sub>), 28.12 (C1), 30.07, 31.81, 31.96, 32.36 (C7), 32.65 (C15), 34.45, 37.08, 37.37 (C2), 37.96, 38.27, 38.47 (C12), 39.77 (C4), 41.06, 50.37 (C9), 56.41, 57.26 (C14), 61.26, 65.55 (C17), 74.24 (C3), 83.55 (C16), 90.72 (C22), 103.39 (2' & 6' of phenyl ring), 122.74 (C6), 128.64 (C27), 134.05 (C5), 136.50 (C26), 137.61 (4' of phenyl ring), 140.06 (C26), 153.63 (3' & 5' of phenyl ring), 170.85 (acetate ester); ESI Mass (MeOH): 621.5 [M+H]<sup>+</sup>, 643.5 [M+Na]<sup>+</sup>, 659.4 [M+K]<sup>+</sup>;

**2.2.9. Synthesis of (22β)-3β-Acetoxy-furost-5-en-26-aldoxime (14)**

Aldehyde **8** (100 mg, 0.22 mmol) was taken in ethanol (10 mL). To this dry pyridine (0.5 mL) and hydroxyaminehydrochloride (100 mg, 1.43 mmol) was added and refluxed for 2 h. On completion ethanol was evaporated and dil HCl (10 mL) was added to it, extracted with ethyl acetate (20 mLx3), washed with water and dry *in vacuo*. The residue thus obtained was purified through silica gel column using hexane-ethyl acetate as eluants. The desired aldoxime **14** was obtained as creamish white solid.

**14:** Yield = 73 mg (70%), mp = 130–33 °C; <sup>1</sup>H NMR (CDCl<sub>3</sub>): δ 0.78 (s, 3H, 18-CH<sub>3</sub>), 0.97 (s, 3H, 19-CH<sub>3</sub>), 1.07–1.86 (m, 26H, rest of the 2 × CH<sub>3</sub>, 8 × CH<sub>2</sub> and 4 × CH of steroidal ring), 2.01 (s, 3H, CH<sub>3</sub>COO, acetate), 2.31 (bd, 2H, 7-CH<sub>2</sub>), 3.29 (bs, 1H, 22-CH), 4.29 (bs, 1H, 3-CH), 4.59 (bd, 1H, 16-CH), 5.36 (s, 1H, 6-CH), 7.29 (bd, 1H, 26-CH, J = 6.3 Hz). <sup>13</sup>C NMR (CDCl<sub>3</sub>, 75 MHz): δ 16.81 (C18), 18.44, 19.26 (C19), 19.70 (C27), 21.03 (C11), 21.78 (acetate CH<sub>3</sub>), 28.12 (C24), 30.06 (C2), 31.32 (C23), 31.95 (C20), 32.36 (C7), 32.56 (C15), 35.06, 37.08 (C10), 37.38 (C1), 38.24 (C8), 38.47 (C12), 39.78 (C4), 41.07 (C13), 50.39 (C9), 57.28 (C14), 65.46 (C17), 74.32 (C3), 83.62 (C16), 90.39 (C22), 122.75 (C6), 140.06 (C5), 156.46 (C26), 170.01 (acetate ester); ESI Mass (MeOH): 472.4 [M+H]<sup>+</sup>, 494.5 [M+Na]<sup>+</sup>, 510.3 [M+K]<sup>+</sup>; IR (KBr, cm<sup>-1</sup>): 3405, 2948, 1735, 1455, 1371, 1256, 1043.

**2.2.10. (22β)-3β-Acetoxy-furost-5-en-26-aldoxime acetate (15)**

The procedure is same as for **6** starting substrate was **14**.

Yield = 1.0 g (92%), mp = 90–93 °C; <sup>1</sup>H NMR (CDCl<sub>3</sub>): δ 0.79 (s, 3H, 18-CH<sub>3</sub>), 0.99 (s, 3H, 19-CH<sub>3</sub>), 1.02–1.97 (m, 29H, rest of the 2 × CH<sub>3</sub>, 8 × CH<sub>2</sub> and 7 × CH of steroidal ring), 2.02 (s, 6H, 2 × CH<sub>3</sub>-COO, 3 & 26-oxime acetates), 2.30 (bd, 2H, 7-CH<sub>2</sub>, J = 6.9 Hz), 3.29 (bs, 1H, 22-CH), 4.29 (bs, 1H, 3-CH), 4.60 (bd, 1H, 16-CH), 5.36 (s, 1H, 6-CH), 7.50–7.53 (d, 1H, 26-CH, J = 8.1 Hz); <sup>13</sup>C NMR (CDCl<sub>3</sub>, 75 MHz): δ 16.81 (C18), 19.20 (C19), 19.72 (C27), 19.91 (C21), 21.03 (C11), 21.81 (acetate CH<sub>3</sub>), 26.33 (Oxime acetate CH<sub>3</sub>), 28.14 (C1), 30.08 (C23), 31.52 (C20), 31.96, 32.38 (C7), 32.59 (C15), 37.11 (C10), 37.39 (C2), 38.06, 38.28 (C24), 38.49 (C12), 39.77 (C4), 41.09 (C13), 50.40 (C9), 57.29 (C14), 65.32 (C17), 74.29 (C3), 83.83 (C16), 90.14 (C22), 122.74 (C6), 140.12 (C5), 163.46 (C26), 169.16 (Oxime acetate), 170.95 (3-acetate ester); ESI Mass (MeOH): 514.4 [M+H]<sup>+</sup>, 536.3 [M+Na]<sup>+</sup>; IR (KBr, cm<sup>-1</sup>): 2934, 1734, 1454, 1372, 1244.

**2.2.11. Synthesis of (22β)-3β-Acetoxy-27-nor-furost-5-en-25-ketoxime (16)**

The ketoxime **16** was prepared from **9** using the same method as for aldoxime **14**.

Yield = 87 mg (84%), mp = 151–53 °C;  $^1\text{H NMR}$  ( $\text{CDCl}_3$ ):  $\delta$  0.79 (s, 3H, 18- $\text{CH}_3$ ), 0.99 (s, 3H, 19- $\text{CH}_3$ ), 1.02–1.95 (m, 28H, rest of the  $1 \times \text{CH}_3$ ,  $8 \times \text{CH}_2$  and  $5 \times \text{CH}$  of steroidal ring), 1.97 (s, 3H,  $\text{CH}_3\text{COO}$ , acetate), 2.03 (s, 3H, 25- $\text{CH}_3\text{C}=\text{N}-\text{O}$ ), 2.34 (bd, 2H, 7- $\text{CH}_2$ ), 3.33 (bm, 1H, 22-CH), 4.29 (bm, 1H, 16-CH), 4.53 (bm, 1H, 3-CH), 5.36 (s, 1H, 6-CH).  $^{13}\text{C NMR}$  ( $\text{CDCl}_3$ , 75 MHz):  $\delta$  16.80 (C18), 19.20 (C19), 19.72 (C21), 21.04 (C11), 21.81 (acetate  $\text{CH}_3$ ), 28.14 (C1), 30.08 (C26), 30.19 (C23), 31.96 (C8), 32.38 (C7), 32.59 (C15), 33.58 (C24), 37.10 (C10), 37.39 (C2), 38.20 (C20), 38.48 (C12), 39.77 (C4), 41.10 (C13), 50.39 (C9), 57.29 (C14), 65.49 (C17), 74.30 (C3), 83.70 (C16), 89.70 (C22), 122.76 (C6), 140.09 (C5), 158.98 (C25), 170.97 (acetate ester); ESI Mass (MeOH): 458.3  $[\text{M}+\text{H}]^+$ , 480.3  $[\text{M}+\text{Na}]^+$ , 496.4  $[\text{M}+\text{K}]^+$ ; IR (KBr,  $\text{cm}^{-1}$ ): 3382, 2941, 1721, 1448, 1374, 1248.

#### 2.2.12. (22 $\beta$ )-3 $\beta$ -Hydroxy-27-nor-furost-5-en-25-ketoxime-3 $\beta$ ,25-diacetate (**17**)

Procedure as for **6**.

Yield = 57 mg (52%), mp = 113–16 °C;  $^1\text{H NMR}$  ( $\text{CDCl}_3$ ):  $\delta$  0.80 (s, 3H, 18- $\text{CH}_3$ ), 0.96 (s, 3H, 19- $\text{CH}_3$ ), 1.08–1.88 (m, 24H, rest of the  $1 \times \text{CH}_3$ ,  $8 \times \text{CH}_2$  and  $5 \times \text{CH}$  of steroidal ring), 1.98 (s, 3H,  $\text{CH}_3\text{COO}$ , Acetate), 2.03 (s, 3H, 25- $\text{CH}_3\text{COO}$ -, acetate), 2.16 (t, 3H,  $\text{CH}_3\text{CO}$ ), 2.36 (bd, 2H, 7- $\text{CH}_2$ ), 3.30 (bs, 1H, 22-CH), 4.32 (bd, 1H, 16-CH,  $J = 5.4$  Hz), 4.60 (bs, 1H, 3-CH), 5.38 (s, 1H, 6-CH).  $^{13}\text{C NMR}$  ( $\text{CDCl}_3$ , 75 MHz):  $\delta$  16.82 (C18), 19.13 (C19), 19.72 (C21), 20.09, 21.03 (C11), 21.80 (acetate  $\text{CH}_3$ ), 28.04 (C1), 29.89 (C26), 30.08 (C2), 31.97 (C8), 32.37 (C7), 32.57 (C15), 33.76 (C24), 37.10, 37.39 (C23), 38.07, 38.48 (C12), 39.76 (C4), 41.12 (C13), 50.40 (C9), 57.28 (C14), 65.46 (C17), 74.27 (C3), 83.73 (C16), 89.61 (C22), 122.71 (C6), 140.12 (C5), 166.81 (C25), 169.26 (Oxime acetate), 170.90 (3-acetate ester); ESI Mass (MeOH): 500.4  $[\text{M}+\text{H}]^+$ , 538.3  $[\text{M}+\text{K}]^+$ ; IR (KBr,  $\text{cm}^{-1}$ ): 2924, 2369, 1735, 1458, 1371, 1245.

#### 2.2.13. Synthesis of (22 $\beta$ )-25-Hydroxy-3 $\beta$ -yl-27-nor-furost-5-en-3-acetate (**18**)

Ketone **9** (100 mg, 0.23 mmol) was stirred in methanol (5 mL). To this stirred solution sodium borohydride (30 mg, 0.79 mmol) was added and reaction mixture was further stirred for 30 min. On completion, solvent was evaporated *in vacuo* and residue was taken in ethyl acetate ( $2 \times 20$  mL). It was acidified with dil. HCl (5%, 5 mL), washed with water ( $2 \times 10$  mL) and organic layer was dried over anhydrous sodium sulfate. The solvent was evaporated *in vacuo* and residue thus obtained was recrystallised with chloroform-hexane (1:4) to get **18** as mixture of both 25 $\alpha/\beta$ -hydroxy isomers.

**18**: Yield = 86 mg (86%), mp = 159–62 °C;  $^1\text{H NMR}$  ( $\text{CDCl}_3$ ):  $\delta$  0.80 (s, 3H, 18- $\text{CH}_3$ ), 0.95 (s, 3H, 19- $\text{CH}_3$ ), 1.02–1.95 (m, 25H, rest of the  $2 \times \text{CH}_3$ ,  $8 \times \text{CH}_2$  and  $3 \times \text{CH}$  of steroidal ring), 2.03 (s, 3H,  $\text{CH}_3\text{COO}$ , Acetate), 2.30 (s, 1H, 20-CH), 2.32 (bd, 2H, 7- $\text{CH}_2$ ), 3.35 (bs, 1H, 22-CH), 3.79 (m, 1H, 25- $\text{CHOH}$ ), 4.33 (bd, 1H, 16-CH), 4.59 (bs, 1H, 3-CH), 5.36 (s, 1H, 6-CH).  $^{13}\text{C NMR}$  ( $\text{CDCl}_3$ , 75 MHz):  $\delta$  16.80 (C18), 19.08 (C19), 19.71 (C21), 21.03 (C11), 21.81 (acetate  $\text{CH}_3$ ), 23.62 (CH), 24.01 (CH), 28.14 (C1), 30.08 (C23), 31.93 (C8), 32.36 (C7), 32.49 (C15), 36.69 (C20), 37.10 (C10), 37.38 (C2), 38.28 (C24), 38.47 (C12), 39.81 (C4), 41.10 (C13), 50.38 (C9), 57.26 (C14), 65.17 (C17), 67.91/68.75 (C25 $\alpha/\beta$ ), 74.28 (C3), 83.80 (C16), 90.60 (C22), 122.75 (C6), 140.08 (C5), 170.94 (acetate ester); ESI Mass (MeOH): 445.3  $[\text{M}+\text{H}]^+$ , 467.4  $[\text{M}+\text{Na}]^+$ , 483.2  $[\text{M}+\text{K}]^+$ ; IR (KBr,  $\text{cm}^{-1}$ ): 3423, 2935, 1732, 1245.

#### 2.3. Crystal structure determination by X-ray diffraction crystallography

Single crystals of compound **9** ( $\text{C}_{28}\text{H}_{42}\text{O}_4$ ,  $M = 442.6$ ) were obtained by slow evaporation from a 50:50 mixture of chloroform and methanol at 4 °C. The compound crystallized in orthorhombic space group  $P2_12_12_1$  with one molecule in the asymmetric unit.

The unit cell dimensions were determined to be  $a = 6.0194$  (6) Å,  $b = 11.7762$  (14) Å,  $c = 35.229$  (4) Å,  $Z = 4$ ,  $V = 2497.2$  (5) Å<sup>3</sup>,  $D_{\text{calc}} = 1.177$  gm/cm<sup>3</sup>,  $F(000) = 968$ . X-ray diffraction data were collected on a Bruker AXS SMART APEX CCD diffractometer using Mo  $K\alpha$  radiation ( $\lambda = 0.71073$  Å). Data were acquired using  $\omega$  scan mode at room temperature (293 K). The structure was solved by direct methods using SHELXS [7a] and was refined against  $F^2$  with full-matrix least squares method by using SHELXL [7b]. All the non hydrogen atoms were refined anisotropically. Hydrogen atoms were fixed geometrically in idealized positions and were refined as riding over the atoms to which they were bonded. 10149 reflections were measured (5107 independent reflections) with  $R_{\text{int}} = 0.060$ . The final R-value was 0.055 ( $wR = 0.1239$ ) for 2040 observed reflections with  $|I| > 2\sigma|I|$  and for 286 parameters. The goodness-of-fit was 0.902. The largest difference peak was  $0.28 \text{ e}\text{\AA}^{-3}$  and the largest difference hole was  $-0.25 \text{ e}\text{\AA}^{-3}$ . The absolute configuration was chosen based on the known configuration of the starting diosgenin molecule. Crystallographic data (excluding structure factors) have been deposited with the Cambridge Crystallographic Data Centre as supplementary publication number CCDC 967022. Copies of the data can be obtained, free of charge, on application to CCDC, 12 Union Road, Cambridge CB2 1EZ, UK, (fax: +44-(0)1223-336033 or e-mail: deposit@ccdc.cam.ac.uk)

#### 2.4. Biological evaluation

##### 2.4.1. Cytotoxicity evaluation by Sulphorhodamine assay

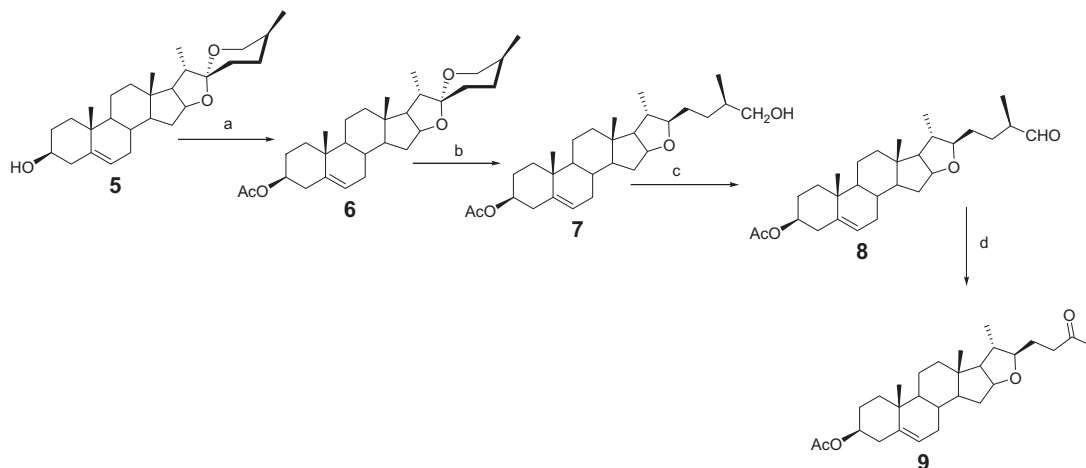
Cytotoxic activity of the compounds was assessed by Sulphorhodamine B dye based plate assay [8]. In brief,  $10^4$  cells/well were added in 96-well culture plates and incubated overnight at 37 °C in 5%  $\text{CO}_2$ . Next day (at 80% confluency), serial dilutions of test compound were added to the wells. Untreated cells served as control. After 48 h, cells were fixed with ice-cold 50% (w/v) Tri-chloro acetic acid (100  $\mu\text{L}$ /well) for 1 h at 4 °C. Cells were then stained with SRB (0.4% w/v in 1% acetic acid, 50  $\mu\text{L}$ /well), washed and air-dried. Bound dye was solubilized with 10 mM Tris base (150  $\mu\text{L}$ /well) and absorbance was read at 540 nm on a plate reader (Biotek, USA). The cytotoxic effect of compound was calculated as% inhibition in cell growth as per formula:  $[1 - (\text{Absorbance of drug treated cells}/\text{Absorbance of untreated cells}) \times 100]$ . Determination of 50% inhibitory concentration ( $\text{IC}_{50}$ ) was based on dose-response curves.

##### 2.4.2. Cell cycle analysis

The effect of most potent compound on cell division cycle was assessed by flow cytometry with PI-stained cellular DNA, as described earlier [9]. Briefly, cells ( $4 \times 10^5$  per well) were seeded in 6-well culture plate and grown overnight at 37 °C in 5%  $\text{CO}_2$ . After exposure to the compound for different time points, cells were harvested by trypsinization and fixed with ice-cold 70% ethanol for 30 min at 4 °C. The pellets were washed with PBS and resuspended in a solution containing PI (20 mg/ml), Triton X100 (0.1%) and RNase (1 mg/ml) in PBS. After distribution of cells in different phases of cell cycle was calculated using "Cell Quest" software.

##### 2.4.3. Western blot assay

Compound treated cells were lysed (30 min, in ice) with cold M-PER (mammalian protein extraction reagent) supplemented with protease inhibitor cocktail. Equal amount of proteins (25  $\mu\text{g}$ ) extracted from the cells treated for different time intervals were separated by 10% SDS-polyacrylamide gel electrophoresis and transferred electrophoretically onto PVDF membranes. The membranes were blocked with 5% nonfat dry milk powder dissolved in Tris-buffered saline (TBS; 20 mM Tris-HCl pH 7.6, 137 mM NaCl) containing 0.1% Tween 20 (TBS-T) for 1 h at room temperature and subsequently incubated overnight with anti-PARP antibody (cat#



**Scheme 1.** (a) Ac<sub>2</sub>O, dry pyridine, dry CHCl<sub>3</sub>, RT, 2 h, 91%; (b) AcOH, NaCNBH<sub>3</sub>, RT, 5 h, 81%; (c) Dry DCM, PCC, reflux, 1 h, 91%; (d) Ethanol, substituted aniline, RT, 2 h, 66–84%.

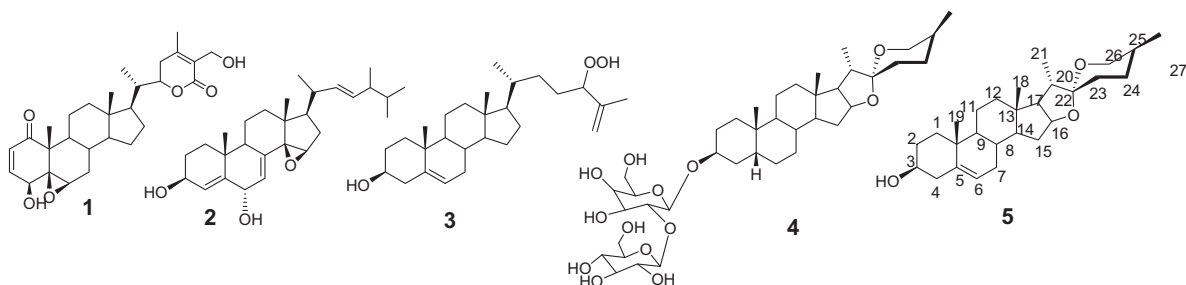


**Fig. 1.** Some of the plant based potent cytotoxic molecules on steroidal framework; **1:** withaferin A, **2:** gymnasterol **3:** 24-hydroxyperoxide desmosterol, **4:** timosaponin A-III, **5:** diosgenin.

**Table 1**  
Effect of various amines on transformation of **8–9**.

Entry	Aldehyde	Amine	Solvent	Reaction time (h)	%Yield of <b>9</b>
1	<b>8</b>	No amine	EtOH	16	No reaction
2	<b>8</b>	3,4,-Dimethoxyaniline	EtOH	2	66
3	<b>8</b>	3,4,5-Trimethoxyaniline	EtOH	2	84
4	<b>8</b>	3,4-Methylenedioxyaniline	EtOH	2	72
5	<b>8</b>	Benzyl amine	EtOH	16	No reaction
6	<b>8</b>	3,4-Methylenedioxybenzyl amine	EtOH	16	No reaction
7	<b>8</b>	Ammonia	EtOH	16	No reaction
8	<b>8</b>	Methylamine	EtOH	16	No reaction
9	<b>8</b>	Ethylamine	EtOH	16	No reaction

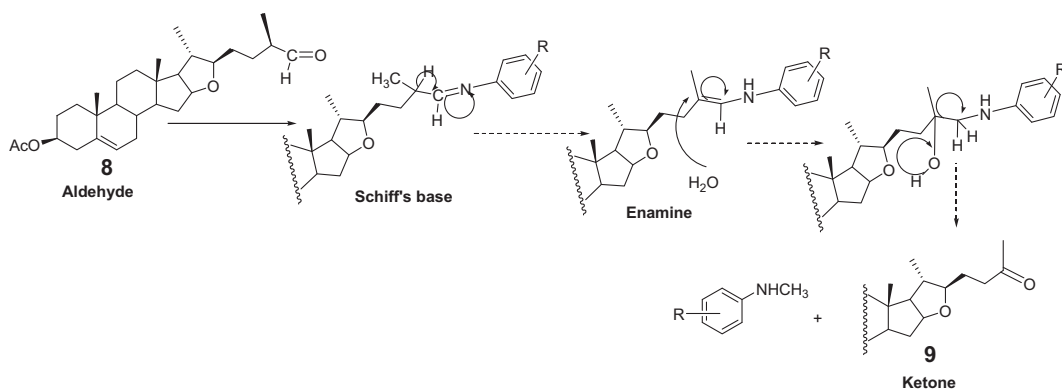


**Fig. 2.** Plausible mechanism of conversion of aldehyde **8** to ketone **9**.

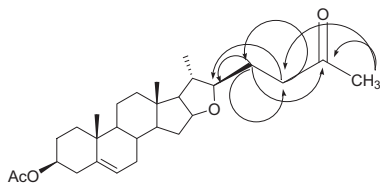


Fig. 3. HMBC correlations of side chain of ketone 9.

9542, Cell Signaling Technology, USA) at 4 °C. After 3 washes with TBS-T, the membranes were incubated with HRP conjugated anti-rabbit antibody for 1 h at room temperature and washed again with TBS-T (x3 times). Proteins were detected with an enhanced chemiluminescence (ECL) reagent and visualized by a chemiluminescence detector (Bio-Rad Laboratories, USA). The densitometry analysis of blots was done by using Bio-Rad Image Lab 4.0 software.

#### 2.4.4. Docking studies

The two dimensional structures of the molecules were constructed with the ChemDraw Ultra. Energy minimization of the compounds was performed with 'ChemBio office' considering MM2/MM3 molecular mechanics parameter up to its lowest stable energy state. This energy minimization process was performed until the energy change was less than 0.001 kcal mol<sup>-1</sup> or the molecules had been updated almost 300 times. The 3D chemical structure of doxorubicin (Positive control) was retrieved from the PubChem compound database at NCBI (<http://www.pubchem.ncbi.nlm.nih.gov>). Crystallographic 3D structures of target proteins (caspase-9: (PDB:1NW9- chain B) and caspase-3: (PDB:3KJF) were retrieved from the Brookhaven Protein Databank (<http://www.pdb.org>) [10,11]. Hydrogen atoms were added to the protein targets to achieve the correct ionization and tautomeric states of amino acid residues such as His, Asp, Ser, and Glu. Molecular docking of the compounds against selected target was achieved using the 'AutoDock Vina'. To perform the automated docking of ligands into the active sites, we used a Lamarckian genetic algorithm [12].

#### 2.4.5. In-vivo acute oral toxicity

In view of potent anti-cancer activity of compound 7 in *in-vitro* model, acute and sub-acute oral toxicity of the same was carried out in Swiss albino mice for its further development into drug product. Experiment was conducted in accordance with the Organization for Economic Co-operation and Development (OECD) test guideline No 423 (1987).

For this experiment, 30 mice (15 male and 15 female) were taken and divided into four groups comprising 3 male and 3 female mice in each group weighing between 20 and 25 g. The animals were maintained at 22 ± 5°C with humidity control and also on an automatic dark and light cycle of 12 hours. The animals were fed with the standard mice feed and provided *ad libitum* drinking

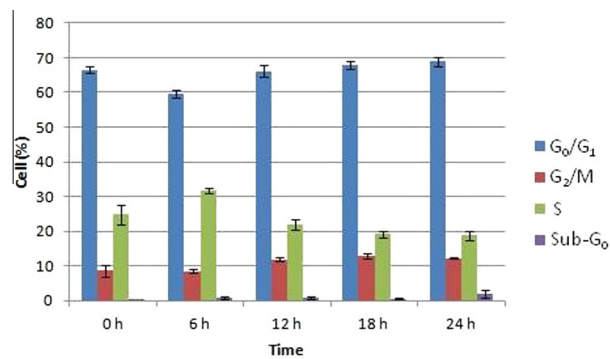


Fig. 5. Cell cycle analysis of compound 7.

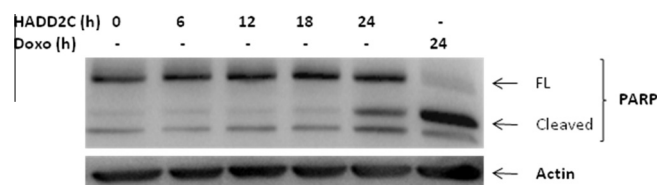


Fig. 6. Cleavage of PARP, a caspase target by compound 7.

water. Mice of group 1 were kept as control and animals of groups 2, 3, 4 and 5 were kept as experimental. The animals were acclimatized for 7 days in the experimental environment prior to the actual experimentation. The test compound was solubilized in dimethyl sulphoxide with few drops of tween 80 and then suspended in caboxymethyl cellulose (0.7%) and was given at 5, 50, 300 and 1000 mg/kg body weight to animals of groups 2, 3, 4 and 5 respectively once orally. Control animals received only vehicle.

The animals were checked for mortality and any signs of ill health at hourly interval on the day of administration of drug and there after a daily general case side clinical examination was carried out including changes in skin, mucous membrane, eyes, occurrence of secretion and excretion and also responses like lachrymation, piloerection respiratory patterns etc. Also changes in gait, posture and response to handling were also recorded [13]. In addition to observational study, body weights were recorded and blood and serum samples were collected from all the animals on 7<sup>th</sup> day of the experiment in acute oral toxicity. The samples were analyzed for total RBC, WBC, differential leucocytes count, hemoglobin percentage and biochemical parameters like ALKP, SGPT, SGOT, total cholesterol, triglycerides, creatinine, bilirubin, serum protein, tissue protein, malonaldehyde and reduced GSH activity. The animals were then sacrificed and were necropsed for any gross pathological changes. Weights of vital organs like liver, heart, kidney etc. were recorded [14].

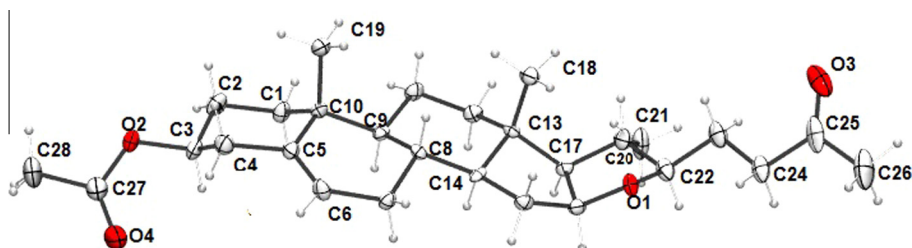


Fig. 4. Molecular conformation of 9 in crystals. Thermal ellipsoids are shown at 50% probability level.

### 2.4.6. Statistical analysis

Statistical analysis was carried out in Microsoft Excel.

## 3. Results and discussion

Scheme 1 denotes the synthetic strategy of these derivatives starting with diosgenin (**5**). Diosgenin **5** was converted to diosgenin acetate **6** by acetylation with acetic anhydride-pyridine in dry chloroform at room temperature. The spectral data of acetate **6** was alike the earlier reports [6a]. The reductive cleavage of ring F of spiroketal linkage was done by using sodium cyanoborohydride in AcOH at room temperature to get the alcohol **7** that pos-

sesses furostenic system. Oxidation of alcohol **7** with pyridinium chlorochromate (PCC) yielded aldehyde **8** (Fig. 1).

We tried to prepare some Schiff's bases onto C<sub>29</sub> aldehyde (**8**), but unexpectedly, we ended with a C<sub>28</sub> ketone (**9**). Aldehyde **8** on treatment with an aromatic amine in ethanol at room temperature afforded product **9** as a ketone in 2 h. Various aromatic amines (3,4-dimethoxyaniline, 3,4,5-trimethoxyaniline, 3,4-methylenedioxyaniline) were tried and every time the same product **9** was obtained in varied yields (66–84%). The reaction of aldehyde **8** with aliphatic amines (MeNH<sub>2</sub> and EtNH<sub>2</sub>) and even with ammonia was unsuccessful. Benzyl amines (BnNH<sub>2</sub> and 3,4-methylenedioxybenzylamine) also did not yield the product **9** (Table 1). It will be worth mentioning that without aromatic amine this transformation does not take place. Aldehyde **8** did not form Schiff's base with

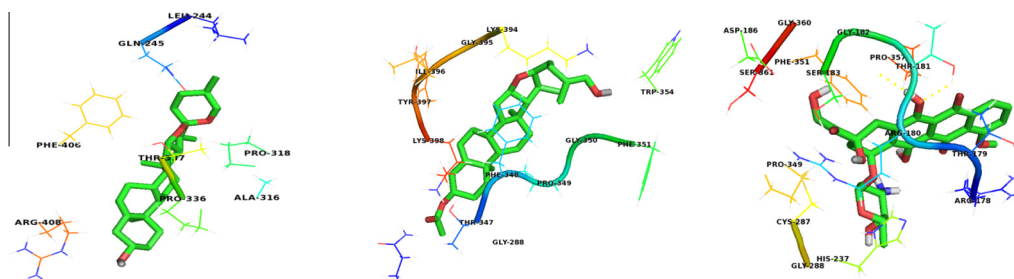


**Fig. 7a.** *In-silico* molecular docking studies elucidating the possible mechanisms of diosgenin (**5**), its derivatives **7**, and positive control doxorubicin with Caspase-9 (PDB: 1NW9-B). The docking studies were carried out using 'AutoDock Vina', using Lamarckian genetic algorithm.

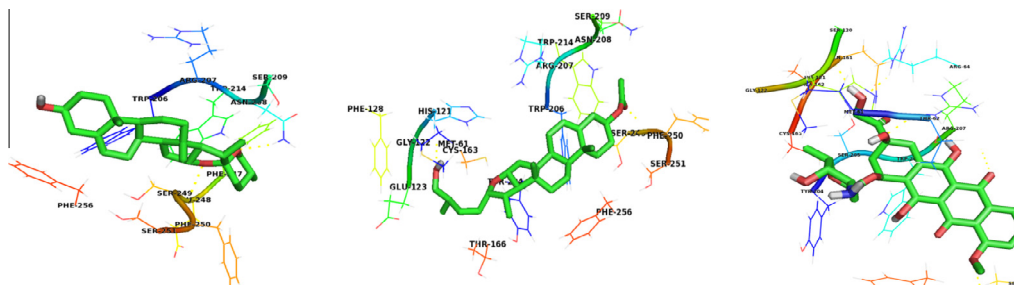


**Fig. 7b.** *In-silico* molecular docking studies elucidating the possible mechanisms of diosgenin (**5**), its derivatives **7**, and positive control doxorubicin with Caspase-3 (PDB: 3KJF). The docking studies were carried out using 'AutoDock Vina', using Lamarckian genetic algorithm.

**Table 2**  
Effect of solvent polarity on transformation of compound **8–9**.

Entry	Aldehyde	Amine	Solvent	Reaction time (t) h	% Yield of <b>9</b>
1	<b>8</b>	3,4,5-Trimethoxyaniline	EtOH	2	84
2	<b>8</b>	3,4,5-Trimethoxyaniline	MeOH	2	73
3	<b>8</b>	3,4,5-Trimethoxyaniline	THF	2	44
4	<b>8</b>	3,4,5-Trimethoxyaniline	Dichloromethane	2	49
5	<b>8</b>	3,4,5-Trimethoxyaniline	Toluene	2	28

**Table 3**  
*In-vitro* cytotoxicities of diosgenin analogs.

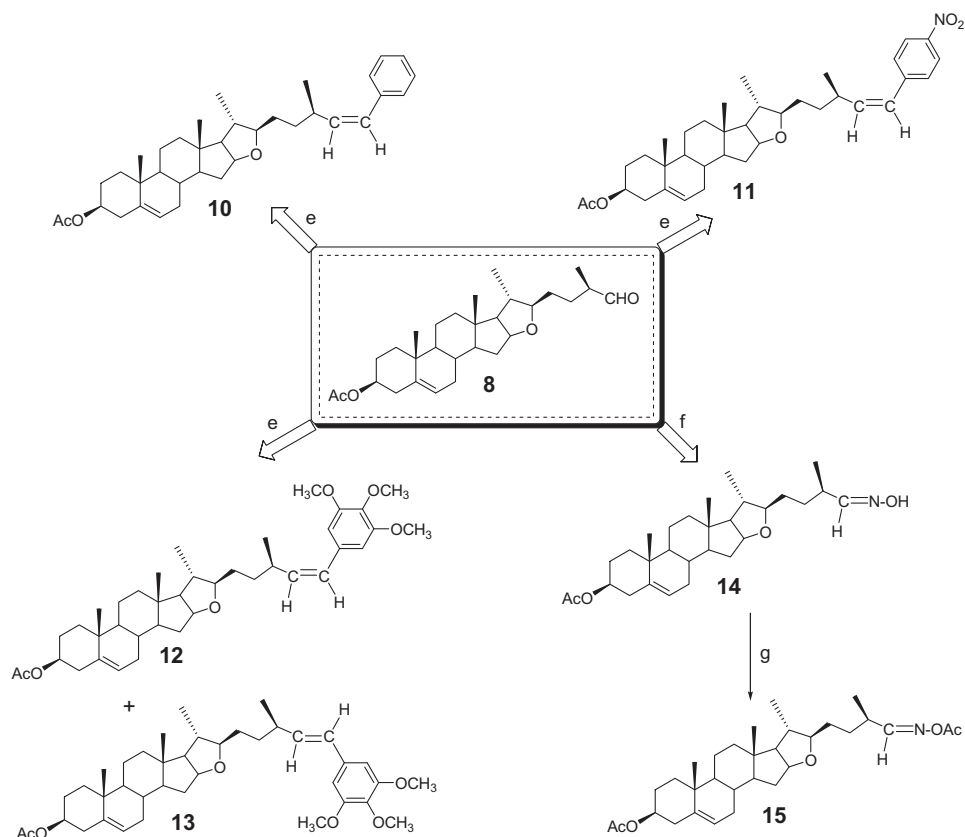
S. no.	Compound no./name	IC <sub>50</sub> (uM) (Mean ± SE) <sup>a</sup>				
		KB	C-33A	DU145	A549	MCF-7
1	<b>7</b>	11.43 ± 1.47	7.54 ± 0.93	>20	>20	10.95 ± 0.73
2	<b>8</b>	17.55 ± 1.25	11.54 ± 0.10	16.826	>20	15.17 ± 1.36
3	<b>14</b>	15.97 ± 1.96	11.18 ± 0.63	17.08 ± 0.09	15.27 ± 1.18	14.53 ± 1.07
4	<b>15</b>	13.96 ± 0.39	12.27 ± 0.38	13.27 ± 0.25	12.56 ± 0.18	14.28 ± 0.20
5	<b>17</b>	17.52	13.15	>20	16.29	18.67
6	Tamoxifen	10.25 ± 1.21	6.94 ± 0.09	12.24 ± 0.28	10.07 ± 0.46	8.54 ± 1.01
7	Podophyllotoxin	<1.25	<1.25	<1.25	<1.25	<1.25

<sup>a</sup> Rest of the compounds have IC<sub>50</sub> > 20 μM, considered inactive.

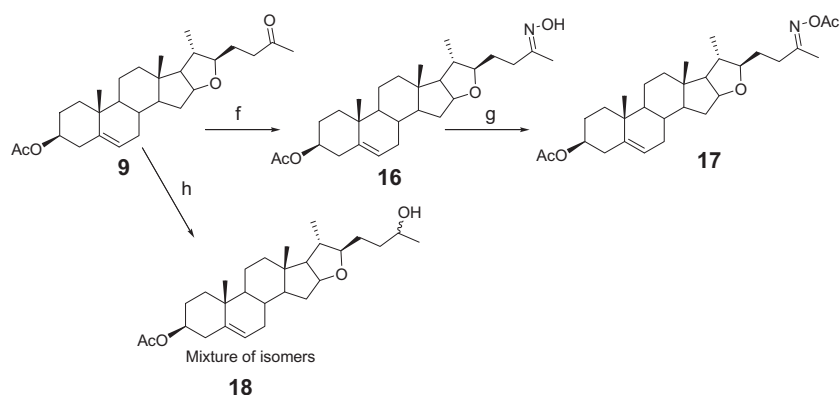
any of these amines. The structure of the ketone **9** was confirmed by 1D NMR ( $^1\text{H}$  &  $^{13}\text{C}$ ), 2D NMR (COSY, HSQC, HMBC), mass and IR spectroscopy. A plausible mechanism is given in Fig. 2.

Compound **9** was obtained as yellow amorphous powder. Its structure was established by spectroscopy. Its molecular formulae  $\text{C}_{28}\text{H}_{42}\text{O}_4$  was determined by its HR-ESI-MS at  $m/z$  443.3139  $[\text{M}+\text{H}]^+$  (Calcd 443.3161).  $^{13}\text{C}$  NMR showed total 28 distinct carbons indicating loss of one carbon as compared to aldehyde **8**. There were 5 methyls ( $\delta$ 16.80, 19.01, 19.71, 21.80, 30.33), 9 methylenes ( $\delta$ 21.02, 27.44, 28.13, 32.37, 32.55, 37.38, 38.48, 39.75, 41.28), 9 methines ( $\delta$ 31.95, 38.24, 50.38, 57.27, 65.39, 74.28, 83.69, 89.53, 122.72) and 5 quaternary carbons ( $\delta$  37.10, 41.09, 140.12, 170.95, 209.24). There was no aldehyde group and a carbonyl group was generated as ketone at  $\delta$ 209.24 ppm. Least change

in the chemical shifts of C1 to C22 suggested possibility of no change in the ring system of the ketone **9**. From HSQC spectrum, chemical shifts of 22-CH ( $\delta$ 3.26 m, 89.53), 23-CH<sub>2</sub> ( $\delta$ 1.72, 27.44), 24-CH<sub>2</sub> ( $\delta$ 2.49–2.61, 41.28) and 26-CH<sub>3</sub> ( $\delta$ 2.13, 30.33) were established. In  $^1\text{H}$ - $^1\text{H}$  COSY spectrum, 22-CH ( $\delta$ 3.26) showed coupling with 23-CH<sub>2</sub> ( $\delta$ 1.72) and 24-CH<sub>2</sub> ( $\delta$ 2.49–2.61) showed coupling with 23-CH<sub>2</sub> ( $\delta$ 1.72). In HMBC correlations, 26-CH<sub>3</sub> protons ( $\delta$ 2.13 ppm) showed correlations with C24 ( $\delta$ 41.28) and C25 ketone ( $\delta$ 209.24). 24-CH<sub>2</sub> protons ( $\delta$ 2.49–2.61) exhibited correlations with C26 ( $\delta$ 30.33) and C23 ( $\delta$ 27.44) carbons. C23-CH<sub>2</sub> protons ( $\delta$ 1.72) showed correlations with C22 ( $\delta$ 89.53), C24 (41.28) and C25 ( $\delta$ 209.24) carbons. HMBC correlations of side chain are shown in Fig. 3. The structure of **29** was finally authenticated by single crystal X-ray crystallography (Fig. 4).



**Scheme 2.** (e) Wittig salt, NaH, dry Toluene, RT, 3–4 h, 62–81%; (f)  $\text{NH}_2\text{OH}\cdot\text{HCl}$ , EtOH, reflux, 2 h, 84%; (g)  $\text{Ac}_2\text{O}$ , dry pyridine, dry  $\text{CHCl}_3$ , RT, 3 h, 92%.



**Scheme 3.** (f)  $\text{NH}_2\text{OH}\cdot\text{HCl}$ , EtOH, reflux, 2 h, 79%; (g)  $\text{Ac}_2\text{O}$ , dry pyridine, dry  $\text{CHCl}_3$ , RT, 3 h, 89%; (h)  $\text{NaBH}_4$ -MeOH, RT, 30 min, 86% (Mix of isomers).



Further, the molecular conformation of compound **9** in crystals is depicted in Fig. 4. All the bond lengths and bond angles are within the accepted range. The crystal packing is stabilized by van der Waals interactions, in the absence of strong hydrogen bond donors in this molecule. However, the ketonic O atom and the methylene group (C24) adjacent to the ketone functionality of symmetry-related molecules are at 3.22Å apart, suggesting a weak C-H...O interaction (O3...H = 2.55Å, C24...O3 = 3.22Å, ∠C24-H...O3 = 125.8°). The ring conformations of compound **9** are very similar to that observed in other diosgenin derivatives and solvates (Figs. 5, 6, 7A, 7B).

The effect of various solvents was also observed, as shown in Table 2. Ethanol was found to be the best solvent. However, methanol was equally good. In case of less polar solvents like THF, dichloromethane and toluene the yield of the product **9** was relatively low (Table 3).

Further, several styrene derivatives were prepared on to **8** aldehyde using Wittig reaction. Various Wittig salts (Benzylidene-triphenylphosphonium bromide) were prepared using triphenylphosphine and corresponding benzylbromide in toluene. Finally the styrene derivatives of diosgenin were obtained by treating wittig salt with aldehyde **8** in sodium hydride/toluene under reflux conditions in 29–68% yields. **8** was transformed to aldoxime (**14**) also and then oxime acetate (**15**) by usual methodologies [15]. All these transformations are depicted in Scheme 2.

Similarly, Scheme 3 shows modification of ketone **9** to various other derivatives. **9** was modified to ketoxime (**16**) and its corresponding acetate (**17**) same as described earlier for aldehyde **8**. The ketone group of **9** was reduced to alcohol (**18**) with sodium borohydride in methanol. Both C25α-OH and C25β-OH isomers were formed in equal ratio as evident from <sup>13</sup>C NMR at δ67.91 and δ68.75 respectively.

All synthesized compounds were evaluated against C33A (Cervical carcinoma), A549 (Lung carcinoma), KB (HeLa contaminant of mouth epidermal carcinoma), MCF-7 (Breast adenocarcinoma), DU145 (prostate carcinoma) human cancer cell lines by Sulphorhodamine assay [7]. Only five of the analogs exhibited significant anticancer activity, rest were inactive at 20 μM concentration.

Cell cycle regulation ensures the fidelity of genomic replication and cell division. G<sub>1</sub>/S and G<sub>2</sub>/M transitions are two major checkpoints to allow the cells to control any modification in DNA con-

tent. Checkpoint loss results in genomic instability and induce carcinogenesis. Induction of cell cycle arrest in cancer cell lines constitutes one of the most prevalent strategies to stop or limit cancer spreading [16]. Our data demonstrate that Compound **7** arrests cells at G<sub>0</sub>/G<sub>1</sub> phase of division cycle which is associated with decrease in G<sub>2</sub>/M population. We also observed accumulation of cells in sub-G<sub>0</sub> phase after treatment confirming induction of apoptosis by the molecule.

Diosgenin and related compounds have been good cytotoxic agents against various human cancer cell lines [17a–f]. Diosgenin and its semisynthetic derivatives induced apoptosis through increased expression of caspase-3 [18a–e]. Caspases are a family of cysteine-aspartic proteases, which are crucial mediators of apoptosis. Among these caspase-3 encoded as CAS3 gene is identified in numerous mammals. It remains as zymogens (procaspase) unless activated biochemically. It cleaves and activates caspases 6, 7 and 9, and the protein itself is processed by caspases 8, 9 and 10. Caspase-3 is necessary for its typical role in apoptosis, where it is responsible for chromatin condensation and DNA fragmentation [19]. PARP is an enzyme involved in DNA repair when cell are exposed to environmental stress [20]. During apoptosis, PARP is cleaved and inactivated by caspases [21,22]. Therefore, cleavage of PARP is a well established marker for detection of apoptosis. In the present study we found cleavage of PARP in MCF-7 cells at 24 h exposure to the Compound **7** implying activation of caspases by the molecule to trigger apoptosis.

The binding affinity obtained in the docking experiment allowed the activity of the diosgenin derivative **7** to be compared to that of the standard anticancer compound doxorubicin (Table 4). The diosgenin and its active derivatives '**7**' showed high binding affinity (high negative docking energy) against known human caspases 9 (–7.3 kcal/mol) and caspase 3 (–7.8 kcal/mol) (PDB: 1NW9-B; PDB: 3KJF). When we compared how the binding site pocket amino acid residues interacted with the derivatives, we found that the in case of CASPASE 9, 'PHE, PRO, THR, GLY, ARG, and HIS' amino acids were in share with positive control doxorubicin. While, in case of CASPASE 3, 'GLN, PHE, TYR, TRP, SER, ALA, GLY and ARG' were in share with doxorubicin.

In acute oral toxicity studies of compound **7**, no observational changes, morbidity and mortality were observed throughout the experimental period up to the dose level of 1000 mg/kg body

**Table 4**  
Molecular interactions of diosgenin (**5**) and its derivative **7** docked with Caspase-9: (PDB: 1NW9-B) and Caspase-3: (PDB: 3KJF) and binding pocket residues (amino acids).

Compound code	Caspase-3 (PDB entry 1pau)		Caspase-9 (PDB entry 1nw9)	
	Binding affinity (Kcal/mol)	Binding pocket amino acids	Binding affinity (kcal/mol)	Binding pocket amino acids
<b>5</b> 	–7.9	ARG(B)-207, ASN(B)-208, GLU(B)-248, PHE(B)-247, PHE(B)-250, PHE(B)-256, SER(B)-209, SER(B)-249, SER(B)-251, TRP(B)-206, TRP(B)-214	–8.7	ALA-316, ARG-408, GLN-245, LEU-244, PHE-406, PRO-318, PRO-336, THR-337
<b>7</b> 	–7.8	CYS(A)-163, GLU(A)-123, GLY(A)-122, HIS(A)-121, MET(A)-61, PHE(A)-128, THR(A)-166, ARG(B)-207, ASN(B)-208, PHE(B)-250, PHE(B)-256, SER(B)-209, SER(B)-249, SER(B)-251, TRP(B)-206, TRP(B)-214, TYR(B)-204	–7.3	GLN-240, GLY-288, GLY-350, GLY-395, ILE-396, LYS-394, LYS-398, PHE-348, PHE-351, PRO-349, THR-347, TRP-354, TYR-397
<b>Doxorubicin</b>	–8.2	ALA(A)-162, ARG(A)-64, CYS(A)-163, GLN(A)-161, GLY(A)-122, HIS(A)-121, MET(A)-61, SER(A)-120, ARG(B)-207, ASP(B)-253, PHE(B)-256, SER(B)-205, SER(B)-251, TRP(B)-206, TYR(B)-204	–8.2	ARG-178, ARG-180, ASP-186, CYS-287, GLY-182, GLY-288, GLY-360, HIS-237, PHE-351, PRO-349, PRO-357, SER-183, SER-361, THR-179, THR-181

**Table 5**

Effect of compound **7** as a single acute oral dose at 5, 50, 300 and 1000 mg/kg body weight on body weight, haemogram and serum biochemical parameters in Swiss albino mice (Mean  $\pm$  SD;  $n = 6$ ) compared to control, 5, 50, 300 and 1000 mg/kg.<sup>a</sup> significant ( $P < 0.05$ ).

Parameters	Dose of compound <b>7</b> at mg/kg body weight as a single oral dose				
	Control	5 mg/kg	50 mg/kg	300 mg/kg	1000 mg/kg
Body weight (gm)	23.32 $\pm$ 0.60	23.31 $\pm$ 0.48	23.95 $\pm$ 0.45	21.92 $\pm$ 0.47	23.10 $\pm$ 0.55
Hemoglobin (gm/dL)	11.23 $\pm$ 0.92	11.44 $\pm$ 0.50	10.94 $\pm$ 0.58	11.51 $\pm$ 1.02	12.10 $\pm$ 0.40
RBC (million/mm <sup>3</sup> )	5.82 $\pm$ 0.19	6.55 $\pm$ 0.30	5.85 $\pm$ 0.31	5.42 $\pm$ 0.34	6.19 $\pm$ 0.30
WBC (1000 <sup>a</sup> /mm <sup>3</sup> )	10.68 $\pm$ 2.14	11.03 $\pm$ 2.24	10.48 $\pm$ 1.76	10.71 $\pm$ 2.52	12.53 $\pm$ 2.77
ALKP (U/L)	222.1 $\pm$ 14.4	259.4 $\pm$ 6.9	263.6 $\pm$ 16.2	239.4 $\pm$ 13.7	139.7 $\pm$ 17.4
SGOT (U/L)	24.44 $\pm$ 2.37	32.49 $\pm$ 3.51	31.50 $\pm$ 2.98	36.04 $\pm$ 3.33	32.54 $\pm$ 3.50
SGPT (U/L)	12.96 $\pm$ 1.96	18.76 $\pm$ 1.79	18.07 $\pm$ 3.20	19.96 $\pm$ 4.63	18.33 $\pm$ 2.27
Albumin (g/dL)	3.60 $\pm$ 0.45	3.08 $\pm$ 0.15	2.98 $\pm$ 0.13	2.87 $\pm$ 0.24	3.27 $\pm$ 0.11
Creatinine (mg/dL)	0.63 $\pm$ 0.11	0.48 $\pm$ 0.09	0.50 $\pm$ 0.07	0.44 $\pm$ 0.05	0.47 $\pm$ 0.08
Triglycerides (mg/dL)	172.21 $\pm$ 17.57	180.55 $\pm$ 19.70	172.73 $\pm$ 19.15	171.74 $\pm$ 19.80	166.89 $\pm$ 17.97
Serum protein (mg/mL)	1.15 $\pm$ 0.13	1.02 $\pm$ 0.08	0.94 $\pm$ 0.08	1.00 $\pm$ 0.08	1.23 $\pm$ 0.09
Cholesterol (mg/dL)	156.4 $\pm$ 35.8	114.3 $\pm$ 21.2	115.9 $\pm$ 23.4	123.8 $\pm$ 25.6	156.4 $\pm$ 28.3

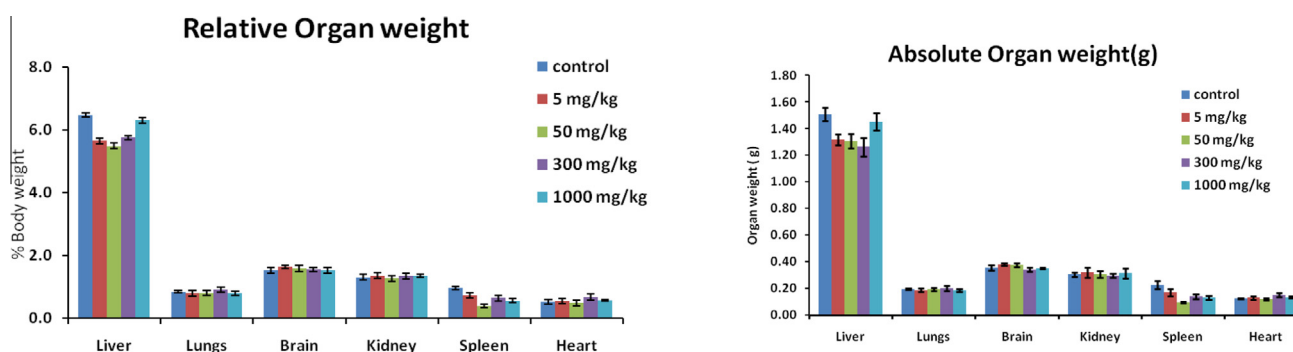


**Fig. 8.** Effect of compound **7** as a single acute oral dose at 5, 50, 300 and 1000 mg/kg on absolute and relative organ weight in Swiss albino mice ( $n = 6$ , Non significant changes were found compared to control).

weight. No morbidity or any other gross observation changes could be noticed in the group of animals treated with the test drug at 1000 mg/kg. Blood and serum samples upon analysis showed non-significant changes in all the parameters studied like total hemoglobin level, RBC count, WBC count, differential leucocytes count, SGPT, creatinine, triglycerides, cholesterol, albumin, serum protein (Table 5 and Fig. 8) except significant changes in ALKP activities in groups of animals treated with the compound at 1000 mg/kg; wherein ALKP activity was decreased significantly compared to control. Animals on gross pathological study showed no changes in any of the organs studied including their absolute and relative weight (Figs. 7a and 7b). Therefore, the experiment showed that compound **7** is well tolerated by the Swiss albino mice up to the dose level of 1000 mg/kg body weight as a single acute

oral dose except significant decrease in ALKP activities in groups treated with compound **7** at 1000 mg/kg. However, sub-acute and or chronic experiment with the test drug needs to be carried out to look for any adverse effect on repeated exposure to compound **7** for its future development [23] Fig. 10.

#### 4. Conclusion

Diosgenin was modified to obtain novel derivatives. The unusual transformation was observed and product has been confirmed. Compound **7** is the most potent derivative of this series which inhibits cell proliferation by arresting the population in  $G_0/G_1$  phase of the cell cycle. The mechanism of antiproliferative action of this molecule is through induction of caspase depended apoptosis pathway. Compound **7** is a non-toxic anticancer furostane derivative of diosgenin. The lead obtained in this study can further be optimized for better activity in future.

#### Acknowledgements

Authors are thankful to the Directors of CSIR-CDRI and CSIR-CIMAP for constant encouragement and support. Spectral data received by spectral The financial support from CSIR is duly acknowledged. TWAS-CSIR fellowship to Mr. A. A. Hamid is duly acknowledged.

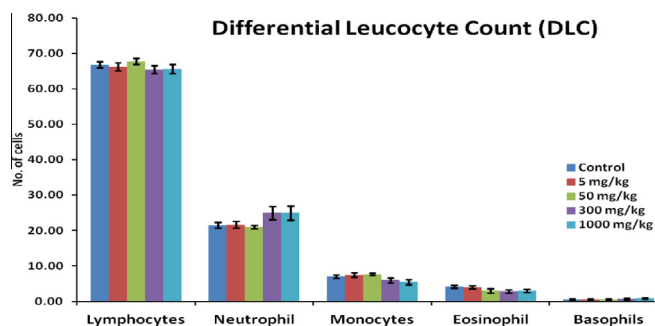


**Fig. 9.** Effect of compound **7** as a single acute oral dose at 5, 50, 300 and 1000 mg/kg body weight on differential leucocytes counts in Swiss albino mice ( $n = 6$ , Non significant changes were found compared to control).

## Appendix A. Supplementary material

Supplementary data associated with this article can be found, in the online version, at <http://dx.doi.org/10.1016/j.steroids.2014.05.025>.

## References

- [1] Cancer Fact sheet N°297 reviewed February 2014.
- [2] Gupta A, Kumar BS, Negi AS. Current status on development of steroids as anticancer agents. *J Steroid Biochem Mol Biol* 2013; 137:242–70 and reference no. 90, 91, 137 and 149 cited therein.
- [3] Kang YJ, Chung HJ, Nam JW, Park HJ, Seo EK, Kim YS, Lee D, Lee SK. Cytotoxic and antineoplastic activity of timosaponin A-III for human colon cancer cells. *J Nat Products* 2011;74:701–6.
- [4] (a) Raju J, Bird RP. Diosgenin, a naturally occurring furostanol saponin suppresses 3-hydroxy-3-methylglutaryl CoA reductase expression and induces apoptosis in HCT-116 human colon carcinoma cells. *Cancer Lett* 2007;255:194–204; (b) Lepage C, Leger DY, Bertrand J, Martin F, Beneytout JL, Liagre B. Diosgenin induces death receptor-5 through activation of p38 pathway and promotes TRAIL-induced apoptosis in colon cancer cells. *Cancer Lett* 2011;301:193–202; (c) Liu MJ, Wang Z, Ju Y, Wong RNS, Wu Qy. Diosgenin induces cell cycle arrest and apoptosis in human leukemia K562 cells with the disruption of Ca<sup>2+</sup> homeostasis. *Cancer Chemother Pharmacol* 2005;55:79–90.
- [5] Nomenclature of Steroids. IUPAC and International Union of Biochemistry-Joint commission on Biochemical Nomenclature, Pure and Applied Chem 1989; 61(10): 1783–822.
- [6] (a) Chaosuancharoen N, Kongkathip N, Kongkathip B. Novel synthetic approach from diosgenin to a 17 $\alpha$ -hydroxy orthoester via a region- and stereo specific rearrangement of an epoxy ester. *Synth Commun* 2004;34:961–83; (b) Rosado-Abon A, Esturau-Escofet N, Flores-A'lamo M, Moreno-Esparza R, Iglesias-Arteaga MA. The crystal structure of diosgenin acetate and its 23-oxygenated derivatives. *J Chem Crystallogr* 2013;43:187–96.
- [7] (a) Sheldrick GM. SHELXS-97. Göttingen, Germany: A program for automatic solution of crystal structures; University of Göttingen; 1997; (b) Sheldrick GM. SHELXL-97. Göttingen, Germany: A program for crystal structure refinement; University of Göttingen; 1997.
- [8] Adaramoye OA, Sarkar J, Singh N, et al. Antiproliferative action of Xylopiya aethiopia fruit extract on human cervical cancer cells. *Phytother Res* 2011;25:1558–63.
- [9] Sarkar J, Singh N, Meena S, Sinha S. Staurosporine induces apoptosis in human papillomavirus positive oral cancer cells at G<sub>2</sub>/M phase by disrupting mitochondrial membrane potential and modulation of cell cytoskeleton. *Oral Oncol* 2009;45:974–9.
- [10] Shiozaki EN, Chai J, Rigotti DJ, Riedl SJ, Li P, Srinivasula SM, Alnemri ES, Fairman R, Shi Y. Mechanism of XIAP-mediated inhibition of caspase-9. *Mol Cell* 2003;11:519–27.
- [11] Wang Z, Watt W, Brooks NA, Harris MS, Urban J, Boatman D, McMillan M, Kahn M, Heinrikson RL, Finzel BC, Wittwer AJ, Blinn J, Kamtekar S, Tomasselli AG. Kinetic and structural characterization of caspase-3 and caspase-8 inhibition by a novel class of irreversible inhibitors. *Biochim Biophys Acta* 2010;1804:1817–31.
- [12] Trott O, Olson AJ. AutoDock Vina: improving the speed and accuracy of docking with a new scoring function, efficient optimization and multithreading. *J Computational Chemistry* 2010;31:455–61.
- [13] Allan JJ, Damodaran A, Deshmukh NS, Goudar KS, Amit A. Safety evaluation of a standardized phytochemical composition extracted from *Bacopa monnieri* in Sprague-Dawley rats. *Food Chemical Toxicol* 2007;45:1928–37.
- [14] Chanda D, Shanker K, Pal A, Luqman S, Bawankule DU, Mani DN, Darokar MP. Safety evaluation of Trikatu, a generic Ayurvedic medicine in Charles Foster rat. *J Toxicol Sci* 2008;34:99–108.
- [15] Furniss BS, Hannaford AJ, Smith PWG, Tatchell AR. Vogel's textbook of practical organic chemistry, fifth ed. England, UK: Addison Wesley Longman Limited, Essex CM20 2JE; 1989.
- [16] Hartwell LH, Weinert TA. Checkpoints: controls that ensure the order of cell cycle events. *Science* 1989;246:629–34.
- [17] (a) Li N, Zhang L, Zeng KW, Zhou Y, Zhang JY, Che YY, Tu PF. Cytotoxic steroidal saponin from *Ophiopogon japonicus*. *Steroids* 2013;78:1–7; (b) Wei G, Wang J, Du Y. Total synthesis of solamargine. *Bioorg Med Chem Lett* 2011;21:2930–3; (c) Huang B, Du D, Zhang R, Wu X, Xing Z, He Y, Huang W. Synthesis, characterisation and biological studies of diosgenyl analogues. *Bioorg Med Chem Lett* 2012;22:7330–4; (d) Perez-Diaz JOH, Rarova L, Ocampo JPM, Magaria-Vergara NE, Farfan N, Strnad M, Santillan R. Synthesis and biological activity of 23-ethylidene-26-hydroxy-22-oxocholestane derivatives from spirostane saponins. *Er J Med Chem* 2012;51:67–78; (e) Fernandez-Herrera MA, Lopez-Munoz H, Hernandez-Vazquez JMV, Sanchez-Sanchez L, Escobar-Sanchez ML, Pinto BM, Sandoval-Ramirez J. Synthesis and selective anticancer activity of steroidal glycoconjugates. *Eur J Med Chem* 2012;54:721–7(f) (a) Li N, Zhang L, Zeng KW, Zhou Y, Zhang JY, Che YY, Tu PF. Cytotoxic steroidal saponin from *Ophiopogon japonicus*. *Steroids* 2013; 78: 1–7; (b) Wei G, Wang J, Du Y. Total synthesis of solamargine. *Bioorg Med Chem Lett* 2011; 21: 2930–2933; (c) Huang B, Du D, Zhang R, Wu X, Xing Z, He Y, Huang W. Synthesis, characterisation and biological studies of diosgenyl analogues. *Bioorg Med Chem Lett* 2012; 22: 7330–7334; (d) Perez-Diaz JOH, Rarova L, Ocampo JPM, Magaria-Vergara NE, Farfan N, Strnad M, Santillan R. Synthesis and biological activity of 23-ethylidene-26-hydroxy-22-oxocholestane derivatives from spirostane saponins. *Er J Med Chem* 2012; 51: 67–78; (e) Fernandez-Herrera MA, Lopez-Munoz H, Hernandez-Vazquez JMV, Sanchez-Sanchez L, Escobar-Sanchez ML, Pinto BM, Sandoval-Ramirez J. Synthesis and selective anticancer activity of steroidal glycoconjugates. *Eur J Med Chem* 2012; 54:721–727; (f) Fernandez-Herrera MA, Sandoval-Ramirez J, Lopez-Munoz H, Sanchez-Sanchez L. Formation of the steroidal 3 $\beta$ -hydroxy-6-oxo-moiety. Synthesis and cytotoxicity on glucoaxogenin. *ARKIVOC* 2009; (xiii): 170–184.
- [18] (a) Tong QY, He Y, Zhao QB, Qing Y, Huang W, Wu XH. Cytotoxicity and apoptosis inducing effect of steroidal saponins from *Dioscorea zingiberensis* Wright against cancer cells. *Steroids* 2012;77:1219–27; (b) Fernandez-Herrera MA, Lopez-Munoz H, Hernandez-Vazquez JMV, Lopez-Davila M, Escobar-Sanchez ML, Sanchez-Sanchez L, Pinto BM, Sandoval-Ramirez J. Synthesis of 26-hydroxy-22-oxocholestanic frameworks from diosgenin and hogenin and their in vitro antiproliferative and apoptotic activity on human cervical cancer CaSki cells. *Bioorg Med Chem* 2010;18:2474–84; (c) Fernandez-Herrera MA, Mohan S, Lopez-Munoz H, Hernandez-Vazquez JMV, Perez-Cervantes E, Escobar-Sanchez ML, Sanchez-Sanchez L, Regla I, Pinto BM, Sandoval-Ramirez J. Synthesis of the steroidal glycoside (25R)-3 $\beta$ ,16 $\beta$ -diacetoxy-12, 22-dioxo-5 $\alpha$ -cholestan-26-yl  $\beta$ -D-glucopyranoside and its anticancer properties on cervicouterine HeLa, CaSki, and ViBo cells. *Eur J Med Chem* 2010;45:4827–37; (d) Fernandez-Herrera MA, Lopez-Munoz H, Hernandez-Vazquez JMV, Lopez-Davila M, Mohan S, Escobar-Sanchez ML, Sanchez-Sanchez L, Pinto BM, Sandoval-Ramirez J. Synthesis and biological evaluation of the glycoside (25R)-3 $\beta$ ,16 $\beta$ -diacetoxy-22-oxocholest-5-en-26-yl  $\beta$ -D-glucopyranoside: a selective anticancer agent in cervicouterine cell lines. *Eur J Med Chem* 2011;46:3877–86; (e) Fernandez-Herrera MA, Sandoval-Ramirez J, Sanchez-Sanchez L, Lopez-Munoz H, Escobar-Sanchez ML. Probing the selective antitumor activity of 22-oxo-26-selenocyancholestan derivatives. *Eur J Med Chem* 2014;74:451–60.
- [19] Porter AG, Jänicke RU. Emerging roles of caspase-3 in apoptosis. *Cell Death Differ* 1999;6:99–104.
- [20] Satoh MS, Lindahl T. Role of poly(ADP-ribose) formation in DNA repair. *Nature* 1992;356:356–8.
- [21] Tewari M, Quan LT, O'Rourke K, Desnoyers S, Zheng Z, Beidler DR, Poiries GG, Salvesen G, Dixit VM. Yama/CPP32 beta, a mammalian homolog of CED-3, is a CrmA-inhibitable protease that cleaves the death substrate poly(ADP-ribose) polymerase. *Cell* 1995;81:801–9.
- [22] Germain M, Affar EB, D'Amours D, Dixit VM, Salvesen GS, Poirier GG. Cleavage of automodified poly(ADP-ribose) polymerase during apoptosis. Evidence for involvement of caspase-7. *J Biol Chem* 1999;274:28379–84.
- [23] Ghosh MN. In: *Fundamentals of Experimental Pharmacology*, 1st ed., Scientific Book Agency, Kolkata; 1984. p. 156.



## Synthesis of diosgenin analogues as potential anti-inflammatory agents



Monika Singh<sup>a,1</sup>, A.A. Hamid<sup>b,d,1</sup>, Anil K. Maurya<sup>a</sup>, Om Prakash<sup>c</sup>, Feroz Khan<sup>c</sup>, Anant Kumar<sup>a</sup>, O.O. Aiyelaagbe<sup>e</sup>, Arvind S. Negi<sup>b,\*\*</sup>, Dnyaneshwar U. Bawankule<sup>a,\*</sup>

<sup>a</sup> Molecular Bioprospection Department, CSIR-Central Institute of Medicinal and Aromatic Plants, Lucknow 226015, India

<sup>b</sup> Medicinal Chemistry Department, CSIR-Central Institute of Medicinal and Aromatic Plants, Lucknow 226015, India

<sup>c</sup> Molecular and Structural Biology Department, CSIR-Central Institute of Medicinal and Aromatic Plants, Lucknow 226015, India

<sup>d</sup> Department of Chemistry, University of Ilorin, Ilorin, Nigeria

<sup>e</sup> Organic Chemistry Unit, Department of Chemistry, University of Ibadan, Ibadan, Nigeria

### ARTICLE INFO

#### Article history:

Received 29 December 2013

Received in revised form 2 April 2014

Accepted 5 April 2014

Available online 9 May 2014

#### Keywords:

Diosgenin

Inflammation

Macrophage

Lipopolysaccharide

Sepsis

Docking

Mice

### ABSTRACT

We herein report the synthesis of diosgenin analogues from commercially available diosgenin as the starting material. The structures of newly synthesised compounds were confirmed by <sup>1</sup>H NMR, <sup>13</sup>C NMR and mass spectrometry. All analogues were evaluated for *in-vitro* anti-inflammatory profile against LPS-induced inflammation in primary peritoneal macrophages isolated from mice by quantification of pro-inflammatory (TNF- $\alpha$ , IL-6 and IL-1 $\beta$ ) cytokines in cell culture supernatant using the ELISA technique followed by *in-vitro* cytotoxicity study. Among the synthesised analogues, analogue **15** [(E) 26-(3',4',5'-trimethoxybenzylidene)-furost-5en-3 $\beta$ -acetate] showed significant anti-inflammatory activity by inhibiting LPS-induced pro-inflammatory cytokines in a dose-dependent manner without any cytotoxicity. Efficacy and safety of analogue **15** were further validated in an *in-vivo* system using LPS-induced sepsis model and acute oral toxicity in mice. Oral administration of analogue **15** inhibited the pro-inflammatory cytokines in serum, attenuated the liver and lung injury and reduced the mortality rate in sepsis mice. Acute oral toxicity study showed that analogue **15** is non-toxic at higher dose in BALB/c mice. Molecular docking study revealed the strong binding affinity of diosgenin analogues to the active site of the pro-inflammatory proteins. These findings suggested that analogue **15** may be a useful therapeutic candidate for the treatment of inflammatory diseases.

© 2014 Elsevier Ltd. All rights reserved.

### 1. Introduction

Inflammation is a complex and an important host defence mechanism in response to different stimuli, such as pathogens, physical injury and chemical injury. At a damaged site, inflammation is initiated by migration of immune cells from blood vessels and release of mediators, followed by recruitment of inflammatory cells and release of reactive oxygen species, reactive nitrogen species and pro-inflammatory cytokines to eliminate foreign pathogens, resolving infection and repairing injured tissues [1]. In general, normal inflammation is rapid and self-limiting, but aberrant resolution and prolonged release of inflammatory mediators lead to chronic

inflammation. Inflammation is linked to a wide range of progressive diseases, including sepsis, auto-immune disorders, neurological diseases, metabolic disorder and cardiovascular disease [2,3] which impose severe social and financial burdens including poor quality of life, high health-care costs and substantial loss of productivity. Sepsis, a life-threatening disease with a high mortality rate, is accompanied by systemic inflammation with excessive production of pro-inflammatory cytokines including tumour necrosis factor- $\alpha$  (TNF- $\alpha$ ) and interleukin-1 $\beta$  (IL-1 $\beta$ ) [4]. Lipopolysaccharide (LPS), an endotoxin and the outer membrane component of Gram-negative bacteria, is a major pathogenic factor in sepsis [5]. LPS has been established for inflammatory research because LPS induces systemic inflammation mimicking the initial clinical features of sepsis [6].

Steroids are very important class of anti-inflammatory agents (SAIA). They suppress immune response through inhibition of NF- $\kappa$ B and by suppression of pro-inflammatory cytokines. They also inhibit production of prostaglandins and leukotrienes. Some of the notable steroidal anti-inflammatory drugs are dexamethasone,

\* Corresponding author. Tel.: +915222718646.

\*\* Corresponding author.

E-mail addresses: [as.negi@cimap.res.in](mailto:as.negi@cimap.res.in) (A.S. Negi), [du.bawankule@cimap.res.in](mailto:du.bawankule@cimap.res.in), [bawankuledu@gmail.com](mailto:bawankuledu@gmail.com) (D.U. Bawankule).

<sup>1</sup> Equal contribution.

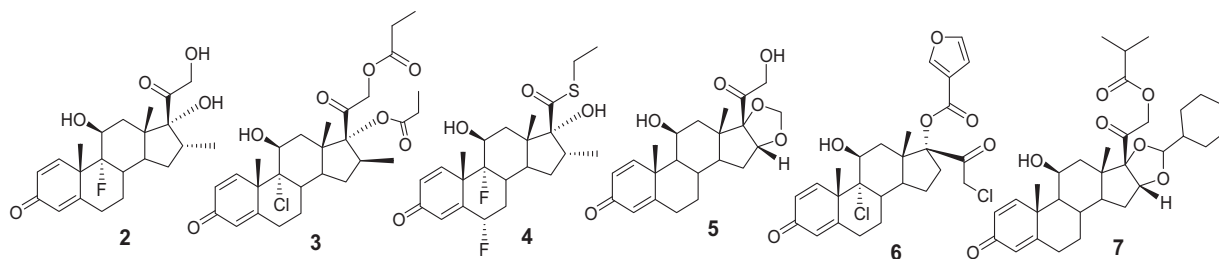


**Fig. 1.** Structures of standard anti-inflammatory steroid drugs; dexamethasone (2), beclomethasone dipropionate (3), fluticasone (4), budesonide (5), mometasone (6) and ciclesonide (7).

beclomethasone dipropionate, fluticasone, budesonide, mometasone, ciclesonide, etc. (Fig. 1). These are used for the management of various human disease conditions linked with inflammation [7].

The majority of natural molecules and their analogues showed potent anti-inflammatory activities and some established themselves as clinical agents for chronic inflammatory disease conditions. Therefore, plant-based natural compounds play a significant role in the development of anti-inflammatory drugs in the pharmaceutical industry which can serve as a good source of lead molecules suitable for further modification during the drug development process.

Diosgenin is a C27 spiroketal steroidal sapogenin abundantly available in nature. It is mainly present in the form of saponin in the plants including *Trigonella*, *Dioscorea* [8], *Costus* [9] and *Smilax* species [10]. In traditional medicine, it is used as an anti-hypercholesterolemia, antihypertriglycerolemia, antidiabetes and antihyperglycemia agent [11]. Several pharmacological reports reveal that diosgenin improves vascular function by increasing aortic eNOS expression in chronic renal failure model in rat [12], inhibits proliferation and induces apoptosis in a wide variety of cancer cell lines [13,14]. The antiproliferative and apoptotic properties are due to its ability to arrest the cell cycle, activate p53, release apoptosis-inducing factor, modulate caspase-3 activity [15] and due to inhibition of the ERK, JNK and phosphoinositide 3-kinase signalling pathways and nuclear factor kappa B activity (NF- $\kappa$ B) [16]. The NF- $\kappa$ B family of transcription factors has been increasingly recognised as a crucial player in many steps of cancer and inflammation [17]. Recently, it has been reported that diosgenin exhibits anti-inflammatory activity due to down-regulation of ICAM-1 expression through NF $\kappa$ B pathway [18]. In the present study, we have synthesised several analogues of diosgenin by modifying at spiroketal ring (Fig. 2) to examine its influences on inflammatory response; we validated the hypothesis using *in-vitro* and *in-vivo* bioassay techniques and it was further confirmed using *in-silico* study.

## 2. Materials and methods

### 2.1. General procedures

The starting substrate diosgenin (purity ~93%) was procured from Sigma Chemicals, USA. All the dry solvents were prepared as

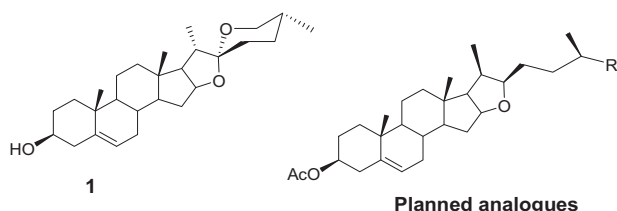


**Fig. 2.** Structures of diosgenin (1) and planned analogues.

per standard methods. Reagents were used as such without any further purification. Reactions were monitored in Merck aluminium sheet silica gel thin layer plates (TLC, 60F<sub>254</sub>), visualised in UV-cabinet ( $\lambda_{\text{max}} = 254$  and 365 nm) and further charred with 2% ceric sulphate in 10% aqueous sulphuric acid with subsequent heating at 80–100 °C. Melting points were determined in open capillaries in E-Z Melt melting point apparatus, Stanford Research System, USA. Solvents were evaporated under reduced pressure at 50 °C in Buchi Rotavapor. Compounds were purified through column chromatography over silica gel (Avra Chemicals, India, 100–200 mesh). NMR experiments were performed on Bruker Avance DRX 300 MHz spectrometer using tetramethylsilane (TMS,  $\delta$  scale, 0.00 ppm) as internal standard. Splitting of peaks are abbreviated as s for singlet, d for doublet, t for triplet, q for quartet, bs for broad singlet and m for multiplet. <sup>1</sup>H and <sup>13</sup>C spectra are reported. Electrospray mass analysis was done on API 3000 Triple Quad LC–MS–MS (Applied Biosystem, USA) mass spectrometer after dissolving samples in methanol or acetonitrile. Nomenclature of diosgenin analogues has been done as per recommendations published by the Joint Commission on the Biochemical Nomenclature (JCBN) of IUPAC [19].

### 2.2. Chemical synthesis

#### 2.2.1. Synthesis of analogues 8 and 17

Acetylation was done as per reported method [20]. Substrate was taken in dry chloroform and pyridine at room temperature and acetic anhydride was added to it. Usual work-up was done after pouring into water.

**Analogue 8** (*3 $\beta$ -Hydroxy-(25R)-Spirost-5-en-3 $\beta$ -acetate*): Yield = 91%, mp = 193–196 °C; <sup>1</sup>H NMR (CDCl<sub>3</sub>),  $\delta$  0.77 (s, 3H, 18-CH<sub>3</sub>), 0.96 (d, 3H, 27-CH<sub>3</sub>), 1.02 (s, 3H, 19-CH<sub>3</sub>), 1.11–2.31 (m, 25H, rest of the 1 $\times$ CH<sub>3</sub>, 8 $\times$ CH<sub>2</sub> and 6 $\times$ CH of steroidal ring), 2.01 (s, 3H, CH<sub>3</sub>COO, acetate), 2.24–2.31 (bd, 2H, 7-CH<sub>2</sub>), 3.38 (m, 2H, 26-CH<sub>2</sub>), 4.37 (bs, 1H, 3-CH), 4.42 (bd, 1H, 16-CH), 5.36 (s, 1H, 6-CH). <sup>13</sup>C NMR (CDCl<sub>3</sub>, 75 MHz);  $\delta$  14.89, 16.64, 17.51, 19.69, 21.20, 21.74, 28.12, 29.19, 30.66, 31.78, 31.80, 32.21, 32.41, 37.10, 37.34, 38.47, 40.10, 40.63, 42.00, 42.68, 50.35, 56.82, 62.52, 67.19, 74.26, 81.16, 109.60, 122.72, 140.05, 170.82; ESI mass (MeOH): 457.3 [M+H]<sup>+</sup>, 479.3 [M+Na]<sup>+</sup>, 495.4 [M+K]<sup>+</sup>.

**Analogue 17** (*Furost-5-en-3 $\beta$ , 26N-diacetoxy-26-aldoxime*): Yield = 92%, mp = 90–93 °C, <sup>1</sup>H NMR (CDCl<sub>3</sub>):  $\delta$  0.79 (s, 3H, 18-CH<sub>3</sub>), 0.99 (s, 3H, 19-CH<sub>3</sub>), 1.02–1.97 (m, 29H, rest of the 2 $\times$ CH<sub>3</sub>, 8 $\times$ CH<sub>2</sub> and 7 $\times$ CH of steroidal ring), 2.02 (s, 6H, 2 $\times$ CH<sub>3</sub>COO, 3 and 26-oxime acetates), 2.30 (bd, 2H, 7-CH<sub>2</sub>, *J* = 6.9 Hz), 3.29 (bs, 1H, 22-CH), 4.29 (bs, 1H, 3-CH), 4.60 (bd, 1H, 16-CH), 5.36 (s, 1H, 6-CH), 7.50–7.53 (d, 1H, 26-CH, *J* = 8.1 Hz); <sup>13</sup>C NMR (CDCl<sub>3</sub>, 75 MHz):  $\delta$  16.81, 19.20, 19.72, 19.91, 21.03, 21.81, 26.33, 28.14, 30.08, 31.52, 31.96, 32.38, 32.59, 37.11, 37.39, 38.06, 38.28, 38.49, 39.77, 41.09, 50.40, 57.29, 65.32, 74.29, 83.83, 90.14, 122.74, 140.12, 163.46, 169.16, 170.95; ESI mass (MeOH): 551 [M+K–1]<sup>+</sup>.

### 2.2.2. Synthesis of (25R) furost-5-en-, 3 $\beta$ -acetoxy, 26-ol (**9**)

Diosgenin 3-acetate (200 mg, 0.44 mmol) was stirred in a 5 mL acetic acid. To this solution, sodium cyanoborohydride (200 mg, 3.17 mmol) was added in portions over a period of 30 min. After 2 h, when the reaction was complete, the reaction mixture was poured in ice-cool water, extracted with ethyl acetate (3  $\times$  30 mL), washed with water and dried over anhydrous sodium sulphate. The organic layer was dried *in-vacuo* to get a crude mass, which was purified through column chromatography over silica gel using hexane-ethyl acetate as eluants. The desired alcohol **9** was obtained at 10–12% ethyl acetate–hexane as white crystalline solid.

Analogue **9**: Yield = 81%, mp = 121–122 °C;  $^1\text{H NMR}$  ( $\text{CDCl}_3$ ):  $\delta$  0.83 (s, 3H, 18- $\text{CH}_3$ ), 0.94 (s, 3H, 19- $\text{CH}_3$ ), 1.03–1.90 (m, 28H, rest of the 2 $\times$  $\text{CH}_3$ , 8 $\times$  $\text{CH}_2$  and 6 $\times$  $\text{CH}$  of steroidal ring), 2.05 (s, 3H,  $\text{CH}_3\text{COO}$ , acetate), 2.35 (bd, 2H, 7- $\text{CH}_2$ ), 3.36 (bs, 1H, 22-CH), 3.48 (m, 2H, 27- $\text{CH}_2\text{OH}$ ), 4.34 (bs, 1H, 3-CH), 4.63 (bs, 1H, 16-CH), 5.40 (s, 1H, 6-CH).  $^{13}\text{C NMR}$  ( $\text{CDCl}_3$ , 75 MHz):  $\delta$  16.80, 17.00, 19.30, 19.69, 21.03, 21.77, 28.13, 30.46, 30.82, 31.94, 32.36, 32.59, 36.08, 37.07, 37.37, 38.28, 38.46, 39.78, 41.07, 50.39, 57.28, 65.48, 68.27, 74.28, 83.57, 90.71, 122.74, 140.04, 170.91; ESI mass (MeOH): 459.4 [M+H] $^+$ , 481.3 [M+Na] $^+$ , 497.4 [M+K] $^+$ .

### 2.2.3. Synthesis of furost-5-en-3 $\beta$ -acetoxy 26-al (**10**)

Alcohol **9** (200 mg, 0.43 mmol) was taken in 10 mL methylene chloride. To this stirred solution, pyridinium chlorochromate (PCC, 200 mg, 0.93 mmol) was added and further stirred for an hour. On completion, solvent was evaporated and residue was dissolved in ethyl acetate. It was acidified with dil. HCl and washed with water. The organic layer was dried over anhydrous sodium sulphate and dried *in-vacuo*. The residue thus obtained was recrystallised with chloroform–hexane (1:3) to get aldehyde **10** as brown coloured solid.

Analogue **10**: Yield = 91%, mp = 119–123 °C;  $^1\text{H NMR}$  ( $\text{CDCl}_3$ ):  $\delta$  0.80 (s, 3H, 18- $\text{CH}_3$ ), 0.93 (s, 3H, 19- $\text{CH}_3$ ), 1.16–1.97 (m, 28H, rest of the 2 $\times$  $\text{CH}_3$ , 8 $\times$  $\text{CH}_2$  and 6 $\times$  $\text{CH}$  of steroidal ring), 2.16 (s, 3H,  $\text{CH}_3\text{COO}$ , Acetate), 2.46 (bd, 2H, 7- $\text{CH}_2$ ), 3.45 (bs, 1H, 22-CH), 4.44 (bs, 1H, 3-CH), 4.73 (bd, 1H, 16-CH), 5.50 (s, 1H, 6-CH), 9.75 (s, 1H, 26-CHO).  $^{13}\text{C NMR}$  ( $\text{CDCl}_3$ , 75 MHz):  $\delta$  13.78, 16.79, 19.22, 19.71, 21.03, 21.77, 28.15, 30.07, 31.11, 31.96, 32.37, 32.59, 37.09, 37.39, 38.26, 38.48, 39.77, 41.08, 46.72, 50.41, 57.29, 65.44, 74.28, 83.28, 90.11, 122.73, 140.09, 170.91, 205.54; ESI mass (MeOH): 457.3 [M+H] $^+$ , 479.3 [M+Na] $^+$ , 495.4 [M+K] $^+$ ; ESI-HRMS: 457.33181 (calculated), and 457.3311 (observed) for  $\text{C}_{29}\text{H}_{45}\text{O}_4$ .

### 2.2.4. Synthesis of 27-nor- furost-5-en- 3 $\beta$ -acetoxy-25-one (**11**)

Aldehyde **10** (200 mg, 0.44 mmol) was taken in 10 mL ethanol. To this stirred solution, 3,4,5-trimethoxyaniline (200 mg, 1.09 mmol) was added and further stirred for 2 h at room temperature. The solvent was evaporated and the residue was dissolved in ethyl acetate and washed with water. The organic phase was dried over anhydrous sodium sulphate and dried *in-vacuo* to get a residue. It was purified through silica gel column eluting with ethyl acetate:hexane. The desired ketone **11** was obtained at 8–10% ethyl acetate–hexane as creamish white solid.

Analogue **11**: Yield = 84%, mp = 138–140 °C;  $^1\text{H NMR}$  ( $\text{CDCl}_3$ ):  $\delta$  0.79 (s, 3H, 18- $\text{CH}_3$ ), 0.98 (s, 3H, 19- $\text{CH}_3$ ), 1.02–1.87 (m, 23H, rest of the 1 $\times$  $\text{CH}_3$ , 8 $\times$  $\text{CH}_2$  and 4 $\times$  $\text{CH}$  of steroidal ring), 1.95 (s, 3H,  $\text{CH}_3\text{COO}$ , acetate), 2.13 (s, 3H, 26- $\text{CH}_3\text{CO}$ ), 2.32 (d, 1H, 7- $\text{CH}_2$ ,  $J=6.3$  Hz) 2.51–2.63 (bd, 2H, 24- $\text{CH}_2$ ), 3.26–3.29 (bs, 1H, 22-CH), 4.24–4.29 (bs, 1H, 16-CH), 4.47 (bd, 1H, 3-CH), 5.35 (s, 1H, 6-CH).  $^{13}\text{C NMR}$  ( $\text{CDCl}_3$ , 75 MHz):  $\delta$  16.80, 19.01, 19.71, 21.02, 21.80, 27.44, 28.13, 30.33, 31.95, 32.37, 32.55, 37.10, 37.38, 38.24, 38.48, 39.75, 41.09, 41.28, 50.38, 57.27, 65.39, 74.28, 83.69, 89.53, 122.72, 140.12, 170.95, 209.24; ESI mass (MeOH): 443.3 [M+H] $^+$ , 465.4 [M+Na] $^+$ ,

481.3 [M+K] $^+$ ; ESI-HRMS: 443.31616 (calculated) and 443.3139 (observed) for  $\text{C}_{28}\text{H}_{43}\text{O}_4$ .

### 2.2.5. Synthesis of Wittig products **12–15**

2.2.5.1. Synthesis of (22 $\beta$ )-(E)-26-benzylidene-3 $\beta$ -yl-furost-5-en-3-acetate (**12**). Sodium hydride (200 mg, 8.3 mmol) was washed with dry hexane and taken in 10 mL dry toluene. To this Wittig salt (150 mg, 0.34 mmol) was added and refluxed for 20 min. To this aldehyde **10** (100 mg, 0.22 mmol) was added and further refluxed for 4 h. Toluene was evaporated under vacuum and residue was taken in ethyl acetate, washed with water and dried over anhydrous sodium sulphate. The organic layer was dried *in-vacuo* to get a crude mass, which was purified through silica gel column eluting with ethyl acetate–hexane. The desired product was obtained as yellowish viscous liquid.

Analogue **12**: Yield = 68%, oil;  $^1\text{H NMR}$  ( $\text{CDCl}_3$ ):  $\delta$  0.73 (s, 3H, 18- $\text{CH}_3$ ), 0.95 (s, 3H, 19- $\text{CH}_3$ ), 1.02–1.95 (m, 26H, rest of the 2 $\times$  $\text{CH}_3$ , 7 $\times$  $\text{CH}_2$  and 6 $\times$  $\text{CH}$  of steroidal ring), 1.99 (s, 3H,  $\text{CH}_3\text{COO}$ , acetate), 2.23 (d, 2H, 4- $\text{CH}_2$   $J=5.4$  Hz), 2.30 (bd, 2H, 7- $\text{CH}_2$ ), 3.23 (bd, 1H, 22-CH), 4.22 (bs, 1H, 16-CH), 4.51 (bs, 1H, 3-CH), 5.28 (s, 1H, 6-CH), 5.96 (dd, 1H, 26-CH,  $J=15.6$  Hz and 7.8 Hz), 6.26 (d, 1H, 28-CH,  $J=15.6$  Hz), 7.12 (m, 5H, aromatic protons of phenyl ring).  $^{13}\text{C NMR}$  ( $\text{CDCl}_3$ , 75 MHz):  $\delta$  16.83, 19.39, 19.72, 21.06, 21.79, 28.16, 30.06, 31.85, 31.99, 32.40, 32.66, 34.48, 37.12, 37.41, 38.04, 38.31, 38.51, 39.82, 41.10, 50.44, 57.31, 65.60, 74.33, 83.58, 90.82, 122.77, 126.39, 127.15, 128.73, 128.83, 137.05, 138.33, 140.09, 170.97; ESI mass (MeOH): 531.5 [M+H] $^+$ , 553.5 [M+K] $^+$ , 569.6 [M+K] $^+$ .

Analogue **13** (z) 26-(4'-nitrobenzylidene)-furost-5-en-3 $\beta$ -acetate: Yield = 62%, oil;  $^1\text{H NMR}$  ( $\text{CDCl}_3$ ):  $\delta$  0.71 (s, 3H, 18- $\text{CH}_3$ ), 0.96 (s, 3H, 19- $\text{CH}_3$ ), 1.05–1.88 (m, 26H, rest of the 2 $\times$  $\text{CH}_3$ , 7 $\times$  $\text{CH}_2$  and 6 $\times$  $\text{CH}$  of steroidal ring), 2.02 (s, 3H,  $\text{CH}_3\text{COO}$ , acetate), 2.21 (bs, 2H, 4- $\text{CH}_2$ ), 2.30 (bd, 2H, 7- $\text{CH}_2$ ), 3.20 (bd, 1H, 22-CH), 4.20 (bs, 1H, 16-CH), 4.50 (bs, 1H, 3-CH), 5.26 (bs, 1H, 6-CH), 6.29 (m, 1H, 26-CH), 6.79 (d, 1H, 28-CH,  $J=9.0$  Hz), 7.33–8.05 (m, 4H, aromatic protons of phenyl ring).  $^{13}\text{C NMR}$  ( $\text{CDCl}_3$ , 75 MHz):  $\delta$  16.80, 19.29, 19.69, 20.62, 21.01, 21.81, 28.11, 29.74, 31.38, 31.95, 32.35, 32.99, 34.01, 37.09, 37.36, 38.22, 38.45, 39.74, 41.10, 50.37, 57.27, 65.40, 74.50, 83.69, 90.54, 122.77, 123.92, 124.33, 126.80, 130.53, 134.03, 140.04, 142.28, 143.26, 162.83, 171.85; ESI mass (MeOH): 576.6 [M+H] $^+$ , 574.6 [M-H] $^+$ , 598.6 [M+Na] $^+$ , 614.5 [M+K] $^+$ .

Analogue **14** (z) 26-(3',4',5'-trimethoxybenzylidene)-furost-5-en-3 $\beta$ -acetate: Yield = 29%, oil;  $^1\text{H NMR}$  ( $\text{CDCl}_3$ ):  $\delta$  0.79 (s, 3H, 18- $\text{CH}_3$ ), 0.95 (s, 3H, 19- $\text{CH}_3$ ), 1.04–1.87 (m, 29H, rest of the 2 $\times$  $\text{CH}_3$ , 8 $\times$  $\text{CH}_2$  and 7 $\times$  $\text{CH}$  of steroidal ring), 2.02 (s, 3H,  $\text{CH}_3\text{COO}$ , acetate), 2.29 (bd, 2H, 7- $\text{CH}_2$ ), 3.85 (s, 9H, 3 $\times$  $\text{OCH}_3$ ), 4.28 (bd, 1H, 22-CH), 4.61 (bs, 1H, 3-CH), 5.39 (t, 1H, 6-CH), 6.28 (d, 1H, 27-CH,  $J=11.4$  Hz), 6.32 (bd, 1H, 26-CH), 6.50 (d, 2H, 2' and 6'-CH of phenyl ring).  $^{13}\text{C NMR}$  ( $\text{CDCl}_3$ , 75 MHz):  $\delta$  16.83, 19.41, 19.71, 21.03, 21.82, 28.14, 30.06, 31.97, 32.37, 32.61, 33.39, 35.13, 37.10, 37.39, 38.29, 38.48, 39.77, 41.06, 50.38, 56.42, 57.28, 61.30, 65.51, 74.30, 83.58, 90.71, 106.17, 122.77, 128.05, 133.94, 139.38, 140.09, 153.27, 170.97; ESI mass (MeOH): 621.5 [M+H] $^+$ , 643.4 [M+K] $^+$ , 659.4 [M+K] $^+$ .

Analogue **15** (E) 26-(3',4',5'-trimethoxybenzylidene)-furost-5-en-3 $\beta$ -acetate: Yield = 52%, oil;  $^1\text{H NMR}$  ( $\text{CDCl}_3$ ):  $\delta$  0.77 (s, 3H, 18- $\text{CH}_3$ ), 0.94 (s, 3H, 19- $\text{CH}_3$ ), 1.04–1.84 (m, 30H, rest of the 2 $\times$  $\text{CH}_3$ , 9 $\times$  $\text{CH}_2$  and 6 $\times$  $\text{CH}$  of steroidal ring), 1.99 (s, 3H,  $\text{CH}_3\text{COO}$ , acetate), 2.29 (bd, 2H, 7- $\text{CH}_2$ ), 3.84 (s, 9H, 3 $\times$  $\text{OCH}_3$ ), 4.10 (bd, 1H, 22-CH,  $J=7.1$  Hz), 4.27 (bs, 1H, 16-CH), 4.54 (bs, 1H, 3-CH), 5.33 (s, 1H, 6-CH), 5.98 (dd, 1H, 26-CH,  $J=15.6$  Hz and 7.8 Hz), 6.22 (d, 1H, 27-CH,  $J=15.9$  Hz), 6.54 (s, 2H, 2' and 6'-CH of phenyl ring).  $^{13}\text{C NMR}$  ( $\text{CDCl}_3$ , 75 MHz):  $\delta$  16.83, 19.41, 19.70, 21.01, 21.77, 28.12, 30.07, 31.81, 31.96, 32.36, 32.65, 34.45, 37.08, 37.37, 37.96, 38.27, 38.47, 39.77, 41.06, 50.37, 56.41, 57.26, 61.26, 65.55, 74.24, 83.55, 90.72, 103.39, 122.74, 128.64, 134.05, 136.50, 137.61, 140.06, 153.63, 170.85; ESI mass (MeOH): 621.5 [M+H] $^+$ , 643.5 [M+Na] $^+$ , 659.4 [M+K] $^+$ .

### 2.2.6. General synthesis of aldoxime **16**

Analogue **16** *Furost-5-en-3 $\beta$ -acetoxy 26-aldoxime*: Yield = 70%, mp = 130–133 °C; <sup>1</sup>H NMR (CDCl<sub>3</sub>):  $\delta$  0.78 (s, 3H, 18-CH<sub>3</sub>), 0.97 (s, 3H, 19-CH<sub>3</sub>), 1.07–1.86 (m, 26H, rest of the 2 $\times$ CH<sub>3</sub>, 8 $\times$ CH<sub>2</sub> and 4 $\times$ CH of steroidal ring), 2.01 (s, 3H, CH<sub>3</sub>COO, acetate), 2.31 (bd, 2H, 7-CH<sub>2</sub>), 3.29 (bs, 1H, 22-CH), 4.29 (bs, 1H, 3-CH), 4.59 (bd, 1H, 16-CH), 5.36 (s, 1H, 6-CH), 7.29 (bd, 1H, 26-CH,  $J$  = 6.3 Hz). <sup>13</sup>C NMR (CDCl<sub>3</sub>, 75 MHz):  $\delta$  16.81, 18.44, 19.26, 19.70, 21.03, 21.78, 28.12, 30.06, 31.32, 31.95, 32.36, 32.56, 35.06, 37.08, 37.38, 38.24, 38.47, 39.78, 41.07, 50.39, 57.28, 65.46, 74.32, 83.62, 90.39, 122.75, 140.06, 156.46, 170.01; ESI mass (MeOH): 472.4 [M + H]<sup>+</sup>, 494.5 [M + Na]<sup>+</sup>, 510.3 [M + K]<sup>+</sup>.

## 2.3. Pharmacology

### 2.3.1. Cell culture

Primary cell culture was carried out as described previously [21]. In brief, the macrophage cells were collected from the peritoneal cavities of mice (8-week-old female Swiss albino mice) after an intra peritoneal injection of 1.0 mL of 1% peptone (BD Biosciences, USA) 3 days before harvesting. Mice were euthanised by cervical dislocation under ether anaesthesia and peritoneal macrophages were obtained by intra-peritoneal injection of phosphate buffer saline (PBS; pH 7.4). Membrane debris was removed by filtering the cell suspensions through sterile gauze. The viability of the cells was determined by trypan blue exclusion and the viable macrophage cells at the concentration of 0.5  $\times$  10<sup>6</sup> live cells/mL were used for the experimentation. Cells were grown in tissue culture plates in DMEM (Dulbecco modified Eagle medium, Sigma) supplemented with 10% foetal bovine serum with 1 $\times$  stabilised antibiotic–antimycotic solution (Sigma) in a CO<sub>2</sub> incubator at 37 °C with 5% CO<sub>2</sub> and 90% relative humidity.

### 2.3.2. Quantification of pro-inflammatory cytokines

Cells were pretreated with 1 and 10  $\mu$ g/mL of diosgenin analogues and standard anti-inflammatory drug dexamethasone (Sigma, USA), respectively, for 30 min. The cells were stimulated with lipopolysaccharide (LPS, *E. coli* 055:B5 Sigma, USA; 1  $\mu$ g/mL). After incubation with LPS for 24 h, supernatants were collected and immediately frozen at –80 °C. Harvested supernatants were tested for quantification of pro-inflammatory cytokines using mouse-specific enzyme immuno assay (EIA) kits (BD Biosciences, USA) following the manufacturer's protocol. Briefly, the ELISA plates were coated (100  $\mu$ L per well) with specific mouse TNF- $\alpha$ , IL-1 $\beta$  and IL-6 capture antibody and incubated overnight at 4 °C. The plate was blocked with 200  $\mu$ L/well assay diluents. Culture supernatant and standard (100  $\mu$ L) were added into the appropriate coated wells and incubated for 2 h at room temperature (20–25 °C). After incubation, the plates were washed thoroughly 5 times with wash buffer. 100  $\mu$ L of detecting solution (detection antibody and streptavidin HRP) was added into each well. The plates were sealed and incubated for 1 h at RT and then washed thoroughly 5 times with wash buffer. 100  $\mu$ L of tetramethylbenzidine (TMB) substrate solution was added to each well and the plate was incubated (without plate sealer) for 30 min at room temperature in the dark. Finally, 50  $\mu$ L of stop solution (2 N H<sub>2</sub>SO<sub>4</sub>) was added to each well. The colour density was measured at 450 and 570 nm using a microplate reader (Spectramax; Molecular Devices, USA). Subtracted absorbance was measured at 570 nm from absorbance 450 nm. The values of TNF- $\alpha$ , IL-1 $\beta$  and IL-6 were expressed as pg/mL. The percentage (%) inhibition of pro-inflammatory cytokine production was calculated as follows: %inhibition =  $100 \times \frac{\text{concentration of vehicle control} - \text{concentration of test treatment}}{\text{OD of concentration of vehicle control}}$  where vehicle control indicates cells treated with vehicle in LPS-induced inflammation.

### 2.3.3. Cytotoxicity evaluation

Effect of diosgenin analogues on cytotoxicity was carried out in peritoneal macrophage cells using 3-(4,5-dimethylthiazol-2-yl)-2,5-diphenyltetrazolium (MTT) assay. Peritoneal macrophage cells (0.5  $\times$  10<sup>6</sup> cells/well) isolated from mice were suspended in DMEM medium (Sigma, USA) containing 10% heat-inactivated foetal bovine serum (Gibco, USA) and incubated in a 96-well culture plate at 37 °C in 5% CO<sub>2</sub> in an incubator and left overnight to attach. Cells were treated (1, 10 and 30  $\mu$ g/mL) and incubated for 24 h at 37 °C in 5% CO<sub>2</sub>. Thereafter, 20  $\mu$ L aliquots of MTT solution (5 mg/mL in PBS) were added to each well and left for 4 h. Then, the MTT-containing medium was carefully removed and the formazan crystals formed were solubilised in DMSO (100  $\mu$ L) for 10 min. The culture plate was placed on a micro-plate reader (Spectramax; Molecular Devices, USA) and the absorbance was measured at 550 nm. The amount of colour produced is directly proportional to the number of viable cells. Cell cytotoxicity was calculated as the percentage of MTT absorption as percentage (%) of survival = (mean experimental absorbance/mean control absorbance  $\times$  100).

### 2.3.4. In-vivo study

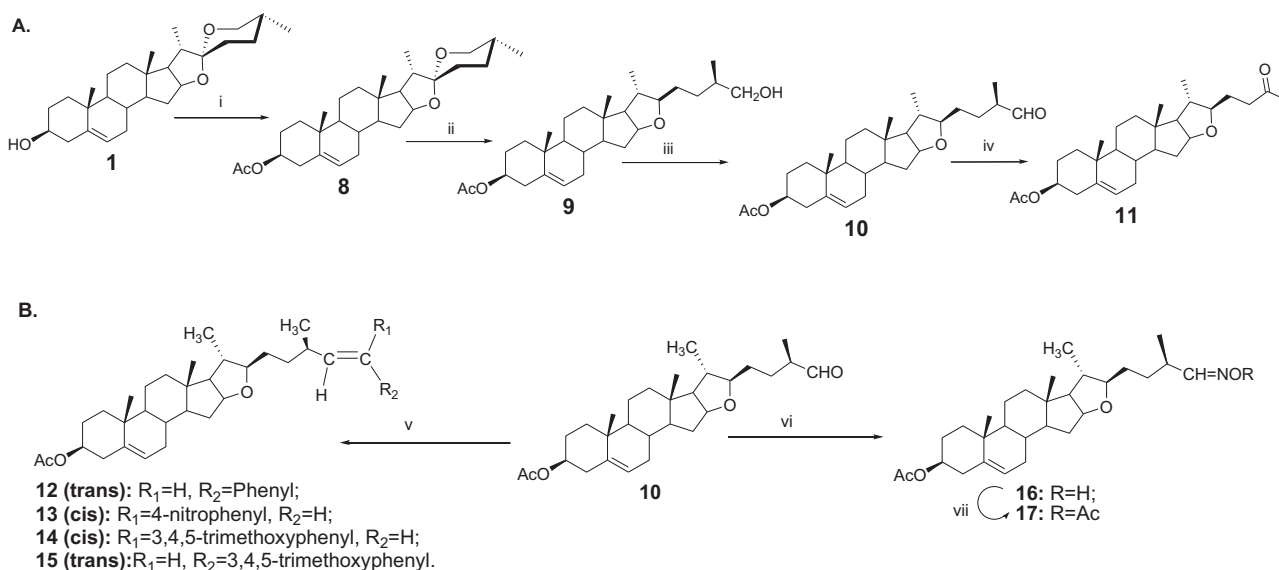
Animal experiments were carried out as per the approved protocol by the Institutional Animal Ethics Committee (IAEC) followed by the Committee for the Purpose of Control and Supervision of Experimental Animals (CPCSEA), Government of India (Registration no.: 400/01/AB/CPCSEA).

**2.3.4.1. LPS-induced sepsis model in mice.** BALB/c mice, 6–8 weeks of age, and weighing 18–22 g, were procured from the institute's animal house and acclimatised to the animal room for a week prior to experiment. The mice were fed with the standard mice feed and *ad libitum* drinking water under standard environmental conditions of 22  $\pm$  3 °C, 12:12 dark-to-light cycle. After 1 week of adaptation, the mice were randomly divided into six groups of six mice each. Sepsis was induced in the experimental mice except normal group of mice by intra-peritoneal (i.p.) injection of LPS (5 mg/kg) in normal saline. Analogue **15** was dissolved in 0.7% carboxymethyl cellulose (CMC) to obtain a uniform suspension and administered orally 24 h and 2 h before LPS injection.

- Group 1: Normal control administered CMC
- Group 2: Vehicle control administered CMC + LPS
- Group 3: Analogue **15** (3 mg/kg) + LPS
- Group 4: Analogue **15** (10 mg/kg) + LPS
- Group 5: Analogue **15** (30 mg/kg) + LPS

Blood was collected 2 h after LPS administration from orbital plexus and serum was separated and stored at –80 °C until analysis. Pro-inflammatory cytokines (IL-1 $\beta$ , IL-6 and TNF- $\alpha$ ) from serum were quantified using commercially available mouse-specific enzyme immune assay kits (BD Biosciences, USA) by following the manufacturer's instruction.

**2.3.4.2. Histopathology examination.** Liver and lung samples were obtained 24 h after LPS challenge. Tissues were collected and fixed in 10% buffered formalin. After fixation, tissues were rinsed with water, dehydrated with graded concentration of ethanol and embedded in paraffin wax. The samples were sectioned into 5  $\mu$ m thick and mounted on glass slides. The sections were then de-waxed using xylene and ethanol, and stained with haematoxylin and eosin (H&E stain). A representative area was selected for qualitative light microscopic analysis under 100 $\times$  magnification.



**Scheme 1.** (i) Ac<sub>2</sub>O, dry pyridine, CHCl<sub>3</sub>, RT, 2 h, 91%; (ii) AcOH, NaCNBH<sub>4</sub>, RT, 3 h, 81%; (iii) dry DCM, PCC, reflux, 1 h, 91%; (iv) ethanol, 3,4,5-trimethoxyaniline, RT, 2 h, 84%; (v) Wittig salt, NaH, toluene, reflux, 3–4 h, 29–68%; (vi) NH<sub>2</sub>OH·HCl, EtOH, reflux, 2 h, 70%; (vii) Ac<sub>2</sub>O, dry pyridine, dry CHCl<sub>3</sub>, RT, 92%.

**2.3.4.3. Survival study.** The second set of experiments was performed to examine the effect of analogue **15** on LPS-induced lethality in mice. The female BALB/c mice were divided into five groups ( $n=6$ ). The treatment group received analogue **15** orally at doses of 3, 10 and 30 mg/kg, 24 and 2 h before injection of LPS, the LPS group received an intraperitoneal injection at a dose of 15 mg/kg, and the control group received the equal amount of vehicle instead of analogue **15**. Survival of mice was monitored every 12 h for 5 days.

### 2.3.5. Acute oral toxicity study

Acute oral toxicity study of the analogue **15** was done on BALB/c male mice as described previously [22]. For this study, mice administered orally with analogue **15** (300 mg/kg body weight) were considered as the test group and mice treated with corresponding volume of vehicle (0.7% carboxymethyl cellulose [CMC]) were considered the control group. Mice were observed individually, after dosing, at least once during the first 30 min, periodically during the first 24 h and daily thereafter for a total of 7 days.

### 2.4. Molecular docking

Two-dimensional molecular structures were drawn with the ChemDraw Ultra and energy minimization was performed with MM2/MM3 molecular mechanics parameter until achieving the lowest stable energy state. This energy minimization process was performed until the energy change was less than 0.001 kcal mol<sup>-1</sup> or the molecules had been updated almost 300 times [23]. The 3D chemical structure of known drug was collected from the PubChem compound database of NCBI, USA (<http://www.pubchem.ncbi.nlm.nih.gov>). Crystallographic 3D structures of target proteins TNF- $\alpha$  (PDB: 2AZ5), IL-6 (PDB: 1ALU) and IL-1 $\beta$  (PDB: 9ILB) were retrieved from the Brookhaven Protein Databank (PDB) (<http://www.pdb.org>). Hydrogen atoms were added to the protein targets to achieve the correct ionisation and tautomeric states of amino acid residues such as His, Asp, Ser and Glu. Molecular docking of the compounds against selected target was achieved using the 'AutoDock Vina' software. To perform the automated docking of ligands into the active sites, we used a Lamarckian genetic algorithm [24].

### 2.5. Statistical analysis

Results were presented as the means  $\pm$  SE and analysed using GraphPad Prism 4. The ANOVA followed by Tukey's multiple comparison test was used to assess the statistical significance of vehicle vs treatment groups. Results are presented as the means  $\pm$  SE. Differences with a  $p$  value < 0.05 were considered significant.

## 3. Results

### 3.1. Chemistry

The synthetic strategy was depicted as Scheme 1. Diosgenin (**1**) was acetylated with acetic anhydride–pyridine system in dry chloroform to get diosgenin 3-acetate (**8**) at room temperature. The spiroketal bond was reduced with sodium cyanoborohydride in acetic acid to get a primary alcohol (**9**). The alcohol **9** was oxidised to its corresponding aldehyde (**10**) by treating it with pyridinium chlorochromate (PCC) in dichloromethane.

Further, while preparing Schiff's bases of aldehyde **10** with an aromatic amine, ketone **11** was obtained unexpectedly. Compound **10** was reacted with an aromatic amine (aniline/3,4-methylenedioxyaniline/3,4,5-trimethoxyaniline) in ethanol and each time it was transformed to ketone **11**. We did not do any mechanistic study to establish this transformation. However, it is assumed that after the formation of a Schiff's base, it was converted to an enamine. Further decomposition of enamine by water might have converted it to ketone **11**. The structure of **11** was established by 1D, 2D NMR, ESI-HRMS and finally by X-ray crystallography.

Diverse analogues were prepared on aldehyde **10**. Three different Wittig salts (benzyltriphenylphosphonium bromide, 4-nitrobenzyltriphenylphosphonium bromide, 3,4,5-trimethoxybenzyltriphenylphosphonium bromide) were treated with sodium hydride–toluene system to get styrene type analogues (**12–15**) at C27 of steroidal framework of aldehyde **10**. Aldoxime (**16**) and oxime-acetate (**17**) were also prepared on **10** by treating with hydroxylamine hydrochloride and then acetylating. All these diosgenin analogues were confirmed through spectroscopy.



**Table 1**  
Effect of diosgenin analogues on production of pro-inflammatory cytokines in LPS-induced inflammation in macrophage cells.

Analogues	Dose ( $\mu\text{g/mL}$ )	Pro-inflammatory cytokine (pg/mL)		
		TNF- $\alpha$	IL-6	IL-1 $\beta$
Normal	–	68.17 $\pm$ 9.67	93.52 $\pm$ 5.14	22.65 $\pm$ 4.09
Vehicle	–	1301.07 $\pm$ 93.68 <sup>#</sup>	912.63 $\pm$ 21.71 <sup>#</sup>	103.08 $\pm$ 8.72 <sup>#</sup>
Diosgenin				
<b>1</b>	1	1138.74 $\pm$ 77.05 <sup>ns</sup>	792.58 $\pm$ 49.25 <sup>ns</sup>	96.50 $\pm$ 3.18 <sup>ns</sup>
	10	1052.72 $\pm$ 93.68 <sup>*</sup>	693.69 $\pm$ 16.10 <sup>*</sup>	81.33 $\pm$ 7.23 <sup>ns</sup>
<b>8</b>	1	1192.86 $\pm$ 79.42 <sup>ns</sup>	777.13 $\pm$ 15.17 <sup>ns</sup>	98.00 $\pm$ 6.18 <sup>ns</sup>
	10	794.84 $\pm$ 13.09 <sup>*</sup>	718.24 $\pm$ 19.70 <sup>*</sup>	87.33 $\pm$ 4.98 <sup>ns</sup>
<b>9</b>	1	1077.04 $\pm$ 66.6 <sup>ns</sup>	841.72 $\pm$ 61.28 <sup>ns</sup>	92.46 $\pm$ 7.47 <sup>ns</sup>
	10	801.94 $\pm$ 53.08 <sup>*</sup>	774.53 $\pm$ 61.50 <sup>ns</sup>	82.46 $\pm$ 6.06 <sup>ns</sup>
<b>10</b>	1	1037.36 $\pm$ 43.22 <sup>ns</sup>	822.39 $\pm$ 30.99 <sup>ns</sup>	98.67 $\pm$ 6.94 <sup>ns</sup>
	10	810.96 $\pm$ 24.37 <sup>*</sup>	781.33 $\pm$ 34.57 <sup>ns</sup>	93.45 $\pm$ 4.09 <sup>ns</sup>
<b>11</b>	1	1227.5 $\pm$ 58.02 <sup>ns</sup>	740.96 $\pm$ 57.40 <sup>ns</sup>	88.67 $\pm$ 10.27 <sup>ns</sup>
	10	1155.38 $\pm$ 45.14 <sup>ns</sup>	727.53 $\pm$ 52.43 <sup>*</sup>	83.61 $\pm$ 6.13 <sup>ns</sup>
<b>12</b>	1	1049.54 $\pm$ 73.35 <sup>ns</sup>	599.58 $\pm$ 13.33 <sup>*</sup>	98.60 $\pm$ 4.70 <sup>ns</sup>
	10	548.76 $\pm$ 58.51 <sup>*</sup>	569.58 $\pm$ 32.86 <sup>*</sup>	82.67 $\pm$ 8.42 <sup>ns</sup>
<b>13</b>	1	1013.42 $\pm$ 46.32 <sup>*</sup>	551.97 $\pm$ 27.30 <sup>*</sup>	98.65 $\pm$ 4.45 <sup>ns</sup>
	10	623.78 $\pm$ 63.25 <sup>*</sup>	540.14 $\pm$ 33.92 <sup>*</sup>	95.33 $\pm$ 7.54 <sup>ns</sup>
<b>14</b>	1	971.20 $\pm$ 75.12 <sup>*</sup>	557.82 $\pm$ 16.70 <sup>*</sup>	97.00 $\pm$ 1.77 <sup>ns</sup>
	10	458.94 $\pm$ 55.30 <sup>*</sup>	465.60 $\pm$ 12.43 <sup>*</sup>	84.67 $\pm$ 2.34 <sup>ns</sup>
<b>15</b>	1	950.220 $\pm$ 33.90 <sup>*</sup>	517.61 $\pm$ 25.54 <sup>*</sup>	93.50 $\pm$ 5.18 <sup>ns</sup>
	10	307.56 $\pm$ 65.03 <sup>*</sup>	387.61 $\pm$ 16.01 <sup>*</sup>	69.00 $\pm$ 8.15 <sup>*</sup>
<b>16</b>	1	1215.66 $\pm$ 54.18 <sup>ns</sup>	758.15 $\pm$ 52.4 <sup>ns</sup>	96.0 $\pm$ 6.24 <sup>ns</sup>
	10	1178.92 $\pm$ 61.79 <sup>ns</sup>	687.64 $\pm$ 34.12 <sup>*</sup>	94.44 $\pm$ 5.26 <sup>ns</sup>
<b>17</b>	1	1067.20 $\pm$ 63.58 <sup>ns</sup>	667.26 $\pm$ 57.24 <sup>*</sup>	92.50 $\pm$ 7.23 <sup>ns</sup>
	10	493.38 $\pm$ 45.40 <sup>*</sup>	591.70 $\pm$ 16.89 <sup>*</sup>	70.67 $\pm$ 8.02 <sup>*</sup>
Dexamethasone	1	439.48 $\pm$ 57.49 <sup>*</sup>	313.85 $\pm$ 50.57 <sup>*</sup>	88.50 $\pm$ 2.73 <sup>ns</sup>
	10	177.04 $\pm$ 35.18 <sup>*</sup>	163.74 $\pm$ 10.18 <sup>*</sup>	57.66 $\pm$ 8.85 <sup>*</sup>

$n = 3$ ,  $p < 0.05$ .

<sup>#</sup> normal vs vehicle.

<sup>\*</sup> vehicle vs treatment.

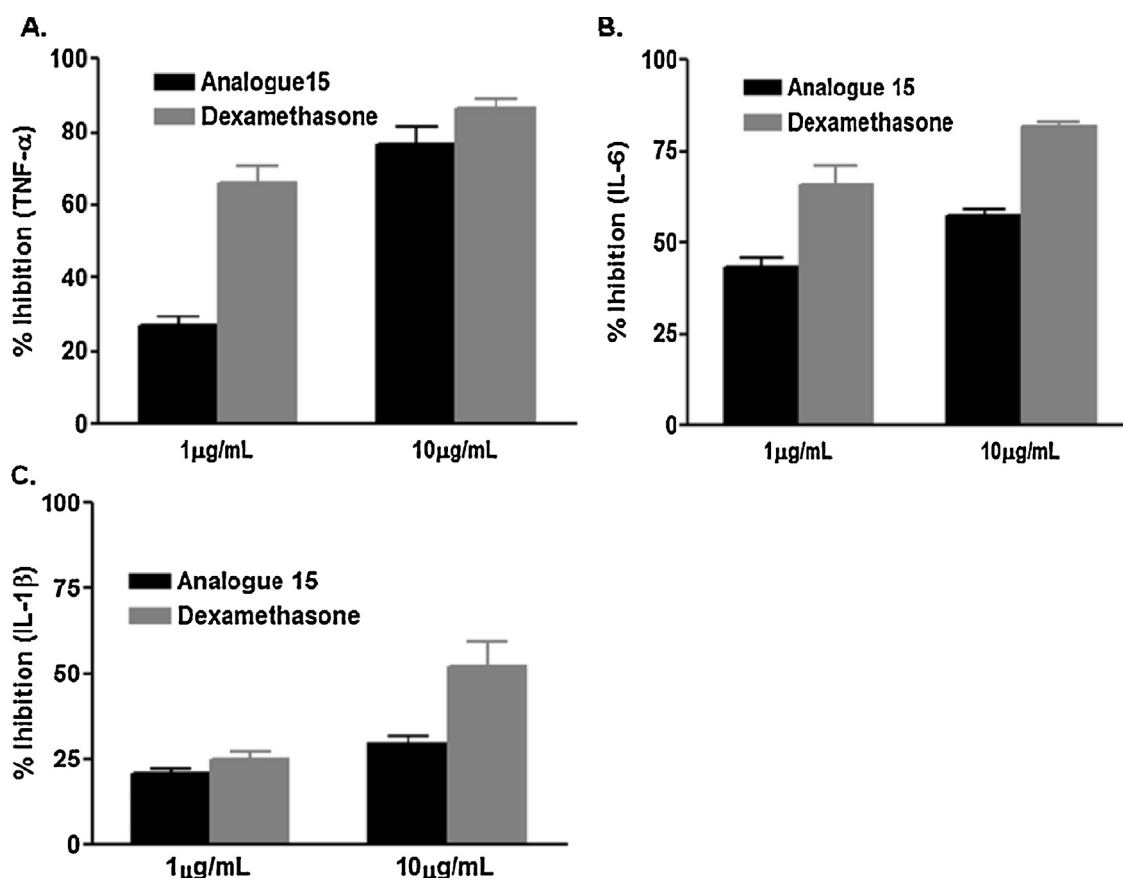


**Fig. 3.** Effect of analogue 15 and dexamethasone on percent (%) inhibition of pro-inflammatory cytokine production in LPS-induced inflammation in macrophage cells. (A) TNF- $\alpha$ ; (B) IL-6; (C) IL-1 $\beta$ .

### 3.2. Pharmacology

#### 3.2.1. Effect of diosgenin analogues on LPS-induced pro-inflammatory cytokines production in macrophages

All the synthesised diosgenin analogues were evaluated for their anti-inflammatory status against the production of pro-inflammatory cytokines (TNF- $\alpha$ , IL-6 and IL-1 $\beta$ ) using ELISA technique in LPS-induced inflammation in macrophage cells at the concentrations of 1 and 10  $\mu$ g/mL.

Production of pro-inflammatory cytokines was significantly ( $p < 0.05$ ) increased in LPS-stimulated cells when compared with normal un-stimulated cells. All the analogues including parent diosgenin exhibited inhibition of pro-inflammatory cytokines production when compared with vehicle treated LPS-stimulated cells (Table 1).

Among the all analogues, analogue **15** [(E) 26-(3',4',5'-trimethoxybenzylidene)-furost-5en-3 $\beta$ -acetate] possessed significant inhibition of TNF- $\alpha$ , IL-1 $\beta$  and IL-6 at both the concentration (Table 1). The percent inhibition of pro-inflammatory cytokines by analogue **15** in comparison to dexamethasone, a standard anti-inflammatory steroid drug is depicted in Fig. 3. These pro-inflammatory cytokines are the mediators of various acute and chronic inflammation linked diseases. Based on this study, analogue **15** was chosen for its further validation for evaluation of efficacy and safety in *in-vivo* system using LPS-induced sepsis as a systemic inflammation model and acute oral toxicity respectively in mice.

#### 3.2.2. In-vitro cytotoxicity profile of diosgenin analogues

We first examined the *in-vitro* cytotoxicity profile of all synthesised diosgenin analogues using MTT assay in peritoneal macrophage cells isolated from mice. The significant change in percent live cell population was not observed ( $p < 0.05$ ) at any concentration of diosgenin analogues treatment when compared with normal cells. Results are summarised in Table 2.

#### 3.2.3. Effect of analogue 15 on pro-inflammatory cytokine production in sepsis model of mice

To substantiate the physiological function of analogue **15** in *in-vivo* system, we examine the therapeutic anti-inflammatory effect of analogue **15** in a mouse model of sepsis, a systemic inflammatory condition. Serum level of pro-inflammatory cytokines (TNF- $\alpha$ , IL-6 and IL-1 $\beta$ ) was significantly increased in LPS-challenged vehicle-treated mice when compared to normal mice. Oral administration of analogue **15** before LPS challenge significantly ( $p < 0.05$ ) inhibited TNF- $\alpha$  and IL-6 production in a dose-dependent manner at dose rates of 3, 10 and 30 mg/kg body weight. The higher pretreatment dose (10 and 30 mg/kg) could also inhibit the IL-1 $\beta$  production in serum (Fig. 4).

#### 3.2.4. Histopathological changes in lung and liver tissues

To elucidate the effect of analogue **15** on lung and liver injuries in sepsis model of mice, histopathological examination of liver and lung tissue section was performed. Significant damage was observed in liver and lung tissues as evidenced by inflammatory cell infiltration in LPS-challenged vehicle-treated mice when compared with normal mice. Pretreatment of analogue **15** ameliorated the tissue damage in a dose-dependent manner (Fig. 5).

#### 3.2.5. Effect of analogue 15 on LPS-induced mortality in mice

The survival study was conducted to assess the protective effect of analogue **15** on LPS-induced mortality in mice. We monitored its effect on survival of mice for 5 days at 12 h. All the mice in LPS-challenged vehicle-treated group died within 48 h. Pretreatment of analogue **15** resulted in a markedly improved survival in

**Table 2**

Effect of diosgenin analogues on percent (%) cell viability in macrophage cells using MTT assay.

Analogues	Dose ( $\mu$ g/mL)	% Cell viability
Diosgenin		
<b>1</b>	1	104.31 $\pm$ 5.97
	10	101.18 $\pm$ 1.97
	30	97.73 $\pm$ 1.78
<b>8</b>	1	104.25 $\pm$ 9.05
	10	99.62 $\pm$ 1.77
	30	97.80 $\pm$ 3.08
<b>9</b>	1	99.42 $\pm$ 2.66
	10	96.87 $\pm$ 3.71
	30	93.34 $\pm$ 1.39
<b>10</b>	1	105.40 $\pm$ 2.41
	10	101.81 $\pm$ 4.85
	30	95.17 $\pm$ 5.81
<b>11</b>	1	102.22 $\pm$ 2.66
	10	99.63 $\pm$ 4.48
	30	94.47 $\pm$ 6.09
<b>12</b>	1	101.62 $\pm$ 3.56
	10	97.92 $\pm$ 2.64
	30	96.62 $\pm$ 5.34
<b>13</b>	1	100.25 $\pm$ 2.87
	10	98.20 $\pm$ 0.90
	30	97.13 $\pm$ 1.18
<b>14</b>	1	101.33 $\pm$ 3.55
	10	99.65 $\pm$ 1.96
	30	98.25 $\pm$ 2.78
<b>15</b>	1	103.28 $\pm$ 6.28
	10	100.78 $\pm$ 2.67
	30	96.73 $\pm$ 2.11
<b>16</b>	1	104.21 $\pm$ 4.19
	10	100.94 $\pm$ 3.67
	30	94.51 $\pm$ 4.40
<b>17</b>	1	102.83 $\pm$ 3.30
	10	97.26 $\pm$ 2.69
	30	97.57 $\pm$ 4.17
Dexamethasone		
	1	99.87 $\pm$ 3.92
	10	96.11 $\pm$ 5.55
	30	93.78 $\pm$ 8.71

$n = 3$ .

dose-dependent manner at 5 days and these animals are still survived (Fig. 6).

### 3.3. Acute oral toxicity study

The acute toxicity study showed that a single oral administration of analogue **15** (300 mg/kg) did not produce any mortality, behavioural changes (gait, posture, fur, depression and panting) in the mice as compared to the control group. Similarly, no significant changes were recorded in body weight, organ weight, serum biochemical (total bilirubin, creatinine, triglycerides, SGOT and glucose) as well as haematology parameters (total RBCs and total WBCs) of the treated group when compared to the control group. The representative results are depicted in Table 3 and Fig. 7.

#### 3.3.1. Molecular interaction study of diosgenin analogues through docking

*In-vitro* and *in-vivo* anti-inflammatory profiles of diosgenin analogues were further confirmed by molecular docking experiments. The aim of the molecular interaction study was to explore the molecular interaction of diosgenin analogues with pro-inflammatory cytokine receptors. The interaction study was compared with dexamethasone, a standard steroidal anti-inflammatory drug (Table 4).

The studied molecules show molecular interaction with TNF- $\alpha$  (PDB: 2AZ5), IL-6 (PDB: 1ALU) and IL-1 $\beta$  (PDB: 9ILB). The representative molecular interaction results of analogue **15** and dexamethasone are depicted in Fig. 8.

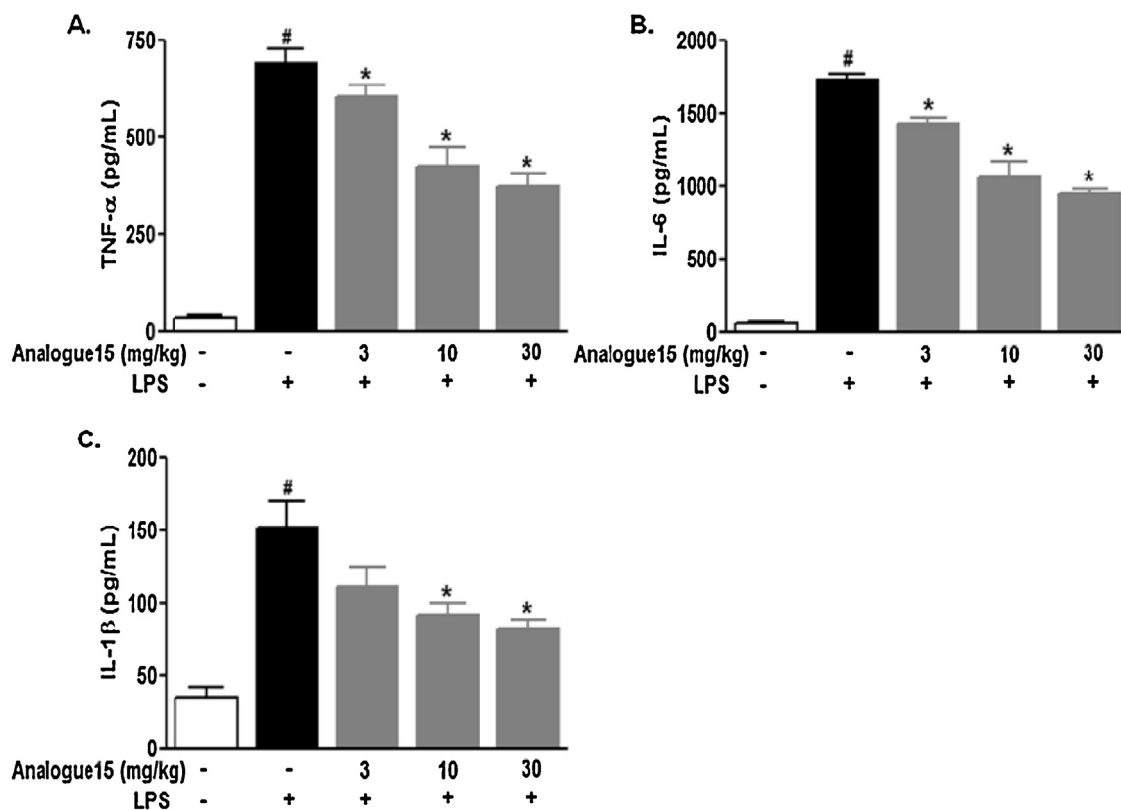


**Fig. 4.** Effect of analogue **15** on pro-inflammatory cytokine production in sepsis model of mice. (A) TNF- $\alpha$ ; (B) IL-6; (C) IL-1 $\beta$ . Data are expressed as mean  $\pm$  SEM: \* $p$  < 0.05; vehicle vs treatment; # vehicle vs normal; (Tukey's multiple comparison test);  $n$  = 6.

TNF- $\alpha$  interaction study found that residues Tyr-119, Leu-120, Gly-121, Leu-57, Tyr-59, Ser-60, Gly-122 and Tyr-151 were commonly shared by dexamethasone and diosgenin analogue **15**. Similarly analysis of binding pocket residues of IL-6 interacted with the diosgenin analogue **15**, and dexamethasone shared Asn-63, Leu-64, Pro-65, Glu-93, Val-96, Tyr-97, Pro-139, Thr-143, Asn-144, Leu-147 and Lys-150 residues. IL-1 $\beta$  interaction with the diosgenin analogue **15** and dexamethasone revealed the common residues as Leu-57, Ile-58, Tyr-59, Ser-60, Gln-61, Asn-63, Leu-64, Pro-65, Gly-122, Tyr-151, Ile-155, Tyr-119, Leu-120 and Gly-121.

#### 4. Discussion

There has been increasing interest in the discovery and development of novel pharmaceuticals from natural origin that have the same or better efficacy accompanied by less side effects. The majority of natural molecules and their analogues showed potent anti-inflammatory activities and some established themselves as clinical agents for chronic inflammatory disease conditions. Therefore, plant-based natural compounds play a significant role in the development of anti-inflammatory drugs in the pharmaceutical industry which can serve as good lead molecules suitable

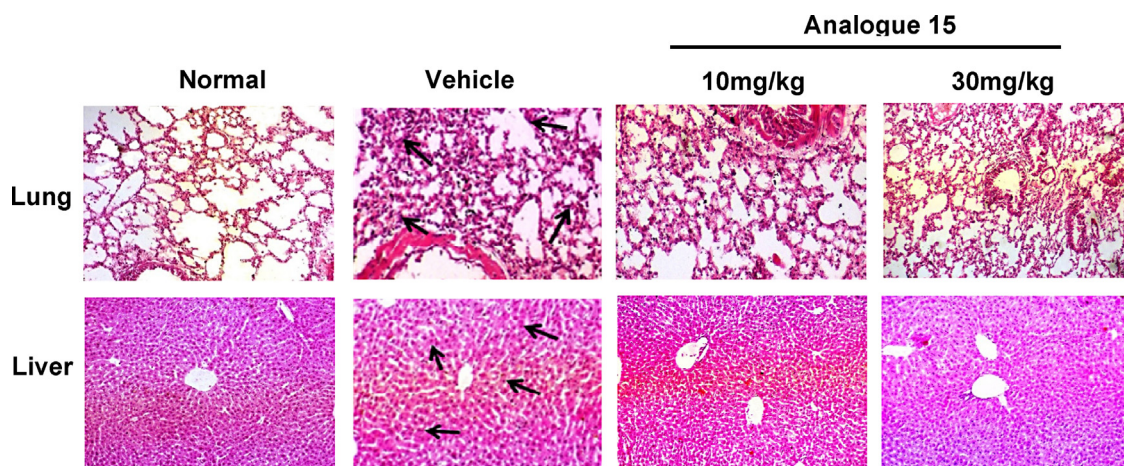


**Fig. 5.** Representative microphotograph of lung and liver (H&E stain, 100 $\times$ ) sections from the mice. Arrows indicate leukocyte infiltration.

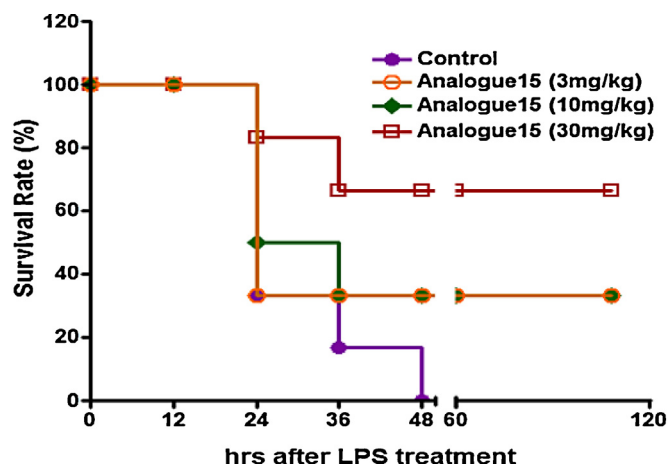


Fig. 6. Effect of analogue 15 on LPS-induced mortality in mice.

for further modification during the drug development process. Diosgenin (DG) is a C27 spiroketal steroidal saponin abundantly available in nature. It is mainly present in the form of saponin in the plants [25]. Previous investigations have shown that diosgenin plays an important pharmacological role including anti-inflammatory activity [18]. In present study, we have reported the influence of synthesised analogues of diosgenin by modifying at spiroketal ring on LPS-induced inflammatory response; an *in-vitro*, *in-vivo* study and it was further confirmed using *in-silico* study.

We have evaluated the *in-vitro* anti-inflammatory status of the synthesised diosgenin analogues against the

production of pro-inflammatory cytokines (TNF- $\alpha$ , IL-6 and IL-1 $\beta$ ). Synthesised analogues along with parent diosgenin exhibited inhibition of pro-inflammatory cytokines productions in LPS-stimulated cells without any cytotoxic effect as assessed by MTT assay. Several previous studies reported that diosgenin, a parent molecule, reduces the production of inflammatory mediators by inhibiting CK2, JNK, NF- $\kappa$ B and AP-1 activation [18,26]. This study, to our knowledge, provides the first evidence that synthesised analogues of diosgenin modifies at spiroketal ring exhibiting anti-inflammatory activity by inhibiting the production of pro-inflammatory cytokines in LPS-induced inflammation in macrophage cells. Pro-inflammatory cytokines, namely, TNF- $\alpha$ , IL-1 $\beta$  and IL-6, in LPS-induced macrophages, are known to have profound effects on the regulation of immune reactions, haematopoiesis and inflammation [27]. Overproduction of these cytokines has been implicated in the pathogenesis of many disease processes. The control of macrophage overproduction of these mediators should greatly facilitate the treatment of many inflammation-linked diseases such as sepsis, rheumatoid arthritis and autoimmune diabetes [16,17].

Among all analogues, analogue 15 [(E) 26-(3',4',5'-trimethoxybenzylidene)-furost-5en-3 $\beta$ -acetate] possessed significant ( $p < 0.05$ ) inhibition of pro-inflammatory cytokines (TNF- $\alpha$ , IL-6 and IL-1 $\beta$ ) at both the concentrations. It would also be interesting to evaluate its therapeutic effect in *in-vivo* systemic inflammation model. To substantiate the physiological function of most potent analogue, we have further evaluated the therapeutic efficacy and safety profile of analogue 15 in *in-vivo* system using LPS-induced sepsis and acute oral toxicity respectively in mice. Sepsis is marked by a systemic inflammatory response. Persistent or inappropriate or overproduction of multiple pro-inflammatory mediators such as TNF- $\alpha$  and IL-6 leads to severe injury and

Table 3

Effect of analogue 15 on acute toxicity at 300 mg/kg as a single oral dose in BALB/c mice.

Parameters studied	0th day		7th day	
	Control	Experimental	Control	Experimental
Body weight (g)	21.85 $\pm$ 0.36	21.80 $\pm$ 0.40	22.53 $\pm$ 0.49	22.6 $\pm$ 0.361
SGOT (U/L)	32.30 $\pm$ 4.34	31.56 $\pm$ 3.21	31.50 $\pm$ 5.34	31.06 $\pm$ 8.42
SGPT (U/L)	23.46 $\pm$ 4.01	22.45 $\pm$ 3.02	23.83 $\pm$ 7.53	21.96 $\pm$ 3.28
Cholesterol (mg/dL)	101.03 $\pm$ 1.33	105 $\pm$ 2.87	103.0 $\pm$ 1.69	100.28 $\pm$ 1.58
Triglycerides (mg/dL)	147.09 $\pm$ 7.28	128.47 $\pm$ 5.71	106.93 $\pm$ 7.14	108.69 $\pm$ 4.67
Haemoglobin (g/dL)	14.81 $\pm$ 2.11	14.96 $\pm$ 1.34	13.42 $\pm$ 1.51	14.44 $\pm$ 0.86
RBC (million/mm <sup>3</sup> )	7.31 $\pm$ 1.17	7.80 $\pm$ 1.33	7.58 $\pm$ 0.38	7.21 $\pm$ 0.41
WBC (thousands/mm <sup>3</sup> )	4.09 $\pm$ 0.12	4.35 $\pm$ 0.75	5.51 $\pm$ 0.19	4.32 $\pm$ 0.34

Data are expressed as mean  $\pm$  S.E.M.,  $n = 6$ .

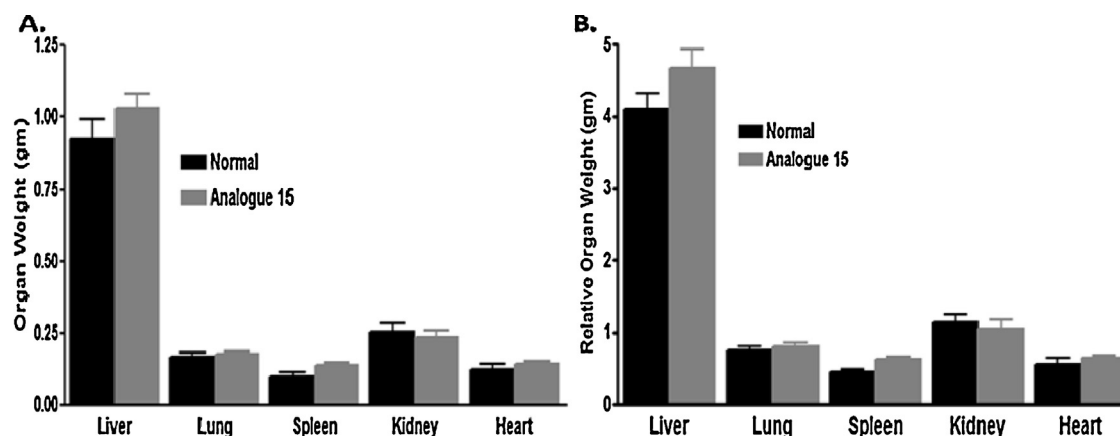
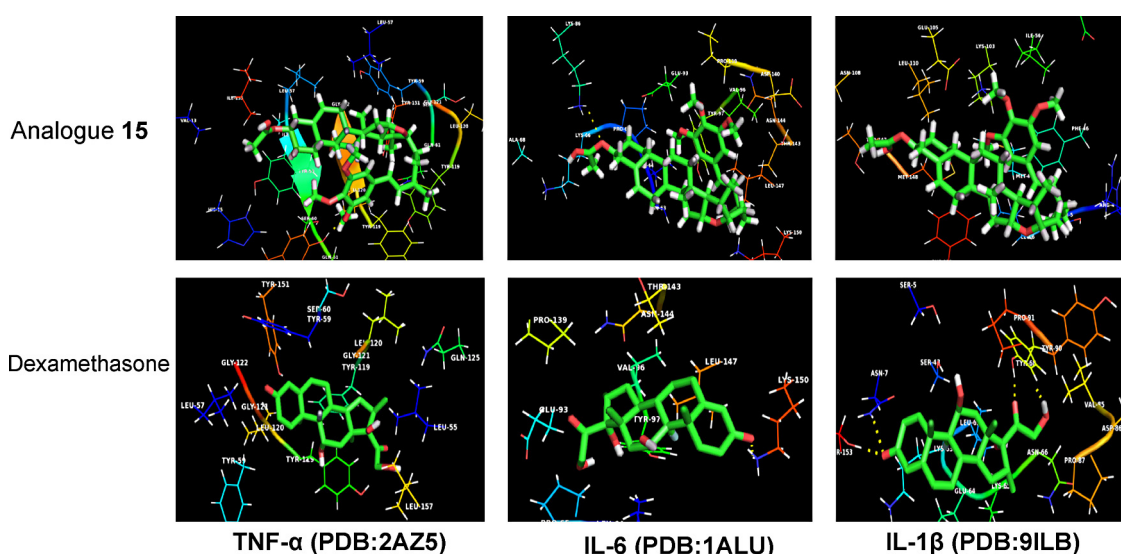


Fig. 7. Effect of analogue 15 as a single acute oral dose at 300 mg/kg on (A) absolute and (B) relative organ weight in BALB/c albino mice ( $n = 6$ , non significant changes were found compared to control).

**Table 4**  
Binding affinity (kcal mol<sup>-1</sup>) and interacting residual information of diosgenin derivatives with respect to the anti-inflammatory targets TNF-α (PDB: 2AZ5), IL-6 (PDB: 1ALU) and IL-1β (PDB: 9ILB).

Protein	Ligands	Binding affinity (kcal mol <sup>-1</sup> )	Pocket residues
TNF-α (2AZ5)	Analyse 15	-9	Gln(C)-61, Gly(C)-121, Gly(C)-122, Ile(C)-58, Ile(C)-155, Leu(C)-57, Leu(C)-120, Ser(C)-60, Tyr(C)-59, Tyr(C)-119, Tyr(C)-151, Gly(D)-121, Leu(D)-57, Leu(D)-120, Ser(D)-60, Tyr(D)-59, Tyr(D)-119, Tyr(D)-151
	Dexamethasone	-7.9	Gln(B)-125, Leu(B)-55, Leu(B)-157, Gly(C)-121, Gly(C)-122, Leu(C)-57, Leu(C)-120, Tyr(C)-59, Tyr(C)-119, Gly(D)-121, Leu(D)-120, Ser(D)-60, Tyr(D)-59, Tyr(D)-119, Tyr(D)-151
IL-6 (1ALU)	Analyse 15	-6	Asn-63, Leu-64, Pro-65, Lys-66, Lys-86, Glu-93, Val-96, Tyr-97, Pro-139, Asp-140, Thr-143, Asn-144, Leu-147, Lys-150
	Dexamethasone	-6.4	Asn-61, Asn-63, Asn-144, Glu-93, Leu-64, Leu-147, Lys-150, Pro-65, Pro-139, Thr-143, Tyr-97, Val-96
IL-1β (9ILB)	Analyse 15	-5.7	Arg-4, Asn-108, Glu-51, Glu-105, Ile-56, Leu-6, Leu-110, Lys-103, Met-44, Met-148, Phe-46, Phe-150, Ser-5
	Dexamethasone	-7.4	Asn-7, Asn-66, Asp-86, Glu-64, Leu-62, Lys-63, Lys-65, Pro-87, Pro-91, Ser-43, Ser-153, Tyr-68, Tyr-90, Val-85



**Fig. 8.** Analogue 15 and dexamethasone docked on target protein; TNF-α (PDB: 2AZ5), IL-6 (PDB: 1ALU) and IL-1β (PDB: 9ILB).

increased mortality in sepsis [28,29]. Thus, regulation of multiple mediators could be more beneficial than suppression of single mediator. In fact, the clinical trials targeting single inflammatory cytokine have been proved ineffective in the treatment of sepsis [30,31]. In LPS-induced sepsis model study in mice, we demonstrated that the oral administration of analogue 15 before LPS challenge significantly ( $p < 0.05$ ) inhibited TNF-α and IL-6 production in dose-dependent manner at the dose rate of 3, 10 and 30 mg/kg body weight and higher dose (30 mg/kg) is required to inhibit ( $p < 0.05$ ) the IL-1β production in serum. Pretreatment of analogue 15 also ameliorated the lung and liver injuries in sepsis model of mice as an evidence of histopathological examination as well as it helps to improve the survival of mice in lethal sepsis model. Overproduction of TNF-α and IL-1β leads to tissue damage [32,33], multiple organ failure and finally causes lethal sepsis [21]. Therefore, agents attenuating the production of pro-inflammatory cytokines may have potential as treatments for prevention of lethal sepsis [22].

Molecular interaction study of diosgenin analogue 15 with pro-inflammatory targets (TNF-α, IL-6 and IL-1β) through docking showed high binding affinity i.e. low docking energy. Several previous reports also concluded that the molecules having high binding affinity with targeted protein exhibited therapeutic efficacy [34,35].

## 5. Conclusion

Collectively, we demonstrated that diosgenin analogues inhibit the production of pro-inflammatory cytokines in both *in-vitro* and *in-vivo* condition, it was further confirmed with docking study. This finding confirms the suitability of diosgenin analogues as candidates for further investigation towards the management of inflammation related diseases.

## Conflict of interest

There are no conflicts of interest.

## Acknowledgements

We acknowledge the Council of Scientific and Industrial Research (CSIR) (Grant Nos. BSC0121 and BSC0203), New Delhi, India for financial support through XII FYP networking projects BSC0121 and BSC0203. We are thankful to Director, CSIR-Central Institute of Medicinal and Aromatic Plants, Lucknow, India for rendering essential research facilities and support. CSIR-Senior Research Fellowship to Ms. Monika Singh and TWAS-CSIR fellowship to Mr. A.A. Hamid are duly acknowledged.

## References

- [1] R. Medzhitov, Origin and physiological roles of inflammation, *Nature* 454 (2008) 428–435.
- [2] P.C. Calder, R. Albers, J.M. Antoine, S. Blum, R. Bourdet-Sicard, G.A. Ferns, G. Folkerts, P.S. Friedmann, G.S. Frost, F. Guarner, M. Lovik, S. Macfarlane, P.D. Meyer, L. M'Rabet, M. Serafini, E.W. Van, L.J. Van, D.W. Vas, S. Vidry, B.M. Winkhofer-Roob, J. Zhao, Inflammatory disease processes and interactions with nutrition, *Br. J. Nutr.* 101 (2009) S1–S45.
- [3] M. Guha, N. Mackman, LPS induction of gene expression in human monocytes, *Cell. Signal.* 13 (2001) 85–94.
- [4] H.K. de Jong, T. van der Poll, W.J. Wiersinga, The systemic proinflammatory response in sepsis, *J. Innate Immun.* 2 (2010) 422–430.
- [5] B. Beutler, E.T. Rietschel, Innate immune sensing and its roots: the story of endotoxin, *Nat. Rev. Immunol.* 3 (2003) 169–176.
- [6] K. Doi, A. Leelahavanichkul, P.S. Yuen, R.A. Star, Animal models of sepsis and sepsis-induced kidney injury, *J. Clin. Invest.* 119 (2009) 2868–2878.
- [7] P.J. Barnes, How corticosteroids control inflammation: Quintiles Prize Lecture 2005, *Br. J. Pharmacol.* 148 (2006) 245–254.
- [8] J. Raju, R. Mehta, Cancer chemopreventive and therapeutic effects of diosgenin, a food saponin, *Nutr. Cancer* 61 (2009) 27–35.
- [9] M.M. Gupta, S.U. Farooqui, R.N. Lal, Distribution and variation of diosgenin in different parts of *Costus speciosus*, *J. Nat. Prod.* 44 (1981) 486–489.
- [10] B. Shao, H. Guo, Y. Cui, M. Ye, J. Han, D. Guo, Steroidal saponins from *Smilax china* and their anti-inflammatory activities, *Phytochemistry* 68 (2007) 623–630.
- [11] M.A. McAnuff, W.W. Harding, F.O. Omoruyi, H. Jacobs, E.Y. Morrison, H.N. Asemota, Hypoglycemic effects of steroidal saponins isolated from Jamaican bitter yam, *Dioscorea polygonoides*, *Food Chem. Toxicol.* 43 (2005) 1667–1672.
- [12] J. Manivannan, E. Balamurugan, T. Silambarasan, B. Raja, Diosgenin improves vascular function by increasing aortic eNOS expression, normalize dyslipidemia and ACE activity in chronic renal failure rats, *Mol. Cell. Biochem.* 384 (2013) 113–120.
- [13] P.S. Chen, Y.W. Shih, H.C. Huang, H. Cheng, W. Diosgenin, A steroidal saponin, inhibits migration and invasion of human prostate cancer PC-3 cells by reducing matrix metalloproteinase expression, *PLoS ONE* 6 (2011) e20164.
- [14] F. Li, P.P. Fernandez, P. Rajendran, K.M. Hui, G. Sethi, Diosgenin a steroidal saponin, inhibits STAT3 signaling pathway, leading to suppression of proliferation and chemosensitization of human hepatocellular carcinoma cells, *Cancer Lett.* 292 (2010) 197–207.
- [15] C. Corbiere, B. Liagre, F. Terro, J.L. Beneytout, Induction of antiproliferative effect by diosgenin through activation of p53, release of apoptosis-inducing factor (AIF) and modulation of caspase-3 activity in different human cancer cells, *Cell Res.* 14 (2004) 188–196.
- [16] S. Shishodia, B.B. Aggarwal, Diosgenin inhibits osteoclastogenesis, invasion, and proliferation through the downregulation of Akt, I kappa B kinase activation and NF-kappa B-regulated gene expression, *Oncogene* 25 (2006) 1463–1473.
- [17] B. Hoesel, J.A. Schmid, The complexity of NF-kB signaling in inflammation and cancer, *Mol. Cancer* 12 (2013) 1–15.
- [18] J.X. Song, L. Ma, J.P. Kou, B.Y. Yu, Diosgenin reduces leukocyte adhesion and migration linked with inhibition of intercellular adhesion molecule-1 expression and NF-kb p65 activation in endothelial cells, *Chin. J. Nat. Med.* 10 (2012) 142–149.
- [19] Nomenclature of Steroids, IUPAC and International Union of Biochemistry-Joint commission on Biochemical Nomenclature, *Pure and Applied Chemistry*, vol. 61, No. 10, 1989, pp. 1783–1822.
- [20] B.S. Furniss, A.J. Hannaford, P.W.G. Smith, A.R. Tatchell, Vogel's textbook of practical organic chemistry, fifth edition, Addison Wesley Longman Limited Essex CM20 2JE, England, UK, 1989.
- [21] D.U. Bawankule, S.K. Chattopadhyay, A. Pal, K. Saxena, S. Yadav, U. Faridi, M.P. Darokar, A.K. Gupta, S.P. Khanuja, Modulation of inflammatory mediators by coumarinolignoids from *Cleome viscosa* in female swiss albino mice, *Inflammopharmacology* 6 (2008) 272–277.
- [22] D. Chanda, K. Shanker, A. Pal, S. Luqman, D.U. Bawankule, D. Mani, M.P. Darokar, Safety evaluation of Trikatu, a generic Ayurvedic medicine in Charles Foster rats, *J. Toxicol. Sci.* 34 (2009) 99–108.
- [23] S. Parihar, A. Kumar, A.K. Chaturvedi, N.K. Sachan, S. Luqman, B. Changkija, M. Manohar, O. Prakash, D. Chanda, F. Khan, C.S. Chanotiya, K. Shanker, A. Dwivedi, R. Konwar, A.S. Negi, Synthesis of combretastatin A4 analogues on steroidal framework and their anti-breast cancer activity, *J. Steroid Biochem. Mol. Biol.* 137 (2013) 332–344.
- [24] O. Trott, A.J. Olson, AutoDock Vina: improving the speed and accuracy of docking with a new scoring function, efficient optimization and multithreading, *J. Comput. Chem.* 31 (2010) 455–461.
- [25] M. Gao, L. Chen, H. Yu, Q. Sun, J. Kou, B. Yu, Diosgenin down-regulates NF-kB p65/p50 and p38MAPK pathways and attenuates acute lung injury induced by lipopolysaccharide in mice, *Int. Immunopharmacol.* 15 (2013) 240–245.
- [26] D.H. Jung, H.J. Park, H.E. Byun, Y.M. Park, T.W. Kim, B.O. Kim, S.H. Um, S. Pyo, Diosgenin inhibits macrophage-derived inflammatory mediators through downregulation of CK2, JNK, NF-kappaB and AP-1 activation, *Int. Immunopharmacol.* 10 (2010) 1047–1054.
- [27] I. Christiaens, D.B. Zaragoza, L. Guilbert, S.A. Robertson, B.F. Mitchell, D.M. Olson, Inflammatory processes in preterm and term parturition, *J. Reprod. Immunol.* 79 (2008) 50–57.
- [28] M.G. Netea, J.W. van der Meer, M. van Deuren, B.J. Kullberg, Proinflammatory cytokines and sepsis syndrome: not enough, or too much of a good thing? *Trends Immunol.* 24 (2003) 254–258.
- [29] C. Gerard, B.J. Rollins, Chemokines disease, *Nat. Immunol.* 2 (2001) 108–115.
- [30] E. Abraham, K. Reinhart, S. Opal, I. Demeyer, C. Doig, A.L. Rodriguez, R. Beale, P. Svoboda, P.F. Laterre, S. Simon, B. Light, H. Spapen, J. Stone, A. Seibert, C. Peckelsen, C. De Deyne, R. Postier, V. Pettilä, A. Artigas, S.R. Percell, V. Shu, C. Zwingelstein, J. Tobias, L. Poole, J.C. Stolzenbach, A.A. Creasey, Efficacy and safety of tifacogin (recombinant tissue factor pathway inhibitor) in severe sepsis: a randomized controlled trial, *J. Am. Med. Assoc.* 290 (2003) 238–247.
- [31] P. Qiu, X. Cui, A. Barochia, Y. Li, C. Natanson, P.Q. Eichacker, The evolving experience with therapeutic TNF inhibition in sepsis: considering the potential influence of risk of death, *Expert Opin. Invest. Drugs* 20 (2011) 1555–1564.
- [32] T. Yan, Q. Li, H. Zhou, Y. Zhao, S. Yu, G. Xu, Z. Yin, Z. Li, Z. Zhao, Gu-4 suppresses affinity and avidity modulation of CD11b and improves the outcome of mice with endotoxemia and sepsis, *PLoS ONE* 7 (2012) e30110.
- [33] H. Li, Y. Wang, H. Zhang, B. Jia, D. Wang, H. Li, D. Lu, R. Qi, Y. Yan, Hu. Wang, Yohimbine enhances protection of berberine against LPS-Induced mouse lethality through multiple mechanisms, *PLoS ONE* 7 (2012) e52863.
- [34] S. Sharma, S.K. Chattopadhyay, D.K. Yadav, F. Khan, S. Mohanty, A. Maurya, D.U. Bawankule, QSAR, docking and in vitro studies for anti-inflammatory activity of cleomiscosin A methyl ether derivatives, *Eur. J. Pharm. Sci.* 47 (2012) 952–964.
- [35] D.K. Yadav, V. Mudgal, J. Agrawal, A.K. Maurya, D.U. Bawankule, C.S. Chanotiya, F. Khan, S.T. Thul., Molecular docking and ADME studies of natural compounds of Agarwood oil for topical anti-inflammatory activity, *Curr. Comput. Aided Drug Des.* 9 (2013) 360–370.